IMAGE-GUIDED ABLATION OF TUMORS

EDITED BY: Jie Yu, Wei Yang and Mattia Squarcia
PUBLISHED IN: Frontiers in Oncology

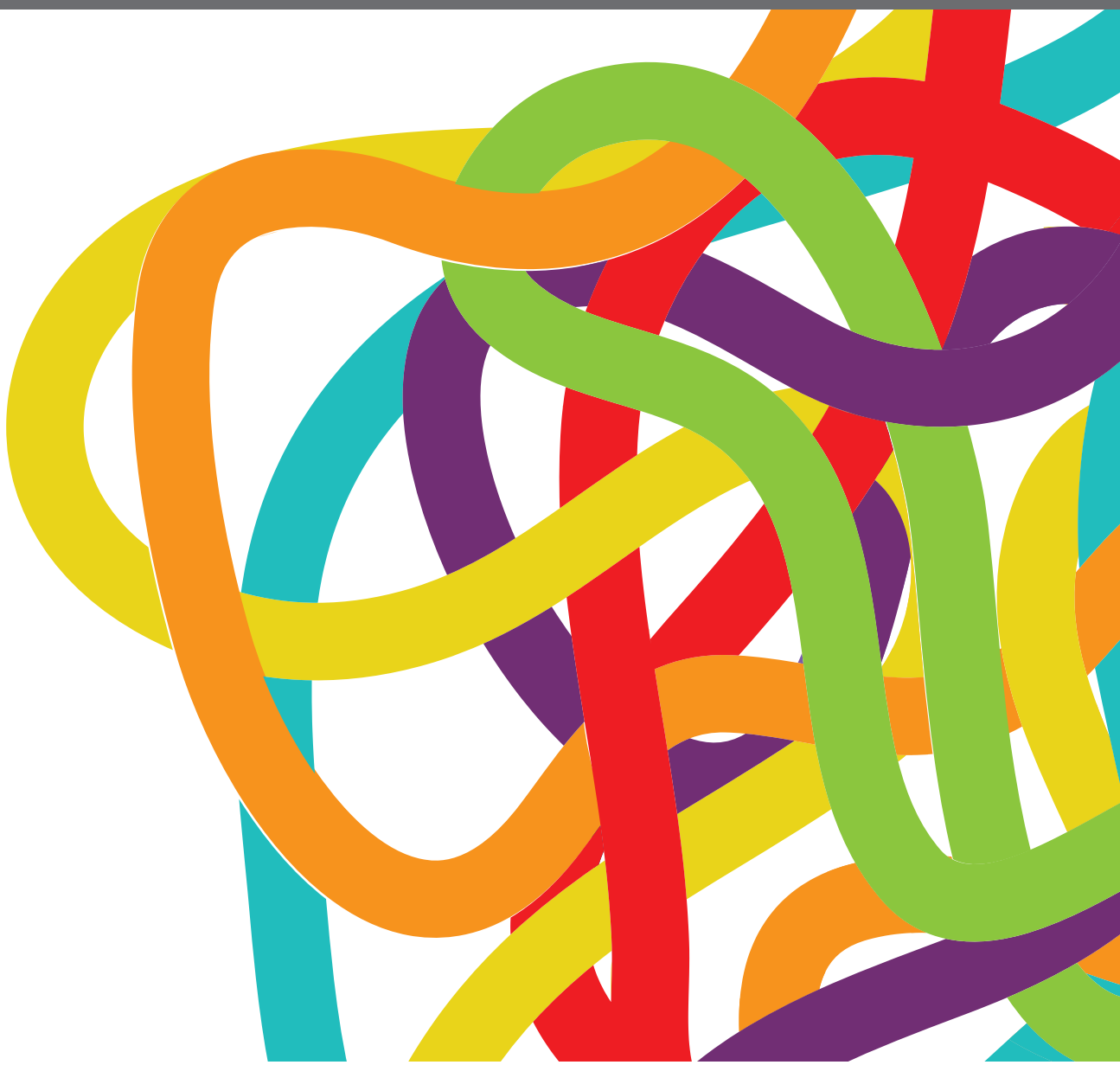

frontiers Research Topics

ISSN 1664-8714
ISBN 978-2-88974-561-6
DOI 10.3389/978-2-88974-561-6

About Frontiers

Frontiers is more than just an open-access publisher of scholarly articles: it is a pioneering approach to the world of academia, radically improving the way scholarly research is managed. The grand vision of Frontiers is a world where all people have an equal opportunity to seek, share and generate knowledge. Frontiers provides immediate and permanent online open access to all its publications, but this alone is not enough to realize our grand goals.

Frontiers Journal Series

The Frontiers Journal Series is a multi-tier and interdisciplinary set of open-access, online journals, promising a paradigm shift from the current review, selection and dissemination processes in academic publishing. All Frontiers journals are driven by researchers for researchers; therefore, they constitute a service to the scholarly community. At the same time, the Frontiers Journal Series operates on a revolutionary invention, the tiered publishing system, initially addressing specific communities of scholars, and gradually climbing up to broader public understanding, thus serving the interests of the lay society, too.

Dedication to Quality

Each Frontiers article is a landmark of the highest quality, thanks to genuinely collaborative interactions between authors and review editors, who include some of the world's best academicians. Research must be certified by peers before entering a stream of knowledge that may eventually reach the public - and shape society; therefore, Frontiers only applies the most rigorous and unbiased reviews.
Frontiers revolutionizes research publishing by freely delivering the most outstanding research, evaluated with no bias from both the academic and social point of view. By applying the most advanced information technologies, Frontiers is catapulting scholarly publishing into a new generation.

What are Frontiers Research Topics?

Frontiers Research Topics are very popular trademarks of the Frontiers Journals Series: they are collections of at least ten articles, all centered on a particular subject. With their unique mix of varied contributions from Original Research to Review Articles, Frontiers Research Topics unify the most influential researchers, the latest key findings and historical advances in a hot research area! Find out more on how to host your own Frontiers Research Topic or contribute to one as an author by contacting the Frontiers Editorial Office: frontiersin.org/about/contact

IMAGE-GUIDED ABLATION OF TUMORS

Topic Editors:
Jie Yu, People's Liberation Army General Hospital, China
Wei Yang, Peking University Cancer Hospital, China
Mattia Squarcia, Hospital Clínic de Barcelona, Spain

Citation: Yu, J., Yang, W., Squarcia, M., eds. (2022). Image-Guided Ablation of Tumors. Lausanne: Frontiers Media SA. doi: 10.3389/978-2-88974-561-6

Table of Contents

frontiers in Oncology

ORIGINAL RESEARCH
published: 10 June 2020
doi: 10.3389/fonc.2020.00842

Stereotactic Image-Guided Microwave Ablation for Malignant Liver Tumors—A Multivariable Accuracy and Efficacy Analysis

Pascale Tinguely[1], Lorenz Frehner[1], Anja Lachenmayer[1], Vanessa Banz[1], Stefan Weber[2], Daniel Candinas[1] and Martin H. Maurer[3]*

[1] Department of Visceral Surgery and Medicine, Inselspital, Bern University Hospital, University of Bern, Bern, Switzerland, [2] ARTORG Center for Biomedical Engineering Research, University of Bern, Bern, Switzerland, [3] Department of Diagnostic, Interventional and Pediatric Radiology, Inselspital, Bern University Hospital, University of Bern, Bern, Switzerland

Background: Therapeutic success of thermal ablation for liver tumors depends on precise placement of ablation probes and complete tumor destruction with a safety margin. We investigated factors influencing targeting accuracy and treatment efficacy of percutaneous stereotactic image-guided microwave ablation (SMWA) for malignant liver neoplasms.

Materials and methods : All consecutive patients treated with SMWA for malignant liver tumors over a 3-year period were analyzed. A computed tomography-based navigation system was used for ablation probe trajectory planning, stereotactic probe positioning, and validation of probe positions and ablation zones. Factors potentially influencing targeting accuracy [target positioning error (TPE)] and treatment efficacy within 6 months [ablation site recurrence (ASR)] were analyzed in a multivariable regression model, including challenging lesion locations (liver segments I, VII, and VIII; subphrenic location).

Results: Three hundred one lesions (174 hepatocellular carcinomas, 87 colorectal liver metastases, 17 neuroendocrine tumors, and 23 others) were targeted in 191 interventions in 153 patients. The median TPE per ablation probe was 2.9 ± 2.3 mm ($n = 384$). Correction of ablation probe positions by repositioning was necessary in 4 out of 301 lesions (1%). Factors significantly influencing targeting accuracy were cirrhosis (R 0.67, CI 0.22–1.12) and targeting trajectory length (R 0.21, CI 0.12–0.29). Factors significantly influencing early ASR were lesion size >30 mm (OR 5.22, CI 2.44–11.19) and TPE >5 mm (OR 2.48, CI 1.06–5.78). Challenging lesion locations had no significant influence on targeting accuracy or early ASR.

Conclusions: SMWA allows precise and effective treatment of malignant liver tumors even for lesions in challenging locations, with treatment efficacy depending on targeting accuracy in our model. Allowing for many tumors to be safely reached, SMWA has the potential to broaden treatment eligibility for patients with otherwise difficult to target tumors.

Keywords: liver neoplasms, interventional radiology, ablation techniques, stereotaxic techniques, computer-assisted therapies

OPEN ACCESS

Edited by:
Wei Yang,
Peking University Cancer Hospital, China

Reviewed by:
Hao Wu,
Peking University Cancer Hospital, China
Jin-yu Wu,
Harbin First Hospital, China

****Correspondence:***
Pascale Tinguely
pascale.tinguely@insel.ch

Specialty section:
This article was submitted to Cancer Imaging and Image-directed Interventions, a section of the journal Frontiers in Oncology

Received: *13 February 2020*
Accepted: *28 April 2020*
Published: *10 June 2020*

Citation:
Tinguely P, Frehner L, Lachenmayer A, Banz V, Weber S, Candinas D and Maurer MH (2020) Stereotactic Image-Guided Microwave Ablation for Malignant Liver Tumors—A Multivariable Accuracy and Efficacy Analysis. Front. Oncol. 10:842. doi: 10.3389/fonc.2020.00842

INTRODUCTION

For patients with malignant liver tumors, thermal ablation is a locally destructive, low-morbidity, and potentially curative treatment option, particularly for hepatocellular carcinoma (HCC) and colorectal liver metastases (CRLM) (1, 2). Radiofrequency ablation (RFA) or microwave ablation (MWA) are increasingly used for non-resectable disease (3), in combined treatment approaches (4), or even as an alternative to surgery (5–7), with repeat therapy sessions well-tolerated in the case of hepatic recurrence (8).

The crucial factor for successful ablative treatment is complete tumor ablation with an adequate safety margin (9), while avoiding injury to critical intrahepatic and perihepatic structures. This is highly dependent on the precision with which the ablation probes are guided toward and positioned within the target lesions to subsequently generate adequate ablation zones. Safe percutaneous targeting is often precluded when using conventional ultrasonography (US) or computed tomography (CT) guidance (10), especially for tumors located in challenging intrahepatic positions such as in the liver dome (11), in a subcapsular location, or in proximity to the liver hilum or heart (12). Ablation of such difficult to target tumors results in an increased risk of complications and associated higher recurrence rates (13, 14), especially if multiple re-positionings of ablation probes are necessary to achieve adequate probe positions. Several techniques have been proposed to target tumors located in the liver dome, such as artificially induced pneumothorax (15), pleural effusion (16), or ascites (17), an epicardial fat pad approach (18), combined imaging techniques (19), or mathematic models (20), with varying degrees of reliability.

Advanced image-guided navigation technologies aiming to enhance precision and safety in the targeting of liver tumors have been introduced (21). First clinical reports on stereotactic percutaneous ablation of liver tumors are available (22–25), as well as several comparative studies highlighting the accuracy and efficiency of using navigation technology vs. conventional image guidance for tumor targeting (26, 27). While little is known about factors influencing targeting accuracy and therapeutic efficacy when using such navigation systems for stereotactic tumor targeting, they likely facilitate accessibility and treatment of traditionally difficult to target liver tumors (28). Our group has previously reported the benefits of using stereotactic image-guided microwave ablation (SMWA) in the treatment of HCC (29). The aim of the current study was to investigate factors influencing targeting accuracy and treatment efficacy when using SMWA for malignant liver tumors in a multivariable model that includes challenging lesion locations.

MATERIALS AND METHODS

Patient Population

Data from all consecutive patients treated with SMWA for malignant liver tumors at our institution between January 2015 and December 2017 were prospectively collected and analyzed retrospectively. The study protocol was approved by the Regional Ethical Review Board (KEK-Nr 2017-01038). All patients were discussed at the weekly multidisciplinary tumor board meeting. SMWA and the use of stereotactic navigation technology represent the standard approach at our institution for all patients in whom percutaneous thermal ablation for malignant liver tumors is indicated. Thermal ablation therapy was indicated for patients with (i) unresectable disease due to comorbidities or lesion location, but in whom local ablation was considered a potentially curative treatment due to adequate response to chemotherapy or stable disease, (ii) HCC awaiting liver transplantation as part of a bridge to transplant or down-staging approach, (iii) resectable CRLM as part of a prospective multi-center trial investigating ablation as an alternative to resection (30), or (iv) multiple liver lesions as part of a multimodal treatment approach of combined ablation and resection. A maximum of five lesions were treated in one intervention to limit overall intervention time and generally lesions up to 5 cm in diameter were included for SMWA.

Material and Procedural Technique

All interventions were performed in the interventional radiology CT suite (SOMATOM Definition Flash, Siemens Healthineers, Erlangen, Germany), by a joint interdisciplinary team consisting of one of four radiologists and one of four surgeons. A commercially available navigation system (CAS-ONE, CAScination AG, Bern, Switzerland) was used to plan ablation probe trajectories, position ablation probes, and validate ablation probe positions and ablation zones. The system utilizes optical tracking of the patient's abdominal surface via six skin fiducials that are rigidly co-registered to available image data (24, 26). Procedures were performed under general anesthesia with patients positioned on a vacuum mattress, using high-frequency jet ventilation for respiratory motion control (31). This quasi-static scenario ensures patient immobility and minimal displacement of the diaphragm and provides the basis for accurate and automatic rigid fusion of all performed CT scans (32). If insufficient fusion quality between scans was suspected upon visual inspection, a manual point-based registration was additionally performed. The four main procedural steps are described and illustrated in **Figure 1**.

A planning CT scan using a predefined multi-phase imaging protocol ($2 \times 64 \times 0.6$ mm; 280-ms gantry rotation time; pitch factor, 0.6; tube voltage, 100 kV) was performed after delivery of intravenous contrast medium (Ultravist® Bayer Healthcare, Berlin, Germany). The scan window of this first planning scan included all previously placed skin fiducials. The planning imaging where the target lesions were best detectable was transferred to the navigation system. After navigated ablation probe positioning, a second non-enhanced CT scan was performed for validation of the correct ablation probe position. Native scans were repeated for each targeted lesion to evaluate the respective probe positions before ablation. MWA (Acculis MTA System, AngioDynamics, Latham, NY, USA) was performed with energy and time settings adapted to the lesion diameter. A final contrast-enhanced CT scan with three phases and intravenous contrast medium was performed for immediate confirmation of adequate treatment of all target lesions. A minimal ablation margin of 5–10 mm was considered sufficient

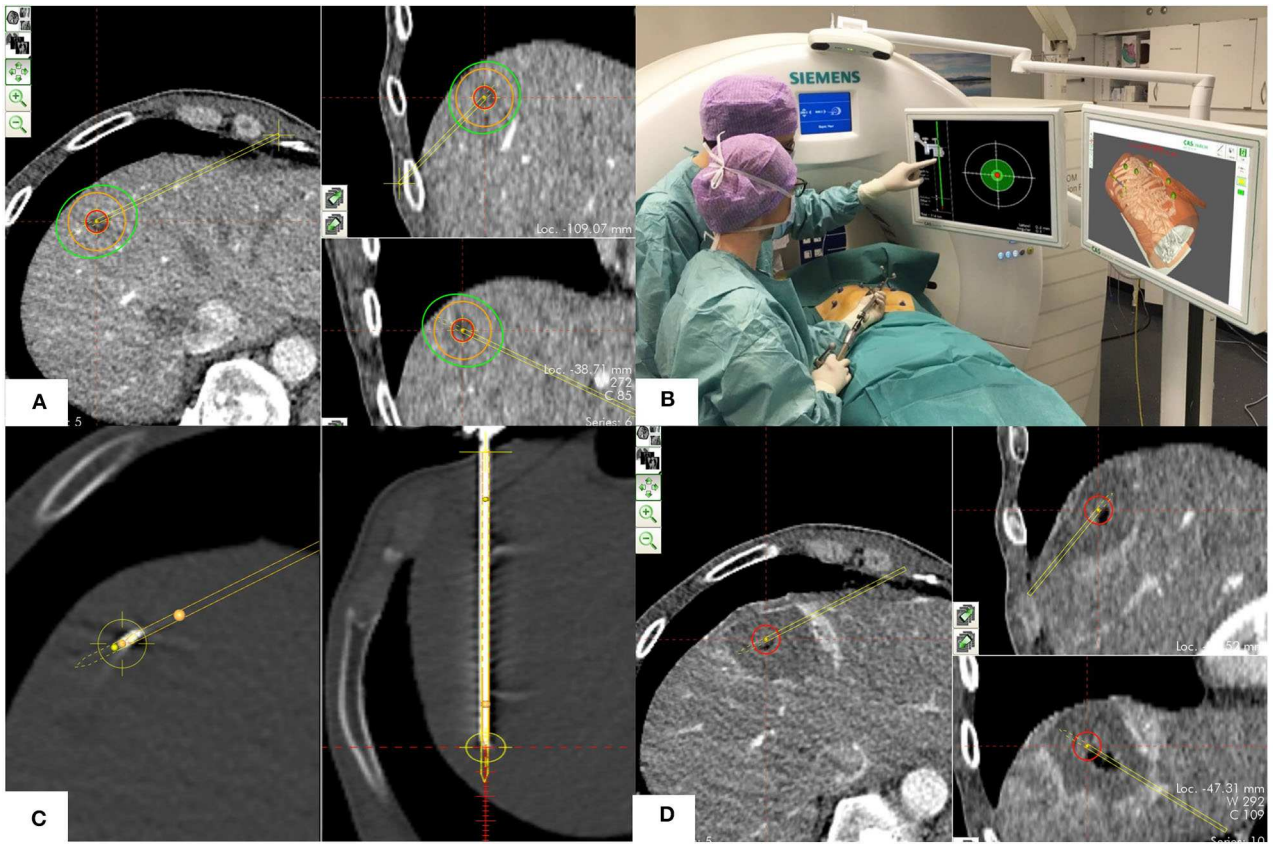

FIGURE 1 | Procedural technique including the four phases of SMWA. **(A)** Planning phase: Planning of the optimal ablation probe trajectory by selecting the skin entry point and the intrahepatic target point using the navigation system's planning module. The target tumor is depicted in red, the planned ablation margin is in orange, and the simulated ablation zone according to the manufacturer's prediction is in green. **(B)** Navigation phase: Navigated alignment of the aiming device along the planned trajectory, with the cross-hair viewer indicating the trajectory direction. The trajectory depth for consecutive ablation probe positioning is indicated in millimeters. **(C)** Ablation probe validation and ablation phase: After insertion of the ablation probe, its positional accuracy relative to the planned trajectory is verified in the validation scan and calculated in millimeters. If satisfactory, microwave ablation is performed. **(D)** Ablation zone validation phase: A sufficient ablation zone is verified by direct overlay of pre- and post-ablation images using the validation module, allowing immediate estimation of the completeness of ablation.

(33, 34). Prophylactic antibiotics were administered routinely. If safe, all medical staff including anesthesia left the IR suite during CT scanning.

Assessment of Accuracy and Procedural Efficiency

The navigation system software allows recording and calculation of the exact targeting accuracies, trajectory-specific parameters, and duration of individual procedural steps, data that were extracted from the navigation system's log file data. Angles of the ablation probe trajectories were calculated as indicated in **Figure 2A**. Targeting accuracy was assessed as the targeting errors resulting after ablation probe positioning, defined as the deviance between the planned trajectory and the achieved ablation probe position, and was calculated as shown in **Figure 2B**. Targeting accuracies were reported as sub-millimetric values resulting from statistical computation, as visual assessment was limited by the image resolution of the CT imaging. A large lateral error implied the *repositioning* of the ablation probe, defined as the full retraction of the ablation probe, repeat navigated alignment of the aiming device and probe re-insertion. Contrarily, longitudinal errors were easily corrected by advancement or retraction of the probe along the same trajectory line. For this reason, the lateral targeting error was defined as the primary target positioning error (TPE) (27). The navigation system software allows for the precise planning of multiple ablation probes in excentric positions as opposed to a single probe in the tumor center, enabling the generation of larger ablation zones. This positioning of multiple parallel ablation probes was defined as *planned overlapping ablation* and was mostly applied for lesions >3 cm.

Durations of the overall procedure and of individual procedural steps were recorded. When multiple ablation probes were positioned per intervention, the durations were calculated for each probe and added to obtain the total time per phase per intervention. Clinical complications within 90 days were assessed and graded according to the Clavien-Dindo classification (35). Radiological complications without clinical symptoms as diagnosed on the first post-ablation scan or on

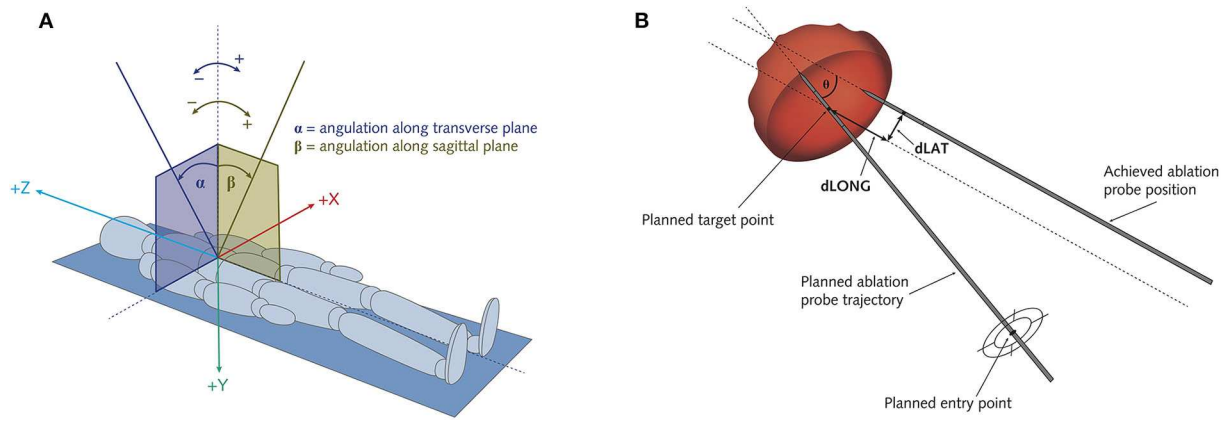

FIGURE 2 | Schematic illustration of the assessment of ablation probe trajectory angles **(A)** and of targeting errors of the positioned ablation probes **(B)**. **(A)** Alpha angle α: angulation along transverse plane. Beta angle β: angulation along sagittal plane. **(B)** Theta θ: Angular error. dLat: Lateral error = target positioning error (TPE). dLong: Longitudinal error.

imaging within the same hospitalization were recorded. Length of hospital stay was calculated from the day of SMWA to the day of discharge.

Assessment of Treatment Efficacy

All imaging results were reviewed and interpreted by an independent radiologist specialized in liver imaging. *Immediate re-ablation* was defined as the repeat ablation of one lesion, due to incomplete tumor coverage after ablation zone validation, at the end of the same treatment session. *Technical success* was reported according to the standardized criteria suggested by Ahmed et al. (36) and defined as complete tumor coverage by the ablation zone as assessed on the final CT scan with intravenous contrast on the day of intervention, including immediate re-ablations. The first follow-up imaging (MRI or CT) was carried out at 1–3 months, with re-imaging every 2–4 months thereafter in patients with stable disease. Early *ablation site recurrence (ASR)* was defined as the presence of morphologically detectable tumor tissue within 10 mm from the edge of the ablation zone, on any of the follow-up imaging performed within 6 months (including the first follow-up imaging), in lesions with initial complete tumor coverage. Subgroup analyses were performed for lesions located in *challenging locations*, defined as the superior dorsal liver segments VII/VIII, segment I and a subphrenic location (<10 mm from the diaphragm). The appearance of new intrahepatic lesions on follow-up imaging was documented.

Statistical Analysis

Continuous data were reported as median, interquartile range (IQR), and standard deviation (SD), and categorical data were reported as number and percentage. Regression analysis was performed to identify factors potentially influencing targeting accuracy and early ASR per targeted lesion. As multiple lesions were ablated in the same individual patients and we focused on per-lesion outcomes, we included repeated measure analyses in our model. Generalized estimating equations (GEE) using an exchangeable correlation structure and a robust estimator of covariance were applied. The resulting regression coefficients and odds ratios (OR) are comparable to coefficients and OR resulting from classic regression models, with the benefit of accounting for intra-class correlations. All factors thought to potentially influence the precision with which ablation probes were positioned along the planned trajectory were analyzed using univariable and multivariable linear GEE, with all covariates included in the multivariable model. For lesions with multiple ablation probe insertions (immediate re-ablations or planned parallel insertions) per ablated lesion, average values were used for continuous variables (targeting errors, trajectory lengths and angles). Results of all tested variables were reported as regression coefficients with 95% Wald confidence intervals (CIs). All available factors thought to potentially influence early ASR were analyzed using univariable and multivariable binary logistic GEE, with results reported as OR and 95% Wald CI. The threshold for statistical significance was set to the level $\alpha = 0.05$. SPSS Statistics (Version 24.0.0, SPSS Inc.) was used for all statistical analyses.

RESULTS

In 3 years, a total of 301 lesions were treated with SMWA in 191 interventions in 153 patients. Lesion characteristics and ablation parameters per lesion are described in **Table 1**. The number of ablated tumors per intervention ranged from 1 to 5 and maximum lesion size ranged from 4 to 60 mm. Of the 301 treated lesions, 54 (18%) were local recurrences after prior treatment of the same lesion, including previous thermal ablation ($n = 33$), trans-arterial (chemo-)embolization ($n = 10$), or resection ($n = 11$). For 25 lesions (8%), multiple parallel needles were placed to create larger ablation zones. Correction of probe positions with probe repositioning was necessary in 4 out of 301 lesions (1%). Two example cases of SMWA for lesions in challenging intrahepatic locations in liver segment VII and segment I are illustrated in **Figures 3**, **4**, respectively.

TABLE 1 | Lesion and ablation characteristics per ablated lesion ($n = 301$).

Lesion entity	
Hepatocellular carcinoma	174 (58)
Colorectal liver metastases	87 (29)
Neuroendocrine metastases	17 (6)
Others	23 (8)
Lesion size	
Diameter [mm][a]	15 (11–21)
Tumor size >30 mm	29 (10)
Lesion location	
Segments II–IV	100 (33)
Segments V/VI	59 (20)
Segments VII/VIII	136 (45)
Segment I	6 (2)
Subcapsular location[b]	175 (59)
Subphrenic location[b]	71 (24)
Vessel proximity[c]	103 (34)
IVC	7 (2)
Organ proximity[b]	23 (8)
Gallbladder	5 (2)
Other (colon/stomach/kidney/heart)	18 (6)
Ablation parameters per lesion	
Cumulative ablation time[d] [min]	4 (3–6)
Ablation energy	
60/80 W	6 (2)
100 W	271 (94)
120 W	12 (4)
Number of ablation probes per lesion	
1	233 (77)
2	56 (19)
3–5	12 (4)
Planned overlapping ablations	25 (8)
Number of parallel ablation probes	2 (2–3)
Immediate re-ablations	48 (16)
Ablation probe repositionings	4 (1)

Categorical data are shown as number and percentage, and numerical data are shown as median and interquartile range. [a]Maximal diameter measured in a transverse plane. [b]Edge of the tumor located within 10 mm of the respective structure. [c]Edge of the tumor located within 5 mm to an intrahepatic artery, vein, or portal vein of a minimum diameter of 3 mm. [d]Addition of all ablation times per lesions treated in one session (including re-ablations and planned overlapping ablations).

Targeting Accuracy

Median TPE per positioned ablation probe ($n = 384$) was 2.9 mm (IQR 1.7–4.5 mm, SD 2.3 mm). When the ablation probes were positioned in lesions located in segments VII or VIII ($n = 178$), segment I ($n = 6$), or in a subphrenic location ($n = 71$), median TPE was 3.5 mm (SD 2.3 mm), 3.1 mm (SD 1.8 mm), and 4.0 mm (SD 2.4 mm), respectively. All targeting errors and trajectory-specific parameters per positioned ablation probe are summarized in **Table 2**.

Univariable and multivariable analyses of factors influencing TPE are shown in **Table 3**. In the multivariable model, underlying liver cirrhosis (linear regression coefficient R 0.668, CI 0.218–1.119) and targeting trajectory length (R 0.205, CI 0.118–0.291) had a statistically significant influence on TPE. This implies a mean increase in TPE of 0.7 mm for lesions targeted in a cirrhotic vs. a non-cirrhotic liver, and of 0.2 mm for each additional centimeter of targeting trajectory length. Contrarily, challenging intrahepatic lesion locations such as a subphrenic, superior dorsal, or segment I lesion location, an intercostal targeting trajectory or varying targeting trajectory angles did not significantly influence TPE (**Table 3**).

Procedural Efficiency and Safety

Procedural efficiency and safety are summarized in **Table 4**. Median overall duration of SMWA from first to last CT scan was 64 min (IQR 46–82 min, SD 33 min).

In the 191 SMWA interventions, a total of 10 (5%) clinical complications occurred. These included six grade I–II complications, of which were one fever of unknown origin, one skin infection at the ablation probe entry site, one case of ascites, one case of transient brachial plexus paralysis due to arm positioning in a cachectic patient, and two cases of severe lower thoracic/upper abdominal pain due to pleuritis and a small perihepatic hematoma, respectively. Three grade IIIa complications included one pneumothorax and one pleural effusion, both requiring chest drainage, and one case of intrahepatic abscess, which was drained percutaneously. A second case of a suspected intrahepatic abscess with fever underwent surgical resection of segments VI and VII (grade IIIb complication); however, histologic analyses did not confirm the presence of intrahepatic infection. Median length of hospital stay was 1 day (range, 0–13).

Treatment Efficacy

Immediate re-ablations due to insufficient tumor coverage after ablation zone validation were performed in 48 (16%) lesions. The rate of complete tumor coverage on the day of intervention (technical success) was 96% (290/301 lesions). In the remaining 11 lesions, immediate re-ablation was judged to be unsafe, due to an increased risk of injury to critical structures or an already large ablation zone with risk of secondary infection. In the subgroup of lesions located in challenging locations, technical success was achieved in 97% (155 of 160) of the lesions. In the subgroup of 25 lesions targeted with multiple parallel ablation probes, technical success was 96% (23 of 24 lesions), with the one remaining large (41 mm) lesion located in proximity to a main portal vein bifurcation. This lesion was planned for future resection and was thus knowingly insufficiently ablated.

Overall ASR within 6 months, including the first follow-up imaging, was 22% (49 out of 227 previously completely ablated lesions with available 6 months follow-up), of which 17 (35%) lesions were successfully re-ablated. Twenty-one of the 49 lesions with ASR (43%) occurred in the setting of simultaneous appearance of new intrahepatic lesions. In the subgroups of lesions located in segment VII or VIII, segment I, or in a subphrenic location, ASR was 16, 23, and 20%, respectively. In the subgroup of lesions that had undergone immediate re-ablation, ASR was 18%. Results from the regression analyses of factors influencing early ASR are summarized in **Table 5**. In the univariable analysis of factors influencing early ASR, colorectal liver metastases and a tumor size >30 mm

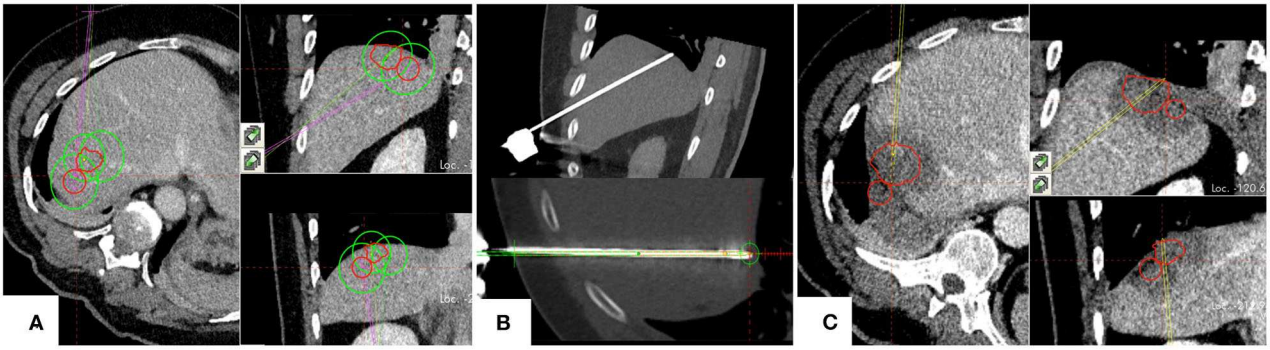

FIGURE 3 | Example case of a patient with hepatocellular carcinoma, treated for two adjacent tumors located in segment VII. **(A)** Planning of targeting trajectories for three parallel ablation probes to create overlapping ablation zones (green) around the target tumors (red). **(B)** Top: positioned ablation probe in an immediate subphrenic position. Bottom: Validation of ablation probe position. **(C)** Complete ablation of both tumors (red) with a sufficient surrounding ablation margin.

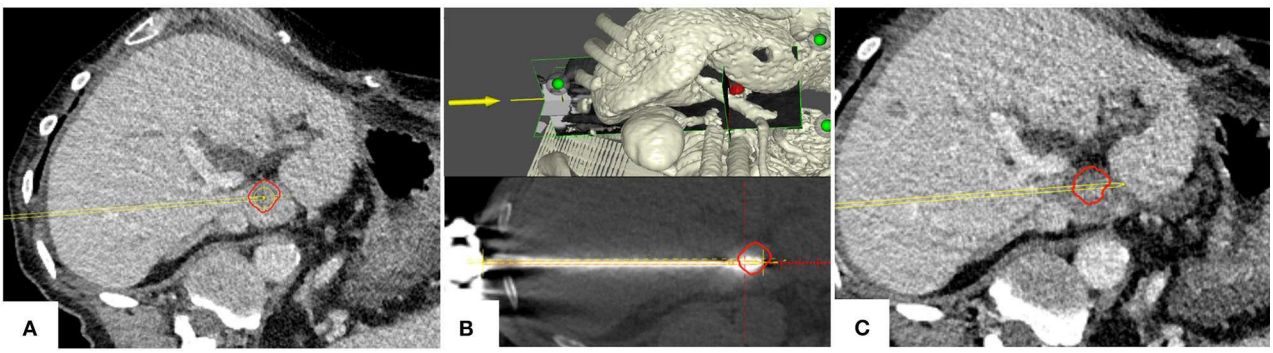

FIGURE 4 | Example case of a patient with a colorectal cancer metastasis (red) located in segment I. **(A)** Planning of targeting trajectory. **(B)** Top: targeting trajectory and tumor in a three-dimensional view. Bottom: Validation of ablation probe position. **(C)** Complete tumor (red) coverage by the ablation zone with a sufficient ablation margin; the adjacent main portal vein branches remain patent.

were statistically significant. In the multivariable model, factors with a significant influence on early ASR were lesion size (>30 mm) and targeting accuracy (TPE >5 mm). Challenging intrahepatic lesion locations or the proximity to intrahepatic vascular structures or adjacent organs were not predictive factors of early ASR (**Table 5**).

DISCUSSION

This study shows that using SMWA for targeting of malignant liver tumors allows precise, efficient, and effective local tumor treatment, without compromise in accuracy or efficacy when targeting lesions located in challenging locations. To our knowledge, this is the first series analyzing factors influencing targeting accuracy and treatment efficacy of stereotactic MWA of malignant liver tumors using a multivariable model to date.

The present work confirms a high overall precision in the positioning of ablation probes when using SMWA, comparable to previously reported TPE values after navigated ablation probe positioning, ranging between 2.9 and 4.0 mm (24, 26). Targeting errors might have been minimally influenced by otherwise non-quantifiable fusion errors between scans, despite optimizing conditions for minimal patient and organ movement during the procedure. Importantly, a superior dorsal (segment VII or VIII), segment I or a subphrenic location did not significantly influence targeting accuracy, confirming the safe

TABLE 2 | Targeting accuracy and trajectory-specific parameters, per ablation probe ($n = 384$).

Targeting trajectory characteristics	
Trajectory length [cm]	11.1 (8.3–13.2)
Intercostal trajectory (*n*, %)	253 (85)
Trajectory angle α [°]	−15 (−46–6)
Trajectory angle β [°]	19 (4–32)
Targeting errors	
Lateral targeting error, TPE [mm]	2.9 (1.7–4.5)
Longitudinal targeting error [mm][a]	1.3 (0.4–2.7)
Angular targeting error [°]	1.8 (1.1–2.7)

Categorical data are shown as number and percentage, and numerical data are shown as median and interquartile range. TPE, target positioning error. [a]Targeting errors prior to correction of ablation probe position (advancement/retraction) before thermal ablation.

TABLE 3 | Linear Generalized Estimating Equations (GEE) analysis of factors influencing target positioning errors, per ablated lesion.

	Univariable analysis		Multivariable analysis	
	***B* (95% CI)**	***p*-value**	***B* (95% CI)**	***p*-value**
Clinical parameters				
Cirrhosis [y/n]	0.791 (0.274, 1.308)	0.003	0.668 (0.218, 1.119)	0.004
Location-specific parameters				
Segments I/VII/VIII [y/n]	0.870 (0.363, 1.377)	<0.001	0.128 (−0.413, 0.670)	0.642
Subphrenic location[a] [y/n]	0.935 (0.293, 1.578)	0.004	0.238 (−0.382, 0.859)	0.415
Subcapsular location[a] [y/n]	0.425 (−0.052, 0.902)	0.081	0.371 (−0.080, 0.821)	0.107
Trajectory-specific parameters				
Trajectory length [per cm]	0.244 (0.166, 0.323)	<0.001	0.205 (0.118, 0.291)	<0.001
Intercostal trajectory [y/n]	1.005 (0.549, 1.461)	<0.001	0.497 (−0.002, 0.997)	0.051
Trajectory angle α[b] [per 10°]	−0.025 (−0.126, 0.077)	0.634	−0.088 (−0.184, 0.009)	0.076
Trajectory angle β[b] [per 10°]	0.286 (0.073, 0.499)	0.008	0.092 (−0.096, 0.280)	0.336

[a]Edge of the tumor located within 10 mm of the respective structure. [b]Calculated per 10° positive deviation from transverse/sagittal plane. B, regression coefficient; CI, confidence interval.

TABLE 4 | Procedural efficiency and safety, per intervention ($n = 191$).

Intervention times	
Overall procedure time [min][a]	64 (46–82)
Trajectory planning [min][(A)]	11 (7–19)
Navigated probe positioning [min][(B)]	7 (4–13)
Validation ablation probe [min][(C)]	8 (4–17)
Validation ablation zone [min][(D)]	4 (2–6)
Radiological parameters	
Radiation dose DLP [mGycm]	1,732 (1,202–2,464)
Complications, *n* (%)	
Radiological	2 (1)
Clinical	10 (5)
Grade I–II	6 (3)
Grade IIIa/b	4 (2)

Categorical data are shown as number and percentage, and numerical data are shown as median and interquartile range. [a]Time from the first to the last CT scan. [(A)]Loading of the first CT scan onto the navigation system until the first switch to the navigation module. [(B)]First switch to the navigation module until the last screen shot taken of the positioned ablation probe. [(C)]First switch to the validation module until the last log file activity before loading the next CT scan. [(D)]First log file activity after the last validation scan until detection of the last log file activity before the end of the procedure. DLP, dose length product.

accessibility of lesions in challenging intrahepatic locations when using SMWA. Also, more complex targeting trajectories such as intercostal trajectories and steep trajectory angles had no significant influence on targeting accuracy in multivariable analysis. Since the proposed navigation technique requires optimal fusion between planning and validation scans to ensure precise navigational information, factors leading to intracorporal displacement of the tumor target compromise accuracy of ablation probe positioning. This explains the significantly higher TPE when targeting lesions in cirrhotic livers, as the associated liver stiffness leads to organ distortion when ablation probes are introduced. The influence of targeting trajectory length on TPE can be explained by the bending of ablation probe shafts when applying longer probes, which represents a known challenge when tracking instruments at their extracorporal end rather than the tip (37). Hence, when targeting tumors in cirrhotic livers or when using long targeting trajectories, giving particular attention to control of the ablation probe position is advocated. An equally important factor for a safe and efficient treatment is accurate positioning of the ablation probes at the first targeting attempt without the need for multiple probe repositioning, which greatly reduces tissue trauma and complications as well as high radiation doses (38, 39). The ablation probe repositioning rate in this study was 1%. Accordingly, patient safety and length of hospital stay were favorable in this work compared to previous studies on MWA of liver tumors (6, 22, 40), with low radiation exposure for patients and no exposure for medical staff.

A further potential benefit of SMWA is the augmented visualization of the completeness of ablation using the ablation zone validation module. The precise overlay of pre- and post-ablation images allows an enhanced visual and 3D interpretation of the tumor coverage by the ablation zone, with the possibility of re-ablation in the same treatment session if necessary. Immediate re-ablation was performed in 48 lesions leading to an overall technical success rate of 96%, which was knowingly not 100% due to safety concerns in the remaining 11 lesions. Comparable technical success rates were shown for lesions in challenging intrahepatic locations, corresponding to previously reported success rates after MWA of tumors in the hepatic dome of between 73 and 94% (20, 41). Due to the possibility of navigated positioning of multiple parallel probes, the same technical success rate was also shown when targeting larger lesions. The ASR rate of 22% in this series lies within the wide range of ASRs of 2–34% reported after MWA of liver tumors (42–44), but was higher than rates reported in other studies (22). This is probably influenced by the definition of ASR (detectable tumor seen on any follow-up imaging after the day of ablation) likely resulting in more lesions being assessed as ASR in our study, which in others might be defined as residual unablated tumor and therefore included in the terms of "primary or secondary technique efficacy"(36). The latter definitions allow a wide range of variability in reported efficacy rates and thus

TABLE 5 | Binary logistic Generalized Estimating Equations (GEE) analysis of factors influencing ablation site recurrence per ablated lesion.

	Univariable analysis		Multivariable analysis	
	OR (95% CI)	***p*-value**	**OR (95% CI)**	***p*-value**
Lesion-specific parameters				
HCC [y/n]	0.622 (0.320, 1.208)	0.161	1.038 (0.322, 3.341)	0.950
CRLM [y/n]	2.224 (1.084, 4.564)	0.029	2.280 (0.650, 7.995)	0.198
Tumor size > 30 mm [y/n]	3.970 (1.962, 8.033)	<0.001	5.221 (2.435, 11.192)	<0.001
Location-specific parameters				
Segments I/VII/VIII [y/n]	1.226 (0.606, 2.481)	0.571	1.339 (0.578, 3.104)	0.496
Subphrenic location[a] [y/n]	0.996 (0.453, 2.190)	0.991	0.564 (0.189, 1.679)	0.303
Subcapsular location[a] [y/n]	1.436 (0.700, 2.944)	0.324	1.532 (0.638, 3.680)	0.340
Vessel proximity[b] [y/n]	1.250 (0.588, 2.656)	0.562	1.053 (0.484, 2.291)	0.896
Organ proximity[a] [y/n]	0.773 (0.214, 2.790)	0.694	0.607 (0.120, 3.068)	0.545
Procedural parameters				
TPE > 5 mm [y/n][c]	1.874 (0.879, 3.994)	0.104	2.480 (1.064, 5.784)	0.035

[a]Edge of the tumor located within 10 mm of the respective structure. [b]Edge of the tumor located within 5 mm to an intrahepatic artery, vein, or portal vein of a minimum diameter of 3 mm. [c] n = 55 lesions. OR, odds ratio; CI, confidence interval; HCC, hepatocellular carcinoma; CRLM, colorectal liver metastases; TPE, target positioning error.

make comparability of efficacy results difficult. Furthermore, we included all patients consecutively treated with MWA for any malignant liver tumors at our tertiary referral center, resulting in an unfiltered group of lesions of multiple sizes, locations, and disease stages. While not analyzed in our model, an aggressive tumor biology and/or advanced disease stage of treated patients can be assumed, since 43% of all lesions with ASR occurred in patients with diffuse intrahepatic disease progression within 6 months. The short follow-up period of 6 months was chosen for a per-lesion analysis of factors influencing early ASR. The high rates of intrahepatic recurrences after initial treatments for CRLM and HCC (70–80%) (7, 45) often imply the need for multiple repeat liver-targeted treatments. Therefore, describing ASRs *per lesion* after long follow-up periods is of limited clinical value and cancer-specific time-to-progression analyses will be more adequate.

To further improve the assessment of complete ablation and technical success, safety margins will be integrated into the immediate ablation zone validation module of the navigation system. We are currently investigating the quantification of tumor coverage by the ablation zone by computed volume segmentation, which will enable refined analyses of liver- and tumor-related factors associated with the expansion of ablation zones (46). This will also allow a true distinction between local recurrence and residual unablated tumor, enabling refined analyses on factors influencing true local tumor recurrence (47). Odisio et al. reported local tumor progression rates of 18% after MWA of CRLM, which were not influenced by a subcapsular lesion location in regression analysis (48). In the present work, early ASR was not affected by a challenging lesion location or subcapsular position; however, a TPE > 5 mm was shown to be an independent predictor of early local tumor control.

A potential limitation of the present study is that the regression model for treatment efficacy focused on location-specific parameters and targeting accuracy, excluding other factors that could also have a potential impact on treatment efficacy. These would primarily be parameters specific to different cancer types, which are difficult to include in the current analysis that involves varying tumor entities. The results presented in this work allow a first estimation regarding a possible enhancement of targeting accuracy and tumor accessibility when using SMWA, especially for lesions in challenging intrahepatic locations. A true superiority of using navigation technology over conventional image guidance for tumor targeting must be confirmed in future well-designed prospective comparative studies. Ultimately, we believe that SMWA has its greatest merit when aiming to efficiently target lesions in challenging intrahepatic locations requiring more complex targeting trajectories. Using SMWA also for easier-to-reach liver tumors, as reported in this series, allows for expertise within the team to increase, so that more challenging lesions can be safely treated. The standardization of the treatment technique also leads to short learning curves and the generation of reproducible and comparable results when using such novel navigation technology.

In conclusion, SMWA allows for accurate targeting and effective treatment of malignant liver tumors, even for lesions in challenging locations, with targeting accuracy independently predicting efficacy in our model. Allowing for many tumors to be safely reached, SMWA might broaden treatment eligibility for patients with otherwise difficult to target tumors.

DATA AVAILABILITY STATEMENT

The datasets generated for this study are available on request to the corresponding author.

ETHICS STATEMENT

The studies involving human participants were reviewed and approved by Kantonale Ethikkomission Bern (KEK), Bern,

Schweiz. All participants gave written informed consent that their data can be used for scientific purposes.

AUTHOR CONTRIBUTIONS

PT: primary investigator, involved in study planning, data collection, data analysis and interpretation, and manuscript writing. LF, AL, VB, SW, and DC: involved in study planning, data collection, data analysis and interpretation, and proofreading of manuscript. MM: involved in study planning, data collection, data analysis and interpretation, manuscript writing, and proofreading of manuscript. All authors provided approval for publication of the content.

FUNDING

PT, SW, and DC report partial funding by the European Union's Horizon 2020 Research and Innovation program under Marie Skłodowska-Curie grant agreement No. 722068, which had no involvement in study design, data collection and analysis, or manuscript preparation.

ACKNOWLEDGMENTS

We thank Lukas Bütikofer from the Clinical Trial Unit in the University of Bern for support in statistical analyses; Jessica Lindemann from Washington University in St. Louis Missouri for proofreading the manuscript; Johan Baijot, Gordana Veljanoska, Fabrice Vermont, and Matthias Peterhans from CAScination AG for support in data extraction.

REFERENCES

1. Bruix J, Reig M, Sherman M. Evidence-Based diagnosis, staging, and treatment of patients with hepatocellular carcinoma. *Gastroenterology*. (2016) 150:835–53. doi: 10.1053/j.gastro.2015.12.041
2. Pathak S, Jones R, Tang JMF, Parmar C, Fenwick S, Malik H, et al. Ablative therapies for colorectal liver metastases: a systematic review. *Colorectal Dis*. (2011) 13:e252–65. doi: 10.1111/j.1463-1318.2011.02695.x
3. Ruers T, Van Coevorden F, Punt CJA, Pierie J-PEN, Borel-Rinkes I, Ledermann JA, et al. Local treatment of unresectable colorectal liver metastases: results of a randomized phase ii trial. *JNCI J Natl Cancer Inst*. (2017) 109:djx015. doi: 10.1093/jnci/djx015
4. Wang X, Hu Y, Ren M, Lu X, Lu G, He S. Efficacy and safety of radiofrequency ablation combined with transcatheter arterial chemoembolization for hepatocellular carcinomas compared with radiofrequency ablation alone: a time-to-event meta-analysis. *Korean J Radiol*. (2016) 17:93–102. doi: 10.3348/kjr.2016.17.1.93
5. Tiong L, Maddern GJ. Systematic review and meta-analysis of survival and disease recurrence after radiofrequency ablation for hepatocellular carcinoma. *Br J Surg*. (2011) 98:1210–24. doi: 10.1002/bjs.7669
6. Luo W, Zhang Y, He G, Yu M, Zheng M, Liu L, et al. Effects of radiofrequency ablation versus other ablating techniques on hepatocellular carcinomas: a systematic review and meta-analysis. *World J Surg Oncol*. (2017) 15:126. doi: 10.1186/s12957-017-1196-2
7. Hof J, Wertenbroek MWJLAE, Peeters PMJG, Widder J, Sieders E, de Jong KP. Outcomes after resection and/or radiofrequency ablation for recurrence after treatment of colorectal liver metastases. *Br J Surg*. (2016) 103:1055–62. doi: 10.1002/bjs.10162
8. Engstrand J, Nilsson H, Jansson A, Isaksson B, Freedman J, Lundell L, et al. A multiple microwave ablation strategy in patients with initially unresectable colorectal cancer liver metastases - a safety and feasibility study of a new concept. *Eur J Surg Oncol*. (2014) 40:1488–93. doi: 10.1016/j.ejso.2014.05.003
9. Sala M, Llovet JM, Vilana R, Bianchi L, Solé M, Ayuso C, et al. Initial response to percutaneous ablation predicts survival in patients with hepatocellular carcinoma. *Hepatology*. (2004) 40:1352–60. doi: 10.1002/hep.20465
10. Kim J-E, Kim Y-S, Rhim H, Lim HK, Lee MW, Choi D, et al. Outcomes of patients with hepatocellular carcinoma referred for percutaneous radiofrequency ablation at a tertiary center: analysis focused on the feasibility with the use of ultrasonography guidance. *Eur J Radiol*. (2011) 79:e80–4. doi: 10.1016/j.ejrad.2011.03.090
11. Kambadakone A, Baliyan V, Kordbacheh H, Uppot RN, Thabet A, Gervais DA, et al. Imaging guided percutaneous interventions in hepatic dome lesions: tips and tricks. *World J Hepatol*. (2017) 9:840–49. doi: 10.4254/wjh.v9.i19.840
12. Filippiadis DK, Spiliopoulos S, Konstantos C, Reppas L, Kelekis A, Brountzos E, et al. Computed tomography-guided percutaneous microwave ablation of hepatocellular carcinoma in challenging locations: safety and efficacy of high-power microwave platforms. *Int J Hyperthermia*. (2018) 34:863–9. doi: 10.1080/02656736.2017.1370728
13. Curley SA, Marra P, Beaty K, Ellis LM, Vauthey JN, Abdalla EK, et al. Early and late complications after radiofrequency ablation of malignant liver tumors in 608 patients. *Ann Surg*. (2004) 239:450–8. doi: 10.1097/01.sla.0000118373.31781.f2
14. Mulier S, Ni Y, Jamart J, Ruers T, Marchal G, Michel L. Local recurrence after hepatic radiofrequency coagulation: multivariate meta-analysis and review of contributing factors. *Ann Surg*. (2005) 242:158–71. doi: 10.1097/01.sla.0000171032.99149.fe
15. Hermida M, Cassinotto C, Piron L, Assenat E, Pageaux G-P, Escal L, et al. Percutaneous thermal ablation of hepatocellular carcinomas located in the hepatic dome using artificial carbon dioxide pneumothorax: retrospective evaluation of safety and efficacy. *Int J Hyperthermia*. (2018) 35:90–6. doi: 10.1080/02656736.2018.1477206
16. Zhang D, Liang P, Yu X, Cheng Z, Han Z, Yu J, et al. The value of artificial pleural effusion for percutaneous microwave ablation of liver tumour in the hepatic dome: a retrospective case-control study. *Int J Hyperthermia*. (2013) 29:663–70. doi: 10.3109/02656736.2013.833347
17. Kang TW, Rhim H, Lee MW, Kim Y, Choi D, Lee WJ, et al. Radiofrequency ablation for hepatocellular carcinoma abutting the diaphragm: comparison of effects of thermal protection and therapeutic efficacy. *AJR Am J Roentgenol*. (2011) 196:907–13. doi: 10.2214/AJR.10.4584
18. Brennan DD, Ganguli S, Brecher CW, Goldberg SN. Thinking outside the abdominal box: safe use of the epipericardial fat pad window for percutaneous radiofrequency ablation of hepatic dome tumors. *J Vasc Interv Radiol*. (2008) 19:133–6. doi: 10.1016/j.jvir.2007.08.023
19. Basile A, Calcara G, Montineri A, Brisolese V, Lupattelli T, Patti MT. Application of a new combined guiding technique in RF ablation of subphrenic liver tumors. *Eur J Radiol*. (2008) 66:321–4. doi: 10.1016/j.ejrad.2007.06.006
20. Gao F, Wang G-B, Xiang Z-W, Yang B, Xue J-B, Mo Z-Q, et al. A preoperative mathematic model for computed tomographic guided microwave ablation treatment of hepatic dome tumors. *Oncotarget*. (2016) 7:25949–59. doi: 10.18632/oncotarget.8299
21. Peterhans M, vom Berg A, Dagon B, Inderbitzin D, Baur C, Candinas D, et al. A navigation system for open liver surgery: design, workflow and first clinical applications. *Int J Med Robot*. (2011) 7:7–16. doi: 10.1002/rcs.360
22. Widmann G, Schullian P, Haidu M, Bale R. Stereotactic radiofrequency ablation (SRFA) of liver lesions: technique effectiveness, safety, and interoperator performance. *Cardiovasc Intervent Radiol*. (2012) 35:570–80. doi: 10.1007/s00270-011-0200-4
23. Bale R, Widmann G, Schullian P, Haidu M, Pall G, Klaus A, et al. Percutaneous stereotactic radiofrequency ablation of colorectal liver metastases. *Eur Radiol*. (2012) 22:930–7. doi: 10.1007/s00330-011-2314-0
24. Engstrand J, Toporek G, Harbut P, Jonas E, Nilsson H, Freedman J. Stereotactic CT-guided percutaneous microwave ablation of liver tumors with

the use of high-frequency jet ventilation: an accuracy and procedural safety study. *AJR Am J Roentgenol*. (2017) 208:193–200. doi: 10.2214/AJR.15.15803
25. Bale R, Schullian P, Eberle G, Putzer D, Zoller H, Schneeberger S, et al. Stereotactic radiofrequency ablation of hepatocellular carcinoma: a histopathological study in explanted livers. *Hepatology*. (2018) 70:840–50. doi: 10.1002/hep.30406
26. Beyer LP, Lürken L, Verloh N, Haimerl M, Michalik K, Schaible J, et al. Stereotactically navigated percutaneous microwave ablation (MWA) compared to conventional MWA: a matched pair analysis. *Int J Comput Assist Radiol Surg*. (2018) 13:1991–7. doi: 10.1007/s11548-018-1778-7
27. Beyer LP, Pregler B, Nießen C, Schicho A, Haimerl M, Jung EM, et al. Stereotactically-navigated percutaneous irreversible electroporation (IRE) compared to conventional IRE: a prospective trial. *Peer J*. (2016) 4:e2277. doi: 10.7717/peerj.2277
28. Schullian P, Putzer D, Laimer G, Levy E, Bale R. Feasibility, safety, and long-term efficacy of stereotactic radiofrequency ablation for tumors adjacent to the diaphragm in the hepatic dome: a case-control study. *Eur Radiol*. (2020) 30:950–60. doi: 10.1007/s00330-019-06399-y
29. Lachenmayer A, Tinguely P, Maurer MH, Frehner L, Knöpfli M, Peterhans M, et al. Stereotactic image-guided microwave ablation of hepatocellular carcinoma using a computer-assisted navigation system. *Liver Int*. (2019) 39:1975–85. doi: 10.1111/liv.14187
30. https://clinicaltrials.gov/ct2/show/NCT02642185?term=MAVERRIC&cntry=SE&rank=1.
31. Galmén K, Freedman J, Toporek G, Gozdzik W, Harbut P. Clinical application of high frequency jet ventilation in stereotactic liver ablations - a methodological study. *F1000Res*. (2018) 7:773. doi: 10.12688/f1000research.14873.2
32. Denys A, Lachenal Y, Duran R, Chollet-Rivier M, Bize P. Use of high-frequency jet ventilation for percutaneous tumor ablation. *Cardiovasc Intervent Radiol*. (2014) 37:140–6. doi: 10.1007/s00270-013-0620-4
33. Lencioni R, de Baere T, Martin RC, Nutting CW, Narayanan G. Image-guided ablation of malignant liver tumors: recommendations for clinical validation of novel thermal and non-thermal technologies - a western perspective. *Liver Cancer*. (2015) 4:208–14. doi: 10.1159/000367747
34. Wang X, Sofocleous CT, Erinjeri JP, Petre EN, Gonen M, Do KG, et al. Margin size is an independent predictor of local tumor progression after ablation of colon cancer liver metastases. *Cardiovasc Intervent Radiol*. (2013) 36:166–75. doi: 10.1007/s00270-012-0377-1
35. Dindo D, Demartines N, Clavien P-A. Classification of surgical complications: a new proposal with evaluation in a cohort of 6336 patients and results of a survey. *Ann Surg*. (2004) 240:205–13. doi: 10.1097/01.sla.0000133083.54934.ae
36. Ahmed M, Solbiati L, Brace CL, Breen DJ, Callstrom MR, Charboneau JW, et al. Image-guided tumor ablation: standardization of terminology and reporting criteria–a 10-year update. *Radiology*. (2014) 273:241–60. doi: 10.1148/radiol.14132958
37. Tinguely P, Schwalbe M, Fuss T, Guensch DP, Kohler A, Baumgartner I, et al. Multi-operational selective computer-assisted targeting of hepatocellular carcinoma-Evaluation of a novel approach for navigated tumor ablation. *PLoS ONE*. (2018) 13:e0197914. doi: 10.1371/journal.pone.0197914
38. Rathmann N, Haeusler U, Diezler P, Weiss C, Kostrzewa M, Sadick M, et al. Evaluation of radiation exposure of medical staff during CT-guided interventions. *J Am Coll Radiol*. (2015) 12:82–9. doi: 10.1016/j.jacr.2014.04.012
39. Heerink WJ, Ruiter SJS, Pennings JP, Lansdorp B, Vliegenthart R, Oudkerk M, et al. Robotic versus freehand needle positioning in ct-guided ablation of liver tumors: a randomized controlled trial. *Radiology*. (2019) 290:826–32. doi: 10.1148/radiol.2018181698
40. Groeschl RT, Pilgrim CHC, Hanna EM, Simo KA, Swan RZ, Sindram D, et al. Microwave ablation for hepatic malignancies: a multiinstitutional analysis. *Ann Surg*. (2014) 259:1195–200. doi: 10.1097/SLA.0000000000000234
41. Asvadi NH, Anvari A, Uppot RN, Thabet A, Zhu AX, Arellano RS. CT-guided percutaneous microwave ablation of tumors in the hepatic dome: assessment of efficacy and safety. *J Vasc Interv Radiol*. (2016) 27:496–502. doi: 10.1016/j.jvir.2016.01.010
42. Meijerink MR, Puijk RS, van Tilborg AAJM, Henningsen KH, Fernandez LG, Neyt M, et al. Radiofrequency and microwave ablation compared to systemic chemotherapy and to partial hepatectomy in the treatment of colorectal liver metastases: a systematic review and meta-analysis. *Cardiovasc Intervent Radiol*. (2018) 41:1189–204. doi: 10.1007/s00270-018-1959-3
43. Mahnken AH, Pereira PL, de Baère T. Interventional oncologic approaches to liver metastases. *Radiology*. (2013) 266:407–30. doi: 10.1148/radiol.12112544
44. Urbonas T, Anderson EM, Gordon-Weeks AN, Kabir SI, Soonawalla Z, Silva MA, et al. Reddy S. Factors predicting ablation site recurrence following percutaneous microwave ablation of colorectal hepatic metastases. *HPB*. (2019) 21:1175–84. doi: 10.1016/j.hpb.2019.01.007
45. Lencioni R. Loco-regional treatment of hepatocellular carcinoma. *Hepatology*. (2010) 52:762–3. doi: 10.1002/hep.23725
46. Praktiknjo M, Krabbe V, Pohlmann A, Sampels M, Jansen C, Meyer C, et al. Evolution of nodule stiffness might predict response to local ablative therapy: a series of patients with hepatocellular carcinoma. *PLoS ONE*. (2018) 13:e0192897. doi: 10.1371/journal.pone.0192897
47. Kaye EA, Cornelis FH, Petre EN, Tyagi N, Shady W, Shi W, et al. Volumetric 3D assessment of ablation zones after thermal ablation of colorectal liver metastases to improve prediction of local tumor progression. *Eur Radiol*. (2018) 29:2698–705. doi: 10.1007/s00330-018-5809-0
48. Odisio BC, Yamashita S, Huang SY, Harmoush S, Kopetz SE, Ahrar K, et al. Local tumour progression after percutaneous ablation of colorectal liver metastases according to RAS mutation status. *Br J Surg*. (2017) 104:760–8. doi: 10.1002/bjs.10490

Conflict of Interest: SW and DC are co-founders and shareholders of CAScination AG, manufacturer of the navigation technology used for SMWA in this study.

The remaining authors declare that the research was conducted in the absence of any commercial or financial relationships that could be construed as a potential conflict of interest.

frontiers in Oncology

ORIGINAL RESEARCH
published: 24 July 2020
doi: 10.3389/fonc.2020.01150

Multiple-Electrode Switching-Based Radiofrequency Ablation vs. Conventional Radiofrequency Ablation for Single Early-Stage Hepatocellular Carcinoma Ranging From 2 to 5 Cm

Guang-liang Huang[1†], Ming Liu[1†], Xiao-er Zhang[1], Bao-xian Liu[1], Ming Xu[1], Man-xia Lin[1], Ming Kuang[1,2], Ming-de Lu[1,2] and Xiao-yan Xie[1]*

[1] Department of Medical Ultrasonics, Institute for Diagnostic and Interventional Ultrasound, The First Affiliated Hospital of Sun Yat-sen University, Guangzhou, China, [2] Department of Liver Surgery, The First Affiliated Hospital of Sun Yat-sen University, Guangzhou, China

OPEN ACCESS

Edited by:
Jie Yu,
People's Liberation Army General Hospital, China

Reviewed by:
Hyunchul Rhim,
Sungkyunkwan University, South Korea
Min Woo Lee,
Sungkyunkwan University, South Korea

***Correspondence:**
Xiao-yan Xie
xxy1992sys@163.com

[†]These authors have contributed equally to this work

Specialty section:
This article was submitted to Cancer Imaging and Image-directed Interventions, a section of the journal Frontiers in Oncology

Received: 21 February 2020
Accepted: 08 June 2020
Published: 24 July 2020

Citation:
Huang G, Liu M, Zhang X, Liu B, Xu M, Lin M, Kuang M, Lu M and Xie X (2020) Multiple-Electrode Switching-Based Radiofrequency Ablation vs. Conventional Radiofrequency Ablation for Single Early-Stage Hepatocellular Carcinoma Ranging From 2 to 5 Cm. Front. Oncol. 10:1150. doi: 10.3389/fonc.2020.01150

Purpose: To retrospectively compare the treatment outcome of multiple-electrode switching-based radiofrequency ablation (switching RFA) and the conventional RFA for early-stage hepatocellular carcinoma (HCC).

Methods: A total of 122 patients with single early-stage HCC ranging from 2.1 to 5.0 cm received ultrasonography-guided percutaneous RFA as the first-line treatment. Seventy-one patients underwent switching RFA, and 51 underwent conventional RFA. Tumor response, major complication, local tumor progression (LTP), and overall survival (OS) were compared between the two groups. Log-rank tests and Cox regression models were used for univariate and multivariate analyses to identify predictors of LTP and OS.

Results: The rate of initial local complete response rates were 100% (71/71) in the switching RFA group and 98.0% (50/51) in the conventional RFA group ($P > 0.05$). No major complication occurred in the switching RFA group, whereas two in the conventional RFA group. After a median follow-up period of 45.9 months (range, 9.8–60.0 months), the rates of LTP in the switching RFA and conventional RFA groups were 19.7% (14/71) and 41.2% (21/51), respectively. The cumulative LTP rates at 1, 3, and 5 years were 11.3, 20.5, and 20.5% for switching RFA and 17.6, 38.7, and 46.7% for conventional RFA, respectively ($p < 0.001$). Switching RFA was an independent factor associated with a lower LTP rate ($p = 0.022$). Five-year OS rates were 75.8% after switching RFA vs. 66.2% after conventional RFA ($p = 0.363$). Extrahepatic recurrence was a significant prognostic factor for OS in multivariable analysis.

Conclusion: Compared with conventional RFA, switching RFA provides a high local tumor control for single early-stage HCC. An ongoing randomized trial might help to clarify the role of this approach for the treatment of HCC.

Keywords: radiofrequency ablation, hepatocellular carcinoma, multiple-electrode switching, local tumor progression, treatment outcome

INTRODUCTION

Radiofrequency ablation (RFA) has been widely used in the treatment of early-stage hepatocellular carcinoma (HCC) (1–4). Compared with surgical resection, the higher local tumor progression (LTP) rate is regarded as a considerable shortcoming of RFA in the treatment of HCC (5, 6). Because of the limited coagulated necrosis induced by RFA, the ability of local control of HCC with RFA greatly depends on tumor size (7–9). To achieve complete ablation of HCC and sufficient safety margin, overlapping ablations are required (10–12). For conventional RFA with one electrode, the electrode is repositioned and reactivated in untreated tumor sites adjacent to the prior ablation zone after each ablation. The hyperechogenicity caused by the early radiofrequency (RF) electrode frequently obscures the tumor boundaries, rendering the reposition of the electrode under ultrasound (US) guidance, which is technically challenging and time consuming even for a relatively small tumor. A multiple-electrode switching system was introduced and enabled to simultaneously use up to three RF electrodes, between which the power is sequentially switched when an impedance spike is encountered, instead of temporarily switching the system off as it occurs in the conventional RF device (13, 14). The problem mentioned earlier can be potentially remedied with the introduction of such a multiple-electrode switching system. Several previous reports have shown the encouraging results of multiple-electrode switching-based RFA for the treatment of HCC. However, all these studies were single-arm studies without direct comparison with conventional RFA (15–17). The aim of this study was thus to retrospectively compare the treatment outcome of multiple-electrode switching-based RFA (switching RFA) and the conventional RFA with a single electrode for early-stage HCC.

PATIENTS AND METHODS

Patients

From August 2009 to August 2014, a total of 122 patients (105 men, 17 women; mean age 56.3 ± 12.6 years, range: 27.0–85.0 years) with HCC were enrolled in this retrospective study (**Figure 1**). The diagnosis of HCC was based on the noninvasive diagnostic criteria of the American Association for the Study of Liver Diseases (AASLD) or biopsy. The inclusion criteria comprised: (a) adult patients with early-stage HCC and declined resection recommendation; (b) single HCC with 2.1–5.0 cm in diameter, treated by conventional cool-tip electrode RFA system or multiple-electrode switching RFA system; (c) liver function status at Child–Pugh class A or B; (d) platelet count over 50×10^9/l; and (e) prothrombin time ratio >50%. Exclusion criteria include (a) presence of multiple HCCs; (b) presence of vascular invasion or extrahepatic metastases at pre-procedure imaging study; (c) previous treatment for HCC; (d) ongoing anticoagulant treatment that cannot be stopped; and (e) tumor in close proximity to the hepatic hilum. The study was conducted with the approval of the institutional ethics board. Written informed consent was obtained from each patient before treatment.

Radiofrequency Ablation

US-guided percutaneous RFA was performed under local anesthesia and sedation. Vital signs were continuously monitored during the procedure. Two of the authors (X.Y. X. and M. K., who have 10 and 8 years of experience with RFA, respectively) performed the ablation. RFA was carried out with the Cool-tip^{TM} system (Valleylab, Boulder, CO, USA). For conventional RFA, a 17-gauge internally cooled electrode with a 2- to 3-cm-long exposed metallic tip was used. Grounding was achieved by attaching a dispersive pad to each of the patient's thighs. Overlapping ablation technique was used, and the generator was set at the maximum power of 200 W in the impedance automatic mode for 8–12 min. For switching RFA, two or three internally cooled electrodes (Covidien, Boulder, CO) were used, and two grounding pads were placed on each of the patient's thighs. The generator was set at the maximum power of 200 W in the impedance switching mode for 16–24 min. The selection of electrode number and the length of exposed electrode tip was primarily determined based on tumor size and tumor location. Generally, two RF electrodes were used for tumors 2.1–3.0 cm, and three for tumors 3.1–5.0 cm in diameter, with an interelectrode distance of 1.0–2.0 cm. Regardless of the ablation with or without a multiple-electrode switching system, the needle track was carefully treated with the electrode being retracted by a 1-cm increment to prevent bleeding and tumor seeding. Contrast-enhanced US was performed immediately after the RFA procedure in order to obtain complete tumor ablation and a 5-mm safety margin as far as possible.

Evaluation of Treatment Response and Follow-Up

Local efficacy was assessed by a conventional evaluation modality of contrast-enhanced CT or MRI performed 1 month after ablation. According to the CT/MRI results, a response to RFA was classified as complete or incomplete ablation. Complete ablation was defined as non-enhancement in the ablated zone with or without peripheral enhancing rim. Incomplete ablation was indicated when the tissue was still enhanced at the tumor site, and additional ablation was given. If the tumor was still viable after additional ablation, RFA was considered a failure, and the patient was referred for other therapies. The follow-up protocol included contrast-enhanced US performed at 3-month intervals and contrast-enhanced CT performed every 6 months. LTP was defined as the regrowth of the tumor inside the initially completely ablated nodule. All the ablation-related complications were classified according to the Society of Interventional Radiology Reporting Standards for image-guided tumor ablation (18). The follow-up duration was defined as the interval between the first RF ablation and either the incidence of the event or the last visit before December 31, 2018. The follow-up for survival analysis was terminated at 60 months. Liver transplantation was censored on the date of surgery.

Statistical Analysis

Statistical analysis was performed using the SPSS 16.0 software package. A p-value of <0.05 indicated statistical significance. Continuous data were expressed as the mean ± standard

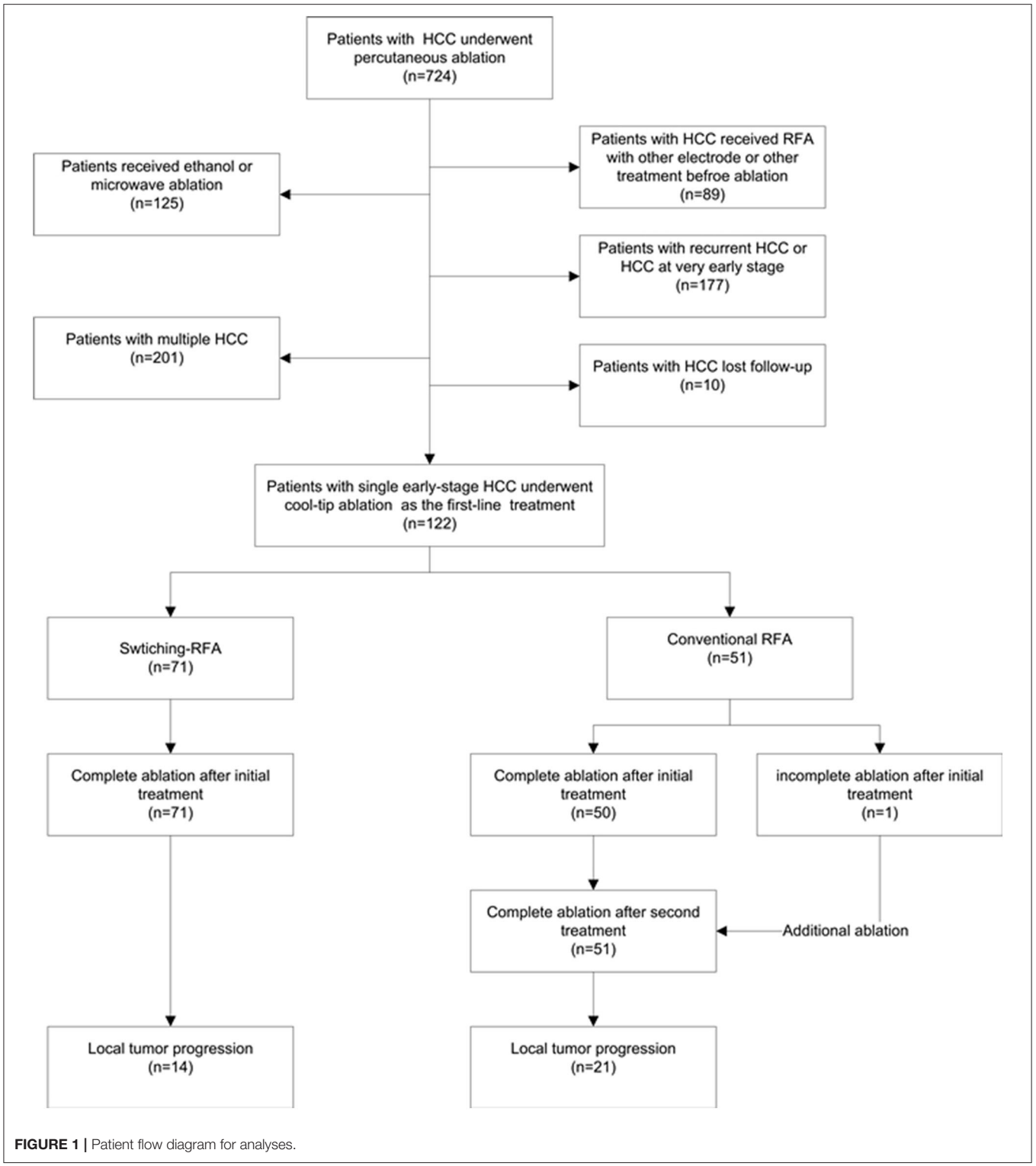

FIGURE 1 | Patient flow diagram for analyses.

deviation. The chi-squared test or Fisher exact tests were used to compare patients' baseline characteristics. Data on survival were evaluated by the Kaplan–Meier method. The relationship between each of the variables and LTP or overall survival (OS) was estimated by the log-rank test. The variables included age, sex, presence of hepatitis B or C virus infection, Child–Pugh class for liver function, alanine aminotransferase, total bilirubin, albumin, prothrombin time, platelet, serum alpha-fetoprotein, tumor location (perivascular or subcapsular), tumor size, and treatment methods. The variables with a p-value of <0.10 in the

log-rank test were introduced in a multivariate Cox proportional hazards model. Perivascular HCC was defined as an index tumor abutting the first- or second-degree branches of a portal or hepatic vein that are 3 mm or greater in diameter. Subcapsular tumor was defined as an index tumor being <1.0 cm from the liver capsule.

RESULTS

Patients

Of the 122 eligible patients, 71 (mean age, 55.5 ± 12.2 years; range, 27–80 years) underwent switching RFA, whereas 51 (mean age, 57.4 ± 13.1 years; range, 27–80 years) underwent conventional RFA. The tumor sizes were 2.8 ± 0.5 cm (range, 2.1–4.4 cm) in the switching RFA group and 2.8 ± 0.7 cm (range, 2.1–4.6 cm) in the conventional RFA group. Among 26 perivascular tumors, 18 (69.2%) tumors were abutting portal vein, 6 (23.1%) abutting hepatic vein, and 2 (7.6%) abutting inferior vena cava. The baseline clinical characteristics of the two groups are compared in **Table 1**. No significant differences were observed between the two groups in sex, age, Child–Pugh class, presence of hepatitis B/C virus infection, serum total bilirubin, serum albumin, tumor size, and tumor location (perivascular or subcapsular tumor), whereas the serum alanine aminotransferase level, prothrombin time, platelet count, and the serum alpha-fetoprotein level differed significantly.

TABLE 1 | Baseline characteristics of patients with single early-stage HCC.

Characteristics	Switching-RFA ($n = 71$)	Conventional RFA ($n = 51$)	*P*-value
Gender (male/female)	64/7	41/10	0.125
Age (y)			
≤65	58	36	0.150
>65	13	15	
Child-Pugh (A/B)	69/2	48/3	0.704
Hepatitis B/C (±)	67/4	48/3	1.000
Serum ALT level			
≤40 U/L	46	22	0.018
>40 U/L	25	29	
Serum total bilirubin			
≤34.2 mg/dl	65	49	0.531
>34.2 mg/dl	6	2	
Serum albumin			
≤35 g/L	13	16	0.095
>35 g/L	58	35	
Prothrombin time			
≤14 s	64	37	0.011
>14 s	7	14	
Platelet count			
$\leq 100 \times 10^9$/L	13	20	0.010
$>100 \times 10^9$/L	58	31	
Serum AFP level			
≤200 ng/ml	64	36	0.006
>200 ng/ml	7	15	
Tumor size			
2.1–3.0 cm	50	35	0.832
3.1–5.0 cm	21	16	
Perivascular (+/–)	18/53	8/43	0.198
Subcapsular (+/–)	21/50	22/29	0.122

Tumor Response

In the switching RFA group, complete ablation was achieved in all tumors in a single session of RFA (**Figure 2**). In the conventional RFA group, complete ablation was achieved in 50 of 51 tumors in a single session of RFA. One residual tumor reached complete ablation after additional treatment. The rates of initial local complete ablation were 100% (71/71) in the switching RFA group and 98.0% (50/51) in the conventional RFA group ($P = 0.418$).

Major Complications

No ablation-related death occurred. No major complication was observed in the switching RFA group, whereas two (2/51, 3.9%) major complications were observed in the conventional RFA group. One patient in the conventional RFA group developed obstructive jaundice as a result of the injury of the bile duct. The patient received percutaneous transhepatic catheter drainage and stent placement. Another patient required US-guided percutaneous gallbladder catheter drainage and antibiotics due to the acute cholecystitis.

Local Tumor Progression

The overall median follow-up period for all patients was 45.9 months (range, 9.8–60.0 months), with median follow-up periods of 43.0 months (range, 9.8–60.0 months) and 55.3 months (range, 10.3–60.0 months) for switching RFA group and conventional RFA group, respectively ($p = 0.107$). The LTP rate in the switching RFA group was 19.7% (14/71) vs. 41.2% (21/51) in the conventional RFA group ($p = 0.010$). According to the Kaplan–Meier method, the cumulative LTP rates at 1, 3, and 5 years were 11.3, 20.5, and 20.5% for switching RFA and 17.6, 38.7, and 46.7% for conventional RFA, respectively (**Figure 3**). Risk factors for LTP of HCC were analyzed by the log-rank test, which revealed that the treatment method was significantly associated with LTP ($p = 0.018$). Other factors associated with LTP are described in **Table 2**. In a multivariable analysis, the treatment method was identified as an independent predictor of LTP (HR = 2.209; 95% CI: 1.123–4.346; $p = 0.022$) (**Table 3**). LTP was treated by repeat RFA ($n = 16$), ethanol ablation ($n = 1$), liver transplantation ($n = 1$), surgical resection ($n = 2$), and TACE ($n = 1$) in the conventional RFA group, whereas repeat RFA ($n = 11$), liver transplantation ($n = 1$), and surgical resection ($n = 2$) in the switching RFA group.

Distant Recurrence

Intrahepatic distant recurrence had occurred in 25 of 71 (35.2%) patients in the switching RFA group and in 31 of 51 (60.8%) patients in the conventional RFA group ($p = 0.005$). Extrahepatic recurrence was found in 10 of 71 (14.1%) patients in the switching RFA group and in 11 of 51 (21.6%) patients in the conventional RFA group ($p = 0.280$).

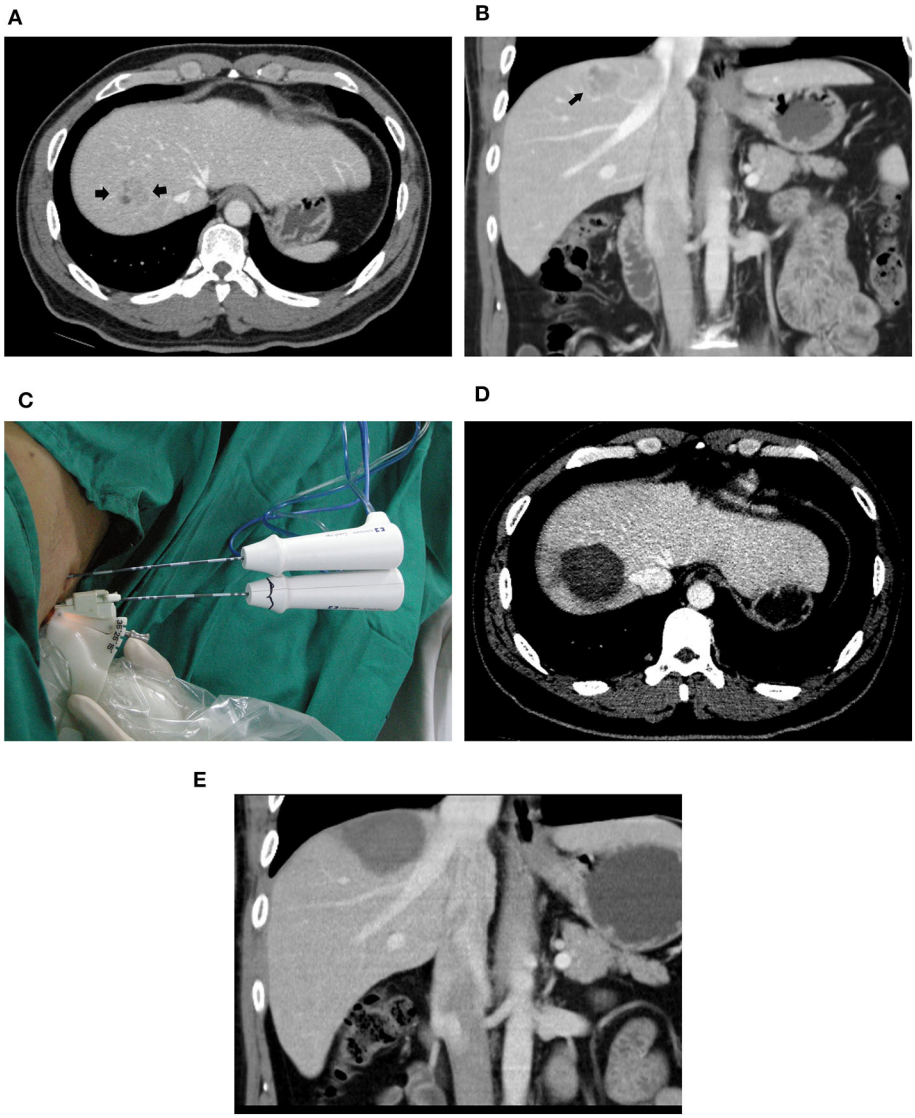

FIGURE 2 | A 39-year-old male patient with HCC who underwent radiofrequency ablation with a multiple-electrode switching system. Pre-ablation CT scans showed a 2.6-cm tumor (arrowhead) in the segment VIII of the liver in the transverse **(A)** and coronal **(B)** view. **(C)** Ultrasound-guided RFA using the multiple-electrode switching system was performed with two RF electrodes for 16 min. CT scans obtained 1 month after ablation showed that the tumor was completely ablated in the transverse **(D)** and coronal **(E)** view.

Overall Survival Rates

Ten (14.1%) of 71 patients in the switching RFA group and 13 (25.5%) of 51 patients in the conventional group died during the observation period. The estimated 5-year OS rates were 75.8% in the switching RFA group and 66.2% in the conventional RFA group ($p = 0.363$). Of the factors evaluated for association with OS in univariate analysis (**Table 4**), the following three factors were statistically significant: LTP ($p = 0.004$), intrahepatic recurrence ($p = 0.002$), and extrahepatic recurrence ($p = 0.000$). Extrahepatic recurrence was found to be a significant risk factor in the Cox proportional hazards regression model (hazard ratio = 15.850; 95% CI: 6.169–40.722; $p < 0.001$; **Table 5**).

DISCUSSION

The present study demonstrated that both switching RFA and conventional RFA achieved satisfactory tumor response for single HCC, ranging from 2.1 to 5.0 cm. Switching RFA appeared to be superior in local control of HCC compared with conventional RFA, whereas similar OS was achieved after both treatments.

Previous studies have reported the LTP rate to be as high as 40% in patients with early-stage HCC, especially for the intermediate-sized HCC (19). It has been reported that HCC micrometastases may still exist as far as 1 cm from the main tumor, including the small encapsulated tumors (20). Therefore, at least 0.5 cm of the ablation margin is required for local

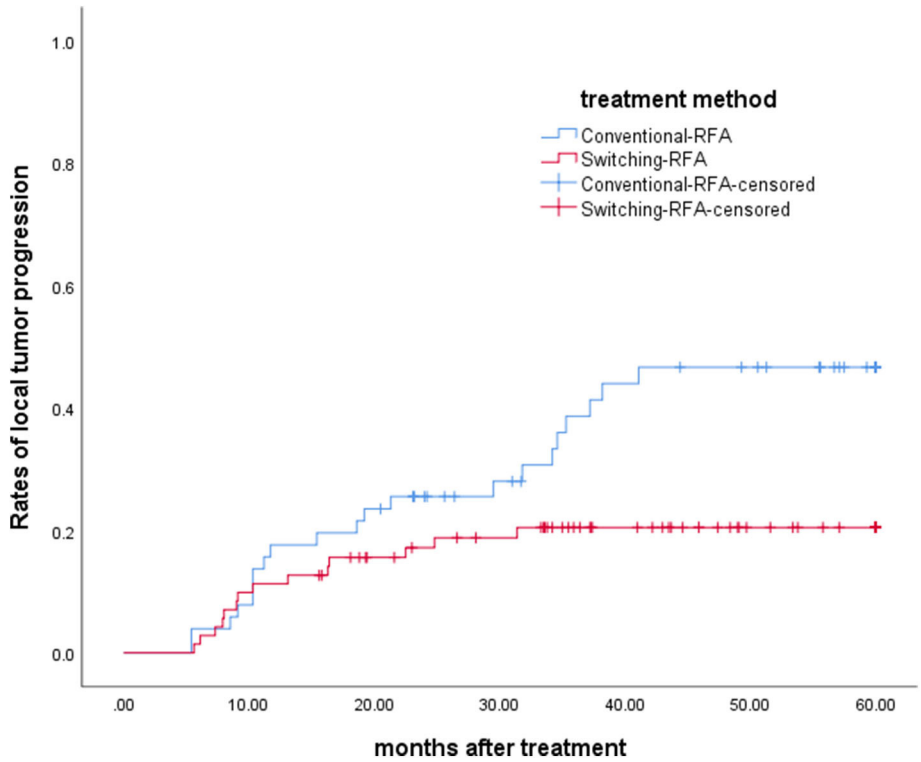

FIGURE 3 | Cumulative LTP survival curves in patients treated with switching RFA or conventional RFA.

TABLE 2 | Univariate analysis of risk factors for local tumor progression of HCC after ablation.

Variables	Local tumor progression *P*-value
Gender (male)	0.790
Age (>65 years)	0.601
Hepatitis B/C virus infection (+/–)	0.382
Child-Pugh class (A/B)	0.173
Serum ALT level (>40 U/L)	0.438
Serum total bilirubin (>34.2 mg/dl)	0.077
Serum albumin (>35 g/L)	0.089
Platelet count (>100 × 10^9/L)	0.773
Prothrombin time (>14 s)	0.703
Serum AFP level (>200 ng/ml)	0.962
Tumor size (2.1–3.0/3.1–5.0 cm)	0.598
Perivascular (+/–)	0.129
Subcapsular (+/–)	0.665
Treatment methods (switching/non-switching)	0.018

+, positive; –, negative; ALT, alanine aminotransferase; AFP, alpha-fetoprotein.

TABLE 3 | Multivariate analysis of risk factors for local tumor progression of HCC after ablation.

Variables	*P*-value	Risk ratio (95% CI)
Treatment methods	0.022	2.209 (1.123–4.346)
Serum albumin	0.151	NA
Serum total bilirubin	0.096	NA

NA, not applicable.

ablative therapy (21–23). However, the commonly used RFA devices show limited ability to create a large ablation zone. To overcome the limitations of conventional RFA, other techniques, including microwave ablation (24), expandable RF electrode (24), and clustered RF electrode (12), have been proposed. In theory, Microwave ablation is more efficient than RFA and less influenced by the heat-sink effect. However, the relatively high complication rate limits its clinical use for the tumor close to the critical structures. Expandable electrodes can create a large ablation zone, but it is difficult to see all the time under US-guided RFA. Multiple-electrode switching RFA system enabled the creation of significantly larger ablation zones compared with conventional RFA system with a single-electrode *in vivo* experiment study (14). In the present study, the LTP rates at 1, 3, and 5 years were 11.3, 20.6, and 20.6% in the switching RFA group, as compared with 17.6, 38.7, and 46.7% in the conventional RFA group, respectively. Switching RFA provided a better local tumor control than conventional RFA. The result was further supported by the multivariate analysis, which highlighted switching RFA as an independent factor associated with LTP. Previous studies reported that tumor size

TABLE 4 | Univariate analysis of risk factors for overall survival of HCC after ablation.

Variables	Overall survival *P*-value
Gender (male)	0.219
Age (>65 years)	0.334
Hepatitis B/C virus infection(+/–)	0.481
Child-Pugh class (A/B)	0.241
Serum ALT level (>40 U/L)	0.088
Serum total bilirubin (>34.2 umol/L)	0.151
Serum albumin (>35 g/L)	0.451
Platelet count (>100 $\times 10^9$/L)	0.452
Prothrombin time (>14 s)	0.689
Serum AFP level (>200 ng/ml)	0.197
Tumor size (2.1–3.0/3.1–5.0 cm)	0.798
Perivascular tumor	0.158
Subcapsular	0.114
Treatment methods (switching/non-switching)	0.363
Local tumor progression	0.004
Intrahepatic recurrence (+/–)	0.002
Extrahepatic recurrence (+/–)	0.000

+, positive; –, negative; ALT, alanine aminotransferase; AFP, alpha-fetoprotein.

TABLE 5 | Multivariate analysis of risk factors for overall survival of HCC after ablation.

Variables	*P*-value	Risk ratio (95% CI)
Extrahepatic recurrence	0.000	15.850 (6.169–40.722)
Local tumor progression	0.256	NA
Intrahepatic recurrence	0.337	NA
Serum ALT level	0.532	NA

NA, not applicable.

and tumor location (subcapsular/perivascular location) were two predisposing factors to LTP of HCC (3, 25, 26). However, no such correlations were detected in our cohorts.

In the present study, no major complication was observed in the switching RFA group, whereas two major complications occurred in the conventional RFA group. As we mentioned before, the gas induced by the ablation will disturb the reposition of the electrode. Under such circumstances, we had to count the scale marks from both electrode and puncture line and tried to ensure a uniform depth in which a shift of punctate was inevitable, but it cannot be predicted. The likelihood of injuring the neighboring vital structure, such as portal branches, biliary ducts, or gastrointestinal tract, increases. Multiple electrodes in this new system can be inserted into the predetermined location, minimizing the possibility of damaging the important neighboring structure. That could be the reason why no major complication was observed in the switching RFA group in the present study. Although the rate of major complications did not differ between two groups, theoretically, patients may benefit from the multiple-electrode switching-based RFA, and we believe that it can be significant between two groups if large cohorts were analyzed, especially when more large tumors were included.

Interestingly, we found that the LTP rate and the intrahepatic recurrence rate in the switching RFA group were both lower than those in the conventional RFA group; however, no significant differences in OS were observed. Only extrahepatic recurrence was found to be a significant prognostic factor for OS in multivariable analysis. The reason could be explained that most patients with LTP or intrahepatic recurrence were eligible for rescue treatment. However, the estimated overall 5-year survival rate in the switching RFA group was higher than that in the conventional RFA group.

The main limitation of our study is its retrospective nature, which may induce selection bias. Ideally, randomized multicenter controlled clinical trials are needed to provide a complete evaluation of switching RFA for the treatment of HCC. Second, it should be made aware that the outcome of the RFA for HCC is heavily dependent on the expertise of the operators and that we focused only on patients with a single HCC, which may result in differences in the prognostic factors for OS.

In conclusion, our findings from this study demonstrate that the multiple-electrode switching-based RFA is safe and effective in treating single early-stage hepatocellular carcinoma. Compared with conventional RFA, switching RFA provides a high local tumor control for HCC. An ongoing randomized trial might help to clarify the role of this approach for the treatment of HCC.

DATA AVAILABILITY STATEMENT

All datasets generated for this study are included in the article/supplementary material.

ETHICS STATEMENT

The studies involving human participants were reviewed and approved by Institutional Review Board approval was obtained from the First Affiliated Hospital of Sun Yat-sen University. The patients/participants provided their written informed consent to participate in this study. Written informed consent was obtained from the individual(s) for the publication of any potentially identifiable images or data included in this article.

AUTHOR CONTRIBUTIONS

GH and XZ accumulated the patients' data and wrote the main manuscript text. BL and MLiu analyzed the results. MX and MLin prepared all figures. MLu and MK conducted the therapy and exam. XX conceived the study, was responsible for the study planning, data analyze and manuscript preparation. All authors wrote and reviewed the main manuscript.

FUNDING

This work was funded by the National Natural Science Foundation of China, Grant Number: 81501493.

REFERENCES

1. Marrero JA, Kulik LM, Sirlin CB, Zhu AX, Finn RS, Abecassis MM, et al. Diagnosis, staging, and management of hepatocellular carcinoma: 2018 practice guidance by the American association for the study of liver diseases. *Hepatology.* (2018) 68:723–50. doi: 10.1002/hep.29913
2. Lee S, Kang TW, Cha DI, Song KD, Lee MW, Rhim H, et al. Radiofrequency ablation vs. surgery for perivascular hepatocellular carcinoma: propensity score analyses of long-term outcomes. *J Hepatol.* (2018) 69:70–8. doi: 10.1016/j.jhep.2018.02.026
3. Kutlu OC, Chan JA, Aloia TA, Chun YS, Kaseb AO, Passot G, et al. Comparative effectiveness of first-line radiofrequency ablation versus surgical resection and transplantation for patients with early hepatocellular carcinoma. *Cancer.* (2017) 123:1817–27. doi: 10.1002/cncr.30531
4. Peng ZW, Zhang YJ, Chen MS, Lin XJ, Liang HH, Shi M. Radiofrequency ablation as first-line treatment for small solitary hepatocellular carcinoma: Long-term results. *Eur J Surg Oncol.* (2010) 36:1054–60. doi: 10.1016/j.ejso.2010.08.133
5. Hong SN, Lee SY, Choi MS, Lee JH, Koh KC, Paik SW, et al. Comparing the outcomes of radiofrequency ablation and surgery in patients with a single small hepatocellular carcinoma and well-preserved hepatic function. *J Clin Gastroenterol.* (2005) 39:247–52. doi: 10.1097/01.mcg.0000152746.72149.31
6. Gravante G, Overton J, Sorge R, Bhardwaj N, Metcalfe MS, Lloyd DM, et al. Radiofrequency ablation versus resection for liver tumours: an evidence-based approach to retrospective comparative studies. *J Gastrointest Surg.* (2011) 15:378–87. doi: 10.1007/s11605-010-1377-6
7. N'Kontchou G, Mahamoudi A, Aout M, Ganne-Carrie N, Grando V, Coderc E, et al. Radiofrequency ablation of hepatocellular carcinoma: long-term results and prognostic factors in 235 Western patients with cirrhosis. *Hepatology.* (2009) 50:1475–83. doi: 10.1002/hep.23181
8. Lam VW, Ng KK, Chok KS, Cheung TT, Yuen J, Tung H, et al. Risk factors and prognostic factors of local recurrence after radiofrequency ablation of hepatocellular carcinoma. *J Am Coll Surg.* (2008) 207:20–9. doi: 10.1016/j.jamcollsurg.2008.01.020
9. Mulier S, Ni Y, Jamart J, Ruers T, Marchal G, Michel L. Local recurrence after hepatic radiofrequency coagulation: multivariate meta-analysis and review of contributing factors. *Ann Surg.* (2005) 242:158–71. doi: 10.1097/01.sla.0000171032.99149.fe
10. de Baere T, Rehim MA, Teriitheau C, Deschamps F, Lapeyre M, Dromain C, et al. Usefulness of guiding needles for radiofrequency ablative treatment of liver tumors. *Cardiovasc Intervent Radiol.* (2006) 29:650–4. doi: 10.1007/s00270-005-0187-9
11. Chen MH, Yang W, Yan K, Zou MW, Solbiati L, Liu JB, et al. Large liver tumors: protocol for radiofrequency ablation and its clinical application in 110 patients–mathematic model, overlapping mode, and electrode placement process. *Radiology.* (2004) 232:260–71. doi: 10.1148/radiol.2321030821
12. Park MJ, Kim YS, Rhim H, Lim HK, Lee MW, Choi D. A comparison of US-guided percutaneous radiofrequency ablation of medium-sized hepatocellular carcinoma with a cluster electrode or a single electrode with a multiple overlapping ablation technique. *J Vasc Interv Radiol.* (2011) 22:771–9. doi: 10.1016/j.jvir.2011.02.005
13. Brace CL, Sampson LA, Hinshaw JL, Sandhu N, Lee FT Jr. Radiofrequency ablation: simultaneous application of multiple electrodes via switching creates larger, more confluent ablations than sequential application in a large animal model. *J Vasc Interv Radiol.* (2009) 20:118–24. doi: 10.1016/j.jvir.2008.09.021
14. Laeseke PF, Sampson LA, Haemmerich D, Brace CL, Fine JP, Frey TM, et al. Multiple-electrode radiofrequency ablation creates confluent areas of necrosis: *in vivo* porcine liver results. *Radiology.* (2006) 241:116–24. doi: 10.1148/radiol.2411051271
15. Laeseke PF, Frey TM, Brace CL, Sampson LA, Winter TC 3rd, Ketzler JR, et al. Multiple-electrode radiofrequency ablation of hepatic malignancies: initial clinical experience. *AJR Am J Roentgenol.* (2007) 188:1485–94. doi: 10.2214/AJR.06.1004
16. Woo S, Lee JM, Yoon JH, Joo I, Kim SH, Lee JY, et al. Small- and medium-sized hepatocellular carcinomas: monopolar radiofrequency ablation with a multiple-electrode switching system-mid-term results. *Radiology.* (2013) 268:589–600. doi: 10.1148/radiol.13121736
17. Tan Y, Jiang J, Wang Q, Guo S, Ma K, Bie P. Radiofrequency ablation using a multiple-electrode switching system for hepatocellular carcinoma within the Milan criteria: long-term results. *Int J Hyperthermia.* (2018) 34:298–305. doi: 10.1080/02656736.2017.1330495
18. Ahmed M, Solbiati L, Brace CL, Breen DJ, Callstrom MR, Charboneau JW, et al. Image-guided tumor ablation: standardization of terminology and reporting criteria–a 10-year update. *Radiology.* (2014) 273:241–60. doi: 10.1148/radiol.14132958
19. Morimoto M, Numata K, Kondou M, Nozaki A, Morita S, Tanaka K. Midterm outcomes in patients with intermediate-sized hepatocellular carcinoma: a randomized controlled trial for determining the efficacy of radiofrequency ablation combined with transcatheter arterial chemoembolization. *Cancer.* (2010) 116:5452–60. doi: 10.1002/cncr.25314
20. Shi M, Zhang CQ, Zhang YQ, Liang XM, Li JQ. Micrometastases of solitary hepatocellular carcinoma and appropriate resection margin. *World J Surg.* (2004) 28:376–81. doi: 10.1007/s00268-003-7308-x
21. Kim YS, Lee WJ, Rhim H, Lim HK, Choi D, Lee JY. The minimal ablative margin of radiofrequency ablation of hepatocellular carcinoma (> 2 and < 5 cm) needed to prevent local tumor progression: 3D quantitative assessment using CT image fusion. *AJR Am J Roentgenol.* (2010) 195:758–65. doi: 10.2214/AJR.09.2954
22. Ye J, Huang G, Zhang X, Xu M, Zhou X, Lin M, et al. Three-dimensional contrast-enhanced ultrasound fusion imaging predicts local tumor progression by evaluating ablative margin of radiofrequency ablation for hepatocellular carcinoma: a preliminary report. *Int J Hyperthermia.* (2019) 36:55–64. doi: 10.1080/02656736.2018.1530460
23. Jiang C, Liu B, Chen S, Peng Z, Xie X, Kuang M. Safety margin after radiofrequency ablation of hepatocellular carcinoma: precise assessment with a three-dimensional reconstruction technique using CT imaging. *Int J Hyperthermia.* (2018) 34:1135–1141. doi: 10.1080/02656736.2017.1411981
24. Hoffmann R, Rempp H, Erhard L, Blumenstock G, Pereira PL, Claussen CD, et al. Comparison of four microwave ablation devices: an experimental study in *ex vivo* bovine liver. *Radiology.* (2013) 268:89–97. doi: 10.1148/radiol.13121127
25. Kim YS, Rhim H, Cho OK, Koh BH, Kim Y. Intrahepatic recurrence after percutaneous radiofrequency ablation of hepatocellular carcinoma: analysis of the pattern and risk factors. *Eur J Radiol.* (2006) 59:432–41. doi: 10.1016/j.ejrad.2006.03.007
26. Lai ZC, Liang JY, Chen LD, Wang Z, Ruan SM, Xie XY, et al. Do hepatocellular carcinomas located in subcapsular space or in proximity to vessels increase the rate of local tumor progression? A meta-analysis. *Life Sci.* (2018) 207:381–5. doi: 10.1016/j.lfs.2018.06.016

Conflict of Interest: The authors declare that the research was conducted in the absence of any commercial or financial relationships that could be construed as a potential conflict of interest.

frontiers in Oncology

ORIGINAL RESEARCH
published: 26 August 2020
doi: 10.3389/fonc.2020.01464

The Perfusion Features of Recurrent Hepatocellular Carcinoma After Radiofrequency Ablation Using Contrast-Enhanced Ultrasound and Pathological Stemness Evaluation: Compared to Initial Tumors

Jin-Yu Wu[1,2†], Xiu-Mei Bai[2†], Hong Wang[2], Qian Xu[1], Song Wang[2], Wei Wu[2], Kun Yan[2] and Wei Yang[2]*

[1] Department of Ultrasound, the First Hospital of Harbin, Harbin, China, [2] Key Laboratory of Carcinogenesis and Translational Research (Ministry of Education/Beijing), Department of Ultrasound, Peking University Cancer Hospital and Institute, Beijing, China

OPEN ACCESS

Edited by:
Fu Wang,
Xidian University, China

Reviewed by:
Xin-Wu Cui,
Huazhong University of Science and Technology, China
Yuming Jiang,
Stanford University, United States
Ming Xu,
First Affiliated Hospital of Sun Yat-sen University, China

***Correspondence:**
Wei Yang
13681408183@163.com

[†] These authors have contributed equally to this work

Specialty section:
This article was submitted to Cancer Imaging and Image-directed Interventions, a section of the journal Frontiers in Oncology

Received: 27 March 2020
Accepted: 09 July 2020
Published: 26 August 2020

Citation:
Wu J-Y, Bai X-M, Wang H, Xu Q, Wang S, Wu W, Yan K and Yang W (2020) The Perfusion Features of Recurrent Hepatocellular Carcinoma After Radiofrequency Ablation Using Contrast-Enhanced Ultrasound and Pathological Stemness Evaluation: Compared to Initial Tumors. Front. Oncol. 10:1464. doi: 10.3389/fonc.2020.01464

Objective: To investigate the perfusion features of local recurrence in hepatocellular carcinoma (HCC) after radiofrequency ablation (RFA) with contrast-enhanced ultrasound (CEUS) and pathological correlation, as well as to compare with those of initial HCC.

Methods: From 2010 to 2018, 42 patients with recurrent HCC after RFA were enrolled in this study. The initial HCC patients included 32 males and 10 females with an average age of 58.2 ± 8.1 years. The CEUS images for initial HCC lesions and local recurrence after RFA were compared. The perfusion features were analyzed, including enhancement time, process, boundary, morphology, washout time, washout degree, feeding vessels, and internal necrosis. H&E staining and CD133/EpCAM staining were performed with biopsy samples for the stemness study.

Results: According to CEUS, 59.5% of initial HCC lesions had centripetal enhancement, and 61.9% of recurrent HCC lesions had homogeneous enhancement in the arterial phase ($p < 0.001$). A total of 73.8% of initial HCC lesions had well-defined margins at the peak, and 81.0% of recurrent HCC lesions had poorly defined margins ($p < 0.001$). A total of 78.6% of initial HCC lesions had regular morphology at the peak, and 83.3% of recurrent HCC lesions were irregular ($p < 0.001$). Feeding vessels were more frequently found in initial HCC lesion (71.4%) than in recurrent HCCs (38.1%, $p = 0.002$). In the late phase, 60% of initial HCCs had marked washout while 83.3% of recurrent HCC lesion had marked washout ($p = 0.019$). A total of 31.3% of the initial HCC lesions had internal necrosis areas while only 7.1% of recurrent HCC lesions had internal necrosis areas ($p = 0.035$). In tumors 3–5 cm in size, the washout time of recurrent HCCs was shorter than that of initial HCCs (50.3 ± 13.5 s vs. 75.6 ± 45.8 s, $p = 0.013$). Pathological staining showed that the tumor stem cell markers (CD133 and EpCAM) were both highly expressed in recurrent samples compared with initial tumor samples (CD133+: 19 vs. 5%, $p = 0.002$; EpCAM+:15 vs. 6%, $p = 0.005$).

Conclusions: Recurrent HCC after RFA had more homogeneous enhancement with a poorly defined border, marked washout, and fewer less feeding vessels and inner necrosis areas compared to initial HCC. The stemness study also found upregulated stemness in recurrent HCC. These specific features might be related to the aggressive biological behavior of recurrent HCC.

Keywords: hepatocellular carcinoma, radiofrequency ablation, recurrence, contrast-enhanced ultrasound, cancer stem cell

INTRODUCTION

In recent years, radiofrequency ablation (RFA) has been widely applied to cure cancers, including liver, kidney, and lung tumors. RFA has been performed as a first-line treatment for hepatocellular carcinoma (HCC) and patients' 5-year survival rates have reached 67.9% (1). Compared to surgical resection, however, RFA has higher local recurrence rates (2, 3), and the second RFA treatment becomes more difficult in the case of large recurrent lesions or recurrent lesions in high-risk locations. Therefore, the accurate evaluation of local recurrence in HCC is an important issue for achieving early diagnosis and conducting timely repeat treatment. Currently, contrast-enhanced computed tomography (CT) and magnetic resonance imaging (MRI) are considered the standard modalities for evaluating RFA efficacy (4, 5). However, CT enhancement involves radioactive radiation, and it is not feasible to use MRI repeatedly in a short period. Contrast-enhanced ultrasound (CEUS) imaging is recognized as the revolution of traditional ultrasound examination and can overcome several limitations of conventional grayscale and color ultrasound techniques (6). Unlike enhanced CT and MRI, CEUS is able to demonstrate dynamic changes in hepatic blood flow in real time (6–10). Furthermore, CEUS provides visible information on the vascular density and structures of lesions and liver tissue (11).

Studies assessing the histopathological features of primary HCC with the perfusion pattern of CEUS are increasing (12–14). Fan et al. (12) showed that ∼98% of primary HCC had enhancement in the arterial phase and portal phase with CEUS findings. Wilson et al. (15) reported that washout at parenchymal phase or late phase was another important diagnostic clue for HCC. Based on clinical diagnostic criteria, primary HCC can be diagnosed when the lesion has fast in and fast out features in enhanced images. However, reports on the perfusion features of CEUS in terms of the local recurrence of HCC after local ablation are rare. Recent studies have demonstrated that incomplete RFA of HCC can initiate malignant transition (16, 17). It is not clear whether local recurrent HCC after RFA has specific perfusion characteristics and pathological changes compared to initial tumors. Thus, this study aimed to investigate the difference in CEUS characteristics and pathological features between local recurrent HCC after RFA treatment and initial HCC and to summarize the specific features of recurrent HCC. The results might provide more information about biological behavior after local recurrence and advice for appropriate treatment.

MATERIALS AND METHODS

Patients

From 2010 to 2018, 1,118 consecutive HCC patients received ultrasound-guided percutaneous RFA treatment in our center. The inclusion criteria of liver tumors for ultrasound-guided percutaneous RFA (local curative purpose) were as follows: (1) a tumor size of no more than 5 cm and a tumor number of no more than 3; (2) no direct tumor invasion of adjacent organs or tumor thrombi in the main or lobar portal system; (3) a tumor not invading a main bile duct or being obviously exophytic; (4) a tumor accessible via a percutaneous approach; (5) an international standard ratio < 1.6 and a platelet count $> 50{,}000/\mu l$; and (6) no extrahepatic metastasis or local extrahepatic metastasis with good control before RFA.

After RFA treatment, the patients received close follow-up. During the follow-up period, 66 patients were diagnosed with local recurrence after RFA. The inclusion criteria for this study were as follows: (1) the patients had local recurrent HCC after RFA in our center; (2) the patients received CEUS examinations for both initial HCC and recurrent HCC tumors; and (3) the initial tumor or recurrent tumor was not treated by previous therapies such as TACE, radiotherapy, or PEI in 1 month before CEUS examination. Regularly, the HCC patients underwent enhanced CT/MRI in the first month after RFA. The enhanced area around or within the ablation zone was defined as residual tumor at the initial evaluation. Then, the patients with residual tumors would receive the second RFA or other therapies. Furthermore, the patients who had completely sufficient ablation continued the follow-up protocol. The enhanced area around or within the ablation zone during follow-up was defined as local recurrence. Finally, 42 patients who met the inclusion criteria were enrolled in this study: 32 males and 10 females with an average age of 58.2 ± 8.1 years old (range: 35–80 years old). Initial HCC and local recurrent lesions were diagnosed by biopsy (which included 17 initial HCC cases and 13 recurrent HCC cases) and clinical diagnosis (nodule size $\geq$1 cm, two kinds of imaging modalities with a typical enhanced performance, which included 25 initial HCC cases and 29 recurrent HCC cases). Among them, 11 patients underwent biopsy for both initial HCC and recurrent HCC.

Ultrasound Equipment

Low mechanical index (MI) and real-time contrast-enhanced harmonic ultrasound examination were performed in this study. The contrast-enhanced agent was SonoVue (Bracco

SpA, Italy) suspension, which contained 6.07 mg/ml sulfur hexafluoride (SF6) stabilized by a phospholipid shell (microbubble concentration: 5 mg/ml). The mean diameter of the microbubbles was 2.5 μm. The SonoVue suspension was administered through the cubital vein by bolus injection (2 ml in 1–3 s). The GE LOGIQ E9 ultrasound system (General Electric, Milwaukee, WI, USA) was used for this study. The probe frequency ranged from 2.5 to 6.0 MHz. The MI used in CEUS scanning ranged from 0.11 to 0.14.

CEUS Examination Method

First, the liver was scanned with conventional grayscale ultrasound to identify the lesions' number and location. The size, morphology, border, echogenicity, echotexture, and flow features of the lesions were observed. Then, the examination was switched to a low-MI harmonic pulse-inversion CEUS mode. After injection of the contrast agent, the lesions were scanned continually for a duration of 5–6 min. The enhancement pattern and washout degree of the lesions were noted and recorded. After acquiring the vascular perfusion information for the target lesion, the whole liver was scanned quickly to detect abnormal washout lesions. The abnormal washout lesions required repeat injection of contrast agent if necessary. CEUS dynamic clips and single-frame static images were stored in an ultrasonic instrument hard disk for further analysis.

Imaging Analysis

All CEUS images and clips were reviewed retrospectively, and the perfusion patterns of CEUS were analyzed by two radiologists with more than 10 years of experience in liver CEUS (W. J. Y. and Y. W.). The blinded radiologists read the CEUS imaging results, without the information of the pathologic and clinical materials. The two radiologists would discuss and make an agreement in each case. The perfusion features between the two groups were compared.

Based on our definition, the arterial phase of CEUS was started with enhancement in the hepatic artery. The peak occurred when the lesion reached its highest echogenicity. The late phase referred to the whole liver parenchyma, reached the highest level of enhancement and was gradually washed out. The CEUS examination time for one injection was 5–6 min. The CEUS features of the liver lesions included enhancement in the arterial phase, the presence of a feeding artery, lesion margins and morphology at the peak of enhancement, the washout degree in the late phase, and the presence of necrosis areas inside the lesion.

Centripetal enhancement was defined as the first enhancement of the lesion in the periphery and then a gradual filling toward the center. Centrifugal enhancement was defined as the first enhancement of the lesion in the center, gradually reaching the periphery. Homogeneous enhancement referred to the rapid enhancement of the entire lesion and showed a significant increase in echogenicity compared to the same level of liver tissue. A well-defined margin was defined as a distinct difference between the lesion and the surrounding liver. Marked washout was defined as a lesion with almost no enhancement or mostly washed out contrast agent within 2 min after contrast injection (18). A feeding vessel was identified in the arterial phase when contrast flowed directly through the vessel from the hepatic hilum to the lesion. Internal necrosis was considered if no contrast agent entered the area from the arterial to the late phase. Regular lesions had a round shape with well-defined margins.

Phase of Enhancement

The enhancement pattern should be described separately for the different phases, which for the liver comprise the arterial, portal venous, and the late phases. "Wash in" used for both qualitative and quantitative analyses, referred to the period of progressive enhancement within a region of interest from the arrival of microbubbles in the field of view to "peak enhancement," which referred to the arterial phase in this study. The "washout phase" referred to the period of reduction in enhancement that followed peak enhancement, which referred to portal phase to the late phase (19).

Time–Intensity Curve Analysis

Time–intensity curve (TIC) analysis was performed as a quantitative tool to analyze the difference between the initial HCC and recurrent HCC lesions. The stored DICOM data were evaluated using the built-in TIC analysis software of the LOGIQ E9 system (GE, USA). A region of interest (ROI), mainly including the liver lesion, was selected to obtain the TIC. The ROI sampling frame was chosen in lesions around the central and liver tissues as same a depth as possible to avoid the great vessels and tumor necrosis area. The enhanced time was calculated from the time of contrast agent injection to the contrast agents arrived lesions. The peak time was considered from the contrast agents injected to the contrast agent reaching the maximum level. The washout time referred to lesions with echo intensities lower than the time needed for the liver parenchyma.

Pathological Evaluation

Eleven patients underwent biopsy for initial HCC before RFA and for recurrent HCC after RFA. Pathological specimens were fixed in formalin and were routinely processed and embedded in paraffin. All tumor slices were subjected to hematoxylin and eosin (H&E) staining for gross pathologic examination. CD133 and EpCAM are regarded as important surface markers of cancer stem cells in HCC (20). CD133 (allophycocyanin, Miltenyi Biotec) and EpCAM (fluorescein isothiocyanate, Stem cell Technologies) immunofluorescent (IF) staining were performed for tumor stemness evaluation. The stained slices were reviewed by an experienced pathologist. Slides were imaged and analyzed by using a microscope (Olympus BX41, Olympus, Japan) and imaging software (Micron; Westover Scientific). The temporal evolution of cellular morphology and the spatial distribution of protein expression were determined first. Quantitative analysis was performed by accounting for the percentage of positively stained cells per high-powered field within the tumor zone. Five random high-powered fields were analyzed for a minimum of five specimens for each marker and were scored in a blinded fashion to remove observer bias. The percentage of CD133/EpCAM-positive cells was evaluated with pathological initial HCC and

recurrent HCC samples and was compared to observe the changes after RFA treatment.

Statistical Analysis

All data are expressed as the mean ± standard deviation. The significance of differences in the baseline characteristics, enhancement patterns, ITC parameters, and pathological results were compared by the chi-squared test or independent-sample *t*-test. Statistical significance was defined as a p-value < 0.05. All data analysis was performed by using SPSS statistical software 24.0 (SPSS, Chicago, IL, USA).

RESULTS

General Features

The enrolled HCC patients included 32 males and 10 females with an average age of 58.2 ± 8.1 years (35–80 years) and an average lesion size of 3.1 ± 1.3 cm (1.0–5.0 cm). There were 38 patients with solitary lesions, and four had multiple lesions. The largest tumor was used to evaluate the CEUS features. The etiologies of liver disease included hepatitis B in 34 patients, hepatitis C in 4, alcoholic liver disease in 2, and absence of liver disease in 2. Of them, 31 (73.8%) patients had abnormal serum ALT/AST levels, and 15 (35.7%) patients had elevated AFP levels before RFA treatment. Thirty (71.4%) patients had Child-Pugh class A and 12 (28.6%) had class B. During the follow-up, these recurrent tumors occurred 2–65 months after initial RFA. With the exception of the tumor size, there was no significant difference in other clinical characteristics between the initial HCC and recurrent HCC groups (**Table 1**).

TABLE 1 | The basic characteristics of initial HCC and recurrent HCC patients.

Varies	Initial HCC	Recurrent HCC	*p*-value
No. of patients	42	42	
Gender			1.0
Male	32 (76.2)	32 (76.2)	
Female	10 (23.8)	10 (23.8)	
Age			
Mean	58.2 ± 8.1	58.7 ± 7.9	0.875
≤60 years	25 (59.5)	23 (54.8)	0.659
>60 years	17 (40.5)	19 (45.2)	
Tumor size*			
Mean	3.1 ± 1.3	2.5 ± 1.0	0.012
≤3 cm	20 (47.6)	31 (73.8)	0.014
3.1–5 cm	22 (52.4)	11 (26.2)	
Etiology of liver disease			0.776
HBV	34 (81.0)	35 (83.3)	
HCV	4 (9.5)	4 (9.5)	
Alcoholic liver	2 (4.8)	2 (4.8)	
Absence of liver disease	2 (4.8)	1 (2.4)	
Liver cirrhosis			0.763
None	7 (16.7)	6 (14.3)	
Yes	35 (83.3)	36 (85.7)	
Serum ALT/AST			0.474
Normal	31 (73.8)	28 (66.7)	
Elevated	11 (26.2)	14 (33.3)	
Child–Pugh class			0.355
Child-push A	30 (71.4)	26 (61.9)	
Child-push B	12 (28.6)	16 (38.1)	
Serum AFP level			0.818
≤20 ng/ml	27 (64.3)	28 (66.7)	
>20 ng/ml	15 (35.7)	14 (33.3)	

HCC, hepatocellular carcinoma; HBV, hepatitis B virus; HCV, hepatitis C virus; ALT, alanine aminotransferase; AST, aspartate transaminase; AFP, alpha-fetoprotein. Numbers in parentheses are percentages.
**Statistically significant.*

Comparison of CEUS Perfusion Features

Of the 42 initial HCCs, all tumors had arterial phase enhancement, and 40 tumors had washout in the portal phase or late phase. On the other hand, all 42 recurrent HCC lesions showed arterial phase enhancement and washout in the portal phase or late phase. The comparison of CEUS findings is summarized in **Table 2**. In the arterial phase of CEUS, 59.5% of the initial HCC lesions showed centripetal enhancement, while 61.9% of the recurrent HCC lesions showed homogeneous enhancement ($p < 0.001$). At the peak, 73.8% of the initial HCC lesions had well-circumscribed margins, while 81.0% of the recurrent HCC lesions had poorly defined margins ($p < 0.001$). A total of 78.6% of the initial HCC lesions had regular morphology at the peak, while 83.3% of the recurrent HCC lesions were irregular ($p < 0.001$). Feeding vessels were more frequently visualized in initial HCC lesions (71.4%) than in recurrent HCC lesions (38.1%, $p = 0.002$). In the portal phase or late phase, 60% of initial HCCs had marked washout while 83.3% of recurrent HCCs had marked washout ($p = 0.019$). Thirty-one percent of the initial HCCs had internal necrosis areas, while only 7.1% of recurrent HCCs had internal necrosis areas ($p = 0.035$) (**Figures 1**, **2**).

Comparison of CEUS Quantitative Parameters

Quantitative analysis of the TIC showed that there was no significant difference between initial HCC and recurrent HCC lesions in terms of enhancement time (16.5 ± 3.3 s vs. 17.4 ± 3.1 s, $p = 0.256$), peak time (23.7 ± 4.6 s vs. 24.4 ± 5.0 s, $p = 0.384$), and washout time (74.7 ± 38.6 s vs. 58.4 ± 18.5 s, $p = 0.186$). We further divided cases into two subgroups based on tumor size. In <3 cm tumors, there was no significant difference in TIC parameters between initial HCC and recurrent HCC lesions ($p = 0.084$, $p = 0.913$, and $p = 0.076$). In tumors 3–5 cm in size, the washout time in recurrent HCCs was shorter than that in initial HCCs (50.3 ± 13.5 s vs. 75.6 ± 45.8 s, $p = 0.013$) (**Table 3**).

TABLE 2 | The comparison of the perfusion features of CEUS between initial and recurrent HCC tumors.

Perfusion features		Initial HCC	Recurrent HCC	*p*-value
Arterial phase				
Enhancement		42 (100)	42 (100)	1.0
Enhance process*				<0.001
	Centrifugal	4 (9.5)	4 (9.5)	
	Centripetal	25 (59.5)	6 (14.3)	
	Homogeneous	8 (19.0)	26 (61.9)	
	Others	5 (11.9)	6 (14.3)	
Morphology at peak*				<0.001
	Regular	33 (78.6)	7 (16.7)	
	Irregular	9 (21.4)	35 (83.3)	
Margin at peak*				<0.001
	Well defined	31 (73.8)	8 (19.0)	
	Poor defined	11 (26.2)	34 (81.0)	
Feeding vessels*				0.002
	Yes	30 (71.4)	16 (38.1)	
	No	12 (28.6)	26 (61.9)	
PV or late phase				
Washout		40[#] (95.2)	42 (100)	0.494
Degree of washout*	Marked	24 (60.0)	35 (83.3)	0.019
	Mild	16 (40.0)	7 (16.7)	
Inner necrosis area*				0.035
	Yes	10 (31.3)	3 (7.1)	
	No	32 (68.7)	39 (92.9)	

CEUS, contrast-enhanced ultrasound; HCC, hepatocellular carcinoma; PV, portal vein. Numbers in parentheses are percentages.

** Statistically significant.*

[#] Two initial HCCs showed no marked or mild washout in the PV or late phase.

Pathological Results

The HE staining results of HCC samples demonstrated that a more intensive cell distribution was detected in the recurrent HCC than in the initial tumor in the same patient (**Figure 3A**). Moreover, IF staining showed that the tumor stem cell markers CD133 and EpCAM were both highly expressed in recurrent samples compared with the expression in initial tumors (CD133+: 19 vs. 5%, $p = 0.002$; EpCAM+:15 vs. 6%, $p = 0.005$) (**Figure 3B**).

DISCUSSION

RFA, along with surgical resection and liver transplantation, has been recognized as one of the radical therapies for HCC, especially for small HCC. However, regardless of technical success, local tumor recurrence affects long-term survival after radical treatment (3, 21). In our center, the local recurrence rate of HCC after RFA in 10 years was 13.8% (21). The mechanisms of malignant behaviors from recurrent HCC after RFA have been increasingly reported (22). Early detection and diagnosis of local recurrence in HCC patients' follow-up have become important issues (5, 9, 23–26). A previous study (27) indicated that isoenhancement in all vascular phase patterns on CEUS was found in >50% of recurrent lesions, indicating a high risk of HCC. This suggests that recurrent lesions may be different from initial HCC lesion in terms of perfusion patterns. However, the comparison between initial HCC and recurrent HCC of CEUS performance has not been yet reported.

As previously reported, the performance of HCC is mainly fast-in and fast-out on CEUS and dynamically enhanced CT images (28, 29). Microvascular density in recurrent disease is significantly higher on CEUS evaluation than on CECT/MRI ($p < 0.05$) (9). Recurrent tumors have the characteristics of incipient lesions. Our study showed that all local recurrent lesions had different levels of enhancement, and all were consistent with the characteristics of malignant performance. However, the artery-portal phase enhancement and late washout pattern were not sufficient to assess the characteristics of recurrence after RFA treatment.

In our study, we analyzed in more detail the CEUS performance for recurrent HCC after RFA and compared it with that for initial HCC before treatment. The results showed the unique performance of the enhancement process, pattern, lesion border, internal necrosis, and feeding vessels. Reported animal studies have showed that thermal ablation promotes a large degree of blood sinus expansion surrounding the ablation

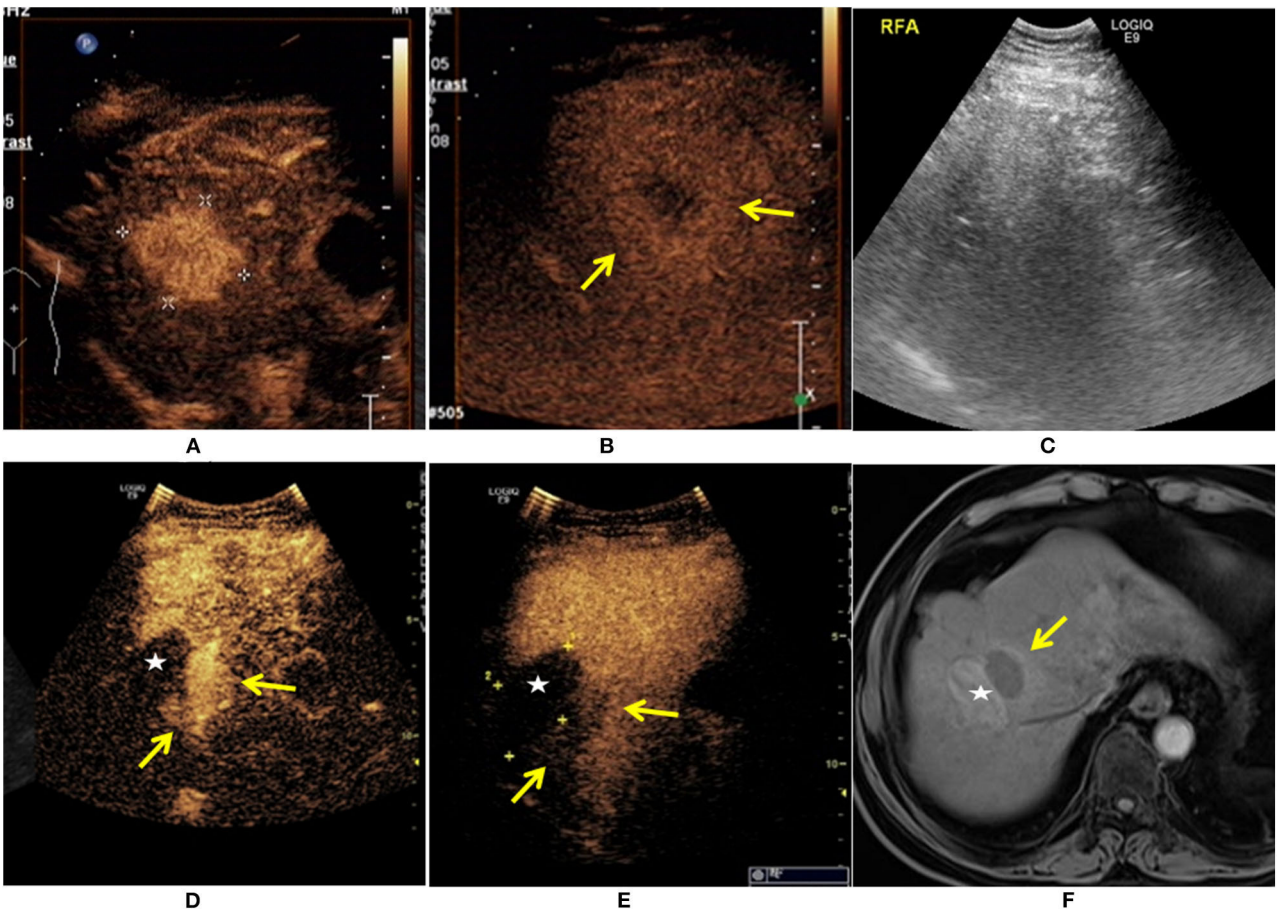

FIGURE 1 | A 65-year-old man was diagnosed with HCC. The patient had a 30-year history of hepatitis B. The contrast-enhanced ultrasound (CEUS) showed a single lesion measuring 4.1 × 3.6 cm in size (+) enhanced at arterial phase **(A)**, and the mild washout in lesion was found at the late phase (⇑) **(B)**. The patient received ultrasound-guided radiofrequency ablation (RFA) treatment **(C)**. Eleven months after RFA, there was an irregular enhancement (⇑) around the ablation zone (★), and marked washout at the late phase (⇑) **(D,E)**. The local recurrence after RFA was also demonstrated at enhanced MRI (⇑) **(F)**.

area and results in microvascular structure disorder hyperplasia. Kong et al. reported (16) that angiogenesis produced by altered cells after hyperthermia treatment through the HIF1α/VEGFA pathway could be one of the vital factors causing the rapid growth of residual HCC after RFA. With the wide application of CEUS in the clinic, especially the application of microvascular flow imaging (30, 31), Kang et al. demonstrated (31) significantly higher sensitivity and accuracy than color Doppler imaging and power Doppler imaging for the detection of intratumoral vascularity in suspected residual or recurrent HCCs. Benefiting from our center's regular follow-up after RFA treatment, local tumor recurrence can be found in the earlier stage. Therefore, the tumor size in the recurrent HCC group was smaller than that in the initial HCC group. The difference in tumor size might partly be attributed to the different patterns of blood perfusion on CEUS imaging. The tumor was larger, and the frequency of the feeding artery was increased. The absence of feeding vessels between initial HCC and recurrent HCC was significantly different ($p = 0.002$). Additionally, 31.3% of the initial HCC lesions had internal necrosis areas, while only 7.1% of recurrent HCC had internal necrosis areas ($p = 0.035$). Accordingly, in the arterial phase, the enhancement process was different [initial HCC group: centripetal (59.5%), recurrent HCC group: homogeneous (61.9%), $p < 0.001$].

In addition to tumor size, incomplete RFA enhanced the invasiveness and metastasis of residual cancer in HCC cells (17, 32). The aggressive biological behavior of recurrent tumors might cause poorly defined margins and irregular lesions on CEUS. In the diagnostic algorithm for focal liver lesions on CEUS, washout was an important feature and was highly suggestive of malignancy. Kitao et al. (33) reported that during multistep hepatocarcinogenesis, the drainage vessels of HCC changed from hepatic veins to hepatic sinusoids, and then to portal veins in the course of dedifferentiation. They (33) suggested that the drainage vessels of HCC changed from hepatic veins to hepatic sinusoids, which may be correlated with the onset of tumor washout on CEUS. Accordingly, when the hepatic sinusoids became the main drainage vessels, late washout occurred. In advanced lesions, the portal veins became the main drainage vessels, and fast washout was frequently seen. Our study showed that the washout time

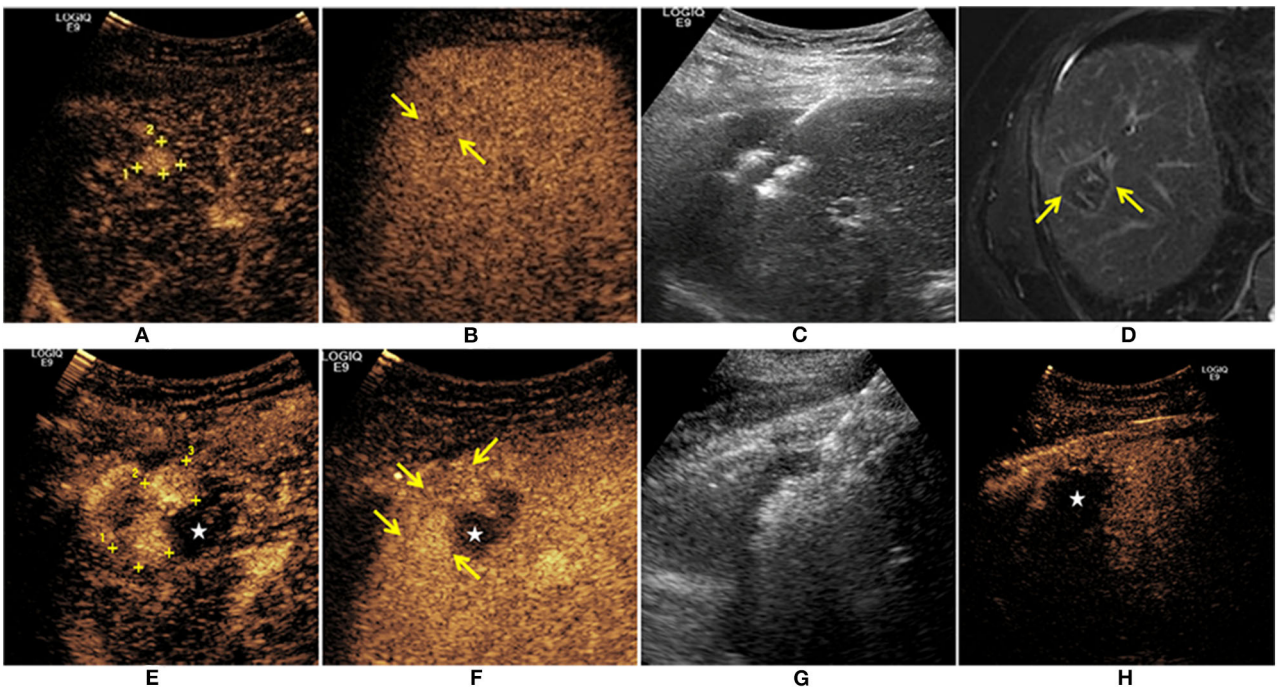

FIGURE 2 | A 59-year-old man was diagnosed with HCC. The CEUS showed a single lesion (+) enhanced at arterial phase **(A)**, and the mild washout in the lesion was found at the late phase (⇑) **(B)**. The patient received ultrasound-guided RFA treatment **(C)**. One month after treatment, there was no residual tumor on MR imaging (⇑) **(D)**. Thirteen months after RFA, there were irregular nodules enhanced (+) at the upper edge of the ablation zone (★) **(E)**. Mild washout was found at the late phase (⇑) **(F)**. The second RFA for this recurrent HCC was performed under ultrasound guidance **(G)**. Immediate CEUS after RFA treatment showed that there was no enhancement in the ablation zone (★) **(H)**.

TABLE 3 | The comparison of the quantitative parameters of TIC between initial HCC and recurrent HCC tumors.

Group	Tumor size: 1.0–3.0 cm				Tumor size: 3.1–5.0 cm			
	n	ET (s)	PT (s)	WT (s)	*n*	ET (s)	PT (s)	WT (s)*
Initial HCC	20	15.8 ± 4.1	23.2 ± 5.3	74.1 ± 39.7	22	17.4 ± 3.7	24.6 ± 5.8	75.6 ± 45.8
Recurrent HCC	31	18.1 ± 3.7	24.3 ± 4.2	63.8 ± 29.1	11	17.0 ± 4.0	24.5 ± 5.3	50.3 ± 13.5
p value	—	0.084	0.913	0.076	—	0.925	0.874	0.013

TIC, time–intensity curve; HCC, hepatocelluar carcinoma; ET, enhance time; PT, peak time; WT, washout time.
**Statistically significant.*

in recurrent HCCs was shorter than that in initial HCCs with a tumor size of 3–5 cm (50.3 ± 13.5 s vs. 75.6 ± 45.8 s, $p = 0.013$) and the marked washout rate was higher in recurrent HCCs (83.3 vs. 60%, $p = 0.019$), which is consistent with previous studies. The clinical significance of our CEUS study on recurrent HCC was as follows: first, a summary of the perfusion features of recurrent HCC on CEUS would help to differentiate diagnosis between recurrent HCC and other diseases, such as inflammatory reactions. Second, investigating the difference in perfusion features of recurrent HCC compared with initial HCC would help to understand the biological behavior of recurrent HCC. Third, identifying the tumor range and feeding vessels also provided useful information to plan the treatment protocol for local therapy.

Additionally, we found that the tumor stem cell markers (CD133 and EpCAM) were both highly expressed in recurrent HCCs compared with initial HCCs (CD133+: 19 vs. 5%, $p = 0.002$; EpCAM+: 15 vs. 6%, $p = 0.005$). These results provide a reference for clinical practice. According to a previous study (26), the expression levels of basic fibroblast growth factor in recurrent HCC were significantly higher than those in non-recurrent HCC ($p < 0.05$) and were associated with HCC recurrence after RFA. Thus, the biological behavior of recurrent HCCs is more aggressive than that of primary HCCs. It would be more difficult to treat recurrent lesions with local ablation. Additionally, the safety ablation margins should have been larger when we performed the second RFA session.

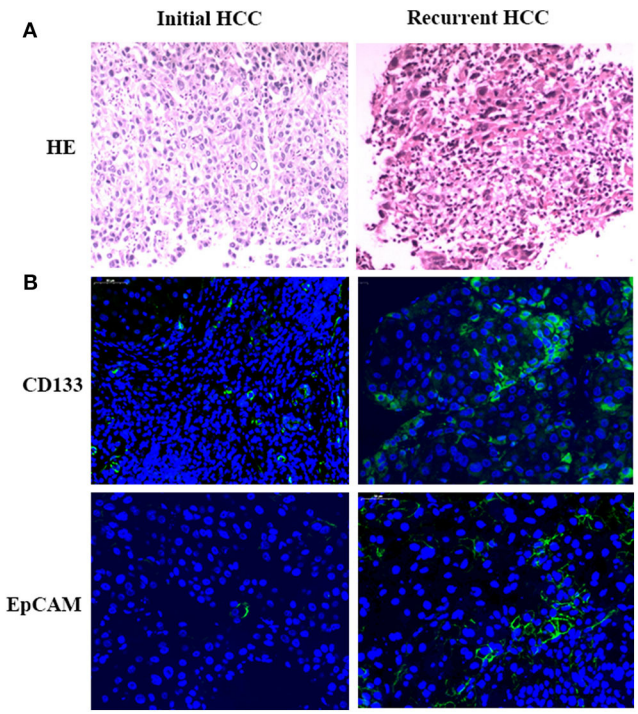

FIGURE 3 | Pathological results. Tumor samples obtained from initial and recurrent HCC patients treated with RFA were examined by H&E staining. H&E staining showed the more intensive cell distribution detected in recurrent HCC compared with the initial tumor in the same patient **(A)**. Immunofluorescence staining was used for detecting the expression of CD133 and EpCAM in HCC tumor samples **(B)**. Positive cells were stained with green signal; nuclei were stained with DAPI (Blue). Magnification: 400×.

There were some limitations in our study. First, the study was retrospective with some inevitable bias due to a single center. Second, recurrent tumors in difficult locations might have been missed by CEUS because of the inherent limitation of CEUS examination. In addition, due to the small sample size, we did not further analyze the degree of HCC differentiation or the local recurrence time (early recurrence vs. late recurrence). The local recurrence rate after RFA in our center was low. More patient data need to be collected in further studies.

In conclusion, recurrent HCC after RFA had more homogeneous enhancement, a poorly defined border, marked washout, and fewer feeding vessels and inner necrosis areas. These specific perfusion features might reflect the aggressive biological behavior and higher expression of cancer stem cell markers in recurrent HCC. Additionally, the analysis of CEUS findings for local recurrence after RFA would be useful for the differential diagnosis between inflammatory reaction and tumor recurrence as well as for identifying recurrence early. Furthermore, the perfusion feature in local recurrence of HCC would help to design optimal treatment strategies.

DATA AVAILABILITY STATEMENT

All datasets presented in this study are included in the article/supplementary material.

ETHICS STATEMENT

The studies involving human participants were reviewed and approved by the institutional review board of Peking University Cancer Hospital. The patients/participants provided their written informed consent to participate in this study.

AUTHOR CONTRIBUTIONS

WW and KY performed the patient's CEUS examinations. J-YW, X-MB, and WY helped to design the study and reviewed the images and performed the statistical analysis. HW and SW organized and analyzed the imaging database. J-YW, X-MB, and QX wrote the first draft of the manuscript. All authors contributed to the article and approved the submitted version.

FUNDING

This work was funded by the National Natural Science Foundation of China (Nos. 81773286 and 81971718) and Capital Medical Development Program (No. 2018-2-2154).

ACKNOWLEDGMENTS

We sincerely thank all participants in the study for their cooperation.

REFERENCES

1. Lee DH, Lee JM, Lee JY, Kim SH, Yoon JH, Kim YJ, et al. Radiofrequency ablation of hepatocellular carcinoma as first-Line treatment: long-term results and prognostic factors in 162 patients with cirrhosis. *Radiology.* (2014) 270:900–9. doi: 10.1148/radiol.13130940
2. Ueno M, Hayami S, Shigekawa Y, Kawai M, Hirono S, Okada K, et al. Prognostic impact of surgery and radiofrequency ablation on single nodular HCC ≤5 cm: cohort study based on serum HCC markers. *J Hepatol.* (2015) 63:1352–9. doi: 10.1016/j.jhep.2015.07.013
3. Rahbari NN, Mehrabi A, Mollberg NM, Muller SA, Koch M, Buchler MW, et al. Hepatocellular carcinoma: current management and perspectives for the future. *Ann Surg.* (2011) 253:453–69. doi: 10.1097/SLA.0b013e31820d944f
4. Shimizu R, Tamai H, Mori Y, Shingaki N, Maeshima S, Nuta J, et al. The arterial tumor enhancement pattern on contrast-enhanced computed tomography is associated with primary cancer death after radiofrequency ablation for small hepatocellular carcinoma. *Hepatol Int.* (2016) 10:328–39. doi: 10.1007/s12072-015-9678-1
5. Zheng SG, Xu HX, Lu MD, Xie XY, Xu ZF, Liu GJ, et al. Role of contrast-enhanced ultrasound in follow-up assessment after ablation for hepatocellular carcinoma. *World J Gastroenterol.* (2013) 19:855–65. doi: 10.3748/wjg.v19.i6.855

6. Rennert J, Wiesinger I, Beyer LP, Schicho A, Stroszczynski C, Wiggermann P, et al. Color coded perfusion analysis and microcirculation imaging with contrast enhanced ultrasound (CEUS) for post-interventional success control following thermal ablative techniques of primary and secondary liver malignancies. *Clin Hemorheol Microcirc.* (2019) 73:73–83. doi: 10.3233/CH-199224
7. Feng Y, Qin XC, Luo Y, Li YZ, Zhou X. Efficacy of contrast-enhanced ultrasound washout rate in predicting hepatocellular carcinoma differentiation. *Ultrasound Med Biol.* (2015) 41:1553–60. doi: 10.1016/j.ultrasmedbio.2015.01.026
8. Wiesinger I, Wiggermann P, Zausig N, Beyer LP, Salzberger B, Stroszczynski C, et al. Percutaneous treatment of malignant liver lesions: evaluation of success using contrast- enhanced ultrasound (CEUS) and perfusion software. *Ultraschall Med.* (2018) 39:440–7. doi: 10.1055/s-0043-119353
9. Liu LF, Ding ZL, Zhong JH, Li HX, Liu JJ, Li H. Contrast-enhanced ultrasound to monitor early recurrence of primary hepatocellular carcinoma after curative treatment. *BioMed Res Int.* (2018) 2018:1–8. doi: 10.1155/2018/8910562
10. Liu LN, Xu HX, Zhang YF, Xu JM. Hepatocellular carcinoma after ablation: the imaging follow-up scheme. *World J Gastroenterol.* (2013) 19:797–801. doi: 10.3748/wjg.v19.i6.797
11. Wiesinger I, Beyer LP, Zausig N, Verloh N, Wiggermann P, Stroszczynski C, et al. Evaluation of integrated color-coded perfusion analysis for contrast-enhanced ultrasound (CEUS) after percutaneous interventions for malignant liver lesions: first results. *Clin Hemorheol Microcirc.* (2018) 69:59–67. doi: 10.3233/CH-189131
12. Fan ZH, Chen MH, Dai Y, Wang YB, Yan K, Wu W, et al. Evaluation of primary malignancies of the liver using contrast-enhanced sonography: correlation with pathology. *Am J Roentgenol.* (2006) 186:1512–9. doi: 10.2214/AJR.05.0943
13. Ogawa S, Kumada T, Toyoda H, Ichikawa H, Kawachi T, Otobe K, et al. Evaluation of pathological features of hepatocellular carcinoma by contrast-enhanced ultrasonography: comparison with pathology on resected specimen. *Eur J Radiol.* (2006) 59:74–81. doi: 10.1016/j.ejrad.2006.02.003
14. Von Herbay A, Vogt C, Westendorff J, Haussinger D, Gregor M. Correlation between SonoVue enhancement in CEUS, HCC differentiation and HCC diameter: analysis of 130 patients with hepatocellular carcinoma (HCC). *Ultraschall Med.* (2009) 30:544–50. doi: 10.1055/s-0028-1109745
15. Wilson SR, Burns PN. An algorithm for the diagnosis of focal liver masses using microbubble contrast-enhanced pulse-inversion sonography. *Am J Roentgenol.* (2006) 186:1401–12. doi: 10.2214/AJR.04.1920
16. Kong J, Kong J, Pan B, Ke S, Dong S, Li X, et al. Insufficient radiofrequency ablation promotes angiogenesis of residual hepatocellular carcinoma via HIF-1alpha/VEGFA. *PLoS ONE.* (2012) 7:e37266. doi: 10.1371/journal.pone.0037266
17. Zhang N, Wang L, Chai ZT, Zhu ZM, Zhu XD, Ma DN, et al. Incomplete radiofrequency ablation enhances invasiveness and metastasis of residual cancer of hepatocellular carcinoma cell HCCLM3 via activating beta-catenin signaling. *PLoS ONE.* (2014) 9:e115949. doi: 10.1371/journal.pone.0115949
18. CEUS LI-RADS® v2017. Available online at: https://www.acr.org/Clinical-Resources/Reporting-and-Data-Systems/LI-RADS/CEUS-LI-RADS-v2017 (accessed September 12, 2017).
19. Claudon M, Dietrich CF, Choi BI, Cosgrove DO, Kudo M, Nolsøe CP, et al. Guidelines and good clinical practice recommendations for contrast enhanced ultrasound (CEUS) in the liver –update 2012. *Ultraschall Med.* (2013) 34:11–29. doi: 10.1016/j.ultrasmedbio.2012.09.002
20. Jang JW, Song Y, Kim SH, Kim JS, Kim KM, Choi EK, et al. CD133 confers cancer stem-like cell properties by stabilizing EGFR-AKT signaling in hepatocellular carcinoma, *Cancer Lett*. (2017) 389:1–10. doi: 10.1016/j.canlet.2016.12.023
21. Yang W, Yan K, Goldberg SN, Ahmed M, Lee JC, Wu W, et al. Ten-year survival of hepatocellular carcinoma patients undergoing radiofrequency ablation as a first-line treatment. *World J Gastroenterol.* (2016) 22:2993–3005. doi: 10.3748/wjg.v22.i10.2993
22. Zhang R, Ma M, Lin XH, Liu HH, Chen J, Chen J, et al. Extracellular matrix collagen I promotes the tumor progression of residual hepatocellular carcinoma after heat treatment. *BMC Cancer.* (2018) 18:901. doi: 10.1186/s12885-018-4820-9
23. Liu M, Lin MX, Lu MD, Xu ZF, Zheng KG, Wang W, et al. Comparison of contrast-enhanced ultrasound and contrast-enhanced computed tomography in evaluating the treatment response to transcatheter arterial chemoembolization of hepatocellular carcinoma using modified RECIST. *Eur Radiol.* (2015) 25:2502–11. doi: 10.1007/s00330-015-3611-9
24. Zhong J, Su Z, Zhang Y, Zhang H. Contrast-enhanced ultrasonography versus contrast-enhanced computed tomography for assessment of residual tumor from hepatocellular carcinoma treated with transarterial chemoembolization: a meta-analysis. *J Ultrasound Med.* (2018) 37:1881–90. doi: 10.1002/jum.14534
25. Zhou G, Cai ZQ, Luo J, Hu ZX, Luo H, Wu H, et al. Prognostic value of enhancement rate by enhanced ultrasound in hepatitis B virus-positive hepatocellular carcinoma undergoing radiofrequency ablation. *Asia Pac J Clin Oncol.* (2019) 15:238–43. doi: 10.1111/ajco.13157
26. Gao Y, Zheng DY, Cui Z, Ma Y, Liu YZ, Zhang W. Predictive value of quantitative contrast-enhanced ultrasound in hepatocellular carcinoma recurrence after ablation. *World J Gastroenterol.* (2015) 21:10418–26. doi: 10.3748/wjg.v21.i36.10418
27. Leoni S, Piscaglia F, Granito A, Borghi A, Galassi M, Marinelli S, et al. Characterization of primary and recurrent nodules in liver cirrhosis using contrast-enhanced ultrasound: which vascular criteria should be adopted? *Ultraschall Med.* (2013) 34:280–7. doi: 10.1055/s-0033-1335024
28. Egger C, Goertz RS, Strobel D, Lell M, Neurath MF, Knieling F, et al. Dynamic contrast-enhanced ultrasound (DCE-US) for easy and rapid evaluation of hepatocellular carcinoma compared to dynamic contrast-enhanced computed tomography (DCE-CT)–a pilot study. *Ultraschall Med.* (2012) 33:587–92. doi: 10.1055/s-0032-1325545
29. Goetti R, Reiner CS, Knuth A, Klotz E, Stenner F, Samaras P, et al. Quantitative perfusion analysis of malignant liver tumors: dynamic computed tomography and contrast-enhanced ultrasound. *Invest Radiol.* (2012) 47:18–24. doi: 10.1097/RLI.0b013e318229ff0d
30. Bae JS, Lee JM, Jeon SK, Jang S. Comparison of microflow imaging with color and power Doppler imaging for detecting and characterizing blood flow signals in hepatocellular carcinoma. *Ultrasonography.* (2020) 39:85–93. doi: 10.14366/usg.19033
31. Kang HJ, Lee JM, Jeon SK, Ryu H, Han JK. Microvascular flow imaging of residual or recurrent hepatocellular carcinoma after transarterial chemoembolization: comparison with color/power doppler imaging. *Kor J Radiol.* (2019) 20:1114–23. doi: 10.3348/kjr.2018.0932
32. Tan L, Chen S, Wei G, Li Y, Liao J, Jin H, et al. Sublethal heat treatment of hepatocellular carcinoma promotes intrahepatic metastasis and stemness in a VEGFR1-dependent manner. *Cancer Lett.* (2019) 460:29–40. doi: 10.1016/j.canlet.2019.05.041
33. Kitao A, Zen Y, Matsui O, Gabata T, Nakanuma Y. Hepatocarcinogenesis: multistep changes of drainage vessels at CT during arterial portography and hepatic arteriography–radiologic-pathologic correlation. *Radiology.* (2009) 252:605–14. doi: 10.1148/radiol.2522081414

Conflict of Interest: The authors declare that the research was conducted in the absence of any commercial or financial relationships that could be construed as a potential conflict of interest.

frontiers in Oncology

ORIGINAL RESEARCH
published: 04 September 2020
doi: 10.3389/fonc.2020.01408

Risk Factor Analysis of Acute Kidney Injury After Microwave Ablation of Hepatocellular Carcinoma: A Retrospective Study

Yongfeng Yang[1†], Fangyi Liu[1†], Jie Yu[1], Zhigang Cheng[1], Zhiyu Han[1], Jianping Dou[1], Jie Hu[1], Ze Wang[2], Haigang Gao[3], Qiao Yang[4], Jing Tian[5], Yongjie Xu[6], Xiaoli Bai[7], Liping Lu[8] and Ping Liang[1]*

[1] Department of Interventional Ultrasound, Chinese PLA General Hospital, Beijing, China, [2] Special Clinic Department, The 985th Hospital of Chinese People's Liberation Army Joint Logistic Support Force, Taiyuan, China, [3] Ultrasonic Diagnosis Department, The 991st Hospital of Chinese People's Liberation Army Joint Logistic Support Force, Xiangyang, China, [4] Ultrasound Department, Zunhua People's Hospital, Zunhua, China, [5] Tianjin Institute of Urology, The Second Hospital of Tianjin Medical University, Tianjin, China, [6] Department of Diagnostic Ultrasound, PLA Strategic Support Force Characteristic Medical Center, Beijing, China, [7] Ultrasound Department, Hohhot Mongolian Hospital of Traditional Chinese Medicine, Hohhot, China, [8] Department of Ultrasonography, Nanhai Hospital of Southern Medical University, Foshan, China

OPEN ACCESS

Edited by:
Fu Wang,
Xidian University, China

Reviewed by:
Xiang Jing,
Tianjin Third Central Hospital, China
Chao An,
Sun Yat-sen University Cancer Center (SYSUCC), China

***Correspondence:**
Ping Liang
liangping301@126.com

[†] These authors have contributed equally to this work

Specialty section:
This article was submitted to Cancer Imaging and Image-directed Interventions, a section of the journal Frontiers in Oncology

Received: *05 March 2020*
Accepted: *03 July 2020*
Published: *04 September 2020*

Citation:
Yang Y, Liu F, Yu J, Cheng Z, Han Z, Dou J, Hu J, Wang Z, Gao H, Yang Q, Tian J, Xu Y, Bai X, Lu L and Liang P (2020) Risk Factor Analysis of Acute Kidney Injury After Microwave Ablation of Hepatocellular Carcinoma: A Retrospective Study. Front. Oncol. 10:1408. doi: 10.3389/fonc.2020.01408

Objectives: Acute kidney injury (AKI) is a recently observed side effect in patients after microwave ablation (MWA) of hepatocellular carcinoma (HCC) and is associated with negative outcomes. The aim of this study is to explore the risk factors of affecting the occurrence of AKI (stages 1b, 2, and 3), because they have a higher mortality rate than patients with AKI (stage 1a) and without AKI.

Materials and methods: In this retrospective study, a total of 1,214 patients with HCC who were treated with MWA under ultrasound (US) guidance in our department between January 2005 and November 2017 were enrolled. We evaluated the influence of 20 risk factors. Univariate and multivariate analysis were used for statistical analysis. The possible risk factors of AKI after MWA for HCC were summarized.

Results: AKI, AKI (stage 1a), and AKI (stages 1b, 2, and 3) after MWA were found in 34, 15, and 19 patients (2.80, 1.24, and 1.57%), respectively. Among 34 patients with AKI, 10 cases with AKI (stage 1a) and 6 cases with AKI (stages 1b, 2, and 3) recovered before their discharge without any treatment for AKI and 9 cases with AKI (stages 1b, 2, and 3) with further treatment. Four cases who had chronic renal failure before MWA of liver accepted renal dialysis. By univariate analysis, the number of antenna insertions ($P = 0.027$, OR = 3.3), MWA time ≥20 min ($P = 0.029$, OR = 4.3), creatinine (Cr)-pre above the upper limit of the reference value ($P < 0.001$, OR = 35.5), albumin (Alb)-pre ($P = 0.030$, OR = 0.9), and red blood cell (RBC)-pre ($P < 0.001$, OR = 0.3) were significant risk factors. By multivariate analysis, Cr-pre ≥ 110 μmol/L ($P < 0.001$, OR = 31.4) and MWA time ≥20 min ($P = 0.043$ OR = 9.9) were the independent risk factors.

Conclusion: AKI (stages 1b, 2, and 3) is a relatively serious complication after MWA for HCC, which is related to MWA time and Cr-pre. It requires attention by clinicians. So it is of great necessity to assess the Cr-pre level and reduce the MWA time to <20 min to minimize the risk of AKI after MWA for HCC.

Keywords: acute kidney injury, microwave ablation, hepatocellular carcinoma, complication, risk factor analysis

INTRODUCTION

Microwave ablation (MWA) is an important therapy for the focal HCC with single or up to three nodules (<3 cm), which is recommended by the 2018 Barcelona Clinic Liver Cancer (BCLC) system (1). As a minimally invasive therapy, MWA is safe with a low incidence of major complications, which was 0–2.7% (2–4), including 1.7% pleural effusion requiring thoracentesis, 1.4% tumor seeding, 0.4% liver abscess and empyema, 0.1% hemorrhage requiring arterial embolization, and 0.1% bile duct injury (5). Acute kidney injury (AKI) after MWA of HCC has been a recently observed complication, which is diagnosed by the following criteria—Stage 1: Creatinine ≥1.5 times baseline or increase of ≥0.3 mg/dl within any 48-h period (1a: Creatinine < 1.5 mg/dl, 1b: Creatinine ≥ 1.5 mg/dl); Stage 2: Creatinine ≥ 2.0 times baseline; Stage 3: Creatinine ≥ 3.0 times baseline or increase to ≥4.0 mg/dl or acute dialysis (6–9). Ding et al. reported that the accidence of AKI is 23.6% for the large liver tumor (>5 cm) after MWA (10). Most importantly, the patients with AKI and creatinine >1.5 mg/dl (stages 1b, 2, and 3) present a worse clinical outcome. They had a higher mortality rate than patients with AKI stage 1a (Cr < 1.5 mg/dl) and without AKI. This fact reinforces that small elevations in the value of creatinine, especially when they exceed 1.5 mg/dl, have a great impact on the morbidity and mortality of patients with cirrhosis (6, 11). Furthermore, despite most of them having recovered, a few cases after RFA of metastasis liver cancer developed the renal failure, requiring intensive care unit admission and a prolonged hospital stay (12). Ong et al. summarized that the accidence of renal failure after MWA of liver tumors was 1.7% (13). Although there are reports in the existing literature regarding AKI after MWA of liver tumors including HCC, metastasis, and hemangioma, there are seldom exclusive reports on AKI for HCC in particular. Therefore, we determined the risk factors of AKI after MWA of HCC to prevent the occurrence of severe complications.

Patients

The clinical data of 1,214 adult patients admitted for HCC with histopathological diagnosis and treated with ultrasound-guided percutaneous MWA from January 2005 to November 2017 were reviewed in this study.

Evaluation Methods

Blood tests including routine, biochemistry, and coagulation function tests were conducted before and after MWA. In 1,214 patients, hepatic and renal functions were tested on the first day after MWA. Data of the MWA maximum diameter, the MWA parameter, and all blood test results of patients in this study were obtained from our departmental database. MWA energy was calculated by the equation E = P * T, where P and T were ablation power and time, respectively. The MWA zone was spherical in shape. The maximum diameter in the three dimensions of the tumor was measured using ultrasound. The comorbidity score was the pre-operation assessment of other diseases except for HCC such as diabetes, cardiovascular diseases, or AIDS using the Charlson comorbidity index (CCI) that included 19 diseases as well as the age of the patient (14). According to the anatomical segment of the liver, the location of the tumor was separated into four sections including the left lateral lobe, the left inner lobe (including the caudate lobe), the right anterior segment, and the right posterior segment. Because there were just nine patients whose tumor located in the caudate lobe, we attributed the caudate lobe into the left inner lobe to narrow deviation. The number of antenna insertions was defined as the total number of antenna placements in each patient during ablation.

MWA Equipment and Technology

The MWA unit used was a 100 W two-cooled-shaft system (KY-2000, Kangyou Medical, Nanjing, China) with frequencies of 2,450 and 915 MHz. The antennae (KY-2450-T11b, KY-2450B-T3, 89 KY-2450B-T7 and KY-2450B-QT) were percutaneously inserted into the tumor and placed at a designated location under ultrasound guidance. When the distance of tumor to the important structure such as the main bile, gallbladder, and bowel was <5 mm, the thermocouple needles can be inserted at the margin of those structure to monitor temperature in real time. To reduce the risk of the bleeding and the seeding of tumor, the MW emission was continued until the antennae were withdrawn to below the skin entrance site after the MWA of the tumor (4).

Statistical Analysis

Data analysis was performed using EmpowerStats (Version 3.4.3) for Windows, and the continuous data were expressed as β (95%CI) *P*-value/OR (95%CI) *P*-value. All of the analyses were performed with statistical software package R (http://R-project.org, The R-foundation) and EmpowerStats (http://empowerstats.com, X&Y Solutions. Inc., Boston, MA). Data of two groups were analyzed between the group A (no AKI and AKI 1a) and group B (AKI stage 1b,2,3) by using the Student *t* test for unpaired data and Fisher exact test as appropriate. Twenty related risk factors, including gender, age, comorbidity scores, biochemical parameters, and blood routine before treatment like alanine transaminase (ALT)-pre, glutamic oxaloacetic transaminase (AST)-pre, ALB-pre, STB-pre, Cr-pre, Hb-pre, platelet (PLT)-pre, white blood cell (WBC)-pre, lymphocyte (LY)-pre, red blood cell (RBC)-pre, the location of

TABLE 1 | Baseline characteristic of acute kidney injury (AKI) (stages 1b, 2, and 3).

Variation	Total	No AKI and AKI 1A	AKI 1B,2, and 3	*P*-value
Patients no.	1,214	1,195	19	
Age(year)	58.4 ± 10.8	58.4 ± 10.8	56.8 ± 11.4	0.535
Gender				0.798
Female	228 (18.8%)	224 (18.7%)	4 (21.1%)	
Male	986 (81.2%)	971 (81.3%)	15 (78.9%)	
ALT-pre(U/L)	32.7 ± 24.5	32.7 ± 24.4	32.8 ± 29.6	0.977
AST-pre(U/L)	33.7 ± 25.6	33.7 ± 25.8	31.1 ± 14.4	0.67
ALB-pre(g/L)	39.5 ± 5.0	39.5 ± 5.0	37.1 ± 5.6	**0.036**
STB-pre(mol/L)	16.8 ± 9.4	16.8 ± 9.4	13.9 ± 7.3	0.176
Cr-pre(μmol/L)	77.1 ± 58.0	74.1 ± 37.1	261.5 ± 314.2	**<0.001**
				<0.001
<110	1,182 (97.4%)	1,171 (98.0%)	11 (57.9%)	
≧110	32 (2.6%)	24 (2.0%)	8 (42.1%)	
HB-pre(g/L)	135.1 ± 18.7	135.4 ± 18.4	118.2 ± 23.9	**<0.001**
PLT-pre(10^9/L)	119.6 ± 59.3	119.6 ± 59.5	120.1 ± 48.6	0.973
LY-pre(10^9/L)	0.4 ± 2.2	0.4 ± 2.2	0.3 ± 0.1	0.829
WBC-pre(10^9/L)	4.7 ± 4.7	4.7 ± 4.8	4.6 ± 2.0	0.925
NE-pre(10^9/L)	0.6 ± 0.1	0.6 ± 0.1	0.6 ± 0.1	0.096
RBC-pre(10^{13}/L)	4.3 ± 0.6	4.3 ± 0.6	3.8 ± 0.9	**<0.001**
MWA time(s)	723.2 ± 457.4	721.6 ± 457.9	825.8 ± 423.1	0.325
				0.164
<600	568 (46.8%)	563 (47.1%)	5 (26.3%)	
≧600, <900	322 (26.5%)	315 (26.4%)	7 (36.8%)	
≧900, <1,200	163 (13.4%)	161 (13.5%)	2 (10.5%)	
≧1,200	161 (13.3%)	156 (13.1%)	5 (26.3%)	
Comorbidity scores				0.597
0	172 (14.2%)	169 (14.2%)	3 (16.7%)	
1	245 (20.2%)	243 (20.4%)	2 (11.1%)	
2	276 (22.8%)	273 (22.9%)	3 (16.7%)	
3	224 (18.5%)	221 (18.5%)	3 (16.7%)	
≧4	294 (24.3%)	287 (24.1%)	7 (38.9%)	
The location of tumor				0.476
The left lateral lobe	147 (12.1%)	145 (12.1%)	2 (10.5%)	
Left inner lobe(including caudate lobe)	158 (13.0%)	157 (13.1%)	1 (5.3%)	
Right anterior segment	445 (36.7%)	435 (36.4%)	10 (52.6%)	
Right posterior segment	464 (38.2%)	458 (38.3%)	6 (31.6%)	
Maximum diameter of tumor (cm)	3.0 ± 1.5	3.0 ± 1.5	3.5 ± 1.9	0.100
				0.497
≦3	776 (63.9%)	766 (64.1%)	10 (52.6%)	
>3, ≦5	324 (26.7%)	318 (26.6%)	6 (31.6%)	
>5	114 (9.4%)	111 (9.3%)	3 (15.8%)	
Tumor no.				0.994
Solitary	829 (68.3%)	816 (68.3%)	13 (68.4%)	
Multiple	384 (31.7%)	378 (31.7%)	6 (31.6%)	
MWA energy(J)	38,473.7 ± 26,042.4	38,373.5 ± 26,052.7	44,763.2 ± 25,258.4	0.289
The number of electrodes				0.354
1	274 (22.6%)	272 (22.8%)	2 (10.5%)	
2	840 (69.2%)	824 (69.0%)	16 (84.2%)	
≧3	100 (8.2%)	99 (8.3%)	1 (5.3%)	
The number of antenna insertions				0.078
1–2	634 (52.2%)	628 (52.6%)	6 (31.6%)	
3–4	359 (29.6%)	349 (29.2%)	10 (52.6%)	
≧5	221 (18.2%)	218 (18.2%)	3 (15.8%)	

Results in table, Mean + SD/N (%). the Cr-pre, 1 mg/dl = 88.4 μmol/L.
Bold values represent P < 0.05.

TABLE 2 | Baseline and univariate analysis of maximum diameter for patients with solitary tumor.

Variation	Total	No AKI and AKI 1A	AKI(stages 1B, 2, and 3)	*P*-value	OR (95%CI) *P*-value
Tumor No.	829	816	13		
Maximum diameter of tumor (cm)	3.0 ± 1.6	3.0 ± 1.5	3. ± 2.1	0.047	
				0.114	
≦3	529 (63.8%)	524 (64.2%)	5 (38.5%)		1
>3, ≦5	217 (26.2%)	212 (26.0%)	5 (38.5%)		2.5 (0.7, 8.6) 0.156
>5	83 (10.0%)	80 (9.8%)	3 (23.1%)		3.9 (0.9, 16.8) 0.064

tumor, the maximum diameter of tumor, MWA energy, MWA time, and the number of antenna insertions, were analyzed using the univariate and multivariate logistic regression model method.

RESULTS

Basic Analysis

Among all 1,214 patients after MWA of HCC, 19 patients had AKI (stages 1b, 2, and 3), and the accidence was 1.57%. The biochemical parameters and blood routine before treatment of all patients, tumor characteristic, and MWA parameters were described. The mean maximum diameter of tumor for 829 patients with solitary tumor with AKI vs. without AKI was 3.0 vs. 3.8 cm, respectively. The mean ALT, AST, and STB for the 19 patients were 32.8 U/L, 31.1 U/L, and 13.9 μmol/L, respectively. The mean ALT, AST, and STB for 1,195 patients without AKI were 32.7 U/L, 33.7 U/L, and 16.8 μmol/L. Most *P*-values were >0.05 except Hb-pre, RBC-pre, and Alb-pre. There were no significant differences between the groups. The basic characteristic is shown in **Table 1**.

Risk Factors of AKI

By univariate analysis, the number of antenna insertions ($P = 0.027$, OR = 3.3), MWA time ≥ 20 min ($P = 0.029$, OR = 4.3), Cr-pre above the upper limit of the reference value ($P < 0.001$, OR = 35.5), Alb-pre ($P = 0.030$, OR = 0.9), and RBC-pre ($P < 0.001$, OR = 0.3) were significant risk factors. The maximum diameter of tumor for patients with solitary tumor was analyzed by univariate analysis separately (**Table 2**). While by univariate and multivariate analysis, Cr-pre ≥ 110 μmol/L ($P < 0.001$, OR = 31.4) and MWA time ≥20 min ($P = 0.043$ OR = 9.9) were the independent risk factors associated with AKI (stages 1b, 2, and 3) (**Tables 3**, **4**).

DISCUSSION

AKI (stage 1a) is a transient and controlled complication for most patients after MWA of HCC, but AKI (stages 1b, 2, and 3) needs further treatment. According to our research, among 34 patients with AKI after MWA, 10 cases with AKI (stage 1a) and 6 cases with AKI (stages 1b, 2, and 3) recovered before their discharge without any treatment for AKI whose mean post-operation Cr level was 123.2 μmol/L. Five cases with AKI (stage 1a) and nine cases with AKI (stages 1b, 2, and 3) recovered after further treatment of renal conservation: (1) the diuretic-furosemide or/and spironolactone and (2) sodium bicarbonate injection. Their mean post-operation Cr was 169.8 μmol/L. Then, four cases accepted the renal dialysis who had the chronic renal failure before MWA of liver whose mean post-operation Cr level was 947.4 μmol/L. Hence, most cases of AKI after MWA for HCC had a good recovery unless with chronic kidney disease (CKD), but the hospital stay was prolonged (10). What is worse, the patients with AKI (stages 1b, 2, and 3) had a higher mortality rate than patients with AKI stage 1a (Cr < 1.5 mg/dl) and without AKI. Lins et al. reported that the mortalities of the cirrhotic patient group with (A) no AKI, (B) AKI (stage 1a), (C) AKI (stage 1b), and (D) AKI (stages 2 and 3) were 11.8, 12.5, 33.3, and 52.4%, respectively (6). Fagundes et al. presented that the survival rates of groups B, C, and D were 84, 68, and 36%, respectively ($p < 0.001$) (11). Furthermore, Rodriguez et al. reported that three patients after radiofrequency ablation (RFA) of metastasis liver cancer developed renal failure, requiring intensive care unit admission and a prolonged hospital stay (12), even though there was no report about acute renal failure after MWA of HCC without preexisting CKD. It is still of great necessity to pay much attention to the risk factor of AKI (stages 1b, 2, and 3) after MWA to prevent the severe complication happening and improve the survival.

This study shows that the statistically significant risk factors for AKI (stages 1b, 2, and 3) after MWA for HCC were 3 ≤ the number of antenna insertions ≤ 4 ($P = 0.027$, OR = 3.3) RBC-pre ($P < 0.001$, OR = 0.3). For the patients with multiple tumors, Hb-pre ($P < 0.001$, OR = 0.9) were also significant risk factors. MWA time ≥ 20 min ($P = 0.029$, OR = 4.3) was the independent risk factor by multivariate analysis. As we know, the thermal effect of ablation can lead to the destruction of RBC and the release of Hb to the circulation system. When the quantity of cell-free Hb exceeds the liver detoxification threshold, some Hb will cross the glomerular filtration membrane, reach the renal tubules, and cause renal tubular necrosis that ultimately leads to AKI (15–18). The ablation of large tumors took longer time and more antenna insertions, and more Hb was released into the circulation system. Therefore, patients who had a high HB-pre level and RBC-pre and took longer time were more prone to having AKI than those who have a small tumor. Hence, the number of antenna insertions should be reduced for treating large and multiple tumors. It is recommended that the MWA time is controlled within 20 min.

TABLE 3 | Univariate analysis for acute kidney injury (AKI) (stages 1b, 2, and 3) for risk factors.

Exposure	Solitary	Total
Gender	1	1
Female		
Male	0.9 (0.2, 3.2) 0.817	0.9 (0.3, 2.6) 0.800
Age(year)	1.0 (0.9, 1.0) 0.507	1.0 (0.9, 1.0) 0.531
Comorbidity scores		
0	1	1
1	0.5 (0.1, 2.9) 0.418	0.5 (0.1, 2.8) 0.401
2	0.2 (0.0, 2.0) 0.177	0.6 (0.1, 3.1) 0.558
3	0.5 (0.1, 3.2) 0.481	0.8 (0.2, 3.8) 0.742
≧4	0.8 (0.2, 3.5) 0.725	1.4 (0.4, 5.4) 0.647
The location of tumor		
The left lateral lobe	1	1
Left inner lobe(including caudate lobe)	1.0 (0.1, 16.5) 0.989	0.5 (0.0, 5.1) 0.528
Right anterior segment	2.3 (0.3, 18.9) 0.438	1.7 (0.4, 7.7) 0.510
Right posterior segment	1.4 (0.2, 12.8) 0.757	0.9 (0.2, 4.7) 0.946
Maximum diameter of tumor (cm)		
≦3	1	1
>3, ≦5	2.5 (0.7, 8.6) 0.156	1.4 (0.5, 4.0) 0.476
>5	3.9 (0.9, 16.8) 0.064	2.1 (0.6, 7.6) 0.275
ALT-pre(U/L)	1.0 (1.0, 1.0) 0.715	1.0 (1.0, 1.0) 0.982
AST-pre(U/L)	1.0 (1.0, 1.0) 0.873	1.0 (1.0, 1.0) 0.660
ALB-pre(g/L)	0.9 (0.8, 1.0) 0.083	**0.9 (0.8, 1.0) 0.030**
STB-pre(mol/L)	1.0 (0.9, 1.1) 0.776	1.0 (0.9, 1.0) 0.171
Cr-pre(μmol/L)	1.0 (1.0, 1.0) < 0.001	1.0 (1.0, 1.0) < 0.001
<110	1	1
≧110	**19.7 (5.5, 70.0) < 0.001**	**35.5 (13.1, 96.0) < 0.001**
HB-pre(g/L)	1.0 (0.9, 1.0) 0.027	1.0 (0.9, 1.0) < 0.001
PLT-pre(10^9/L)	1.0 (1.0, 1.0) 0.993	1.0 (1.0, 1.0) 0.965
LY-pre(10^9/L)	0.1 (0.0, 35.9) 0.428	0.0 (0.0, 0.6) 0.029
WBC-pre(10^9/L)	0.9 (0.6, 1.3) 0.674	1.0 (0.9, 1.1) 0.929
NE-pre(10^9/L)	1.4 (0.0, 286.8) 0.912	41.4 (0.5, 3,189.7) 0.093
RBC-pre(10^{13}/L)	0.4 (0.2, 1.1) 0.069	**0.3 (0.1, 0.6) < 0.001**
The number of electrodes		
1	1	1
2	1.5 (0.3, 7.0) 0.594	2.6 (0.6, 11.6) 0.197
≧3	0.9 (0.1, 9.5) 0.897	1.4 (0.1, 15.6) 0.803
MWA time(s)		
<600	1	1
≧600, <900	1.2 (0.2, 6.4) 0.806	2.9 (0.9, 9.6) 0.082
≧900, <1,200	2.4 (0.5, 12.8) 0.290	1.6 (0.3, 8.7) 0.574
≧1,200	5.7 (1.5, 21.8) 0.011	**4.3 (1.2, 15.8) 0.029**
The number of antenna insertions		
1–2	1	1
3–4	**4.1 (1.3, 13.0) 0.018**	**3.3 (1.1, 9.6) 0.027**
≧5	1.5 (0.2, 12.9) 0.717	1.7 (0.4, 7.6) 0.478
MWA energy(J)	1.0 (1.0, 1.0) 0.047	1.0 (1.0, 1.0) 0.266

Results in table, β (95%CI) P value/OR (95%CI) P value. Bold values represent P < 0.05.

TABLE 4 | Multivariate analysis of acute kidney injury (AKI) (stages 1b, 2, and 3) for risk factors.

Exposure	Solitary	Total
ALB-pre(g/L)	0.9 (0.8, 1.0) 0.081	0.9 (0.8, 1.0) 0.091
STB-pre(mol/L)	1.0 (0.9, 1.0) 0.436	1.0 (0.9, 1.0) 0.186
Cr-pre(μmol/L)		
<110	1	1
≧110	41.0 (6.9, 243.4) < 0.001	**31.4 (8.2, 120.2) < 0.001**
HB-pre(g/L)	1.0 (0.9, 1.0) 0.245	1.0 (0.9, 1.0) 0.600
NE-pre(10^9/L)	0.1 (0.0, 40.8) 0.435	10.5 (0.1, 1,712.3) 0.366
RBC-pre(10^{13}/L)	3.5 (0.6, 19.4) 0.150	1.3 (0.3, 5.8) 0.713
MWA time(s)		
<600	1	1
≧600, <900	0.6 (0.0, 7.3) 0.656	1.7 (0.3, 10.2) 0.564
≧900, <1,200	1.0 (0.1, 16.4) 0.990	0.9 (0.1, 10.2) 0.924
≧1,200	11.5 (0.7, 180.5) 0.081	**9.9 (1.1, 91.3) 0.043**
The number of antenna insertions		
1–2	1	1
3–4	4.2 (0.4, 45.7) 0.233	3.0 (0.5, 16.9) 0.222
≧5	0.3 (0.0, 8.6) 0.508	0.4 (0.0, 4.2) 0.406
Maximum diameter of tumor (cm)		
≦3	1	1
>3, ≤5	1.7 (0.4, 8.4) 0.503	1.4 (0.4, 4.8) 0.636
>5	1.7 (0.2, 14.1) 0.636	0.9 (0.2, 4.8) 0.857

Results in table, β (95%CI) P value/OR (95%CI) P value. Bold values represent P < 0.05.

Additionally, another independent risk factor was Cr-pre above the upper limit of the reference value ($P < 0.001$, OR = 31.4). In our analysis, there were six patients with AKI after MWA for HCC with CKD, and the preoperative Cr in these patients were higher than the upper level of the reference range (110 μmol/l). Multivariate analysis showed that Cr-pre > 110 μmol/L was an independent risk factor. The present literature showed that the mortality of people who had CKD with AKI was higher than those without AKI (19, 20), especially for critically ill patients with CKD (21). Therefore, when Cr-pre is above the upper limit of the reference value, the clinician should assess the patient's magnitude of benefit from MWA and then decide whether to do it. It was noted that the Alb-pre ($P = 0.030$, OR = 0.9) was also a significant risk factor. It was revealed that the infection before MWA could make it easier to AKI for patients. Then, the low levels of STB-pre and Alb-pre were also significant risk factors. The mechanism was still unclear.

Therefore, to avoid complications of AKI (stages 1b, 2, and 3), the independent risk factors reported in this study should be emphasized in the preoperative evaluation. Clinicians should pay attention to the Cr-pre and the need for long MWA time. Appropriate measures should be taken including preoperative evaluation of renal function, intraoperative and postoperative administration of fluid, appropriate timing of diuresis, and urine alkalization (10, 17, 22). Furthermore, patient survival should actively involve not only the preservation of their kidney health but also postdischarge follow-up of kidney function because severe AKI predisposes patients to faster progression of CKD

later on—especially when they had multiple hits of AKI or preexisted CKD (23).

The innovation of the study is that the risk factor of the maximum diameter of tumor in patients with single nodule was analyzed separately, and the interference of cases with multiple tumors on this factor was excluded. It is because the maximum diameter is just referred to the largest one among multiple tumors for them. That cannot reflect the relation of the size of tumor to the AKI accurately.

There are three limitations of this research. First, this is a retrospective study. To provide further evidence for the conclusion, prospective studies are still needed. Then, the clinical data were just collected from a single institution. Finally, we designed this study to assess the Cr only on the first day after MWA in the hospital; we did not evaluate the occurrence of late AKI. So the occurrence incidence of the AKI after MWA of HCC we obtained may be lower than the true value.

DATA AVAILABILITY STATEMENT

All datasets generated for this study are included in the article/supplementary material.

ETHICS STATEMENT

The studies involving human participants were reviewed and approved by Ethics Committee of PLA General Hospital. The patients/participants provided their written informed consent to participate in this study.

AUTHOR CONTRIBUTIONS

YY, FL, and PL made substantial contributions to the research design, analysis, and interpretation of data. FL contributed a lot to the data analysis and appropriate method to the research. ZC and ZH took part in the building of the clinical database. JY provided the instruction for statistical analysis by EmpowerStats (Version 2019-11-18). JD, JH, ZW, HG, QY, JT, YX, XB, and LL performed the clinical collection. YY and FL drafted the manuscript. All authors contributed to the article and approved the submitted version.

FUNDING

This work was supported by Grants 81627803, 81971625, 91859201, and 81871374 from the National Scientific Foundation Committee of China, Grant JQ18021 from the National Scientific Foundation Committee of Beijing, Fostering Funds for National Distinguished Young Scholar Science Fund, and the National Clinical Research Center for Geriatric Diseases (NCRCG-PLAGH-2019011) of Chinese PLA General Hospital, and Grant 2018ZX10723-204 from the National Key R&D Program of Ministry of Science and Technology of China.

ACKNOWLEDGMENTS

This work was supported by NHC Key Laboratory of Echinococcosis Prevention and Control (Xizang Center for Disease Control and Prevention).

REFERENCES

1. Ayuso C, Rimola J, Vilana R, Burrel M, Darnell A, García-Criado Á, et al. Diagnosis and staging of hepatocellular carcinoma (Hcc): current guidelines. *Eur J Radiol.* (2018) 101:72–81. doi: 10.1016/j.ejrad.2018.01.025
2. Ding J, Jing X, Liu J, Wang Y, Wang F, Wang Y, et al. Comparison of two different thermal techniques for the treatment of hepatocellular carcinoma. *Eur J Radiol.* (2013) 82:1379–84. doi: 10.1016/j.ejrad.2013.04.025
3. Francica G, Meloni MF, Riccardi L, de Sio I, Terracciano F, Caturelli E, et al. Ablation treatment of primary and secondary liver tumors under contrast-enhanced ultrasound guidance in field practice of interventional ultrasound centers. A multicenter study. *Eur J Radiol.* (2018) 105:96–101. doi: 10.1016/j.ejrad.2018.05.030
4. Liang P, Wang Y, Yu X, Dong B. Malignant liver tumors: treatment with percutaneous microwave ablation–complications among cohort of 1136 patients. *Radiology.* (2009) 251:933–40. doi: 10.1148/radiol.2513081740
5. Wang XH, Yu J, Liang P, Yu XL, Cheng ZG, Han ZY, et al. Percutaneous cooled-tip microwave ablation under ultrasound guidance for primary liver cancer: analysis of major complications in 693 patients. *Chin J Oncol.* (2012) 34:945–49. doi: 10.3760/cma.j.issn.0253-3766.2012.12.014
6. Lins PR, Padilha WS, Pimentel CF, Batista MC, de Gois AF. Risk factors, mortality and acute kidney injury outcomes in cirrhotic patients in the emergency department. *BMC Nephrol.* (2018) 19:277–77. doi: 10.1186/s12882-018-1061-8
7. Kellum JA, Lameire N, KDIGO AKI Guideline Work Group. Diagnosis, evaluation, and management of acute kidney injury: a Kdigo summary (part 1). *Crit Care.* (2013) 17:204. doi: 10.1186/cc11454
8. Mehta RL, Kellum JA, Shah SV, Molitoris BA, Ronco C, Warnock DG, et al. Acute kidney injury network: report of an initiative to improve outcomes in acute kidney injury. *Crit Care.* (2007) 11:R31. doi: 10.1186/cc5713
9. Piano S, Rosi S, Maresio G, Fasolato S, Cavallin M, Romano A, et al. Evaluation of the acute kidney injury network criteria in hospitalized patients with cirrhosis and ascites. *J Hepatol.* (2013) 59:482–89. doi: 10.1016/j.jhep.2013.03.039
10. Ding M, Ma S, Tang X, Wang T, Qi X, Chi J, et al. Oliguric acute kidney injury after microwave ablation of large liver tumors: incidence and preventive measures. *Int J Hyperthermia.* (2019) 35:141–9. doi: 10.1080/02656736.2018.1487589
11. Fagundes C, Barreto R, Guevara M, Garcia E, Solà E, Rodríguez E, et al. A modified acute kidney injury classification for diagnosis and risk stratification of impairment of kidney function in cirrhosis. *J Hepatol.* (2013) 59:474–81. doi: 10.1016/j.jhep.2013.04.036
12. Rodriguez J, Tellioglu G, Siperstein A, Berber E. Myoglobinuria after laparoscopic radiofrequency ablation of liver tumors. *J Gastrointest Surg.* (2010) 14:664–7. doi: 10.1007/s11605-009-1118-x
13. Ong SL, Gravante G, Metcalfe MS, Strickland AD, Dennison AR, Lloyd DM. Efficacy and safety of microwave ablation for primary and secondary liver malignancies: a systematic review. *Eur J Gastroenterol Hepatol.* (2009) 21:599–605. doi: 10.1097/MEG.0b013e328318ed04
14. Dias A, Teixeira-Lopes F, Miranda A, Alves M, Narciso M, Mieiro L, et al. Comorbidity burden assessment in older people admitted to a Portuguese University Hospital. *Aging Clin Exp Res.* (2015) 27:323–28. doi: 10.1007/s40520-014-0280-5
15. Billings IV FT, Ball SK, Roberts II LJ, Pretorius M. Postoperative acute kidney injury is associated with hemoglobinemia and an

enhanced oxidative stress response. *Free Radic Biol Med.* (2011) 50:1480–7. doi: 10.1016/j.freeradbiomed.2011.02.011
16. Deuel JW, Schaer CA, Boretti FS, Opitz L, García-Rubio I, Baek JH, et al. Hemoglobinuria-related acute kidney injury is driven by intrarenal oxidative reactions triggering a heme toxicity response. *Cell Death Dis.* (2016) 7:e2064. doi: 10.1038/cddis.2015.392
17. Qi K, Zhang XG, Liu SW, Yin Z, Chen XM, Wu D. Reversible acute kidney injury caused by paroxysmal nocturnal hemoglobinuria. *Am J Med Sci.* (2011) 341:68–70. doi: 10.1097/MAJ.0b013e3181f515b9
18. Verbeek DE, Waanders F, Mulder AB, Bierman WF, Croles FN. Quiz page may 2014: acute kidney injury with red urine. *Am J Kidney Dis.* (2014) 63:A21–4. doi: 10.1053/j.ajkd.2013.09.024
19. Chawla LS, Amdur RL, Amodeo S, Kimmel PL, Palant CE. The severity of acute kidney injury predicts progression to chronic kidney disease. *Kidney Int.* (2011) 79:1361–9. doi: 10.1038/ki.2011.42
20. Wang HE, Jain G, Glassock RJ, Warnock DG. Comparison of absolute serum creatinine changes versus kidney disease: improving global outcomes consensus definitions for characterizing stages of acute kidney injury. *Nephrol Dial Transpl.* (2013) 28:1447–54. doi: 10.1093/ndt/gfs533
21. Goldberg R, Dennen P. Long-term outcomes of acute kidney injury. *Adv Chronic Kidney Dis.* (2008) 15:297–307. doi: 10.1053/j.ackd.2008.04.009
22. Rewa O, Bagshaw SM. Acute kidney injury–epidemiology, outcomes and economics. *J Nat Rev Nephrol.* (2014) 10:193. doi: 10.1038/nrneph.2013.282
23. Vanmassenhove J, Kielstein J, Jörres A, Van Biesen W. Management of patients at risk of acute kidney injury. *Lancet.* (2017) 389:2139–51. doi: 10.1016/S0140-6736(17)31329-6

Conflict of Interest: The authors declare that the research was conducted in the absence of any commercial or financial relationships that could be construed as a potential conflict of interest.

The reviewer CA declared a past co-authorship with several of the authors ZH, JD, JY, PL, ZC, and FL to the handling Editor.

frontiers in Oncology

ORIGINAL RESEARCH
published: 14 September 2020
doi: 10.3389/fonc.2020.01764

Hepatocellular Carcinoma Within the Milan Criteria: A Novel Inflammation-Based Nomogram System to Assess the Outcomes of Ablation

Shuanggang Chen[1,2†], Weimei Ma[2,3†], Fei Cao[1,2†], Lujun Shen[1,2†], Han Qi[1,2], Lin Xie[1,2], Ying Wu[1,2] and Weijun Fan[1,2]*

[1] Department of Minimally Invasive Interventional Therapy, Sun Yat-sen University Cancer Center, Guangzhou, China, [2] State Key Laboratory of Oncology in South China, Collaborative Innovation Center of Cancer Medicine, Sun Yat-sen University, Guangzhou, China, [3] Department of Imaging Medicine, Sun Yat-sen University Cancer Center, Guangzhou, China

OPEN ACCESS

Edited by:
Jie Yu,
People's Liberation Army General Hospital, China

Reviewed by:
Yuming Jiang,
Stanford University, United States
Xin Ye,
Shandong University, China

***Correspondence:**
Weijun Fan
fanwj@sysucc.org.cn

[†] These authors have contributed equally to this work

Specialty section:
This article was submitted to Cancer Imaging and Image-directed Interventions, a section of the journal Frontiers in Oncology

Received: 23 March 2020
Accepted: 06 August 2020
Published: 14 September 2020

Citation:
Chen S, Ma W, Cao F, Shen L, Qi H, Xie L, Wu Y and Fan W (2020) Hepatocellular Carcinoma Within the Milan Criteria: A Novel Inflammation-Based Nomogram System to Assess the Outcomes of Ablation. Front. Oncol. 10:1764. doi: 10.3389/fonc.2020.01764

Objectives: Few studies based on pretreatment inflammation-based scores focused on assessing the prognosis of hepatocellular carcinoma (HCC) patients within the Milan Criteria after ablation. This study aimed to construct a nomogram based on a novel inflammation-based score for those patients.

Methods: A total of 635 HCC patients within the Milan Criteria after ablation meeting the inclusion and exclusion criteria were included in the study. The novel inflammation-based score—Albumin-Platelet Score (APS)—was constructed by Cox proportional-hazards modeling. The nomogram based on APS was constructed by multivariate analysis and the "rms" R package. The performance of the APS and the nomogram were assessed by time-dependent receiver operating characteristic and the concordance index (C-index).

Results: The APS was an integrated indicator based on peripheral albumin level and platelet counts, which was significantly superior to other inflammation-based scores (neutrophil to lymphocyte ratio, platelet to lymphocyte ratio, Prognostic Nutritional Index, modified Glasgow Prognostic Score, Glasgow Prognostic Score, Prognostic Index, and C-reactive protein/albumin ratio) in predicting the long-term prognosis of those patients undergoing ablation ($P < 0.05$). An easy-to-use nomogram based on three pretreatment clinical variables (i.e., the APS, tumor size, and age) was constructed and further improved significantly the performance in predicting the prognosis in patients within the Milan Criteria after ablation ($P < 0.05$). The C-index of nomogram for overall survival was 0.72 (95% CI 0.66, 0.77). The calibration plots with 1000 cycles of bootstrapping were well matched with the idealized 45° line.

Conclusion: The APS was a better inflammation-based prognostic system than others. Also, the nomogram based on the APS improved the performance of predicting the prognosis of HCC patients within the Milan Criteria after ablation.

KEY POINTS

- The Albumin-Platelet Score (APS) consisted of peripheral platelet counts and albumin level.
- The APS was superior to other inflammation-based scores in the performance of predicting the prognosis of hepatocellular carcinoma (HCC) patients within the Milan Criteria after ablation.
- The nomogram based on the APS improved the performance of predicting the prognosis of HCC patients within the Milan Criteria after ablation.

Keywords: hepatocellular carcinoma, nomogram, ablation techniques, inflammatory biomarkers, the Milan Criteria

INTRODUCTION

Hepatocellular carcinoma (HCC) accounts for 70–90% of liver cancer that was the fourth cancer-related death cause worldwide in 2018 (1). At present, the mainstream treatment of HCC within Milan Criteria (one lesion ≤5 cm or three lesions ≤3 cm without vascular invasion or extrahepatic metastasis) is still liver transplantation and surgical resection (2). However, with its advantages of minimal invasiveness and cost-effectiveness, local ablation treatment is recommended by the National Comprehensive Cancer Network as an optional first-line curative therapy for early HCC (3, 4).

Inflammation is considered as a hallmark of cancer, and more and more evidence has shown that inflammation is closely related to the progression, recurrence, and survival of patients with HCC (5, 6). Recently, different inflammation-based scores, such as the Glasgow Prognostic Score (GPS), modified Glasgow Prognostic Score (mGPS), Prognostic Index (PI), Prognostic Nutritional Index (PNI), neutrophil to lymphocyte ratio (NLR), platelet to lymphocyte ratio (PLR), and C-reactive protein/albumin ratio (CAR), have been proposed and been also thought to predict the prognosis of HCC, which mainly calculate quantitative values of plasma neutrophil count, total lymphocyte count, platelet count, albumin level and C-reactive protein (CRP) level, or the ratio or combination between the two indicators; however, those inflammation-based scores are not adequate to predict the overall survival (OS) of HCC patients (7–13). Besides, to our knowledge, the vast majority of studies on these pretreatment inflammation-based markers have not targeted patients with HCC within the Milan Criteria for ablation therapy. Therefore, we systematically analyzed the pre-treatment clinical characteristics and the inflammatory indicators included in these inflammation-based scores of patients with HCC within the Milan Criteria of ablation therapy and integrate a novel combination of inflammatory indicators—APS. Also, we hypothesized that the nomogram based on the APS could improve the performance of predicting the prognosis. To test this hypothesis, we constructed a simple and clinically applicable nomogram based on the APS to assess the prognosis of HCC patients within the Milan Criteria after curative ablation.

Abbreviations: AFP, alpha-fetoprotein; ALB, albumin; ALBI, albumin-bilirubin; ALT, alanine aminotransferase; APS, Albumin-Platelet Score; AST, aspartate transaminase; AUC, area under the curve; CAR, C-reactive protein/albumin ratio; C-index, Harrell's concordance index; CRP, C-reactive protein; GPS, Glasgow Prognostic Score; HBV, hepatitis B virus; HCC, hepatocellular carcinoma; mGPS, modified Glasgow Prognostic Score; MWA, microwave ablation; NLR, neutrophil to lymphocyte ratio; OS, overall survival; PI, Prognostic Index; PLR, platelet to lymphocyte ratio; PLT, platelet; PNI, Prognostic Nutritional Index; PT, prothrombin time; RFA, radiofrequency ablation; ROC, receiver operating characteristic; TACE, transarterial chemoembolization; TBIL, total bilirubin; WBC, white blood cell.

MATERIALS AND METHODS

We retrospectively analyzed the data of 694 HCC patients within the Milan Criteria at the Sun Yat-sen University Cancer Center (SYSUCC) between June 2004 and October 2019. The inclusion criteria included (1) patients with HCC diagnosis confirmed by radiologic imaging studies or histopathological examination, (2) HCC treated with initial radiofrequency ablation (RFA) or microwave ablation (MWA), and (3) HCC treated with curative ablation. The exclusion criteria were (1) severe coagulation disorders and renal dysfunction, (2) patients who receive cryoablation or percutaneous ethanol injection (PEI), (3) patients

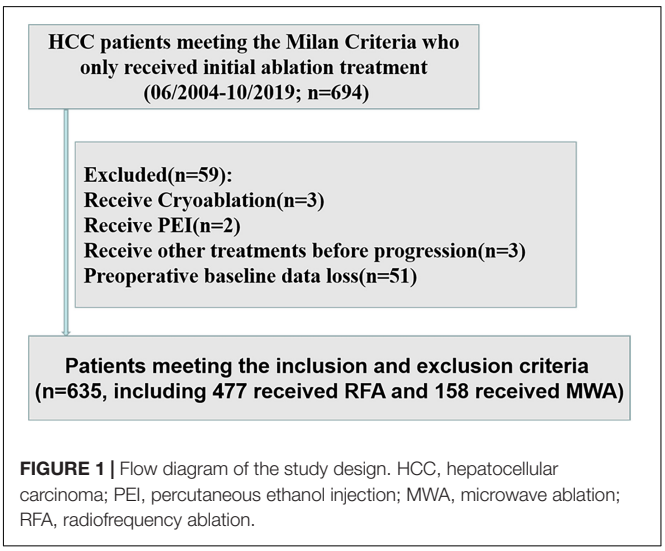

FIGURE 1 | Flow diagram of the study design. HCC, hepatocellular carcinoma; PEI, percutaneous ethanol injection; MWA, microwave ablation; RFA, radiofrequency ablation.

TABLE 1 | Systemic inflammation-based prognostic scores.

Scoring systems	Score
GPS	
CRP (≤10 mg/L) and albumin (≥35 g/L)	0
CRP (≤10 mg/L) and albumin (<35 g/L)	1
CRP (>10 mg/L) and albumin (≥35 g/L)	1
CRP (>10 mg/L) and albumin (<35 g/L)	2
mGPS	
CRP (≤10 mg/L)	0
CRP (>10 mg/L) and albumin (≥35 g/L)	1
CRP (>10 mg/L) and albumin (<35 g/L)	2
PI	
CRP (≤10 mg/L) and WBC (≤10 × 10^9/L)	0
CRP (≤10 mg/L) and WBC (>10 × 10^9/L)	1
CRP (>10 mg/L) and WBC (≤10 × 10^9/L)	1
CRP (>10 mg/L) and WBC (>10 × 10^9/L)	2
PNI	
Albumin (g/L) + 5 × total lymphocyte count (×10^9/L) ≥ 45	0
Albumin (g/L) + 5 × total lymphocyte count (×10^9/L) < 45	1
NLR	
Neutrophil count (×10^9/L): lymphocyte count (×10^9/L) < 3	0
Neutrophil count (×10^9/L): lymphocyte count (×10^9/L) ≥ 3	1
PLR	
Platelet count (× 10^9/L): lymphocyte count (×10^9/L) < 150	0
Platelet count (× 10^9/L): lymphocyte count (×10^9/L) ≥ 150	1
CAR	
CRP (mg/L): albumin (g/L) < 0.05	0
0.05 ≤ CRP (mg/L): albumin (g/L) < 0.1	1
CRP (mg/L): albumin (g/L) ≥ 0.1	2
APS	
Albumin > 37.7 g/L, PLT > 80 × 10^9/L	1
Albumin > 37.7 g/L, PLT ≤ 80 × 10^9/L	2
Albumin ≤ 37.7 g/L, PLT > 80 × 10^9/L	2
Albumin ≤ 37.7 g/L, PLT ≤ 80 × 10^9/L	3

WBC, white blood cell; PLT, platelet; CRP, C-reactive protein; GPS, Glasgow Prognostic Score; NLR, neutrophil to lymphocyte ratio; mGPS, modified Glasgow Prognostic Score; PI, Prognostic Index; PLR, platelet to lymphocyte ratio; PNI, Prognostic Nutritional Index; CAR, C-reactive protein/albumin ratio; APS, Albumin-Platelet Score.

TABLE 2 | Demographic and clinical characteristics of the enrolled patients.

Variables	*N* = 635 or median (*n*% or interquartile Q_1–Q_3)
Gender (male vs. female)	531 vs. 104 (83.6 vs. 16.4)
Age (years)	57.74 ± 12.35
ALB (g/L)	42.10 (39.00, 45.10)
Cirrhosis (absent vs. present)	282 vs. 353 (44.4 vs. 55.6)
HBV infection (absent vs. present)	62 vs. 573 (9.8 vs. 90.2)
TBIL (μmol/L)	14.30 (10.90, 20.20)
WBC (×10^9/L)	5.26 (4.18, 6.50)
Neutrophil count (×10^9/L)	2.80 (2.10, 3.75)
Lymphocyte count (×10^9/L)	1.60 (1.20, 2.06)
Monocyte count (×10^9/L)	0.40 (0.30, 0.50)
Prothrombin time (s)	12.20 (11.50, 13.10)
PLT (×10^9/L)	131.00 (87.00, 177.00)
CRP (mg/L)	1.25 (0.66, 2.59)
ALT (U/L)	32.00 (22.10, 47.90)
AST (U/L)	32.40 (25.00, 44.60)
AFP (<37.15 ng/ml vs. ≥ 37.15 ng/ml)	328 vs. 307 (51.7 vs. 48.3)
Tumor size (<3.5 cm vs. ≥3.5 cm)	573 vs. 62 (90.2 vs. 9.8)
Tumor numbers (solitary vs. multiple)	577 vs. 58 (90.9 vs. 9.1)
Treatment (RFA vs. MWA)	477 vs. 158 (75.1 vs. 24.9)
ALBI grade (1 vs. 2 vs. 3)	438 vs. 194 vs. 3 (69.0 vs. 30.5 vs. 0.5)
GPS before treatment (0/1/2)	543 vs. 84 vs. 8 (85.5 vs. 13.2 vs. 1.3)
NLR before treatment (0/1)	530 vs. 105 (83.5 vs. 16.5)
mGPS before treatment (0/1/2)	601 vs. 26 vs. 8 (94.6 vs. 4.1 vs. 1.3)
PI before treatment (0/1/2)	596 vs. 31 vs. 8 (93.9 vs. 4.9 vs. 1.2)
PLR before treatment (0/1)	586 vs. 49 (92.3 vs. 7.7)
PNI before treatment (0/1)	502 vs. 133 (79.1 vs. 20.9)
CAR before treatment (0/1/2)	429 vs. 100 vs. 106 (67.6 vs. 15.7 vs. 16.7)

ALB, albumin; HBV, hepatitis B virus; TBIL, total bilirubin; WBC, white blood cell; PLT, platelet; CRP, C-reactive protein; ALT, alanine aminotransferase; AST, aspartate transaminase; ALBI, albumin-bilirubin; GPS, Glasgow Prognostic Score; NLR, neutrophil to lymphocyte ratio; mGPS, modified Glasgow Prognostic Score; PI, Prognostic Index; PLR, platelet to lymphocyte ratio; PNI, Prognostic Nutritional Index.

who receive other treatments for HCC except ablation before progression, and (4) patients with preoperative baseline data loss (**Figure 1**). After the application of these inclusion and exclusion criteria, a total of 635 HCC patients within the Milan Criteria were included in the study. The study was conducted in accordance with the Declaration of Helsinki and was approved by the SYSUCC Hospital Ethics Committee.

Baseline Data Collection and Inflammation-Based Prognostic Scores

We collected the baseline data of those patients before initial ablation, including patient characteristics, imaging, biochemistry, tumor markers, coagulation, and blood routine. Important clinical data included patient characteristics (gender, age, HBV infection, treatment), imaging (tumor size, tumor numbers, cirrhosis), biochemistry [albumin (ALB), CRP, total bilirubin (TBIL), alanine aminotransferase (ALT), aspartate transaminase (AST)], tumor markers (alpha-fetoprotein), and coagulation [prothrombin time (PT)] blood routine [white blood cell (WBC), neutrophil, lymphocyte, monocyte, platelet]. The albumin-bilirubin (ALBI) score was defined as −0.085 × (albumin g/L) + 0.66 × log (TBIL μmol/L) (14). The APS, mGPS, GPS, PNI, PI, PLR, NLR, and CAR were constructed as described in **Table 1**.

Treatment Protocols

Microwave ablation and radiofrequency ablation procedures were performed under real-time ultrasound (US) or CT by radiologists who had at least 5 years of experience in interventional therapy. Both therapies were administered after analgesia (50–60 mg propofol and 0.05–0.1 mg fentanyl) and local anesthesia (5–15 mL 1–2% lidocaine) by anesthesiologists. According to the location, size, and number of the lesions, radiologists chose the number of ablation antennas, the power and corresponding time and whether to adjust the needle

TABLE 3 | Univariate and multivariate of the prognostic factors for overall survival based on time-dependent Cox regression analyses.

Variable	Number of cases	Univariate analysis		Multivariate analysis	
		HR (95% CI)	*P*-value	HR (95% CI)	*P*-value
Gender (female vs. male)	104 vs. 531	1.44 (0.90–2.31)	0.125	–	–
Tumor size (≥3.5 cm vs. <3.5 cm)	62 vs. 573	1.75 (1.10–2.80)	0.019	2.09 (1.29–3.37)	0.003
AFP level (≥37.15 ng/ml vs. <37.15 ng/ml)	307 vs. 328	1.44 (0.98–2.10)	0.060	–	0.162
HBV infection (present vs. absent)	573 vs. 62	1.68 (0.78–3.61)	0.185	–	–
Numbers (multiple vs. solitary)	58 vs. 577	1.29 (0.70–2.33)	0.423	–	–
Treatment (MWA vs. RFA)	158 vs. 477	1.02 (0.64–1.61)	0.949	–	–
Cirrhosis (present vs. absent)	353 vs. 282	1.59 (1.08–2.36)	0.019	–	0.994
PT (s) (≥13.6 vs. <13.6)	104 vs. 531	2.69 (1.80–4.01)	<0.001	–	0.100
ALB (≤37.7 g/L vs. >37.7 g/L)	120 vs. 515	3.20 (2.19–4.68)	<0.001	2.76 (1.84–4.16)	<0.001
TBIL (≥28.3 μmol/L vs. <28.3 μmol/L)	66 vs. 569	2.22 (1.38–3.58)	0.001	–	0.359
WBC (≤4.24 × 10^9/L vs. >4.24 × 10^9/L)	175 vs. 460	1.71 (1.16–2.52)	0.007	–	0.955
Neutrophil (≤2.41 × 10^9/L vs. >2.41 × 10^9/L)	231 vs. 404	1.65 (1.14–2.40)	0.009	–	0.437
Lymphocyte (≤1.43 × 10^9/L vs. >1.43 × 10^9/L)	250 vs. 385	1.54 (1.06–2.23)	0.025	–	0.867
Monocyte (≥0.64 × 10^9/L vs. <0.64 × 10^9/L)	57 vs. 578	1.37 (0.80–2.32)	0.250	–	–
PLT (≤80 × 10^9/L vs. >80 × 10^9/L)	134 vs. 501	2.57 (1.75–3.77)	<0.001	2.04 (1.36–3.05)	0.001
CRP (≥1.81 mg/L vs. <1.81 mg/L)	230 vs. 405	1.82 (1.26–2.65)	0.002	–	0.413
ALT (≥52.5 U/L vs. <52.5 U/L)	127 vs. 508	1.00 (0.63–1.59)	0.998	–	–
AST (≥41.0 U/L vs. <41.0 U/L)	200 vs. 435	2.15 (1.48–3.12)	<0.001	–	0.132
Age (years)	635	1.03 (1.01–1.04)	0.001	1.03 (1.01–1.05)	<0.001
ALBI grade before treatment			<0.001		0.316
1	438	Reference		Reference	
2	194	2.91 (1.99–4.25)	<0.001	–	0.196
3	3	3.03 (0.42–22.02)	0.273	–	0.623
NLR before treatment (1 vs. 0)	105 vs. 530	1.23 (0.77–1.99)	0.387	–	–
PLR before treatment (1 vs. 0)	49 vs. 586	0.95 (0.42–2.17)	0.908	–	–
PNI before treatment (1 vs. 0)	133 vs. 502	2.39 (1.63–3.53)	<0.001	–	0.535
mGPS before treatment			0.084		0.946
0	601	Reference		Reference	
1	26	1.31 (0.53–3.21)	0.557	–	0.897
2	8	3.03 (1.12–8.25)	0.030	–	0.753
GPS before treatment			<0.001		0.405
0	543	Reference		Reference	–
1	84	2.95 (1.93–4.53)	<0.001	–	0.179
2	8	3.67 (1.34–10.05)	0.011	–	0.753
PI before treatment			0.128		–
0	596	Reference		–	–
1	31	1.96 (0.99–3.87)	0.054	–	–
2	8	0.56 (0.08–4.01)	0.563	–	–
CAR before treatment			0.004		0.845
0	429	Reference	–	Reference	–
1	100	1.67 (1.03–2.71)	0.037	–	0.758
2	106	2.03 (1.30–3.18)	0.002	–	0.566

ALB, albumin; HBV, hepatitis B virus; TBIL, total bilirubin; WBC, white blood cell; PLT, platelet; CRP, C-reactive protein; ALT, alanine aminotransferase; AST, aspartate transaminase; ALBI, albumin-bilirubin; GPS, Glasgow Prognostic Score; NLR, neutrophil to lymphocyte ratio; mGPS, modified Glasgow Prognostic Score; PI, Prognostic Index; PLR, platelet to lymphocyte ratio; PNI, Prognostic Nutritional Index.

position in order to eliminate tumors. The basic principles of ablation treatment are as follows. For tumors with a maximum diameter of ≤3.0 cm, a single antenna was usually used. For tumors with a maximum diameter of >3.0 cm, multiple antennas were usually used to acquire adequate ablation necrosis. The end point of ablation was defined as having a security boundary that extended at least 5–10 mm beyond the tumor boundary.

Microwave ablation equipment: a microwave delivery system (FORSEA; Qinghai Microwave Electronic Institute, Nanjing, China) was used during MWA therapy. This system consisted of an MTC-3 microwave generator (FORSEA) with a frequency of

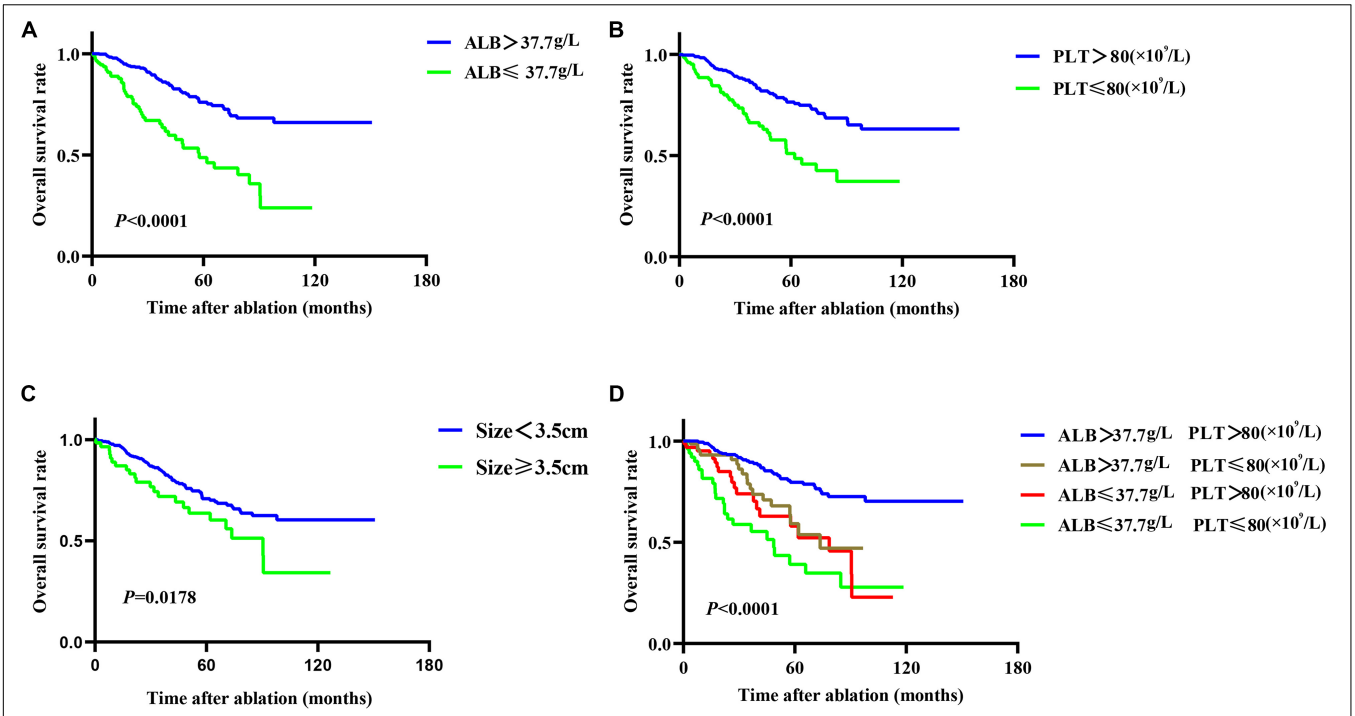

FIGURE 2 | Kaplan–Meier plots for independent prognostic factors of overall survival (OS) in patients with HCC within the Milan Criteria after RFA. **(A,B)** Patients with reduced albumin (ALB) and platelet (PLT) level had lower OS rate than did those with higher ALB and PLT level. **(C)** Patients with tumor size ≥3.5 cm had lower OS rate than did those with size <3.5 cm. **(D)** Different combinations of ALB and PLT showed the different median OS, but the OS of the two combinations of (ALB > 37.7 g/L, PLT ≤ 80 × 10^9/L) and (ALB ≤ 37.7 g/L, PLT > 80 × 10^9/L) did not reach statistical difference (P = 0.397).

2450 MHz, a power output of 10–150 W, a flexible low-loss cable, and a 15- or 18-cm 14G or 16G cooled-shaft antenna.

Radiofrequency ablation equipment: radiofrequency system (RF 2000; RadioTherapeutics, Mountain View, CA, United States) and a needle electrode with a 15G insulated cannula with 10 hook-shaped expandable electrode tines with a diameter of 3.5 cm at expansion (LeVeen; RadioTherapeutics).

Following Up

Follow-up included the imaging examination, serum AFP, the liver function, and the physical examination. Patients underwent a re-examination approximately 1 month after RFA or MWA treatment using abdominal contrast material-enhanced CT, US, or MRI. If there were no obvious signs of recurrence, those patients were followed up once every 3 months for the first 2 years. If recurrence was still not observed, the follow-up visits were allowed to extend to once every 6 months from 2 to 5 years after RFA or MWA and then to once every 12 months after 5 years. If recurrence was detected, the patients were allowed to treat with RFA or MWA, transarterial chemoembolization (TACE), systemic chemotherapy, targeted therapy, or supportive treatment according to the patient's physical condition, liver function, and the tumor staging at the time of tumor recurrence. Technical success was defined as the diameter of the non-enhanced area being greater than that of the treated nodule. The end point, OS, was defined as the interval time from the start of initial RFA or MWA treatment to death by any cause.

Statistical Analysis

Continuous variables that met the normal distribution were described by mean ± SD, otherwise by median and quartile. Continuous variables were compared by using the t-test or Mann–Whitney U test. Binary variables were compared by using the χ^2 test or the Fisher exact test. Also, ordinal categorical variables were compared by using the Kruskal–Wallis H test. The optimal cut-off value of baseline variables was calculated by "survivalROC" R package (15). Those baseline variables were included in a time-dependent Cox proportional-hazards modeling for univariate analysis. Variables satisfying $P < 0.1$ in univariate analysis were introduced into the multivariate time-dependent Cox proportional-hazards modeling. The OS rate between the different groups were compared by Kaplan–Meier curves and log-rank test. The abilities to predict prognosis of the variables with respect to OS were compared by time-dependent receiver operating characteristic (ROC) curves and the estimated area under the curve (AUC). The concordance index (C-index) and time-dependent ROC were analyzed by using the "survival" and "timeROC" R package (16). A nomogram was constructed based on the results of multivariate time-dependent Cox proportional-hazards modeling and by the "rms" R package. The C-index, the internal validation with 1000 sets of bootstrap samples, and the calibration curve were used to demonstrate ability to predict prognosis of the nomogram model. Analyses were two-sided, and $P < 0.05$ indicated statistical significance. Statistical analyses were

TABLE 4 | Multivariate of the prognostic factors for overall survival based on time-dependent Cox regression analyses.

Variable	Number of cases	Multivariate analysis	
		HR (95% CI)	*P*-value
Cirrhosis (present vs. absent)	353 vs. 282	–	0.954
PT (s) (≥13.6 vs. <13.6)	104 vs. 531	–	0.088
TBIL (≥28.3 μmol/L vs. <28.3 μmol/L)	66 vs. 569	–	0.335
WBC (≤4.24 × 10^9/L vs. >4.24 × 10^9/L)	175 vs. 460	–	0.819
Lymphocyte (≤1.43 × 10^9/L vs. >1.43 × 10^9/L)	250 vs. 385	–	0.687
CRP (≥1.81 mg/L vs. <1.81 mg/L)	230 vs. 405	–	0.316
AST (≥41.0 U/L vs. <41.0 U/L)	200 vs. 435	–	0.119
ALB (≤37.7 g/L vs. >37.7 g/L)	120 vs. 515	–	0.357
PLT (≤80 × 10^9/L vs. >80 × 10^9/L)	134 vs. 501	–	0.357
Neutrophil (≤2.41 × 10^9/L vs. >2.41 × 10^9/L)	231 vs. 404	–	0.514
PNI before treatment (1 vs. 0)	133 vs. 502	–	0.725
AFP level (≥37.15 ng/ml vs. <37.15 ng/ml)	307 vs. 328	–	0.141
Size (≥3.5 cm vs. <3.5 cm)	62 vs. 573	1.99 (1.24–3.22)	0.005
Age (years)	635	1.03 (1.01–1.05)	<0.001
mGPS before treatment			0.977
0	601	Reference	–
1	26	–	0.863
2	8	–	0.888
GPS before treatment			0.251
0	543	Reference	–
1	84	–	0.100
2	8	–	0.888
ALBI grade before treatment			0.230
1	438	Reference	
2	194	–	0.129
3	3	–	0.556
CAR before treatment			0.737
0	429	Reference	
1	100	–	0.806
2	106	–	0.435
APS before treatment			<0.001
1 grade	433	Reference	–
2 grade	150	2.52 (1.64–3.87)	<0.001
3 grade	52	5.51 (3.35–9.05)	<0.001

ALB, albumin; HBV, hepatitis B virus; TBIL, total bilirubin; WBC, white blood cell; PLT, platelet; CRP, C-reactive protein; AST, aspartate transaminase; ALBI, albumin-bilirubin; GPS, Glasgow Prognostic Score; NLR, neutrophil to lymphocyte ratio; mGPS, modified Glasgow Prognostic Score; PNI, Prognostic Nutritional Index.

conducted using SPSS version 25.0 (IBM, United States) and R version 3.6.1[1].

RESULTS

Patient Characteristics

A total of 635 HCC patients within the Milan Criteria meeting the inclusion and exclusion criteria were included in this study. The mean age of those patients was 57.74 years (57.74 ± 12.35 years). The median size was 2.30 cm (range: 0.70–5.00 cm). A total of 577 (90.9%) and 58 (9.1%) of HCC patients had solitary and multiple tumors, respectively. There were 573 (90.2%) patients with hepatitis B virus (HBV) infection and 353 (55.6%) patients with cirrhosis, respectively. A total of 477 (75.1%) and 158 (24.9%) of HCC patients were treated with RFA and MWA, respectively. Other clinical characteristics and the inflammation-based scores are depicted in **Table 2**.

Optimal Cut-Off Value of Baseline Variables

The optimal cut-off value of baseline variables was calculated by survival ROC, which could fit Cox proportional-hazards modeling to the status and the time of survival. The optimal cut-off value of tumor size, AFP level, PT, ALB, TBIL, WBC, neutrophil, lymphocyte, monocyte, platelet, C-reactive protein (CRP), ALT, and AST were 3.5 cm, 37.15 ng/ml, 13.6 s, 37.7 g/L, 28.3 μmol/L, 4.24 × 10^9/L, 2.41 × 10^9/L, 1.43 × 10^9/L, 0.64 × 10^9/L, 80 × 10^9/L, 1.81 mg/L, 52.5 U/L, and 41.0 U/L, respectively.

[1]https://www.r-project.org/

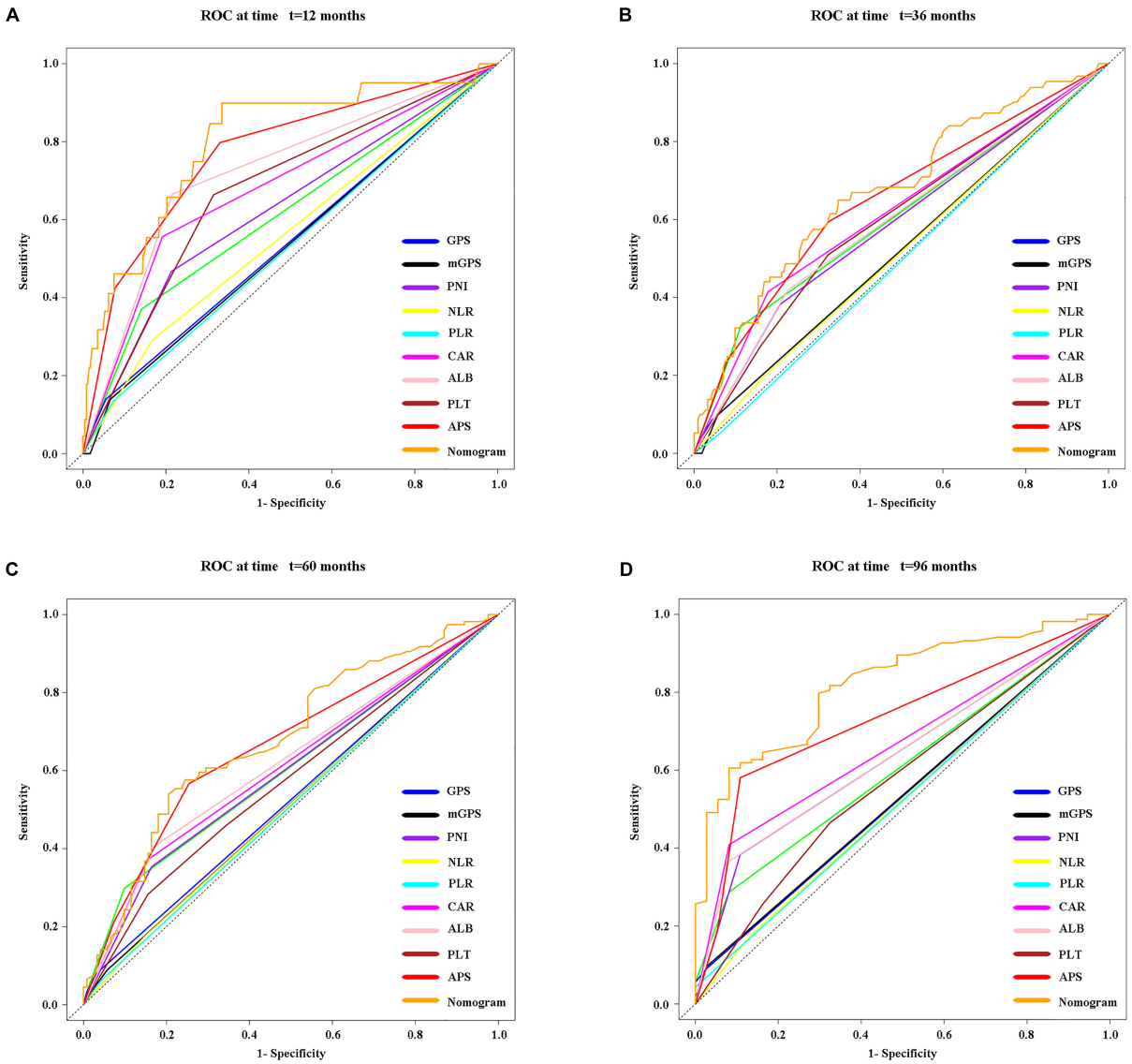

FIGURE 3 | Time-dependent receiver operating characteristic (timeROC) curves at 1 **(A)**, 3 **(B)**, 5 **(C)**, and 8 **(D)** years of OS based on different inflammation-based scores, variables (i.e., ALB and PLT) that built the APS, and the nomogram based on the three pretreatment clinical variables, including the APS level, tumor size, and age.

TABLE 5 | Comparison of the performance and discriminative ability between the preoperative blood-related prognostic factors.

Score	1-year AUC (95% CI)	3-year AUC (95% CI)	5-year AUC (95% CI)	8-year AUC (95% CI)	C-index (95% CI)
ALB	0.68 (0.57, 0.79)	0.62 (0.55, 0.68)	0.61 (0.55, 0.67)	0.66 (0.59, 0.73)	0.64 (0.59, 0.69)
PLT	0.72 (0.62, 0.83)	0.60 (0.53, 0.66)	0.62 (0.56, 0.68)	0.64 (0.57, 0.71)	0.61 (0.56, 0.67)
PLR	0.53 (0.46, 0.60)	0.49 (0.46, 0.52)	0.51 (0.48, 0.54)	0.52 (0.50, 0.54)	0.50 (0.47, 0.53)
mGPS	0.54 (0.47, 0.62)	0.52 (0.49, 0.56)	0.52 (0.49, 0.56)	0.53 (0.49, 0.58)	0.52 (0.49, 0.55)
PI	0.54 (0.46, 0.61)	0.52 (0.48, 0.56)	0.52 (0.48, 0.55)	0.53 (0.49, 0.58)	0.52 (0.49, 0.55)
NLR	0.56 (0.46, 0.66)	0.51 (0.46, 0.57)	0.51 (0.46, 0.56)	0.52 (0.45, 0.59)	0.52 (0.48, 0.57)
PNI	0.63 (0.52, 0.74)	0.59 (0.52, 0.65)	0.59 (0.53, 0.66)	0.64 (0.56, 0.71)	0.60 (0.55, 0.65)
GPS	0.61 (0.51, 0.72)	0.61 (0.55, 0.67)	0.60 (0.54, 0.66)	0.61 (0.54, 0.67)	0.60 (0.55, 0.65)
CAR	0.68 (0.57, 0.78)	0.60 (0.52, 0.67)	0.57 (0.50, 0.64)	0.57 (0.48, 0.67)	0.60 (0.54, 0.65)
APS	0.77 (0.67, 0.88)	0.65 (0.58, 0.72)	0.66 (0.59, 0.73)	0.73 (0.65, 0.81)	0.67 (0.62, 0.73)
Nomogram	0.80 (0.70, 0.91)	0.67 (0.60, 0.75)	0.68 (0.61, 0.75)	0.82 (0.75, 0.89)	0.71 (0.66, 0.77)

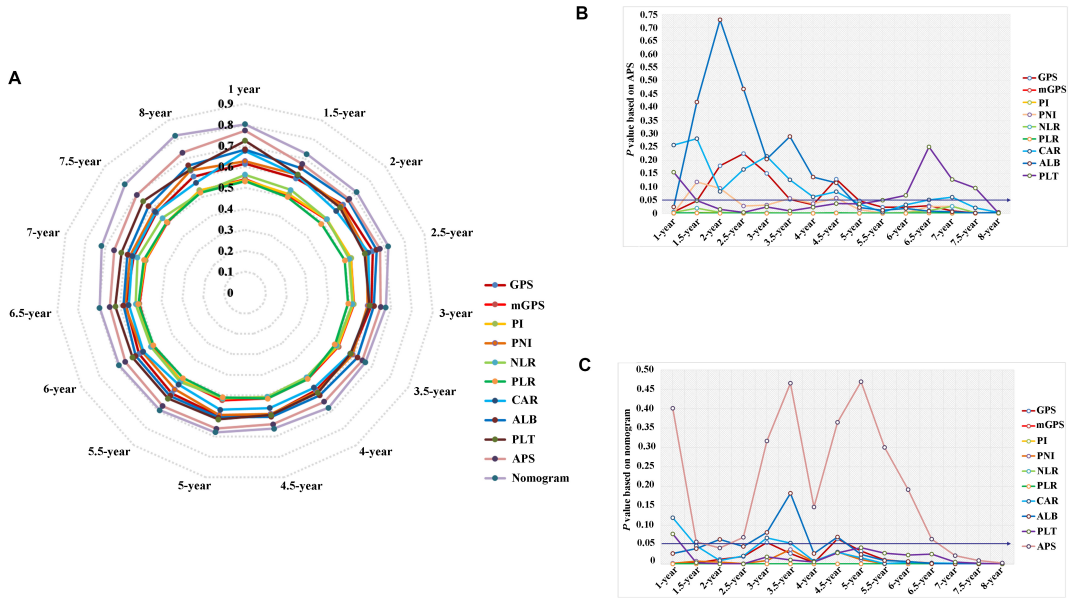

FIGURE 4 | The comparison of serial trends of their performance and discrimination of different inflammation-based scores, variables that built the APS, and the nomogram by the estimated area under the curve (AUC) values **(A)**, and the corresponding *P*-value based on APS **(B)** and the nomogram **(C)**.

Establishment of the Inflammation-Based Score—APS

Twenty-seven variables (gender, tumor size, tumor numbers, AFP level, HBV infection, treatment method, cirrhosis, PT, ALB, TBIL, WBC, neutrophil, lymphocyte, monocyte, PLT, CRP, ALT, AST, age, ALBI grade, NLR, PLR, PNI, mGPS, GPS, PI, CAR) were included in the time-dependent Cox proportional-hazards modeling one by one for univariate analysis, and we introduced those variables satisfying $P < 0.1$ in univariate analysis into the multivariate time-dependent Cox proportional-hazards modeling, and found that only four variables (tumor size, ALB, PLT, age) were independent prognostic factors of OS (**Table 3** and **Figure 2A–C**). Therefore, we combined ALB with PLT (i.e., ALB + PLT) to construct a novel inflammation-based prognostic score. The OS rate between the different groups of ALB + PLT was compared by Kaplan–Meier curves and log-rank test (**Figure 2D**). As shown in **Figure 2D**, we combined (ALB $>$ 37.7 g/L, PLT $\leq$ 80 $\times$ 10^9/L) and (ALB $\leq$ 37.7 g/L, PLT $>$ 80 $\times$ 10^9/L) of ALB + PLT and recorded it as APS 2 level. We then included those variables satisfying $P < 0.1$ in univariate analysis and APS into proportional-hazards modeling for multivariate analysis, and found that only three variables (tumor size, APS, age) were independent prognostic factors for the OS of HCC patients within the Milan Criteria after ablation (**Table 4**).

The Performance and Discrimination of the APS

Time-dependent ROC curves at 1, 3, 5, and 8 years of OS were constructed to compare the performance of the other inflammation-based scores and variables (i.e., ALB and PLT) that built APS, which suggested that APS was superior to other factors (**Figure 3**). The details of the corresponding AUC values and C-index values of those variables for OS prediction are depicted in **Table 5**, which showed that the AUC values and C-index value (0.67; 95% CI 0.62, 0.73) of APS was higher than that of others. To further prove the performance and discrimination of APS, the AUC values (**Figure 4A**) and corresponding *P*-value based on APS (**Figure 4B**) of those inflammation-based scores, ALB, and PLT at different times were calculated to compare the sequential trends of their performance and discrimination, which showed that APS was significantly superior to other factors in predicting the long-term prognosis.

Correlations Between Patient Characteristics and the APS

The relationship between the APS and patient characteristics is summarized in **Table 6**. The higher APS was significantly associated with female ($P = 0.006$); cirrhosis ($P < 0.001$); PT $\geq$ 13.6 s ($P < 0.001$); TBIL $\geq$ 28.3 μmol/L ($P < 0.001$); WBC $\leq$ 4.24 $\times$ 10^9/L ($P < 0.001$); neutrophil $\leq$ 2.41 $\times$ 10^9/L ($P < 0.001$); lymphocyte $\leq$ 1.43 $\times$ 10^9/L ($P < 0.001$); CRP $\geq$ 1.81 mg/L ($P < 0.001$); AST $\geq$ 41.0 U/L ($P < 0.001$); older patients ($P < 0.001$); increased ALBI grade ($P < 0.001$); and increased PNI, mGPS, GPS, and CAR ($P < 0.001$). Besides, patients with cirrhosis have significantly reduced WBC ($P < 0.001$), neutrophil ($P < 0.001$), and lymphocyte ($P < 0.001$) counts than patients without cirrhosis (**Figure 5**).

Construction and Validation of Nomogram Based on the APS

Three variables (APS, tumor size, age), which were independent prognostic factors of OS, were integrated to construct a novel nomogram for predicting prognosis (**Figure 6**). The C-index

TABLE 6 | Clinical characteristics of patients in relation to APS.

Variables	APS 1 grade *N* = 433	APS 2 grade *N* = 150	APS 3 grade *N* = 52	*P*-value
Gender (female vs. male)	57 vs. 376	35 vs. 115	12 vs. 40	0.006
Tumor size (≥3.5 cm vs. <3.5 cm)	39 vs. 394	18 vs. 132	5 vs. 47	0.567
AFP level (≥37.15 ng/ml vs. <37.15 ng/ml)	198 vs. 235	79 vs. 71	30 vs. 22	0.127
HBV infection (present vs. absent)	392 vs. 41	134 vs. 16	47 vs. 5	0.913
Numbers (multiple vs. solitary)	33 vs. 400	17 vs. 133	8 vs. 44	0.105
Treatment (MWA vs. RFA)	101 vs. 332	39 vs. 111	18 vs. 34	0.192
Cirrhosis (present vs. absent)	193 vs. 240	118 vs. 32	42 vs. 10	<0.001
PT(s) (≥13.6 vs. <13.6)	21 vs. 412	47 vs. 103	36 vs. 16	<0.001
TBIL (≥28.3 μmol/L vs. <28.3 μmol/L)	21 vs. 412	24 vs. 126	21 vs. 31	<0.001
WBC (≤4.24 × 10^9/L vs. >4.24 × 10^9/L)	69 vs. 364	72 vs. 78	34 vs. 18	<0.001
Neutrophil (≤2.41 × 10^9/L vs. >2.41 × 10^9/L)	111 vs. 322	83 vs. 67	37 vs. 15	<0.001
Lymphocyte (≤1.43 × 10^9/L vs. >1.43 × 10^9/L)	130 vs. 303	80 vs. 70	40 vs. 12	<0.001
Monocyte (≥0.64 × 10^9/L vs. <0.64 × 10^9/L)	39 vs. 394	14 vs. 136	4 vs. 48	0.938
CRP (≥1.81 mg/L vs. <1.81 mg/L)	129 vs. 304	68 vs. 82	33 vs. 19	<0.001
ALT (≥52.5 U/L vs. <52.5 U/L)	84 vs. 349	29 vs. 121	14 vs. 38	0.428
AST (≥41.0 U/L vs. <41.0 U/L)	95 vs. 338	69 vs. 81	36 vs. 16	<0.001
Age (years)	57 (48–66)*	60 (52–69)*	59 (51–66)*	0.039
ALBI grade before treatment				<0.001
1	385	53	0	–
2	48	95	51	–
3	0	2	1	–
NLR before treatment (1 vs. 0)	65 vs. 368	30 vs. 120	10 vs. 42	0.316
PLR before treatment (1 vs. 0)	40 vs. 393	7 vs. 143	2 vs. 50	0.108
PNI before treatment (1 vs. 0)	17 vs. 416	67 vs. 83	49 vs. 3	<0.001
mGPS before treatment				<0.001
0	416	141	44	–
1	17	6	3	–
2	0	3	5	–
GPS before treatment				<0.001
0	416	111	16	–
1	17	36	31	–
2	0	3	5	–
PI before treatment				0.064
0	411	141	44	–
1	18	7	6	–
2	4	2	2	–
CAR before treatment				<0.001
0	326	85	18	–
1	54	33	13	–
2	53	32	21	–

*ALB, albumin; HBV, hepatitis B virus; TBIL, total bilirubin; WBC, white blood cell; PLT, platelet; CRP, C-reactive protein; ALT, alanine aminotransferase; AST, aspartate transaminase; ALBI, albumin-bilirubin; GPS, Glasgow Prognostic Score; NLR, neutrophil to lymphocyte ratio; mGPS, modified Glasgow Prognostic Score; PI, Prognostic Index; PLR, platelet to lymphocyte ratio; PNI, Prognostic Nutritional Index. *These data represent the median (interquartile Q1–Q3).*

for the nomogram for assessment of OS after ablation was 0.72 (95% CI 0.66, 0.77). The calibration plots for probability of survival at 1, 3, 5, and 8 years with 1000 cycles of bootstrapping were well matched with the idealized 45° line (**Figure 7**). Besides, we calculated individualized scores of each patient, which was the total score for those three prognostic variables. Time-dependent ROC curves at different times of OS, the AUC and C-index values, and the corresponding *P*-value suggested that the novel inflammation-based nomogram system improved the performance and discrimination in predicting the short-term or long-term prognosis of HCC patients within the Milan Criteria after curative ablation (**Figures 3**, **4C**). Besides, the time-dependent ROC curves also showed that compared with age, tumor size, and the American Joint Committee on Cancer (AJCC) 8th staging system (3), the novel inflammation-based nomogram system has obvious advantages in predicting prognosis of HCC patients within the Milan Criteria after curative ablation at 1 year [compared with age ($P < 0.001$), tumor

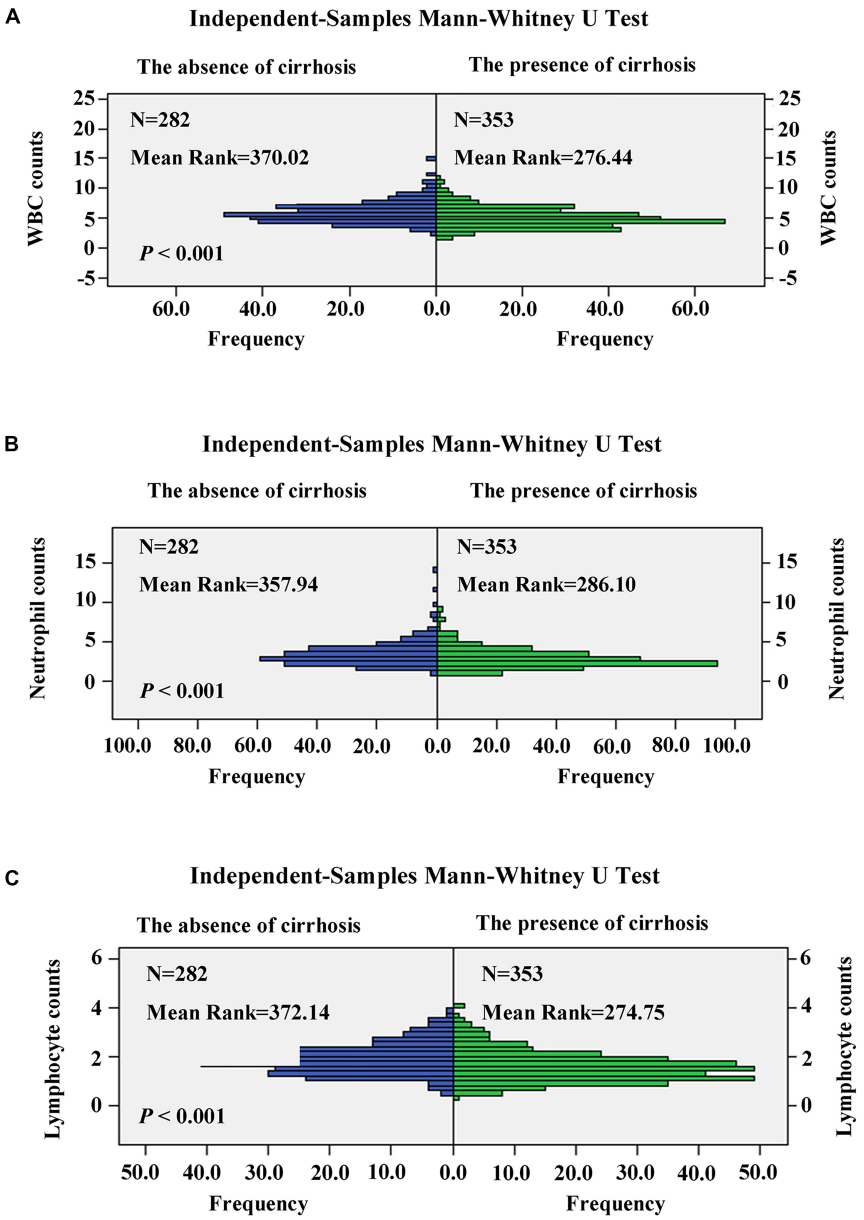

FIGURE 5 | Comparison of white blood cell (WBC) **(A)**, neutrophil **(B)**, and lymphocyte **(C)** counts in patients with cirrhosis and non-cirrhosis by the independent-samples Mann–Whitney U test.

size ($P = 0.004$), and AJCC 8th staging system ($P = 0.031$)], 3 years [compared with age ($P = 0.004$), tumor size ($P < 0.001$), and AJCC 8th staging system ($P = 0.028$)], and 5 years [compared with age ($P = 0.010$), tumor size ($P < 0.001$), and AJCC 8th staging system ($P < 0.001$)] of OS (**Figure 8**).

DISCUSSION

In this study, we firstly found a novel inflammation-based score system—Albumin-Platelet Score (APS)—that has a significant advantage over others in predicting the long-term prognosis by systematically analyzing the pre-treatment clinical characteristics and the inflammatory indicators included in these inflammation-based scores (i.e., NLR, PLR, PNI, mGPS, GPS, PI, and CAR). Also, the nomogram based on the APS further improved the performance of predicting the prognosis of HCC patients within the Milan Criteria after ablation.

As we all know, inflammation promotes bad prognosis of HCC through induction of thrombocytopenia, lymphopenia, and resistance to chemotherapy (17–19). Therefore, inflammation-based prediction systems have great potential in predicting the prognosis of HCC patients (7–13). Especially in China, most cases of HCC are caused by potentially chronic HBV infection.

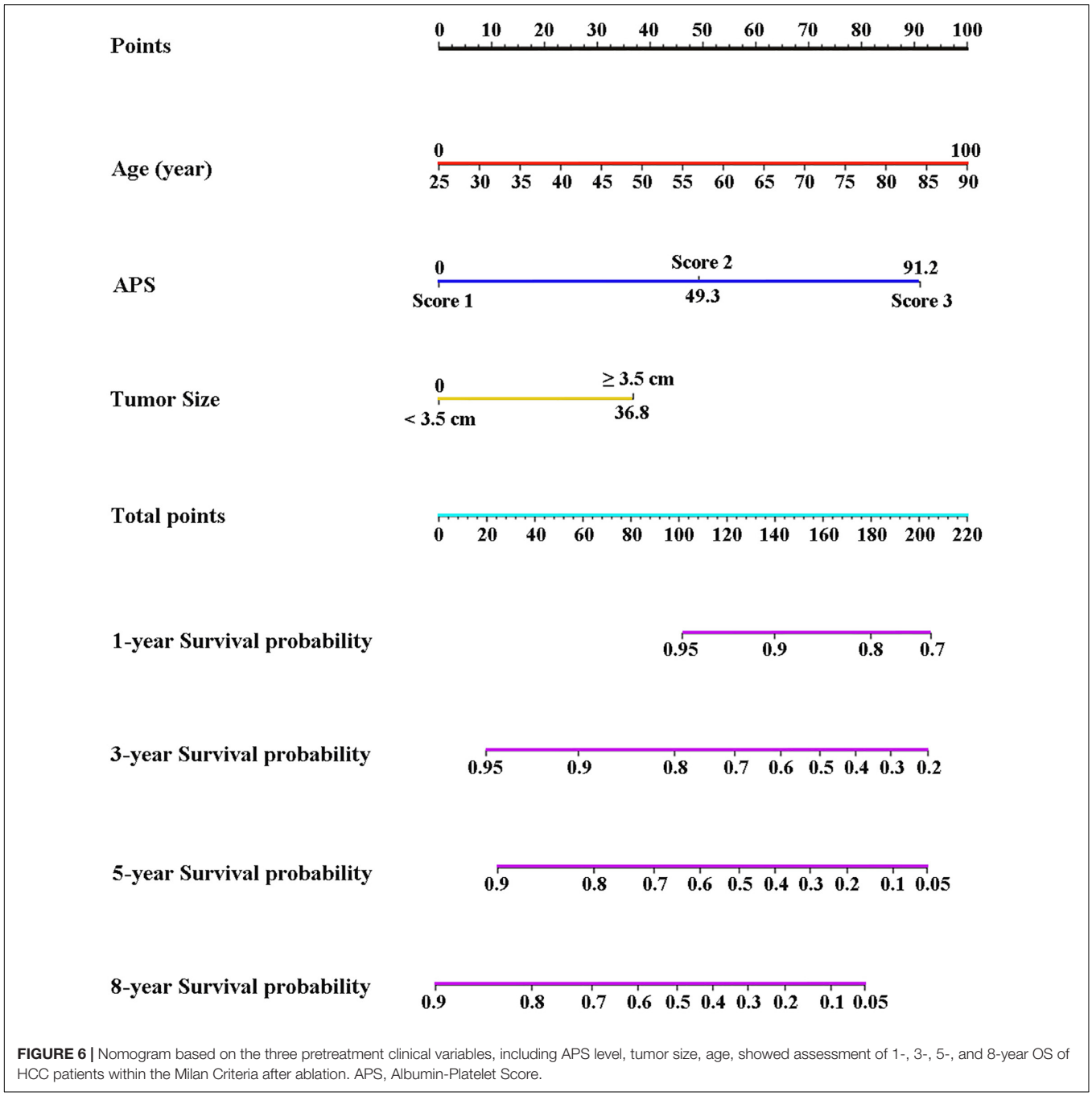

FIGURE 6 | Nomogram based on the three pretreatment clinical variables, including APS level, tumor size, age, showed assessment of 1-, 3-, 5-, and 8-year OS of HCC patients within the Milan Criteria after ablation. APS, Albumin-Platelet Score.

However, few studies based on pretreatment inflammation-based markers focused on assessing the prognosis of HCC patients within the Milan Criteria after curative ablation. To bridge the gap, we systematically analyzed the pre-treatment clinical characteristics to find a significant pre-treatment inflammation-based markers to choose a more ideal treatment for HCC patients within the Milan Criteria.

The APS was an integrated indicator based on peripheral ALB level and PLT counts. In this study, reduced ALB level (ALB $\leq$ 37.7 g/L) and PLT counts (PLT $\leq$ 80 $\times$ 10^9/L) were independent predictors of OS in HCC patients within the Milan Criteria after curative ablation. Platelets were involved in the pathogenesis of chronic liver disease through hemostasis and inflammatory processes. Kondo et al. (20) reported an important outcome of the accumulation of platelets in the liver with chronic hepatitis causing thrombocytopenia and liver fibrosis through the activation of hepatic stellate cells (HSCs). Therefore, thrombocytopenia was considered as an important feature of chronic liver disease and cirrhosis. In addition, thrombocytopenia was associated closely with the development of hepatocarcinogenesis (21). Furthermore, some studies suggested that thrombocytopenia was regarded as an

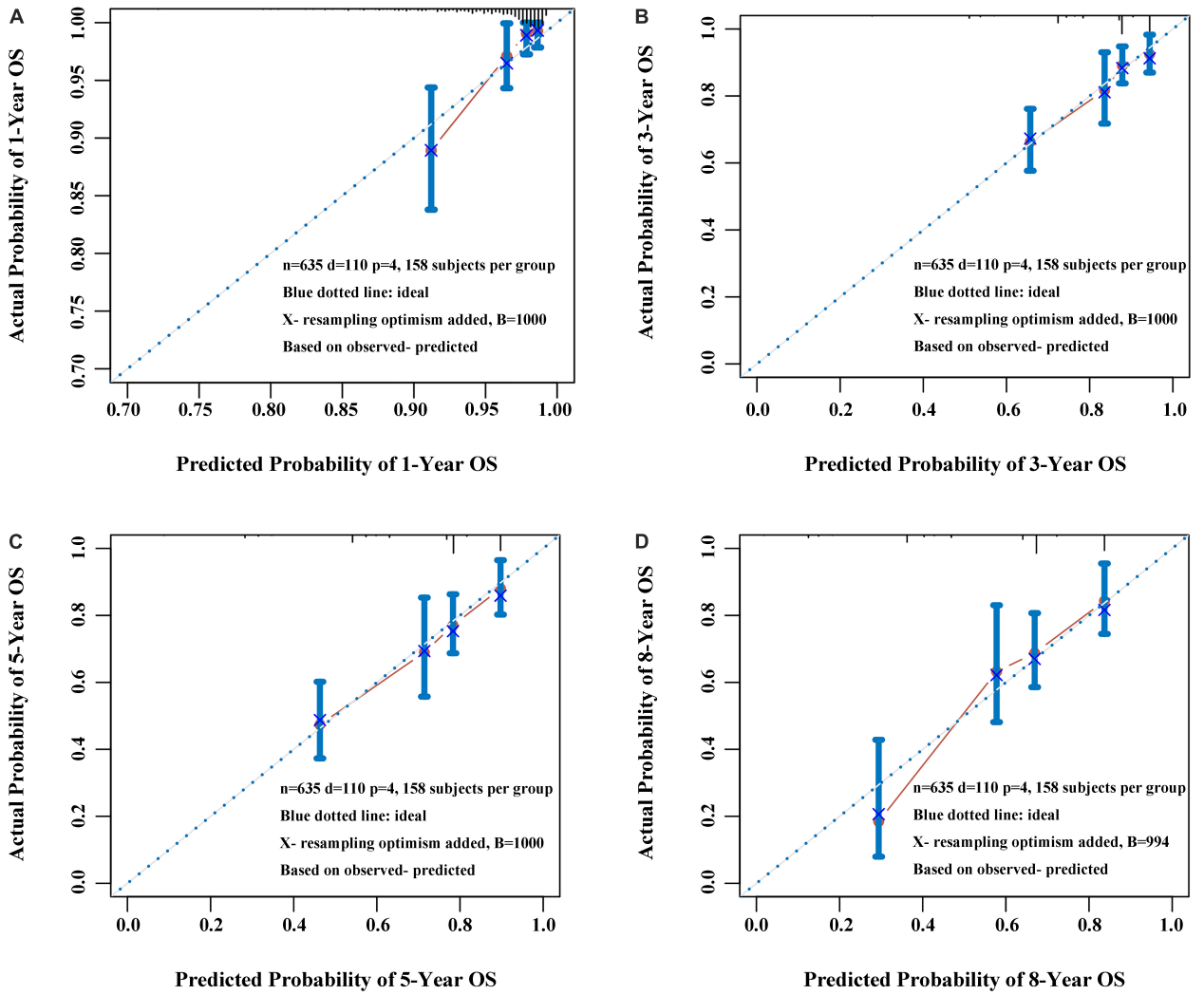

FIGURE 7 | Calibration plot of the nomogram at 1 year **(A)**, 3 years **(B)**, 5 years **(C)**, and 8 years **(D)**. The calibration curves were well matched with the idealized 45° line.

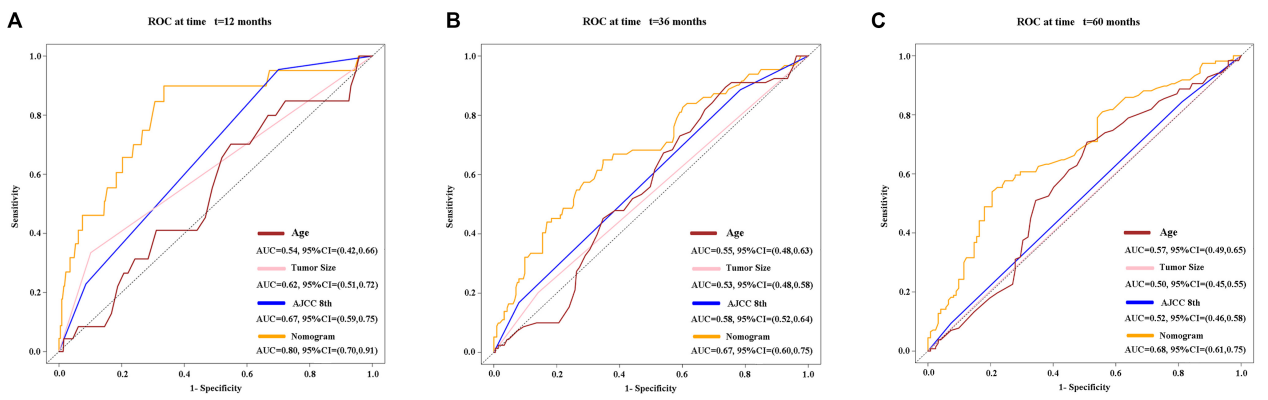

FIGURE 8 | Time-dependent receiver operating characteristic (timeROC) curves at 1 **(A)**, 3 **(B)**, and 5 **(C)** years of overall survival based on the nomogram, age, tumor size, and AJCC 8th staging system. AJCC, American Joint Committee on Cancer.

inexpensive, valuable predictor for the recurrence, and survival in patients with HCC (22, 23). ALB was an important component of various liver function evaluation indicators, such as Child–Turcotte–Pugh classification, ALBI grade, and some inflammation-based score systems, such as GPS, mGPS, and PNI, and they were closely related to the prognosis of HCC (9, 10, 12, 14, 24). Therefore, the APS was an important predictive indicator of the efficacy of HCC undergoing ablation theoretically and practically. Besides, we conducted a correlation analysis between patient characteristics and the APS, and found that among HCC patients within the Milan Criteria after curative ablation with a higher APS, more patients had reduced WBC, neutrophil, and lymphocyte counts; increased CRP level; increased PNI, mGPS, GPS, and CAR; increased ALBI grade; cirrhosis; and increased AST and TBIL, suggesting a higher APS often with poorer immune response, an elevated inflammation status, and worse liver functional reserve. We also found that patients with cirrhosis have significantly reduced WBC, neutrophil, and lymphocyte counts than patients without cirrhosis, which suggested that leukopenia, neutropenia, and lymphopenia were also considered as important features of chronic liver disease and cirrhosis in HCC patients within the Milan Criteria, similar to the thrombocytopenia. In fact, some studies showed the HBV-encoded regulatory HBX protein was able to transactivate the IL-8 promoter, which promoted the IL-8 expression and elicited granulocytes, NK cells, and T-cell chemotaxis at the inflammatory regions, contributing to the development of liver damage (25–28). Therefore, we assumed that the accumulation of neutrophil in the liver with chronic hepatitis was also one of the important causes of neutropenia in early-stage HCC.

Based on the significance of APS, we established an easy-to-use nomogram based on three pretreatment clinical variables, including APS level, tumor size, and age, to assess the prognosis of HCC patients within the Milan Criteria after curative ablation. We also found that the novel inflammation-based nomogram system significantly improved the performance and discrimination in predicting the short-term or long-term prognosis of HCC patients within the Milan Criteria after curative ablation. Also, the nomogram system has more obvious advantages than AJCC 8th staging system in predicting OS of HCC patients within the Milan Criteria after curative ablation.

Besides, there are some considerations to consider when constructing the nomogram. To reduce the expected error in the predicted probability below 10%, the numbers of survival and death should be greater than 10 times the numbers of variables constructing the nomogram (29). The number of deaths was 110, which was more than 36.7 times the number of variables in our study. Considering the insufficient number of cases in the external validation group, we applied the internal validation with 1000 sets of bootstrap samples and its calibration curve and well verified the nomogram. Therefore, the nomogram system can help clinicians make good decisions, improve patient–physician communication, and even choose suitable HCC patients for clinical trials.

Although our findings were significant, there were several limitations to our study. First, the study was a retrospective study mainly based on HBV-infected population, so whether the APS could also predict the prognosis well in non-HBV-predominated HCC patients within the Milan Criteria after curative ablation is a question worthy of further verification. Second, the number of patients with mGPS 3 level, GPS 3 level, and PI 3 level were quite less, which may weaken the ability of mGPS, GPS, and PI in predicting the prognosis. Third, although the ideal cut-off values for these pre-treatment baseline variables were based on survival ROC, which could fit Cox proportional-hazards modeling to the status and the time of survival, this was a single-center study. Therefore, the prospective and multicentric external verification will be conducted to further verify this novel inflammation-based score—APS—and the nomogram based on the APS.

CONCLUSION

This study is the first to find the novel inflammation-based score—APS—that was a better inflammation-based prognostic system than others (i.e., NLR, PLR, PNI, mGPS, GPS, PI, and CAR). Also, the nomogram based on the APS improved the performance of predicting the prognosis of HCC patients within the Milan Criteria after ablation.

DATA AVAILABILITY STATEMENT

The raw data supporting the conclusions of this article will be made available by the authors, without undue reservation.

ETHICS STATEMENT

The studies involving human participants were reviewed and approved by the research ethics committee of the Sun Yat-sen University Cancer Center (SYSUCC). Written informed consent for participation was not required for this study in accordance with the national legislation and the institutional requirements.

AUTHOR CONTRIBUTIONS

SC and WF conceived and designed this study. WF provided the study material and access to patients. SC, WM, FC, LS, HQ, LX, and YW acquired the data. SC, WM, FC, LS, HQ, LX, YW, and WF analyzed the data and drafted the manuscript. All authors contributed to the draft and critically reviewed or revised the manuscript.

FUNDING

This work was funded by the National Natural Science Foundation of China (Grant Number 81771954).

ACKNOWLEDGMENTS

We would like to thank Ms. Binyan Shen for her support of SC.

REFERENCES

1. Bray F, Ferlay J, Soerjomataram I, Siegel RL, Torre LA, Jemal A. Global cancer statistics 2018: globocan estimates of incidence and mortality worldwide for 36 cancers in 185 countries. *CA Cancer J Clin*. (2018) 68:394–424. doi: 10.3322/caac.21492
2. Mazzaferro V, Regalia E, Doci R, Andreola S, Pulvirenti A, Bozzetti F, et al. Liver transplantation for the treatment of small hepatocellular carcinomas in patients with cirrhosis. *N Engl J Med*. (1996) 334:693–9. doi: 10.1056/nejm199603143341104
3. Benson AB, D'Angelica MI, Abbott DE, Abrams TA, Alberts SR, Anaya DA, et al. Guidelines insights: hepatobiliary cancers, version 2.2019. *J Natl Compr Canc Netw*. (2019) 17:302–10.
4. Cucchetti A, Piscaglia F, Cescon M, Colecchia A, Ercolani G, Bolondi L, et al. Cost-effectiveness of hepatic resection versus percutaneous radiofrequency ablation for early hepatocellular carcinoma. *J Hepatol*. (2013) 59:300–7. doi: 10.1016/j.jhep.2013.04.009
5. Hanahan D, Weinberg RA. Hallmarks of cancer: the next generation. *Cell*. (2011) 144:646–74. doi: 10.1016/j.cell.2011.02.013
6. Wang C, He W, Yuan Y, Zhang Y, Li K, Zou R, et al. Comparison of the prognostic value of inflammation-based scores in early recurrent hepatocellular carcinoma after hepatectomy. *Liver Int*. (2020) 40:229–39. doi: 10.1111/liv.14281
7. Chen J, Fang A, Chen M, Tuoheti Y, Zhou Z, Xu L, et al. A novel inflammation-based nomogram system to predict survival of patients with hepatocellular carcinoma. *Cancer Med*. (2018) 7:5027–35. doi: 10.1002/cam4.\break1787
8. Li X, Han Z, Cheng Z, Yu J, Yu X, Liang P. Clinical significance of preoperative platelet-to-lymphocyte ratio in recurrent hepatocellular carcinoma after thermal ablation: a retrospective analysis. *Int J Hyperthermia*. (2015) 31:758–63. doi: 10.3109/02656736.2015.1068958
9. Abe T, Tashiro H, Kobayashi T, Hattori M, Kuroda S, Ohdan H. Glasgow prognostic score and prognosis after hepatectomy for hepatocellular carcinoma. *World J Surg*. (2017) 41:1860–70. doi: 10.1007/s00268-017-3909-7
10. Chen H, Hu N, Chang P, Kang T, Han S, Lu Y, et al. Modified glasgow prognostic score might be a prognostic factor for hepatocellular carcinoma: a meta-analysis. *Panminerva Med*. (2017) 59:302–7.
11. Chen TM, Lin CC, Huang PT, Wen CF. Neutrophil-to-lymphocyte ratio associated with mortality in early hepatocellular carcinoma patients after radiofrequency ablation. *J Gastroenterol Hepatol*. (2012) 27:553–61. doi: 10.1111/j.1440-1746.2011.06910.x
12. Man Z, Pang Q, Zhou L, Wang Y, Hu X, Yang S, et al. Prognostic significance of preoperative prognostic nutritional index in hepatocellular carcinoma: a meta-analysis. *HPB*. (2018) 20:888–95. doi: 10.1016/j.hpb.2018.03.019
13. Sanghera C, Teh JJ, Pinato DJ. The systemic inflammatory response as a source of biomarkers and therapeutic targets in hepatocellular carcinoma. *Liver Int*. (2019) 39:2008–23. doi: 10.1111/liv.14220
14. Johnson PJ, Berhane S, Kagebayashi C, Satomura S, Teng M, Reeves HL, et al. Assessment of liver function in patients with hepatocellular carcinoma: a new evidence-based approach-the albi grade. *J Clin Oncol*. (2015) 33:550–8. doi: 10.1200/jco.2014.57.9151
15. Heagerty PJ, Zheng Y. Survival model predictive accuracy and roc curves. *Biometrics*. (2005) 61:92–105. doi: 10.1111/j.0006-341x.2005.030814.x
16. Rodriguez-Alvarez MX, Meira-Machado L, Abu-Assi E, Raposeiras-Roubin S. Nonparametric estimation of time-dependent roc curves conditional on a continuous covariate. *Stat Med*. (2016) 35:1090–102. doi: 10.1002/sim.6769
17. El-Serag HB, Rudolph KL. Hepatocellular carcinoma: epidemiology and molecular carcinogenesis. *Gastroenterology*. (2007) 132:2557–76. doi: 10.1053/j.gastro.2007.04.061
18. Kurebayashi Y, Ojima H, Tsujikawa H, Kubota N, Maehara J, Abe Y, et al. Landscape of immune microenvironment in hepatocellular carcinoma and its additional impact on histological and molecular classification. *Hepatology*. (2018) 68:1025–41. doi: 10.1002/hep.29904
19. Ringelhan M, Pfister D, O'Connor T, Pikarsky E, Heikenwalder M. The immunology of hepatocellular carcinoma. *Nat Immunol*. (2018) 19:222–32. doi: 10.1038/s41590-018-0044-z
20. Kondo R, Yano H, Nakashima O, Tanikawa K, Nomura Y, Kage M. Accumulation of platelets in the liver may be an important contributory factor to thrombocytopenia and liver fibrosis in chronic hepatitis c. *J Gastroenterol*. (2013) 48:526–34. doi: 10.1007/s00535-012-0656-2
21. Kumada T, Toyoda H, Kiriyama S, Sone Y, Tanikawa M, Hisanaga Y, et al. Incidence of hepatocellular carcinoma in hepatitis c carriers with normal alanine aminotransferase levels. *J Hepatol*. (2009) 50:729–35. doi: 10.1016/j.jhep.2008.11.019
22. Pang Q, Zhang JY, Song SD, Qu K, Xu XS, Liu SS, et al. Thrombocytopenia as an inexpensive, valuable predictor for survival in patients with hepatocellular carcinoma. *Scand J Gastroenterol*. (2014) 49:1507–8. doi: 10.3109/00365521.2014.962076
23. Pang Q, Qu K, Bi JB, Liu SS, Zhang JY, Song SD, et al. Thrombocytopenia for prediction of hepatocellular carcinoma recurrence: systematic review and meta-analysis. *World J Gastroenterol*. (2015) 21:7895–906. doi: 10.3748/wjg.v21.i25.7895
24. Llovet JM, Bru C, Bruix J. Prognosis of hepatocellular carcinoma: the bclc staging classification. *Semin Liver Dis*. (1999) 19:329–38. doi: 10.1055/s-2007-1007122
25. Mahe Y, Mukaida N, Kuno K, Akiyama M, Ikeda N, Matsushima K, et al. Hepatitis b virus x protein transactivates human interleukin-8 gene through acting on nuclear factor kb and ccaat/enhancer-binding protein-like cis-elements. *J Biol Chem*. (1991) 266:13759–63.
26. Zimmermann HW, Seidler S, Gassler N, Nattermann J, Luedde T, Trautwein C, et al. Interleukin-8 is activated in patients with chronic liver diseases and associated with hepatic macrophage accumulation in human liver fibrosis. *PLoS One*. (2011) 6:e21381. doi: 10.1371/journal.pone.0021381
27. Gehring AJ, Koh S, Chia A, Paramasivam K, Chew VS, Ho ZZ, et al. Licensing virus-specific t cells to secrete the neutrophil attracting chemokine cxcl-8 during hepatitis b virus infection. *PLoS One*. (2011) 6:e23330. doi: 10.1371/journal.pone.0023330
28. Mukaida N. Pathophysiological roles of interleukin-8/cxcl8 in pulmonary diseases. *Am J Physiol Lung Cell Mol Physiol*. (2003) 284:L566–77. doi: 10.1152/ajplung.00233.2002
29. Iasonos A, Schrag D, Raj GV, Panageas KS. How to build and interpret a nomogram for cancer prognosis. *J Clin Oncol*. (2008) 26:1364–70. doi: 10.1200/JCO.2007.12.9791

Conflict of Interest: The authors declare that the research was conducted in the absence of any commercial or financial relationships that could be construed as a potential conflict of interest.

frontiers in Oncology

ORIGINAL RESEARCH
published: 24 September 2020
doi: 10.3389/fonc.2020.573316

Assessment of Ablative Margin After Microwave Ablation for Hepatocellular Carcinoma Using Deep Learning-Based Deformable Image Registration

Chao An[1], Yiquan Jiang[1], Zhimei Huang[1], Yangkui Gu[1], Tianqi Zhang[1], Ling Ma[2] and Jinhua Huang[1]**

[1] Department of Minimal Invasive Intervention, State Key Laboratory of Oncology in South China, Collaborative Innovation Center for Cancer Medicine, Sun Yat-sen University Cancer Center, Guangzhou, China, [2] College of Software, Nankai University, Tianjin, China

OPEN ACCESS

Edited by:
Wei Yang,
Peking University Cancer Hospital, China

Reviewed by:
Fangyi Liu,
People's Liberation Army General Hospital, China
Kun Yan,
Peking University Cancer Hospital, China

***Correspondence:**
Jinhua Huang
huangjh@sysucc.org.cn
Ling Ma
maling@nankai.edu.cn

Specialty section:
This article was submitted to Cancer Imaging and Image-directed Interventions, a section of the journal Frontiers in Oncology

Received: *16 June 2020*
Accepted: *14 August 2020*
Published: *24 September 2020*

Citation:
An C, Jiang Y, Huang Z, Gu Y, Zhang T, Ma L and Huang J (2020) Assessment of Ablative Margin After Microwave Ablation for Hepatocellular Carcinoma Using Deep Learning-Based Deformable Image Registration. Front. Oncol. 10:573316. doi: 10.3389/fonc.2020.573316

Aim: To assess the ablative margin (AM) after microwave ablation (MWA) for hepatocellular carcinoma (HCC) with a deep learning-based deformable image registration (DIR) technique and analyze the relation between the AM and local tumor progression (LTP).

Patients and Methods: From November 2012 to April 2019, 141 consecutive patients with single HCC (diameter $\leq$ 5 cm) who underwent MWA were reviewed. Baseline characteristics were collected to identify the risk factors for the determination of LTP after MWA. Contrast-enhanced magnetic resonance imaging scans were performed within 1 month before and 3 months after treatment. Complete ablation was confirmed for all lesions. The AM was measured based on the margin size between the tumor region and the deformed ablative region. To correct the misalignment, DIR between images before and after ablation was achieved by an unsupervised landmark-constrained convolutional neural network. The patients were classified into two groups according to their AMs: group A (AM $\leq$ 5 mm) and group B (AM $>$ 5 mm). The cumulative LTP rates were compared between the two groups using Kaplan–Meier curves and the log-rank test. Multivariate analyses were performed on clinicopathological variables to identify factors affecting LTP.

Results: After a median follow-up period of 28.9 months, LTP was found in 19 patients. The mean tumor and ablation zone sizes were 2.3 $\pm$ 0.9 cm and 3.8 $\pm$ 1.2 cm, respectively. The mean minimum ablation margin was 3.4 $\pm$ 0.7 mm (range, 0–16 mm). The DIR technique had higher AUC for 2-year LTP without a significant difference compared with the registration assessment without DL ($P = 0.325$). The 6-, 12-, and 24-month LTP rates were 9.9, 20.6, and 24.8%, respectively, in group A, and 4.0, 8.4, and 8.4%, respectively, in group B. There were significant differences between the two groups ($P = 0.011$). Multivariate analysis showed that being >65 years of age ($P = 0.032$, hazard ratio (HR): 2.463, 95% confidence interval (CI), 1.028–6.152) and AM $\leq$ 5 mm ($P = 0.010$, HR: 3.195, 95% CI, 1.324–7.752) were independent risk factors for LTP after MWA.

Conclusion: The novel technology of unsupervised landmark-constrained convolutional neural network-based DIR is feasible and useful in evaluating the ablative effect of MWA for HCC.

Keywords: microwave ablation, deep learning-based deformable image registration, ablative margin, hepatocellular carcinoma, local tumor progression

INTRODUCTION

Image-guided percutaneous thermal ablation (PTA) is a widely prevalent minimally invasive therapy for early-stage hepatocellular carcinoma (HCC) (1–3). Both microwave ablation (MWA) and radiofrequency ablation (RFA) offer a shorter operative duration, less bleeding, and fewer complications than surgery (4–6). Despite many advantages, the therapeutic effect of PTA is still hampered by local tumor progression (LTP) (7). Accumulating data shows that untreated micrometastases from the primary tumor, the ensuing spread along intrasegmental branches, and vascular invasion can lead to LTP. Previous studies have reported that the LTP rate ranged from 5.1 to 20.7% in patients with a liver malignancy who underwent different ablation modalities (8, 9). Numerous clinical studies have found that a minimum ablation margin (AM) is an independent predictor of LTP after ablation for HCC (10–12). Most micrometastases in previous reports were found to be more than 5 mm away from the boundary of target lesions, and a thermal field range that extends outside the tumor border with a 5–10-mm safe margin should be developed. To improve ablative efficacy, accurate AM assessment would deliver important feedback to the operator during the procedure.

For the assessment of the surgical margin, the margin size refers to the distance from the edge of the neoplasm to the transected tissue (13). Similarly, the AM was measured by the distance among the radiographic borders of the tumor and the ablation zone based on 2D pre- and post-ablative images (14). Traditionally, radiologists typically assess the AM by comparison of the pre- and post-ablation images side by side based on anatomical markers. However, this method fails to measure the AM conveniently and accurately. Instead, pre- and post-ablative images can be registered, and the AM can be measured immediately. However, these registration techniques still have two major issues: first, due to the breathing motion of the liver and heating-stimulated tissue deformation (15, 16), the registration error between the pre- and post-ablation images is augmented; second, there is no specific cutoff value for the optimal safety boundary value. Therefore, precise assessment in the AM and image registration play a vital role in improving the predictive accuracy of LTP after PTA.

Deep learning (DL) is a subspecialty of machine learning that has achieved impressive performance in diagnosis, prediction, and decision-making. In recent years, DL has been applied to image registration and DL-based registration methods can be divided into two categories: one method is to utilize a deep neural network to estimate the similarity between the two images of pre- and post-ablation and drive iterative optimization, and the other method utilizes a deep regression network to predict the transformation parameters. The former methods only use deep learning for the similarity measurement, but they still need the traditional registration method for iterative optimization and cannot perform real-time registration. The latter methods take advantage of DL and address the challenges of non-rigid registration. Balakrishnan et al. (17) proposed an unsupervised learning-based deformable image registration method for MR brain registration. They used a convolutional neural network-based framework, VoxelMorph, to map an input image pair to a deformation field that aligns these images. Zhao et al. (18) presented recursive cascaded networks for deformable image registration. They warped the moving image successively by each cascade recursively in an unsupervised manner and finally aligned to the fixed image.

The goal of this study was to develop and explore AMs using registration between pre- and post-ablation MRI images based on DL, which overcomes the limitations of the current techniques and increases the AM accuracy assessment post-MWA in early-stage HCC.

MATERIALS AND METHODS

Patient Selection

The protocol was reviewed and granted approval through the institutional review board. The necessity to acquire informed consent was waived. For our cohort study, 289 treatment-naïve patients with HCC (tumor diameter $\leq$ 5 cm) who subsequently were administered computed tomography-guided percutaneous microwave ablation (CT-PMWA) from November 2012 to April 2019 were reviewed. The patients were monitored from time of treatment until death or April 2020. A diagnosis of HCC was established as per recommendations of the European Association for the Study of the Liver (EASL) (19). To avoid any confounding factors that might cause LTP, we designed strict inclusion and exclusion criteria (**Figure 1**). The inclusion and exclusion criteria are described in **Supplementary Material A1**. The ablation area covering the tumor focus was examined by comparing the real-time images that were acquired after the procedure with the enhanced scan image that were acquired prior to treatment to confirm complete ablation. The AM is defined as the shortest distance from the edge of the tumor to the edge of the ablation zone. These patients had undergone necessary follow-up examinations.

Pre- and Post-ablative MRI and Follow-Up

All pre-ablation magnetic resonance image (MRI) scans were performed within 1 month (mean, 12.8 $\pm$ 2.2 days; range, 1–29 days) before the MWA procedure. The post-ablation MRI

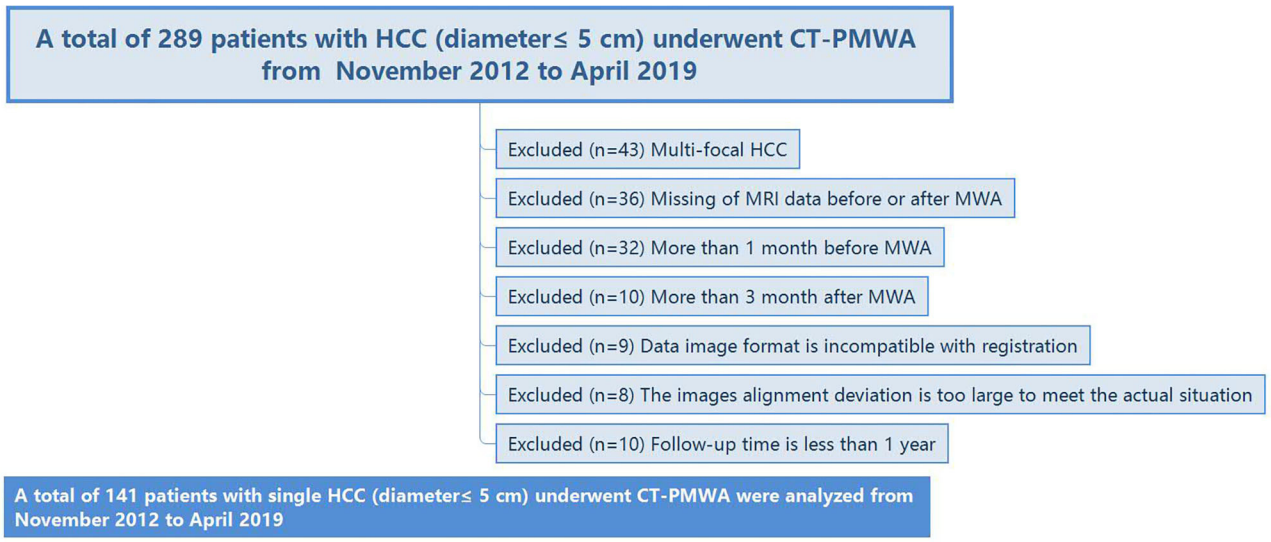

FIGURE 1 | Flow diagram shows the study patient accrual process.

scans were also performed within 3 months (mean, 34.5 ± 10.5 days; range, 25–82 days) following the MWA procedure. Two GE 750w 3.0T MRI scanners were used (GE Healthcare, Waukesha, WI). MRI image parameters used for registration are shown in **Supplementary Material A2**. Contrast-enhanced MR images were obtained through the use of a T1-weighted 3D gradient-echo sequence prior to and 30, 60, and 90 s post-intravenous administration of 0.1 mmol/kg gadopentetate dimeglumine (Bayer HealthCare Pharmaceuticals, Berlin, Germany). The patients were monitored using a contrast-enhanced imaging (i.e., MRI or CT) at 3-month intervals within 1 year and 6-month intervals beyond 1 year, and the follow-up period was not <1 year.

MWA Procedures

Ablation was conducted through three interventional radiologists (JH, ZH, and CA, with 25, 10, and 5 years of experience with MWA, respectively). All MWA procedures were carried out under CT guidance, the microwave antenna was localized into the tumor, and the deployment degree scale was established based on the tumor size and shape. Patients were asked to lie in a supine or prone position on the scanning bed based on the location of their lesions. Every MWA procedure was carried out using local and intravenous anesthesia. Post-anesthesia, a 15-gauge, 18-cm MWA antenna (MTC-3C, Nanjing Qinghai Research Institute of Microwave Electric, China) was introduced into the tumor at a pre-set angle. In order to make sure that the position of the ablation electrode was adequate, CT image scanning was carried out once more before the ablation surgery. The settings for the power and ablation times were established as per the standard guidelines that were recommended by the manufacturer. Each MWA session utilized an overlapping technique to make sure the entire tumor was eliminated.

Definition of Local Tumor Progression and Technique Effectiveness

LTP was characterized based on the imaging results of the abnormal nodular, disseminated, and/or atypical patterns of peripheral enhancement around the ablation site in MWA-treated patients. The efficacy of the technique was described as comprehensive local necrosis at 1 month post-treatment (20).

Image Registration Procedure

The MRI–MRI image fusion was carried out utilizing a commercial image fusion system (MyLab Twice, Esoate, Genoa, Italy) (11). One set of MRI images prior to MWA that demonstrated hepatic vessels clearly and HCC lesions within the portal vein or delay phase were chosen. Next, the images in DICOM format were imported into the image fusion system. An additional set of MRI images post-MWA with clear hepatic vessels and ablative zones in DICOM format were also imported within the image fusion system. HCC lesions in the MRI scans before MWA were manually outlined, and a 5-mm AM was automatically established. The system labeled the HCC lesion and AM through the use of various colors (**Figure 2**).

Deep Learning-Based Deformable Image Registration

To reduce the registration errors due to breathing motion and heating-induced tissue deformation, we present a deep learning-based deformable image registration (DIR) algorithm based on an unsupervised end-to-end deep spatial transformed similarity network (STS-net) for the ablation images. The architecture of our proposed registration method is given in **Figure 3**. The registration network, STS-net, contains a spatial transformer network (ST-net) and a similarity network (S-net). The ST-net performs explicit spatial transformations of moving images according to fixed images, and the S-net calculates the

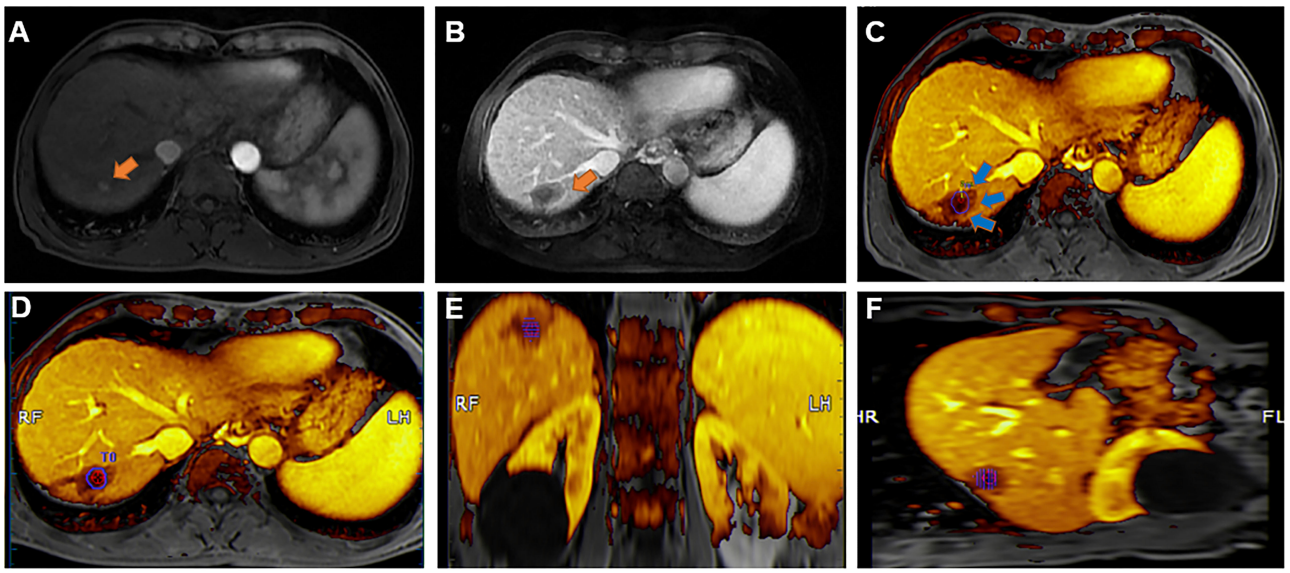

FIGURE 2 | An example of margin assessment based on MR-MR fusion. **(A)** Co-registered pre-ablation MR images show the tumor zone (orange arrow); **(B)** Co-registered post-ablation MR images show the ablation zone (orange arrow). **(C)** Achievement of registration between the tumor and ablation zones (blue arrow). **(D–F)**. Segmented tumor (red) and theoretical 5 mm (blue) margin contours overlaid on the ablation zone on the axial, sagittal, and coronal MR images.

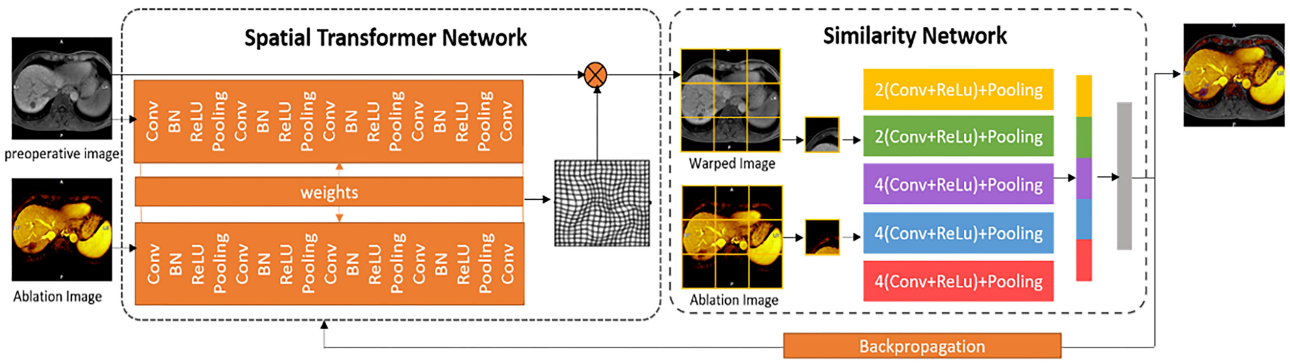

FIGURE 3 | The non-rigid DIR STS-net. Two neural network (left: spatial transformer network and right: similarity network). The orange frame is a non-rigid transformation parameter generation framework in which there are three parts: The localization network specified by a Siamese network, grid generator, and sampler. The blue frame is a similarity calculation framework where the deep multiscale features from the transformed pre-operative image and ablation image are extracted by a convolutional neural network, and their similarity is backpropagated to the orange frame for more accurate registration.

similarity between pairs of transformed moving images and fixed images. By backpropagating the similarity from the S-Net, the ST-net can achieve the optimized spatial transformation for unsupervised registration.

The ST-net forms a spatial transformer. First, a Siamese network, which includes two identical convolutional neural networks that share the same set of weights with a final regression layer, is designed to create the non-rigid transformation parameters that minimize the difference between the pair of images. Next, the predicted spatial transformation parameters are utilized to generate a sampling grid to obtain the rigid and non-rigid transformations. Finally, the sampler achieves the warped image sampled from the original moving image at the grid points. For a better transformation, we use the differentiable image sampler, which takes the set of sampling points, and an input image U to produce a transformed moving image V. The transformed image V can be determined using

$$V_i = \sum_{n}^{H} \sum_{m}^{W} U_{nm} \max(0, 1 - |x_i - m|) \max\left(0, 1 - \left|y_i - n\right|\right) \quad (1)$$

where H and W are the height and width of the image, respectively; the (x_i, y_i) coordinates define the spatial location of pixel i in the input image, and $\max(a, b)$ is a function returning the larger value between value a and value b. The bilinear

sampling kernel is used to obtain the value at a particular pixel in image V.

The S-net measures the similarity metric between the paired images. For a more accurate measurement, the whole images are divided into regions, and the similarities between the paired regions are calculated and combined. First, the deep feature is extracted by a convolutional neural network. The regions are passed through a stack of convolutional layers to capture the notion of left, right, up, down, and center, are linearly transformed, and are passed through five max-pooling layers to maintain the local translation invariance property, for a set of feature maps. Then, the multiscale features are fused to form a fully connected layer. Finally, the similarity of deep features from the paired images is calculated in the sum of the similarity between the paired deep features of regions with the normalized cross-correlation. The similarity as the loss function is backpropagated to the ST-net for more accurate registration of ablation images. The loss function can be defined by

$$LOSS = -\sum_{i=1}^{N} \frac{D(F_{wi}, F_{ai})}{\sqrt{D(F_{wi}, F_{wi}) \times D(F_{ai}, F_{ai})}}, \quad (2)$$

where F_{wi} and F_{ai} are the features of the ith block of the warped image and ablation image, respectively, which are extracted from the fully connected layer, D (a, b) is a function returning the dot product of vector a and vector b, and N is the number of blocks in the warped image.

The proposed network can learn changes in the position and deformation of the liver according to the pair of the pre- and post-ablation images and apply the transformation on the pre-operative image to obtain the warped image with the deformation. By backpropagating the similarity and correcting the deformation iteratively until the minimum dissimilarity is reached, the pre-operative image is finally aligned to the ablation image.

Statistical Analysis

Continuous variables were evaluated through the Mann–Whitney U-tests, while categorical variables were assessed through the Pearson $\chi 2$ or Fisher's exact tests. LTP was then determined utilizing the Kaplan–Meier method using a log-rank test. Univariate and multivariate analyses of independent risk factors for LTP were evaluated using a forward stepwise Cox regression model. The variation in prediction power among the metrics was determined by comparing the area under the receiver operating characteristic curve utilizing DeLong's method. SPSS 22.0 (SPSS, Chicago, IL) and RMS package for the R environment 3.5.1 (http://www.r-project.org/) were utilized for all statistical analyses. A two-sided $P < 0.05$ was the threshold for statistical significance.

RESULTS

Baseline Characteristics

After layer-by-layer screening according to the above exclusion criteria, 141 patients (17 females and 124 males; mean age, 55.2 ± 10.8 years) using single HCC (mean diameter, 2.3 ± 0.9 cm) were enrolled. All HCC lesions underwent deep learning-based deformable image registration (DIR), and the success rate of registration was 100% (141/141). The median image registration time cost was 183.5 s, and the mean registration error was 1.6 ± 0.8 mm, which is significantly lower than that of the registration method without DL (2.8 ± 1.1 mm, $P = 0.003$). The patient and tumor characteristics are demonstrated in **Table 1**. The mean maximum tumor and ablation zone sizes were 2.3 ± 0.9 cm and 3.8 ± 1.2 cm, respectively. The median maximum tumor and ablation zone volumes were 47.8 and 102.6 ml, respectively. The mean minimum ablation margin was 3.4 ± 0.7 mm (range, 0–16 mm). In total, 80 patients successfully achieved a 5-mm safe margin, and 61 patients failed to achieve 5-mm safe margins.

TABLE 1 | Baseline characteristics of patients undergoing CT-PMWA.

Characteristics	No. of patients (n = 141)
Age (y)[a]	55.2 ± 10.8 (26–82)
Gender	
Female	17 (12.1)
Male	124 (87.9)
Comorbid disease	
Absence	41 (29.1)
Presence	100 (70.9)
Maximum tumor diameter (cm)[a]	2.3 ± 0.9
Maximum ablation zone diameter (cm)[a]	3.8 ± 1.2
Tumor volume (ml)*	47.8 (16.3–352.8)
Ablation zone volume (ml)*	102.6 (76.5–892.6)
Child–Pugh class	
A	140 (99.3)
B	1(0.7)
Location of tumor	
Left S1/S2/S3/S4	2/2/3/6
Right S5/S6/S7/S8	35/34/24/35
Abutting major vessels	
Presence	25 (17.7)
Absence	116 (82.3)
Biochemical tests	
AFP (ng/ml)*	32.7 (6.3–22352.8)
ALP (U/L)*	86.1 (49.0–241.6)
AST (U/L)[a]	36.1 ± 10.8
ALT(U/L)[a]	37.7 ± 11.6
TBIL (μmol/l)[a]	15.6 ± 3.9
Ablation margin	
≤5 mm	61 (43.3)
>5 mm	80 (56.7)
Ablation duration (min)[a]	8.7 ± 1.6
Ablation power (W) [a]	58.2 ± 1.2

Unless otherwise indicated, numbers in parentheses are the range.
[a] Values are mean value ± standard deviation (range).
**Values are median (range); AFP, alpha-fetoprotein; AST, aspartate aminotransferase; ALT, alanine transaminase; ALB, serum albumin; TBIL, total bilirubin; MWA, microwave ablation.*

TABLE 2 | Comparison between DIR and conventional registration assessment.

DIR	Conventional registration				Total
	AM ≤ 5 mm		AM > 5 mm		
	LTP	Non-LTP	LTP	Non-LTP	
AM ≤ 5 mm	8	34	8	11	61
AM > 5 mm	3	26	0	51	80
Total	11	60	8	62	141

AM, ablative margin; DIR, deep learning-based deformable image registration; LTP, local tumor progression.

Comparison Between DIR and Conventional Registration Assessment

Using the conventional registration technique without DL, after registration based on the intrahepatic structure landmark, in three of these cases, significant deviations were visible due to heating-induced tissue deformation. However, 11 cases were misaligned due to breathing motion. If these incorrect registrations were followed, seven patients were considered not to reach the ablation margin. As there is only a limited amount of cases in categories "AM > 10 mm" and "AM = 0 mm," we divided these patients into two groups for statistical analysis and comparison between DIR and conventional registration without DL. **Table 2** shows the comparative results. Compared with registration without DL, DIR was classified into a proportion of ablations as AM ≤ 5 mm (61 vs. 70), and others as margin >5 mm (80 vs. 71). The statistical analysis results demonstrated that the minimum AM calculated utilizing the DIR technique had increased discrimination power for 2-year LTP without a significant difference compared with the registration assessment without DL (AUC, 0.728 vs. 0.705, respectively; $P = 0.325$).

Ablative Margin and Tumor Size

According to tumor size, we divided these patients into two groups: the <3-cm and 3–5-cm groups. The mean AM size was similar to that in the 3–5-cm group, demonstrating no significant differences ($P = 0.403$). The correlation between the minimal AM (average of the measured margins by the observers) and tumor size is demonstrated in **Figure 4**.

Midterm Local Tumor Progression After CT-PMWA

The median follow-up period was 28.9 months (range, 12.3–89.2 months). In total, 13.5% of patients (19/141) had experienced confirmed LTP. Based on follow-up imaging, the efficacy rate of this technique was 98.6%. These patients were separated into two groups including (1) patients with an ablation area that fully covers the tumor but fails to attain the 5-mm safe margin (group A) and (2) patients with an ablation area that completely covers the tumor and effectively achieves the 5-mm safe margin (group B). With the DIR technique, of the 61 HCC patients in group A, 16 experienced LTP, whereas three patients experienced LTP in group B. In the conventional registration technique, of the 70 HCC patients in group A, 11 were found to have LTP, whereas eight were found to have LTP in group B. According to DIR, the cumulative 6-, 12-, and 24-month LTP rates of group A were 9.9, 20.6, and 24.8%, respectively, for group A and 4.0, 8.4, and 8.4%, respectively (**Figure 5A**), showing a significant difference ($P = 0.011$) between the groups. According to conventional registration without DL, the cumulative 6-, 12-, and 24-month LTP rates were 7.7, 18.8, and 23.1%, respectively, for group A and 4.0, 8.4, and 8.4%, respectively, for group B (**Figure 5B**), showing a significant difference ($P = 0.025$) among the two groups.

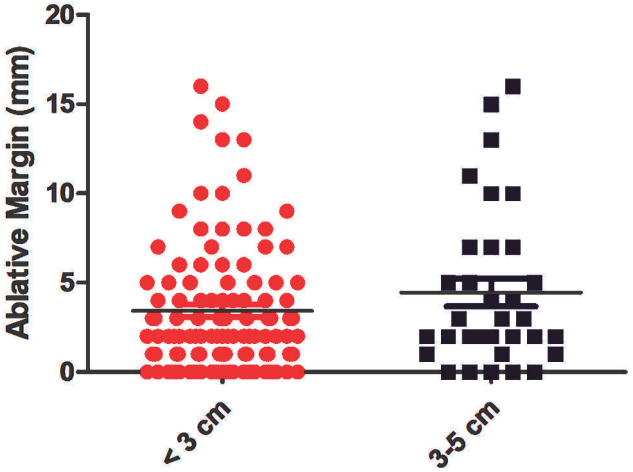

FIGURE 4 | The correlation between the minimal (ablative margin) AM and tumor size. The histogram shows that there is no statistical difference in the AM between the <3-cm group and 3–5-cm group.

Univariate and Multivariate Analyses for LTP

Eight potential risk factors (sex, age, comorbidities, cirrhosis, AFP, tumor size, location abutting major vessels, and AM) for LTP were examined through univariate and multivariate analyses (**Table 3**). Univariate analysis demonstrated statistical significance between the LTP rates dependent on age [hazard ratio (HR) = 2.891; 95% confidence interval (CI): 1.298, 6.439; $P = 0.009$] and AM (HR = 2.426; 95% CI: 1.081, 5.444; $P = 0.027$). The multivariate analysis showed that older age (HR = 2.463; 95% CI: 1.028, 6.152; $P = 0.032$) and an AM ≤ 5 mm (HR = 3.195; 95% CI: 1.324, 7.752; $P = 0.010$) were significant LTP risk factors.

DISCUSSION

Registering the pre- and post-ablation images has been a promising alternative to conventional side-by-side assessment for AMs, which has many advantages as follows (21–23): (1) faster and more accurate measurement of safety boundaries and (2) clearer observation of the spatial relationship between the tumor and ablation zone. Therefore, an increasing number of registration methods have emerged for evaluating AMs. Soichiro Tani et al. (24) reported that a non-rigid intensity-based registration was used to develop a 3D distance map

TABLE 3 | Factors associated with LTP according to univariate and multivariate analysis.

Factors	No. of patients	Univariate analysis		multivariate analysis	
		HR (95% CI)	*P*-value	HR (95% CI)	*P*-value*
Age (years)		2.891 (1.298, 6.439)	0.009	2.463 (1.028, 6.152)	0.032
<65	113				
≥65	29				
Gender		2.839 (0.462, 4.524)	0.513	…	…
Male	124				
Female	17				
Comorbidities		2.129 (0.651, 6.961)	0.211	…	…
Absence	41				
Presence	100				
Cirrhosis		2.129 (0.651, 6.961)	0.211	…	…
Absence	51				
Presence	90				
Tumor size(cm)		1.864 (0.824, 4.219)	0.135	…	…
<3	108				
3–5	33				
Abutting major vessels		1.018 (0.501, 2.068)	0.960	…	…
Absence	116				
Presence	25				
AFP (ng/mL)		1.585 (0.667, 3.830)	0.292	…	…
≤200	112				
>200	29				
Ablative margin (mm)		2.426 (1.081, 5.444)	0.011	3.195 (1.324, 7.752)	0.010
≤5	61				
>5	80				

*Data in parentheses are 95% confidence intervals. *P-values were determined with Cox proportional hazards regression models. P < 0.05 indicated a significant difference. LTP, local tumor progression; HR, hazard ratio; CI, confidence intervals; AFP, α-fetoprotein.*

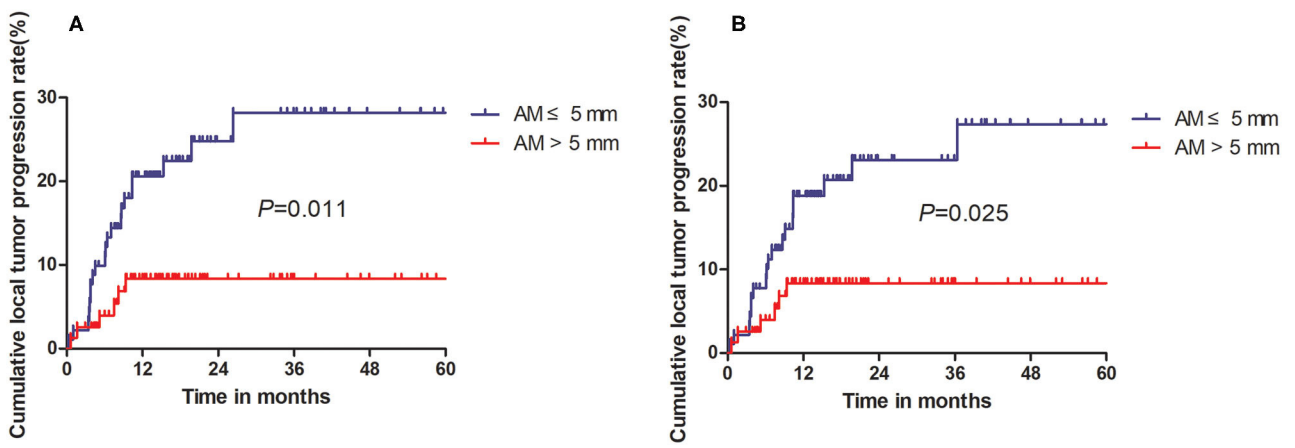

FIGURE 5 | Kaplan–Meier curves comparing local tumor recurrence between the AM ≤ 5-mm and AM > 5-mm groups. **(A)** Comparison of LTP based on deep learning-based deformable image registration (DIR) technique. **(B)** Comparison of LTP based on registration without deep learning.

encompassing the tumor and computed the ablation volume to identify the area with insufficient margins. Elena A. Kaye et al. (25) suggested that the generation of new 3D assessment metrics can easily measure the volume of tissue at-risk post-ablation and predicted LTP. However, a crucial issue remains unresolved. The pre- and post-image misalignment of the liver due to the breathing motion and heating-stimulated tissue deformation may result in incorrect AM measurements (26, 27). To effectively

reduce this measurement error, we use DL methods for optimal registration in this study.

In this study, we introduced the MRI registration method, which is semi-automated and interactive, utilizing a commercial image-processing software that is utilized in clinic in radiology and interventional oncology. An additional 5-mm boundary beyond the tumor can be automatically calculated and depicted. Although this method can effectively shorten the AM assessment time and decrease the evaluation bias of different radiologists, it is still unable to achieve the most accurate registration between the tumor and ablation zone. The difficulty of traditional registration methods is the design of similarity measures and the selection and matching of features. The unsupervised DL-based registration method proposed in this paper can use the derivable spatial transformer to optimize the image similarity between pre- and post-ablative MRI images. Our method does not avoid the extraction of handcrafted features, the matching design, and the similarity measure, and it also uses extensive clinical data that has not been annotated by medical experts. In addition, our DIR method uses the Siamese spatial transformer network to obtain the non-rigid transformation parameters more accurately than other methods and uses backpropagation to continuously optimize the similarity of the paired pre- and post-ablative images to minimize the distance between them (28–30). The proposed registration method can make full use of the advantages of deep neural networks to achieve better registration performance than previous methods.

The obtained AM in patients with solitary HCC from CT-PMWA were analyzed. Of the 144 patients, 7.8% of patients (11/141) patients had suboptimal co-registration results from differences in liver position and/or shape. Interestingly, all the suboptimal co-registrations were improved by DL and eventually reached sufficient integration. Because several patients had inaccurate AMs when using the conventional registration technique, the predictive power of the AM for LTP may weaken. However, the DIR technique has more powerful prediction ability than conventional registration techniques based on better AUC values for the prediction of LTP.

In this study, there were three major findings. First, using DL-based registration can improve the predictive power. The higher AUC value compared with the conventional registration technique and the cumulative LTP rate of patients in the $\leq$5-mm AM group being significantly increased compared to the $>$5-mm AM group can explain the advantage of DL-based registration; second, the minimal AM size was not affected as the tumor diameter increased when patients underwent CT-PMWA, and the reason may be that MWA can generate a larger ablative zone easily; third, in addition to the AM, older age ($>$65 years old) was also a risk factor for LTP and deserved our attention before ablation treatment.

Our study has several limitations. First, assessment of the technique utilizing the diagnostic pre- and post-ablation MRI images with a 5-mm slice thickness limits the accuracy of the slice direction assessment. Optimally, further studies should try to acquire thinner slices. Secondly, the DIR of potential value for intra-ablation use would require a prospective study in an HCC patient cohort with similar characteristics. In fact, post-ablation imaging will possibly be obtained using the ablation applicator that remains in the tissue, which introduces a degree of beam hardening artifact that impacts segmentation performance. Third, our study design is a limitation, as the person evaluating the novel technique was not blinded to the LTP-associated outcomes and may be subjected to bias. Future studies will be focused on the assessment and adjustment of this technique for intraprocedural utilization. Final, no blinded valued method may cause biases and the larger sample and further perspective studies can be needed.

In conclusion, non-rigid DIR permits us to quantitatively assess the adequacy of the AM post-CT-PMWA. This method can help predict LTP at an earlier time point, including immediately after the ablation procedure and lead to an improvement in patient care.

DATA AVAILABILITY STATEMENT

The datasets used and/or analyzed during the current study are available from the corresponding author on reasonable request.

ETHICS STATEMENT

The studies involving human participants were reviewed and approved by the institutional review board of Sun Yat-sen University Cancer Center. The patients provided their written informed consent to participate in this study. Written informed consent was obtained from the individual(s) for the publication of any potentially identifiable images or data included in this article.

AUTHOR CONTRIBUTIONS

CA participated in the data analysis and drafted the manuscript. JH and YG conceived of the study and carried out the editorial support for this manuscript. JH, ZH, and TZ participated in the ablation procedure. LM provided deep learning-based deformable image registration method. YJ provided assistance in data analysis. All authors read and approved the final manuscript.

FUNDING

This work was supported by the National Scientific Foundation Committee of China (Grant No. 81871374); Sun Yat-sen University Clinical Trial 5010 Project (No. 2016002), and Guangzhou Science and Technology Program (No. 201704020134).

SUPPLEMENTARY MATERIAL

The Supplementary Material for this article can be found online at: https://www.frontiersin.org/articles/10.3389/fonc.2020.573316/full#supplementary-material

REFERENCES

1. Kamal A, Elmoety A, Rostom Y, Shater MS, Lashen SA. Percutaneous radiofrequency versus microwave ablation for management of hepatocellular carcinoma: a randomized controlled trial. *J Gastrointest Oncol.* (2019) 10:562–71. doi: 10.21037/jgo.2019.01.34
2. Yang BS, Liu LX, Yuan M, Hou YB, Li QT, Zhou S, et al. Multiple imaging modality-guided radiofrequency ablation combined with transarterial chemoembolization for hepatocellular carcinoma in special locations. *Diagn Interv Radiol.* (2020) 26:131–9. doi: 10.5152/dir.2019.18540
3. Hermida M, Cassinotto C, Piron L, Aho-Glélé S, Guillot C, Schembri V, et al. Multimodal percutaneous thermal ablation of small hepatocellular carcinoma: predictive factors of recurrence and survival in western patients. *Cancers.* (2020) 12:313. doi: 10.3390/cancers12020313
4. Si MB, Yan PJ, Hao XY, Du ZY, Tian HW, Yang J, et al. Efficacy and safety of radiofrequency ablation versus minimally invasive liver surgery for small hepatocellular carcinoma: a systematic review and meta-analysis. *Surg Endosc.* (2019) 33:2419–29. doi: 10.1007/s00464-019-06784-0
5. He W, Li B, Zheng Y, Zou R, Shen J, Cheng D, et al. Resection vs. ablation for alpha-fetoprotein positive hepatocellular carcinoma within the milan criteria: a propensity score analysis. *Liver Int.* (2016) 36:1677–87. doi: 10.1111/liv.13166
6. Liu W, Zou R, Wang C, Qiu J, Shen J, Liao Y, et al. Microwave ablation versus resection for hepatocellular carcinoma within the milan criteria: a propensity-score analysis. *Ther Adv Med Oncol.* (2019) 11:1758835919874652. doi: 10.1177/1758835919874652
7. Hirooka M, Ochi H, Koizumi Y, Tokumoto Y, Hiraoka A, Kumagi T, et al. Local recurrence of hepatocellular carcinoma in the tumor blood drainage area following radiofrequency ablation. *Mol Clin Oncol.* (2014) 2:182–6. doi: 10.3892/mco.2013.229
8. Brunello F, Carucci P, Gaia S, Rolle E, Brunocilla PR, Castiglione A, et al. Local tumor progression of hepatocellular carcinoma after microwave percutaneous ablation: a preliminary report. *Gastroenterology Res.* (2012) 5:28–32. doi: 10.4021/gr401w
9. Yu J, Liang P, Yu XL, Cheng ZG, Han ZY, Mu MJ, et al. Local tumour progression after ultrasound-guided microwave ablation of liver malignancies: risk factors analysis of 2529 tumours. *Eur Radiol.* (2015) 25:1119–26. doi: 10.1007/s00330-014-3483-4
10. Hocquelet A, Trillaud H, Frulio N, Papadopoulos P, Balageas P, Salut C, et al. Three-dimensional measurement of hepatocellular carcinoma ablation zones and margins for predicting local tumor progression. *J Vasc Interv Radiol.* (2016) 27:1038–45.e2. doi: 10.1016/j.jvir.2016.02.031
11. Wang XL, Li K, Su ZZ, Huang ZP, Wang P, Zheng RQ. Assessment of radiofrequency ablation margin by MRI-MRI image fusion in hepatocellular carcinoma. *World J Gastroenterol.* (2015) 21:5345–51. doi: 10.3748/wjg.v21.i17.5345
12. Koda M, Tokunaga S, Miyoshi K, Kishina M, Fujise Y, Kato J, et al. Ablative margin states by magnetic resonance imaging with ferucarbotran in radiofrequency ablation for hepatocellular carcinoma can predict local tumor progression. *J Gastroenterol.* (2013) 48:1283–92. doi: 10.1007/s00535-012-0747-0
13. Wakai T, Shirai Y, Sakata J, Valera VA, Korita PV, Akazawa K, et al. Appraisal of 1 cm hepatectomy margins for intrahepatic micrometastases in patients with colorectal carcinoma liver metastasis. *Ann Surg Oncol.* (2008) 15:2472–81. doi: 10.1245/s10434-008-0023-y
14. Shady W, Petre EN, Do KG, Gonen M, Yarmohammadi H, Brown KT, et al. Percutaneous microwave versus radiofrequency ablation of colorectal liver metastases: ablation with clear margins (A0) provides the best local tumor control. *J Vasc Interv Radiol.* (2018) 29:268–75.e1. doi: 10.1016/j.jvir.2017.08.021
15. Choi GW, Suh Y, Das P, Herman J, Holliday E, Koay E, et al. Assessment of setup uncertainty in hypofractionated liver radiation therapy with a breath-hold technique using automatic image registration-based image guidance. *Radiat Oncol.* (2019) 14:154. doi: 10.1186/s13014-019-1361-6
16. Fabian S, Spinczyk D. Target registration error minimization for minimally invasive interventions involving deformable organs. *Comput Med Imaging Graph.* (2018) 65:4–10. doi: 10.1016/j.compmedimag.2017.01.008
17. Dalca AV, Balakrishnan G, Guttag J, Sabuncu MR. Unsupervised learning of probabilistic diffeomorphic registration for images and surfaces. *Med Image Anal.* (2019) 57:226–36. doi: 10.1016/j.media.2019.07.006
18. Zhao S, Lau T, Luo J, Chang EI, Xu Y. Unsupervised 3D end-to-end medical image registration with volume tweening network. *IEEE J Biomed Health Inform.* (2020) 24:1394–404. doi: 10.1109/JBHI.2019.2951024
19. European Association for the Study of the Liver. Electronic address: easloffice@easloffice.eu, European Association for the Study of the Liver. EASL Clinical Practice Guidelines: Management of hepatocellular carcinoma. *J Hepatol.* (2018) 69:182–236. doi: 10.1016/j.jhep.2018.03.019
20. Ahmed M, Solbiati L, Brace CL, Breen DJ, Callstrom MR, Charboneau JW, et al. Image-guided tumor ablation: standardization of terminology and reporting criteria–a 10-year update. *Radiology.* (2014) 273:241–60. doi: 10.1148/radiol.14132958
21. Yoon JH, Lee JM, Klotz E, Woo H, Yu MH, Joo I, et al. Prediction of local tumor progression after radiofrequency ablation (RFA) of hepatocellular carcinoma by assessment of ablative margin using pre-RFA MRI and post-RFA CT registration. *Korean J Radiol.* (2018) 19:1053–65. doi: 10.3348/kjr.2018.19.6.1053
22. Fu T, Li Q, Liu D, Ai D, Song H, Liang P, et al. Local incompressible registration for liver ablation surgery assessment. *Med Phys.* (2017) 44:5873–88. doi: 10.1002/mp.12535
23. Shyn PB, Tremblay-Paquet S, Palmer K, Tatli S, Tuncali K, Olubiyi OI, et al. Breath-hold PET/CT-guided tumour ablation under general anaesthesia: accuracy of tumour image registration and projected ablation zone overlap. *Clin Radiol.* (2017) 72:223–9. doi: 10.1016/j.crad.2016.10.017
24. Tani S, Tatli S, Hata N, Garcia-Rojas X, Olubiyi OI, Silverman SG, et al. Three-dimensional quantitative assessment of ablation margins based on registration of pre- and post-procedural MRI and distance map. *Int J Comput Assist Radiol Surg.* (2016) 11:1133–42. doi: 10.1007/s11548-016-1398-z
25. Kaye EA, Cornelis FH, Petre EN, Tyagi N, Shady W, Shi W, et al. Volumetric 3D assessment of ablation zones after thermal ablation of colorectal liver metastases to improve prediction of local tumor progression. *Eur Radiol.* (2019) 29:2698–705. doi: 10.1007/s00330-018-5809-0
26. Lv J, Yang M, Zhang J, Wang X. Respiratory motion correction for free-breathing 3D abdominal MRI using CNN-based image registration: a feasibility study. *Br J Radiol.* (2018) 91:20170788. doi: 10.1259/bjr.20170788
27. Menys A, Hamy V, Makanyanga J, Hoad C, Gowland P, Odille F, et al. Dual registration of abdominal motion for motility assessment in free-breathing data sets acquired using dynamic MRI. *Phys Med Biol.* (2014) 59:4603–19. doi: 10.1088/0031-9155/59/16/4603
28. Weick S, Breuer K, Richter A, Exner F, Ströhle SP, Lutyj P, et al. Non-rigid image registration of 4D-MRI data for improved delineation of moving tumors. *BMC Med Imaging.* (2020) 20:41. doi: 10.1186/s12880-020-00439-6
29. Ohashi Y, Takashima H, Ohmori G, Harada K, Chiba A, Numasawa K, et al. Efficacy of non-rigid registration technique for misregistration in 3D-CTA fusion imaging. *Radiol Med.* (2020) 125:618–24. doi: 10.1007/s11547-020-01164-4
30. Yang F, Ding M, Zhang X. Non-rigid multi-modal 3D medical image registration based on foveated modality independent neighborhood descriptor. *Sensors.* (2019) 19:4675. doi: 10.3390/s19214675

Conflict of Interest: The authors declare that the research was conducted in the absence of any commercial or financial relationships that could be construed as a potential conflict of interest.

frontiers in Oncology

ORIGINAL RESEARCH
published: 07 October 2020
doi: 10.3389/fonc.2020.546883

Microwave Ablation Versus Nipple Sparing Mastectomy for Breast Cancer ≤5 cm: A Pilot Cohort Study

Jie Yu[1], Zhi-yu Han[1], Ting Li[2], Wen-zhe Feng[3], Xiao-ling Yu[1], Yan-chun Luo[1], Han Wu[4], Jian Jiang[1], Jian-dong Wang[5] and Ping Liang[1]**

[1] Department of Interventional Ultrasound, Chinese PLA General Hospital, Beijing, China, [2] Department of Ultrasound, People's Hospital of Sanya, Sanya, China, [3] Department of Laboratory Medicine, The Fourth Hospital of Baotou City, Baotou, China, [4] Department of Ultrasound, Qingdao Municipal Hospital, Qingdao, China, [5] Department of General Surgery, Chinese PLA General Hospital, Beijing, China

OPEN ACCESS

Edited by:
Youyong Kong,
Southeast University, China

Reviewed by:
Ying Huang,
ShengJing Hospital of China Medical University, China
Xiang Jing,
Tianjin Third Central Hospital, China
Kun Yan,
Peking University Cancer Hospital, China

***Correspondence:**
Ping Liang
liangping301@126.com
Jian-dong Wang
wangjiandong@188.com

Specialty section:
This article was submitted to Cancer Imaging and Image-directed Interventions, a section of the journal Frontiers in Oncology

Received: 30 March 2020
Accepted: 21 September 2020
Published: 07 October 2020

Citation:
Yu J, Han Z-y, Li T, Feng W-z, Yu X-l, Luo Y-c, Wu H, Jiang J, Wang J-d and Liang P (2020) Microwave Ablation Versus Nipple Sparing Mastectomy for Breast Cancer ≤5 cm: A Pilot Cohort Study. Front. Oncol. 10:546883. doi: 10.3389/fonc.2020.546883

Objectives: Compared with nipple sparing mastectomy (NSM), microwave ablation (MWA) is one relatively new modality indicated for selected breast cancer with nipple sparing and with little of evidence-based medical research for decision-making. The objective of this study was to compare the effect of ultrasound-guided percutaneous MWA and NSM for breast cancer.

Materials and Methods: A retrospective cohort study was conducted in a single institution from 2014 to 2020. Women with invasive ductal carcinoma of the breast ≤ 5cm treated by MWA or NSM were enrolled. The primary end point was tumor progression and secondary end points included survival, cosmetic results, and complications.

Results: 21 patients in the MWA group and 43 in the NSM group were evaluated. The mean tumor size was 2.3 cm (range, 0.3–5.0 cm). Median follow-up was 26.7 months (range, 14.6–62.5 months). The mean age of MWA was 24 years older than that of the NSM group. All the patients achieved technique effectiveness. One local tumor progression and one ipsilateral breast recurrence occurred at 42 and 28 months after MWA, respectively. One ipsilateral breast recurrence and two bone metastasis occurred at 31.2, 34, and 30.5 months after NSM. Two groups had no significant difference in tumor progression ($P = 0.16$). No participants in both groups developed cancer related death ($P > 0.99$) and major complications ($P > 0.99$). However, MWA needed less hospitalization time ($P < 0.001$) and achieved better cosmetic results ($P < 0.001$).

Conclusions: MWA achieved similar short term effect for breast cancer control and better cosmetic satisfaction compared with NSM in selected patients. MWA provides appropriate option for elderly patients who are unfit for surgery.

Keywords: breast cancer, nipple, breast-sparing surgery, microwaves, ablation techniques

HIGHLIGHTS

- As techniques with nipple sparing, microwave ablation achieved satisfactory effect in treating breast tumors ≤5 cm compared with nipple sparing mastectomy during a 26.7-month follow-up.
- Microwave ablation achieved better cosmetic satisfaction compared with nipple sparing mastectomy.
- MWA could be considered as an alternative minimally invasive treatment in early stage tumors and in the elderly cases considered unfit for surgery.

INTRODUCTION

Among females, breast cancer (BC) is the most commonly diagnosed cancer (24.2% of the total cancer cases) and the leading cause of cancer death (15.0% of the total cancer deaths) worldwide (1). Surgical management of BC has undergone a dramatic evolution over the past four decades from radical mastectomy toward breast-conserving techniques such as oncoplastic lumpectomy, nipple sparing mastectomy (NSM), and the sentinel lymph node (SLN) evaluations, which provide great aesthetic satisfaction and less aggression for early-stage BCs patients (2–4). NSM of BC was firstly applied in the 1990s and by now has become an acceptable method among several breast-conserving techniques. The clinical requirements toward an even less invasive approach compared to the standard breast-conserving surgery have promoted studies investigating image-guided percutaneous ablation treatment of BC (5). As the application in other solid tumors, numerous potential ablation approaches including radiofrequency ablation (RFA), cryoablation, laser ablation, high-intensity focused ultrasound (US) and microwave ablation (MWA) have been tried in BC treatment since 1994 (6–10). There are many reasons for ablation treatment of BC, including lower cost, less morbidity, less hospitalization, better cosmetic results, and appropriate option for elderly patients with comorbidities that led to their unfit for surgery.

MWA is an exciting advance among thermal ablation techniques and has been widely used for the treatment of liver cancer (11, 12). Compared with other thermal ablation techniques, the potential advantages of MWA include larger ablation area and higher intratumoral temperatures produced by active heating (13). However, only two literatures have been published on MWA of BC patients with the initially satisfactory results since 2012 (10, 14).

MWA and NSM share the common advantage of nipple and areola sparing, and they are technically feasible for small to moderate size BC if the tumor with no clinical nipple or skin involvement (15). However, ablation is more controversial for less of evidence-based medical research for decision-making. Especially for MWA with the advantage of high thermal efficacy and potentially strong deactivation for tumor compared with other thermal ablation methods, its clinical effectiveness is to be investigated urgently. Therefore, we performed this cohort study to investigate the efficacy of ultrasound-guided percutaneous MWA without surgery as a local treatment for BC and to comparatively assess the preliminary results of MWA and NSM for treating BC.

Abbreviations: MWA, microwave ablation; NSM, nipple sparing mastectomy; BC, breast cancer; US, ultrasound; SLN, sentinel lymph node; RFA, radiofrequency ablation; LTP, local tumor progression; TE, technique effectiveness; CEUS, contrast enhanced US; CEMRI, contrast enhanced magnetic resonance image; ALN, axillary lymph node; NPV, negative predictive value; CCI, Charlson comorbidity index.

MATERIALS AND METHODS

Study Design and Participants

The electronic clinical records system of our hospital was checked to collect all consecutive patients who underwent percutaneous MWA or NSM for BC between October, 2014 and May, 2020. This retrospective study was approved by the institutional review board of our hospital. All the patients provided written informed consent for treatment and the informed consent for data for publication was waived by the review board as no individual information would be explored. Data were monitored by two clinicians (HW and TL, with three and five years of experience in ablation, respectively) and a statistician (Y-CL, with three years of statistical experience).

Inclusion criteria for both two groups were women, with invasive ductal carcinoma with histologic confirmation, with tumor size ≤5cm, the distance from the tumor to the nipple ≥2cm, and with no direct tumor involvement of the nipple, areola, skin, and pectoralis on imaging or physical examination, and no extensive vascular carcinoma thrombus. In addition, for the NSM group, with no significant ptosis was required, and for the MWA group the tumor was clearly visible on US was required.

Exclusion criteria were patients who were pregnant or breastfeeding, imaging suspicion of multifocality or extensive intraductal carcinoma, and previous surgery, neoadjuvant or radiation therapy of the ipsilateral breast. All the patients in the MWA group were unresectable patients for comorbidities or patients who refused surgery. Patients who met all inclusion criteria and none of the exclusion criteria were enrolled in the study.

Pre-Procedure Evaluation

The pre-procedure evaluation and other research details are given in **Appendix E1**. Prior to the procedure the number and location of BC masses were evaluated by combination of conventional US, contrast enhanced US (CEUS), and magnetic resonance image (CEMRI). The data were analyzed by doctors JY (10-year experience in interventional radiology) and Z-yH (15-year experience in interventional radiology). Core needle biopsy was performed prior to the MWA to evaluate the pathological diagnosis of the BC and all the suspicious SLN and axillary lymph node (ALN) (based on CEUS and CEMRI) under US guidance.

Treatments

The treatment decision was made in consensus by a team of experienced radiologists, surgeons, and oncologists in BC. The patients who were poor surgical candidates or whose preference was minimal invasion would be arranged for MWA. NSM was performed under general anesthesia as previously described for patients who elected to undergo this procedure (4, 16). Following NSM, six patients chose no reconstruction, and 37 patients were performed 1-stage tissue expander placement and 2-stage implant reconstruction.

US-Guided MWA

US guidance was performed with a GE LOGIQ E9 scanner (GE Medical Systems US & Primary Care Diagnostics, Wauwatosa, USA) with 9.0 MHz Convex array transducer. The microwave unit (KY-2000, Kangyou Medical, Nanjing, China) is capable of producing 100 W of power at 2,450 MHz. The MWA procedure under local anesthesia and other study details are given in **Appendix E2**.

Management of Lymph Nodes

For NSM, SLN biopsy and/or ALN dissection were performed as well as the NSM incision. ALN dissection was based on the intraoperative frozen section examination of SLN. For MWA, all the histological positive SLNs and ALNs by biopsy were ablated with moving shot technique.

Follow-Up and Imaging Evaluation

For the MWA group, within 1–3 days after the procedure, conventional US, CEUS, and CEMRI were performed to evaluate the treatment efficacy. For both groups, conventional US was repeated for its convenience and cheapness to monitor breast at 3-month intervals during the first year after MWA or NSM and then at 6-month intervals thereafter. CEUS/MRI was performed for breast at 6-month intervals, and when US with suspicious breast lesions after MWA or NSM during follow-up (CEMRI was preferred for its accuracy in breast diagnosis, and CEUS was performed for the patients without MRI indications). Brain MRI/computed tomography, lung computed tomography, and emission computed tomography were performed for patients to evaluate systematic metastasis.

The definition of technical success and effectiveness was in **Appendix E3**. The cosmetic result was categorized as bad, moderate, good, or very good. The prespecified primary outcome measure was tumor progression (including LTP, ipsilateral breast recurrence, and systematic metastasis) evaluated according to biopsy and histological results. Prespecified secondary outcome measures were cancer specified survival, overall survival, cosmetic results, ablation volume reduction, and postoperative complications associated with the procedure and treatment.

STATISTICAL ANALYSIS

The two treatment modalities were compared for patient and tumor characteristics, treatment parameters, the risk of breast recurrence, distant metastasis, and survival. Differences for categorical variables between groups were analyzed with the chi-square test or Fisher test when the assumption of number of cases per cell in the contingency tables, multiplied by two, is not fulfilled and the Student t test or non-parametric Wilcoxon rank sum test for continuous variables. Multiple clinical variables were evaluated for their potential association with tumor progression using a Cox proportional hazards regression model in univariable and multivariable analyses. We excluded each non-significant parameter with a P-value > 0.05 to finally obtain significantly independent factors. Survival and tumor progression were analyzed using the Kaplan–Meier method and compared using the log-rank test. Statistical analysis was performed using Empower(R) (www.empowerstats.com, X&Y Solutions, Inc. Boston MA). All tests were two sided, with $P < 0.05$ considered statistically significant.

RESULTS

Patients

During the study period, 2,770 patients with BC were assessed for eligibility for this study (**Figure 1**). Among them, 64 were enrolled in the study (21 in the MWA group and 43 in the NSM group) and no patient was lost to follow-up. The overall mean age was 47.8 years (range, 22–90 years) for the overall patients, but the mean age of the MWA group was 24 years older than that of the NSM group. Baseline characteristics of the patients are presented in **Table 1**. There was a good consistence for the tumor size, number, location, and histological type among the baseline data, but inconsistence remained for age, menopausal status, and Charlson comorbidity index (17). The MWA group had significantly more elderly patients with more comorbidities.

Treatments

In the MWA group, 21 patients with 22 tumors received 25 session treatments. Nineteen nodules were successfully treated in one MWA session, and three nodules were in two sessions. Eighteen patients were treated by MWA for advanced age or poor surgical candidates with comorbidities and three patients for preference to minimal invasion. All the patients in the NSM group underwent one operation. Four patients were performed ablation of 18 SLN/ALNs. 43 patients in the NSM group were performed SLN biopsy and 10 patients were performed ALN dissection (total 43 positive ALN) (**Table 3**). After MWA and NSM, local radioactive and systemic adjuvant treatments were performed and described in **Table 2**. The MWA group had significantly less patients receiving adjuvant systemic treatment ($P = 0.03$) for intolerance.

All the patients achieved technical success, and the efficacy was evaluated by CEMRI/US (**Figure 2**). The operative time of the NSM group was significantly longer than that of the MWA group ($P < 0.001$). Estimated blood loss was more in the NSM group ($P < 0.001$), but no subjects in both groups needed blood transfusion treatment (**Table 3**).

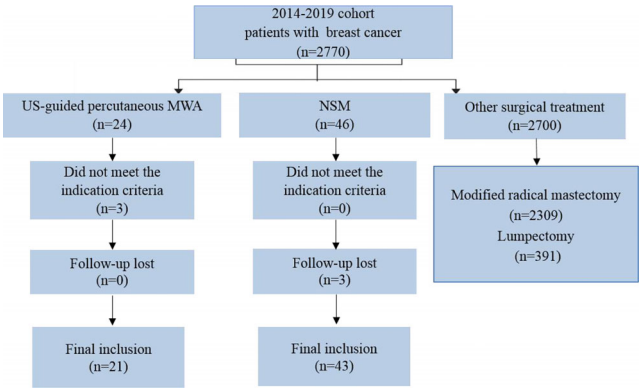

FIGURE 1 | Flow of study inclusion. A total of 2,770 patients were examined with breast cancer, and 64 patients with ≤5 cm tumors treated with US-guided percutaneous MWA or NSM were finally included. US, ultrasound; MWA, microwave ablation; NSM, nipple sparing mastectomy.

TABLE 1 | Baseline characteristics for patients in the study group.

Parameter	MWA	NSM	*P* value
Patients (n)	21	43	
Age (yr)	64.8 ± 16.0	39.4 ± 7.5	<0.001
	(33–90)	(22–55)	
Menopausal status (Y/N)	Mar-18	42/1	<0.001
Charlson comorbidity index	3.5(0–11)	0.1 (0–2)	<0.001
Mean max size (cm)	2.4 ± 1.3	2.3 ± 1.2	0.81
	(0.9–5.0)	(0.3–5.0)	
<2.0 cm	7 (33.3%)	18 (41.9%)	0.81
2.1–3.0 cm	9 (42.9%)	13 (30.2%)	
3.1–4.0 cm	3 (14.3%)	8 (18.6%)	
4.1–5.0 cm	2 (9.5%)	4 (9.3%)	
Tumor Number (%)			0.27
1	20 (95.2%)	37 (86.0%)	
2	1 (4.8%)	6 (14.0%)	
Tumor Location (%)			0.42
Left	9 (42.9%)	23 (53.5%)	
Right	12 (57.1%)	20 (46.5%)	
TNM Stage			0.32
T1N0M0	4 (19.0%)	12 (27.9%)	0.44
T1N1M0	6 (28.8%)	5 (11.6%)	0.09
T1N2M0	0 (0.0%)	2 (4.7%)	0.32
T2N0M0	9 (42.9%)	16 (37.2%)	0.66
T2N1M0	0 (0.0%)	4 (9.3%)	0.15
T2N2M0	2 (9.5%)	4 (9.3%)	0.98
Subrogate molecular subtype*			0.04
Luminal A	9 (42.9%)	7 (16.3%)	0.02
Luminal B			
HER2 negative	4 (19.0%)	24 (55.8%)	0.007
HER2 positive	3 (14.3%)	6 (14.0%)	1
HER2 enriched (nonluminal)	0 (0.0%)	2 (4.7%)	0.31
Triple negative	2 (9.5%)	2 (4.7%)	0.46
Undefined	3 (14.3%)	2 (4.7%)	0.19

Except where indicated, data are numbers of participants, with percentages in parentheses.
MWA, microwave ablation; NSM, nipple sparing mastectomy.
**Luminal A: estrogen receptor (ER) and progesterone receptor (PR) positive, Ki67 level <20%, and human epidermal growth factor receptor type 2 (HER2) negative.*
Luminal B (HER2 negative): ER positive and HER2 negative (PR < 20% or Ki67 ≥ 20%).
Luminal B (HER2 positive): ER and HER2 positive (PR < 20% or Ki67 ≥ 20%).
HER2 enriched (nonluminal): ER and PR negative and HER2 positive.
Triple negative: ER, PR, and HER2 negative.

TABLE 2 | Adjuvant treatment.

Parameter	MWA (*n* = 21)	NSM (*n* = 43)	*P* value
Adjuvant systemic therapy	7 (33.3%)	31 (72.1%)	0.03
Only endocrine therapy	2 (9.5%)	9 (20.9%)	0.33
Only chemotherapy	3 (14.3%)	9 (20.9%)	0.49
Endocrine therapy +Chemotherapy	2 (9.5%)	13 (30.2%)	0.008
Adjuvant radiation therapy	3 (14.3%)	7 (16.3%)	0.31
Only lymph node irradiation	1 (4.8%)	0 (0.0%)	0.15
Breast+ lymph node irradiation	2 (9.5%)	7 (16.3%)	0.47

Numbers are numbers of participants, with percentages in parentheses.
MWA, microwave ablation; NSM, nipple sparing mastectomy.

Recurrence and Survival

The median follow-up was 26.7 months (range, 14.6–62.5 months) for overall patients. Two patients were performed core needle biopsy for their MRI results showed suspicious tumor progression around the ablation zone but achieving negative pathological diagnosis. Totally, tumor progression occurred in five patients for the two groups, which achieved consistency between MRI and pathology. Among the 51 patients with MRI and follow-up assessment, the negative predictive value (NPV), specificity and sensitivity of MRI was 100% (95% confidence interval [CI], 88.7–96.1%), 95.8% (95% CI, 86–98.8%), and 100% (95% CI, 43.9–100%).

One patient was diagnosed as LTP (1/22, 4.5%) at 42 months after MWA. She refused detection of tumor molecular subtype and all adjuvant treatments for 94 years old. Then she died from pulmonary heart disease at 47 months after MWA. Another 78-year old patient with molecular subtype of triple negative was diagnosed with ipsilateral breast recurrence at 28 months after MWA. She didn't receive any treatment for fracture. No patient was diagnosed with contralateral breast or systemic recurrence in the MWA group during the follow-up. Another patient (81Y) died from cardiac arrest at 9 months after MWA. All the patients were alive in the NSM group, but one patient had ipsilateral breast recurrence at 31.2 months after NSM and was treated with mastectomy. Two patients had bone metastasis at 34 and 4 months after NSM and

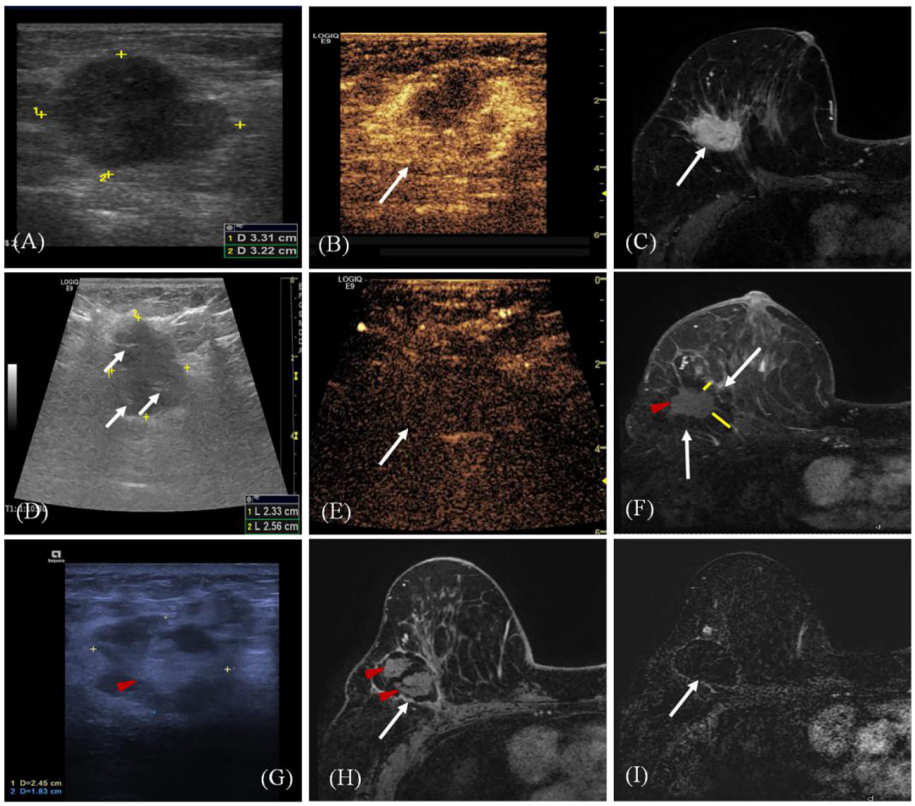

FIGURE 2 | A 68-year old woman with invasive ductal carcinoma of the right breast. **(A)** Ultrasound (US) scan before microwave ablation (MWA) shows the hypoechoic mass (arrow) with size of 3.3 cm × 3.2 cm. **(B)** Contrast-enhanced US before MWA shows the mass is hyper-enhanced (arrow) in arterial phase. **(C)** Transverse contrast-enhanced magnetic resonance imaging (MRI) shows hyperintensity masses (arrow) before MWA in arterial phase. **(D)** US scan shows the heterogeneously hypoechoic mass (marker) with size of 2.6 cm × 2.3 cm immediately after MWA (ghost size). Hyperechoic needle tracts can be seen in the ablated mass (arrow). **(E)** Contrast-enhanced US immediately after MWA shows the mass is non-enhanced (arrow) in arterial phase. (F) Contrast-enhanced MRI image shows hyperintensity ghost of mass (red arrow) and the peripheral hypointensity treatment zone (white arrow) in arterial phase three days after MWA. The ablation margin is from 1.2 to 2.2 cm (yellow lines) which can be measured in the hospital information system. **(G)** US scan shows the heterogeneously ablation zone (marker) shrinks to the size of 2.5 cm × 1.8 cm at 18 months after MWA. Ghost of mass (arrow) is surrounded by hypoechoic adipose tissue. **(H)** Contrast-enhanced MRI image shows treatment zone (white arrow) is non-enhanced with clear capsule and the central hyperintensity ghost of mass (red arrow) in arterial phase at 18 months after MWA. **(I)** MRI silhouette shows no signal for the ablation zone with clear fibrous capsule and margin (arrow).

were controlled stably by chemotherapy of docetaxel plus cyclophosphamide. They both had the molecular subtype of Luminal B. There was no difference in tumor progression and overall survival between the two groups (**Table 3**, **Figure 3**). There was no ALN and SLN progression in all the patients.

Univariate and Multivariable Analysis for Tumor Progression and Survival

On univariable analysis, age (hazard ratio (HR): 1.0; 95% CI: 1.0, 1.1; P = 0.05), CCI (HR: 1.7; 95% CI: 1.1, 2.6; P = 0.03), therapy method (HR: 17.3; 95% CI: 1.5, 204.3; P = 0.02), and menopausal (HR: 17.3; 95% CI: 1.5, 204.3; P = 0.02) demonstrated an association with tumor progression (**Table 4**). CCI (HR: 1.5; 95% CI: 1.0, 2.4; P = 0.04) demonstrated an association with overall survival (**Table S1**). However, we couldn't find an independent predictor of tumor progression or survival in multivariable analyses (**Table 4**, **Tables S1**, **S2**).

Volume Reduction of Ablation Zone

Because some ablated tumor ghosts were not clear in the US and MRI image after one month of MWA, we calculated the volume of tumor before MWA and ablation zone by using CEMRI or CEUS if MRI was not feasible (**Appendix E4**). Compared with that of one day after MWA, the 1, 6, and 12-month median volume reduction rate of ablation zone was 35% (0–56%), 56% (0–95%), and 67 (0–97%). Volume of ablation zone showed a rapid reduction during the first 6 months after MWA and then reached stability (**Table 5**, **Figure 4**).

Complications and Cosmetic Satisfaction

The safety of MWA and NSM appeared very good. Treatment was well tolerated, and there were no major complications and other adverse effects in all the patients (**Appendix E4**). For MWA, 100% of the patients reported excellent cosmetic satisfaction. For NSM, two (4.7%) patients reported bad

TABLE 3 | Postoperative outcomes and follow-up.

Parameter	MWA (*n* = 21)	NSM (*n* = 43)	*P* value
Postoperative hospitalization time (days)	2 (1–5)	4 (2–18)	<0.001
Operative time (min)	29.9 (23.7–69.2)	130 (53–275)	<0.001
Estimated blood loss (ml)	2.0 ± 0.5	139.0 ± 100.0 (20–600)	<0.001
Fever >38> (%)	0 (0.0%)	1 (2.4%)	0.48
Major complication (%)	0 (0.0%)	0 (0.0%)	>0.99
Follow-up (mons)	15.7 (5.0–47.1)	19 (4.6–58.5)	0.51
All cause death (%)	2 (9.6%)	0 (0.0%)	0.197
BC related death (%)	0 (0.0%)	0 (0.0%)	>0.99
LTP (%)	1 (4.8%)	0 (0.0%)	0.15
Isiplateral breast recurrence (%)	1 (4.8%)	1 (2.3%)	0.16
Systemic metastasis (%)	0 (0.0%)	1 (2.4%)	0.48
Costs (RMB)	25,223.5 (17,663.7–41,722.1)	22,586.5 (13,285.7–37,297.3)	0.23
Number of ablated/ resected lymph nodes	0.9 (0–7)	1.3 (0–12)	0.51
Cosmetic satisfaction			<0.001
Bad (%)	0 (0.0%)	1 (2.4%)	
Moderate (%)	0 (0.0%)	10 (23.8%)	
Good (%)	0 (0.0%)	30 (71.4%)	
Very good (%)	21 (100.0%)	1 (2.4%)	

MWA, microwave ablation; NSM, nipple sparing mastectomy.

TABLE 4 | Univariable and multivariable analyses of predictors of tumor progression after treatment.

Parameter	Univariable		Multivariable	
	HR (95%CI)	*P* Value	HR (95%CI)	*P* Value
Age (yr)	1.0 (1.0, 1.1)	0.05	0.9 (0.6,1.4)	0.69
Tumor size (cm)	0.8 (0.3, 2.1)	0.67	1.0 (0.1, 9.0)	0.99
Comorbidity Index	1.7 (1.1, 2.6)	0.03	1.5 (0.4,5.4)	0.49
Therapy method				
NSM	1		1	
MWA	17.3 (1.5, 204.3)	0.02	1.0 (1.0, 1.0)	NA
Menopausal				
No	1		1	
Yes	17.3 (1.5, 204.3)	0.02	81.0 (0.0, inf.)	0.68
Postoperative Chemotherapy				
No	1			
Yes	1.8 (0.1, 30.8)	0.69		
Postoperative Radiotherapy				
No	1			
Yes	0.0 (0.0, inf)	0.99	.	
Postoperative Endocrinotherapy				
No	1			
Yes	0.0 (0.0, inf)	0.99		

cosmetic satisfaction, and 10 (23.3%) patients with moderate cosmetic satisfaction (**Table 3**).

DISCUSSION

Different from previous studies mainly focusing on ablation of BC ≤2.0 cm, our study enrolled patients with BC ≤5.0 cm because 12 (12/21, 57.1%) patients with the age older than 65 years had tumors 2.0–5.0 cm, and they lost the chance of surgery for comorbidities. Although few patients received adjuvant treatments for the old age in the MWA group, tumor progression including breast recurrences and distant metastatic recurrences has no significant difference during median 26.7 months follow-up. The only LTP patient was treated as the first case with small BC (max diameter 1.1 cm) in the MWA group, so the LTP might be attributed to the problem of limited experience to enlarge the ablation zone at the beginning of the technique, and the 94-year old patient without the chance of MRI evaluation. The favorable efficacy of MWA was better cosmetic satisfaction and less invasion with local anesthesia, shorter

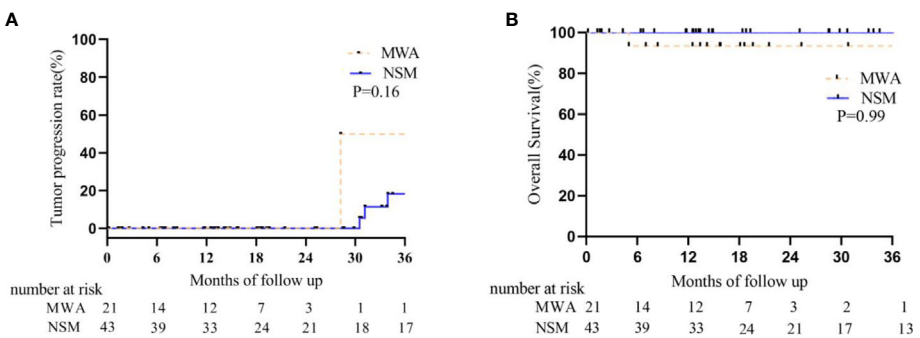

FIGURE 3 | Kaplan–Meier estimates for tumor progression and survival between BC patients who underwent MWA and NSM. **(A)** Tumor progression rate. The 1-, 2-, and 3-year intra- and extra-breast recurrence rate were 0, 0, 50% in the MWA group and 0, 0, 18.3% in the NSM group, respectively (P = 0.08). **(B)** Cumulative overall survival rate. The 1-, 2-, and 3-year overall survival rate were 93.3, 93.3, 93.3% in the MWA group and 100, 100, 100% in the NSM group, respectively (P = 0.99).

hospitalization time and operative time, and only means 2 ml blood loss. The clinical advantage was evident when the results of the two treatment groups were analyzed in ≤5.0 cm BC patients.

The treatment for early BC has evolved significantly since the past decade. Several randomized clinical trials have clarified a similar survival outcome between breast-conserving therapy and mastectomy (18–20). NSM is deemed as an extension of breast-conserving surgery. It is considered appropriate and oncologically safe if patients are carefully selected based on the long lasting literature data (19, 21, 22). A large number of studies have investigated RFA of BC followed by surgical resection and confirmed a high occurrence of complete tumor necrosis ranging from 80 to 100% (23). However, the evaluation of curative efficacy of ablation without subsequent surgical excision is very limited, and the comparative data from ablation alone *versus* surgery are absent.

MWA is a relatively new technique for BC with advantages of higher thermal efficiency and the potential for more complete inactivation of the tumor. The preliminary results showed 95% of patients with BC <3.0 cm could achieve complete tumor coagulation after MWA confirmed by microscopic examination (14). However, apart from BC <3.0 cm, unresectable larger tumors in senile patients were to be treated urgently by less invasive techniques. Therefore, according to our knowledge, we performed the first study comparing the ablation of BC ≤5.0 cm without subsequent excision with NSM. Both techniques are nipple sparing modalities.

The evaluation for tumor necrosis depended on the CEMRI/CEUS in all the patients who underwent MWA in our study. Pathological findings by core needle biopsy were performed only if there were suspicious lesions on image. MRI is a sensitive image for diagnosis of the breast lesion (24). It has been used to predict tissue damage after BC ablation, and previous studies suggested MRI was suitable for long-term follow-up of ablation of BC with a NPV of 92.2–97.7% (25–27). MRI evaluated the efficacy of MWA with the NPV of 100% and specificity of 95.8% in our study. And CEUS provided a good auxiliary check for 13 patients without MRI indications in our study.

According to the latest report from systematic review of imaging-guided percutaneous ablation of 1,168 BCs with the mean size from 11 to 31 mm, pooled technical success was 96% (95% CI 94–97%) and pooled TE was 75% (67–81%). RFA showed the best TE of 82% (95% CI 74–88%) and followed by

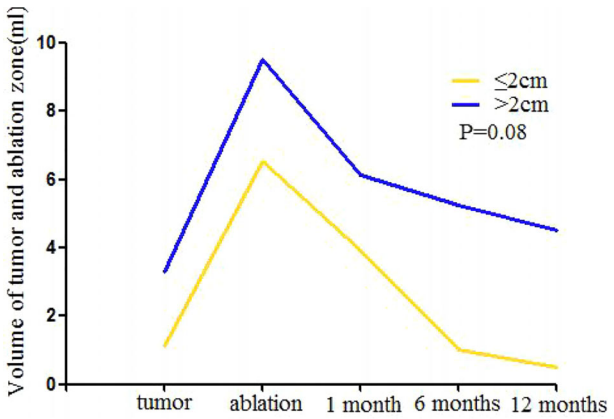

FIGURE 4 | Mean volume of mass ≤ 2.0cm and >2.0cm at baseline (time of MWA) and at follow-up after treatment. One month after MWA the increased volume shows the enlarged ablation zone compared with index mass. The ablation area will shrink significantly during the 6 months after MWA and then reach stability gradually for both groups. After 6 months, the volume of mass ≤ 2.0 cm reached the level of before MWA, the volume of mass >2.0 cm was larger than the index mass continuously. There is no significant difference between two groups in volume reduction after MWA (P = 0.08).

TABLE 5 | Volume change of tumor and ablation zone.

	Tumor volume (ml)	volume of ablation zone (ml)	*P* value (compared with baseline)	*P* value (compared with immediately)	*P* value (compared with 1 month)	P value (compared with 6 months)
All tumors						
Baseline	2.1 (0.4–13.0)					
Immediately after MWA	NA	7.8 (0.5–64.7)	0.001			
1 month after MWA	NA	4.8 (0.5–51.6)	0.01	0.03		
6 months after MWA	NA	2.3 (0.2–9.1)	0.59	0.005	0.05	
12 months after MWA	NA	1.7 (0.2–6.1)	0.26	0.001	0.02	0.29
Tumor ≤2cm						
Baseline	1.1 (0.4–3.0)					
Immediately after MWA	NA	6.5 (0.5–14.5)	0.008			
1 month after MWA	NA	3.9 (0.5–9.8)	0.01	0.07		
6 months after MWA	NA	1.0 (0.2–9.1)	0.47	0.02	0.06	
12 months after MWA	NA	0.5 (0.2–5.6)	0.31	0.01	0.04	0.3
Tumor>2cm						
Baseline	3.3 (1.6–13.0)					
Immediately after MWA	NA	9.5 (1.8–64.7)	0.005			
1 month after MWA	NA	6.1 (0.8–51.6)	0.01	0.04		
6 months after MWA	NA	5.2 (1.6-–8.8)	0.53	0.03	0.34	
12 months after MWA	NA	4.5 (4.2–4.8)	0.35	0.02	0.26	0.6

NA, not available for some ablated lesions were not clear in image.

cryoablation, LA, and HIFU only with 49% (95% CI 26–74). And the study concluded tumor size did not influence the TE. According to another meta-analysis including 15 clinical trials to assess the effect of RFA of BC with a total of 404 patients, pooled results showed that 89% of patients achieved TE, and several studies reported the LTP ranging from 1.37 to 14.29%. Compared with other ablation techniques, MWA of BC ≤5.0 cm achieved 100% TE and 4.5% LTP in our study, which was even superior to the previous report of ablation of <3.0 cm BC. Furthermore, the present results were from MWA of BC with relatively long follow-up information.

Just as NSM, ablation is a modality with nipple and areola sparing while with less invasion. According to this pilot study, two relatively new techniques for BC achieved similar effect. MWA used the technique by combining moving shot with fixed ablation, which showed the potential to completely eradicate the tumors with safety margin >1cm. And CEMRI/CEUS was the key image to improve the effect of MWA. Three nodules achieved complete ablation in the second session by MRI evaluation with residual tumor after the first MWA session, and totally 18 malignant lymph nodes in four patients were successfully ablated under CEUS and MRI evaluation. Certainly, this led to the slightly higher cost of MWA than that of NSM.

LIMITATION

Our study has some limitations. First, we used a cohort approach, and this was a single center retrospective study with only limited participating patients and follow-up, which might lead to bias of results. Second, the margin status and tumor cell viability after MWA were not evaluated by surgery. We performed CEMRI and CEUS to improve diagnosis accuracy, which need to accumulate the experience for future ablation evaluation without surgery. Third, we only performed percutaneous biopsy for suspicious SLN and ALN on image because of patients' refusal for surgery, which might potentially lead to positive lymph nodes missing. In conclusion, US guided percutaneous MWA and NSM seem to provide similar results for BC, with a favorable success rate and low risk of major complications. MWA could be considered as an alternative minimal-invasive treatment in early stage BC and in the elderly cases considered unfit for surgery. However, this warrants further investigation.

DATA AVAILABILITY STATEMENT

All datasets presented in this study are included in the article/ **Supplementary Material**.

ETHICS STATEMENT

The studies involving human participants were reviewed and approved by Chinese PLA General Hospital. The patients/ participants provided their written informed consent to participate in this study.

AUTHOR CONTRIBUTIONS

JY, PL and J-dW have full access to all of the data in the study and take responsibility for the integrity of the data and the accuracy of the data analysis. PL, JY, and J-dW contributed to the conception and design of the study. PL, JY, Z-yH, TL, HW, and JJ finished the acquisition of data. JY, Y-cL, and W-zF performed the statistical analysis and interpretation. JY wrote the draft of the manuscript. PL and J-dW finished the critical revision of the manuscript for important intellectual content. All authors contributed to the article and approved the submitted version.

SUPPLEMENTARY MATERIAL

The Supplementary Material for this article can be found online at: https://www.frontiersin.org/articles/10.3389/fonc.2020.546883/full#supplementary-material

REFERENCES

1. Bray F, Ferlay J, Soerjomataram I, Siegel RL, Torre LA, Jemal A. Global cancer statistics 2018: GLOBOCAN estimates of incidence and mortality worldwide for 36 cancers in 185 countries. *CA: Cancer J Clin* (2018) 68:394–424. doi: 10.3322/caac.21492
2. De La Cruz L, Blankenship SA, Chatterjee A, Geha R, Nocera N, Czerniecki BJ, et al. Outcomes After Oncoplastic Breast-Conserving Surgery in Breast Cancer Patients: A Systematic Literature Review. *Ann Surg Oncol* (2016) 23:3247–58. doi: 10.1245/s10434-016-5313-1
3. van Maaren MC, de Munck L, de Bock GH, Jobsen JJ, van Dalen T, Linn SC, et al. 10 year survival after breast-conserving surgery plus radiotherapy compared with mastectomy in early breast cancer in the Netherlands: a population-based study. *Lancet Oncol* (2016) 17:1158–70. doi: 10.1016/s1470-2045(16)30067-5
4. Zarba Meli E, Cattin F, Curcio A, Manna E, Samorani D, Tognali D, et al. Surgical delay may extend the indications for nipple-sparing mastectomy: A multicentric study. *Eur J Surg Oncol* (2019) 45:1373–7. doi: 10.1016/j.ejso.2019.02.014
5. Fleming MM, Holbrook AI, Newell MS. Update on Image-Guided Percutaneous Ablation of Breast Cancer. *AJR Am J Roentgenol* (2017) 208:267–74. doi: 10.2214/ajr.16.17129
6. Brem RF. Radiofrequency Ablation of Breast Cancer: A Step Forward. *Radiology* (2018) 289:325–6. doi: 10.1148/radiol.2018181784
7. Harries SA, Amin Z, Smith ME, Lees WR, Cooke J, Cook MG, et al. Interstitial laser photocoagulation as a treatment for breast cancer. *Br J Surg* (1994) 81:1617–9. doi: 10.1002/bjs.1800811118
8. Lanza E, Palussiere J, Buy X, Grasso RF, Beomonte Zobel B, Poretti D, et al. Percutaneous Image-Guided Cryoablation of Breast Cancer: A Systematic Review. *J Vasc Interv Radiol JVIR* (2015) 26:1652–1657.e1651. doi: 10.1016/j.jvir.2015.07.020
9. Peek MC, Ahmed M, Napoli A, ten Haken B, McWilliams S, Usiskin SI, et al. Systematic review of high-intensity focused ultrasound ablation in the treatment of breast cancer. *Br J Surg* (2015) 102:873–882; discussion 882. doi: 10.1002/bjs.9793

10. Zhou W, Jiang Y, Chen L, Ling L, Liang M, Pan H, et al. Image and pathological changes after microwave ablation of breast cancer: a pilot study. *Eur J Radiol* (2014) 83:1771–7. doi: 10.1016/j.ejrad.2014.06.015
11. Giorgio A, Gatti P, Montesarchio L, Merola MG, Amendola F, Calvanese A, et al. Microwave Ablation in Intermediate Hepatocellular Carcinoma in Cirrhosis: An Italian Multicenter Prospective Study. *J Clin Trans Hepatol* (2018) 6:251–7. doi: 10.14218/jcth.2018.00013
12. Liang P, Yu J, Yu XL, Wang XH, Wei Q, Yu SY, et al. Percutaneous cooled-tip microwave ablation under ultrasound guidance for primary liver cancer: a multicentre analysis of 1363 treatment-naive lesions in 1007 patients in China. *Gut* (2012) 61:1100–1. doi: 10.1136/gutjnl-2011-300975
13. Yu J, Liang P, Yu X, Liu F, Chen L, Wang Y. A comparison of microwave ablation and bipolar radiofrequency ablation both with an internally cooled probe: results in ex vivo and in vivo porcine livers. *Eur J Radiol* (2011) 79:124–30. doi: 10.1016/j.ejrad.2009.12.009
14. Zhou W, Zha X, Liu X, Ding Q, Chen L, Ni Y, et al. US-guided percutaneous microwave coagulation of small breast cancers: a clinical study. *Radiology* (2012) 263:364–73. doi: 10.1148/radiol.12111901
15. Cil TD, McCready D. Modern Approaches to the Surgical Management of Malignant Breast Disease: The Role of Breast Conservation, Complete Mastectomy, Skin- and Nipple-Sparing Mastectomy. *Clinics Plast Surg* (2018) 45:1–11. doi: 10.1016/j.cps.2017.07.002
16. Smith BL, Coopey SB. Nipple-Sparing Mastectomy. *Adv Surg* (2018) 52:113–26. doi: 10.1016/j.yasu.2018.03.008
17. Charlson ME, Pompei P, Ales KL, MacKenzie CR. A new method of classifying prognostic comorbidity in longitudinal studies: development and validation. *J Chronic Dis* (1987) 40:373–83. doi: 10.1016/0021-9681(87)90171-8
18. Jacobson JA, Danforth DN, Cowan KH, d'Angelo T, Steinberg SM, Pierce L, et al. Ten-year results of a comparison of conservation with mastectomy in the treatment of stage I and II breast cancer. *New Engl J Med* (1995) 332:907–11. doi: 10.1056/nejm199504063321402
19. Romanoff A, Zabor EC, Stempel M, Sacchini V, Pusic A, Morrow M. A Comparison of Patient-Reported Outcomes After Nipple-Sparing Mastectomy and Conventional Mastectomy with Reconstruction. *Ann Surg Oncol* (2018) 25:2909–16. doi: 10.1245/s10434-018-6585-4
20. Veronesi U, Salvadori B, Luini A, Banfi A, Zucali R, Del Vecchio M, et al. Conservative treatment of early breast cancer. Long-term results of 1232 cases treated with quadrantectomy, axillary dissection, and radiotherapy. *Ann Surg* (1990) 211:250–9.
21. Ashikari AY, Kelemen PR, Tastan B, Salzberg CA, Ashikari RH. Nipple sparing mastectomy techniques: a literature review and an inframammary technique. *Gland Surg* (2018) 7:273–87. doi: 10.21037/gs.2017.09.02
22. Galimberti V, Morigi C, Bagnardi V, Corso G, Vicini E, Fontana SKR, et al. Oncological Outcomes of Nipple-Sparing Mastectomy: A Single-Center Experience of 1989 Patients. *Ann Surg Oncol* (2018) 25:3849–57. doi: 10.1245/s10434-018-6759-0
23. Chen J, Zhang C, Li F, Xu L, Zhu H, Wang S, et al. A meta-analysis of clinical trials assessing the effect of radiofrequency ablation for breast cancer. *OncoTargets Ther* (2016) 9:1759–66. doi: 10.2147/ott.S97828
24. Saadatmand S, Geuzinge HA, Rutgers EJT, Mann RM, de Roy van Zuidewijn DBW, Zonderland HM, et al. MRI versus mammography for breast cancer screening in women with familial risk (FaMRIsc): a multicentre, randomised, controlled trial. *Lancet Oncol* (2019) 20:1136–47. doi: 10.1016/s1470-2045(19)30275-x
25. Machida Y, Shimauchi A, Igarashi T, Fukuma E. MRI Findings After Cryoablation of Primary Breast Cancer Without Surgical Resection. *Acad Radiol* (2019) 26:744–51. doi: 10.1016/j.acra.2018.07.012
26. Schwartzberg B, Lewin J, Abdelatif O, Bernard J, Bu-Ali H, Cawthorn S, et al. Phase 2 Open-Label Trial Investigating Percutaneous Laser Ablation for Treatment of Early-Stage Breast Cancer: MRI, Pathology, and Outcome Correlations. *Ann Surg Oncol* (2018) 25:2958–64. doi: 10.1245/s10434-018-6623-2
27. Yoshinaga Y, Enomoto Y, Fujimitsu R, Shimakura M, Nabeshima K, Iwasaki A. Image and pathological changes after radiofrequency ablation of invasive breast cancer: a pilot study of nonsurgical therapy of early breast cancer. *World J Surg* (2013) 37:356–63. doi: 10.1007/s00268-012-1820-9

Conflict of Interest: The authors declare that the research was conducted in the absence of any commercial or financial relationships that could be construed as a potential conflict of interest.

frontiers in Oncology

ORIGINAL RESEARCH
published: 16 October 2020
doi: 10.3389/fonc.2020.553556

Ten-Year Outcomes of Percutaneous Radiofrequency Ablation for Colorectal Cancer Liver Metastases in Perivascular vs. Non-Perivascular Locations: A Propensity-Score Matched Study

Binbin Jiang[1], Hongjie Luo[2], Kun Yan[1], Zhongyi Zhang[1], Xiaoting Li[3], Wei Wu[1], Wei Yang[1] and Minhua Chen[1]*

[1] Key Laboratory of Carcinogenesis and Translational Research (Ministry of Education/Beijing), Department of Ultrasound, Peking University Cancer Hospital & Institute, Beijing, China, [2] Department of Hepatobiliary, Pancreatic and Minimally Invasive Surgery, Zhengzhou Central Hospital Affiliated to Zhengzhou University, Zhengzhou, China, [3] Key Laboratory of Carcinogenesis and Translational Research (Ministry of Education/Beijing), Department of Radiology, Peking University Cancer Hospital & Institute, Beijing, China

OPEN ACCESS

Edited by:
Freimut Dankwart Juengling, Universität Bern, Switzerland

Reviewed by:
Paulo Herman, University of São Paulo, Brazil
Kumar Pichumani, Houston Methodist Research Institute, United States

***Correspondence:**
Kun Yan
ydbz@vip.sina.com

Specialty section:
This article was submitted to Cancer Imaging and Image-directed Interventions, a section of the journal Frontiers in Oncology

Received: 19 April 2020
Accepted: 25 September 2020
Published: 16 October 2020

Citation:
Jiang BB, Luo HJ, Yan K, Zhang ZY, Li XT, Wu W, Yang W and Chen MH (2020) Ten-Year Outcomes of Percutaneous Radiofrequency Ablation for Colorectal Cancer Liver Metastases in Perivascular vs. Non-Perivascular Locations: A Propensity-Score Matched Study. Front. Oncol. 10:553556. doi: 10.3389/fonc.2020.553556

Purpose: To compare long-term outcomes of percutaneous radiofrequency ablation for colorectal liver metastases in perivascular versus non-perivascular locations.

Methods: This retrospective study included 388 consecutive patients with colorectal liver metastases (246 men, 142 women; age range 27–86 years) who underwent percutaneous radiofrequency ablation between January 2006 and December 2018. Propensity-score matching was performed for groups with perivascular and non-perivascular colorectal liver metastases. Rates of accumulative local tumor progression, overall survival, intra/extrahepatic recurrence, and complications were compared between the two groups.

Results: We successfully matched 104 patients each in the perivascular and non-perivascular groups (mean age: 60.1 ± 11.5 and 60.1 ± 11.3 years, respectively). Cumulative local tumor progression rates at 6 months, 1 years, 3 years, and 5 years, respectively, were 8.8%,14.8%, 18.9%, and 18.9% in the perivascular group and 8.8%, 13.1%, 15.5%, and 15.5% in the non-perivascular group. The 1-, 3-, 5-, and 10-year overall survival rates, respectively, were 91.3%, 45.6%, 23.9%, and 18.7% in the perivascular group and 88.0%, 47.2%, 27.2%, and 22.6% in the non-perivascular group. No significant between-group differences were detected in cumulative local tumor progression (p=0.567, hazard ratio: 1.224) or overall survival (p = 0.801, hazard ratio: 1.047). The major complication rate was 1.0% (1/104, p > 0.999) in both groups. Tumor size was the only independent prognostic factor for local tumor progression

(hazard ratio: 2.314; p = 0.002). On multivariate analysis for overall colorectal liver metastases, tumor diameter >3 cm, tumor location in the right colon, multiple tumors, and extrahepatic metastases before radiofrequency ablation (hazard ratios: 2.046, 1.920, 1.706, and 1.892, respectively; all $p < 0.001$) and intrahepatic recurrence (hazard ratio: 1.564; p = 0.002) were associated with poor overall survival.

Conclusion: Cumulative local tumor progression, overall survival, and major complications rates did not differ significantly between perivascular and non-perivascular colorectal liver metastases after percutaneous radiofrequency ablation. For perivascular colorectal liver metastases, percutaneous radiofrequency ablation is a safe and effective treatment option.

Keywords: colorectal cancer, liver metastases, perivascular locations, radiofrequency ablation, treatment outcome

INTRODUCTION

The liver is the most frequent site of metastases from colorectal cancer (1), and surgical resection is a standard treatment for colorectal liver metastases (CLM). However, only 10–20% of patients with CLM are eligible for tumor resection due to high tumor burden and clinical complications (2). The National Comprehensive Cancer Network (NCCN)guidelines and European Society for Medical Oncology (ESMO) consensus guidelines recommended ablation as a local curative option for patients with metastatic colorectal cancer to the degree that all visible tumors can be eradicated (3, 4). Radiofrequency ablation (RFA) is an effective treatment in patients with CLM and can achieve high local control rates (5, 6). RFA finds widespread application for liver cancer due to its safety and low rate of major complications (1.3–7%) (6–8).

Tumor location close to the subcapsular region, diaphragm, gastrointestinal tract, and large blood vessels (9, 10) may be a key factor affecting ablation results because it may not permit a sufficient ablative margin and potentially influence tumor necrosis, resulting in high rates of local tumor progression (LTP). In addition, a randomized phase II trial study demonstrated that aggressive RFA treatment can prolong overall survival (OS) in patients with unresectable CLM (11).

The therapeutic outcome of RFA for liver tumors near large blood vessels remains controversial (12–15). A study reported (12) that perivascular location was a prognostic factor in patients with CLM who underwent RFA; perivascular location was associated with higher LTP rates, possibly attributable to the heat sink effect wherein blood flow dispels thermal energy away from the targeted tissue, leading to a reduced coagulation volume and an inadequate ablation margin (16). However, inconsistent conclusions have been reported in the literature; one study reported that RFA for CLM close to large hepatic vessels was safe and effective, perivascular location was not a risk factor for LTP (13). Furthermore, no guidelines are available for RFA for the treatment of perivascular CLM.

This study aimed to use propensity-score matching to compare the long-term outcomes of percutaneous RFA for perivascular and non-perivascular CLM and to identify the risk factors of patients with CLM underwent percutaneous RFA.

MATERIALS AND METHODS

Patient Selection

The institutional review board of the hospital approved this study, and the requirement for informed consent was waived because of the retrospective study design. Between January 2006 and December 2018, 452 patients with CLM were treated with ultrasound-guided RFA in our hospital. Of these, we identified 388 consecutive patients (mean age: 59.4 ± 11.0 years, range: 27–86) with CLM who underwent percutaneous RFA, either determined by a consensus of a multidisciplinary team or who refused surgery, were enrolled in the study. The eligibility criteria included: (a) tumor size ≤ 5 cm in diameter and the number of liver metastases ≤ 9; (b) conventional ultrasound or contrast-enhanced ultrasonography (CEUS) showing hepatic metastasis and treatment with percutaneous RFA under US-guidance; (c) absence of uncontrolled extrahepatic disease; (d) normal coagulation status and a liver function Child-Pugh A and B; (e) reported technical effectiveness of RFA; and (f) > 12-month follow-up. Exclusion criteria: (a) significant direct tumor invasion of adjacent organs or tumor thrombi in the main or lobar portal system; (b) the distance between the tumor and the first-level branch of the bile duct (common liver duct, left and right liver ducts) is ≤ 0.5cm; and (c) patients with serious diseases, such as congestive heart failure, myocardial infarction, and stroke in the past 6 months (**Figure 1**).

Definition of Perivascular CML

In the absence of a standard definition, we defined a perivascular hepatic tumor as an index tumor having any contact with the first- or second-degree branches of a portal or hepatic vein (13, 15), with an axial diameter ≥ 3 mm (based on previous experimental and clinical studies) (17, 18).

If the index tumor was located near more than one large vessel, the largest vessel was selected as the reference vessel. Pre-treatment computed tomography (CT) or magnetic resonance

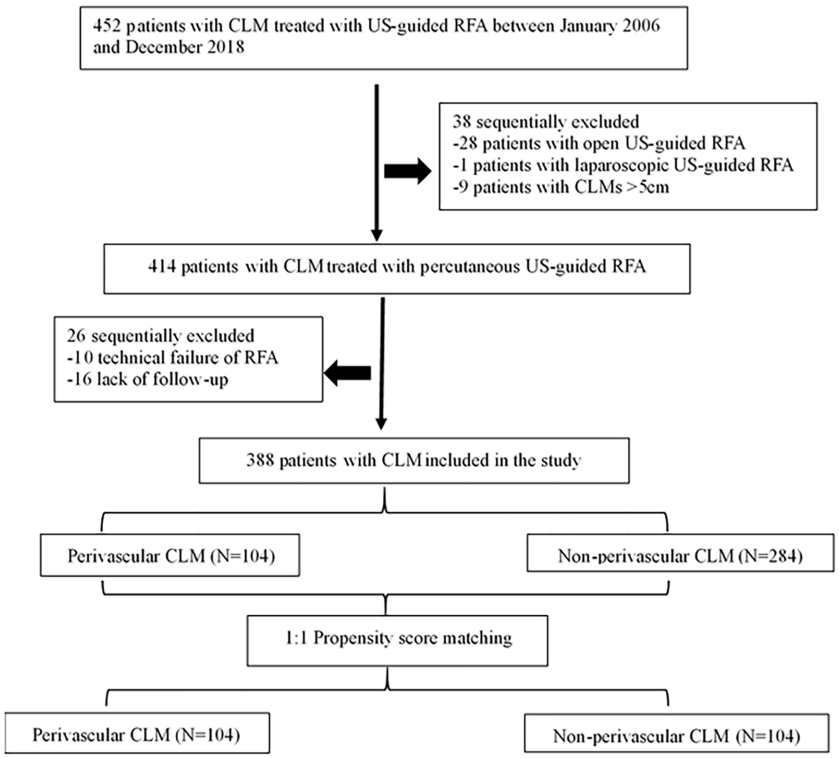

FIGURE 1 | Flow diagram of patient selection for the study. CLM, colorectal liver metastases; US-guided, ultrasound-guided; RFA, radiofrequency ablation.

imaging (MRI) results were reviewed by blinded radiologists with > 5 years of experience. All tumors were retrospectively categorized into the perivascular or non-perivascular group.

RFA Procedure

Prior to RFA, all patients underwent US or enhanced US to assess the feasibility of US-guided percutaneous RFA. The treatment plan was determined by least three experts on RFA, according to the clinical conditions. All RFA procedures were conducted under real-time US guidance by four radiologists (CMH, YK, WW, and YW) who had > 10 years of experience in US-guided interventional procedures. For tumors abutting large vessels, treatment protocols were similar to the protocols that have been previously reported (19). All ablations were undertaken using the available RFA system: Celon Lab Power ablation system (Olympus, Germany); the Valleylab system (Tyco Healthcare, North Haven, CT); or the RITA Model 1500x ablation system (AngioDynamics, Latham, NY), according to the manufacturer's instructions. Real-time ultrasound systems, Aloka ultrasound systems (Alokaα-10, Tokyo, Japan) or GE systems (E9, GE, United States), were used for scanning the lesion with 3.5–5.0 MHz convex probes and needle-guide devices for RFA procedures. As previously described (20), one physician located and guided the lesions in real time, while another inserted the electrode needle into the tumor. Most RFA devices can create an ablation sphere with a maximum diameter of 5 cm in the liver, but when the tumor diameter exceeds 3 cm, a strategy involving multiple overlapping ablations is employed (21). The post-RFA follow-up included routine tracking of the ablated lesions.

Follow-Up and Outcomes

Within a month before performing RFA, enhanced CT or MRI and US of the abdomen were conducted. At 1month post-RFA, enhanced CT was performed to determine lesion persistence to evaluate the effectiveness of RFA. For follow-up, patients were examined with contrast-enhanced US, enhanced CT, or MRI every 3 months in the first 2 years after RFA and every 6 months thereafter. The following definitions used in our study are based on the standardization recommended by the International Working Group on Image-Guided Tumor Ablation (22). Technical effectiveness referred to the ablation area completely covering the tumor during the first enhanced imaging follow-up 1month post-RFA. LTP was defined as the appearance of new lesions at the edge of the ablation zones wherein the RFA had been technically effective. OS was calculated from the start of ablation treatment to death or the last follow-up. Intrahepatic recurrence was defined as a lesion with characteristics similar to those of the primary lesion but without contact with the original ablation zone in the liver. A major complication was an event

that led to substantial morbidity and disability, increased the level of care, resulted in hospital admission, or lengthened hospital stay.

Statistical Analysis

To reduce the effect of selection bias and baseline imbalances between the perivascular and non-perivascular groups, we performed propensity-score matching for the clinical characteristics of each group based on each patient's propensity-score, which was estimated *via* logistic regression (23). The caliper value was 0.02 to performed propensity-score matching. Standardized mean differences of <0.10 indicated minute differences. Variables including age, sex, tumor size, primary location, T stage, lymph node metastases, time to liver metastases, number of liver metastases, history of resection for liver metastases pre-RFA, and extrahepatic metastases achieved the balance between the perivascular and non-perivascular groups after propensity-score matching.

The Wilcoxon rank sum test or independent *t*-test was used for continuous variables, and the chi-square test or Fisher exact test was used for categorical variables. The rates of LTP, OS, and intrahepatic and extrahepatic recurrence were estimated by the Kaplan–Meier method with the log-rank test. Univariate and multivariate analyses of all data were carried out using a Cox proportional hazards regression model for LTP and OS. Statistical analyses were conducted using SPSS 22.0 (SPSS Inc., Chicago, IL) and R version 2.15.x (R Foundation for Statistical Computing, Vienna, Austria). Differences with a p value < 0.05 were considered statistically significant.

RESULTS

Baseline Characteristics

Baseline characteristics of all CLM patients (n = 388; mean age: 59.4 ± 11.0 years, range: 27–86) and lesions (n = 388; mean size: 2.4 ± 1.0 cm, range: 0.6–4.9 cm) are presented in **Table 1**. The median follow-up period was 45.0 (range: 0–161) months for CLM. At the first enhanced imaging follow-up that was performed 1-month post-RFA, the rate of technical effectiveness was 97.6% (404/414) for CLM treated with RFA. The perivascular group showed higher proportions of primary left colon lesions (88.5% vs. 78.9%; p = 0.031) and male patients (72.1% vs. 60.2%; p = 0.031) than the non-perivascular group. The baseline characteristics were well balanced between the two groups (**Table 1**).

Comparison of Outcomes Before Propensity-Score Matching

LTP and OS

During follow-up, LTP occurred in 18 of 104 patients (17.3%) in the perivascular group and 42 of 284 patients (14.8%) in the non-perivascular group (p = 0.543). Moreover, 38.9% (7/18) of patients with LTP were treated with RFA and 44.4% (8/18)

TABLE 1 | Demographic and clinical characteristics of patients with colorectal liver metastases (CLM).

Variable	Perivascular	Before Matching			After Matching		
		Non-perivascular	*p*	St.MD	Non-perivascular	*p*	St.MD
	(n = 104)	(n =284)	Value		(n = 104)	Value	
Age at enrollment (year)*	60.14 ± 11.51	59.14 ± 10.86	0.427	0.091	60.11 ± 11.25	0.981	0.060
No. of men	75(72.1)	171(60.2)	0.031	0.264	75(72.1)	1.000	0.000
Tumor size (cm)+	2.3(1.8–3.2)	2.2(1.6-3.0)	0.157	0.111	2.4(1.8–3.2)	0.827	0.043
≤3cm	75(72.1)	219(77.1)	0.309			73(70.2)	0.760
>3cm	29(27.9)	65(22.9)				31(29.8)	
Primary location			0.031	0.299		1.000	0.000
Right colon	12(11.5)	60(21.1)				12(11.5)	
Left colon	92(88.5)	224(78.9)				92(88.5)	
T3-4 stage	99(95.2)	272(95.8)	0.783	0.027	98(94.2)	0.757	0.045
Lymph node metastasis	82(78.8)	204(71.8)	0.164	0.171	84(80.8)	0.730	0.047
Synchronous liver metastasis	57(54.8)	132(46.5)	0.146	0.167	52(50.0)	0.488	0.096
No. of liver metastases			0.437	0.089		0.576	0.077
Single	47(45.2)	141(49.6)				43(41.3)	
Multiple	57(54.8)	143(50.4)				61(58.7)	
Liver metastases resection pre-RFA	39(37.5)	113(39.8)	0.682	0.047	41(39.4)	0.776	0.040
Extrahepatic metastases pre-RFA	34(32.7)	100(35.2)	0.644	0.053	38(36.5)	0.560	0.082
Type of peritumoral vessel							
Portal vein	52(50.0)						
Hepatic vein	52(50.0)						

Unless indicated otherwise, data are the number of patients, with percentages in parentheses. Values of standardized mean differences less than 0.10 indicate better balance.

**Data are means ± standard deviations, were analyzed using the two-sample t test.*

+Data are medians, with interquartile ranges in parentheses, were analyzed using Wilcoxon rank sum test.

The categorical variables were analyzed using the x^2 test or Fisher exact test.

CLM, colorectal liver metastases; RFA, radiofrequency ablation; No. of liver metastases, number of liver metastases; St.MD, Standardized mean difference.

underwent chemotherapy due to multiple or recurrent lesions. The cumulative LTP rates at 6 months, 1 years, 3 years, and 5 years were 8.8%, 14.8%, 18.9%, and 18.9% in the perivascular group and 6.9%, 11.2%, 19.7%, and 21.4% in the non-perivascular groups, respectively (p = 0.823). As of July 31, 2019, 70 of 104 (67.3%) patients in the perivascular group and 137 of 284 (48.2%) patients in the non-perivascular group had died. The 1-, 3-, 5-, and 10-year OS rates were 91.3%, 45.6%, 23.9%, and 18.7% in the perivascular group and 85.0%, 51.9%, 25.6% and 21.3% in the non-perivascular group (p = 0.798).

Intrahepatic and Extrahepatic Recurrence

In the perivascular and non-perivascular groups, 57 of 104 (54.8%) patients and 128 of 284 (45.1%) patients, respectively, had intrahepatic recurrence (p = 0.089); 60–70% of patients with intrahepatic recurrence received chemotherapy. The 1-, 3-, 5-, and 10-year intrahepatic recurrence rates were 33.3%, 56.8%, 60.1%, and 76.1% in the perivascular group and 32.8%, 55.6%, 59.0%, and 72.7% in the non-perivascular group (p = 0.705). Extrahepatic recurrence was identified in 49 patients (47.1%) in the perivascular group and 117 patients (41.2%) in the non-perivascular group. The 1-, 3-, 5-, and 10-year cumulative rates of extrahepatic metastases were 26.8%, 48.8%, 55.6%, and 60.1% in the perivascular group and 24.5%, 49.2%, 61.6%, and 65.5% in the non-perivascular group (p = 0.962).

Complications

Six (1.5%) major complications occurred in 388 patients within 30 days of RFA, as summarized in **Table 2**. There was one RFA-related death (0.3%) in an 84-year-old man with a history of cerebral hemorrhage and diabetes and a 4.6-cm tumor situated close to the hepatic vein. The patient developed abdominal hemorrhage and biliary effusion 3 days after RFA. Despite active treatment, the patient eventually died of septic shock 9 days after RFA. One of the three patients with liver abscess and one patient with pleural effusion were treated with percutaneous catheterization drainage; the other patients showed improvement with symptomatic treatment. The rate of major complications was 1.0% (1 of 104 patients) in the perivascular group and 1.8% (5 of 284 patients) in the non-perivascular group, with no significant intergroup difference (p > 0.999; **Table 2**).

Comparison of Therapeutic Outcomes After Propensity-Score Matching

In the matched cohort, 104 perivascular CLM patients were all enrolled after propensity-score matching. In the non-perivascular group, LTP occurred in 14 of 104 patients (13.5%, p = 0.442; **Table 3**). The subsequent treatment modalities for patients are shown in **Table 3**. The cumulative LTP rates at 6 months, 1 year, 3 years, and 5 years were 8.8%, 13.1%, 15.5%, and

TABLE 2 | Incidence of major complications.

Major complications	Overall Data*		Matched Data+	
	Perivascular (n=104)	Non-perivascular (n=284)	Perivascular (n=104)	Non-perivascular (n=104)
Major Complications	1(1.0)	5(1.9)	1(1.0)	1(1.0)
Hepatic abscess	0	3(1.1)	0	1(1.0)
Acute cholecystitis	0	1(0.4)	0	0
Pleural effusion requiring drainage	1(1.0)	0	1(1.0)	0
Liver rupture	0	1(0.4)	0	0
Tumor seeding	0	0	0	0
Treatment-related death	1	0	1	0

data are the number of patients, with percentages in parentheses.
**p > .999; +p > .999.*
p obtained by using Fisher exact test.

TABLE 3 | treatment modalities for patients with local tumor progression (LTP) and intrahepatic recurrence in matched groups.

Treatment Modalities	Local Tumor Progression*		Intrahepatic Recurrence+	
	Perivascula r (n=18)	Non-perivascular (n=14)	Perivascular (n=57)	Non-perivascular (n=46)
Resection	2(11.1)	4(28.6)	4(7.0)	4(8.7)
RFA	7(38.9)	5(35.7)	3(5.3)	3(6.5)
Radiotherapy	1(5.6)	1(7.1)	2(3.5)	3(6.5)
Resection + radiotherapy	0	0	1(1.8)	0
TACE	0	0	3(5.3)	0
RFA+TACE	0	0	1(1.8)	0
Gamma Knife Treatment	0	0	2(3.5)	0
Chemotherapy	8(44.4)	4(28.6)	39(68.4)	35(76.1)
Best supportive care	0	0	2(3.5)	1(2.2)

Data are the number of patients, with percentages in parentheses.
**p value between two groups was.442, +p value between two groups was .127.*
p value obtained by using the $x\chi^2$ test.
RFA, radiofrequency ablation; TACE, transcatheter arterial chemoembolization.

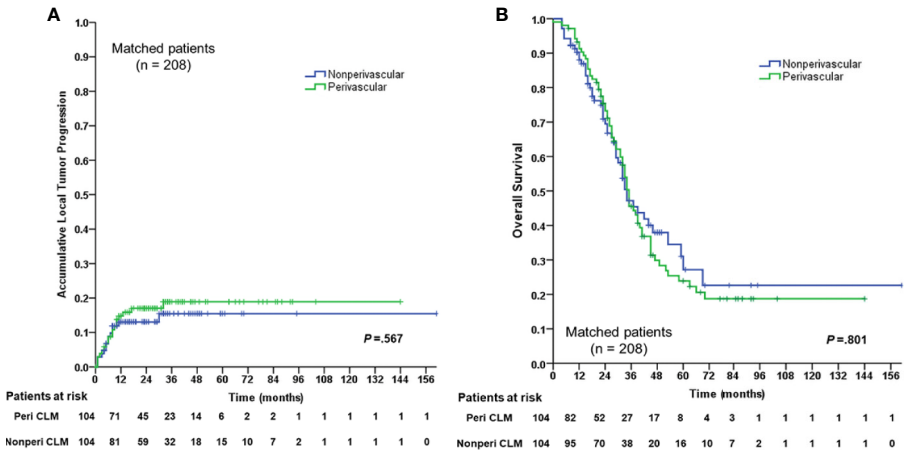

FIGURE 2 | Cumulative LTP)rate and OS rate curves for the perivascular CLM and the non-perivascular CLM in matched data. **(A)** Cumulative local tumor progression in matched data. **(B)** Overall survival in matched data. The local tumor progression and overall survival were estimated by the Kaplan-Meier method with the log-rank test. LTP, local tumor progression; OS, overall survival; Peri CLM, perivascular colorectal liver metastases.

15.5%, respectively (p = 0.567; **Figure 2**); 51 of 104 (49.0%) patients died. The 1-, 3-, 5-, and 10-year OS rates were 88.0%, 47.2%, 27.2%, and 22.6%, respectively (p = 0.801; **Figure 2**), without significant differences in LTP and OS rates between the perivascular and non-perivascular groups.

In the non-perivascular group, 46 of 104 CLM patients (44.2%) showed intrahepatic recurrence (p = 0.127, **Table 3**). The subsequent treatment modalities for patients with intrahepatic recurrence in both groups are shown in **Table 3**. The 1-, 3-, 5-, and 10-year intrahepatic recurrence rates were 30.2%, 56.3%, 59.4%, and 59.4%, respectively (p = 0.589). Moreover, 40.4% (42/104) of CLM patients showed extrahepatic recurrence during follow-up. The 1-, 3-, 5-, and 10-year extrahepatic recurrence rates were 22.8%, 47.4%, 58.9%, and 58.9%, respectively (p = 0.830). The rate of major complications was 1.0% (1 of 104 patients; p > 0.999; **Table 2**) in both groups.

Analysis of Risk Factors Associated With Outcomes

The 6-month, 1-year, 3-year, and 5-year cumulative LTP rates were 7.4%, 12.2%, 19.3%, and 20.3%, respectively. The 1-, 3-, 5-, and 10-year OS rates were 86.7%, 49.5%, 25.2%, and 20.4%, respectively, for the overall CLM patients in the study. Multivariate analysis of all patients (n = 388), the results of

TABLE 4 | Univariable and multivariable analyses of prognostic factors for local tumor progression (LTP) and overall survival (OS) for overall colorectal liver metastases (CLMs).

Variable	Local tumor progression				Overall survival			
	Univariate analysis		Multivariate analysis		Univariate analysis		Multivariate analysis	
	HR (95%CI)	p	HR (95%CI)	p	HR (95%CI)	p	HR (95%CI)	p
Age (yr)	1.527(0.911–2.559)	.109	1.447(0.860–2.435)	.164	1.241(0.932–1.652)	.139	1.131(0.841–1.521)	.415
Tumor size (cm)	2.230(1.324–3.756)	.003	2.314(1.354–3.955)	.002	1.831(1.370–2.446)	<.001	2.046(1.511–2.769)	<.001
Sex	0.888(0.522–1.509)	.660			0.886(0.668–1.175)	.402		
Primary location	0.908(0.472–1.748)	.773			1.647(1.179–2.302)	.003	1.920(1.348–2.733)	<.001
T stage	0.994(0.311–3.177)	.992			1.763(0.829–3.748)	.141	1.351(0.614–2.972)	.454
Lymph node metastasis	0.649(0.384–1.098)	.107	0.627(0.361–1.091)	.098	1.887(1.326–2.685)	<.001	1.352(0.917–1.991)	.127
Synchronous liver metastasis	1.385(0.829–2.314)	.214			1.126(0.867–1.479)	0.396		
No. of liver metastases	0.600(0.357–1.011)	.055	0.692(0.403–1.187)	0.181	1.882(1.419–2.497)	<.001	1.706(1.265–2.300)	<.001
Liver metastasis resection pre-RFA	1.384(0.803–2.386)	.242			0.918(0.691–1.219)	.555		
Extrahepatic metastases	1.150(0.661–2.001)	.620			1.942(1.462–2.579)	<.001	1.892(1.413–2.533)	<.001
Perivascular location	1.065(0.612–1.851)	.825			1.038(0.778–1.386)	.800		
Intrahepatic recurrence	1.033(0.623–1.714)	.900			1.688(1.275–2.236)	<.001	1.564(1.171–2.088)	0.002
Extrahepatic recurrence	1.224(0.730–2.052)	.444			0.828(0.630–1.088)	.175		
LTP	–	–	–		1.053(0.746–1.488)	.768		

Data in parentheses are 95% confidence intervals. The Cox proportional hazards regression model was used for the univariable and multivariable analysis. Variables with p<0.15 in univariable analyses were included in the multivariable model.

LTP, local tumor progression; OS, overall survival; RFA, radiofrequency ablation; CLM, colorectal liver metastases; No. of liver metastases, number of liver metastases; HR, hazard ratio; CI, confidence interval.

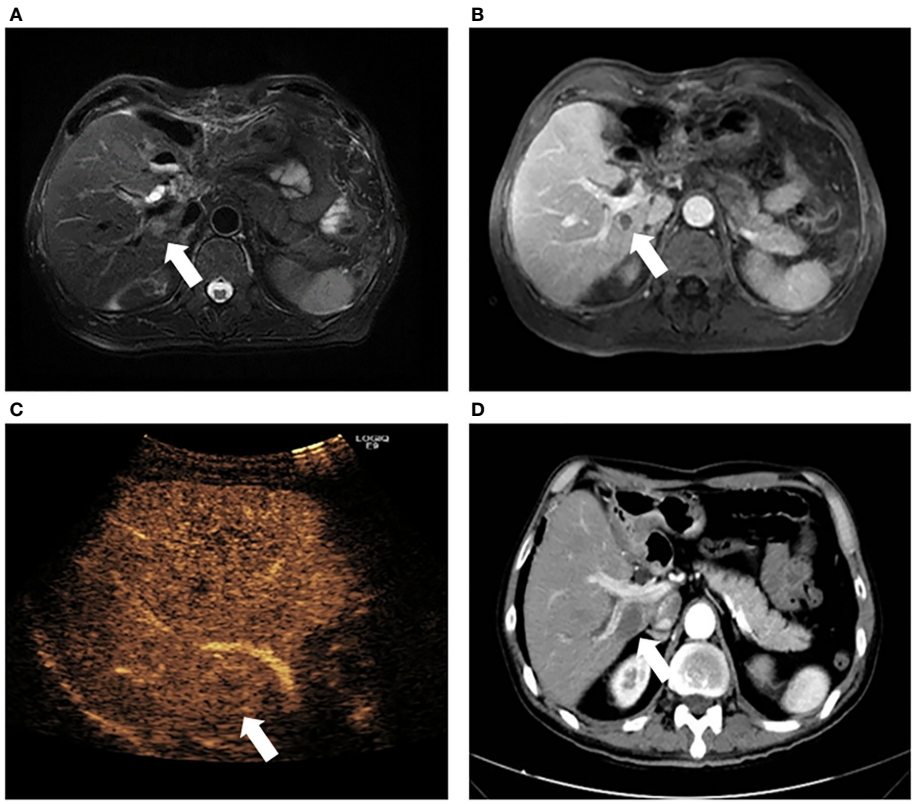

FIGURE 3 | Images in a 61-year-old-man who underwent radiofrequency ablation (RFA) for periportal CLM. **(A)** Axial MRI T2-weighted images shows a 2.2-cm lesion of high signal intensity (arrow) in segment VII before RFA. **(B)** Axial enhanced MRI image shows that the lesion (arrow) washes out in equilibrium phase; **(C)** contrast-enhanced ultrasonography (CEUS) image before RFA shows that the index tumor (arrow) is in contact with the portal vein. The patient underwent RFA, and obtained technical effectiveness 1 month after RFA. **(D)** Axial enhanced CT image shows no local tumor progression around the ablation zone 17 months after RFA. CLM, colorectal liver metastases; US, ultrasound; RFA, radiofrequency ablation.

which were expressed as hazard ratios (HRs) and 95% confidence intervals (CIs), showed that tumor size was an independent prognostic factor for LTP (HR: 2.314, 95% CI: 1.354–3.955, $p = 0.002$) (**Table 4**). In addition, tumor size (HR: 2.046, 95% CI: 1.511–2.769, $p < 0.001$), primary tumor location (HR: 1.920, 95% CI: 1.348–2.733, $p < 0.001$), number of liver metastases (HR: 1.706, 95% CI: 1.265–2.300, $p < 0.001$), extrahepatic metastases pre-RFA (HR: 1.892, 95% CI: 1.413–2.533, $p < 0.001$), and intrahepatic recurrence (HR: 1.564, 95% CI: 1.171–2.088, $p = 0.002$) were independent prognostic factors for OS in patients with CLM (**Table 4**).

Subgroup Analysis for the Type of Peritumoral Vessels

The type of peritumoral vessels was classified as periportal and perihepatic vessels in 52 (50.0%) and 52 (50.0%) patients, respectively (**Figures 3**, **4**). Furthermore, 7 of 52 patients (13.5%) and 11 of 52 patients (21.2%) in the periportal and perihepatic groups, respectively, showed LTP. The 6-month, 1-year, 3-year, and 5-year cumulative LTP rates were 5.8%, 9.8%, 14.1% and 14.1%, respectively, in the periportal group and 11.9%, 19.9%,23.4%, and 23.4%, respectively, in the perihepatic group ($p = 0.285$). In both groups, 35 of 52 patients (67.3%) with CLM died. The OS rates at 1, 3, 5, and 10 years were 92.2%, 43.4%, 22.5%, and 19.3%, respectively, in the periportal group and 90.3%, 47.6%, 24.8%, and 17.7%, respectively, in the perihepatic group ($p = 0.920$). The differences in LTP and OS between the periportal and perihepatic groups were not significant.

DISCUSSION

We identified that patients with CLM who underwent percutaneous RFA had similar rates of cumulative LTP, OS, and major complications in the perivascular and non-perivascular groups, both before and after propensity-score matching. This indicates that percutaneous RFA can be safe and effective for perivascular CLM.

Surgical resection is a standard treatment for patients with CLM (4), RFA cannot completely replace surgery, because of the low progression-free survival for lesions > 3cm (24). However, ESMO guidelines (3) recommend RFA as a curative option to eradicate all visible liver tumors, for patients with resectable lesions located deep in the liver where surgical resection would

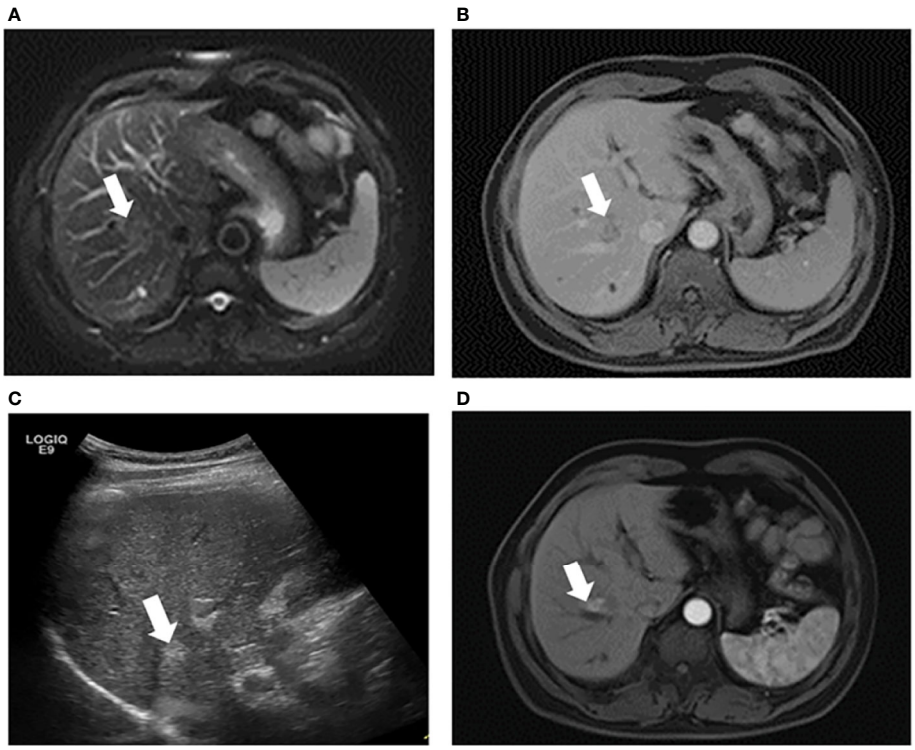

FIGURE 4 | Images in a 53-year-old-man who underwent RFA for perihepatic CLM. **(A)** Axial MRI T2-weighted images shows a 2.6-cm lesion of high signal intensity (arrow) in segment VIII before RFA. The index tumor abuts the hepatic vein. **(B)** Axial enhanced MRI image shows that the lesion (arrow) washes out in equilibrium phase; **(C)** US image before RFA shows that the index tumor (arrow) is in contact with the hepatic vein. The patient underwent RFA, obtained technical effectiveness 1 month after RFA. **(D)** Axial enhanced MRI image showed local tumor progression around the ablation zone 6 month after RFA. CLM, colorectal liver metastases; US, ultrasound; RFA, radiofrequency ablation.

lead to a great loss of liver volume, with recurrence of lesions after liver surgical resection, for patients who are intolerant to surgery (advanced age, associated co-morbidity), and for patients who refused surgery. In this study, RFA demonstrated its safety in lesions adjacent to blood vessels.

It is generally believed that an inadequate ablation margin is an independent predictor of LTP after ablation for CLM (25–28). Investigators in previous studies have suggested (12, 14, 17) that perivascular location of a liver tumor was a risk factor for LTP after RFA, because of the inability to achieve an adequate margin in such cases, as blood flow dispels thermal energy away from the lesions. However, some studies (13, 15) showed that perivascular location should not be considered a risk factor for LTP after RFA. In our study, perivascular location was defined with respect to two criteria:1) the vessel diameter ≥ 3 mm. The appropriate cut-off of 3mm was based on the results of previously published animal experiments and clinical research (16, 17, 29–31), which showed an inverse correlation between vessel diameter and the degree of heat sink effect. Sink effect may occur over 3 mm in vessel diameter and cause incomplete ablation; and 2) any contact with first- or second-degree branches of a portal or hepatic vein based on CT/MRI. The latter criterion was accepted by most clinical studies (15, 29–32). The cumulative LTP rates after RFA were not significantly different between perivascular CLM and non-perivascular CLM patients in line with the previous studies (13, 15).

There are some possible reasons for the similar outcomes in the perivascular and non-perivascular groups: firstly, the equipment used for multipolar RFA (13, 33) for perivascular liver tumors has gradually improved, resulting in better local tumor control. Second, the "supplementary ablation," "accumulative multiple ablations," (34) and "multi-step ablation" (35) techniques are helpful in achieving local tumor control. Furthermore, physician expertise and experience facilitate successful ablation.

Previous studies (36) have demonstrated that insufficient RFA enhanced the metastatic ability of tumor cells, which was mediated by signaling and dissemination of cancer cells, leading to recurrence. However, there were no significant differences in intrahepatic and extrahepatic recurrence rates after RFA between the perivascular and non-perivascular groups. Therefore, this indicated that RFA techniques may offer sufficient ablation for both perivascular and non-perivascular CLMs. The effect of RFA on perivascular CLM was similar to that on non-perivascular CLM.

The zone of ablation is larger near the hepatic vein than near the portal vein because of different flow velocity (37); patients with tumors located near the main portal vein branch are at risk for rapid tumor progression after RFA (38). However, we found

no significant differences between the periportal vessel and perihepatic vessel groups, which suggests that improved treatment strategies have a greater influence on the planning of the RFA target volume than the heat sink effect.

Previous studies have reported (6, 39) that 5-year OS rates ranged from 21% to 31% in patients with CLM treated with RFA; the LTP rates were in the range of 9–42% (40). We found similar outcomes in CLM patients treated by RFA. In this study, tumor size was the only independent prognostic factor for LTP. In addition, several prognostic factors of poor OS were identified: a tumor diameter > 3 cm, tumor location in the right colon, multiple tumors, extrahepatic metastases pre-RFA, and intrahepatic recurrence. These concur with previously reported prognostic factors (6, 13, 41–43), except for intrahepatic recurrence; this may be the reason that these investigators did not conduct further analysis into the relationship between intrahepatic recurrence and OS. However, intrahepatic recurrence may indicate the presence of more tumor cells in the blood, resulting in poor OS.

Complication rates between patients with perivascular and non-perivascular CLM treated with percutaneous RFA did not differ before or after propensity-score matching, which is consistent with previous results (15). Percutaneous RFA did not increase biliary complications, even when periportal tumors were possibly close to biliary duct structures in our study. This was because of the strict enrollment criteria and operating procedures. If the distance between the tumor and the first-level branch of the bile duct (common hepatic duct, left and right hepatic ducts) was ≤ 0.5 cm, patients did not meet the inclusion criteria for treatment with RFA. If a safe margin and a needle access route could possibly be obtained, patients were considered for treatment with RFA, and real-time ultrasound guidance was required during RFA to ensure that there was no damage to the bile duct. Therefore, perivascular CLM can be safely treated with RFA. Although there was one treatment-related death in this study, this patient had multiple RFA-related risk factors, including older age, multiple comorbidities, a large tumor, and a problematic tumor location. Hence, indications should always be evaluated carefully before RFA and treated prudently.

This study had several limitations. First, it was retrospective study. Although we conducted a propensity-score matched analysis to balance the baseline characteristics of patients, we cannot exclude the possibility of bias in terms of other confounding factors, such as the experience of the physician. Second, we failed to consider that other problematic tumor locations, such as locations close to the liver surface or the diaphragm, may influence the outcome of ablation. However, a study (34) reported that individualized treatment strategies can ensure that patients with problematic locations achieve outcomes similar to those of patients with non-problematic tumor locations. Finally, there is no universal consensus on the definition of perivascular tumors. Our definition of a perivascular tumor was consistent with that used in previous reports (13, 15, 17); however, this needs validation in future studies.

In conclusion, there were no significant differences in the rates of cumulative LTP, OS, and major complications between patients with perivascular CLM and non-perivascular CLM treated with percutaneous RFA. Thus, the findings provide evidence-based medical evidence that percutaneous RFA is a safe and effective treatment option for perivascular CLM.

DATA AVAILABILITY STATEMENT

The raw data supporting the conclusions of this article will be made available by the authors, without undue reservation.

ETHICS STATEMENT

The studies involving human participants were reviewed and approved by the Research Ethics Committee of the Peking University Cancer Hospital. Written informed consent for participation was not required for this study in accordance with the national legislation and the institutional requirements.

AUTHOR CONTRIBUTIONS

KY, BJ, and HL conceived and designed the experiments. KY, ZZ, WW, WY, and MC performed clinical studies. BJ, HL, ZZ, and XL performed the data analysis and statistical analysis. BJ, HL, KY, and ZZ edited manuscript. All authors contributed to the article and approved the submitted version.

FUNDING

This research was supported by Beijing Municipal Science and Technology Commission (grant no. Z151100004015186) and The capital health research and development of special (grant no.2020-2-2152).

REFERENCES

1. Luo D, Liu Q, Yu W, Ma Y, Zhu J, Lian P, et al. Prognostic value of distant metastasis sites and surgery in stage IV colorectal cancer: a population-based study. *Int J Colorectal Dis* (2018) 33(9):1241–9. doi: 10.1007/s00384-018-3091-x
2. Ruers T, Bleichrodt RP. Treatment of liver metastases, an update on the possibilities and results. *Eur J Cancer (Oxford Engl 1990)* (2002) 38(7):1023–33. doi: 10.1016/s0959-8049(02)00059-x
3. Yoshino T, Arnold D, Taniguchi H, Pentheroudakis G, Yamazaki K, Xu RH, et al. Pan-Asian adapted ESMO consensus guidelines for the management of patients with metastatic colorectal cancer: a JSMO-ESMO initiative endorsed by CSCO, KACO, MOS, SSO and TOS. *Ann Oncol* (2018) 29(1):44–70. doi: 10.1093/annonc/mdx738
4. Benson AB, Venook AP, Al-Hawary MM, Cederquist L, Chen YJ, Ciombor KK, et al. NCCN Guidelines Insights: Colon Cancer, Version 2.2018. *J Natl Compr Cancer Netw JNCCN* (2018) 16(4):359–69. doi: 10.6004/jnccn.2018.0021

5. Vietti Violi N, Duran R, Demartines N, Sempoux C, Guiu B, Bize PE, et al. Local recurrence rate in patients with colorectal cancer liver metastasis after wedge resection or percutaneous radiofrequency ablation. *Int J Hyperthermia* (2018) 34(7):1020–8. doi: 10.1080/02656736.2017.1372644
6. Shady W, Petre EN, Gonen M, Erinjeri JP, Brown KT, Covey AM, et al. Percutaneous Radiofrequency Ablation of Colorectal Cancer Liver Metastases: Factors Affecting Outcomes–A 10-year Experience at a Single Center. *Radiology* (2016) 278(2):601–11. doi: 10.1148/radiol.2015142489
7. Solbiati L, Ahmed M, Cova L, Ierace T, Brioschi M, Goldberg SN. Small liver colorectal metastases treated with percutaneous radiofrequency ablation: local response rate and long-term survival with up to 10-year follow-up. *Radiology* (2012) 265(3):958–68. doi: 10.1148/radiol.12111851
8. Gillams A, Goldberg N, Ahmed M, Bale R, Breen D, Callstrom M, et al. Thermal ablation of colorectal liver metastases: a position paper by an international panel of ablation experts, The Interventional Oncology Sans Frontieres meeting 2013. *Eur Radiol* (2015) 25(12):3438–54. doi: 10.1007/s00330-015-3779-z
9. Sartori S, Tombesi P, Macario F, Nielsen I, Tassinari D, Catellani M, et al. Subcapsular liver tumors treated with percutaneous radiofrequency ablation: a prospective comparison with nonsubcapsular liver tumors for safety and effectiveness. *Radiology* (2008) 248(2):670–9. doi: 10.1148/radiol.2482071690
10. Song I, Rhim H, Lim HK, Kim YS, Choi D. Percutaneous radiofrequency ablation of hepatocellular carcinoma abutting the diaphragm and gastrointestinal tracts with the use of artificial ascites: safety and technical efficacy in 143 patients. *Eur Radiol* (2009) 19(11):2630–40. doi: 10.1007/s00330-009-1463-x
11. Ruers T, Van Coevorden F, Punt CJ, Pierie JE, Borel-Rinkes I, Ledermann JA, et al. Local Treatment of Unresectable Colorectal Liver Metastases: Results of a Randomized Phase II Trial. *J Natl Cancer Inst* (2017) 109(9):9. doi: 10.1093/jnci/djx015
12. Shady W, Petre EN, Do KG, Gonen M, Yarmohammadi H, Brown KT, et al. Percutaneous Microwave versus Radiofrequency Ablation of Colorectal Liver Metastases: Ablation with Clear Margins (A0) Provides the Best Local Tumor Control. *J Vasc Intervent Radiol JVIR* (2018) 29(2):268–75.e1. doi: 10.1016/j.jvir.2017.08.021
13. Snoeren N, Nijkamp MW, Berendsen T, Govaert KM, van Kessel CS, Borel Rinkes IH, et al. Multipolar radiofrequency ablation for colorectal liver metastases close to major hepatic vessels. *Surg J R Colleges Surg Edinburgh Ireland* (2015) 13(2):77–82. doi: 10.1016/j.surge.2013.11.013
14. Mulier S, Ni Y, Jamart J, Ruers T, Marchal G, Michel L. Local recurrence after hepatic radiofrequency coagulation: multivariate meta-analysis and review of contributing factors. *Ann Surg* (2005) 242(2):158–71. doi: 10.1097/01.sla.0000171032.99149.fe
15. Kang TW, Lim HK, Lee MW, Kim YS, Choi D, Rhim H. Perivascular versus nonperivascular small HCC treated with percutaneous RF ablation: retrospective comparison of long-term therapeutic outcomes. *Radiology* (2014) 270(3):888–99. doi: 10.1148/radiol.13130753
16. Lu DS, Raman SS, Vodopich DJ, Wang M, Sayre J, Lassman C. Effect of vessel size on creation of hepatic radiofrequency lesions in pigs: assessment of the "heat sink" effect. *AJR Am J Roentgenol* (2002) 178(1):47–51. doi: 10.2214/ajr.178.1.1780047
17. Lu DS, Raman SS, Limanond P, Aziz D, Economou J, Busuttil R, et al. Influence of large peritumoral vessels on outcome of radiofrequency ablation of liver tumors. *J Vasc Intervent Radiol JVIR* (2003) 14(10):1267–74. doi: 10.1097/01.rvi.0000092666.72261.6b
18. Seror O, N'Kontchou G, Muhammad M, Barrucand C, Tin Tin Htar M, Assaban M, et al. The impact of large vessel proximity on effectiveness of radiofrequency ablation of hepatocellular carcinoma: a controlled study. *J Radiol* (2007) 88(9 Pt 1):1157–64. doi: 10.1016/s0221-0363(07)89927-6
19. Yang W, Yan K, Wu GX, Wu W, Fu Y, Lee JC, et al. Radiofrequency ablation of hepatocellular carcinoma in difficult locations: Strategies and long-term outcomes. *World J Gastroenterol* (2015) 21(5):1554–66. doi: 10.3748/wjg.v21.i5.1554
20. Jiang BB, Yan K, Zhang ZY, Yang W, Wu W, Yin SS, et al. The value of KRAS gene status in predicting local tumor progression of colorectal liver metastases following radiofrequency ablation. *Int J Hyperthermia* (2019) 36(1):211–19. doi: 10.1080/02656736.2018.1556818
21. Chen MH, Yang W, Yan K, Zou MW, Solbiati L, Liu JB, et al. Large liver tumors: protocol for radiofrequency ablation and its clinical application in 110 patients–mathematic model, overlapping mode, and electrode placement process. *Radiology* (2004) 232(1):260–71. doi: 10.1148/radiol.2321030821
22. Ahmed M, Solbiati L, Brace CL, Breen DJ, Callstrom MR, Charboneau JW, et al. Image-guided tumor ablation: standardization of terminology and reporting criteria–a 10-year update. *J Vasc Intervent Radiol JVIR* (2014) 25(11):1691–705.e4. doi: 10.1016/j.jvir.2014.08.027
23. Pattanayak CW, Rubin DB, Zell ER. Propensity score methods for creating covariate balance in observational studies. *Rev Espanola Cardiol* (2011) 64(10):897–903. doi: 10.1016/j.recesp.2011.06.008
24. Wang LJ, Zhang ZY, Yan XL, Yang W, Yan K, Xing BC. Radiofrequency ablation versus resection for technically resectable colorectal liver metastasis: a propensity score analysis. *World J Surg Oncol* (2018) 16(1):207. doi: 10.1186/s12957-018-1494-3
25. Wang X, Sofocleous CT, Erinjeri JP, Petre EN, Gonen M, Do KG, et al. Margin size is an independent predictor of local tumor progression after ablation of colon cancer liver metastases. *Cardiovasc Intervent Radiol* (2013) 36(1):166–75. doi: 10.1007/s00270-012-0377-1
26. Sotirchos VS, Petrovic LM, Gönen M, Klimstra DS, Do RK, Petre EN, et al. Colorectal Cancer Liver Metastases: Biopsy of the Ablation Zone and Margins Can Be Used to Predict Oncologic Outcome. *Radiology* (2016) 280(3):949–59. doi: 10.1148/radiol.2016151005
27. Kaye EA, Cornelis FH, Petre EN, Tyagi N, Shady W, Shi W, et al. Volumetric 3D assessment of ablation zones after thermal ablation of colorectal liver metastases to improve prediction of local tumor progression. *Eur Radiol* (2019) 29(5):2698–705. doi: 10.1007/s00330-018-5809-0
28. Calandri M, Yamashita S, Gazzera C, Fonio P, Veltri A, Bustreo S, et al. Ablation of colorectal liver metastasis: Interaction of ablation margins and RAS mutation profiling on local tumour progression-free survival. *Eur Radiol* (2018) 28(7):2727–34. doi: 10.1007/s00330-017-5273-2
29. Lu DS, Yu NC, Raman SS, Limanond P, Lassman C, Murray K, et al. Radiofrequency ablation of hepatocellular carcinoma: treatment success as defined by histologic examination of the explanted liver. *Radiology* (2005) 234(3):954–60. doi: 10.1148/radiol.2343040153
30. Feng Y, Wang L, Lv H, Shi T, Xu C, Zheng H, et al. Microwave ablation versus radiofrequency ablation for perivascular hepatocellular carcinoma: a propensity score analysis. *HPB Off J Int Hepatol Pancreato Biliary Assoc* (2020) S1365-182X(20)31118-7. doi: 10.1016/j.hpb.2020.08.006
31. Kang TW, Lim HK, Cha DI. Percutaneous ablation for perivascular hepatocellular carcinoma: Refining the current status based on emerging evidence and future perspectives. *World J Gastroenterol* (2018) 24(47):5331–37. doi: 10.3748/wjg.v24.i47.5331
32. Lee S, Kang TW, Cha DI, Song KD, Lee MW, Rhim H, et al. Radiofrequency ablation vs. surgery for perivascular hepatocellular carcinoma: Propensity score analyses of long-term outcomes. *J Hepatol* (2018) 69(1):70–8. doi: 10.1016/j.jhep.2018.02.026
33. Hocquelet A, Aube C, Rode A, Cartier V, Sutter O, Manichon AF, et al. Comparison of no-touch multi-bipolar vs. monopolar radiofrequency ablation for small HCC. *J Hepatol* (2017) 66(1):67–74. doi: 10.1016/j.jhep.2016.07.010
34. Chen MH, Yang W, Yan K, Hou YB, Dai Y, Gao W, et al. Radiofrequency ablation of problematically located hepatocellular carcinoma: tailored approach. *Abdominal Imaging* (2008) 33(4):428–36. doi: 10.1007/s00261-007-9283-4
35. Kotoh K, Nakamuta M, Morizono S, Kohjima M, Arimura E, Fukushima M, et al. A multi-step, incremental expansion method for radio frequency ablation: optimization of the procedure to prevent increases in intra-tumor pressure and to reduce the ablation time. *Liver Int Off J Int Assoc Study Liver* (2005) 25(3):542–7. doi: 10.1111/j.1478-3231.2005.01051.x
36. Zhang N, Li H, Qin C, Ma D, Zhao Y, Zhu W, et al. Insufficient radiofrequency ablation promotes the metastasis of residual hepatocellular carcinoma cells via upregulating flotillin proteins. *J Cancer Res Clin Oncol* (2019) 145(4):895–907. doi: 10.1007/s00432-019-02852-z
37. Frericks BB, Ritz JP, Albrecht T, Valdeig S, Schenk A, Wolf KJ, et al. Influence of intrahepatic vessels on volume and shape of percutaneous thermal ablation zones: in vivo evaluation in a porcine model. *Invest Radiol* (2008) 43(4):211–8. doi: 10.1097/RLI.0b013e31815daf36
38. Kang TW, Lim HK, Lee MW, Kim YS, Rhim H, Lee WJ, et al. Aggressive Intrasegmental Recurrence of Hepatocellular Carcinoma after Radiofrequency Ablation: Risk Factors and Clinical Significance. *Radiology* (2015) 276(1):274–85. doi: 10.1148/radiol.15141215

39. Hamada A, Yamakado K, Nakatsuka A, Uraki J, Kashima M, Takaki H, et al. Radiofrequency ablation for colorectal liver metastases: prognostic factors in non-surgical candidates. *Japanese J Radiol* (2012) 30(7):567–74. doi: 10.1007/s11604-012-0089-0
40. Stang A, Fischbach R, Teichmann W, Bokemeyer C, Braumann D. A systematic review on the clinical benefit and role of radiofrequency ablation as treatment of colorectal liver metastases. *Eur J Cancer (Oxford Engl 1990)* (2009) 45(10):1748–56. doi: 10.1016/j.ejca.2009.03.012
41. Gu Y, Huang Z, Gu H, Gao F, Zhang T, Huang S, et al. Does the Site of the Primary Affect Outcomes When Ablating Colorectal Liver Metastases with Radiofrequency Ablation? *Cardiovasc Intervent Radiol* (2018) 41(6):912–9. doi: 10.1007/s00270-018-1937-9
42. Yamashita S, Odisio BC, Huang SY, Kopetz SE, Ahrar K, Chun YS, et al. Embryonic origin of primary colon cancer predicts survival in patients undergoing ablation for colorectal liver metastases. *Eur J Surg Oncol J Eur Soc Surg Oncol Br Assoc Surg Oncol* (2017) 43(6):1040–9. doi: 10.1016/j.ejso.2017.01.007
43. Wang Y, Zheng J, Chen H, Hu C, Sun B, Wang H, et al. A prognostic nomogram for colorectal cancer liver metastases after percutaneous thermal ablation. *Int J Hyperthermia* (2018) 34(6):853–62. doi: 10.1080/02656736.2017.1368095

Conflict of Interest: The authors declare that the research was conducted in the absence of any commercial or financial relationships that could be construed as a potential conflict of interest.

frontiers in Oncology

ORIGINAL RESEARCH
published: 20 October 2020
doi: 10.3389/fonc.2020.540239

The Learning Curve for Thermal Ablation of Liver Cancers: 4,363-Session Experience for a Single Central in 18 Years

Xiang Jing[1,2*], *Yan Zhou*[1,2], *Jianmin Ding*[1,2], *Yijun Wang*[2,3], *Zhengyi Qin*[4], *Yandong Wang*[1,2] *and Hongyu Zhou*[1,2]

[1] Department of Ultrasound, Tianjin Third Central Hospital, Tianjin, China, [2] Tianjin Institute of Hepatobiliary Disease, Tianjin Key Laboratory of Extracorporeal Life Support for Critical Diseases, Artificial Cell Engineering Technology Research Center, Tianjin Third Central Hospital, Tianjin, China, [3] Department of Hepatobiliary Surgery, Tianjin Third Central Hospital, Tianjin, China, [4] Department of Ultrasound, The Third Central Clinical College of Tianjin Medical University, Tianjin, China

OPEN ACCESS

Edited by:
Mattia Squarcia,
Hospital Clínic de Barcelona, Spain

Reviewed by:
Xudong Shen,
Guizhou Medical University, China
Kun Yan,
Peking University Cancer Hospital, China
Ernest Belmonte,
Hospital Clínic de Barcelona, Spain

***Correspondence:**
Xiang Jing
dr.jingxiang@aliyun.com

Specialty section:
This article was submitted to Cancer Imaging and Image-directed Interventions, a section of the journal Frontiers in Oncology

Received: 04 March 2020
Accepted: 22 September 2020
Published: 20 October 2020

Citation:
Jing X, Zhou Y, Ding J, Wang Y, Qin Z, Wang Y and Zhou H (2020) The Learning Curve for Thermal Ablation of Liver Cancers: 4,363-Session Experience for a Single Central in 18 Years. Front. Oncol. 10:540239. doi: 10.3389/fonc.2020.540239

This study aimed to explore the special efforts required to achieve proficiency in performing thermal ablation of liver cancers, including tumors in difficult locations, and clarify the effects of handing-down teaching on the corresponding process. Major complications of patients receiving percutaneous thermal ablation of liver cancer were analyzed. Polynomial fitting was used to describe the connection between major complication rates and special experience. Learning curve of major complications was plotted both for the whole group and for each operator, respectively. Tumors in difficult locations were further studied. A total of 4,363 thermal ablation sessions were included in this study. 143 of 4,363 patients had major complications, corresponding to an incidence rate of 3.27%. 806 thermal ablation sessions were performed for tumors in difficult locations. The major complication rate of these sessions is 6.33%. According to the trend of the learning curve of the 4363 patients, the experience of the whole group can be classified into five stages, that is, the high-risk, relatively stable, unstable, proficient and stable periods. A learning curve for an individual operator can be classified into the high-risk, proficient and stable periods. The major complication rates for the chronologically first, second and third operator of the group are 3.23, 3.35, and 3.31%, respectively. The special experience needed to bypass the first stage corresponds to 410, 510, and 440 sessions, the second stage, 1850, 850, and 870 sessions, by the three operators, respectively. The major complication rates for the tumors in difficult locations for the first, second and third operator were 7.04, 5.53, and 5.98%, respectively. For the tumors in difficult locations, the special experience needed to bypass the first stage corresponds to 150, 130, and 140 sessions, the second stage, 290, 175, and 185 sessions, by the three operators, respectively. In conclusion, the learning process of an operator percutaneous

thermal ablation for liver cancer can be classified into three stages. The major complication rate for tumors in difficult locations were higher than that for all tumors. Handing-down teaching can make an operator arrive at the third stage earlier but not the second stage.

Keywords: learning curve, thermal ablation, liver cancer, major complication, handing-down teaching

INTRODUCTION

Local thermal ablation techniques—including radiofrequency ablation, microwave ablation, laser ablation, and high intensity focused ultrasound (HIFU)—is widely used for the treatment of liver tumors in clinical practice (1–3). Among them, radiofrequency and microwave ablation are the most popular techniques (4, 5). Patients with liver cancer benefit significantly from the minimally invasive therapy. Previous studies show that the long-term outcome of patients treated by thermal ablation is comparable with that of surgical resection (6, 7). The major complications and perioperative mortality, however, were significantly lower in patients undergoing local thermal ablation (8, 9).

Major complication is a highly concerned evaluating indicator for thermal ablation. Although major complication may occur occasionally, an experienced operator, advanced equipment and use of assisting methods may help to significantly reduce the risk of major complication. Previous studies found that the rate of complication for thermal ablation ranges from 1.3 to 10.0% (10–13). With the increase of special experience and the development of equipment, the rate of complication will decrease. However, the major complication rates in different hospitals, countries, and areas are distinct (12–15). Therefore, similar to other minimally invasive treatments, thermal ablation for liver cancers is experience-dependent.

Thermal ablation is often regarded as a simple technique of inserting a needle to "burn" the tumor, without getting much attention to the details, assisting methods and skills. Despite minimal invasion of thermal ablation, its major complication is non-trivial and sometimes may lead to death (16, 17). Avoiding major complication by improving the special skill of the operators, therefore, is crucial. However, to our best knowledge, there is a lack of extensive study about the special efforts required to achieve proficiency in performing thermal ablation and reduce major complication.

A few studies have explored the learning process of the early period of thermal ablation (18–20). However, the number of patients enrolled in previous studies is small, which is far from sufficient to investigate the connection between special experience and possible major complication, with the rate of the latter being 2.0–4.0% (11, 13).

To bridge the aforementioned gap, in this paper, we studied the learning curve for thermal ablation of more than 4,000 sessions of liver cancers in our central. The effect of handing-down teaching on accelerating the learning process is clarified. Moreover, the special efforts required for treating tumors in difficult location are discussed.

MATERIALS AND METHODS

Patients

The clinical data of patients undergoing thermal ablation for liver cancer from December 2001 to December 2019 were analyzed. The aim of all the thermal ablation is the radical treatment. The recommended indications for thermal ablation in our central were (1) patients having a solitary tumor with a size of ≤5 cm or multiple tumors (no more than 5) with a maximum size of ≤3 cm; (2) patients without portal vein tumor thrombus or extrahepatic metastasis; (3) patients with liver function of a Child-pugh classification A or B; (4) patients with a platelet count of $\geq 50\times10^9$/L or INR ≤ 1.7. For patients that do not meet the aforementioned criteria, thermal ablation was decided on a case-by-case basis by the clinician. For patients with liver dysfunction or coagulation disorders, radical thermal ablation was performed after the liver function or coagulation function was improved. Patients (1) receiving thermal ablation for benign tumors, (2) receiving laparoscopic-assisted or open thermal ablation, or (3) undergoing thermal ablation combined with liver resection were excluded. A total of 4,363 patients with 4,363 percutaneous thermal ablation sessions were included in this study.

Equipment

RFA procedures were performed using mono-polar RFA with cooled-shaft needles or umbrella electrodes without cooled-shaft needles (Mianyang Lide electronics co. LTD, Mianyang, China). The length of the electrodes ranged from 15 to 20 cm with a 2- or 3-cm active tip. The power was 200 W, and the frequency was 480 kHz. Cool-tip RFA system (Radionics, Burlington, MA, US) and RITA RFA system (Angio Dynamics. US) were adopted.

MWA procedures were carried out using an MTC-3 or MTC-3CA microwave therapy instrument (Forsea Microwave & Electronic Research Institute, Nanjing, China) with a frequency of 2,450 MHz. The MW antenna was a 14 G unipolar cooled-shaft needle with a 15-cm length and a 1.5-cm long active tip.

The ultrasound systems used for guidance were ALOKA5000 (Aloka, Tokyo, Japan), Philips iU22, Philips IU Elit, and Philips epic7 (Philips, Bothell, WA, USA), having a convex array probe with a frequency of 1.0–5.0 MHz.

Ablation Procedures

Different ablation strategies were used depending on the size, morphology, and location of the tumor. Generally, for tumors ≤2 cm, single-point ablation was performed, whereas for tumors >2 cm, multi-point overlapping ablation was conducted. In addition, the safe margin for complete ablation of the tumor

was 0.5 cm, unless the tumor was in a difficult location. Before 2005, the immediate efficacy was assessed based on the hyperechoic region covering the tumor or the clinical experience of the operator. After 2005, CEUS was performed 15 to 20 min after thermal ablation to determine the immediate efficacy. For residual tumors determined by CEUS, supplementary ablation was performed. All the patients received contrast enhanced CT/MR to evaluate complete ablation one month after thermal ablation. All the treatments were performed by X. Jing, J. Ding, or Y. Wang individually. Among them, X. Jing was the first operator in our central, and J. Ding and Y. Wang was the second and third. The last two operators had more than 3-year experience of interventional ultrasound and more than 1,000 ultrasound guided procedures before doing thermal ablation. All the treatments were performed by free hand.

Definition of Tumor Located in Difficult Locations

We defined a tumor in difficult location if the tumor is (1) within 5 mm from important tissues or organs (including diaphragm, gallbladder, biliary tract, large vessels, right kidney, and gastrointestinal tract), (2) within 5 mm from the liver capsule, and (3) an exophytic tumor.

Ancillary Protocols for Tumors in Difficult Locations

(1) Artificial Ascites and Difficult Locations: For tumors adjacent to the extrahepatic tissues or organs, percutaneous puncture catheter drainage was conducted by inserting a 21 G or 18 G PTC needle into the adjoining site. If the adjoining site can restore water, then production of artificial ascites was undertaken. If the adjoining site cannot restore water, then the tissues or organs were prevented from thermal damage by dropping the ice saline solution continuously.

(2) Arterial Hydrothorax: For tumors adjacent to diaphragm or located at liver dome, percutaneous puncture catheter drainage was conducted by inserting an 18 G PTC needle into the pleural cavity. Then, 100–500 mL of fluid was injected into the pleural cavity to obtain the safe and clear puncture path.

(3) Thermal Ablation Combined With PEIT: For tumors adjacent to the large vessels or biliary tract, a 21 G PTC needle was inserted into the side of the tumor close to the vessel or tract. Then, 1– 3 mL dehydrated alcohol was injected into the tumor. The injection of dehydrated alcohol and the thermal ablation were started at the same time.

(4) Tumor Blood Vessel Block: For exophytic tumors, the antenna or elector was inserted into the tumor blood vessel under the guidance of ultrasound or contrast enhanced ultrasound by passing through a portion of normal liver tissue. (If it cannot be performed, then the antenna was inserted into tumor directly). Then, the ablation was performed with a high power until the tumor presents as hypovascularity on CEUS.

(5) Thermal Ablation Combined With TACE: For tumors with a size of ≥5cm or with arteriovenous fistula, TACE was performed 1 or 2 weeks before thermal ablation. When the blood supply of the tumor was reduced and the patient was with liver function of a Child-pugh classification A or B, the radical thermal ablation was conducted.

(6) Image-Fusion and Navigation Systems: For lesions invisible on US and CEUS but detected by CECT or CEMRI, the antenna or elector was inserted under the guidance of US/CEUS-CECT/CEMRI fusing imaging.

It should be noted that in the early period of the development of our group, the same strategy (without assisting method or combined therapy) was performed for all the tumors, no matter whether they located in difficult location or not, because the aforementioned ancillary protocols were not established.

Classification of Complications

Complications after thermal ablation were assessed according to the clinical symptoms, imaging findings and results of laboratory examinations. The definition of a major complication was a complication that requires further treatment, threatens the life of the patient, leads to substantial morbidity and disability, or results in a lengthened hospital stay (21). All other complications were considered to be minor.

Calculation of Learning Curve

The learning curves were calculated for the entire group and each operator, respectively. All the tumors and tumors in difficult locations were considered, respectively. The major complication rates were calculated based on moving averages of 50 samples. Polynomial fitting was used to describe the relationship between major complication rates and special experience. The periods of learning curve were identified based on the trend of the curve and the major complication rates. Complication rates of 4 and 2% were the cut-off values for identifying periods of the learning curves of all ablation sessions. Complication rates of 6 and 4% were the cut-off values for identifying periods of the learning curves of ablation sessions of tumors in difficult locations.

Statistical Analysis

Continuous variables are expressed as the mean ± standard error and categorical variables as frequencies and percentages. The x^2-test or Fisher test was used to compare categorical data between different groups. For all tests, a p value < 0.05 was considered to indicate statistical significance. Statistical analyses were performed using the SPSS software (Version 17.0, IBM, Armonk, NY, USA).

RESULTS

A total of 4,363 patients undergoing percutaneous thermal ablation were included in this study. 143 of 4,363 patients had major complications with an incidence rate of 3.27% (**Table 1**). Six patients had a combined major complication. A total of 149 major complications occurred. Eight patients died during the

TABLE 1 | Major complications after thermal ablation.

Complication	No. of complications
Hemorrhage	14
Intra-hepatic haematomas	3
Intra-peritoneal bleeding	6
Haemothorax	4
Subphrenic arterial hemorrhage	1
Bile duct injury	26
Biliary stenosis	8
Biloma combined with infection	11
Bile leak	5
Bronchobiliary fistula	2
Liver abscess	23
Diaphragmatic hernia	5
Liver dysfunction	5
Multiple organ failure	4
Intractable pleural effusion	49
Intractable ascites	10
Tumor implantation	6
Severe sepsis	4
Hepato-gastrointestinal fistula	1
gallbladder perforation	1
Massive arterioportal fistula	1

periprocedural time (within 30 days of the thermal ablation) with a mortality of 0.18%. Among the eight patients, four of them died due to multiple organ failure, one died because of infectious shock, two died due to liver dysfunction, and one death happened by acute myocardial infarction after thermal ablation.

The learning curve for thermal ablation of all the 4,363 patients in our central is shown in **Figure 1**. According to the trend of the learning curve, the experience of thermal ablation can be classified into five stages. The first stage was from the first patients to the 350th patient, called high-risk period. The second stage was from the 351th patient to 1150th patient, called relative stable period. The third stage, named unstable period, was from the 1151th patient to 2400th patient. The fourth and fifth stage

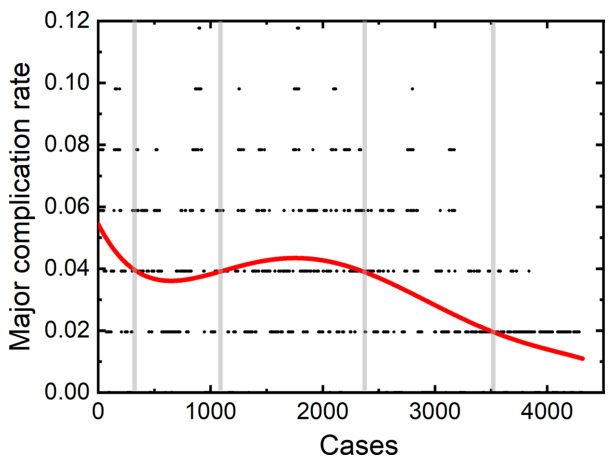

FIGURE 1 | Learning curve for thermal ablation of all the 4,363 patients in our central.

was coined proficient period and stable period, from the 2401th patient to 3500th patient and 3501th patient to 4,363th patient, respectively.

Three operators participated in treating the aforementioned patients. X. Jing was the first operator in our central. He started the first thermal ablation since December 2001 with an experience of the technique for 18 years. J. Ding was the second operator and started his first thermal ablation from the 928th patient in our hospital with an experience of 8 years. The third operator was Y. Wang, who starts his first thermal ablation from the 1227th patient, with an experience of 7.5 year for thermal ablation.

A total of 2,170 thermal ablation sessions were performed by the first operator. Among these sessions, 70 patients (3.23%) had major complications. 1,104 thermal ablation sessions were performed by the second operator with a major complication rate of 3.35% (37/1,104). The third operator achieved 1,089 sessions, with 36 (3.31%) major complications.

The learning curves of each individual operator were depicted in **Figure 2**. The learning process can be classified into the high-risk, proficient and stable periods, according to the cut-off values of major complication rates of 4 and 2%. The experience needed to bypass the first stage corresponds to 410, 510, and 440 patients, and the second stage, 1,850, 850, and 870 patients, respectively.

Among the 4,363 thermal ablation sessions, 806 sessions were performed for tumors in difficult locations with a proportion of 18.47%. 223 of the 806 sessions were with tumors adjacent to the large vessels or biliary tract (the first and second branch of biliary duct). Among the above 223 sessions, 159 ablation sessions were assisted with PEI. 57 of the 806 sessions were with tumors close to gallbladder. Hydro-dissection technique was used in 39 of the 57 sessions. 462 of the 806 sessions were with tumors located under liver capsule, including 351 sessions with tumors adjacent to diaphragm and 201 sessions with exophytic tumors. Among the 462 sessions, artificial ascites technique and arterial hydrothorax technique were used in 221 and 123 sessions, respectively. 61 of the 806 sessions were with tumors close to gastrointestinal tract. Artificial ascites technique was used in 45 of the 61 sessions. Artificial ascites technique was used in 3 sessions with tumors close to right kidney. The incidence rate of major complications in patients with a tumor in a difficult location was 6.33% (51/806). The rest 3,557 sessions correspond to 92 major complications with an incidence rate of 2.59%. The learning curve for thermal ablation of tumors in difficult locations was shown in **Figure 3**.

Among the 806 difficult sessions, 355 ones were performed by the first operator, with a major complication rate of 7.04%. 217 and 234 sessions were achieved by the second and third operator, respectively. 12 of 217 and 14 of 234 sessions correspond to major complications, with complication rates of 5.53 and 5.98%, respectively. The second and third operator started the thermal ablation for tumors in the difficult location from the 104th and 141th patients, respectively. According to the major complication rates at the cut-off values of 6 and 4%, a learning curve for thermal ablation of tumors in difficult locations of an individual operator was classified into the high-risk, proficient, and stable

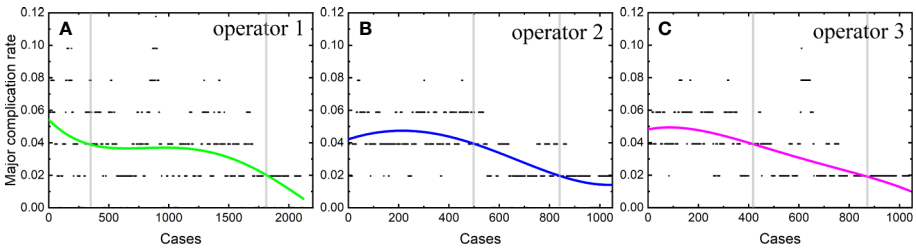

FIGURE 2 | Learning curves of the operator 1 **(A)**, operator 2 **(B)** and operator 3 **(C)**.

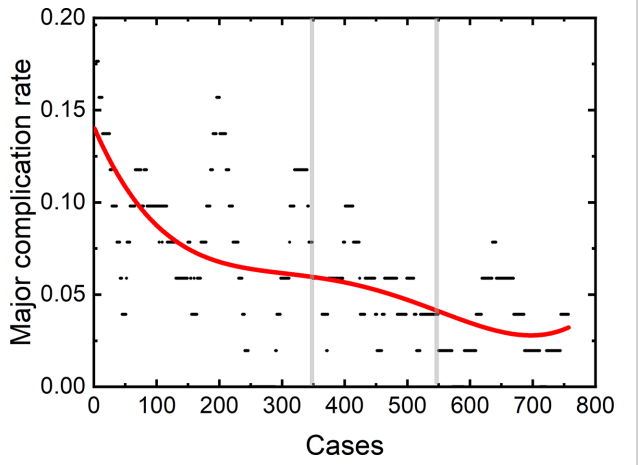

FIGURE 3 | Learning curve for 806 sessions of tumors in difficult locations.

periods (**Figure 4**). The experience required to bypass the first stage corresponds to 150, 130, and 140 patients and the second, 290, 175, and 185, for the three operators, respectively.

DISCUSSION

The major complication rate of our central for the 4,363 radical thermal ablations of liver cancers was 3.27%, similar to those reported in previous studies (9, 22). According to the learning curve of individual operators in our hospital, the learning process can be classified into three stages, namely, the high-risk, proficient, and stable periods. The experience required to bypass the first period corresponds to similar number of patients for the three operators, which was not affected by handing-down teaching. However, handing-down teaching can significantly reduce experience needed to bypass the second period, as mirrored by the length of this period of the three operators. The peak value of the complication rate for thermal ablation of tumors in difficult locations is also reduced due to the handing-down teaching.

Recently, thermal ablation is widely used for primary and metastatic liver tumors and is popular with clinician due to its minimal invasion and safety (23, 24). Besides, thermal ablation is easy to learn, so that clinician in different professions started to use this therapy to treat liver cancer. In China, thermal ablation can be performed by clinician in the departments of interventional ultrasound, interventional radiography, and hepatobiliary surgery etc. However, the learning process of this technique does not attract the same attention as laparoscopic liver resection, robotic-assisted laparoscopic colorectal surgery, and laparoscopic cholecystectomy (25–27). Previous studies mentioned that the complication rates range from 1.3 to 10% (10–13). Although the risk of complications can be reduced by improving our ablation skills, using assisted methods or developing equipment. Assisted methods and ablation strategy have been reported to achieve complete ablation and reduce major complications in previous studies (28–32). The learning process of this technique has not been well studied. In our study, the learning curve of this

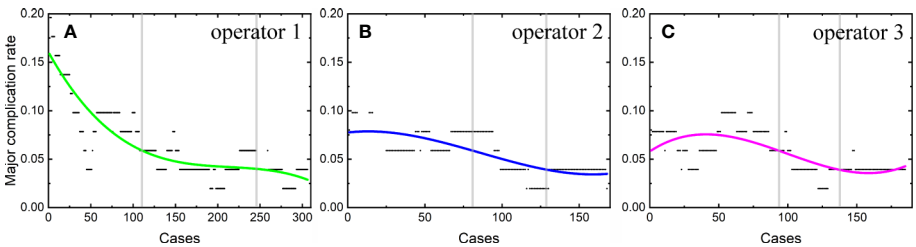

FIGURE 4 | Learning curve for thermal ablation of tumors in difficult locations of the operator 1 **(A)**, operator 2 **(B)** and operator 3 **(C)**.

technique has been explored, and the influence of handing-down teaching on the learning process has been analyzed.

The learning curve of 4,363 thermal ablation sessions in our single central shows five stages, namely, the high-risk, relative stable, unstable, proficient, and stable periods. A peak value of major complication rate of 5.5% appeared in the first stage. Then, the major complication rates decrease. The stable period of our group, with a major complication rate of 2% similar to a previous study (11), is after the relative stable, unstable, and proficient period. 1,150 patients in the first stage were treated by the first operator only. The major complication rate shows a mild trend of increase in the third stage, which may be caused by the new participants of the second and third operators. The second and third operators started their individual thermal ablation from the 928^{th} and 1227^{th} patients, which corresponds to the third stage (1151^{th}–2400^{th}). After that, the major complication rate decreased rapidly for the following 1,000 patients and became stable at 2%, which indicates that all the operators were skillful enough to perform thermal ablation.

We further plotted the learning curve for thermal ablation of each operator. According to the trends of the curves and the complication rates, we classified the learning process into three stages, according to the cut-off values of major complication rates of 4 and 2%. The first stage is the high-risk period with a major complication rate higher than 4%, the second stage is the proficient period having a rate higher than 2%, and the third stage with a stable complication rate of 2% is called the stable period. The results of our study demonstrate that the experience corresponding to about 400 to 500 patients were needed to bypass the first period. Under the guidance of handing-down teaching, the experience needed in the first period did not decrease for the second and third operator. Different from the first period, the required experience reduced significantly in the second period by the handing-down teaching. The first operator arrived at the stable period when treating the 1800^{th} patient, while the experience corresponding to only half number of patients was needed for the second and third operator. This result indicates that the handing-down teaching has an important effect on learning thermal ablation.

We found that the risk of major complication highly depends on the location of tumors, in agreement with a previous study (28). Patients with tumors in difficult locations have a high major complication rate, in accordance with previous results (28, 31). The major complication was usually caused by (1) puncturing the non-tumor tissues by electrode or antenna, (2) thermal damage. It has been reported that patients with tumors close to biliary duct or with tumors adjacent to diaphragm have a higher major complication rate (28, 33). In our study, the major complication rate of patients with tumors in difficult locations is 2.5 times as large as that of patients without a tumor located in difficult locations. Therefore, understanding the learning process of difficult thermal ablation is very important. We calculated the learning curve of 806 difficult thermal ablation sessions. Our results demonstrate that the peak value of major complication rate in the early period of 806 difficult sessions was higher than that of all the sessions (about 14 vs. 5.5%). Different from the trend of learning curve for all the sessions, the major complication rate for thermal ablation for tumors in difficult locations decreases rapidly and becomes stable at 4%. The second and third operators started their difficult ablation from the 104^{th} and 141^{th} patient with a tumor located in difficult locations, respectively. Besides, the trend of the learning curve was not affected by the participant of the second and third operators. Without any fluctuations, the complication rate on the learning curve for thermal ablations of tumors in difficult locations decreases gradually.

The learning curves for thermal ablations of tumors in difficult locations of each operator were calculated. The learning process was classified into three stages, namely, the high-risk, proficient and stable periods, according to the trend of curve and the cut-offs of complication rates of 6 and 4%. The handing-down teaching also shows an effect on the second period but a negligible effect on the first period. The experience of thermal ablation needed to bypass the second period were significantly reduced under the guidance of the teacher (the first operator: 290, the second operator: 175, and the third operator: 185). Furthermore, the peak values of major complication rates for thermal ablations of tumors in difficult locations were lower for "students" (the second and third operators) compared with that for the "teacher" (the first operator). The peak values of major complication rates for the second and third operators were about 8 to 9% compared with 16% for the first operator. All the above results indicate that thermal ablation for liver cancer is experience-dependent. The handing-down teaching can shorten the learning process and reduce peak value of the major complication rate.

The learning process of thermal ablation for liver cancer presents three stages. The first stage, namely, the high-risk period was the early stage of learning. Both in the learning processes of the team or individual operators, the highest major complication rates appear in the first stage. The experience needed to bypass the first stage of the learning process for all the patients and for patients with tumors in difficult locations was shown in our study. The beginner should pay more attention to the treatment of patients in the first stage. We found that the number of patients relevant to the first stage was stable, which may be determined by this technology itself. Thermal ablation for liver cancer is a minimally invasive treatment and easy-to-learn to perform, which shows low dependence on experience. Besides, the dependence on experience was concealed in the early stage due to the large portion of easy cases enrolled. We thought that the first learning stage of thermal ablation only means "operator can do it" not "operator can achieve it". After the first stage, more cases of patients with tumors in difficult locations were performed in the second stage, namely, proficient stage. The effects of handing-down teaching for thermal ablation are significant in the second stage. Less experience of thermal ablation was needed to bypass the second stage under handing-down teaching and to arrive at the stable period. Except for reducing the need of experience, handing-down teaching can also reduce the peak value of the major complication rate in patients with tumors in difficult locations. However, it should be pointed out that all the operators in our central had an experience of more than 1,000 ultrasound-guided procedures, and all the thermal ablation were performed with the

free-hand technique, which may have effects on the learning process of thermal ablation. To our knowledge, thermal ablation was performed by two operators with puncture trestle in some centrals (28, 34). Thus, the learning curve of thermal ablation in different central may be distinct.

Thermal ablation is not only experience-dependent but also equipment- and assisting method-dependent. In recent years, various assisting methods have been developed to reduce the risk of major complication. For example, PEIT and PTCD with intraductal chilled saline perfusion were used for tumors adjacent to large vessels or biliary duct (35, 36). Electrode or antenna deployed parallel to vessels can be also used to avoid damage of large vessels (28). For large tumors with rich blood supply, TACE can be performed before thermal ablation to weaken the influence of "heat sink effect" (37). The invisible lesions on US or CEUS were regarded as a contraindication for percutaneous US-guided thermal ablation. Now such lesions can be ablated under the guidance of US/CEUS-CECT/CEMRI fusing imaging (38–40). The No-Touch technique is used by inserting multiples electrodes around the periphery of the tumor and activating them sequentially to perform ablation with a sufficient peritumoural margin and decrease the risk of needle-path tumor implantation by avoiding direct puncture of the tumor (41, 42). The major complications in our hospital show that some major complications may largely appear in a specific period of time, such as skin burn or diaphragm damage. Among the 143 major complications in our central, only one case of several skin burns happened in the early stage of thermal ablation. The MTC-3CA microwave therapy instrument was performed for this patient. Although a cooled-shaft needle was used, the ablation antenna works in parallel with water-cooled circle. We turned on the ablation energy but not water-cooled circle, which caused the skin burn of patients. After that, the manufacturer changed the ablation antenna working in series with water-cooled circle and the skin burn never happens in our hospital. Most of the diaphragm damage also happened in the early stage of thermal ablation for the lack of effective assisting method. When the artificial ascites or pleural effusion technique has been developed, the major complications about diaphragm significantly decreased during the ablation procedure by using such assisting methods. Therefore, advanced equipment and effective assisting methods have the same importance as the experience of thermal ablation for reducing the risk of major complications.

Some limitations present in our study. First, although all the treatments in our central aim to achieve the radical treatment outcome, we focused on the learning curve about the major complication of thermal ablation but not the complete ablation rate or prognosis in this study. Second, considering the similarities of the two types of thermal ablation technologies, i.e., microwave ablation and radiofrequency ablation, they were not analyzed respectively.

CONCLUSION

The learning process of thermal ablation is classified into the high-risk, proficient and stable periods. The major complication rate of patients with tumors in difficult locations are higher than that of patients without a tumor in difficult locations. The major complication rate is stabilized at 2% for thermal ablation of all the tumors and 4% for thermal ablation of tumors in difficult locations. Handing-down teaching can reduce the experience needed to bypass the second period and reduce the peak value of major complication rate for patients with tumors in difficult locations. Our results can help the operators, especially beginners, achieve proficiency in an efficient fashion.

DATA AVAILABILITY STATEMENT

The datasets generated for this study are available on request to the corresponding author.

ETHICS STATEMENT

The studies involving human participants were reviewed and approved by Tianjin Third Central Hospital Institutional Review Board. Written informed consent for participation was not required for this study in accordance with the national legislation and the institutional requirements.

AUTHOR CONTRIBUTIONS

YZ and XJ designed the study and wrote the manuscript. JD and ZQ collected data. HZ, YW, and YW supervised the findings of this study. All authors contributed to the article and approved the submitted version.

FUNDING

This work was supported the Tianjin Science and Technology Commission (nos. 17ZXMFSY00050 and No.17YFZCSY01070).

REFERENCES

1. Heimbach JK, Kulik LM, Finn RS, Sirlin CB, Abecassis MM, Roberts LR, et al. AASLD guidelines for the treatment of hepatocellular carcinoma. *Hepatology* (2018) 67:358–80. doi: 10.1002/hep.29086
2. European Association for the Study of the Liver. Electronic address: easloffice@easloffice.eu, European Association for the Study of the Liver. EASL Clinical Practice Guidelines: Management of hepatocellular carcinoma. *J Hepatol* (2018) 69:182–236. doi: 10.1016/j.jhep.2018.03.019
3. Elliott R, Ram S, Khanna V. Classification and Current Treatment of Hepatocellular Carcinoma. *Am J Intervent Radiol* (2018) 2:8. doi: 10.25259/AJIR-21-2018
4. An C, Li X, Zhang M, Yang J, Cheng Z, Yu X, et al. 3D visualization ablation planning system assisted microwave ablation for hepatocellular carcinoma

(Diameter >3): a precise clinical application. *BMC Cancer* (2020) 20:44. doi: 10.1186/s12885-020-6519-y

5. Jiang A-N, Wang S, Yang W, Zhao K, Bai X-M, Zhang Z-Y, et al. The Role of a Curved Electrode with Controllable Direction in the Radiofrequency Ablation of Liver Tumors Behind Large Vessels. *Cardiovasc Intervent Radiol* (2019) 42:893–904. doi: 10.1007/s00270-019-02182-0
6. Ng KKC, Chok KSH, Chan ACY, Cheung TT, Wong TCL, Fung JYY, et al. Randomized clinical trial of hepatic resection versus radiofrequency ablation for early-stage hepatocellular carcinoma. *Br J Surg* (2017) 104:1775–84. doi: 10.1002/bjs.10677
7. Shi J, Sun Q, Wang Y, Jing X, Ding J, Yuan Q, et al. Comparison of microwave ablation and surgical resection for treatment of hepatocellular carcinomas conforming to Milan criteria. *Jf Gastroenterol Hepatol* (2014) 29:1500–7. doi: 10.1111/jgh.12572
8. Ding J, Jing X, Liu J, Wang Y, Wang F, Wang Y, et al. Complications of thermal ablation of hepatic tumours: comparison of radiofrequency and microwave ablative techniques. *Clin Radiol* (2013) 68:608–15. doi: 10.1016/j.crad.2012.12.008
9. Maeda M, Saeki I, Sakaida I, Aikata H, Araki Y, Ogawa C, et al. Complications after Radiofrequency Ablation for Hepatocellular Carcinoma: A Multicenter Study Involving 9,411 Japanese Patients. *Liv Cancer* (2020) 9(1):50–62. doi: 10.1159/000502744
10. Chua JME, Lam YMP, Tan BS, Tay KH, Gogna A, Irani FG, et al. Single-centre retrospective review of risk factors for local tumour progression and complications in radiofrequency ablation of 555 hepatic lesions. Singapore. *Med J* (2019) 60:188–92. doi: 10.11622/smedj.2019036
11. Livraghi T, Solbiati L, Franca Meloni M, Scott Gazelle G, Halpern EF, Nahum Goldberg S. Treatment of Focal Liver Tumors with Percutaneous Radio-frequency Ablation: Complications Encountered in a Multicenter Study. *Radiology* (2003) 226:441–51. doi: 10.1148/radiol.2262012198
12. Kong W-T, Zhang W-W, Qiu Y-D, Zhou T, Qiu J-L, Zhang W, et al. Major complications after radiofrequency ablation for liver tumors: analysis of 255 patients. *World J Gastroenterol* (2009) 15:2651–6. doi: 10.3748/wjg.15.2651
13. Liang P, Wang Y, Yu X, Dong B. Malignant Liver Tumors: Treatment with Percutaneous Microwave Ablation—Complications among Cohort of 1136 Patients. *Radiology* (2009) 251:933–40. doi: 10.1148/radiol.2513081740
14. Fang C, Cortis K, Yusuf GT, Gregory S, Lewis D, Kane P, et al. Complications from percutaneous microwave ablation of liver tumours: a pictorial review. *Br J Radiol* (2019) 92:20180864. doi: 10.1259/bjr.20180864
15. Kasugai H, Osaki Y, Oka H, Seki T, Kudo M. Severe complications of radiofrequency ablation therapy for hepatocellular carcinoma: analysis of 3,891 ablations in 2,614 patients. *Oncology* (2007) 72:72–5. doi: 10.1159/000111710
16. Moumouh A, Hannequin J, Chagneau C, Rayeh F, Jeanny A, Weber-Holtzscherer A, et al. A tamponade leading to death after radiofrequency ablation of hepatocellular carcinoma. *Eur Radiol* (2005) 15:234–7. doi: 10.1007/s00330-004-2485-z
17. Melikian R, Minocha J. Septic Shock and Death after Microwave Ablation of Hepatocellular Carcinoma in a Liver Transplant Patient with a Bilioenteric Anastomosis. *Semin Intervent Rad* (2019) 36:137–41. doi: 10.1055/s-0039-1688430
18. Poon RT, Ng KK, Lam CM, Ai V, Yuen J, Fan ST, et al. Learning Curve for Radiofrequency Ablation of Liver Tumors. *Ann Surg* (2004) 239:441–9. doi: 10.1097/01.sla.0000118565.21298.0a
19. Yan TD, King J, Sjarif A, Glenn D, Steinke K, Morris DL. Learning curve for percutaneous radiofrequency ablation of pulmonary metastases from colorectal carcinoma: a prospective study of 70 consecutive cases. *Ann Surg Oncol* (2006) 13:1588–95. doi: 10.1245/s10434-006-9010-3
20. Hildebrand P, Leibecke T, Kleemann M, Mirow L, Birth M, Bruch HP, et al. Influence of operator experience in radiofrequency ablation of malignant liver tumours on treatment outcome. *Eur J Surg Oncol* (2006) 32:430–4. doi: 10.1016/j.ejso.2006.01.006
21. Burke DR, Lewis CA, Cardella JF, Citron SJ, Drooz AT, Haskal ZJ, et al. Quality improvement guidelines for percutaneous transhepatic cholangiography and biliary drainage. *J Vasc Intervent Radiol* (2003) 14: S243–6. doi: 10.1016/j.jvir.2010.01.012
22. Yu J, Liang P, Yu X-L, Cheng Z-G, Han Z-Y, Liu F-Y. Comparison of cooled-probe microwave and radiofrequency ablation treatment in incipient hepatocellular carcinoma: A phase III randomized controlled trial with 6-year follow-up. *J Clin Oncol* (2016) 34:4068–8. doi: 10.1200/JCO.2016.34.15_suppl.4068
23. Huang Q, Zeng Q, Long Y, Tan L, Zheng R, Xu E, et al. Fusion imaging techniques and contrast-enhanced ultrasound for thermal ablation of hepatocellular carcinoma - A prospective randomized controlled trial. *Int J Hyperthermia* (2019) 36:1207–15. doi: 10.1080/02656736.2019.1687945
24. Gennaro N, Mauri G, Varano GM, Monfardini L, Pedicini V, Poretti D, et al. Thermal Ablations for Colorectal Liver Metastases. *Dig Dis Intervent* (2019) 03:117–25. doi: 10.1055/s-0039-1688724
25. Sultana A, Nightingale P, Marudanayagam R, Sutcliffe RP. Evaluating the learning curve for laparoscopic liver resection: a comparative study between standard and learning curve CUSUM. *HPB* (2019) 21:1505–12. doi: 10.1016/j.hpb.2019.03.362
26. Bokhari MB, Patel CB, Ramos-Valadez DI, Ragupathi M, Haas EM. Learning curve for robotic-assisted laparoscopic colorectal surgery. *Surg Endosc* (2011) 25:855–60. doi: 10.1007/s00464-010-1281-x
27. Moore MJ, Bennett CL. The learning curve for laparoscopic cholecystectomy. The Southern Surgeons Club. *Am J Surg* (1995) 170:55–9. doi: 10.1016/S0002-9610(99)80252-9
28. Yang W, Yan K, Wu G-X, Wu W, Fu Y, Lee J-C, et al. Radiofrequency ablation of hepatocellular carcinoma in difficult locations: Strategies and long-term outcomes. *World J Gastroenterol* (2015) 21:1554–66. doi: 10.3748/wjg.v21.i5.1554
29. Liu F, Yu X, Cheng Z, Han Z, Sun Y, Liang P, et al. Comparison of ultrasonography-guided percutaneous microwave ablation for subcapsular and nonsubcapsular hepatocellular carcinoma. *Eur J Radiol* (2017) 91:93–8. doi: 10.1016/j.ejrad.2017.04.002
30. Chen S, Peng Z, Lin M, Chen Z, Hu W, Xie X, et al. Combined percutaneous radiofrequency ablation and ethanol injection versus hepatic resection for 2.1–5.0 cm solitary hepatocellular carcinoma: a retrospective comparative multicentre study. *Eur Radiol* (2018) 28:3651–60. doi: 10.1007/s00330-018-5371-9
31. An C, Cheng Z, Yu X, Han Z, Liu F, Li X, et al. Ultrasound-guided percutaneous microwave ablation of hepatocellular carcinoma in challenging locations: oncologic outcomes and advanced assistive technology. *Int J Hyperthermia* (2020) 37:89–100. doi: 10.1080/02656736.2019.1711203
32. Ding J, Zhou Y, Wang Y, Jing X, Wang F, Wang Y. Percutaneous microwave ablation of exophytic tumours in hepatocellular carcinoma patients: Safe or not? *Liver Int* (2017) 37:1365–72. doi: 10.1111/liv.13426
33. Lin M-X, Ye J-Y, Tian W-S, Xu M, Zhuang B-W, Lu M-D, et al. Risk Factors for Bile Duct Injury After Percutaneous Thermal Ablation of Malignant Liver Tumors: A Retrospective Case–Control Study. *Dig Dis Sci* (2017) 62:1086–94. doi: 10.1007/s10620-016-4312-1
34. Ye J, Huang G, Zhang X, Xu M, Zhou X, Lin M, et al. Three-dimensional contrast-enhanced ultrasound fusion imaging predicts local tumor progression by evaluating ablative margin of radiofrequency ablation for hepatocellular carcinoma: a preliminary report. *Int J Hyperthermia* (2019) 36:55–64. doi: 10.1080/02656736.2018.1530460
35. Li X, Yu J, Liang P, Yu X, Cheng Z, Han Z, et al. Ultrasound-guided percutaneous microwave ablation assisted by three-dimensional visualization operative treatment planning system and percutaneous transhepatic cholangial drainage with intraductal chilled saline perfusion for larger hepatic hilum hepatocellular (D ≥ 3 cm): preliminary results. *Oncotarget* (2017) 8:79742–9. doi: 10.18632/oncotarget.19275
36. Li M, Li Z, Gao Y, Tian J, Chen M, Dong J. Safety and efficacy of percutaneous radiofrequency ablation combined with percutaneous ethanol injection for hepatocellular carcinoma in high-risk locations. *Adv Ultrasound Diagn Ther* (2018) 2:5–16.
37. Chen Q-W, Ying H-F, Gao S, Shen Y-H, Meng Z-Q, Chen H, et al. Radiofrequency ablation plus chemoembolization versus radiofrequency ablation alone for hepatocellular carcinoma: A systematic review and meta-analysis. *Clin Res Hepatol Gastroenterol* (2016) 40:309–14. doi: 10.1016/j.clinre.2015.07.008
38. Ahn SJ, Lee JM, Lee DH, Lee SM, Yoon J-H, Kim YJ, et al. Real-time US-CT/MR fusion imaging for percutaneous radiofrequency ablation of hepatocellular carcinoma. *J Hepatol* (2017) 66:347–54. doi: 10.1016/j.jhep.2016.09.003
39. Hakime A, Yevich S, Tselikas L, Deschamps F, Petrover D, De Baere T. Percutaneous Thermal Ablation with Ultrasound Guidance. Fusion Imaging

Guidance to Improve Conspicuity of Liver Metastasis. *Cardiovasc Intervent Radiol* (2017) 40:721–7. doi: 10.1007/s00270-016-1561-5

40. Calandri M, Ruggeri V, Carucci P, Mirabella S, Veltri A, Fonio P, et al. Thermal ablation with fusion imaging guidance of hepatocellular carcinoma without conspicuity on conventional or contrast-enhanced US: surrounding anatomical landmarks matter. *Radiol Med* (2019) 124:1043–8. doi: 10.1007/s11547-019-01057-1
41. Petit A, Hocquelet A, N'kontchou G, Varin E, Sellier N, Seror O, et al. No-Touch Multi-bipolar Radiofrequency Ablation for the Treatment of Subcapsular Hepatocellular Carcinoma ≤ 5 cm Not Puncturable via the Non-tumorous Liver Parenchyma. *Cardiovasc Intervent Radiol* (2020) 43:273–83. doi: 10.1007/s00270-019-02357-9
42. Seror O, N'Kontchou G, Nault J-C, Rabahi Y, Nahon P, Ganne-Carrié N, et al. Hepatocellular Carcinoma within Milan Criteria: No-Touch Multibipolar Radiofrequency Ablation for Treatment—Long-term Results. *Radiology* (2016) 280:611–21. doi: 10.1148/radiol.2016150743

Conflict of Interest: The authors declare that the research was conducted in the absence of any commercial or financial relationships that could be construed as a potential conflict of interest.

frontiers in Oncology

REVIEW
published: 29 October 2020
doi: 10.3389/fonc.2020.580431

Thermal Ablation of Benign Thyroid Nodules and Papillary Thyroid Microcarcinoma

Xiao-Wan Bo[1,2,3], *Feng Lu*[1,2,3], *Hui-Xiong Xu*[1,2,3], *Li-Ping Sun*[1,2,3]* *and Kun Zhang*[1]*

[1] Department of Medical Ultrasound, Shanghai Tenth People's Hospital, Ultrasound Research and Education Institute, Tongji University Cancer Center, Shanghai Engineering Research Center of Ultrasound Diagnosis and Treatment, Tongji University School of Medicine, Shanghai, China, [2] Thyroid Institute, Tongji University School of Medicine, Shanghai, China, [3] Department of Medical Ultrasound, Shanghai Center for Thyroid Diseases, Shanghai, China

Due to the increasing rates of physical examination and application of advanced ultrasound machines, incidences of benign thyroid nodules (BTNs) and papillary thyroid microcarcinoma (PTMC) were dramatically up-regulated in recent years. Thermal ablation (TA) has been widely used and regarded as a safe and effective method to eliminate or reduce BTNs and recurrent low-risk PTMC. However, conclusions using TA to treat primary PTMC are controversial. Recently, several long-term and prospective studies on TA treatment of BTNs and primary PTMC have been reported. Here, we review current literatures and progress on TA treatment of BTNs and PTMC and underline the way to get the best treatment outcomes, providing a comprehensive insight into the research progresses in this field.

Keywords: thyroid nodules, benign thyroid nodules, primary papillary thyroid microcarcinoma, recurrent papillary thyroid microcarcinoma, thermal ablation

OPEN ACCESS

Edited by:
Wei Yang,
Peking University Cancer Hospital, China

Reviewed by:
Yi Dong,
Fudan University, China
Jie Ren,
The Third Affiliated Hospital of Sun Yat-Sen University, China

***Correspondence:**
Li-Ping Sun
sunliping_s@126.com
Kun Zhang
zhang1986kun@126.com

Specialty section:
This article was submitted to Cancer Imaging and Image-directed Interventions, a section of the journal Frontiers in Oncology

Received: *06 July 2020*
Accepted: *21 September 2020*
Published: *29 October 2020*

Citation:
Bo X-W, Lu F, Xu H-X, Sun L-P and Zhang K (2020) Thermal Ablation of Benign Thyroid Nodules and Papillary Thyroid Microcarcinoma. Front. Oncol. 10:580431. doi: 10.3389/fonc.2020.580431

INTRODUCTION

Thyroid nodules are frequently detected due to the application of ultrasound examination in recent years (1–5). Most of the nodules are benign thyroid nodules (BTNs) or papillary thyroid microcarcinoma (PTMC). Of note, papillary thyroid carcinoma (PTC) is the most common thyroid cancer but features excellent prognosis and low mortality rate (5, 6). Though active surveillance was recommended for the low-risk PTMC, patients with low-risk PTMC often received aggressive over-treatments (7). Thyroidectomy is the first-line treatment method for BTNs and PTMC according to the 2015 ATA guidelines and 2016 Chinese expert consensus and guidelines (4, 5, 7–9). However, limitations remain unavoidable in reality. On one hand, a few patients may feel fear about or not be appropriate for surgery. On the other hand, thyroidectomy will leave permanent scars and require long-time levothyroxine sodium tablets after surgery, which will cause patients, especially young females, to worry about this treatment. Therefore, alternative minimally surgical techniques or non-surgical invasive treatment methods for thyroid nodules are needed.

Percutaneous chemical ablation (ethanol ablation [EA] or polidocanol injection) was usually used to treat cystic or predominantly cystic BTNs (10–15). Thermal ablation (TA), including radiofrequency ablation (RFA), microwave ablation (MWA), laser ablation (LA), and high intensity focused ultrasound (HIFU), were generally applied for solid or mixed BTNs (15–17). TA therapy for

BTNs has been widely utilized across many countries with good efficacy and safety, as revealed by multi-center studies, longitudinal observational studies, guidelines, as well as meta-analyses (18–23). Nevertheless, not all BTNs were appropriate for TA therapy. Long ablation time or multiple ablation operations are needed for the nodules with large sizes. Moreover, fine-needle aspirations (FNA) or core needle biopsy (CNB) was performed to diagnose the thyroid nodules before ablation. However, false negatives may occur in FNA or CNB as they were not the gold standard.

TA was also used for the treatment of recurrent PTMC (24–27). However, the conclusions related to TA of primary PTMC were controversial. Some prospective or retrospective but long-term follow-up studies reported that TA was an effective and safe method for the selected low-risk PTMC (28–30). Before RFA, patients should have no local invasion, regional lymph node, and distant metastasis. Ultrasound and computed tomography (CT) were often used to detect the regional lymph node and distant metastasis (31). However, some regional lymph node metastasis is difficult to detect.

In this present study, we will review the latest progress in TA treatment of BTNs and PTMC to summarize the efficacy and safety of TA techniques, analyze factors related to the efficacy of ablation, and explore future research directions of this topic.

PATIENTS INCLUDED

The selection of patients before TA is related to the safety and efficacy of TA treatment.

Patients With BTNs

Patients included for TA are as follows: patients with symptomatic or cosmetic problems; patients fearing malignancy; refusal of or contraindications to surgery or radioiodine therapy. The nodules included for TA are as follows: cytological confirmation of a benign thyroid nodule on two separate ultrasound-guided biopsies (ultrasound-guided FNA or CNB); no malignant US findings; solid, predominantly solid, or cystic thyroid nodules; thyrotoxicosis in cases of autonomously functioning thyroid nodules (1, 16, 17, 21–23).

The exclusion criteria are as follows: pregnant women; history of radiation to the neck; follicular neoplasm; severe bleeding tendency because of coagulation disorder; severe heart failure/liver failure/respiratory failure or renal failure; no puncture route judged by US; nodules with heavy calcifications (1, 16, 17, 21–23).

Patients With PTMC

The inclusion criteria are as follows: refusal of or contraindications to surgery (e.g., age > 80 years or a co-morbidity such as cardiovascular disease, history of stroke, central nervous system vascular malformation, other malignancy, and immunocompromised state); confirmation of PTMC on ultrasound-guided biopsy; no evidence of gross extrathyroidal extension or metastasis (lymphatic or distant metastasis) on both ultrasound and contrast-enhanced computed tomography (CT); either multiple or solitary PTMCs (1, 25–31).

The exclusion criteria are consistent with those patients with BTNs. Moreover, multiple nodules or those PTMCs without ablation safety margin (less than 2 mm away from the thyroid capsule) were also excluded for TA treatment (1, 25–31).

The Basic Principle of TA

The basic principle of TA is to use the heat energy generated by RF electrode needle, MW antenna, LA fiber, or HIFU to generate coagulative necrosis of the nodules. The coagulation necrotic tissue cells are dissolved and liquefied by hydrolytic enzymes, and they are finally absorbed by lymphocyte and blood vessels. Then the ablation zone gradually decreases and finally disappears completely.

TA TREATMENT OF BTNS

RFA

RFA was first reported for the treatment of BTNs in 2006 (32). In the past 10 years, the safety and efficacy of RFA therapy has been validated by some prospective randomized controlled trials (RCTs) and multicenter researches (18–23, 33). The volume reduction rates (VRR) of BTNs were 66.8%–68%, 63%–74.3%, and 70%–82% at 3, 6, and 12 months after RFA, respectively (22, 34–37). Accordingly, therapeutic success (defined as VRR>50%) can be achieved three months after RFA. Intriguingly, some long-term follow-up studies were reported on the efficacy of RFA for BTNs recently (22, 37). For example, a prospective multicenter study indicated that the mean VRR was 80.3%, 84.3%, 89.2%, 91.9%, and 95.3% at 12, 24, 36, 48, and 60 months after RFA treatment (22). Similarly, another retrospective longitudinal observational study reported that the mean VRR was 63%, 67.4%, 66.7%, 66.9%, and 66.9% at the 1-, 2-, 3-, 4-, and 5-year follow-up, respectively (37). Collectively, these long-term follow-up studies showed that VRR remained stable at least one year after RFA.

The symptom and cosmetic problems are the main reasons that patients with BTNs chose to accept treatment. After RFA, patients' symptom and cosmetic scores were significantly decreased during the follow-up period (22, 34–37). No related deaths were found during and after RFA and the major complication rate was less than 2% (1). Complications such as voice change, pain, hematoma, vomiting, nodule rupture, and Horner syndrome were mostly received after RFA treatment (1). Nevertheless, RFA therapy had fewer complications and pains, preservation of thyroid function as compared with surgery, alongside reduced hospitalization days and increased patients' satisfaction after RFA (22, 38, 39). Moreover, as patients usually get satisfactory results 3 months after treatment and remain stable at 12 months after RFA, RFA could be considered as the first-line treatment for BTNs for selected patients.

MWA

Ultrasound-guided percutaneous MWA that was first introduced in 2012 (40) and 2013 in China (41) ranks as the second approach for BTNs treatment. Similar to RFA, MWA is also effective and safe in decreasing the symptom and cosmetic scores for BTNs, even for large (≥3 cm) benign thyroid nodules (18, 42–45). The VRR was 54.3%–75.1%, 68.7%–85.2%, and 88.6%–96.4% at the 3-, 6-, and 12-month follow-up after ablation (17, 42, 44). RFA and MWA showed approximately identical results considering VRR at 3 months follow-up (46). However, RFA showed higher VRRs at the 6- and 12-month follow-up (45). MWA exhibits advanced advantages compared to thyroid lobectomy including faster recovery, fewer complications, more complete thyroid function preservation, superior esthetic results, less physiologic disruption, less expense, and lower systemic stress response (17, 47–49). In summary, MWA should be also considered as one of the first-line treatments for BTNs, especially for larger BTNs since MWA is expected to be more effective based on previous studies. However, more long-term follow-up studies are needed.

LA

In 2006, ultrasound-guided LA was first introduced for treating patients with BTNs-bearing who are inoperable or unwilling to operate (50). The safety and efficacy of LA of BTNs also have been widely demonstrated, accompanied with significant and persistent volume reduction and local symptom improvement (16, 51–53). The VRR was 55%, 49%–53%, 59%–84% at 3, 6, 12 months follow-up after LA, respectively (51, 54–56). A three-year multicenter prospective randomized trial showed that the VRR was 59%, 60%, and 57% at 1, 2, and 3 years after LA, respectively (56). Compared to RFA and MWA, LA showed similar efficacy and safety considering VRR at 3-months follow-up (56–58). However, the VRR was lower than RFA, but higher than MWA at 6-months follow-up as well as subsequent follow-ups (58–60). From previous literatures, the VRR was relatively low in LA for BTNs. Long-term follow-up studies are also lacking, and more prospective randomized trials are needed to observe efficacy in the future.

HIFU

HIFU was first reported for the treatment of BTNs in 2011 (61). Subsequently, Lang et al. demonstrated that the mean VRR was 68.87% after 12-month post-HIFU for 22 patients by using nodule volume as the sole determinant of ablation success in a prospective study (62). Lang et al. reported that the mean VRR at 3, 6, 12, 18, and 24 months was 51.32%, 62.99%, 68.66%, 69.76%, and 70.41%, respectively, after HIFU treatment for 108 patients (63). The pooled VRR was 17.59%, 48.93%, and 60.43% at 1, 3, and 6 months after HIFU for BTNs in a systematic review and meta-analysis (64). However, for larger nodules (>20 ml), additional operations were needed at 3–6 months after initial HIFU treatment (65, 66). Compared with open lobectomy, HIFU treatment benefits patients with less treatment time, shortened hospitalization duration, and lower medical cost (67). Noticeably, as a novel and relatively less frequently applied method, HIFU treatment has some drawbacks for the treatment of BTNs, e.g., patients should be stable during HIFU treatment, and longer ablation time and multiple ablation times are needed for patients with large BTNs. Thus, HIFU may be not suitable for patients with large BTNs.

At last, from the long-term retrospective and perspective studies (**Table 1**), RFA showed more effective consequences in reducing nodule volume compared to LA for the treatment of BTNs. Nevertheless, no studies were found on MWA or HIFU for BTNs with more than 2-years follow-up. In addition, few major complications (0%–4.2%) emerged after TA in these long-term follow-up studies (**Table 1**). The most common complications are voice change, vocal cord paresis, laryngeal nerve palsy, intraoperative hemorrhage, and Horner syndrome according to these long-term follow-up studies (**Table 1**). Nevertheless, some nodules regrowth (4.1%–20.4%) after TA still occurred in these studies (**Table 1**). Thus, more prospective and long-term studies are needed in TA treatment of BTNs to obtain the comprehensive conclusions.

TA TREATMENT OF PTMC

RFA

RFA could be considered as an alternative method of reoperation objective to recurrent thyroid cancers, as revealed by multiple studies (24–27). For example, Kim et al. reported comparable recurrence-free survival rates between RFA and reoperation for either 1 year (96.0% vs. 92.2%) or 3 year (92.6% vs. 92.2%) groups. The post-treatment complication rates (e.g., hoarseness and hypocalcemia) did not differ significantly between the RFA and reoperation groups (24). In another report, Zhang et al. revealed that the mean VRR was 54%, 81%, 92%, 96%, and 100% at the 1-, 3-, 6-, 12-, and 18-month after RFA, respectively. No residual or recurrent tumor or complications were found during the follow-up period (26). Chung et al. reported that the VRR of RFA for recurrent PTCs was 99.5%, wherein 91.3% of the nodules completely disappeared in the mean 80-months follow-up period (27).

Recently, two studies showed that RFA was also an effective and safe method for primary low-risk PTMC with no local tumor progression or distant metastasis during long-term follow-up (68, 69). As a paradigm, Cho et al. reported that the complete disappearance rates of primary low-risk PTMC were 98.8% and 100% at the 24- and 60-month follow-up after RFA. During the follow-up period, no local tumor progression and lymphatic or distant metastasis were observed. Concurrently, no patients underwent delayed surgery (68). Zhang et al. found that RFA showed similar oncologic outcomes after over 5 years' follow-up, whereas RFA displayed shorter operation and hospitalization time, lower complications, and less total cost compared with surgery (69). In one study with a large population, 91.4% (139/152) of the ablated low-risk PTMCs completely disappeared with no local or distant recurrence during the mean 39-months follow-up period (31). In terms of health-related life quality, US-guided RFA offers more advantages than surgery, supporting the conclusion that RFA can serve as an alternative strategy for PTMC (70).

TABLE 1 | Overview of studies with long-term follow-up on TA treatment of BTNs.

First author/ reference no.	Study design	Journal	Country	Case	Method	Nodule volume (ml)	VRR (%) at the 1-, 3-, 6-, 12-, 24-, 36-, 48-, 60-, 72-month	Major complication rate (%)	Regrowth rate (%)
Valcavi (2010) (53)	RCS	Thyroid	Italy	122	LA	23.1 ± 21.3	6.2, NR, 47.5, 50.6, 51.6, 47.8	0	9
Papini (56)	RCT	J Clin Endocrinol Metab	Italy	101	LA	6-17	NR, NR, 49, 59, 60, 57	0.9	NR
Jung (22)	PCS	Korean J Radiol	Korea	345	RFA	14.2 ± 13.2	44.4, NR, NR, 80.3, 84.3, 89.2, 91.9, 95.3	1	NR
Deandrea (37)	RCS	J Clin Endocrinol Metab	Italy	215	RFA	20.9	NR, NR, 56.2, 63, 67.4, 66.7, 66.9, 66.9, 72	0	4.1
Aldea (33)	PCS	J Vasc Interv Radiol	Spain	24	RFA	NR	33.0, 52.1, 56.8, 68.8, 69.9, 76.8,	4.2	NR
Lang (63)	RCS	Eur Radiol	China	136	HIFU	13.09	NR, 51.3, 63.0, 68.7, 70.4	3.7	20.4
Hu (45)	RCS	J Cancer Res Ther	China	100 vs. 72	MWA vs. RFA	13.0 vs. 10.7	24.0, 54.8, 68.7, 75.8 vs. 22.7, 56.1, 77.9, 85.4	4 vs. 2.8	NR

TA, thermal ablation; BTNs, benign thyroid nodules; VRR: volume reduction rates; RCS, retrospective cohort study; PCS, prospective cohort study; RCT, randomized controlled trial; LA, laser ablation; RFA, radiofrequency ablation; HIFU, high intensity focused ultrasound; MWA, microwave ablation; NR, not reported.

MWA

In 2014, Yue et al. first used ultrasound-guided percutaneous MWA for treatment with PTMC, and in a mean 11-months' follow-up study, all tumors were completely ablated at a single session and no serious complications occurred (71). Similarly, Teng et al. performed MWA for 21 PTMCs and found that 95.2% of nodules were completely absorbed with no recurrent nodule after 3 years' follow-up (72). A systematic review and meta-analysis reported that MWA showed significant improvements in nodule volume, clinical symptom scores, and beauty scores between the baseline and final follow-up visits. However, common adverse effects such as hematomas, unbearable pain, and transient or permanent voice change were reported in corresponding 3.8%, 2.2%, and 4.6% of patients from the 33 original articles, but none of these incidents resulted in patients' hospitalization or death (43). In a 5-year follow-up report, 98.9% of nodules that were diagnosed to be primary PTMC were completely ablated by MWA, with a VRR of 99.37% (30). In a prospective study, 119 unifocal PTMC patients were treated with MWA, VRR was 99.4%, and 93.9% of nodules went into complete remission after mean 37-months follow-up. No residual or recurrent nodules after MWA was observed (29). In a large-cohort study consisting of 185 patients with 206 primary PTMCs, the mean VRR at 21-months follow-up was 98.65% after MWA treatment and 84.5% of nodules were fully absorbed (73). Collectively, these evidences suggest MWA is safe and effective in primary PTMC treatment and offer a new alternative choice for clinical treatment.

LA

Papini et al. first used LA for local PTMC treatment in an otherwise inoperable patient with thyroid gland at high surgical risk, indicating LA was a safe and effective ablative method (74). Zhou et al. reported that 96.7% (29/30) of the nodules were successfully ablated after a single session. After 1-year follow-up, 33.3% of the ablation zones disappeared, and the remaining 66.67% zones are scar-like nodules. No local recurrence or distant metastases were found in the last follow-up (9). In a retrospective study, the VRR of 81 solitary PTMC treated with LA was 98.4% after mean 49-months follow-up. Compared with surgical group, the patients in the LA group showed shorter hospital stay and procedure time and lower complication and recurrence rates (75). In another retrospective study, 37 patients with primary PTMC were treated with LA, and 32.4% of the treated nodules disappeared and only one patient suffered from cervical lymph node metastasis during 2-years follow-up (76). In summary, LA is also a useful approach for treating primary PTMC.

Interestingly, in the last three years, some long-term follow-up studies summarized that no local recurrence was found after TA of primary PTMC; the recurrence rates in the remaining thyroid were also very low, and few major complications (0%–2.4%) were found during and after the procedure (**Table 2**). The most common complications are voice change and hoarseness (**Table 2**). More than 90% of tumors completely disappeared at the last follow-up period (**Table 2**). However, there are still some nodules requiring additional ablation owing to the insufficient

TABLE 2 | Overview of studies with long-term follow-up on TA treatment of primary PTMC.

First author/ reference no.	Study design	Journal	Country	Method	Case	Follow-up (months)	Complete disappearance rates (%)	Additional ablation (%)	Local recurrence rate (%)	Recurrence in remaining thyroid (%)	LN or distant metastasis rate (%)	Major complications rate (%)
Teng (72)	RCS	J Cancer Res Clin Oncol	China	MWA	21	36	95.2	0	0	0	0	0
Lim (31)	RCS	Korean J Radiol	Korea	RFA	152	39	91.4	9.8	0	0	0	0.8
Zhou (75)	RCS	Int J Hyperthermia	China	LA	36	49	94.4	0	0	0	5.5 (LN)	0
Yue (29)	PCS	J Clin Endocrinol Metab	China	MWA	119	37	93.9	1	0	0	0.8 (LN)	0
Teng (30)	RCS	Thyroid	China	MWA	41	60	97.6	0	0	0	0	2.4
Cho (68)	RCS	Thyroid	Republic of Korea	RFA	84	72	100	15.5	0	4.1	0	1.4
Zhang (69)	RCS	Thyroid	China	RFA	94	64	NR	0	0	1.1	0	0

TA, thermal ablation; PTMC, papillary thyroid microcarcinoma; LN, lymph node; RCS, retrospective cohort study; PCS, prospective cohort study; MWA, microwave ablation; RFA, radiofrequency ablation; LA, laser ablation; NR, not reported.

safety margins after the first ablation. In addition, there is no report on the usage of HIFU for the treatment of PTMC yet.

DISCUSSION

Eliminating the symptoms or cosmetic problems are the main goals of treating those patients with BTNs. Through systematic and comprehensive reviewing of the field's progress, we know that all current TA techniques are effective in reducing VRR and patients' symptoms or cosmetic problems. Fewer complications or adverse events were reported during and after TA for BTNs. Overall, more prospective, multicenter, and long-term follow-up researches were reported in RFA for BTNs than other TA techniques (18, 19, 21–23). Compared with MWA, LA, or HIFU, RFA showed higher VRRs in studies with long-term follow-up for BTNs. Accordingly, RFA may be the preferred treatment for BTNs, and more studies should be carried out on other TA techniques for BTNs.

The symptoms or cosmetic problems are usually found in patients with large nodules. However, the main factors affecting the incomplete ablation were large size and narrow range adjacent to the danger triangle area or carotid artery or trachea and peripheral blood flow (77). Although the overall successful rate is high, the requirement of second-session TA may occur in those cases that nodules are not completed ablated in the first-session treatment. Under such conditions, the total expenses will increase as multiple ablations proceed, which may augment the economic burden of these patients. In addition, as the nodules are not completely ablated, the therapeutic success is difficult to achieve, and the regrowth tends to occur more frequently (78). To avoid these inconveniences, the BTNs should be ablated as completely as possible in one-session treatment.

In addition, factors related to VRR should be critically assessed. The initial volume, initially predominant solidity, clear ill-defined margins, applied energy, and initial ablation ratio were the possible predictive factors of VRR (78–82). For example, over 70% of initial ablation ratio usually predicts VRR of over 50% after RFA (79). However, Lee et al. reported that the VRR of predominantly cystic vs. predominantly solid nodules was similar at 6-months follow-up in a study consisting of 1,000 patients with 1,619 thyroid nodules (78). Moreover, the hardness of the ablation zone after TA may be another factor affecting the VRR despite no association between them reported currently. Collectively, there are no stable predictors of VRR after TA treatment, and more prospective studies on the factors affecting VRR are needed.

The nodule regrowth in BTNs after TA is a critical concern for patients. It is believed that the factors including larger size, the delivery of lower energy, and incomplete and insufficient ablation of the external border of the nodules correlate with regrowth rates (82, 83). Consistent with this, Wang et al. demonstrated that larger initial volume, more irregular blood vessel, and nodules adjacent to the vital structures were found accessible in the recurrence group (84). Recently, Negro et al. suggested that non-spongiform nodules and 12-month VRR <

50% increased the risk of BTNs regrowth after LA in a 5-year follow-up retrospective study (85).

In light of above analysis, the size and location of the nodule are the main factors that affect complete ablation rate, VRR, and nodule regrowth. Regarding this, patients with too large nodules are more suitable for TA. TA can be considered as the first-line treatment for patients with BTNs featuring medium size, even though the symptoms or cosmetic problems are not obvious. However, the specific volume values of larger nodules are uncertain (20, 37, 82). In addition, the new ablation techniques including artery-first ablation, marginal venous ablation, and hydrodissection technique may be useful to decrease the incomplete ablation rate and repress nodule regrowth (86). Thus, it is speculated that more patients will benefit from TA due to the application of advanced ablation techniques.

Interestingly, the successful ablation rates and VRR of TA for PTMC were higher than TA for BTNs during the follow-up periods. Recent long-term prospective and retrospective studies demonstrated that TA was also effective for primary PTMC due to low complications and recurrences (29, 30, 68, 87). From one recent systematic review and meta-analysis, RFA and MWA for primary PTMC were found to show higher VRR than LA (87). Compared with surgery, TAs need less operation and hospitalization time and have a lower total cost. Patients received better health-related life quality, lower total costs, and stress response (69, 70). The major concerns are the lymphatic or distant metastasis in patients with primary PTMC before and after ablation. Actually, low-risk primary PTMCs are rarely found with metastasis, and most metastasis can be found by careful high-resolution ultrasound and CT examination before ablation (7). Moreover, up to now, there have been few researches reporting the local or distant metastasis after TA.

Although patients with low-risk primary PTMC are not recommended for TA treatment, some patients fear metastasis and desire early treatment. Compared with surgery, patients benefit from TA, typically associating with shorter treatment and hospitalization time, lower complications, and no neck scars. Moreover, RFA, MWA, or LA showed similar efficacy and safety on the basis of previous long-term follow-up studies. Taken together, TA is a promising alternative treatment for patients with low-risk primary PTMC.

Although TA is an effective and safe method for the treatment of BTNs and low-risk primary PTMC, some limitations of TA should also receive more attention. First, TA is not suitable for all types of thyroid nodules comparing with surgery, especially for large BTNs, substernal nodules, and deep located nodules. Second, there are still some nodules with incomplete response and local regrowth in the following-up period, which will need repeated ablation or surgery. Third, some nodules shrunk slowly but failed to completely recede according to the current studies. Accordingly, more studies focusing on improving the effectiveness of ablation and reducing local or distant recurrence of nodules are demanded in the future.

Outlook

In this review, some prospective and prospective clinical studies with long follow-up periods showed that TA was effective and safe for the treatment of BTNs and PTMC. Nevertheless, more prospective randomized controlled trials of large samples comparing TA with surgery with more than five-year follow-up are still absent. Moreover, it is also unsure on whether TA is also effective for the treatment of large PTC or other pathological subtypes of thyroid carcinoma. In addition, the dissolved gas will give birth to bubbles that usually cause strong backscattering ultrasonic signals, which inevitably introduces mistakes into the assessment and monitoring of the ablation process and lesion boundary. To overcome this issue, new imaging technology featuring precise ablation guidance and curative assessment will also be explored. Intriguingly, some fundamental researches on enhancing thermal sensitivity using some enhancement agents were highlighted to improve the utilization efficiency of thermal energy, elevate treatment biosafety, and magnify the ablation outcomes. These impressive cases pave a solid foundation to clinical translation of these enhancement agents *via* providing theoretical basis and experimental experiences, e.g., RFA enhancement agents, HIFU enhancement agents, etc.

CONCLUSIONS

Thermal ablation is a promising minimally invasive method and should be considered as the first-line treatment for BTNs and recurrent PTMC. For primary PTMC, TA could be a suitable alternative to surgery for selected patients with low-risk PTMC. However, the suitable included criterion, the ablation equipment selection, and the standard technical operation should be critically evaluated to ensure the best clinical outcomes and complication control after ablation.

AUTHOR CONTRIBUTIONS

All authors: designed and wrote the manuscript. X-WB, FL: drafted the manuscript and prepared the tables. L-PS, KZ, and H-XX: modified the manuscript. All authors contributed to the article and approved the submitted version.

FUNDING

This work was supported by grants from National Natural Science Foundation of China (Grants 82022033, 81771836, 81501473, 81601501 and 81801802), Shanghai Rising-Star Program (Grant 19QA1406800), Shanghai Talent Development Fund (Grant2019040), Fostering Project of Shanghai Municipal Commission of Health and Family Planning for Excellent Young Medical Scholars (Grant 2018YQ31), the Opening Project of Guangxi Key Laboratory of Bio-targeting Theranostics (GXSWBX201801), the Opening Project of State Key Laboratory of High Performance Ceramics and Superfine Microstructure (SKL201811SIC), Shanghai Municipal Health Commission (Grant201640166), and Shanghai "Rising Stars of Medical Talent" Youth Development Program.

REFERENCES

1. Kim JH, Baek JH, Lim HK, Ahn HS, Baek SM, Choi YJ, et al. 2017 Thyroid Radiofrequency Ablation Guideline: Korean Society of Thyroid Radiology. *Korean J Radiol* (2018) 19:632–55. doi: 10.3348/kjr.2018.19.4.632
2. Davies L, Welch HG. Increasing incidence of thyroid cancer in the United States, 1973-2002. *JAMA* (2006) 295:2164–7. doi: 10.1001/jama.295.18.2164
3. Burman KD, Wartofsky L. Clinical practice. Thyroid Nodules. *N Engl J Med* (2015) 373:2347–56. doi: 10.1056/NEJMcp1415786
4. Walsh JP. Managing thyroid disease in general practice. *Med J Aust* (2016) 205:179–84. doi: 10.5694/mja16.00545
5. Wong R, Farrell SG, Grossmann M. Thyroid nodules: diagnosis and management. *Med J Aust* (2018) 209:92–8. doi: 10.5694/mja17.01204
6. McLeod DS, Sawka AM, Cooper DS. Controversies in primary treatment of low-risk papillary thyroid cancer. *Lancet* (2013) 381:1046–57. doi: 10.1016/S0140-6736(12)62205-3
7. Haugen BR, Alexander EK, Bible KC, Doherty GM, Mandel SJ, Nikiforov YE, et al. 2015 American Thyroid Association Management Guidelines for Adult Patients with Thyroid Nodules and Differentiated Thyroid Cancer: The American Thyroid Association Guidelines Task Force on Thyroid Nodules and Differentiated Thyroid Cancer. *Thyroid* (2016) 26:1–133. doi: 10.1089/thy.2015.0020
8. Brito JP, Hay ID, Morris JC. Low risk papillary thyroid cancer. *BMJ* (2014) 348:g3045. doi: 10.1136/bmj.g3045
9. Gao M, Ge M, Ji Q, Cheng R, Lu H, Guan H, et al. 2016 Chinese expert consensus and guidelines for the diagnosis and treatment of papillary thyroid microcarcinoma. *Cancer Biol Med* (2017) 14:203–11. doi: 10.20892/j.issn.2095-3941.2017.0051
10. Park HS, Yim Y, Baek JH, Choi YJ, Shong YK, Lee JH. Ethanol ablation as a treatment strategy for benign cystic thyroid nodules: a comparison of the ethanol retention and aspiration techniques. *Ultrasonography* (2019) 38:166–71. doi: 10.14366/usg.18033
11. Iñiguez-Ariza NM, Lee RA, Singh-Ospina NM, Stan MN, Castro MR. Ethanol Ablation for the Treatment of Cystic and Predominantly Cystic Thyroid Nodules. *Mayo Clin Proc* (2018) 93:1009–17. doi: 10.1016/j.mayocp.2018.05.020
12. Hahn SY, Shin JH, Na DG, Ha EJ, Ahn HS, Lim HK, et al. Ethanol Ablation of the Thyroid Nodules: 2018 Consensus Statement by the Korean Society of Thyroid Radiology. *Korean J Radiol* (2019) 20:609–20. doi: 10.3348/kjr.2018.0696
13. Gong X, Zhou Q, Chen S, Wang F, Wu W, Chen X. Efficacy and safety of ultrasound-guided percutaneous polidocanol sclerotherapy in benign predominantly cystic thyroid nodules: a prospective study. *Curr Med Res Opin* (2017) 33:1505–10. doi: 10.1080/03007995.2017.1325732
14. Sung JY, Baek JH, Kim KS, Lee D, Yoo H, Kim JK, et al. Single-session treatment of benign cystic thyroid nodules with ethanol versus radiofrequency ablation: a prospective randomized study. *Radiology* (2013) 269:293–300. doi: 10.1148/radiol.13122134
15. Lin Y, Li P, Shi YP, Tang XY, Ding M, He Y, et al. Sequential treatment by polidocanol and radiofrequency ablation of large benign partially cystic thyroid nodules with solid components: Efficacy and safety. *Diagn Interv Imaging* (2020) 101:365–72. doi: 10.1016/j.diii.2019.11.005
16. Trimboli P, Castellana M, Sconfienza LM, Virili C, Pescatori LC, Cesareo R, et al. Efficacy of thermal ablation in benign non-functioning solid thyroid nodule: A systematic review and meta-analysis. *Endocrine* (2020) 67:35–43. doi: 10.1007/s12020-019-02019-3
17. Dong P, Wu XL, Sui GQ, Luo Q, Du JR, Wang H, et al. The efficacy and safety of microwave ablation versus lobectomy for the treatment of benign thyroid nodules greater than 4 cm. *Endocrine* (2020). doi: 10.1007/s12020-020-02338-w
18. Jang SW, Baek JH, Kim JK, Sung JY, Choi H, Lim HK, et al. How to manage the patients with unsatisfactory results after ethanol ablation for thyroid nodules: role of radiofrequency ablation. *Eur J Radiol* (2012) 81:905–10. doi: 10.1016/j.ejrad.2011.02.039
19. Baek JH, Lee JH, Sung JY, Bae JI, Kim KT, Sim J, et al. Complications encountered in the treatment of benign thyroid nodules with US-guided radiofrequency ablation: a multicenter study. *Radiology* (2012) 262:335–42. doi: 10.1148/radiol.11110416
20. Huh JY, Baek JH, Choi H, Kim JK, Lee JH. Symptomatic benign thyroid nodules: efficacy of additional radiofrequency ablation treatment session–prospective randomized study. *Radiology* (2012) 263:909–16. doi: 10.1148/radiol.12111300
21. Sung JY, Baek JH, Jung SL, Kim JH, Kim KS, Lee D, et al. Radiofrequency ablation for autonomously functioning thyroid nodules: a multicenter study. *Thyroid* (2015) 25:112–7. doi: 10.1089/thy.2014.0100
22. Jung SL, Baek JH, Lee JH, Shong YK, Sung JY, Kim KS, et al. Efficacy and Safety of Radiofrequency Ablation for Benign Thyroid Nodules: A Prospective Multicenter Study. *Korean J Radiol* (2018) 19:167–74. doi: 10.3348/kjr.2018.19.1.167
23. Deandrea M, Sung JY, Limone P, Mormile A, Garino F, Ragazzoni F, et al. Efficacy and Safety of Radiofrequency Ablation Versus Observation for Nonfunctioning Benign Thyroid Nodules: A Randomized Controlled International Collaborative Trial. *Thyroid* (2015) 25:890–6. doi: 10.1089/thy.2015.0133
24. Kim JH, Yoo WS, Park YJ, Park DJ, Yun TJ, Choi SH, et al. Efficacy and Safety of Radiofrequency Ablation for Treatment of Locally Recurrent Thyroid Cancers Smaller than 2 cm. *Radiology* (2015) 276:909–18. doi: 10.1148/radiol.15140079
25. Suh CH, Baek JH, Choi YJ, Lee JH. Efficacy and Safety of Radiofrequency and Ethanol Ablation for Treating Locally Recurrent Thyroid Cancer: A Systematic Review and Meta-Analysis. *Thyroid* (2016) 26:420–8. doi: 10.1089/thy.2015.0545
26. Zhang M, Luo Y, Zhang Y, Tang J. Efficacy and Safety of Ultrasound-Guided Radiofrequency Ablation for Treating Low-Risk Papillary Thyroid Microcarcinoma: A Prospective Study. *Thyroid* (2016) 26:1581–7. doi: 10.1089/thy.2015.0471
27. Chung SR, Baek JH, Choi YJ, Lee JH. Longer-term outcomes of radiofrequency ablation for locally recurrent papillary thyroid cancer. *Eur Radiol* (2019) 29:4897–903. doi: 10.1007/s00330-019-06063-5
28. Yan L, Lan Y, Xiao J, Lin L, Jiang B, Luo YK. A Long-term outcomes of radiofrequency ablation for unifocal low-risk papillary thyroid microcarcinoma: a large cohort study of 414 patients. *Eur Radiol* (2020). doi: 10.1007/s00330-020-07128-6
29. Yue WW, Qi L, Wang DD, Yu SJ, Wang XJ, Xu HX, et al. US-guided Microwave Ablation of Low-Risk Papillary Thyroid Microcarcinoma: Longer-Term Results of a Prospective Study. *J Clin Endocrinol Metab* (2020) 105:dgaa128. doi: 10.1210/clinem/dgaa128
30. Teng D, Li W, Du J, Wang H, Yang D, Wu X. Effects of Microwave Ablation on Papillary Thyroid Microcarcinoma: A Five-Year Follow-Up Report. *Thyroid* (2020). doi: 10.1089/thy.2020.0049
31. Lim HK, Cho SJ, Baek JH, Lee KD, Son CW, Son JM, et al. US-Guided Radiofrequency Ablation for Low-Risk Papillary Thyroid Microcarcinoma: Efficacy and Safety in a Large Population. *Korean J Radiol* (2019) 20:1653–61. doi: 10.3348/kjr.2019.0192
32. Kim YS, Rhim H, Tae K, Park DW, Kim ST. Radiofrequency ablation of benign cold thyroid nodules: initial clinical experience. *Thyroid* (2006) 16:361–7. doi: 10.1089/thy.2006.16.361
33. Aldea Martínez J, Aldea Viana L, López Martínez JL, Ruiz Pérez E. Radiofrequency Ablation of Thyroid Nodules: A Long-Term Prospective Study of 24 Patients. *J Vasc Interv Radiol* (2019) 30:1567–73. doi: 10.1016/j.jvir.2019.04.022
34. Deandrea M, Garino F, Alberto M, Garberoglio R, Rossetto R, Bonelli N, et al. Radiofrequency ablation for benign thyroid nodules according to different ultrasound features: an Italian multicentre prospective study. *Eur J Endocrinol* (2019) 180:79–87. doi: 10.1530/EJE-18-0685
35. Dobnig H, Amrein K. Monopolar Radiofrequency Ablation of Thyroid Nodules: A Prospective Austrian Single-Center Study. *Thyroid* (2018) 28:472–80. doi: 10.1089/thy.2017.0547
36. Vuong NL, Dinh LQ, Bang HT, Thuy T, Bac NH, Vy TT. Radiofrequency Ablation for Benign Thyroid Nodules: 1-Year Follow-Up in 184 Patients. *World J Surg* (2019) 43:2447–53. doi: 10.1007/s00268-019-05044-5
37. Deandrea M, Trimboli P, Garino F, Mormile A, Magliona G, Ramunni MJ, et al. Long-Term Efficacy of a Single Session of RFA for Benign Thyroid Nodules: A Longitudinal 5-Year Observational Study. *J Clin Endocrinol Metab* (2019) 104:3751–6. doi: 10.1210/jc.2018-02808
38. Ha EJ, Baek JH, Lee JH, Sung JY, Lee D, Kim JK, et al. Radiofrequency ablation of benign thyroid nodules does not affect thyroid function in patients with previous lobectomy. *Thyroid* (2013) 23:289–93. doi: 10.1089/thy.2012.0171

39. Choi Y, Jung SL, Bae JS, Lee SH, Jung CK, Jang J, et al. Comparison of efficacy and complications between radiofrequency ablation and repeat surgery in the treatment of locally recurrent thyroid cancers: a single-center propensity score matching study. *Int J Hyperthermia* (2019) 36:359–67. doi: 10.1080/02656736.2019.1571248
40. Feng B, Liang P, Cheng Z, Yu X, Yu J, Han Z, et al. Ultrasound-guided percutaneous microwave ablation of benign thyroid nodules: experimental and clinical studies. *Eur J Endocrinol* (2012) 166:1031–7. doi: 10.1530/EJE-11-0966
41. Yue W, Wang S, Wang B, Xu Q, Yu S, Yonglin Z, et al. Ultrasound guided percutaneous microwave ablation of benign thyroid nodules: safety and imaging follow-up in 222 patients. *Eur J Radiol* (2013) 82:e11–6. doi: 10.1016/j.ejrad.2012.07.020
42. Khanh HQ, Hung NQ, Vinh VH, Khoi NV, Vuong NL. Efficacy of Microwave Ablation in the Treatment of Large (≥3 cm) Benign Thyroid Nodules. *World J Surg* (2020) 44:2272–9. doi: 10.1007/s00268-020-05432-2
43. Cui T, Jin C, Jiao D, Teng D, Sui G. Safety and efficacy of microwave ablation for benign thyroid nodules and papillary thyroid microcarcinomas: A systematic review and meta-analysis. *Eur J Radiol* (2019) 118:58–64. doi: 10.1016/j.ejrad.2019.06.027
44. Zheng BW, Wang JF, Ju JX, Wu T, Tong G, Ren J. Efficacy and safety of cooled and uncooled microwave ablation for the treatment of benign thyroid nodules: a systematic review and meta-analysis. *Endocrine* (2018) 62:307–17. doi: 10.1007/s12020-018-1693-2
45. Hu K, Wu J, Dong Y, Yan Z, Lu Z, Liu L. Comparison between ultrasound-guided percutaneous radiofrequency and microwave ablation in benign thyroid nodules. *J Cancer Res Ther* (2019) 15:1535–40. doi: 10.4103/jcrt.JCRT_322_19
46. Korkusuz Y, Gröner D, Raczynski N, Relin O, Kingeter Y, Grünwald F, et al. Thermal ablation of thyroid nodules: are radiofrequency ablation, microwave ablation and high intensity focused ultrasound equally safe and effective methods. *Eur Radiol* (2018) 28:929–35. doi: 10.1007/s00330-017-5039-x
47. Yan J, Qiu T, Lu J, Wu Y, Yang Y. Microwave ablation induces a lower systemic stress response in patients than open surgery for treatment of benign thyroid nodules. *Int J Hyperthermia* (2018) 34:606–10. doi: 10.1080/02656736.2018.1427286
48. Liu SY, Guo WH, Yang B, Li YF, Huang XY, Wang XQ, et al. Comparison of stress response following microwave ablation and surgical resection of benign thyroid nodules. *Endocrine* (2019) 65:138–43. doi: 10.1007/s12020-019-01900-5
49. Zhi X, Zhao N, Liu Y, Liu JB, Teng C, Qian L. Microwave ablation compared to thyroidectomy to treat benign thyroid nodules. *Int J Hyperthermia* (2018) 34:644–52. doi: 10.1080/02656736.2018.1456677
50. Cakir B, Topaloglu O, Gul K, Agac T, Aydin C, Dirikoc A, et al. Effects of percutaneous laser ablation treatment in benign solitary thyroid nodules on nodule volume, thyroglobulin and anti-thyroglobulin levels, and cytopathology of nodule in 1 yr follow-up. *J Endocrinol Invest* (2006) 29:876–84. doi: 10.1007/BF03349190
51. Oddo S, Felix E, Mussap M, Giusti M. Quality of Life in Patients Treated with Percutaneous Laser Ablation for Non-Functioning Benign Thyroid Nodules: A Prospective Single-Center Study. *Korean J Radiol* (2018) 19:175–84. doi: 10.3348/kjr.2018.19.1.175
52. Mauri G, Nicosia L, Della Vigna P, Varano GM, Maiettini D, Bonomo G, et al. Percutaneous laser ablation for benign and malignant thyroid diseases. *Ultrasonography* (2019) 38:25–36. doi: 10.14366/usg.18034
53. Valcavi R, Riganti F, Bertani A, Formisano D, Pacella CM. Percutaneous laser ablation of cold benign thyroid nodules: a 3-year follow-up study in 122 patients. *Thyroid* (2010) 20:1253–61. doi: 10.1089/thy.2010.0189
54. Rahal Junior A, Falsarella PM, Mendes GF, Hidal JT, Andreoni DM, Lúcio J, et al. Percutaneous laser ablation of benign thyroid nodules: a one year follow-up study. *Einstein (Sao Paulo)* (2018) 16:eAO4279. doi: 10.31744/einstein_journal/2018AO4279
55. Achille G, Zizzi S, Di Stasio E, Grammatica A, Grammatica L. Ultrasound-guided percutaneous laser ablation in treating symptomatic solid benign thyroid nodules: Our experience in 45 patients. *Head Neck* (2016) 38:677–82. doi: 10.1002/hed.23957
56. Papini E, Rago T, Gambelunghe G, Valcavi R, Bizzarri G, Vitti P, et al. Long-term efficacy of ultrasound-guided laser ablation for benign solid thyroid nodules. Results of a three-year multicenter prospective randomized trial. *J Clin Endocrinol Metab* (2014) 99:3653–9. doi: 10.1210/jc.2014-1826
57. Ben Hamou A, Ghanassia E, Espiard S, Abi Rached H, Jannin A, Correas JM, et al. Safety and efficacy of thermal ablation (radiofrequency and laser): should we treat all types of thyroid nodules? (†). *Int J Hyperthermia* (2019) 36:666–76. doi: 10.1080/02656736.2019.1627432
58. Shi YF, Zhou P, Zhao YF, Liu WG, Tian SM, Liang YP. Microwave Ablation Compared With Laser Ablation for Treating Benign Thyroid Nodules in a Propensity-Score Matching Study. *Front Endocrinol (Lausanne)* (2019) 10:874. doi: 10.3389/fendo.2019.00874
59. Cesareo R, Pacella CM, Pasqualini V, Campagna G, Iozzino M, Gallo A, et al. Laser Ablation Versus Radiofrequency Ablation for Benign Non-Functioning Thyroid Nodules: Six-Month Results of a Randomized, Parallel, Open-Label, Trial (LARA Trial). *Thyroid* (2020) 30:847–56. doi: 10.1089/thy.2019.0660
60. Ha EJ, Baek JH, Kim KW, Pyo J, Lee JH, Baek SH, et al. Comparative efficacy of radiofrequency and laser ablation for the treatment of benign thyroid nodules: systematic review including traditional pooling and bayesian network meta-analysis. *J Clin Endocrinol Metab* (2015) 100:1903–11. doi: 10.1210/jc.2014-4077
61. Esnault O, Franc B, Ménégaux F, Rouxel A, De Kerviler E, Bourrier P, et al. High-intensity focused ultrasound ablation of thyroid nodules: first human feasibility study. *Thyroid* (2011) 21:965–73. doi: 10.1089/thy.2011.0141
62. Lang BH, Woo YC, Wong C. High-Intensity Focused Ultrasound for Treatment of Symptomatic Benign Thyroid Nodules: A Prospective Study. *Radiology* (2017) 284:897–906. doi: 10.1148/radiol.2017161640
63. Lang B, Woo YC, Chiu KW. Two-year efficacy of single-session high-intensity focused ultrasound (HIFU) ablation of benign thyroid nodules. *Eur Radiol* (2019) 29:93–101. doi: 10.1007/s00330-018-5579-8
64. Chung SR, Baek JH, Suh CH, Choi YJ, Lee JH. Efficacy and safety of high-intensity focused ultrasound (HIFU) for treating benign thyroid nodules: a systematic review and meta-analysis. *Acta Radiol* (2020). doi: 10.1177/0284185120909339. 284185120909339.
65. Lang BH, Woo YC, Chiu KW. Single-Session High-Intensity Focused Ultrasound Treatment in Large-Sized Benign Thyroid Nodules. *Thyroid* (2017) 27:714–21. doi: 10.1089/thy.2016.0664
66. Lang B, Woo YC, Chiu KW. Two sequential applications of high-intensity focused ultrasound (HIFU) ablation for large benign thyroid nodules. *Eur Radiol* (2019) 29:3626–34. doi: 10.1007/s00330-019-06021-1
67. Lang B, Wong C, Ma E, Woo YC. Chiu KW. A propensity-matched analysis of clinical outcomes between open thyroid lobectomy and high-intensity focused ultrasound (HIFU) ablation of benign thyroid nodules. *Surgery* (2019) 165:85–91. doi: 10.1016/j.surg.2018.05.080
68. Cho SJ, Baek SM, Lim HK, Lee KD, Son JM, Baek JH. Long-Term Follow-Up Results of Ultrasound-Guided Radiofrequency Ablation for Low-Risk Papillary Thyroid Microcarcinoma: More Than 5-Year Follow-Up for 84 Tumors. *Thyroid* (2020). doi: 10.1089/thy.2020.0106
69. Zhang M, Tufano RP, Russell JO, Zhang Y, Zhang Y, Qiao Z, et al. Ultrasound-Guided Radiofrequency Ablation Versus Surgery for Low-Risk Papillary Thyroid Microcarcinoma: Results of Over 5 Years' Follow-Up. *Thyroid* (2020) 30:408–17. doi: 10.1089/thy.2019.0147
70. Lan Y, Luo Y, Zhang M, Jin Z, Xiao J, Yan L, et al. Quality of Life in Papillary Thyroid Microcarcinoma Patients Undergoing Radiofrequency Ablation or Surgery: A Comparative Study. *Front Endocrinol (Lausanne)* (2020) 11:249. doi: 10.3389/fendo.2020.00249
71. Yue W, Wang S, Yu S, Wang B. Ultrasound-guided percutaneous microwave ablation of solitary T1N0M0 papillary thyroid microcarcinoma: initial experience. *Int J Hyperthermia* (2014) 30:150–7. doi: 10.3109/02656736.2014.885590
72. Teng D, Sui G, Liu C, Wang Y, Xia Y, Wang H. Long-term efficacy of ultrasound-guided low power microwave ablation for the treatment of primary papillary thyroid microcarcinoma: a 3-year follow-up study. *J Cancer Res Clin Oncol* (2018) 144:771–9. doi: 10.1007/s00432-018-2607-7
73. Teng DK, Li HQ, Sui GQ, Lin YQ, Luo Q, Fu P, et al. Preliminary report of microwave ablation for the primary papillary thyroid microcarcinoma: a large-cohort of 185 patients feasibility study. *Endocrine* (2019) 64:109–17. doi: 10.1007/s12020-019-01868-2
74. Papini E, Guglielmi R, Gharib H, Misischi I, Graziano F, Chianelli M, et al. Ultrasound-guided laser ablation of incidental papillary thyroid

microcarcinoma: a potential therapeutic approach in patients at surgical risk. *Thyroid* (2011) 21:917–20. doi: 10.1089/thy.2010.0447
75. Zhou W, Ni X, Xu S, Zhang L, Chen Y, Zhan W. Ultrasound-guided laser ablation versus surgery for solitary papillary thyroid microcarcinoma: a retrospective study. *Int J Hyperthermia* (2019) 36:897–904. doi: 10.1080/02656736.2019.1649475
76. Ji L, Wu Q, Gu J, Deng X, Zhou W, Fan X, et al. Ultrasound-guided percutaneous laser ablation for papillary thyroid microcarcinoma: a retrospective analysis of 37 patients. *Cancer Imaging* (2019) 19:16. doi: 10.1186/s40644-019-0204-x
77. Zhao CK, Xu HX, Lu F, Sun LP, He YP, Guo LH, et al. Factors associated with initial incomplete ablation for benign thyroid nodules after radiofrequency ablation: First results of CEUS evaluation. *Clin Hemorheol Microcirc* (2017) 65:393–405. doi: 10.3233/CH-16208
78. Lee GM, You JY, Kim HY, Chai YJ, Kim HK, Dionigi G, et al. Successful radiofrequency ablation strategies for benign thyroid nodules. *Endocrine* (2019) 64:316–21. doi: 10.1007/s12020-018-1829-4
79. Sim JS, Baek JH, Cho W. Initial Ablation Ratio: Quantitative Value Predicting the Therapeutic Success of Thyroid Radiofrequency Ablation. *Thyroid* (2018) 28:1443–9. doi: 10.1089/thy.2018.0180
80. Lee JH, Kim YS, Lee D, Choi H, Yoo H, Baek JH. Radiofrequency ablation (RFA) of benign thyroid nodules in patients with incompletely resolved clinical problems after ethanol ablation (EA). *World J Surg* (2010) 34:1488–93. doi: 10.1007/s00268-010-0565-6
81. Ahn HS, Kim SJ, Park SH, Seo M. Radiofrequency ablation of benign thyroid nodules: evaluation of the treatment efficacy using ultrasonography. *Ultrasonography* (2016) 35:244–52. doi: 10.14366/usg.15083
82. Cesareo R, Naciu AM, Iozzino M, Pasqualini V, Simeoni C, Casini A, et al. Nodule size as predictive factor of efficacy of radiofrequency ablation in treating autonomously functioning thyroid nodules. *Int J Hyperthermia* (2018) 34:617–23. doi: 10.1080/02656736.2018.1430868
83. Sim JS, Baek JH. Long-Term Outcomes Following Thermal Ablation of Benign Thyroid Nodules as an Alternative to Surgery: The Importance of Controlling Regrowth. *Endocrinol Metab (Seoul)* (2019) 34:117–23. doi: 10.3803/EnM.2019.34.2.117
84. Wang B, Han ZY, Yu J, Cheng Z, Liu F, Yu XL, et al. Factors related to recurrence of the benign non-functioning thyroid nodules after percutaneous microwave ablation. *Int J Hyperthermia* (2017) 33:459–64. doi: 10.1080/02656736.2016.1274058
85. Negro R, Greco G, Deandrea M, Rucco M, Trimboli P. Twelve-Month Volume Reduction Ratio Predicts Regrowth and Time to Regrowth in Thyroid Nodules Submitted to Laser Ablation: A 5-Year Follow-Up Retrospective Study. *Korean J Radiol* (2020) 21:764–72. doi: 10.3348/kjr.2019.0798
86. Park HS, Baek JH, Park AW, Chung SR, Choi YJ, Lee JH. Thyroid Radiofrequency Ablation: Updates on Innovative Devices and Techniques. *Korean J Radiol* (2017) 18:615–23. doi: 10.3348/kjr.2017.18.4.615
87. Choi Y, Jung SL. Efficacy and Safety of Thermal Ablation Techniques for the Treatment of Primary Papillary Thyroid Microcarcinoma: A Systematic Review and Meta-Analysis. *Thyroid* (2020) 30:720–31. doi: 10.1089/thy.2019.0707

Conflict of Interest: The authors declare that the research was conducted in the absence of any commercial or financial relationships that could be construed as a potential conflict of interest.

frontiers in Oncology

ORIGINAL RESEARCH
published: 18 November 2020
doi: 10.3389/fonc.2020.561805

Specific Inhibitor of Matrix Metalloproteinase Decreases Tumor Invasiveness After Radiofrequency Ablation in Liver Tumor Animal Model

An-Na Jiang[1†], *Jing-Tao Liu*[2†], *Kun Zhao*[1], *Hao Wu*[1], *Song Wang*[1], *Kun Yan*[1] *and Wei Yang*[1*]

[1] Key Laboratory of Carcinogenesis and Translational Research (Ministry of Education/Beijing), Department of Ultrasound, Peking University Cancer Hospital & Institute, Beijing, China, [2] Key Laboratory of Carcinogenesis and Translational Research (Ministry of Education/Beijing), Department of Pharmacy, Peking University Cancer Hospital & Institute, Beijing, China

OPEN ACCESS

Edited by:
Fu Wang,
Xidian University, China

Reviewed by:
Chaoyun Pan,
Sun Yat-sen University, China
Xiang Jing,
Tianjin Third Central Hospital, China

***Correspondence:**
Wei Yang
13681408183@163.com

[†]*These authors have contributed equally to this work*

Specialty section:
This article was submitted to Cancer Imaging and Image-directed Interventions, a section of the journal Frontiers in Oncology

Received: *13 May 2020*
Accepted: *19 October 2020*
Published: *18 November 2020*

Citation:
Jiang A-N, Liu J-T, Zhao K, Wu H, Wang S, Yan K and Yang W (2020) Specific Inhibitor of Matrix Metalloproteinase Decreases Tumor Invasiveness After Radiofrequency Ablation in Liver Tumor Animal Model. Front. Oncol. 10:561805. doi: 10.3389/fonc.2020.561805

Objective: To determine whether the specific inhibitor of matrix metalloproteinase (MMP)—batimastat (BB-94)—could decrease the progression of liver tumor after radiofrequency ablation (RFA) and achieve better therapeutic efficacy in an animal model.

Methods: *In vitro* experiments, the proliferation of H22 liver tumor cells was detected by CCK 8 assay and cell migration was detected by Transwell method. *In vivo* experiments, H22 murine liver tumors were used. First, 32 mice with one tumor were randomized into four groups (n = 8 each group): control (PBS only), RFA alone (65°C, 5 min), BB-94 (30 mg/kg), RFA+BB-94. The growth rate of the residual tumor and the end point survival were calculated and the pathologic changes were evaluated. Secondly, a total of 48 tumors in 24 animals (paired tumors) were randomized into three groups (n = 8 each group): control, RFA alone, RFA+BB-94. Each mouse was implanted with two tumors subcutaneously, one tumor was treated by RFA and the other was evaluated for distant metastasis after applying BB-94.

Results: *In vitro*, the proliferation assay demonstrated higher proliferation ability after heat treatment (0.82 ± 0.07 *vs* 1.27 ± 0.08, P = 0.008), and it could be inhibited by BB-94 (1.27 ± 0.08 *vs* 0.67 ± 0.06, P = 0.001). In the cell migration assay, the H22 cells demonstrated enhanced tumor invasiveness in the heat group than the control group (33.7 ± 2.1 *vs* 19.7 ± 4.9, P = 0.011). And it could be significantly suppressed after BB-94 incubation (33.7 ± 2.1 *vs* 23.0 ± 4.6, P = 0.009). With one tumor animal, the growth rate of the residual tumor in the BB-94+RFA group was slower than that in the RFA alone group (P = 0.003). And combination of BB-94 could significantly prolong the survival of the mice (40.3 ± 1.4d *vs* 47.1 ± 1.3d, P = 0.002). The expression of CD31 and VEGF at the coagulation margin were decreased after combined with BB-94. With two tumors animal, the growth of metastasis tumor in the BB-94+RFA group was slower than that in the RFA group (P < 0.001).

Conclusion: BB-94 combined with RFA reduced the invasiveness of the liver tumor and improved the end-point survival. Our data suggested that targeting the MMP process with the specific inhibition could help to increase overall ablation efficacy.

Keywords: liver tumor, radiofrequency ablation, invasiveness, specific inhibitor, matrix metalloproteinase

INTRODUCTION

Hepatocellular carcinoma (HCC) is one common malignant tumor in China and the world. Radiofrequency ablation (RFA) is a safe and effective minimally invasive therapy widely used in the unresectable hepatic tumors. However, due to the limitations of liver function, tumor size, location, and other factors, it is hard to achieve complete ablation and lead to tumor residual in some conditions. The acceleration of residual tumor progression after thermal ablation has been reported (1, 2). These data showed the residual tumor after RFA had more invasive growth, more vascular invasion and less differentiation compared with primary tumors (3). Previous studies indicated that insufficient RFA could induce over-expression of matrix metalloproteinase (MMP) (4). The expression of MMP in macrophages around liver parenchyma coagulation area increased after RFA (5).

MMPs are the member of the zinc-dependent endopeptidases family, which play an important role in the degradation of a vast number of protein targets by cleavage of internal peptide bonds (6, 7). It takes both extracellular matrix components and adhesion receptors as substrates, alters some properties of cells including the responses to the environment, and promote the migration, invasion, and metastasis of potential of tumor cells (8). MMPs could modulate the tumor microenvironment to accelerate cell growth, regulate apoptosis, regulate the bioavailability of vascular endothelial growth factor (VEGF) and promote tumor angiogenesis, and affect tumor progression (9). The specific inhibitor of MMP—Batimastat (BB-94)—is a synthetic low molecular weight metalloproteinase inhibitor, which could bound to MMPs and their catalytically active Zn atoms to inhibit the activity of MMPs (10). It has been reported in prior work that BB-94 was able to reduce tumor growth in the standard prostate cancer model (11).

Hence, we designed this study to investigate the combination of BB-94 and RFA in the treatment of hepatic tumors. We aimed to explore if BB-94 could inhibit the proliferation and migration of the residual tumors after RFA.

METHODS AND MATERIALS

Experimental Overview

The study was approved by the Institutional Animal Care and Use Committee (Peking University, Cancer Hospital) prior to the start. H22 cells (ATCC, Manassas, VA, USA) were cultured in RPMI-1640 medium containing 10% fetal bovine serum (Life Technologies, Carlsbad, CA, USA) and 0.5% penicillin-streptomycin (Life Technologies, CA, USA) at 37°C in humidified atmosphere containing 5% CO_2. BALB/C mice (female, weighing 18–20 g, aged 6–8 weeks, Vital River Experimental Animal Technology, Beijing, China) were used in this study. The research was conducted in five phases to explore the potential synergistic effects of RFA and MMP specific inhibitors (BB-94) (APExBIO Technology, Houston, TX, USA) (**Figure 1**).

Phase 1: Assessment of Cell Proliferation and Migration

The cell proliferation ability was detected by Cell Counting kit-8 assay (CCK-8, APExBIO Technology, Houston, TX, USA). 5×10^3 H22 cells were seeded in 96-well plates of each well and incubated for 24 h. Then 10 μl CCK-8 solution was added in each well. After 4 h incubation, the absorbance value of each well was tested by microplate reader (Thermo, USA) at 450 nm (12).

The cell migration ability was assessed by Transwell assay (Corning, NY, USA). 5×10^5 H22 cells were seeded in the upper chamber of each well in 16-well plates containing 8.0 μm pore size membranes with serum-free RPMI. While RPMI containing 10% fetal bovine serum was in the lower chamber of each well. After 48 h, the cells that reached the bottom of the membrane were stained with Giemsa (Sigma) and counted at ×200 magnification in five randomly selected areas per well (13).

Phase 2: Comparison of Tumor Growth Rates

Totally, 32 mice 32 with tumors were used to compare the tumor growth. On the basis of the previous work (14), the ablation destruction was about 7 mm in diameter, while the tumor over 15 mm had a high risk of spontaneous necrosis. Accordingly, tumors at the range of 10–15 mm in diameter were selected as an appropriate size for insufficient RFA. Then the mice were randomized into the following four groups (n = 8 in each group): (a) control (PBS only); (b) RFA alone (5 min, 65°C); (c) BB-94 alone; (d) BB-94 + RFA. BB-94 (30mg/kg, 200 μl each) was injected intraperitoneally every 2 days for seven times. RFA was performed 24 h after first injection. To mimic the residual tumor during ablation of large tumors in clinical practice, about three-quarters of the tumor was completely ablated. The diameter of the residual tumor and the body weight of each mouse were measured every 2 days. The survival end point was defined as the growth of residual tumor to the diameter of 30 mm or survival of mice after treatment for 60 days, whichever was achieved first. The secondary end point was the tumor local control (i.e. no visible tumor on the abdominal wall).

Phase 3: Assessment of Pathologic Findings

Another 12 mice from the four groups in phase 2 were sacrificed 48 h after the last injection of BB-94 (n = 3 in each group) for

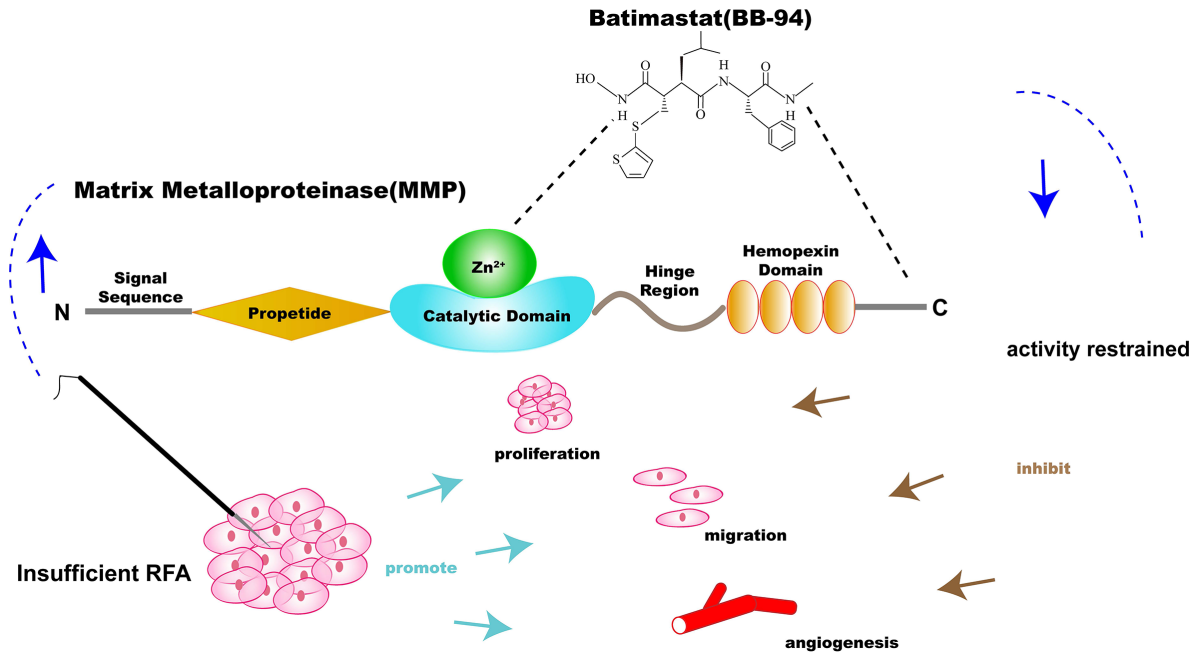

FIGURE 1 | Illustration of the specific inhibitor of matrix metalloproteinase (MMP)—batimastat (BB-94)—combination therapy with RFA for solid tumor. BB-94 could inhibit the activity of MMP, which was upregulated after insufficient RFA and could promote the invasiveness of residual tumor.

pathological analysis. These tumor samples were sectioned along the largest section vertical to RFA electrode. Tissue was fixed in 10% formalin overnight at 4°C, embedded in paraffin, and sliced at a thickness of 5 µm. The tissue was stained with hematoxylin-eosin for gross pathologic examination. The specific immunofluorescence (IF) staining was used to evaluate the expression of Collagen I and TGF-β. Similarly, CD31 and VEGF staining were also performed to assess the angiogenesis. Each specimen was observed for five random high-power fields per parameter and analyzed blindly to the treatment to remove the bias. The expression of CD31 and VEGF were quantified at a magnification of ×400.

Phase 4: Comparison of Tumor Metastasis

Twenty-four mice with paired tumors (10–12 mm) were randomized into the following three experimental groups (n = 8 in each group): (a) control (no treatment); (b) RFA alone (5 min, 65°C); (c) BB-94+RFA. The mice received PBS as control. BB-94 (30mg/kg, 200 µl each) was injected intraperitoneally every 2 days for seven times. RFA was performed 24 h after first injection. Each mouse was implanted with two tumors subcutaneously on the left and right flank in this phase. For each mouse, one tumor was treated with RFA as a mimic of original site and the growth of the other site tumor, as a mimic of metastatic tumors, was then monitored afterwards. The diameter of the tumor and the body weight of each mouse were measured every 2 days. The survival end point was defined as the growth of the other site tumor to the diameter of 30 mm or survival of mice after treatment for 60 days, whichever was achieved first.

Phase 5: Toxicity and Safety Evaluation

Twelve mice were randomized into the four groups in phase 2 but were sacrificed 48 h after the last injection of BB-94 (n = 3 in each group) to obtain important organs sample for toxicity analysis. The major organs (heart, liver, spleen, lung, and kidney) were harvested and fixed with formalin and embedded in paraffin. Then 5-µm sections were cut and stained with hematoxylin eosin (H&E) dyes for gross histopathologic analysis.

Cell Experiments

Heat treatment: H22 cells were seeded in 6-well plates (5×10^4 cells/well) for 24 h, then sealed with parafilm and submerged in a water bath set to 42°C for 6 h which was designed to mimic the effects of insufficient RFA. Meanwhile, the control temperature was set at 37°C.

BB-94 treatment: H22 cells were seeded in 6–well plates (5×10^4 cells/well) for 24 h. Then the cells were treated with BB-94 (1, 2, and 4 µg/ml) and incubated at 37°C. PBS (Life Technologies, Carlsbad, CA, USA) cultured cells were used as the control cells. After 24 h incubation, the cells were rinsed twice and replaced with fresh culture medium.

Animal Model

For all procedures, animals were anesthetized by injecting pentobarbital sodium (45 mg/kg, chemical reagent factory of Foshan, China) intraperitoneally and sacrificed in a CO_2 chamber; and 0.2 ml of H22 cells (at a density of 1×10^7/ml) suspended in serum-free RPMI-1640 and matrigel (1:1) were

injected subcutaneously into the abdominal wall with an 18-gauge needle for each tumor to establish the liver adenocarcinoma model. Animals were observed every 2 or 3 days after injection of cells to monitor the growth of the tumors and ultrasonography was performed before treatment. Thus, the solid nonnecrotic tumors were selected in the study. The longitudinal and transverse directions of the tumor was measured with mechanical calipers every 2 days in the survival studies. The measurement was performed by A-NJ and KZ, with 4 and 3 years of experience, respectively and verified by WY, with 12 years of experience, who was blinded to the treatment group. Tumor volume was calculated as $(D*d)^2*0.5$, where D and d were the two diameters of the tumor measured above.

RFA Procedure

In the animal experiments, the 17-gauge monopolar electrode (ACT1507 electrode; Valleylab, Tyco Healthcare) and the 480-kHz RFA generator (Model CC-1-220; Valleylab, Tyco Healthcare, USA) were used during RFA. The animal was shaved off on the back and applied electrolytic contact gel and then placed on the conventional metallic grounding pad (Cosman Medical, Inc. USA) to complete the RFA circuit. About 0.7 cm of the electrode tip was placed at the center of the tumor first and the RFA generator was set to the tip temperature at 65 ± 2°C and applied for 5 min.

Statistical Analysis

In this study, SPSS 21.0 software (SPSS, Chicago, IL, USA) was used for statistical analysis. $P < 0.05$ was statistically significant. All continuous data were provided as means ± SD. Kruskal Wallis test was used to evaluate the significance of different treatments. When the total P was less than 0.05, Nemenyi test was used for multiple comparison. Kaplan Meier method was used for end-point survival analysis, and log-rank test was used for comparison. When $P < 0.05$, two specific groups were compared by the log-rank test of Bonferroni correction.

RESULTS

Phase 1: Assessment of Cell Proliferation and Migration

In vitro proliferation experiment showed that the proliferation ability of H22 cells after heat treatment was significantly higher than that of the control group (1.27 ± 0.08 *vs* 0.82 ± 0.07, P = 0.008) (**Figure 2A**), and BB-94 could suppress cell growth in a dose-dependent manner (**Figure 2B**). In the cell migration experiment, the migration potential of H22 cells after heat treatment was also significantly higher than that of the control group (33.7 ± 2.1 *vs* 19.7 ± 4.9, P = 0.011) and BB-94 inhibited

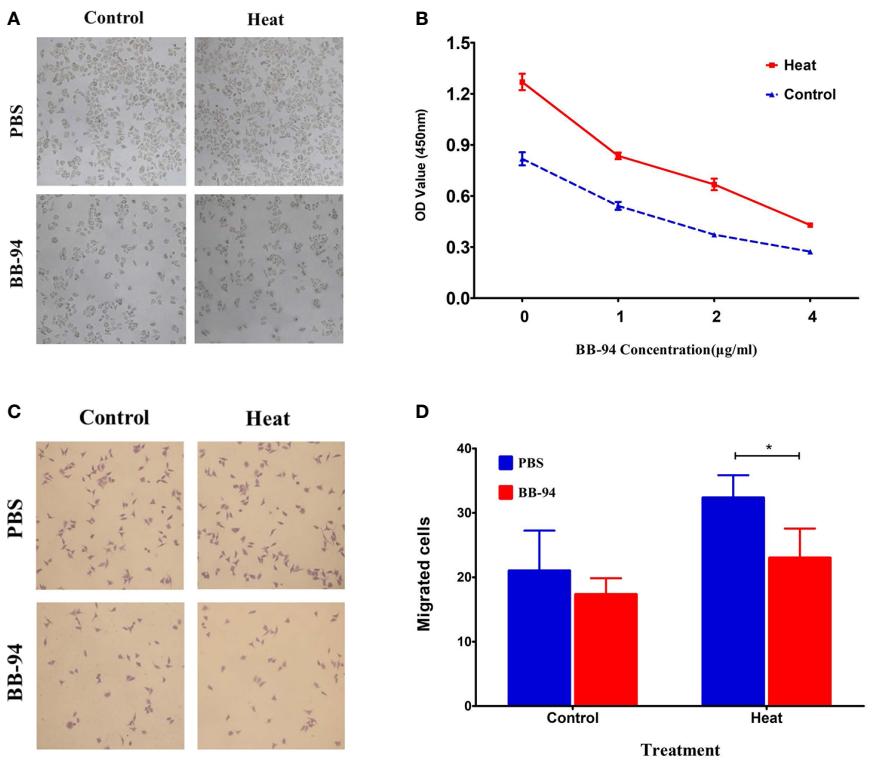

FIGURE 2 | *In vitro* assessment of cell proliferation and migration after different treatment. **(A)** CCK 8 assay demonstrated the proliferation ability after heat and BB-94 treatment. **(B)** Quantitative analysis of the OD value in the different groups at different concentration of BB-94. **(C)** Transwell assay showed the migration potential of the cells in different groups. **(D)** Quantitative analysis of the migrated cells after treatment at 37 and 42°C. *P < 0.05.

the migration of H22 cells (**Figure 2C**). With quantitative analysis, the heat-treated cells showed significantly lower migration potential after treated with BB-94 (33.7 ± 2.1 *vs* 23.0 ± 4.6, P = 0.009) (**Figure 2D**).

Phase 2: Comparison of Tumor Growth Rate

The tumor growth curves (**Figure 3A**) showed the tumor in the BB-94+RFA group grew more slowly than the RFA alone group (P = 0.003) and the tumor in the BB-94 group grew more slowly than the control group (P = 0.015). At 30 days after RFA, the volume of the residual tumor in the BB-94+RFA group was significantly smaller than that in the RFA group (**Figure 3B**) and with lighter tumor weight (1.79 ± 0.10 g *vs* 0.86 ± 0.11 g, P < 0.001) (**Figure 3C**).

Likewise, for end-point survival (**Figure 3D**), the BB-94 group (31.3 ± 1.4 days), the RFA group (40.3 ± 1.4 days), and the BB-94 + RFA group (47.1 ± 1.3 days) had better survival than the control group (25.4 ± 0.2 days) (P < 0.001). The mean survival for mice that received BB-94 was greater than that for mice without BB-94 (RFA *vs* BB-94 + RFA group, P = 0.002; BB-94 *vs* Control, P = 0.004). No organ metastasis was found at the end of follow-up.

Phase 3: Assessment of Pathologic Findings

The center of tumors treated with RFA demonstrated well-defined coagulative necrosis. IF staining in representative slides indicated a gain of more intensive VEGF and CD31 (angiogenesis) after RFA, BB-94 administration significantly inhibited the expression level of VEGF and CD31 (RFA *vs* RFA+BB-94, VEGF: 203.6 ± 12.1/high-power field *vs* 70.2 ± 10.8/high-power field, P < 0.001; CD31:112.6 ± 14.0/high-power field *vs* 60.4 ± 8.5/high-power field, P = 0.003) (**Figure 4A**). Increased collagen I deposition was observed at the periablational zone after RFA, and the expression was decreased with BB-94 administration (**Figure 4B**). Moreover, IF staining revealed that the elevated TGF-β expression in the tumor after RFA was diminished by BB-94 adjuvant treatment (**Figure 4C**).

Phase 4: Comparison of Tumor Metastasis

The tumor growth curves indicated the growth rate of other site tumors in the RFA group was faster than that in the control group (P = 0.006) and in the BB-94+RFA group (P = 0.000) (**Figures 5A, B**). There was no significant difference between the BB-94+RFA group and the control group (P = 0.359). At 20 days after RFA, the volume of the other site tumors in the BB-94+RFA group was significantly smaller than that in the RFA group and with lighter tumor weight (1.79 ± 0.89g *vs* 5.12 ± 0.96 g, P = 0.03) (**Figures 5C, D**).

Phase 5: Toxicity and Safety Evaluation

During the period of follow-up, there were no obvious changes in the health-related parameters after treatment including: body weight (P = 0.095, **Figure 6A**), respiratory status, eating and drinking behaviors, response to stimulations, and general activity level. Additionally, there were no obvious histopathological

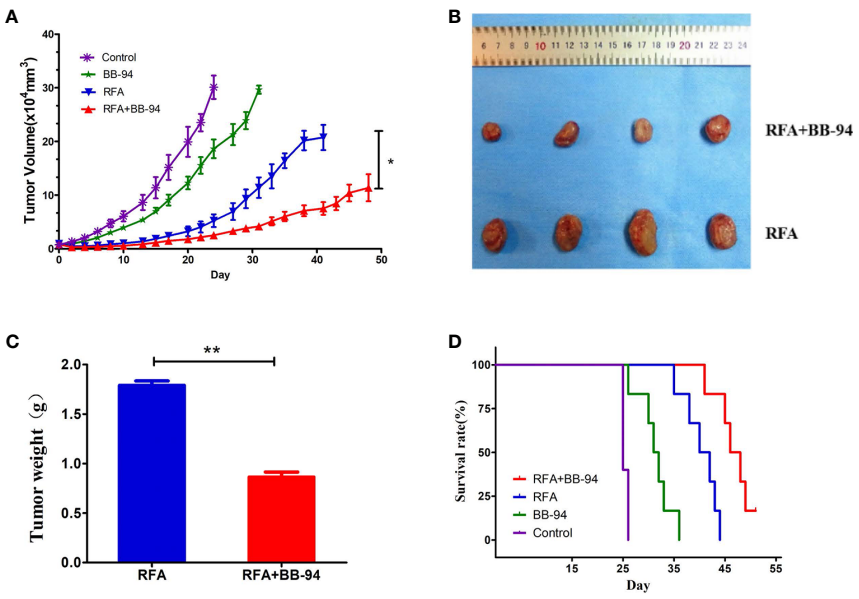

FIGURE 3 | Comparison of tumor growth rate. Long-term outcomes after different treatments. **(A)** The tumor growth curves at different treatment groups. **(B)** The tumors in the RFA group and the BB-94+RFA group 30 days after RFA. **(C)** Quantitative analysis of the tumor weight in the RFA group and the BB-94+RFA group 30 days after RFA. **(D)** The survival curves at different treatment groups. *P < 0.05, **P < 0.01.

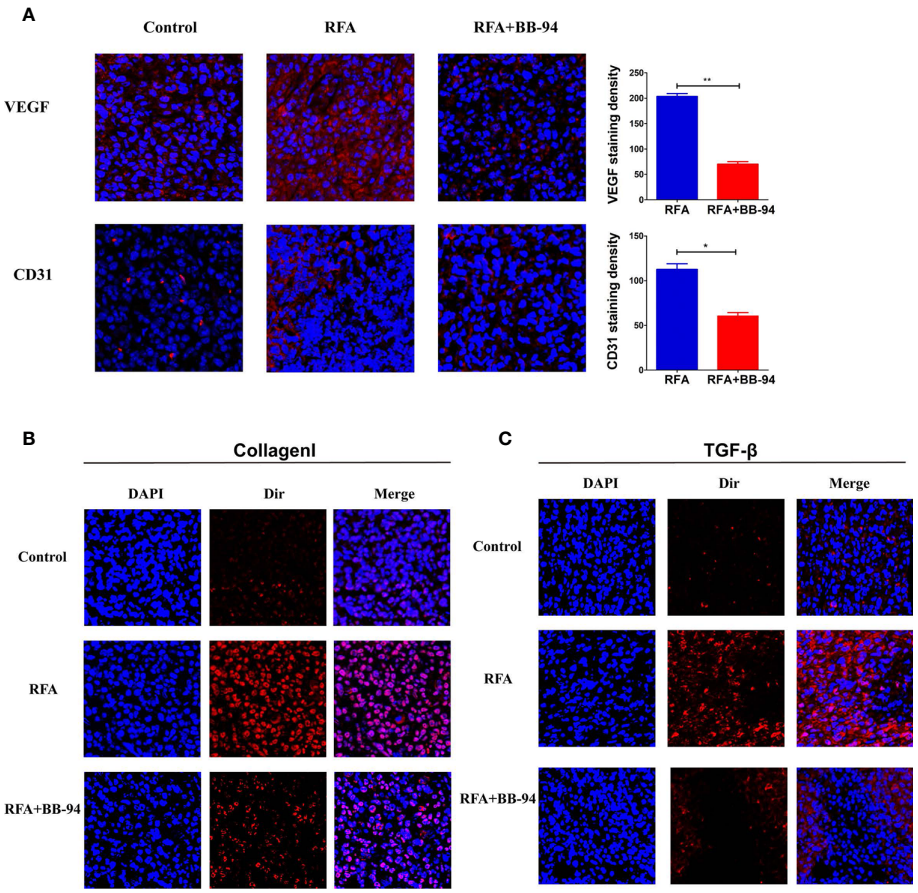

FIGURE 4 | Assessment of pathologic findings was performed 48 h after the last injection of BB-94. (At the magnification of ×200) **(A)** The represented picture of VEGF and CD31 staining after different treatment and the semiqualitative analysis of VEGF and CD31 staining in the RFA group and RFA+BB-94 group. **(B)** The represented picture of Collagen I staining after different treatment. **(C)** The represented picture of TGF-β staining after different treatment. *P < 0.05, **P < 0.01.

changes in heart, liver, spleen, lung, kidney in RFA group, RFA+BB-94 group, and control groups (**Figure 6B**).

DISCUSSION

Hepatocellular carcinoma (HCC) is one of the most common malignant tumors in the world with high morbidity, mortality, and increasing incidence (15). Radiofrequency ablation (RFA) is now an effective method commonly used in the local treatment of tumors. It has the advantages of minimally invasive, easy to operate, and significant curative effect. And RFA showed similar local control, long-term survival, and lower complication rates in patients with small tumors compared with hepatectomy (16). However, due to the factors such as tumor size, location, and liver function, complete ablation is often not possible. Recently, a growing number of studies have shown that residual tumors progress more rapidly after incomplete ablation (2, 17, 18).

Many studies have been reported about the underlying molecular mechanism of the increased tumor invasiveness after RFA, such as the Akt and ERK signaling pathways or through heat shock response by PKCα/Fra-1 pathway (19–21). The accelerated tumor progression after insufficient RFA was driven by many processes, but they all lead to the higher expression of MMPs. MMPs are zinc-dependent endopeptidase involved in the degradation of extracellular matrix (ECM). The MMP family is highly homologous and multidomain, which can be divided into gelatinase, collagenase, stromelysins, matrilysins, and membrane-type MMPs (22–24). MMPs are of great importance in cell proliferation, migration, differentiation, and vascularization. They could break the adhesion between cells and between cells and ECM, degrade ECM protein, promote angiogenesis, and facilitate tumor invasion and metastasis (25–28). Thus, MMPs play an important role in tumor progression after RFA and would be a potential target for treatment.

Therefore, we hypothesized that inhibiting the activities of MMPs may reduce the invasiveness of tumor after RFA. MMPs could be regulated under several levels, such as mRNA expression, proenzyme activation, and the inhibition of tissue inhibitors of metalloproteinases. For exogenous intervention, the

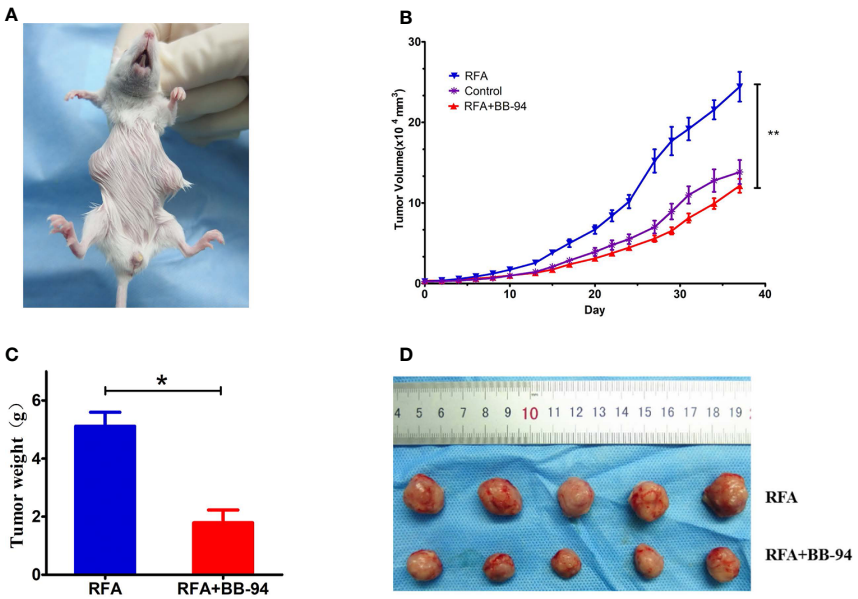

FIGURE 5 | Comparison of tumor metastasis. **(A)** The paired tumors model was used in this phase. One tumor was performed with RFA and the second tumor in other site was regarded as the metastasis tumor. **(B)** The tumor growth curves of other site of tumors at different treatment groups. **(C)** Quantitative analysis of the other site of the tumor weight in the RFA group and the BB-94+RFA group 20 days after RFA. **(D)** The other site of tumors in the RFA group and the BB-94+RFA group 20 days after RFA. *P < 0.05, **P < 0.01.

most direct way is using specific inhibitors to inhibit the enzyme activity. MMP inhibitors have been widely studied in recent years. According to the structure, they can be divided into three categories: collagen or non-collagen peptide analogues, tetracycline derivatives, and bisphosphonates. Among the three categories, the inhibitors of collagen peptide analogues are mainly broad-spectrum inhibitors, and large sample clinical trials have been carried out. Accordingly, as one of the main MMP inhibitors, Batimastat (BB-94), was broadly studied and applied (29, 30). BB-94 is a low molecular weight peptide like collagen substrate analogue, composed of a polypeptide skeleton and an isohydroxamic acid group, which can bind to the MMP and catalytically active Zn atoms to inhibit its activity (9). Therefore, in the present study, we used BB-94 as concomitant agent in combination of RFA treatment to explore its efficacy of decreasing tumor progression.

The present study was designed based on the previous clinical and experimental findings, which indicated that insufficient RFA promoted the invasiveness of residual HCC cells *via* upregulating MMPs (4, 5). Besides, BB-94, the specific inhibitor of MMPs, was reported to inhibit tumor growth (31, 32). The present study aimed to determine the role and mechanisms of BB-94 in the process of residual tumor growth and metastasis after RFA. Initially, the inhibitory role of BB-94 in liver tumor cell growth was identified by CCK8 assays. In addition, the results demonstrated that BB-94 significantly inhibited liver tumor cell migration, as determined by Transwell assays.

We next carried out experiments *in vivo* to further corroborate experimental results *in vitro*. In the animal experiments, we demonstrated two models to evaluate the adjuvant effect of the BB-94. Based on the findings in the previous report, we were not surprised to find that combination therapy could improve the anti-tumor effect. Specifically, RFA combined with BB-94 showed slower tumor growth, while single-treatment group and control group showed positive tumor growth. Because the residual tumor after RFA was relatively small in size, the differences of early growth rate in different groups was not obvious. At 30 days after treatment, differences between RFA and BB-94 in combination with RFA began to become apparent. Best local control occurred in tumors treated with BB-94+RFA. Therefore, the end-point survival rate was consistent with the tumor growth rate, BB-94 in combination with RFA had better survival than the RFA group. No organ metastasis was found at the end of the follow up. Due to the low invasiveness of the H22 cell, we established a two-tumor model to explore the effect of BB-94 on tumor metastasis. We implanted paired tumors subcutaneously, one for ablation in original site and the other tumor was mimic the RFA stimulating distant metastasis. On the basis of findings in prior reports (33), we also found that the unablated tumor grew faster after RFA. While after applying BB-94, the tumor growth was suppressed, similarly to the untreated group (P = 0.359).

Previous studies suggested that MMP may promote tumor growth by regulating tumor angiogenesis, which was crucial for the growth and invasion of solid tumors (34–36), we then examined the two angiogenic markers—VEGF and CD31—in tumor sections. The results indicated that RFA significantly increased the expression of VEGF and CD31. MMPs may

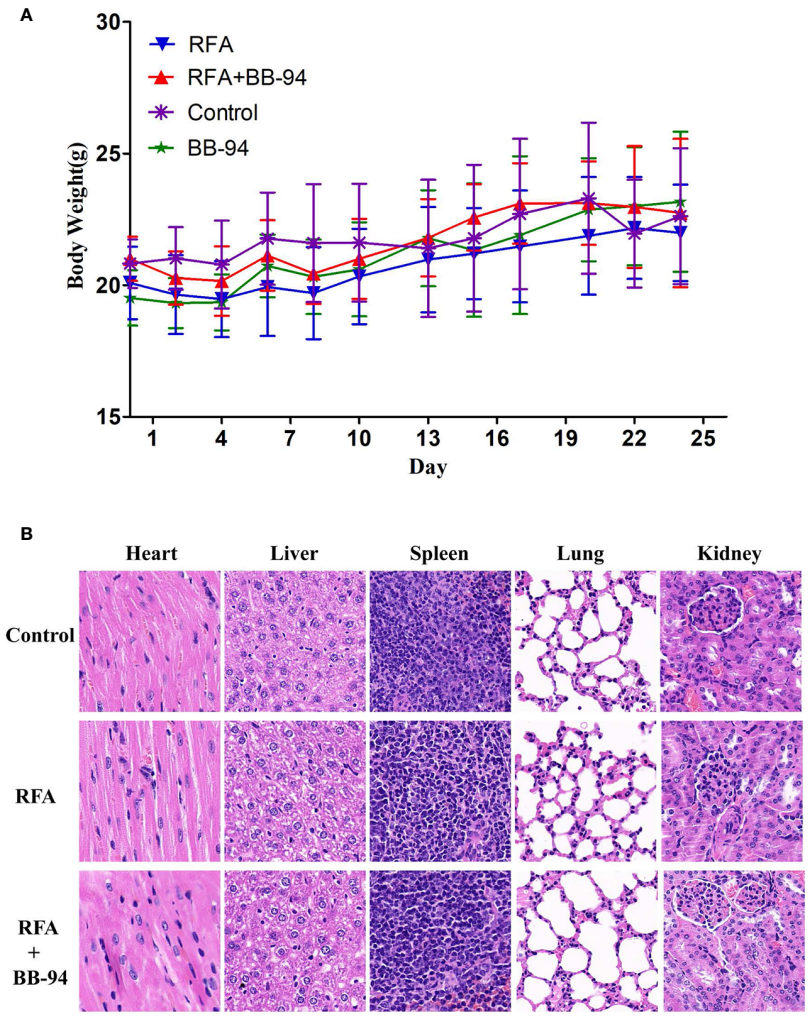

FIGURE 6 | Toxicity and safety evaluation. **(A)** Changes in mice weight after treatment. During the period of follow-up, there were no obvious difference in the bodyweight change after treatment in the four experimental groups ($P > 0.05$). **(B)** Microscopy pathological HE staining demonstrated there was no obvious histopathological changes in heart, liver, spleen, lung, kidney in both RFA and RFA+BB-94 groups.

promote angiogenesis through degradation of basement membrane and ECM components, and stimulating endothelial cell migration and VEGF release, so as to promote the formation of new vessels and increase their permeability (37). And less microvessels were observed after BB-94 applied. TGF-β exhibited higher expression patterns after RFA compared to the control and relatively less staining was identified after treated BB-94. Pathologic findings also suggested that BB-94 may inhibit proliferation and migration after RFA by down regulating TGF-β signaling. RFA could destroy the tumor cells, as well as remodel the tumor microenvironment. Collagen I was one of the extrasellar proteins associated with the increased invasiveness of many solid tumors including HCC (38, 39). Collagen deposition could be seen around the ablation area, which promoted the malignant behaviors of residual tumors. And the result showed BB-94 could have pleiotropic effects, not only inhibiting MMP activity directly but also affecting collagenase production and other cellular activities. During the experiment, the BB-94 showed no special biological toxicity. We preliminarily verified the efficacy of the BB-94 through the cell and animal experiments.

There were some limitations in our study. First, we evaluated the angiogenesis and TGF-β signaling pathway under the combination of RFA and BB-94 in this study. The mechanism of other processes beside MMPs needed to be further explored in the next step. Second, we studied the effect of BB-94 in *in vivo* and *in vitro* experiments with only one cell line model. Although H22 liver tumor model in this study is a well-characterized model that commonly used in the hepatoma related tumor research, however, it should not be excluded that H22 cell is sensitive to the BB-94. So, we should apply in other models to verify the effect carefully. Furthermore, the optimal dose and time of injection is quite important in the combination therapy

and need to be further explored. The detailed strategies to administration of BB-94 need to be optimized and standardized in the future. Last but not least, we established transplantation tumor model to explore the role of BB-94 in liver cancer metastasis, which might not fully recapitulate the liver cancer and the tumor microenvironment. The orthotopic model would be used to reinforce the conclusion of this study for the next experiments.

In conclusion, the specific inhibitor of MMP could help to decrease tumor invasiveness and achieve better overall outcome with combination of RFA. This adjuvant therapy might play an important role in clinical applications of RFA treatment in liver tumors.

DATA AVAILABILITY STATEMENT

The raw data supporting the conclusions of this article will be made available by the authors, without undue reservation.

ETHICS STATEMENT

The animal study was reviewed and approved by Peking University Cancer Hospital.

AUTHOR CONTRIBUTIONS

A-NJ and J-TL have equal contribution to this work. All authors contributed to the article and approved the submitted version.

FUNDING

This research was supported by the National Natural Science Foundation of China (81773286, 81971718) and Capital Characteristic Clinical Application Foundation (No. Z161100000516061).

REFERENCES

1. Wang X, Deng Q, Feng F, Chen S, Jiang J, Xia F, et al. Insufficient radiofrequency ablation promotes hepatocellular carcinoma cell progression via autophagy and the CD133 feedback loop. *Oncol Rep* (2018) 40(1):241–51. doi: 10.3892/or.2018.6403
2. Zhang N, Li H, Qin C, Ma D, Zhao Y, Zhu W, et al. Insufficient radiofrequency ablation promotes the metastasis of residual hepatocellular carcinoma cells via upregulating flotillin proteins. *J Cancer Res Clin Oncol* (2019) 145(4):895–907. doi: 10.1007/s00432-019-02852-z
3. Tajima H, Ohta T, Okamoto K, Nakanuma S, Hayashi H, Nakagawara H, et al. Radiofrequency ablation induces dedifferentiation of hepatocellular carcinoma. *Oncol Lett* (2010) 1(1):91–4. doi: 10.3892/ol_00000016
4. Ke S, Ding XM, Kong J, Gao J, Wang SH, Cheng Y, et al. Low temperature of radiofrequency ablation at the target sites can facilitate rapid progression of residual hepatic VX2 carcinoma. *J Trans Med* (2010) 8:73. doi: 10.1186/1479-5876-8-73
5. Frich L, Bjørnland K, Pettersen S, Clausen OP, Gladhaug IP. Increased Activity of Matrix Metalloproteinase 2 and 9 After Hepatic Radiofrequency Ablation. *J Surg Res* (2006) 135(2):297–304. doi: 10.1016/j.jss.2006.05.010
6. Sternlicht MD, Werb Z. How matrix metalloproteinases regulate cell behavior. *Annu Rev Cell Dev Biol* (2001) 17:463–516. doi: 10.1146/annurev.cellbio.17.1.463
7. Brinckerhoff CE. Matrix metalloproteinases: a tail of a frog that became a prince. *Nat Rev Mol Cell Biol* (2002) 3(3):207–14. doi: 10.1038/nrm763
8. Bourboulia D, Stetlerstevenson WG. Matrix MetalloProteinases (MMPs) andTissue Inhibitors of MetalloProteinases (TIMPs): positive and negative regulators intumor cell adhesion. *Semin Cancer Biol* (2010) 20(3):161–8. doi: 10.1016/j.semcancer.2010.05.002
9. Werb Z. Matrix metalloproteinases: regulators of the tumor microenvironment. *Cell* (2010) 141(1):52–67. doi: 10.1016/j.cell.2010.03.015
10. Chaudhary AK, Pandya S, Ghosh K, Nadkarni A. Matrix metalloproteinase and its drug targets therapy in solid and hematological malignancies: An overview. *Mutat Res* (2013) 753(1):7–23. doi: 10.1016/j.mrrev.2013.01.002
11. Lein M, Jung KD, Le DK, Hasan T, Ortel B, Borchert D, et al. Synthetic inhibitor of matrix metalloproteinases (batimastat) reduces prostate cancer growth in an orthotopic rat model. *Prostate* (2000) 43(2):77–82. doi: 10.1002/(SICI)1097-0045(20000501)43:2<77::AID-PROS1>3.0.CO;2-Q
12. Zhang B, Chen M, Jiang N, Shi K, Qian R. A regulatory circuit of circ-MTO1/miR-17/QKI-5 inhibits the proliferation of lung adenocarcinoma. *Cancer Biol Ther* (2019) 20(8):1127–35. doi: 10.1080/15384047.2019.1598762
13. Zhang N, Wang L, Chai ZT, Zhu ZM, Zhu XD, Ma DN, et al. Incomplete Radiofrequency Ablation Enhances Invasiveness and Metastasis of Residual Cancer of Hepatocellular Carcinoma Cell HCCLM3 via Activating β-Catenin Signaling. *PloS One* (2014) 9(12):e115949. doi: 10.1371/journal.pone.0115949
14. Ahmed M, Monsky WE, Girnun G, Lukyanov A, D'Ippolito G, Kruskal JB, et al. Radiofrequency thermal ablation sharply increases intratumoral liposomal doxorubicin accumulation and tumor coagulation. *Cancer Res* (2003) 63(19):6327–33.
15. Torre LA, Bray F, Siegel RL, Ferlay J, Lortet-Tieulent J, Jemal A. Global cancer statistics, 2012. *CA A Cancer J Clin* (2015) 65(2):87–108. doi: 10.3322/caac.21262
16. Fang Y, Chen W, Liang X, Li D, Lou H, Chen R, et al. Comparison of Long-term Effectiveness and Complications of Radiofrequency Ablation with Hepatectomy for Small Hepatocellular Carcinoma. *J Gastroenterol Hepatol* (2014) 29(1):193–200. doi: 10.1111/jgh.12441
17. Zhang N, Zhu H, Dong YH, Wang L. Establishment of an insufficient radiofrequency ablation orthotopic nude mouse model of hepatocellular carcinoma to study the invasiveness and metastatic potential of residual cancer. *Oncol Lett* (2019) 18(3):2548–53. doi: 10.3892/ol.2019.10552
18. Xu WL, Wang SH, Sun WB, Gao J, Ding XM, Kong J, et al. Insufficient radiofrequency ablation-induced autophagy contributes to the rapid progression of residual hepatocellular carcinoma through the HIF-1α/BNIP3 signaling pathway. *BMB Rep* (2019) 52(4):277–82. doi: 10.5483/BMBRep.2019.52.4.263
19. Zhang Z, Zhang Y, Zhang L, Pei Y, Wu Y, Liang H, et al. Incomplete radiofrequency ablation provokes colorectal cancer liver metastases through heat shock response by PKCα/Fra-1 pathway. *Cancer Biol Med* (2019) 16(3):542–55. doi: 10.20892/j.issn.2095-3941.2018.0407
20. Dong S, Kong J, Kong F, Kong J, Gao J, Ke S, et al. Insufficient radiofrequency ablation promotes epithelial-mesenchymal transition of hepatocellular carcinoma cells through Akt and ERK signaling pathways. *J Trans Med* (2013) 11:273. doi: 10.1186/1479-5876-11-273
21. Zhang N, Ma D, Wang L, Zhu X, Pan Q, Zhao Y, et al. Insufficient Radiofrequency Ablation Treated Hepatocellular Carcinoma Cells Promote Metastasis by Up-Regulation ITGB3. *J Cancer* (2017) 8(18):3742–54. doi: 10.7150/jca.20816
22. Cui N, Hu M, Khalil RA. Biochemical and Biological Attributes of Matrix Metalloproteinases. *Prog Mol Biol Trans Sci* (2017) 147:1–73. doi: 10.1016/bs.pmbts.2017.02.005
23. Nagase H, Visse R, Murphy AG. Structure and function of matrix metalloproteinases and TIMPs. *Cardiovasc Res* (2006) 69(3):562–73. doi: 10.1016/j.cardiores.2005.12.002

24. Huang H. Matrix Metalloproteinase-9 (MMP-9) as a Cancer Biomarker and MMP-9 Biosensors: Recent Advances. *Sensors (Basel)* (2018) 18(10):3249. doi: 10.3390/s18103249
25. Zhang G, Miyake M, Lawton A, Goodison S, Rosser CJ. Matrix metalloproteinase-10 promotes tumor progression through regulation of angiogenic and apoptotic pathways in cervical tumors. *BMC Cancer* (2014) 14:310. doi: 10.1186/1471-2407-14-310
26. García-Irigoyen O, Latasa MU, Carotti S, Uriarte I, Elizalde M, Urtasun R, et al. Matrix metalloproteinase 10 contributes to hepatocarcinogenesis in a novel crosstalk with the stromal derived factor 1/C-X-C chemokine receptor 4 axis. *Hepatology* (2015) 62(1):166–78. doi: 10.1002/hep.27798
27. Mauris J, Woodward AM, Cao Z, Panjwani N, Argüeso P. Molecular basis for MMP9 induction and disruption of epithelial cell-cell contacts by galectin-3. *J Cell Sci* (2014) 127(14):3141–8. doi: 10.1242/jcs.148510
28. Jabłońska-Trypuć A, Matejczyk M, Rosochacki S. Matrix metalloproteinases (MMPs), the main extracellular matrix (ECM) enzymes in collagen degradation, as a target for anticancer drugs. *J Enzyme Inhibit Med Chem* (2016) 31(sup1):177–83. doi: 10.3109/14756366.2016.1161620
29. Li W, Saji S, Sato F, Noda M, Toi M. Potential clinical applications of matrix metalloproteinase inhibitors and their future prospects. *Int J Biol Markers* (2013) 28(2):117–30. doi: 10.5301/JBM.5000026
30. Purcell WT, Rudek MA, Hidalgo M. Development of matrix metalloproteinase inhibitors in cancer therapy. *Hematology/Oncol Clinics North America* (2002) 16(5):1189–227. doi: 10.1016/S0889-8588(02)00044-8
31. Prontera C, Mariani B, Rossi C, Poggi A, Rotilio D. Inhibition of gelatinase A (MMP-2) by batimastat and captopril reduces tumor growth and lung metastases in mice bearing Lewis lung carcinoma. *Int J Cancer* (1999) 81 (5):761–6. doi: 10.1002/(sici)1097-0215(19990531)81:5<761::aid-ijc16>3.0.co;2-1
32. Gu B, Wu D, Li M, Li H, Liang Y. Effects of docetaxel alone or in combination with batimastat against metastasis of mouse forestomach carcinoma. *Chin J Pharmacol Toxicol* (2000) 14(3):177–82.
33. Wang C, Xu L, Liang C, Xiang J, Peng R, Liu Z. Immunological Responses Triggered by Photothermal Therapy with Carbon Nanotubes in Combination with Anti-CTLA-4 Therapy to Inhibit Cancer Metastasis. *Adv Mater* (2014) 26(48):8154–62. doi: 10.1002/adma.201402996
34. Wan J, Wu W, Huang Y, Ge W, Liu S. Incomplete radiofrequency ablation accelerates proliferation and angiogenesis of residual lung carcinomas via HSP70/HIF-1α. *Oncol Rep* (2016) 36(2):659–68. doi: 10.3892/or.2016.4858
35. Kong J, Kong L, Kong J, Ke S, Gao J, Ding X, et al. After insufficient radiofrequency ablation, tumor-associated endothelial cells exhibit enhanced angiogenesis and promote invasiveness of residual hepatocellular carcinoma. *J Trans Med* (2012) 10:230. doi: 10.1186/1479-5876-10-230
36. Nijkamp MW, Hoogwater FJ, Steller EJ, Westendorp BF, van der Meulen TA, Leenders MW, et al. CD95 is a key mediator of invasion and accelerated outgrowth of mouse colorectal liver metastases following radiofrequency ablation. *J Hepatol* (2010) 53(6):1069–1077. doi: 10.1016/j.jhep.2010.04.040
37. Yadav L, Puri N, Rastogi V, Satpute P, Ahmad R, Kaur G. Matrix metalloproteinases and cancer – roles in threat and therapy. *Asian Pac J Cancer Prev* (2014) 15(3):1085–91. doi: 10.7314/APJCP.2014.15.3.1085
38. Yang MC, Wang CJ, Liao PC, Yen CJ, Shan YS. Hepatic stellate cells secrete type I collagen to trigger epithelial mesenchymal transition of hepatoma cells. *Am J Cancer Res* (2014) 4(6):751–63.
39. Hayashi M, Nomoto S, Hishida M, Inokawa Y, Kanda M, Okamura Y, et al. Identification of the collagen type 1 α 1 gene (COL1A1) as a candidate survival-related factor associated with hepatocellular carcinoma. *BMC Cancer* (2014) 14:108. doi: 10.1186/1471-2407-14-108

Conflict of Interest: The authors declare that the research was conducted in the absence of any commercial or financial relationships that could be construed as a potential conflict of interest.

frontiers in Oncology

SYSTEMATIC REVIEW
published: 27 November 2020
doi: 10.3389/fonc.2020.560952

Assessment of Ablation Therapy in Pancreatic Cancer: The Radiologist's Challenge

Vincenza Granata[1], Roberta Grassi[2], Roberta Fusco[1], Sergio Venanzio Setola[1], Raffaele Palaia[3], Andrea Belli[3], Vittorio Miele[4], Luca Brunese[5], Roberto Grassi[2], Antonella Petrillo[1] and Francesco Izzo[3]*

[1] Radiology Division, Istituto Nazionale Tumori, IRCCS, Fondazione G. Pascale, Naples, Italy, [2] Radiology Division, Universita' Degli Studi Della Campania Luigi Vanvitelli, Naples, Italy, [3] Hepatobiliary Surgical Oncology Division, Istituto Nazionale Tumori, IRCCS, Fondazione G. Pascale, Naples, Italy, [4] Department of Radiology, Careggi University Hospital, Florence, Italy, [5] Department of Medicine and Health Sciences "V. Tiberio," University of Molise, Campobasso, Italy

OPEN ACCESS

Edited by:
Mattia Squarcia,
Hospital Clínic de Barcelona, Spain

Reviewed by:
Katsutoshi Sugimoto,
Tokyo Medical University, Japan
Hiroyasu Fujiwara,
Okayama City Hospital, Japan

***Correspondence:**
Roberta Fusco
r.fusco@istitutotumori.na.it

Specialty section:
This article was submitted to Cancer Imaging and Image-directed Interventions, a section of the journal Frontiers in Oncology

Received: 11 May 2020
Accepted: 30 October 2020
Published: 27 November 2020

Citation:
Granata V, Grassi R, Fusco R, Setola SV, Palaia R, Belli A, Miele V, Brunese L, Grassi R, Petrillo A and Izzo F (2020) Assessment of Ablation Therapy in Pancreatic Cancer: The Radiologist's Challenge. Front. Oncol. 10:560952. doi: 10.3389/fonc.2020.560952

This article provides an overview of imaging assessment of ablated pancreatic cancer. Only studies reporting radiological assessment on pancreatic ablated cancer were retained. We found 16 clinical studies that satisfied the inclusion criteria. Radiofrequency ablation and irreversible electroporation have become established treatment modalities because of their efficacy, low complication rates, and availability. Microwave Ablation (MWA) has several advantages over radiofrequency ablation (RFA), which may make it more attractive to treat pancreatic cancer. Electrochemotherapy (ECT) is a very interesting emerging technique, characterized by low complication rate and safety profile. According to the literature, the assessment of the effectiveness of ablative therapies is difficult by means of the Response Evaluation Criteria in Solid Tumors (RECIST) criteria that are not suitable to evaluate the treatment response considering that are related to technique used, the timing of reassessment, and the imaging procedure being used to evaluate the efficacy. RFA causes various appearances on imaging in the ablated zone, correlating to the different effects, such as interstitial edema, hemorrhage, carbonization, necrosis, and fibrosis. Irreversible electroporation (IRE) causes the creation of pores within the cell membrane causing cell death. Experimental studies showed that Diffusion Weigthed Imaging (DWI) extracted parameters could be used to detect therapy effects. No data about functional assessment post MWA is available in literature. Morphologic data extracted by Computed Tomography (CT) or Magnetic Resonance Imaging (MRI) do not allow to differentiate partial, complete, or incomplete response after ECT conversely to functional parameters, obtained with Position Emission Tomography (PET), MRI, and CT.

Keywords: pancreatic cancer, ablation treatment, computed tomography, magnetic resonance imaging, functional imaging

INTRODUCTION

Oncology disease is the second principal cause of death in both men and women. Incidence continues to increase for pancreatic cancer, with an estimated death rate of 81.7% among new cases of 2020 and a 5-year relative survival rate of the 9% (1). The decision regarding resectability status of pancreatic cancer should be made by the multidisciplinary meetings consensus following the acquisition of pancreatic imaging including complete staging. In fact, most patients had locally advanced or metastatic disease at diagnosis, and systemic chemotherapy is usually the main treatment (2–6). Most patients experience relapse after treatment. Furthermore, the "cure rate" for this disease is only 9%, and without treatment, the median survival of patients with metastatic disease is only 3 months. First-line treatment regimens consists of FOLFIRINOX and gemcitabine/albumin-bound nab-paclitaxel, and for patients with BRCA1/2 and PALB2 mutations, gemcitabine/cisplatin. Compared with nab-paclitaxel/gemcitabine, FOLFIRINOX may be associated with a somewhat better response rate and progression-free and overall survival (OS), but it is a difficult regimen that is best reserved for fit patients (3). Despite the latest introduction of new treatment schemes, chemotherapy in advanced pancreatic cancers still correlates to an unfortunate long-term survival and considerable ad interim complications (6, 7). The resectability assessment of Locally Advanced Pancreatic Cancer (LAPC) after neoadjuvant therapy is still challenging. In dedicated cancer centers, patients with persistent LAPC after chemotherapy should be subjected to local treatment if they are in good clinical condition (WHO Performance Status 0–1) and according to Response Evaluation Criteria in Solid Tumors (RECIST) in stable disease after 2–4 months chemotherapy. However, randomized trials to assess the ablative therapies additional value to chemotherapy-alone are lacking and currently there are no completed trials comparing multiple ablative approaches (8). Additionally, there is increasing suggestion that local ablative therapies can induce a systemic anti-tumor response (8).

Today ablative therapies should be used as consolidative treatment in stable disease (9). Assessment after ablative treatment is complicated and is related to the type of treatment used (10–15). Radiofrequency ablation (RFA) and microwave ablation (MWA) are hyperthermic tools that use energy to heat the target area to at least 60°C (16, 17). Although the technological features of RFA and MWA are comparable, the differences occur from the physical phenomenon used to create heat. In fact, RFA is based on thermocoagulation necrosis, while MWA causes cellular death thanks to dielectric heating (16, 17).

The cell membrane permeability changes induced by the application of an external electric field is called electroporation. Electroporation can be applied in either an irreversible (IRE) (14, 18–28) or a reversible manner (11–13, 29, 30), depending on the electrical field strength and duration. IRE is based on alteration of the transmembrane potential, causing the disruption of the lipid bilayer by the creation of small pores ("nanopores"), thus driving the cells toward apoptosis (23). Reversible electroporation can be used in combination with administration of a chemotherapeutic drug (ECT) or also gene therapy and vaccination (Electrogenetransfer, EGT). ECT is based on the electroporation of cells and the associated administration of low doses of a chemotherapeutic agent, especially bleomycin (BLM). An external electrical field is applied to the cell membrane inducing a transient and reversible orientation of its polar molecules, consequently there is an increase in cell permeability with a higher dose of chemotherapeutic agent that can penetrate (11). ECT determines a direct toxic phenomenon and an anti-vascular effect. "This so called 'vascular lock' effect retains the chemotherapeutic agent in the treatment area thereby increasing the treatment effect further" (31). "Furthermore, the type of cell death that is mediated is dependent on the number of intracellular BLM molecules. A few hundred to few thousand molecules lead to a slow mitotic cell death and more internalized molecules lead to a faster pseudoapoptotic cell death" (32).

Several therapies both thermal and non-thermal have the ability to stimulate anti-tumor immunity. The immune-modulatory response evidence is currently the strongest related to radiotherapy, although data is accumulating for high-intensity focused ultrasound, radiofrequency ablation, reversible and irreversible electroporation (33–35).

RECIST are inappropriate to assess locoregional therapies, since existing morphologic response criteria do not offer the sufficient data to assess the efficacy of treatment. Therefore, establishment of response evaluation criteria devoted to ablation therapies is needed in clinical practice, as well as in clinical trials. According to García-Figueiras et al. functional features could predict treatment success before size changes become evident (15).

Our purpose is reporting an overview and update of imaging techniques in the response assessment to ablative therapies in pancreatic cancer.

Abbreviations: ADC, apparent diffusion coefficient; BLM, bleomycin; CT, computed tomography; DCE-MR, dynamic contrast-enhanced MRI; D, diffusion coefficient; Dp, pseudo-diffusion coefficient; DWI, diffusion weigthed imaging; DKI, diffusion kurtosis imaging; ECT, electrochemotherapy; EGT, electrogenetransfer; fp, perfusion fraction; IRE, irreversible electroporation; IVIM, intravoxel incoherent motion; K, kurtosis coefficient; OS, overall survival; LAPC, locally advanced pancreatic cancer; MD, mean diffusivity; MRI, magnetic resonance imaging; MWA, microwave ablation; PR, partial response; PD, progressive disease; PET, position emission tomography; QoL, quality of life; RFA, radiofrequency ablation; RECIST, Response Evaluation Criteria in Solid Tumors; SD, stable diseases.

METHODS

This overview is the result of a self-study without protocol and registration number.

Search Criterion

We assessed several electronic databases: PubMed (US National Library of Medicine, http://www.ncbi.nlm.nih.gov/pubmed), Scopus (Elsevier, http://www.scopus.com/), Web of Science (Thomson

Reuters, http://apps.webofknowledge.com/), and Google Scholar (https://scholar.goo-gle.it/). The following search criteria have been used: "Pancreatic Cancer" AND "Ablative Therapies" AND "Imaging Assessment", "Pancreatic Cancer" AND "RFA" AND "Imaging Assessment, "Pancreatic Cancer" AND "MWA" AND "Imaging Assessment, "Pancreatic Cancer" AND "IRE" AND "Imaging Assessment, "Pancreatic Cancer" AND "ECT" AND "Imaging Assessment." According to our personal decision to assess functional imaging in evaluating ablation treatment, and since only in the last 10 years these diagnostic tool have reached their applicability, the search covered the years from January 2010 to May 2020. Moreover, the references of the found papers were evaluated for papers not indexed in the electronic database. We analyzed all titles and abstracts. The inclusion criteria was: clinical study evaluating radiological assessment of pancreatic cancer after ablative therapies. Articles published in the English language from January 2010 to May 2020 were included. Exclusion criteria were studies with no sufficient reported data, case report, review or editorial letter.

RESULTS

We recognized 140 studies that assessed ablation treatment in pancreatic cancer from January 2010 to May 2020. Ninety-one studies have different topic in respect to the radiological assessment; 5 did not have sufficient data and 8 are case report, review, or letter to editors; so 36 articles were included at the end (**Figure 1**). We included 18 papers for RFA, 3 paper for MWA, 11 paper for IRE, and 4 paper for ECT. **Table 1** reports the mean value and the range of overall survival and the mean value of major complication rates, minor complication rates, mortality rate, and imaging analysis in pancreatic cancer treated with ablation therapies. For IRE and ECT we reported the data of the researches that have assessed significant study population, while for RFA and MWA less patients have been treated so we reported mean value considering each included study.

Radiofrequency Ablation

During RFA, the zone of active tissue heating is restricted to a few millimeters around the active needle, with the remainder of the ablation zone being heated *via* thermal conduction (16). The treatment effectiveness is related to the target size, with the best result for lesions with a size smaller than 3.5 cm (16, 17). Also, some structural characteristics of biological tissues, such as electrical and thermal conductivity, dielectric permittivity, and blood perfusion rate, have effect on the growth of ablation area. The coagulation necrosis extent is linked to the energy deposited correlated to the hepatic blood flow that with its cooling properties affected tumor ablation; this phenomenon is commonly termed "heat sink effect" (20). The heat-sink effect limits the all thermal ablation method's effectiveness since the combined effect of electrical and thermal sink increases the incomplete necrosis risk (17–20, 59).

Today the most application of RFA on pancreatic cancer is the treatment of patients with stage-III, in case of no further systemic therapies response. However, some studies included also stage-IV patients (9). At the best of our knowledge, 18 papers assessed RFA in clinical setting (**Table 1**) (9, 36–51). In most patients RFA was reserved to stages III–IV, and in lower stage in 22 unfit-for-surgery patients. RFA was performed in 158/279 (56.6%) head lesions, in 68/279 (24.4%) body-tail lesions, and in 2 uncinate process lesions. Computed Tomography (CT) scan was the diagnostic tool mostly used to assess the treatment. Fifty-two complications were reported

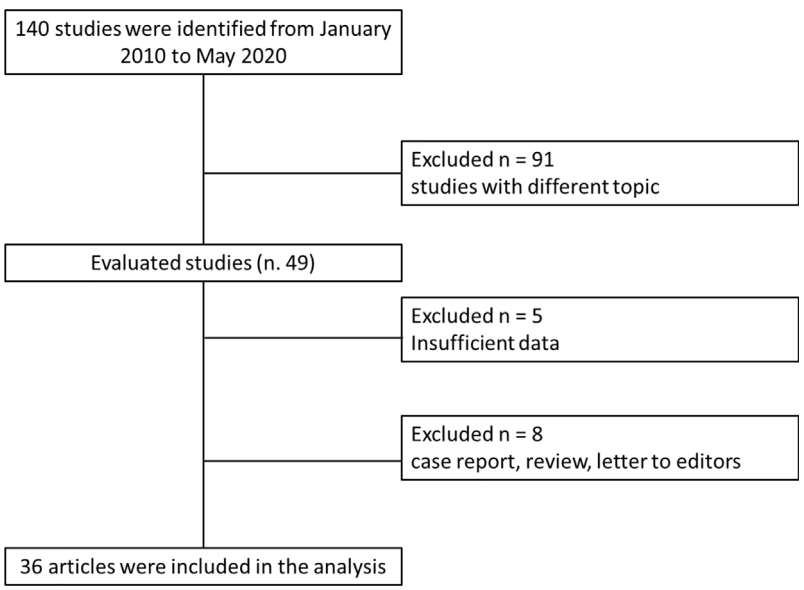

FIGURE 1 | Included and excluded studies in systematic review.

TABLE 1 | Mean value and the range of overall survival and the mean value of major complication rates, minor complication rates, mortality rate, and imaging analysis in pancreatic cancer treated with ablation therapies.

Technique	Authors	Overall Survival (OS)	Major Complication Rates	MinorComplicationRates	MortalityRates	Imaging modality used and radiological response criteria used
RFA	Paiella et al. (9) D'Onofrio et al. (36) Giardino et al. (37) Hadjicostas et al. (38) Ikuta et al. (39) Kallis et al. (40) Lakhtakia (41) Pai (42) Rossi (43) Song et al. (44) Spiliotis et al. (45) Varshney et al. (46) Waung (47) Zou (48) Saccomandi (49) Zou et al. (50) Giardino (51)	23 months (mean value) 9-30 months (range)	1.9% (mean value)	20.2% (mean value)	0.7% (mean value)	CT (no functional data available) No data on MRI
MWA	Carrafiello et al. (52) Ierardi et al. (51) Vogl et al. (53)	–	8.5% (mean value)	8.6% (mean value)	No data reported	CT (no functional data available) No data on MRI
IRE	Martin et al. (20, 21) Kwon et al. (22) Lambert et al. (24) Yan et al. (25) Zhang et al. (26) Scheffer et al. (27) Narayanan et al. (54) Weiss et al. (55) Rombouts et al. (56) Scheffer et al. (57)	24.9 months (mean value) 4.9–85 months (range) [Martin et al. (20)]	1.5% Scheffer 2014 (27)	15% (open approach) 29% (percutaneus approach) Martin et al. (20) Rombouts et al. (56) Scheffer et al. (57)	2% Martin et al. (20) and Rombouts et al. (56)	CT- MRI (functional data available)
ECT	Granata et al. (11–13) Ongoing study by Granata et al. (58)	11.5 months (mean value)	0%	23.1% (mean value)	4.2% (mean value)	CT-MRI (functional data available)

(**Table 1**). The most frequent were pancreatic fistula (12 cases), portal thrombosis (10 cases), and pancreatitis (8 cases). In three patients was reported duodenal injury, and in two patients abdominal bleeding. Two deaths were registered due to hepatic failure (49). In a recent review Paiella et al. reported a good oncological outcome obtained with the use of RFA on pancreatic cancers with a median OS of 30 months for patients treated with RFA, median OS of 25.6 months in the group treated RFA plus systemic therapy (**Table 1**) (9).

Recently, RFA is used as an upfront option, justified on the basis of an immunological antitumoral stimulation (50, 60).

Microwave Ablation

MWA determines a larger zone of active heating (up to 2 cm surrounding the antenna) obtaining more uniform necrosis of the lesion. MWA benefits compared to RFA are: lesion size can be larger for larger area of necrosis determined by MWA; the treatment time is shorter (16). Carrafiello et al. (52) assessed MWA in 10 patients in stage IV, with lesion located in the head of the pancreas (**Table 1**). During the follow-up (mean time 9.2 months, range 3–16 months), the major complications rate was 30% (3 patients). Two patients developed pancreatitis and one patient pseudoaneurysm of the gastroduodenal artery. CT scan was performed up to 15 months after the treatment (**Table 1**). No patients showed a complete response. At 1 month follow-up there were found 1 progressive disease (PD), 1 partial response (PR), and 8 stable diseases (SD). Ierardi et al. (51) assessed feasibility and safety of MWA in LAPC using a new technology of MW with high power (100 W) and frequency of 2,450 MH. They treated five patients with pancreatic head cancer. Follow-up was performed by CT after 1, 3, 6, and, when possible, 12 months. The treatment was feasible in all patients (100%), observing no major complications. Minor complications resolved during the hospital stay (4 days) (**Table 1**). An improvement in Quality of Life (QoL) was observed in all patients (51). Vogl et al. (53) treated 20 pancreatic cancer patients. Seventeen lesions (77.3%) of pancreatic head cancer and 5 (22.7%) of body-tail. The efficacy reported was 100%, without major complications. Minor complications were found in 2 patients (9.1%) (severe local pain correlated to the treatment). PD was documented in one case (10%) of the 10/22 accessible 3-month follow-up MR examinations (**Table 1**).

Altogether, MWA shows promising results, however, it needs further data to improve the knowledge about the efficacy, the safety, and the oncological outcome.

Irreversible Electroporation

IRE induces an electric field across cells in order to alter the cellular transmembrane potential. When a sufficiently high voltage is reached, the cell membrane phospholipid bilayer structure is disrupted, inducing cell apoptosis. The evidence suggests that IRE "leaves supporting tissue largely unaffected, preserving the structure of large blood vessels and bile ducts" (16, 17, 19). Since IRE efficacy is linked to electrical energy delivered; therefore its efficacy is not influenced by the heat-sink effect (16, 17, 19). This suggests safer and more effective ablation of neoplasms adjacent to large vessels or fragile structures (9–18, 20–22, 24–27, 54–56, 59).

Considering this, IRE preserves surrounding tissues and protect the vessels; this characteristic would be an essential feature when the lesion encases the major peripancreatic vessels, in which the use of thermal treatment could be unsafe and inefficacious (9–18, 20–22, 24–27, 54–56, 59).

Currently, IRE is used on stage-III LAPC (18, 27). Narayanan et al. reported three cases of IRE on stage IV (45). Also, several researchers reported the possibility to use IRE, as a technique to reduce R1 resections rate (20, 22, 54, 55). For IRE, two to six electrodes are typically placed around the tumor, with a maximum spacing of 2.0–2.5 cm. IRE has the disadvantage of necessity of general anesthesia. Rombouts et al., in a systematic review, reported complication rate of 13%, and a mortality of 2% (56). The complication rate increases with percutaneous approach (29 *vs* 15%) (20, 56, 57). Martin et al., assessing 200 treated patients, showed an overall rate of adverse events of 37% and a mortality rate of 2% (**Table 1**) (20). The most common complications described are pancreatitis, abdominal pain, bile leakage, pancreatic leakage, duodenal leakage, duodenal ulcer, pneumothorax, hematoma, and deep vein thrombosis (**Table 1**) (6). MR and CT were the diagnostic tool mostly used to assess the treatment. Despite the large number of studies on IRE in pancreatic cancer, only Martin et al. (20) reported an outstanding median Overall Survival (OS) of 24.9 months (range 12.4–85 months). Consequently, there is a need for a greater number of studies that evaluate efficacy in terms of oncological outcomes (**Table 1**).

Electrochemotherapy

ECT is based on the electroporation of cells and the associated administration of low doses of chemotherapy. An external electric field to a cell induces a transient and reversible increase of cells transmembrane potential with a consequent increase of permeability (11–13, 30–32). Formation of the aqueous pores in the lipid bilayer is the widely recognized mechanism, but evidence is growing that individual membrane lipids and proteins changes also contribute at ECT cytotoxic effect (61). The increased accumulation of intracellular drug concentration has actually been shown both *in vitro* and *in vivo* (58, 62–65).

In the clinical setting few papers assessed the safety and efficacy of ECT in LAPC (11–13). Granata et al. (11) evaluated 13 patients with confirmed diagnosis of LAPC (stage III). In 53.8% (7/13) the lesion was on head and in 46.2% (6/13) the lesion was on body-tail. ECT was well tolerated with rapid resolution (4–8 days) of the abdominal pain. No serious adverse events occurred. No heart abnormalities were reported. No clinically significant hemodynamic or serum biologic changes were noted during or following ECT (**Table 1**). CT and MR were employed for the follow-up at 1, 3, 6, and 12 months. In an ongoing study, Granata et al. (58) showed that median OS was 11.5 months with range values of 73 months. At 1 month after ECT 76.0% of patients were in PR and 20.0% were in SD. Today, ECT is recommended during clinical studies in dedicated centres (11–13).

Imaging Analysis

The precise detection and characterization of pancreatic lesion is still difficult. CT and MRI are the main used modalities to assess pancreatic lesions and CT has become the modality of choice in the preoperative setting and staging, so as in treatment planning and follow-up (5). However, approximately 11% of ductal adenocarcinomas are undetected at CT (10). Morever, the pancreatic cancer assessment after neoadjuvant therapy is particularly difficult and as suggested by White et al., CT would miscalculate the resectability, since diagnostic performance seems to be reduced after therapy. Therefore, there are not radiological criteria in order to assess treatment response correlated to histological response (66). The situation becomes more complicated when evaluating effectiveness of ablative therapies, considering that RECIST criteria were not suitable to assess the response (67).

Dimensional Criteria

RECIST 1.1, based on the variation of largest diameter, do not allow to stratify the patients in responders or non-responders after ablation treatment, since after these therapies it is expected that there is an increase in the size of the ablated area. In fact, the primary endpoint of ablation therapy is to obtain a complete necrosis (similar to R0 resection) of liver tumors that is linked to create a safety margin of at least 10 mm round the external margin of the lesion (16, 68). Moreover, the nature of the pancreatic cancer, consisting of a more or less great quantity of cells fixed within a dense and fibrous stroma, reduce diagnostic accuracy when the treated area is measured (69). After effective therapy, it is difficult the differentiation between neoplastic cells and fibrosis and then it is difficult the evaluation with morphological criteria of therapy response. Moreover, a possible locoregional edema induced by treatment or inflammatory changes secondary to biliary drainage could be observed. Therefore, the treatment response evaluation for this cancer type is a serious challenge and the dimensional criteria are unsuitable (69).

Perfusional Assessment

Perfusion CT (CTp) can provide images and quantitative measurements of hemodynamic parameters based on the linear relationship between CT enhancement and iodinated contrast agent concentration (10). Several studies evaluated perfusion CT parameters to characterize and to evaluate the treatment in patient affected by pancreatic cancer; these studies demonstrates that CTp is more able to differentiate the pancreatic disorder respect to density measurements alone. However, no significant differences in the perfusion parameters values were found between acute-chronic pancreatitis and pancreatic adenocarcinoma, then the differential diagnosis by CTp data remains difficult (10).

Dynamic contrast-enhanced (DCE)-MRI allows the calculation of quantitative parameters linked to tumor perfusion, vessel permeability and extracellular-extravascular space composition by the post processing with pharmacokinetic models of the changes in signal intensity over time after the paramagnetic contrast medium injection (69). DCE-MRI can be analyzed by qualitative, semi-quantitative, and quantitative methods (69). DCE-MRI accuracy in the evaluation of pancreatic cancer remains unclear, probably due to the fact that in pancreatic cancer, "poorly represented microvascular components could be clarified by vessel functional impairment often observed in tumors, and by the presence of a prominent stromal matrix that embeds vessels. In addition, activated pancreatic stellate cells yield increasing fibrous stroma in tumor central areas, compressing blood vessels, leading to changes in vascularity and perfusion" (69).

Diffusion Weighted Imaging Assessment

The opportunity to obtain functional parameters by Diffusion Weighted Imaging (DWI) has facilitated the spread of this technique into clinical practice, increasing clinical confidence and decreasing false positives in the detection and characterization of lesions. DW data analysis can be done qualitatively and quantitatively, through the apparent diffusion coefficient (ADC) evaluation using a mono-exponential model at the signal intensity decay over the diffusion b values. DWI signal is linked to water mobility that related to tissue density (69). ADC can be used in the differentiation between benign and malignant tissue. Instead, the Intravoxel incoherent motion (IVIM) method used a more sophisticated process, a bi-exponential model to separately calculate the macroscopic mobility of water movement (contribution to diffusion), and microscopic movement of blood in capillaries (contribution of perfusion). Also IVIM parameters can be analyzed qualitatively and quantitatively (69). Moreover, according to the presence of microstructures, water molecules within biologic tissues exhibit a non-Gaussian phenomenon known as Diffusion Kurtosis Imaging (DKI) (69). Therefore, is possible the calculation of the kurtosis coefficient (K) linked to the deviance of diffusion from a Gaussian approach, and the diffusion coefficient (D) with the correction of non-Gaussian bias.

Since necrosis and perfusion modifications can happen before changes in size during therapy, DWI may aid as an early biomarker of treatment effectiveness (69).

Granata et al. showed that the perfusion-related factors extracted by DWI of pancreatic cancer, perfusion fraction (fp) and pseudo-diffusion coefficient (Dp) (linked to tumoral perfusion), mean diffusivity (MD) (linked to heterogeneous diffusion motion of water molecules in cells interstitial space) values are different from those found in normal pancreatic parenchyma and in peritumoral tissue; in addition these parameters showed better diagnostic performance than ADC (linked both perfusion and diffusion effects). The significantly different of perfusion-related factors value between cancer tissue and normal pancreatic parenchyma might be helpful for determining the most accurate diagnosis. Increased fp and MD values in peritumoral inflammation seem to suggest that DWI-derived parameters fit in the anticipated physiologic phenomena. These findings support the hypothesis that the kurtosis effect could have a better performance to differentiate pancreatic tumors, peritumoral inflammatory tissue, and normal pancreatic parenchyma (69).

Radiomics

The extraction of innumerable quantitative features by biomedical images such as CT, MR, or positron emission tomography (PET) images is known as Radiomics. These features provide data on tumor phenotype as well as cancer microenvironment. The main challenge is the collection and optimal combination of different multimodal data sources in a quantitative method that provides unambiguous clinical parameters that allow in a precise and robust way the prediction of the results according to the upcoming decisions (70). The central hypothesis of radiomics is that individual quantitative voxel-based variables are more sensitively associated with various clinical endpoints than the more qualitative radiological and clinical data more commonly used today (70).

Findings on Radiological Therapeutic Responses to Treatments

It is clear that, considering therapeutic responses to treatments, imaging data are sometimes complicated to understand because it depend on anatomic location, on the method of act of given therapy, on the morphological and functional criteria that are used for each imaging modality (15). In this setting, imaging observations depend highly on the type and method of therapy delivery, the timing of treatment, and the imaging technique being used to observe the effects.

RFA causes heterogeneous appearances on imaging in the ablated areas, correlated to the therapy effects, such as interstitial edema, hemorrhage, carbonization, necrosis, and fibrosis (**Figure 2**).

Experimental studies showed that DWI could be used to detect the efficacy of IRE treatment (71, 72).

The evaluation of the treatment response in terms of lesion dimensional reduction is not appropriate because not always a positive response to treatment is linked to a size reduction; furthermore dimensional criteria do not allow the differentiation of the fibrotic tissue from the residual tumor.

Therefore, an evaluation based only on dimensional data is not appropriate to assess the efficacy of such complex treatments. However, one of the major topics evaluated by papers that we analyzed regarding the ablative techniques is the short- and long-term efficacy based on the tumor dimension reduction. Regarding RFA papers, the results on the follow-up was reported in 12 out of 18 studies for a total of 214 patients (36–41, 43, 45–48). Assessment time was between 7 and 34 months and was mainly performed by means of CT-scan and MRI (seven studies), considering only dimensional criteria (36–41, 43, 45–48). According to Paiella et al. for RFA, and in general for "thermal techniques," the gold standard of imaging is represented by CT with a post-ablative hypointense area observed as result of the treatment (9). However, also pancreatic tumor is hypointense so that a "qualitative assessment" based only human eyes could cause misdiagnosis. A quantitative evaluation based on perfusion evaluation or metabolic analysis allows a more objective reassessment and a more correct stratification of patients in responders and non-responders to treatment (73–77).

Regarding MWA studies, the follow-up was reported in all cases. Assessment time was between 1 and 12 months, performed by CT and MRI, considering dimensional criteria.

At the best of our knowledge no papers in literature reported findings on efficacy of ablation by RFA or MWA using functional radiological approaches such as DWI, DKI, PET. On the contrary in literature are present studies about the evaluation of efficacy by IRE and ECT using several functional radiological parameters in the assessment of the treatment.

Vroomen et al. (14) assessed specific imaging features after IRE for LAPC with contrast-enhanced (ce) MRI and ce-CT, and to explore the correlation of these features with the development of recurrence. They assessed pre and post IRE, for MRI, the Signal Intensity (SI) on T2-Weigthed sequences, on T1-Weigthed sequences (before and after ce, during arterial and venous phase), on DWI and on ADC map; and for CT attenuation in the arterial and portal venous phase. They found that the most remarkable signal alterations after IRE were shown by DWI-b800 and ceMRI. According to Vroomen et al., these features may be useful to establish technical success and predict treatment outcome. Granata et al. (12, 13) assessed morphological (**Figures 3** and **4**) and functional (**Figure 5**) diagnostic parameters to evaluate the efficacy of ECT (61, 78–81). The researchers showed that RECIST criteria were not able to discriminate partial, complete, or incomplete response after

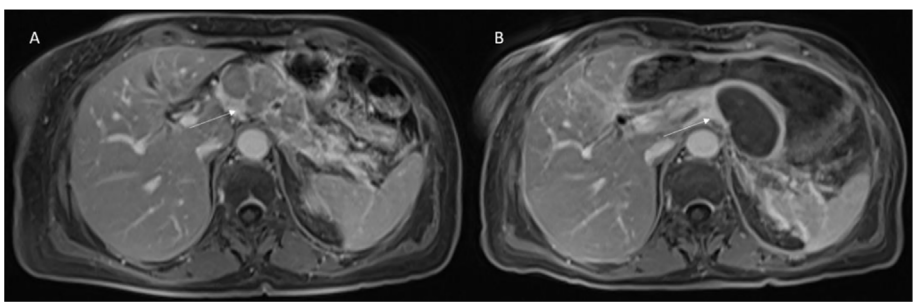

FIGURE 2 | Patient 1 with Body-Tail Pancreatic Cancer. Morphological MRI assessment post-RFA treatment. In **(A)** (VIBE T1-W post-contrast sequence during portal phase in axial plane) pre-treatment evaluation of lesion (arrow). In **(B)** (VIBE T1-W post-contrast sequence during portal phase in axial plane) arrow shows ablated area. Qualitative assessment shows significant differences in SI in pre- and post-treatment sequences.

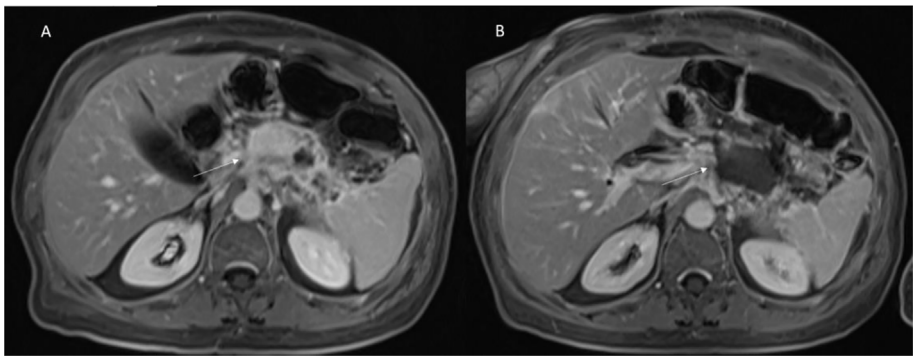

FIGURE 3 | Patient 2 with Body-Tail Pancreatic Cancer. Morphological MRI assessment post-ECT treatment. In **(A)** (VIBE T1-W post-contrast sequence during portal phase in axial plane) pre-treatment evaluation of lesion (arrow). In **(B)** (VIBE T1-W post-contrast sequence during portal phase in axial plane) arrow shows ablated area. Qualitative assessment shows significant differences in SI in pre- and post-treatment sequences.

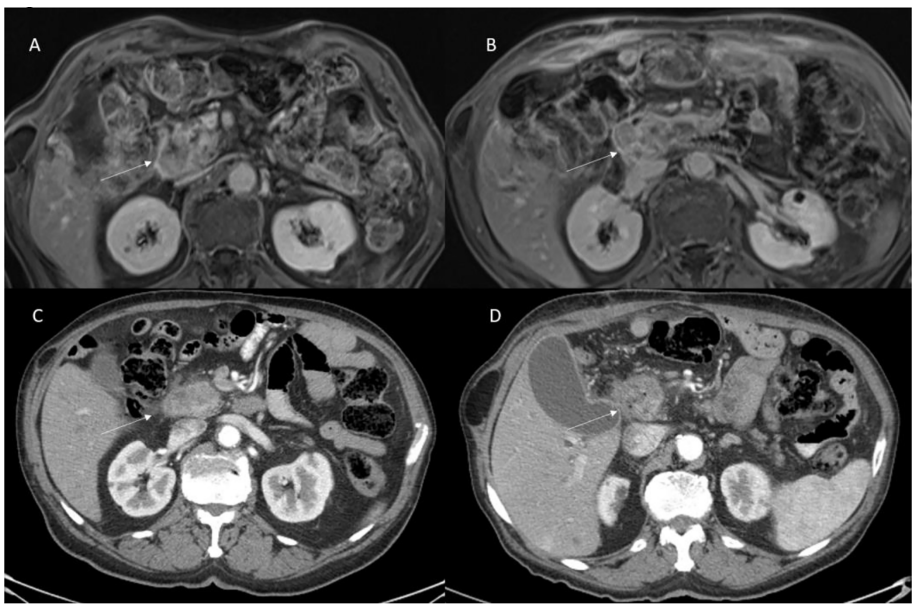

FIGURE 4 | Patient 3 with head pancreatic cancer. Morphological MRI and CT assessment post-ECT treatment. In **(A)** (VIBE T1-W post-contrast sequence during portal phase in axial plane) and **(C)** (CT scan during pancreatic phase of contrast study) the arrow shows lesion. In **(B)** (VIBE T1-W post-contrast sequence during portal phase in axial plane) and **(D)** (CT scan during pancreatic phase of contrast study) the arrow shows ablated area. Qualitative assessment shows no significant differences in SI in pre- and post-treatment sequences and no significant differences in density in pre- and post-CT images.

treatment, conversely using functional parameters, obtained with PET and MRI, it is possible.

CONCLUSIONS

Although new chemotherapeutic schemes have been introduced, advanced pancreatic cancers still correlate with a poor long-term outcome. Local ablative therapies are used in some dedicated cancer centers in patients with LAPC. The assessment of a pancreatic cancer after neoadjuvant treatment is particularly complicated and the condition becomes more difficult when evaluating the effectiveness of ablative therapies, considering that RECIST criteria were not appropriate to assess the treatment. When considering therapy effects, imaging-derived parameters are sometimes complicated to understand, since they depend on anatomic location, on relations between specific tissue characteristics and the mechanism of action of therapy, and on the used techniques. In this setting, imaging features are correlated to the type and method of therapy delivery, the

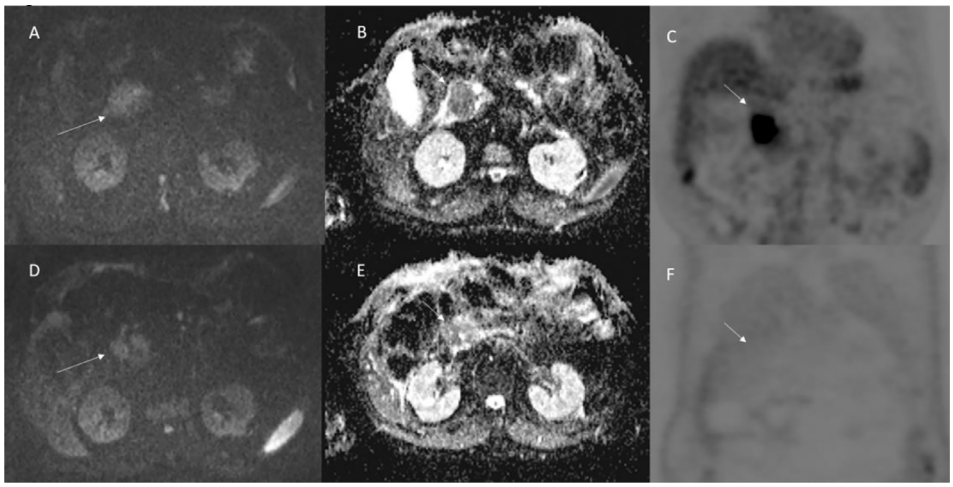

FIGURE 5 | Patient 3 with head pancreatic cancer (the same of **Figure 4**). Functional (DW-MRI and PET) assessment post-ECT treatment. In **(A)** (pre treatment) and **(D)** (post treatment) (b 800 s/mm^2) the lesion (arrow) shows restricted signal so as in ADC map (**B**: pre treatment; and **E**: post treatment) the lesion shows hypointense signal (arrow). This qualitative analysis is indicative of non-responder lesion. The PET (**C**: pre treatment; and **F**: post treatment) assessment shows (arrow) a responder lesion.

timing of treatment, and the imaging technique being used to observe the effects. A "qualitative assessment" based only human eyes should cause misdiagnosis. A quantitative evaluation based on perfusion evaluation or metabolic analysis allows a more objective reassessment and a more correct stratification of patients in responders and non-responders to treatment.

DATA AVAILABILITY STATEMENT

The original contributions presented in the study are included in the article, further inquiries can be directed to the corresponding author.

AUTHOR CONTRIBUTIONS

All authors listed have made a substantial, direct, and intellectual contribution to the work and approved it for publication.

ACKNOWLEDGMENTS

The authors are grateful to Alessandra Trocino, librarian at the National Cancer Institute of Naples, Italy. Moreover, the authors are grateful to Assunta Zazzaro for the collaboration.

REFERENCES

1. Siegel RL, Miller KD, Jemal A. Cancer statistics, 2020. *CA Cancer J Clin* (2020) 70(1):7–30. doi: 10.3322/caac.21590
2. NCCN.org. *NCCN Clinical Practice Guidelines in Oncology (NCCN Guidelines®) Pancreatic Adenocarcinoma Version 1.2020*. (2020). Available at: https://www.nccn.org/professionals/physician_gls/default.aspx.
3. Tempero MA. NCCN Guidelines Updates: Pancreatic Cancer. *J Natl Compr Canc Netw* (2019) 17(5.5):603–5. doi: 10.6004/jnccn.2018.0043
4. Alistar A, Morris BB, Desnoyer R, Klepin HD, Hosseinzadeh K, Clark C, et al. Safety and tolerability of the first-in-class agent CPI-613 in combination with modified FOLFIRINOX in patients with metastatic pancreatic cancer: a single-centre, open-label, dose-escalation, phase 1 trial. *Lancet Oncol* (2017) 18(6):770–8. doi: 10.1016/S1470-2045(17)30314-5
5. Usón Junior PLS, Rother ET, Maluf FC, Bugano DDG. Meta-analysis of Modified FOLFIRINOX Regimens for Patients With Metastatic Pancreatic Cancer. *Clin Colorectal Cancer* (2018) 17(3):187–97. doi: 10.1016/j.clcc.2018.03.007
6. International Agency for Research on Cancer (IARC). http://www.iarc.fr/.
7. Chin V, Nagrial A, Sjoquist K, O'Connor CA, Chantrill L, Biankin AV, et al. Chemotherapy and radiotherapy for advanced pancreatic cancer. *Cochrane Database Syst Rev* (2018) 3(3):CD011044. doi: 10.1002/14651858.CD011044.pub2
8. van Veldhuisen E, van den Oord C, Brada LJ, Walma MS, Vogel JA, Wilmink JW, et al. Locally Advanced Pancreatic Cancer: Work-Up, Staging, and Local Intervention Strategies. *Cancers (Basel)* (2019) 11(7):E976. doi: 10.3390/cancers11070976
9. Paiella S, Salvia R, Ramera M, Girelli R, Frigerio I, Giardino A, et al. Local Ablative Strategies for Ductal Pancreatic Cancer (Radiofrequency Ablation, Irreversible Electroporation): A Review. *Gastroenterol Res Pract* (2016) 2016:4508376. doi: 10.1155/2016/4508376
10. Granata V, Fusco R, Catalano O, Setola SV, de Lutio di Castelguidone E, Piccirillo M, et al. Multidetector computer tomography in the pancreatic adenocarcinoma assessment: an update. *Infect Agent Cancer* (2016) 11:57. eCollection 2016. doi: 10.1186/s13027-016-0105-6
11. Granata V, Fusco R, Piccirillo M, Palaia R, Petrillo A, Lastoria S, et al. Electrochemotherapy in locally advanced pancreatic cancer: Preliminary results. *Int J Surg* (2015) 18:230–6. doi: 10.1016/j.ijsu.2015.04.055
12. Granata V, Fusco R, Setola SV, Piccirillo M, Leongito M, Palaia R, et al. Early radiological assessment of locally advanced pancreatic cancer treated with electrochemotherapy. *World J Gastroenterol* (2017) 23(26):4767–78. doi: 10.3748/wjg.v23.i26.4767
13. Granata V, Fusco R, Setola SV, Palaia R, Albino V, Piccirillo M, et al. Diffusion kurtosis imaging and conventional diffusion weighted imaging to assess electrochemotherapy response in locally advanced pancreatic cancer. *Radiol Oncol* (2019) 53(1):15–24. doi: 10.2478/raon-2019-0004

14. Vroomen LGPH, Scheffer HJ, Melenhorst MCAM, de Jong MC, van den Bergh JE, van Kuijk C, et al. MR and CT imaging characteristics and ablation zone volumetry of locally advanced pancreatic cancer treated with irreversible electroporation. *Eur Radiol* (2017) 27(6):2521–31. doi: 10.1007/s00330-016-4581-2
15. García-Figueiras R, Padhani AR, Baleato-González S. Therapy Monitoring with Functional and Molecular MR Imaging. *Magn Reson Imaging Clin N Am* (2016) 24:261–88. doi: 10.1016/j.mric.2015.08.003
16. Izzo F, Granata V, Grassi R, Fusco R, Palaia R, Delrio P, et al. Radiofrequency Ablation and Microwave Ablation in Liver Tumors: An Update. *Oncologist* (2019) 24(10):e990–1005. doi: 10.1634/theoncologist.2018-0337
17. Pillai K, Akhter J, Chua TC, Shehata M, Alzahrani N, Al-Alem I, et al. Heat sink effect on tumor ablation characteristics as observed in monopolar radiofrequency, bipolar radiofrequency, and microwave, using ex vivo calf liver model. *Med (Baltimore)* (2015) 94(9):e580. doi: 10.1097/MD.0000000000000580
18. Granata V, de Lutio di Castelguidone E, Fusco R, Catalano O, Piccirillo M, Palaia R, et al. Irreversible electroporation of hepatocellular carcinoma: preliminary report on the diagnostic accuracy of magnetic resonance, computer tomography, and contrast-enhanced ultrasound in evaluation of the ablated area. *Radiol Med* (2016) 121(2):122–31. doi: 10.1007/s11547-015-0582-5
19. Granata V, Fusco R, Catalano O, Piccirillo M, De Bellis M, Izzo F, et al. Percutaneous ablation therapy of hepatocellular carcinoma with irreversible electroporation: MRI findings. *AJR Am J Roentgenol* (2015) 204(5):1000–7. doi: 10.2214/AJR.14.12509
20. Martin RC2, Kwon D, Chalikonda S, Sellers M, Kotz E, Scoggins C, et al. Treatment of 200 locally advanced (stage III) pancreatic adenocarcinoma patients with irreversible electroporation: safety and efficacy. *Ann Surg* (2015) 262(3):486–94. discussion 492-4. doi: 10.1097/SLA.0000000000001441
21. Martin RC2, McFarland K, Ellis S. Velanovich V. Irreversible electroporation in locally advanced pancreatic cancer: potential improved overall survival. *Ann Surg Oncol* (2013) 20:S443–9. doi: 10.1245/s10434-012-2736-1
22. Kwon D, McFarland K, Velanovich V, Martin RC2. Borderline and locally advanced pancreatic adenocarcinoma margin accentuation with intraoperative irreversible electroporation. *Surgery* (2014) 156(4):910–20. doi: 10.1016/j.surg.2014.06.058
23. Ansari D, Kristoffersson S, Andersson R, Bergenfeldt M. The role of irreversible electroporation (IRE) for locally advanced pancreatic cancer: a systematic review of safety and efficacy. *Scand J Gastroenterol* (2017) 52 (11):1165–71. doi: 10.1080/00365521.2017.1346705
24. Lambert L, Horejs J, Krska Z, Hoskovec D, Petruzelka L, Krechler T, et al. Treatment of locally advanced pancreatic cancer by percutaneous and intraoperative irreversible electroporation: general hospital cancer center experience. *Neoplasma* (2016) 63(2):269–73. doi: 10.4149/213_150611N326
25. Yan L, Chen YL, Su M, Liu T, Xu K, Liang F, et al. Single-institution Experience with Open Irreversible Electroporation for Locally Advanced Pancreatic Carcinoma. *Chin Med J (Engl)* (2016) 129(24):2920–5. doi: 10.4103/0366-6999.195476
26. Zhang Y, Shi J, Zeng J, Alnagger M, Zhou L, Fang G, et al. Percutaneous Irreversible Electroporation for Ablation of Locally Advanced Pancreatic Cancer: Experience From a Chinese Institution. *Pancreas* (2017) 46(2):e12–4. doi: 10.1097/MPA.0000000000000703
27. Scheffer HJ, Vroomen LG, de Jong MC, Melenhorst MC, Zonderhuis BM, Daams F, et al. Ablation of Locally Advanced Pancreatic Cancer with Percutaneous Irreversible Electroporation: Results of the Phase I/II PANFIRE Study. *Radiology* (2017) 282(2):585–97. doi: 10.1148/radiol.2016152835
28. Izzo F, Ionna F, Granata V, Albino V, Patrone R, Longo F, et al. New Deployable Expandable Electrodes in the Electroporation Treatment in a Pig Model: A Feasibility and Usability Preliminary Study. *Cancers (Basel)* (2020) 12(2):E515. doi: 10.3390/cancers12020515
29. Tafuto S, von Arx C, De Divitiis C, Maura CT, Palaia R, Albino V, et al. Electrochemotherapy as a new approach on pancreatic cancer and on liver metastases. *Int J Surg* (2015) 21:S78–82. doi: 10.1016/j.ijsu.2015.04.095
30. Miklavčič D, Mali B, Kos B, Heller R, Serša G. Electrochemotherapy: from the drawing board into medical practice. *Biomed Eng Online* (2014) 13:29. doi: 10.1186/1475-925X-13-29
31. Mir LM, Tounekti O, Orlowski S. Bleomycin: revival of an old drug. *Gen Pharmacol* (1996) 27(5):745–8. doi: 10.1016/0306-3623(95)02101-9
32. Gehl J, Geertsen PF. Efficient palliation of haemorrhaging malignant melanoma skin metastases by electrochemotherapy. *Melanoma Res* (2000) 10(6):585–9. doi: 10.1097/00008390-200012000-00011
33. Bastianpillai C, Petrides N, Shah T, Guillaumier S, Ahmed HU, Arya M. Harnessing the immunomodulatory effect of thermal and non-thermal ablative therapies for cancer treatment. *Tumour Biol* (2015) 36(12):9137–46. doi: 10.1007/s13277-015-4126-3
34. Neal RE2, Rossmeisl JHJr, Robertson JL, Arena CB, Davis EM, Singh RN, et al. Improved local and systemic anti-tumor efficacy for irreversible electroporation in immunocompetent versus immunodeficient mice. *PloS One* (2013) 8(5):e64559. doi: 10.1371/journal.pone.0064559
35. Longo F, Perri F, Caponigro F, Della Vittoria Scarpati G, Guida A, Pavone E, et al. Boosting the Immune Response with the Combination of Electrochemotherapy and Immunotherapy: A New Weapon for Squamous Cell Carcinoma of the Head and Neck? *Cancers (Basel)* (2020) 12(10):E2781. doi: 10.3390/cancers12102781
36. D'Onofrio M, Barbi E, Girelli R, Tinazzi Martini P, De Robertis R, et al. Variation of tumoral marker after radiofrequency ablation of pancreatic adenocarcinoma. *J Gastrointest Oncol* (2016) 7(2):213–20. doi: 10.3978/j.issn.2078-6891.2015.085
37. Giardino A, Girelli R, Frigerio I, Regi P, Cantore M, Alessandra A, et al. Triple approach strategy for patients with locally advanced pancreatic carcinoma. *HPB (Oxford)* (2013) 15(8):623–7. doi: 10.1111/hpb.12027
38. Hadjicostas P, Malakounides N, Varianos C, Kitiris E, Lerni F, Symeonides P. Radiofrequency ablation in pancreatic cancer. *HPB (Oxford)* (2006) 8(1):61–4. doi: 10.1080/13651820500466673
39. Ikuta S, Kurimoto A, Iida H, Aihara T, Takechi M, Kamikonya N, et al. Optimal combination of radiofrequency ablation with chemoradiotherapy for locally advanced pancreatic cancer. *World J Clin Oncol* (2012) 3(1):12–4. doi: 10.5306/wjco.v3.i1.12
40. Kallis Y, Phillips N, Steel A, Kaltsidis H, Vlavianos P, Habib N, et al. Analysis of Endoscopic Radiofrequency Ablation of Biliary Malignant Strictures in Pancreatic Cancer Suggests Potential Survival Benefit. *Dig Dis Sci* (2015) 60 (11):3449–55. doi: 10.1007/s10620-015-3731-8
41. Lakhtakia S, Ramchandani M, Galasso D, Gupta R, Venugopal S, Kalpala R, et al. EUS-guided radiofrequency ablation for management of pancreatic insulinoma by using a novel needle electrode (with videos). *Gastrointest Endosc* (2016) 83:234–9. doi: 10.1016/j.gie.2015.08.085
42. Pai M, Habib N, Senturk H, Lakhtakia S, Reddy N, Cicinnati VR, et al. Endoscopic ultrasound guided radiofrequency ablation, for pancreatic cystic neoplasms and neuroendocrine tumors. *World J Gastrointest Surg* (2015) 7 (4):52–9. doi: 10.4240/wjgs.v7.i4.52
43. Rossi S, Viera FT, Ghittoni G, Cobianchi L, Rosa LL, Siciliani L, et al. Radiofrequency ablation of pancreatic neuroendocrine tumors: a pilot study of feasibility, efficacy, and safety. *Pancreas* (2014) 43(6):938–45. doi: 10.1097/MPA.0000000000000133
44. Song TJ, Seo DW, Lakhtakia S, Reddy N, Oh DW, Park DH, et al. Initial experience of EUS- guided radiofrequency ablation of unresectable pancreatic can- cer. *Gastrointest Endosc* (2016) 83(2):440–3. doi: 10.1016/j.gie.2015.08.048
45. Spiliotis JD, Datsis AC, Michalopoulos NV, Kekelos SP, Vaxevanidou A, Rogdakis AG, et al. Radiofrequency ablation combined with palliative surgery may prolong survival of patients with advanced cancer of the pancreas. *Langenbecks Arch Surg* (2007) 392(1):55–60. doi: 10.1007/s00423-006-0098-5
46. Varshney S, Sewkani A, Sharma S. Radiofrequency ablation ofunresectable pancreatic carcinoma: feasibility, efficacy and safety. *JOP* (2006) 7:74–8. doi: 10.4251/wjgo.v7.i2.6
47. Waung JA, Todd JF, Keane MG, Pereira SP. Successful management of a sporadic pancreatic insulinoma by endoscopic ultrasound- guided radiofrequency ablation. *Endoscopy* (2016) 48 Suppl 1:E144–5. doi: 10.1055/s-0042-104650
48. Zou YP, Li WM, Zheng F, Li FC, Huang H, Du JD, et al. Intraoperative radiofrequency ablation combined with 125 iodine seed implantation for unresectable pancreatic cancer. *World J Gastroenterol* (2010) 16 (40):5104–10. doi: 10.3748/wjg.v16.i40.5104
49. Saccomandi P, Lapergola A, Longo F, Schena E, Quero G. Thermal ablation of pancreatic cancer: A systematic literature review of clinical practice and pre-clinical studies. *Int J Hyperthermia* (2018) 35(1):398–418. doi: 10.1080/02656736.2018.1506165

50. Waitz R, Solomon SB. Can local radiofrequency ablation of tumors generate systemic immunity against metastatic disease? *Radiology* (2009) 251:1–2. doi: 10.1148/radiol.2511082215
51. Ierardi AM, Biondetti P, Coppola A, Fumarola EM, Biasina AM, Alessio Angileri S, et al. Percutaneous microwave thermosphere ablation of pancreatic tumours. *Gland Surg* (2018) 7(2):59–66. doi: 10.21037/gs.2017.11.05
52. Carrafiello G, Ierardi AM, Fontana F, Petrillo M, Floridi C, Lucchina N, et al. Microwave ablation of pancreatic head cancer: safety and efficacy. *J Vasc Interv Radiol* (2013) 24 (10):1513–20. doi: 10.1016/j.jvir.2013.07.005
53. Vogl TJ, Panahi B, Albrecht MH, Naguib NNN, Nour-Eldin NA, Gruber-Rouh T, et al. Microwave ablation of pancreatic tumors. *Minim Invasive Ther Allied Technol* (2018) 27(1):33–40. doi: 10.1080/13645706.2017.1420664
54. Narayanan G, Hosein PJ, Arora G, Barbery KJ, Froud T, Livingstone AS, et al. Percutaneous irreversible electroporation for downstaging and control of unresectable pancreatic adenocarcinoma. *J Vasc Interventional Radiol* (2012) 23 (12):1613–21. doi: 10.1016/j.jvir.2012.09.012
55. Weiss MJ, Wolfgang CL. Irreversible electroporation: a novel pancreatic cancer therapy. *Curr Problems Cancer* (2013) 37:262–5. doi: 10.1016/j.currproblcancer.2013.10.002
56. Rombouts SJE, Vogel JA, van Santvoort HC, van Lienden KP, van Hillegersberg R, Busch OR, et al. Systematic review of innovative ablative therapies for the treatment of locally advanced pancreatic cancer. *Br J Surg* (2015) 102(3):182–93. doi: 10.1002/bjs.9716
57. Scheffer HJ, Nielsen K, de Jong MC, van Tilborg AA, Vieveen JM, Bouwman AR, et al. Irreversible electroporation for nonthermal tumor ablation in the clinical setting: a systematic review of safety and efficacy. *J Vasc Interventional Radiol* (2014) 25(7):997–1011. doi: 10.1016/j.jvir.2014.01.028
58. Granata V, Fusco R, Palaia R, Belli A, Petrillo A, Izzo F. Comments on Electrochemotherapy with Irreversible Electroporation and FOLFIRINOX Improves Survival in Murine Models of Pancreatic Adenocarcinoma. *Ann Surg Oncol* (2020). doi: 10.1245/s10434-020-09183-66
59. Poulou LS, Botsa E, Thanou I, Ziakas PD, Thanos L. Percutaneous microwave ablation vs radiofrequency ablation in the treatment of hepatocellular carcinoma. *World J Hepatol* (2015) 7(8):1054–63. doi: 10.4254/wjh.v7.i8.1054
60. Giardino A, Innamorati G, Ugel S, Perbellini O, Girelli R, Frigerio I, et al. Immunomodulation after radiofrequency ablation of locally advanced pancreatic cancer by monitoring the immune response in 10 patients. *Pancreatology* (2017) 17(6):962–6. doi: 10.1016/j.pan.2017.09.008
61. Kotnik T, Rems L, Tarek M, Miklavčič D. Membrane Electroporation and Electropermeabilization: Mechanisms and Models. *Annu Rev Biophys* (2019) 48:63–91. doi: 10.1146/annurev-biophys-052118-115451
62. Dežman R, Čemažar M, Serša G, Seliškar A, Erjavec V, Trotovšek B, et al. Safety and Feasibility of Electrochemotherapy of the Pancreas in a Porcine Model. *Pancreas* (2020) 49(9):1168–73. doi: 10.1097/MPA.0000000000001642
63. Girelli R, Prejanò S, Cataldo I, Corbo V, Martini L, Scarpa A, et al. Feasibility and safety of electrochemotherapy (ECT) in the pancreas: a pre-clinical investigation. *Radiol Oncol* (2015) 49(2):147–54. doi: 10.1515/raon-2015-0013
64. Fiorentzis M, Viestenz A, Siebolts U, Seitz B, Coupland SE, Heinzelmann J. The Potential Use of Electrochemotherapy in the Treatment of Uveal Melanoma: In Vitro Results in 3D Tumor Cultures and In Vivo Results in a Chick Embryo Model. *Cancers (Basel)* (2019) 11(9):1344. doi: 10.3390/cancers11091344
65. Fernandes P, O'Donovan TR, McKenna SL, Forde PF. Electrochemotherapy Causes Caspase-Independent Necrotic-Like Death in Pancreatic Cancer Cells. *Cancers (Basel)* (2019) 11(8):1177. doi: 10.3390/cancers11081177
66. Lencioni R, Llovet JM. Modified RECIST (mRECIST) assessment for hepatocellular carcinoma. *Semin Liver Dis* (2010) 30:52–60. doi: 10.1055/s-0030-1247132
67. Kudo M, Ueshima K, Kubo S, Sakamoto M, Tanaka M, Ikai I, et al. Response Evaluation Criteria in Cancer of the Liver (RECICL) (2015 Revised version). *Hepatol Res* (2016) 46(1):3–9. doi: 10.1111/hepr.12542
68. Cassinotto C, Sa-Cunha A, Trillaud H. Radiological evaluation of response to neoadjuvant treatment in pancreatic cancer. *Diagn Interv Imaging* (2016) 97 (12):1225–32. doi: 10.1016/j.diii.2016.07.011
69. Granata V, Fusco R, Sansone M, Grassi R, Maio F, Palaia R, et al. Magnetic Resonance Imaging in the assessment of pancreatic cancer with quantitative parameters extraction by means of Dynamic Contrast Enhanced Magnetic Resonance Imaging, Diffusion Kurtosis Imaging and Intravoxel Incoherent. *Ther Adv Gastroenterol* (2020) 13:1756284819885052. doi: 10.1177/1756284819885052
70. Fusco R, Granata V, Petrillo A. Introduction to Special Issue of Radiology and Imaging of Cancer. *Cancers (Basel)* (2020) 12(9):E2665. doi: 10.3390/cancers12092665
71. Mahmood F, Hansen RH, Agerholm-Larsen B, Gissel H, Ibsen P, Gehl J. Detection of electroporation-induced membrane permeabilization states in the brain using diffusion-weighted MRI. *Acta Oncol* (2015) 54(3):289–97. doi: 10.3109/0284186X.2014.991045
72. Zhang Z, Li W, Procissi D, Tyler P, Omary RA, Larson AC, et al. Rapid dramatic alterations to the tumor microstructure in pancreatic cancer following irreversible electroporation ablation. *Nanomed (Lond)* (2014) 9 (8):1181–9. doi: 10.2217/nnm.13.72
73. Choi H. Response evaluation of gastrointestinal stromal tumors. *Oncologist* (2008) 13:4–7. doi: 10.1634/theoncologist.13-S2-4
74. Tirkes T, Hollar MA, Tann M, Kohli MD, Akisik F, Sandrasegaran K. Response criteria in oncologic imaging: review of traditional and new criteria. *Radiographics* (2013) 33:1323–41. doi: 10.1148/rg.335125214
75. van der Veldt AA, Meijerink MR, van den Eertwegh AJ, Haanen JB, Boven E. Choi response criteria for early prediction of clinical outcome in patients with metastatic renal cell cancer treated with sunitinib. *Br J Cancer* (2010) 102:803–9. doi: 10.1038/sj.bjc.6605567
76. Stacchiotti S, Collini P, Messina A, Morosi C, Barisella M, Bertulli R, et al. High-grade soft-tissue sarcomas: tumor response assessment–pilot study to assess the correlation between radiologic and pathologic response by using RECIST and Choi criteria. *Radiology* (2009) 251:447–56. doi: 10.1148/radiol.2512081403
77. Ding Q, Cheng X, Yang L, Zhang Q, Chen J, Li T, et al. PET/CT evaluation of response to chemotherapy in non-small cell lung cancer: PET response criteria in solid tumors (PERCIST) versus response evaluation criteria in solid tumors (RECIST). *J Thorac Dis* (2014) 6:677–83. doi: 10.3978/j.issn.2072-1439.2014.05.10
78. Cadossi R, Ronchetti M, Cadossi M. Locally enhanced chemotherapy by electroporation: clinical experiences and perspective of use of electrochemotherapy. *Future Oncol* (2014) 10(5):877–90. doi: 10.2217/fon.13.235
79. Aycock KN, Davalos RV. Irreversible Electroporation: Background, Theory, and Review of Recent Developments in Clinical Oncology. *Bioelectricity* (2019) 1:214–34. doi: 10.1089/bioe.2019.0029
80. Geboers B, Scheffer HJ, Graybill PM, Ruarus AH, Nieuwenhuizen S, Puijk RS, et al. High-Voltage Electrical pulses in oncology: Irreversible electroporation, electrochemotherapy, gene electrotransfer, electrofusion, and electroimmunotherapy. *Radiology* (2020) 295:254–72. doi: 10.1148/radiol.2020192190
81. White RR, Paulson EK, Freed KS, Keogan MT, Hurwitz HI, Lee C, et al. Staging of pancreatic cancer before and after neoadju- vant chemoradiation. *J Gastrointest Surg* (2001) 5:626–33. doi: 10.1016/S1091-255X(01)80105-0

Conflict of Interest: The authors declare that the research was conducted in the absence of any commercial or financial relationships that could be construed as a potential conflict of interest.

frontiers in Oncology

CASE REPORT
published: 23 February 2021
doi: 10.3389/fonc.2021.585257

The Role of Real-Time Contrast-Enhanced Ultrasound in Guiding Radiofrequency Ablation of Reninoma: Case Report and Literature Review

Rui Zhang, Ming Xu and Xiao-yan Xie*

Department of Medical Ultrasonics, The First Affiliated Hospital, Institute of Diagnostic and Interventional Ultrasound, Sun Yat-sen University, Guangzhou, China

Background: Reninoma is a rare renal endocrine tumor that can cause secondary hypertension, characterized by hypertension, hypokalemia, high renin and aldosterone with normal aldosterone renin ratio (ARR), and occurs more in young female. Mainstream treatment option is surgery, but is less suitable for small or deep lesions, which makes ablation a promising alternative.

Case presentation: Two young female with typical manifestations of reninoma, including hypertension, hypokalemia, high renin, high aldosterone and normal ARR, were treated successfully with real-time contrast-enhanced ultrasound guided radiofrequency ablation, and contrast-enhanced ultrasound was also performed before and after treatment for diagnosis and postoperative assessment. Afterward, their blood pressure and laboratory tests became normal and remained steady during the follow-up of 32 and 6 months, respectively.

Conclusion: Contrast-enhanced ultrasound guided radiofrequency ablations is a promising alternative for reninoma treatment with comparable safety and efficacy with surgery, and has advantages especially in small or deep lesions.

Keywords: reninoma, case report, secondary hypertension, radiofrequency ablation, contrast-enhanced ultrasound

OPEN ACCESS

Edited by:
Wei Yang,
Peking University Cancer Hospital, China

Reviewed by:
Guolin Ma,
China-Japan Friendship Hospital, China
Xin Li,
People's Liberation Army General Hospital, China

****Correspondence:***
Ming Xu
xuming8@mail.sysu.edu.cn

Specialty section:
This article was submitted to Cancer Imaging and Image-directed Interventions, a section of the journal Frontiers in Oncology

Received: *20 July 2020*
Accepted: *06 January 2021*
Published: *23 February 2021*

Citation:
Zhang R, Xu M and Xie X-y (2021) The Role of Real-Time Contrast-Enhanced Ultrasound in Guiding Radiofrequency Ablation of Reninoma: Case Report and Literature Review. Front. Oncol. 11:585257. doi: 10.3389/fonc.2021.585257

INTRODUCTION

Reninoma, also called juxtaglomerular cell tumor, is a rare cause of secondary hypertension due to the oversecreting renin of juxtaglomerular apparatus. Since the first case reported by Robertson et al. at 1967 (1), nearly 200 cases were described worldwide, and the incidence rate is 0.023% in hypertensive patients at initial diagnosis (2). It often occurs in young adults, especially female, and is characterized by hypertension, hypokalemia, high renin and aldosterone with normal aldosterone renin ratio (ARR). In

Abbreviations: ARR, aldosterone renin ratio; CEUS, contrast-enhanced ultrasound; RFA, radiofrequency ablation; CEMR, contrast-enhanced magnetic resonance; CECT, contrast-enhanced computed tomography; MDT, multiple disciplinary team; MI, mechanical index; ACE, angiotensin-converting enzyme; RCC, renal cell carcinoma; MWA, microwave ablation.

cases with severe or chronic hypertension, target organ damage was observed, such as proteinuria, cardiomyopathy, and retinopathy (2). Most cases of reninoma were considered benign, though metastases and recurrence cases had been reported (3, 4), and pathological evidence as well as FDG-PET/CT did indicate malignancy sometimes (5, 6). The gold standard of diagnosis is histopathological examination, while clinical evidence combined with laboratory tests and imaging can also lead to diagnosis preoperatively. Treatment modalities include surgery, ablation, and medical therapy. Surgery is the main option, while the effect of medical therapy is very uncertain, and ablation is not widely used but considered a potential alternative (2, 7, 8).

Here we presented two reninoma cases admitted in our hospital in Feb. 2018 and Mar. 2020. Their lesions were tackled successfully with real-time contrast-enhanced ultrasound (CEUS) guided radiofrequency ablation (RFA), and CEUS was also performed before and after ablation for diagnosis and postoperative assessment. The treatment outcomes were followed for 32 and 6 months, respectively. To our knowledge, these two cases were the first to use real-time CEUS guided RFA in reninoma treatment and filled the blank of long-term efficacy of ablation.

CASE PRESENTATION

Case 1

A 17-year-old female was admitted to our hospital in *Feb. 2018* with paroxysmal headache, nausea and vomiting for over one year, accompanied with marked hypertension (the highest blood pressure was 190/120 mm Hg) and hypokalemia (serum potassium 2.45–3.18 mmol/L). She tried various antihypertensive regimens such as *Spironolactone* 40 mg, *Benazepril* 10 mg combined with *Amlodipine Besylate* 5 mg; *Indapamide* 1.5 mg combined with *Arolol* 10 mg. When taking drugs, her blood pressure was among 120–140/80–100 mm Hg. She discontinued all medication for one month for diagnostic demand. Contrast-enhanced magnetic resonance (CEMR) and CEUS revealed a 10-mm diameter cortex lesion in the upper pole of the left kidney (**Figure 1**). And the key endocrine parameters were summarized in **Table 1**. Renal veins sampling was performed but failed to detect lateralization. Target organ damage evaluation indicated bilateral ocular fundus arteriosclerosis and moderate proteinuria. We gave her *Spironolactone* 60 mg, 10% *Potassium chloride* 45 ml (oral) and *Adalat* 30 mg after admission. The clinical timeline of Patient 1 was organized in **Supplementary Figure 1**.

Case 2

A 27-year-old female with a 5-year history of poorly controlled hypertension was referred to our hospital in *Mar. 2020*. The highest blood pressure was 179/99 mm Hg. She intermittently used antihypertensive regimens (including *Fosinopril* 10 mg combined with *Metoprolol* 47.5 mg; *Telmisarta* 40 mg combined with *Spironolactone* 40 mg), and her blood pressure was among 120–140/80–90 mm Hg while taking medication, but returned to 170/100 mm Hg after withdrawal, and she stopped taking any medicine for four months for diagnostic need according to the advice of her

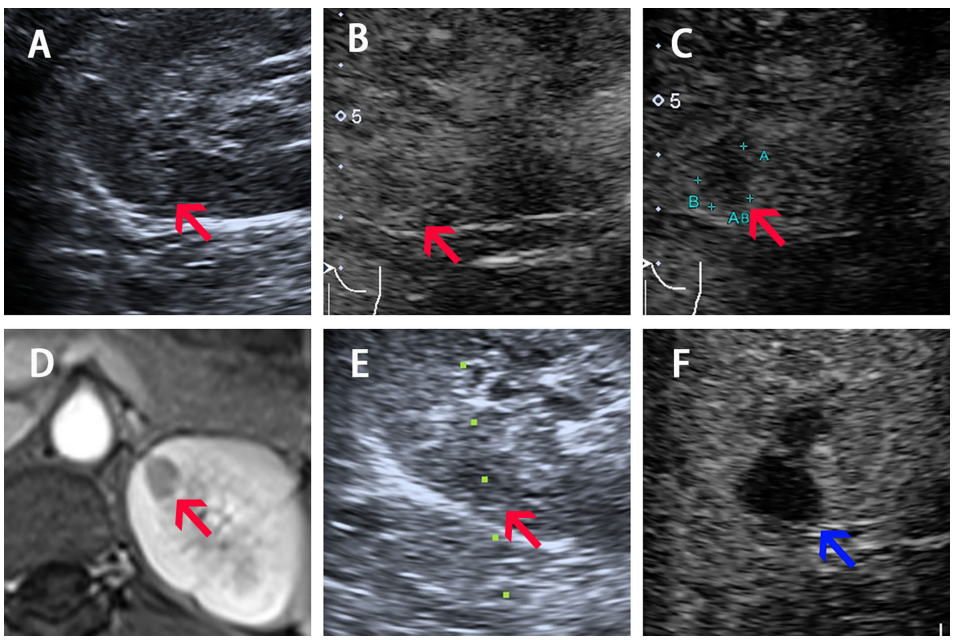

FIGURE 1 | Imaging of Patient 1 before, during, and after ablation procedure. **(A–C)** Ultrasound image acquired in prone position before ablation shows a slight hyperechoic nodule of 10-mm diameter with iso-enhancement in the cortical phase (30 s) and hypo-enhancement in the medulla phase (90 s) (pointed by red arrow). **(D)** Arterial phase of four phases MR before ablation shows a 10-mm diameter nodule (pointed by red arrow) located in the upper pole of left kidney. **(E)** The 17G electrode was implanted into the lesions under real-time CEUS guidance during the ablation (red arrow shows the lesion and the green dotted line shows the puncture path). **(F)** CEUS showed non-enhancement during both cortical and medulla phases postprocedure (pointed by blue arrow).

TABLE 1 | Summary of key indicators before and after ablation.

Indicators	Patient 1			Patient 2			Normal range
	Initial admission	After medicine	After RFA	Initial admission	After medicine	After RFA	
Supine PRA (pg/ml/h)	92.7	88.2	–	60.0	46.2	28.1	4.0–24.0
Supine Aldo (pg/ml)	186.5	289.19	–	314.82	468.17	272.87	10.00–160.00
Supine ARR	2.01	3.28	–	5.25	10.13	9.71	<30
Upright PRA (pg/ml/h)	163.1	147.1	–	138.3	71.5	47.3	4.0–48.0
Upright Aldo (pg/ml)	209.7	216.26	–	1117.83	1174.6	710.13	40.00–310.00
Upright ARR	1.29	1.47	–	8.08	16.42	15.01	<30
Serum K (mmol/L)	2.55	2.71	3.81	2.95	3.28	3.30	3.50–5.30
BP (mmHg)	144/100	123/80	109/73	184/133	155/108	135/96	<140/90

After RFA, 1–2 days postoperatively; PRA, plasma renin activity; Aldo, aldosterone; ARR, aldosterone renin ratio; serum K, serum potassium; BP, blood pressure; -, undone.

doctor. Contrast-enhanced computed tomography (CECT) and CEUS revealed a 6-mm diameter cortex lesion in her right kidney (**Figure 2**). Key endocrine parameters were summarized in **Table 1**. Target organ damage evaluation found nothing except slight proteinuria. We gave her *Terazosin Hydrochloride* 4 mg, *Diltiazem Hydrochloride* 90 mg and oral potassium supplement after admission. The clinical timeline of Patient 2 was organized in **Supplementary Figure 2**.

Multiple Disciplinary Team (MDT) Discussion

MDT discussion was held by endocrinologists, urologists and interventional ultrasound doctors for two patients. Both patients were young female with hypertension, hypokalemia, high renin, high aldosterone and normal ARR. Secondary hypertension caused by endocrine diseases were considered, including pheochromocytoma, Cushing syndrome, congenital adrenal hyperplasia, primary aldosteronism and reninoma. Pheochromocytoma was firstly excluded according to the absence of paroxysmal hypertension or sweating and negative Regitine test in both patients. Cushing syndrome was then ruled out since there were no signs of Cushing appearance and abnormal cortisol level. Congenital adrenal hyperplasia (usually appear as high renin, low aldosterone and decreased ARR) and primary aldosteronism (usually appear as low renin, high aldosterone and increased ARR) were also excluded. Consensus of reninoma diagnosis was finally achieved according to

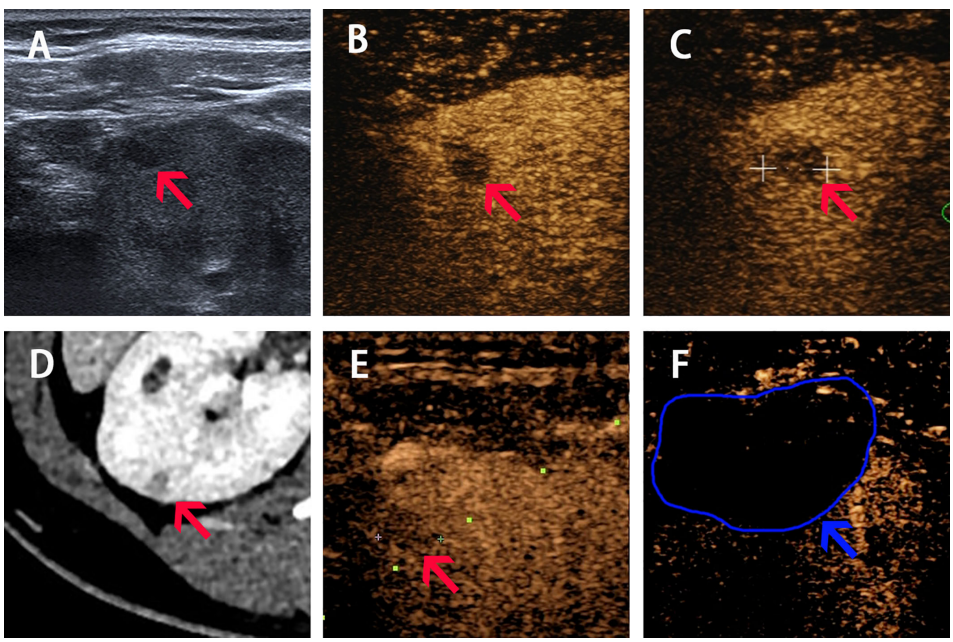

FIGURE 2 | Imaging of Patient 2 before, during and after ablation procedure. **(A–C)** Ultrasound image acquired in prone position before ablation shows a slight hypoechoic nodule of 6-mm diameter with hypo-enhancement in both cortical phase (24 s) and medulla phase (70 s) (pointed by red arrow). **(D)** Arterial phase of CT before procedure shows a 6-mm diameter nodule located in the right kidney (pointed by red arrow). **(E)** The real-time CEUS guided the locating of nodule during ablation (red arrow shows the lesion and the green dotted line shows the puncture path). **(F)** CEUS showed non-enhancement during both cortical and medulla phases postprocedure (pointed by blue arrow and curve).

clinical evidence. Both patients refused preoperative biopsy. Surgery and ablation could be the treatment options for both lesions. However, considering that the lesions were rather small and may have difficulty in intraoperative locating, which could prolong the operation time and thus cause more tissue injury and finally damage renal function, percutaneous RFA guided by real-time CEUS was recommended over surgery. And both patients were aware of MDT discussion recommendation and agreed to receive ablation.

CEUS Examination and Real-Time CEUS Guided RFA Treatment Procedure

The CEUS was performed before RFA. CEUS using a low mechanical index (MI) mode (0.07–0.08) can provide a real-time evaluation of tumor enhancement and location. For case 1, the tumor indicates iso-enhancement and hypo-enhancement during cortical phase and medulla phase. For case 2, the tumor indicates hypo-enhancement in both cortical and medulla phases (**Figures 1** and **2**).

RFA was performed under real-time CEUS guidance using the *Toshiba* ultrasound system. Two physicians who had 10 years of experience performing RFA for renal tumors performed all the procedures. A 20-cm-long, 17-gauge Cool-tip radiofrequency electrode with a 2-cm-long exposed tip (*Covidien Valleylab, Boulder, CO, United States*) was inserted into the targeted tumor. RFA was performed under local anesthesia. The temperature of the ablated tissue was increased to above 60°C and the ablation duration was 12 min for both patients. Immediate CEUS after ablation was done for Patient 2 as shown in **Supplementary Figure 3**. The next day, we performed CEUS for both patients and found the ablation area indicated non-enhancement throughout both cortical and medulla phases, and completely covered the former nodules with satisfactory ablation margin. No intraoperative adverse events occurred and the vital signs remained stable in perioperative period.

Postoperative Results

The laboratory tests 1 to 2 days after RFA were also summarized in **Table 1**. As for Patient 1, the result was delightful, blood pressure and serum tests became normal 12 h after the procedure without any drugs. Patient 2 had a significant decrease of serum renin and aldosterone, her blood pressure and serum potassium remained abnormal without medication, but indeed better than before. Both patients were discharged 3 days after ablation with no discomfort or complications, Patient 2 got take-home medicine (*Valsarta* 160 mg and *Spironolactone* 20 mg) while Patient 1 did not.

Follow-Up

For Patient 1, during the 32-month follow-up after RFA, her blood pressure (100–120/60–80 mm Hg), serum potassium and other endocrine tests were totally normal without any medication, urinary protein turned negative, and headache never occurred. Patient 2 stopped *Spironolactone* 2 weeks after RFA, her blood pressure remains in normal range (100–120/75–85 mm Hg) with *Valsarta 160 mg* according to the latest follow-up (6 months after ablation). Her serum potassium, other endocrine tests and renal ultrasound showed completely normal. Long-term effect still demands follow-up for Patient 2.

DISCUSSION

Reninoma is an uncommon but curable renal endocrine tumor which can cause secondary hypertension. Although it is often considered a benign disease, malignant potentials had shown sometimes (3–6).

To the best of our knowledge, these two cases from our institute were one of the few practices using RFA to treat reninoma, and this is the first report to use real-time CEUS as guidance. Both patients went through RFA successfully, and the postoperative results were delightful. We provided a follow-up of more than 2 years after ablation, which filled the blank of long-term efficacy of RFA. Furthermore, we introduced CEUS into the detecting and follow-up routine, which showed great potential in locating small tumors and indicating the ablation region.

Currently, treatment options for reninoma include surgery, ablation and medical therapy. Medication, such as angiotensin-converting enzyme (ACE) inhibitors, angiotensin II receptor blockers, beta-blockers and *Spironolactone* combined with oral potassium can help control blood pressure and serum potassium (2). However, the use of antihypertensive medications before diagnosis can mask hypokalemia and make reninoma more difficult to recognize (9). And the effect varies from person to person. It is hard to control the blood pressure over years without tackling the oversecreting of renin. Thus, medication is only considered an adjuvant therapy.

Surgery procedures, including nephron sparing partial nephrectomy for superficial or small lesions and radical nephrectomy for deep or large lesions, are the mainstream treatment options. The safety and long-term efficacy have been proved with numerous evidences (2, 7, 8). However, when it comes to small nodules with difficulty in intraoperative locating, surgery may lead to prolonged warm ischemic time as well as operation time, and renal dysfunction consequently. Moreover, using radical nephrectomy to remove deep lesions is in cost of renal dysfunction along with more tissue injury (10, 11).

For these small or deep reninoma, ablation can be an alternative. Ablation for reninoma is not regularly performed currently. Less than five cases of RFA and only one cryoablation have been reported, and none of them provided evidence of long-term efficacy (12–15). However, ablation is actually widely used in other renal tumors, including renal cell carcinoma (RCC), Wilms tumor, adenoma and angioleiomyoma (11, 16). It is considered a type of nephron sparing procedure and recommended mainly in benign tumor or RCC of T1a stage (17). But no randomized controlled trial has been conducted yet

to compare ablation and nephron sparing partial nephrectomy in renal tumors, and the long-term follow-up data lacks in ablation cases.

There are several types of ablations, including RFA, cryoablation and microwave ablation (MWA). RFA is used most frequently and the ablation shape can be controlled precisely. It is preferred to surgery for patients with nodules less than 4 cm or intolerable to surgery, and those requiring better postoperative renal function in cases of solitary kidney, bilateral lesions, or chronic renal insufficiency (17). Cryoablation has less application, according to recent literatures, it may be effective for renal tumors larger than 4 cm, but is more time-consuming (18). MWA has never been reported in reninoma treatment, but it is a potential option with many advantages, such as less affected by vascular heat-sink effect and tissue carbonization, more effective in large nodules, and more uniform thermal field distribution compared to RFA (19).

As we mentioned above, RFA has advantages for small or deep lesions. The reasons are as follows: for small lesion, the image-guidance allows quick and precise locating that leads to appropriate needle implanted angle and satisfactory ablation range; for deep lesions, it can preserve better renal function by less tissue injury. What is more, compared to surgery, RFA has less complications, less postoperative pain, shorter hospitalization time with comparable safety and efficacy (10, 11, 16, 20). The limitations of RFA application include nodules in dangerous sites and tumors larger than 4 cm (17). For nodules near the renal hilum, RFA have higher risk of renal pelvis injury, bleeding or infection, and incomplete ablation due to the heat-sink effect (21).

Up to now, all the reninoma cases reported using RFA were under guidance of CT (12–14). This is the first report to use real-time CEUS during procedure. With superiority in real-time, non-radiant and high sensitivity in blood supply detection facilitated by the pure blood pool contrast agents, CEUS shows more potential in intraoperative guidance and postoperative surveillance than CT. What is more, the use of CEUS through the diagnosis, treatment and follow-up routine makes it convenient and easy to compare the change of lesions.

There are also limitations of this report. First, no histopathology evidence was obtained due to patients' unwillingness; but still, MDT discussion had reached in consensus of reninoma after differential diagnosis. Second, the long-term efficacy of Patients 2 still requires to be further confirmed.

CONCLUSION

In summary, we presented two typical cases of reninoma here, which was the first report of utilizing CEUS guided RFA in treating reninoma worldwide. We showed that real-time CEUS guided RFA is safe and effective in reninoma treatment, and it is a promising alternative to surgery especially in small or deep lesions. More data are still warranted to further confirm the long-term efficacy of RFA compared to surgery.

DATA AVAILABILITY STATEMENT

The raw data supporting the conclusions of this article will be made available by the authors, without undue reservation.

ETHICS STATEMENT

Written informed consent was obtained from the individual(s) and minor(s)' legal guardian/next of kin for the publication of any potentially identifiable images or data included in this article.

AUTHOR CONTRIBUTIONS

Case report design: all authors. Data collecting and patients' follow-up: RZ and MX. Drafting of the manuscript: RZ and MX. Critical revision of the manuscript: MX and X-YX. All authors contributed to the article and approved the submitted version.

FUNDING

Our work is supported by the National Natural Science Foundation of China (81501489)

ACKNOWLEDGMENTS

The authors would like to express their gratitude to Guangliang Huang and Manxia Lin, PhD from the Department of Medical Ultrasonics, Institute of Diagnostic and Interventional Ultrasound, The First Affiliated Hospital of Sun Yat-sen University, for their valuable contributions to the data description of our study.

SUPPLEMENTARY MATERIAL

The Supplementary Material for this article can be found online at: https://www.frontiersin.org/articles/10.3389/fonc.2021.585257/full#supplementary-material

Supplementary Figure 1 | Timeline for Patient 1.

Supplementary Figure 2 | Timeline for Patient 2.

Supplementary Figure 3 | Immediate CEUS after ablation for Patient 2, showed non-enhancement area during both cortical and medulla phases, which completely covered the former 6mm-diameter nodule with satisfactory ablation margin (pointed by blue arrow and curve).

REFERENCES

1. Robertson PW, Klidjian A, Harding LK, Walters G, Lee MR, Robb-Smith AH. Hypertension due to a renin-secreting renal tumour. *Am J Med* (1967) 43 (6):963–76. doi: 10.1016/0002-9343(67)90256-2
2. Wong L, Hsu TH, Perlroth MG, Hofmann LV, Haynes CM, Katznelson L. Reninoma: case report and literature review. *J Hypertension* (2008) 26(2):368–73. doi: 10.1097/HJH.0b013e3282f283f3
3. Duan X, Bruneval P, Hammadeh R, Fresco R, Eble JN, Clark JI, et al. Metastatic juxtaglomerular cell tumor in a 52-year-old man. *Am J Surg Pathol* (2004) 28(8):1098–102. doi: 10.1097/01.pas.0000126722.29212.a7
4. Shera AH, Baba AA, Bakshi IH, Lone IA. Recurrent malignant juxtaglomerular cell tumor: A rare cause of malignant hypertension in a child. *J Indian Assoc Pediatr Surgeons* (2011) 16(4):152–4. doi: 10.4103/0971-9261.86876
5. Kuroda N, Gotoda H, Ohe C, Mikami S, Inoue K, Nagashima Y, et al. Review of juxtaglomerular cell tumor with focus on pathobiological aspect. *Diagn Pathol* (2011) 6:80. doi: 10.1186/1746-1596-6-80
6. Jiang Y, Hou G, Zhu Z, Zang J, Cheng W. Increased FDG Uptake on Juxtaglomerular Cell Tumor in the Left Kidney Mimicking Malignancy. *Clin Nucl Med* (2020) 45(3):252–54. doi: 10.1097/RLU.0000000000002924
7. Liu K, Wang B, Ma X, Li H, Zhang Y, Li J, et al. Minimally Invasive Surgery-Based Multidisciplinary Clinical Management of Reninoma: A Single-Center Study. *Med Sci Monit: Int Med J Exp Clin Res* (2019) 25:1600–10. doi: 10.12659/MSM.913826
8. Mete UK, Niranjan J, Kusum J, Rajesh LS, Goswami AK, Sharma S. Reninoma treated with nephron-sparing surgery. *Urology* (2003) 61(6):1259. doi: 10.1016/S0090-4295(03)00104-3
9. Sierra JT, Rigo D, Arancibia A, Mukdsi J, Nicolai S. Reninoma Masked by the Use of an Angiotensin Receptor Blocker. *Iranian J Kidney Dis* (2016) 10(6):413–15.
10. Hui GC, Tuncali K, Tatli S, Morrison PR, Silverman SG. Comparison of percutaneous and surgical approaches to renal tumor ablation: metaanalysis of effectiveness and complication rates. *J Vasc Intervent Radiol: JVIR* (2008) 19 (9):1311–20. doi: 10.1016/j.jvir.2008.05.014
11. Krokidis ME, Orsi F, Katsanos K, Helmberger T, Adam A. CIRSE Guidelines on Percutaneous Ablation of Small Renal Cell Carcinoma. *Cardiovasc Intervent Radiol* (2017) 40(2):177–91. doi: 10.1007/s00270-016-1531-y
12. Branger N, Maurin C, Daniel L, André M, Coulange C, Vacher-Coponnat H, et al. [Treatment by radiofrequency ablation for a renin-secreting juxtaglomerular tumour: a case report]. *Progres en urologie J l'Association francaise d'urologie la Societe francaise d'urologie* (2014) 24(6):349–52. doi: 10.1016/j.purol.2013.10.001
13. Gil NS, Han JY, Ok SH, Shin IW, Lee HK, Chung YK, et al. Anesthetic management for percutaneous computed tomography-guided radiofrequency ablation of reninoma: a case report. *Korean J Anesthesiol* (2015) 68(1):78–82. doi: 10.4097/kjae.2015.68.1.78
14. Pedicini V, Gennaro N, Muglia R, Saita A, Casale P, Negro A, et al. Renin-dependent hypertension cured with percutaneous radiofrequency ablation. *J Hypertension* (2019) 37(3):653–56. doi: 10.1097/HJH.0000000000002035
15. Maiolino G, Battistel M, Barbiero G, Bisogni V, Rossi GP. Cure With Cryoablation of Arterial Hypertension Due to a Renin-Producing Tumor. *Am J Hypertension* (2018) 31(5):537–40. doi: 10.1093/ajh/hpx213
16. McCarthy CJ, Gervais DA. Decision Making: Thermal Ablation Options for Small Renal Masses. *Semin Intervent Radiol* (2017) 34(2):167–75. doi: 10.1055/s-0037-1602708
17. Ljungberg B, Albiges L, Abu-Ghanem Y, Bensalah K, Dabestani S, Fernández-Pello S, et al. European Association of Urology Guidelines on Renal Cell Carcinoma: The 2019 Update. *Eur Urol* (2019) 75(5):799–810. doi: 10.1016/j.eururo.2019.02.011
18. Miao D, Margolis CA. Genomic correlates of response to immune checkpoint blockade in microsatellite-stable solid tumors. *Vasc Interv Radiol* (2018) 50: (9):1271–81. doi: 10.1016/j.jvir.2013.05.030
19. Crocetti L, Bozzi E, Faviana P, Cioni D, Della Pina C, Sbrana A, et al. Thermal ablation of lung tissue: in vivo experimental comparison of microwave and radiofrequency. *Cardiovasc Intervent Radiol* (2010) 33(4):818–27. doi: 10.1007/s00270-010-9869-z
20. Xing M, Kokabi N, Zhang D, Ludwig JM, Kim HS. Comparative Effectiveness of Thermal Ablation, Surgical Resection, and Active Surveillance for T1a Renal Cell Carcinoma: A Surveillance, Epidemiology, and End Results (SEER)-Medicare-linked Population Study. *Radiology* (2018) 288(1):81–90. doi: 10.1148/radiol.2018171407
21. Veltri A, Calvo A, Tosetti I, Pagano E, Genovesio A, Virzì V, et al. Experiences in US-guided percutaneous radiofrequency ablation of 44 renal tumors in 31 patients: analysis of predictors for complications and technical success. *Cardiovasc Intervent Radiol* (2006) 29(5):811–8. doi: 10.1007/s00270-005-0261-3

Conflict of Interest: The authors declare that the research was conducted in the absence of any commercial or financial relationships that could be construed as a potential conflict of interest.

frontiers in Oncology

ORIGINAL RESEARCH
published: 01 March 2021
doi: 10.3389/fonc.2021.570312

Improving Ablation Safety for Hepatocellular Carcinoma Proximal to the Hilar Bile Ducts by Ultrasound-MR Fusion Imaging: A Preliminary Comparative Study

Yujia You[1†], Yinglin Long[1†], Ronghua Yan[2], Liping Luo[1], Man Zhang[1], Lu Li[1], Qingjing Zeng[1], Kai Li[1], Rongqin Zheng[1] and Erjiao Xu[1,3*]*

[1] Department of Ultrasound, The Third Affiliated Hospital of Sun Yat-Sen University, Guangzhou, China, [2] Department of Radiology, The Eighth Affiliated Hospital of Sun Yat-Sen University, Shenzhen, China, [3] Department of Medical Ultrasonics, The Eighth Affiliated Hospital of Sun Yat-Sen University, Shenzhen, China

Aim: To explore whether ablation safety could be improved by ultrasound (US)-magnetic resonance (MR) fusion imaging for hepatocellular carcinoma (HCC) proximal to the hilar bile ducts (HBDs) through a preliminary comparative study.

Methods: Between January 2014 and June 2019, 18 HCC nodules proximal to the HBDs were included in a US-MR fusion imaging-assisted radiofrequency ablation (RFA) group (study group), while 13 HCC nodules in a similar location were included as a control group. For the study group, the tumor and adjacent bile ducts were outlined on preprocedural MR images. Procedural ablation planning was conducted to assess the feasibility of ablating the tumors while avoiding biliary injury. Such tumors were then ablated under US-MR fusion imaging guidance. The control group nodules were ablated under conventional ultrasound guidance. Baseline characteristics and outcomes were compared between the groups.

Results: After preprocedural assessment, 14 of 18 patients with tumors that were feasible to ablate underwent US-MR fusion imaging-assisted RFA. No biliary complications were observed in these 14 patients; the complication rate was significantly lower in the study group than in the control group (30.8%, 4/13) (P = 0.041). There was no significant difference in the technique efficacy rates [92.9% (13/14) *versus* 100% (13/13), P = 1] or local progression rates [7.1% (1/14) *versus* 7.7% (1/13), P = 1] between the study and control groups.

Conclusions: US-MR fusion imaging may be a non-invasive means for assisting RFA of HCC nodules proximal to the HBDs and ensuring ablation safety.

Keywords: hepatocellular carcinoma (HCC), bile duct, radiofrequency ablation, safety, ultrasonography

OPEN ACCESS

Edited by:
Jie Yu,
People's Liberation Army General Hospital, China

Reviewed by:
Luigi Alessandro Solbiati, Humanitas University, Italy
Kazushi Numata, Yokohama City University Medical Center, Japan

***Correspondence:**
Erjiao Xu
xuerjiao@mail.sysu.edu.cn
Rongqin Zheng
zhengrq@mail.sysu.edu.cn

†These authors have contributed equally to this work and share first authorship

Specialty section:
This article was submitted to Cancer Imaging and Image-directed Interventions, a section of the journal Frontiers in Oncology

Received: *07 June 2020*
Accepted: *15 January 2021*
Published: *01 March 2021*

Citation:
You Y, Long Y, Yan R, Luo L, Zhang M, Li L, Zeng Q, Li K, Zheng R and Xu E (2021) Improving Ablation Safety for Hepatocellular Carcinoma Proximal to the Hilar Bile Ducts by Ultrasound-MR Fusion Imaging: A Preliminary Comparative Study. Front. Oncol. 11:570312. doi: 10.3389/fonc.2021.570312

INTRODUCTION

Radiofrequency ablation (RFA) has been recommended as one of the first-line treatment options for early- or very-early-stage hepatocellular carcinoma (HCC) because this procedure is effective, minimally invasive, and safe (1, 2). However, an HCC nodule location proximal to the hilar bile ducts (HBDs) is considered to be a relative contraindication for RFA since the hilar bile ducts are vulnerable to thermal damage (3, 4). Ablation-related biliary complications (such as bile leakage, biliary stricture and obstruction) occurred in up to 31–46% of patients in previous reports (5, 6); such complications may prolong hospitalization, increase the cost of treatment, and even lead to mortality (7). Since the bile ducts are usually difficult to discern on ultrasound (US) images (the most common guidance tool used for RFA of HCC), this may increase the risk of thermal damage to the bile ducts during US-guided ablation. On the other hand, when operators tend to restrict the ablation area to reduce thermal damage to the HBDs, the reduced complications may be accompanied by higher incidences of residual tumor or local tumor progression (LTP) (8).

To ablate nodules proximal to the HBDs as completely as possible and reduce the risk of thermal biliary damage, several strategies have been employed. Percutaneous ethanol injection (PEI) or transarterial chemoembolization (TACE) with or without RFA is generally used to treat HCC nodules proximal to the hilar bile ducts (9, 10). However, the therapeutic effect of PEI or TACE is limited compared to that of RFA. Another strategy is intraductal chilled saline perfusion through an endoscopic nasobiliary drainage (ENBD) tube or a percutaneous transhepatic cholangial drainage (PTCD) tube to cool the large bile duct during the RFA procedure (11–15). However, both catheterization procedures are invasive and may lead to unexpected pancreatitis. Moreover, percutaneous transhepatic cholangial drainage is usually technically difficult in patients with nondilated intrahepatic bile ducts.

Ultrasound (US)-computed tomography (CT)/magnetic resonance (MR) fusion imaging is a navigation technique that is increasing in popularity that simultaneously combines the real-time capacity of US imaging and the high spatial resolution of CT/MR imaging (16). US-CT/MR fusion imaging has been widely used during US-guided RFA procedures for HCC detection, guidance, and evaluation (17–24). A few studies have integrated the use of a three-dimensional ablation planning system for the ablation procedure for liver tumors to enhance the complete ablation rate and reduce operators' experience dependence (25–27). However, there are no studies evaluating the advantages of ablation planning and fusion imaging for enhancing ablation safety for tumors in high-risk locations.

Since the course of the HBDs is usually more clearly outlined by MR-specific sequences (e.g., T2 or hepatobiliary-phase sequences) than by US or CT images (28), we hypothesize that US-MR fusion imaging (in which a planning module has been integrated) might be helpful during the RFA procedure for HCC nodules proximal to the HBDs. In the planning module, both the tumor and its adjacent HBDs can be outlined easily on MR images and then displayed three-dimensionally; meanwhile, their spatial relationship can be displayed automatically on real-time US images through US-MR fusion imaging. Then, the operator can make an ablation plan (including choosing a puncture path and presetting the electrode placements) and preview the simulated thermal fields to assess the risk of bile duct injury. In addition, the RFA procedure can be performed precisely under the guidance of US-MR fusion imaging according to the preprocedural plan.

Here, we aimed to explore whether ablation safety could be improved by US-MR fusion imaging for HCC nodules adjacent to the HBDs through a preliminary comparative study.

METHODS

Study Design

From January 2014 to June 2019, patients with HCC nodules adjacent to the HBDs were prospectively enrolled into a US-MR fusion imaging-assisted group through a non-randomized study design. This study was approved by the institutional review board of our hospital. Written informed consent was obtained from each patient. To compare the safety of US-MR fusion imaging-assisted RFA for HCC with that of conventional US-guided RFA, patients with HCC nodules adjacent to the HBDs who previously underwent conventional US-guided RFA were retrospectively included as a control group.

The inclusion criteria were as follows: (1) pathological or clinical diagnosis of HCC (29); (2) tumor located within 10 mm proximal to the HBDs (referring to the left hepatic duct, right hepatic duct, and their conjunction); and (3) indications for RFA (29). The exclusion criteria were as follows: (1) patients who were unable or unwilling to participate in follow-up, and (2) patients with pacemakers.

Equipment and Agents

US Machine

A MyLab 90 or MyLab Twice US machine (Esoate, Genoa, Italy) with a convex array probe (CA541, frequency range from 1 to 8 MHz) was used for imaging guidance. The Virtual Navigator (Esoate, Genoa, Italy) electromagnetic positioning system was the main unit of the US machine. A planning module was installed as a system component of the Virtual Navigator.

RFA System

A cool-tip radiofrequency (RF) generator (Covidien, Mansfield, USA) and an internally cooled electrode with a 30-mm tip were used in this study. The RF generator was set in impedance mode with a maximum output. The ablative time for each RF electrode insertion was approximately 4–12 min.

US Contrast Agents (UCAs)

SonoVue (Bracco, Milan, Italy) was used for contrast-enhanced US (CEUS). UCAs were injected as a rapid bolus of 1.0 to 2 ml *via* an antecubital vein, followed by 5 ml of saline solution.

US-MR Fusion Imaging-Assisted RFA

US-MR fusion imaging-assisted RFA was performed by a senior interventional doctor (X.E.J.) with 10 years of experience with RFA and fusion imaging.

Preprocedural Evaluation of Ablation Feasibility Using US-MR Fusion Imaging-Based Planning

MR Image Preparation

Digital image and communication on medicine (DICOM) data from T2-weighted or hepatobiliary phase MR sequences (**Figure 1A**) were selected routinely for US-MR fusion imaging due to clear visualization of the biliary tract and target tumor. DICOM data from MR images were imported into the Virtual Navigator.

Depiction of the Target Tumor and the HBDs

The target tumor was manually outlined in blue, and the course of the adjacent HBDs was depicted automatically or manually in red on the MR images (**Figure 1C**). The relationship between

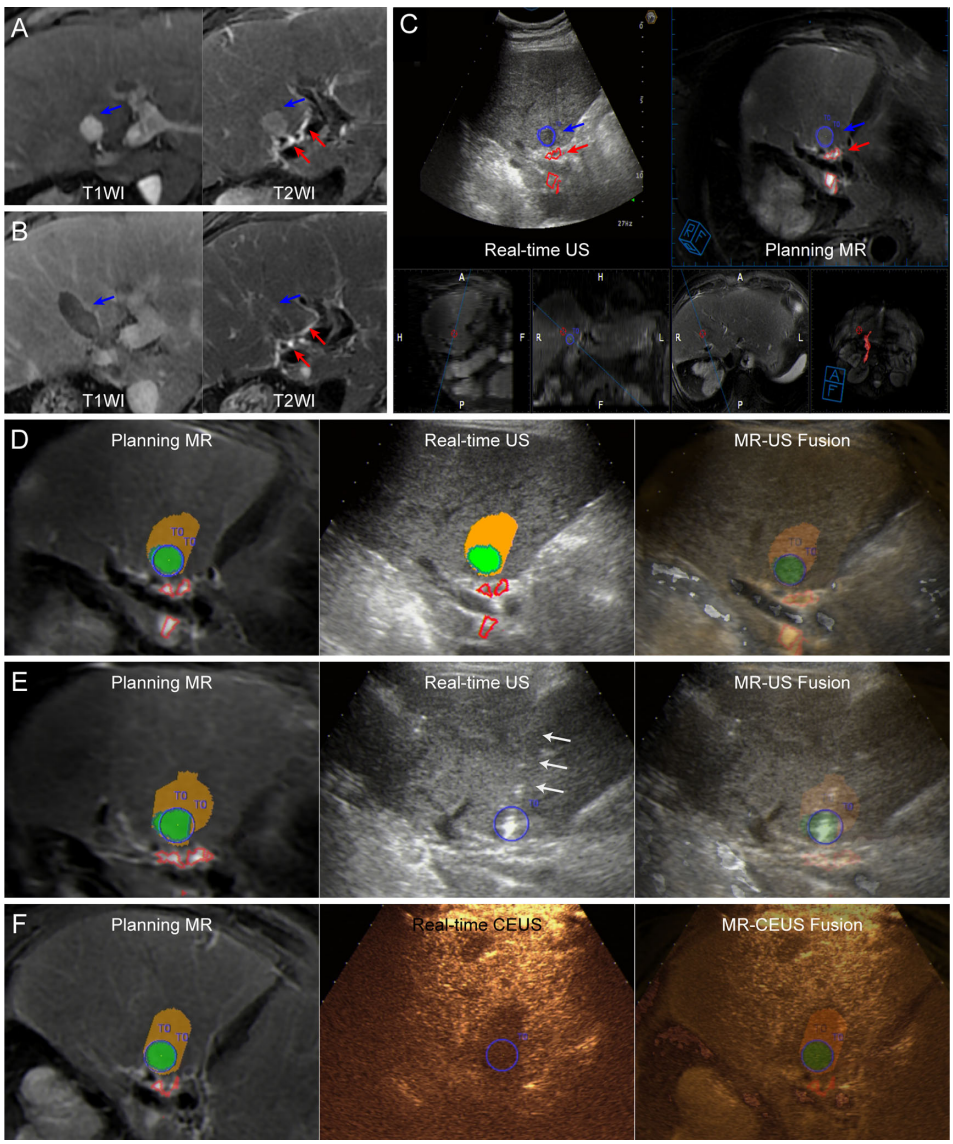

FIGURE 1 | Images from a 72-year-old man diagnosed with HCC adjacent to the right bile duct. **(A)** Preoperative MR images showing the target tumor with a maximum diameter of 16 mm in segment 4 of the liver (blue arrow). Both the target tumor and adjacent bile ducts (red arrows) are displayed clearly on T2WI image (right). **(B)** At the 1-month follow-up MR, the index tumor (blue arrows) was completely ablated without injury to the adjacent bile ducts (red arrows). **(C)** Image depicting the target tumor and adjacent bile ducts. The tumor margins are outlined with red lines, while the ablative margins are outlined with yellow lines. **(D)** Assessment of ablation feasibility based on ablation planning. Simulated thermal fields (STP) are shown in yellow, and when the STP covered the tumor, the overlapping fields are shown in green. One simulated ablation was planned to cover 100% of the tumor volume without overlapping of adjacent bile ducts, and then the tumor was determined to have ablation feasibility. **(E)** Insertion of the electrode (white arrows) under the guidance of US-MR fusion imaging according to the ablation plan. **Supplementary Video 1** completely and dynamically shows the US-MR fusion imaging-guided insertion process. **(F)** Immediate evaluation with MR-CEUS fusion imaging after ablation. The tumor and ablative margins are overlapped by the non-perfusion area.

the marked tumor and the HBDs could be displayed three-dimensionally.

Registration of MR Images and Real-Time US Imaging
Registration was performed by preliminary registration and fine tuning for precise alignment between the MR images and real-time US images. The details of the registration process have been described in previous studies [10]. After successful registration, the MR images could be synchronized with the real-time US images (**Figure 1C**).

Preprocedural Evaluation of Ablation Feasibility
After the registration process, the three-dimensional spatial relationship between the target tumor and the course of the adjacent HBDs could be observed in different planes by moving the probe. The virtual thermal field of the RF electrode with the 30-mm tip was set as an ellipsoid 30 × 20 mm in size in the planning module. Preprocedural planning was carried out by the senior interventional US doctor (X.E.J.). After determination of the entry point on US-MR fusion imaging, one or multiple ellipsoids corresponding to the virtual thermal field were utilized to draft the electrode placement strategy (**Figure 1D**).

The aim of ablation planning was to achieve as much coverage of the target tumor as possible by the simulated thermal field (at least 90% volume) while avoiding coverage of the adjacent HBDs. In addition, in principle, ablations should be planned as few times as possible. Since the spatial relationship among the simulated thermal field, the target tumor and the adjacent bile duct could be observed by three-dimensional visualization, the operator could adjust the electrode placements conveniently to achieve the aim of planning. If the aim of planning could be obtained successfully within five adjustments, RFA was considered feasible. Otherwise, RFA alone was considered infeasible, and other treatment options were considered instead.

Implementation of RFA According to the Preprocedural Plan

All patients underwent RFA under endotracheal general anesthesia. Before implementation of RFA, the registration procedure with US-MR fusion imaging was performed again, and the preprocedural plan was reconfirmed in the operating theater. Subsequently, electrode insertion was performed following the preprocedural plan precisely according to the electrode placement strategy under the guidance of US-MR fusion imaging (**Figure 1E** and **Supplementary Video 1**).

During the RFA procedure, US-MR fusion imaging was used to monitor the hyperechoic area produced by RFA and to assess whether the adjacent HBDs depicted on MR images were covered by the hyperechoic area, aiming to reduce the risk of thermal damage to the bile ducts as much as possible.

Postprocedural Immediate Assessment of the Ablative Effect

Approximately 5–10 min after the procedure, UCAs were administered intravenously to perform CEUS, and CEUS-MR fusion imaging was used to evaluate whether the non-perfusion zone covered the whole target tumor (**Figure 1F**) and whether perfusion of the UCAs in the adjacent bile duct wall was normal. If incomplete ablation was demonstrated by CEUS-MR fusion imaging, supplementary ablation was instantly carried out to achieve complete ablation.

Conventional US-Guided RFA

From January 2014 to June 2019, patients with tumors proximal to the HBDs were treated with the conventional RFA. The ablation procedures were performed by one of three doctors (Z.R.Q, X.E.J., L.K.) with 5 to 10 years of experience with RFA.

Conventional RFA was performed under US guidance, and multiple overlapping ablations were performed to achieve complete ablation. At the end of the ablation procedure, CEUS was used for immediate assessment of the ablative effect.

Postprocedural Surveillance and Follow-Up

After the procedure, US and laboratory examinations were performed regularly to exclude early complications. Biliary tract-related symptoms and signs were also closely surveilled.

One month later, contrast-enhanced CT (CECT) or contrast-enhanced MR (CEMR) was performed to evaluate the technical efficacy and complications (**Figure 1B**). Then, follow-up imaging and laboratory examinations were repeated every 3 months. LTP and ablation-related biliary complications were recorded until December 31, 2019.

Statistical Analysis

SPSS 22.0 (SPSS, Chicago, IL, USA) was used for statistical analysis. Continuous measurement data are presented as the mean ± standard deviation if the data were normally distributed or as the median (range) if the data were not normally distributed. Enumeration data are presented as percentages. Variables in the two independent groups were compared using the two-sample t-test or Mann-Whitney test for continuous variables and Pearson's $\chi 2$ test or Fisher's exact test for categorical variables, while matched data in the groups were compared using the paired t-test or Wilcoxon signed-rank test for continuous variables and the McNemar test for categorical variables. A P value less than 0.05 was considered statistically significant.

RESULTS

Patients and Tumors

A total of 18 patients with 18 tumors proximal to the hilar bile ducts were enrolled in the US-MR fusion imaging-assisted RFA group. A total of 13 patients with 13 tumors were included in the control group. **Figure 2** provides a brief overview of these two groups in a flow chart. The baseline characteristics of the two groups are listed in **Table 1** and their detailed information are listed in **Tables S1** and **S2**.

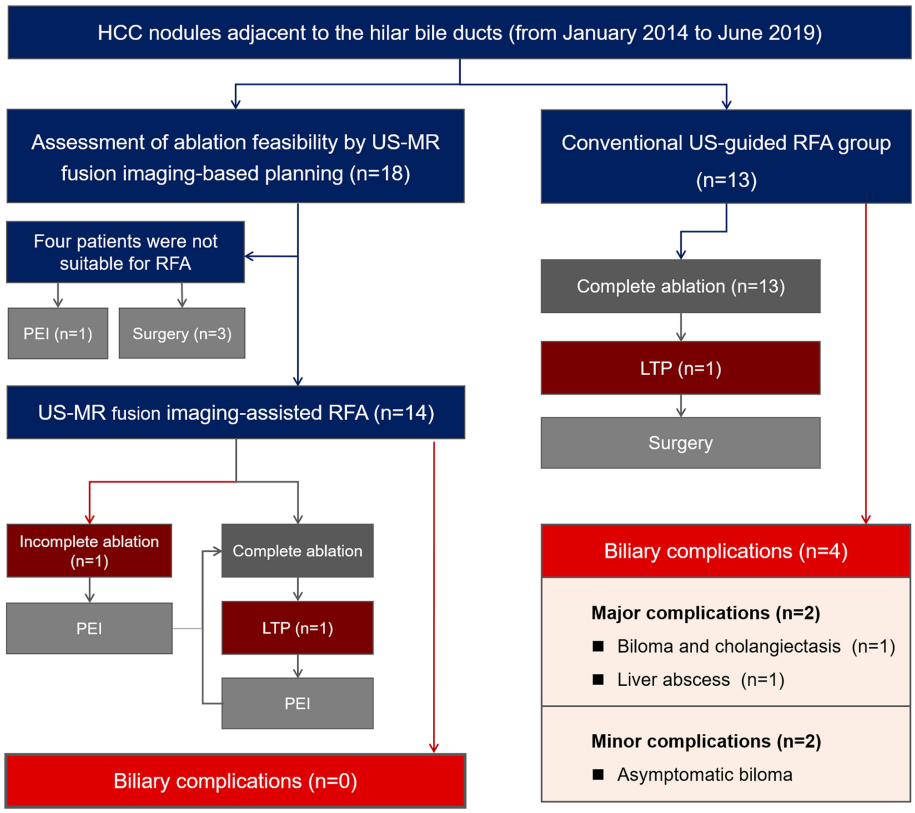

FIGURE 2 | Overview of management and outcome of enrolled patients.

TABLE 1 | Baseline characteristics of enrolled patients and nodules in the US-MR fusion imaging-assisted RFA group and the conventional US-guided RFA group (control group).

Characteristics	US-MR fusion imaging-assisted RFA	Conventional US-guided RFA	*P* value
Patient	N = 14	N = 13	
Age	55 ± 9 (44–72)	53 ± 11 (35–69)	0.633
Gender (male/female)	14/0	11/2	0.222
Primary/recurrent	9/5	3/10	0.054
Diagnosed on pathological/clinical	11/3	5/8	0.054
Cirrhosis (yes/no)	12/2	7/6	0.103
Hepatitis virus infection (HBV/HCV/no)	13/1/0	12/0/1	0.367
AFP (≤200/>200)	13/1	9/4	0.165
PLT (/L)	163 ± 67 (82–279)	130 ± 39 (76–216)	0.139
PT (s)	14.1 ± 1.3 (12.3–17.8)	14.1 ± 1.2 (11.6–16.0)	0.991
ALB (g/L)	39.6 ± 5.8 (31.2–51.5)	40.8 ± 4.3 (35.5–50.2)	0.536
TBil (μmol/L)	14.7 ± 6.2 (7.7–28.5)	13.0 ± 5.6 (5.8–28.7)	0.470
Child Pugh Class (A/B)	13/1	13/0	1
Nodules	N = 14	N = 13	
Single/multiple	10/4	5/8	0.128
Location (left hemiliver/right hemiliver)	8/6	9/4	0.695
Maximum diameter (mm)	21.5 ± 11.2 (9–49)	18.7 ± 9.1 (11–43)	0.482
Adjacent bile duct (biliary confluence/left hepatic duct/right hepatic duct)	5/6/3	3/5/5	0.590
Distance between nodule and bile duct (mm)	**2.5 ± 1.9 (0–6)**	**5.9 ± 1.7 (4–9)**	**<0.001**
Distance <5 mm/5–10 mm	**12/2**	**4/9**	**0.006**

The values was shown in bold since their differences are statistically significant.

US-MR Fusion Imaging-Assisted RFA

Preprocedural Evaluation of Ablation Feasibility With US-MR Fusion Imaging

US-MR fusion imaging registration was successful in all 18 patients. According to the preprocedural plan, four patients failed to achieve the aim of the electrode placement strategy, as coverage of the adjacent HBDs could not be avoided. The ablation feasibility assessment process in one of these four patients is given in **Figure S1** and **Supplementary Video 2**. Surgical resection was recommended for two patients, and the other two patients underwent PEI instead.

In the remaining fourteen patients, RFA was considered feasible, and they underwent the procedure with US-MR fusion imaging guidance. **Figure 3** shows representative images of a patient who underwent US-MR fusion imaging-assisted ablation. The clinical characteristics of these 14 patients and nodules are presented in **Table 1**.

According to the preprocedural plan, 1 to 14 electrode placements (median: two times) were required to cover 90–100% (median: 100%) of the entire target nodule volume. The duration of preprocedural planning was 2–10 min (median: 5 min).

Implementation of RFA According to the Preprocedural Plan and Immediate Evaluation of Technique Success

Each electrode insertion was performed under the guidance of US-MR fusion imaging according to the preprocedural plan. Electrode insertion was performed 1 to 14 times (median: two times) in accordance with the preprocedural plan. The entire ablation procedure required 60–212 min (median: 82 min).

During the RFA procedure, the hyperechoic area was monitored using US-MR fusion imaging. In four of these patients, the ablation process was stopped earlier than planned to avoid the risk of thermal damage, since the hyperechoic area began to cover the marked course of the adjacent HBDs.

After the RFA procedure, the immediate assessment performed *via* CEUS-MR fusion imaging indicated that the non-perfusion zones covered the target nodule in all 14 patients. No supplementary ablation was needed in these patients. The perfusion of the course of the adjacent HBDs was normal during CEUS evaluation.

Comparison of Safety Between the US-MR Fusion Imaging-Assisted RFA Group and the Control Group

Baseline Characteristics of the Control Group

The baseline characteristics of the control group are shown in **Figure 1**. When comparing the baseline characteristics between the control group and the study group, apart from the distance between the tumor and HBDs, no statistically significant differences were observed. The US-MR fusion imaging-assisted RFA group showed a significantly shorter distance between the nodule and the HBDs (2.5 ± 1.9 mm *versus* 5.9 ± 1.7 mm, $P < 0.001$) than the control group.

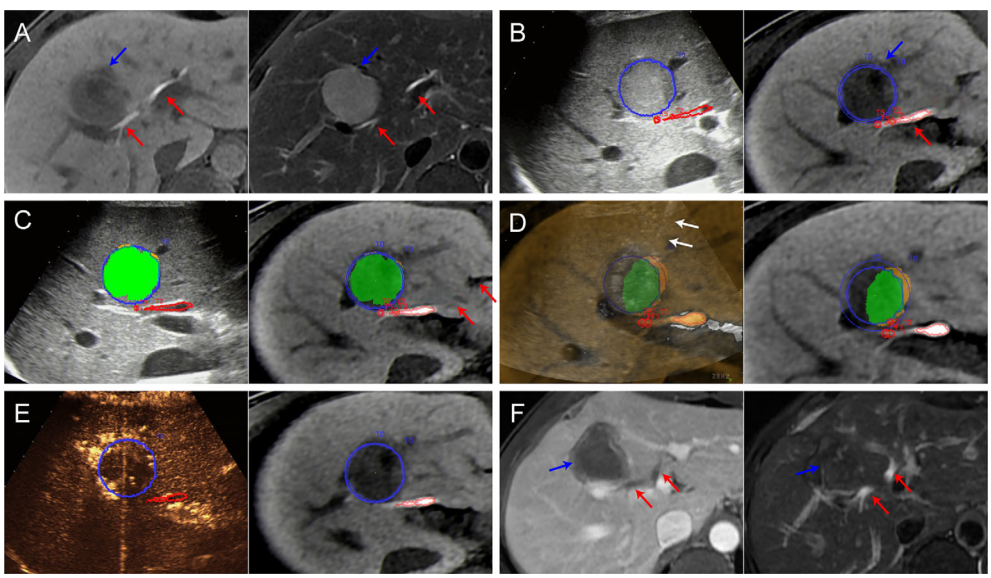

FIGURE 3 | Images from a 44-year-old man diagnosed with HCC adjacent to the right bile duct. **(A)** Preoperative MR images showing the target tumor with a maximum diameter of 36 mm in segment 8 of the liver (blue arrow). Both the hepatobiliary phase (left) and T2WI images (right) clearly display the target tumor and adjacent bile ducts (red arrows). **(B)** Outline of the tumor and adjacent bile ducts. The tumor margins are outlined with red lines, and the ablative margins are outlined with yellow lines. **(C)** Ablation planning. Six simulated ablations were planned to cover 91% of the tumor volume. When the STP covered the tumor, the overlapping fields are presented in green. **(D)** Insertion of the radiofrequency electrode (white arrows) under the guidance of US-MR fusion imaging to implement the plan. **(E)** Immediate evaluation with MR-CEUS fusion imaging after ablation. The tumor and ablative margins are overlapped by the non-perfusion area. **(F)** At the 1-month follow-up MR, the index tumor (blue arrows) was completely ablated without injury to the adjacent bile ducts (red arrows).

Comparisons of Safety and Efficacy

Comparisons of treatment-related results are shown in **Table 2**. The median follow-up periods in the US-MR fusion imaging-assisted RFA group and control group were 13 (range: 7–30) and 32 (range: 3–50) months respectively. During the follow-up period, no biliary complications occurred in the study group. No intrahepatic bile ducts were evidently dilated on follow-up imaging examinations. In the control group, four patients were diagnosed with biliary complications (including two major biliary complications and two minor biliary complications). The biliary complication rate in the control group was significantly higher than that in the study group [30.77% (4/13) *vs* 0% (0/14), $P = 0.041$].

The two patients with major biliary complications were as follows: one patient was diagnosed with a liver abscess and bile fistula several days after the procedure; the other patient was diagnosed with a large biloma (with a maximum diameter of 55 mm) and intrahepatic bile duct dilation 1 month after the procedure. Multiple treatments, such as antibiotic therapy, percutaneous catheter drainage, and surgery, were performed to manage these complications. Two patients with asymptomatic bilomas were diagnosed 1 and 4 months after the procedure. Both of them were not treated and then classified as minor biliary complications.

According to the 1-month follow-up CECT/CEMR, residual tumor was detected in one patient (7.1%) in the study group and in none of the patients in the control group. There was no significant difference between the two groups. In this patient, the tumor could not be eradicated despite several courses of TACE. During the follow-up period, the LTP rate was 7.1% (1/14) in the study group and 7.7% (1/13) in the control group. These two nodules showing LTP were treated with PEI.

DISCUSSION

HCC located in the hepatic hilum has always been a dilemma when considering thermal ablation (11). Even intraductal cooling has been used to assist in ablation of tumors adjacent to the HBDs and to reduce biliary complications; however, this is still an invasive procedure. Here, we proposed a novel non-invasive method (US-MR fusion imaging) to assist the ablation procedure that resulted in satisfactory therapeutic outcomes. The technical efficacy and local tumor recurrence rates of US-MR fusion imaging-assisted RFA are comparable to those in previous reports (5, 10, 11) (technical efficacy rate, 80.0–100.0%; local tumor recurrence rate, 11.8–21.0%) of thermal ablation performed with invasive ancillary procedures, such as intraductal chilled saline perfusion. More importantly, no biliary complications were observed during the follow-up period. Furthermore, patients who underwent traditional US-guided RFA for HCC nodules in the similar location were enrolled as controls for preliminary comparisons. According to the data analysis, the US-MR fusion imaging-assisted RFA group showed a significantly lower biliary complication rate (0 *versus* 30.77%, $P = 0.041$) than the control group.

It's worth noting that the distance between the tumor and adjacent hilar bile ducts has highly important consequences on the therapeutic effect of RFA. Lin et al. reported that a distance from the bile duct within 10 mm was thought to be a high-risk factor for ablation-related biliary complications for HCC nodules (30). RFA is still not recommended for application in HCC nodules adjacent to the HBDs in some clinical treatment guidelines of HCC (29). Theoretically, the injury risk increases with a shortened distance from the hilar bile duct. However, in this study the US-MR fusion imaging-assisted RFA group showed a lower biliary complication rate with a significantly shorter distance between the nodule and the HBDs (2.5 ± 1.9 mm *versus* 5.9 ± 1.7 mm, $P < 0.001$) than the control group. These data showed an increasing number of patients with HCC nodules with a short distance (≤5 mm) from the HBDs underwent RFA, indicating the improved safety with the assistance of US-MR fusion imaging.

The following characteristics of US-MR fusion imaging-assisted RFA contribute to its high ablation safety. First, MR-specific sequences (T2 or hepatobiliary phase sequences) were chosen as reference images for fusion imaging since the target tumor and adjacent HBDs could be displayed clearly on these images (31). Compared with previous reports that used ablation planning based on CT or US images (25, 26), MR has a distinct advantage in displaying the bile ducts. Moreover, after the target tumor and adjacent HBDs were depicted, the outlined structures could be displayed through three-dimensional visualization, to help the operator better understand the spatial relationship between the target tumor and the adjacent HBDs. Second, when performing preprocedure ablation planning, the ablation feasibility of the target tumor could be determined by evaluating the spatial relationship among the simulated thermal field, the target tumor, and the adjacent HBDs. This planning step facilitated the establishment of reasonable and individualized treatment for patients. For tumors that could not be covered by the simulated thermal field without covering the HBDs, RFA alone was considered with a high injury risk. As a result, the

TABLE 2 | Comparisons of treatment-related results between the US-MR fusion imaging-assisted RFA group and the conventional US-guided RFA group.

Characteristics	US-MR fusion imaging-assisted RFA	Conventional US-guided RFA	*P* value
Number of ablations	2 (1–14)	3 (1–10)	0.195
Duration of ablation procedure (min)	89 (60–212)	105 (50–315)	0.923
Biliary complications (yes/no)	**0/14**	**4/9**	**0.041**
Major biliary complications	0	2	
Minor biliary complications	0	2	
Complete ablation (yes/no)	13/1	13/0	1
Local tumor progression (yes/no)	1/13	1/12	1

The values was shown in bold since their differences are statistically significant.

treatment strategy was adjusted as soon as possible. Other means (such as surgery, RFA combined with PEI) may need to be performed to reduce potential biliary complications.

In addition, US-MR fusion imaging played a crucial role in the implementation of the ablation plan, including guiding electrode insertions, monitoring ablation process, and assessing treatment response and bile duct blood supply. With the guidance of US-MR fusion imaging, the electrode could be precisely inserted into the liver according to the planned angle and depth, which would not be affected by the hyperechoic region generated by RFA. With the real-time monitoring of US-MR fusion imaging, the ablation duration could be adjusted timely and flexibly to avoid the injury of the hilar bile ducts. With immediate treatment response assessment of US-MR fusion imaging, it can be timely determined whether supplementary ablation should be needed at the end of the procedure, helping reduce the possibility of residual tumors.

Overall, compared with traditional US-guided ablation, the use of US-MR fusion imaging in multiple links throughout the whole procedure brought changes in many aspects such as the identification of bile ducts, the evaluation method of ablation feasibility, electrode placement strategy, and duration of each ablation. All of these complex factors are conductive to the improved safety in US-MR fusion imaging-assisted ablation.

Apart from the use of fusion imaging, it must be acknowledged that experience may also be a factor that contributes to the favorable results of the study group. However, even the experienced doctors could not have much confidence when ablating the nodules adjacent to the hilar bile ducts which could result in serious complications. US-MR fusion imaging can help the operator assess the ablation feasibility with objective and graphic planning processes other than subjective judgment based on their own experiences, and meanwhile precisely guide the implementation of the ablation planning. Both experienced and inexperienced operators could enhance their confidence in performing ablation and benefit from this technique. Before US-MR fusion imaging was introduced, PEI or combination therapy rather than RFA alone was preferred to the treatment of HCC nodules with a distance ≤5 mm from the HBDs in our center. With the assistance of US-MR fusion imaging and increased operator confidence of performing RFA, an increasing number of HCC nodules proximal to the HBDs could be candidates for RFA. These changes in the treatment strategy brought about by the US-MR fusion imaging-assisted RFA hold the potential to help extend the ablation indications for HCC nodules adjacent to the HBDs in current clinical guidelines.

In this study, RFA was employed in all patients because the thermal field of RFA was well controlled and precise for ablation planning and implementation (32, 33). However, there was one case of residual tumor, possibly because of a registration error occurring when the respiratory phase for fusion during the procedure was inconsistent with that during the registration process (34, 35). To achieve more precise fusion imaging planning and guidance, respiratory phase control should be considered in detail.

The main limitation of our study is that it is a single-center study with a small sample size. After all, early-stage HCC nodules proximal to the hepatic hilum are relatively rare and not frequently referred for US-guided RFA. Another limitation is the short follow-up period of the study group. A larger sample of patients and long-term follow-up are necessary. In addition, US-CT/MR fusion imaging requires high proficiency to ensure the precision of registration, and the planning module is only available in some specific US machines, so popularization is still difficult. However, with the increased attention of fusion imaging, this strategy may be increasingly recognized.

In conclusion, US-MR fusion imaging could be a non-invasive means for assisting in RFA for HCC nodules proximal to the HBDs to ensure ablation safety.

DATA AVAILABILITY STATEMENT

The raw data supporting the conclusions of this article will be made available by the authors, without undue reservation.

ETHICS STATEMENT

The studies involving human participants were reviewed and approved by the institutional review board of Third Affiliated Hospital of Sun Yat-sen University. The patients/participants provided their written informed consent to participate in this study.

AUTHOR CONTRIBUTIONS

RZ and EX contributed to the study design. RY, LPL, MZ, LL, QZ, and KL contributed to data collection. YY and YL performed the statistical analyses and wrote the manuscript. All authors contributed to the article and approved the submitted version.

FUNDING

This work was supported by the National Key Research and Development Program of China under Grant No. 2017YFC0112000; the National Natural Science Foundation of China under Grant No. 81401434; the Science and Technology Planning Project of Guangdong Province, China under Grant Nos. 2017A020215082, 2017A020215137, and 2017B090901034; the Science and Technology Planning Project of Guangzhou, China under Grant No. 201704020164; the Fundamental Research Funds for the Central Universities, China under Grant Nos. 18ykpy05 and 20ykpy37; and Health public welfare scientific research project in Futian District Shenzhen under Grant No. FTWS2020022.

SUPPLEMENTARY MATERIAL

The Supplementary Material for this article can be found online at: https://www.frontiersin.org/articles/10.3389/fonc.2021.570312/full#supplementary-material

REFERENCES

1. Omata M, Cheng AL, Kokudo N, Kudo M, Lee JM, Jia J, et al. Asia-Pacific clinical practice guidelines on the management of hepatocellular carcinoma: a 2017 update. *Hepatol Int* (2017) 11(4):317–70. doi: 10.1007/s12072-017-9799-9
2. European Association for the Study of the Liver. EASL Clinical Practice Guidelines: Management of hepatocellular carcinoma. *J Hepatol* (2018) 69 (1):182–236. doi: 10.1016/j.jhep.2018.03.019
3. Kudo M. Radiofrequency ablation for hepatocellular carcinoma: updated review in 2010. *Oncology* (2010) 78 Suppl 1:113–24. doi: 10.1159/000315239
4. Fu Y, Yang W, Wu JY, Yan K, Wu W, Xing BC, et al. Intrahepatic biliary injuries associated with radiofrequency ablation of hepatic malignancies. *Chin Med J (Engl)* (2011) 124(13):1957–63. doi: 10.3760/cma.j.issn.0366-6999.2011.13.007
5. Felker ER, Lee-Felker SA, Ajwichai K, Tan N, Lu DS, Durazo FA, et al. Intraductal Cooling via a Nasobiliary Tube During Radiofrequency Ablation of Central Liver Tumors Reduces Biliary Injuries. *AJR Am J Roentgenol* (2015) 204(6):1329–35. doi: 10.2214/ajr.14.13788
6. Ohnishi T, Yasuda I, Nishigaki Y, Hayashi H, Otsuji K, Mukai T, et al. Intraductal chilled saline perfusion to prevent bile duct injury during percutaneous radiofrequency ablation for hepatocellular carcinoma. *J Gastroenterol Hepatol* (2008) 23(8 Pt 2):e410–5. doi: 10.1111/j.1440-1746.2007.05091.x
7. Fonseca AZ, Santin S, Gomes LG, Waisberg J, Ribeiro MAJr. Complications of radiofrequency ablation of hepatic tumors: Frequency and risk factors. *World J Hepatol* (2014) 6(3):107–13. doi: 10.4254/wjh.v6.i3.107
8. Jiang K, Zhang WZ, Liu Y, Su M, Zhao XQ, Dong JH, et al. "One-off" complete radiofrequency ablation for hepatocellular carcinoma in a "high-risk location" adjacent to the major bile duct and hepatic blood vessel. *Cell Biochem Biophys* (2014) 69(3):605–17. doi: 10.1007/s12013-014-9840-8
9. Cha DI, Lee MW, Rhim H, Choi D, Kim YS, Lim HK. Therapeutic efficacy and safety of percutaneous ethanol injection with or without combined radiofrequency ablation for hepatocellular carcinomas in high risk locations. *Korean J Radiol* (2013) 14(2):240–7. doi: 10.3348/kjr.2013.14.2.240
10. Guo Y, Zhang Y, Huang J, Chen X, Huang W, Shan H, et al. Safety and Efficacy of Transarterial Chemoembolization Combined with CT-Guided Radiofrequency Ablation for Hepatocellular Carcinoma Adjacent to the Hepatic Hilum within Milan Criteria. *J Vasc Interv Radiol* (2016) 27 (4):487–95. doi: 10.1016/j.jvir.2016.01.002
11. Li X, Yu J, Liang P, Yu X, Cheng Z, Han Z, et al. Ultrasound-guided percutaneous microwave ablation assisted by three-dimensional visualization operative treatment planning system and percutaneous transhepatic cholangial drainage with intraductal chilled saline perfusion for larger hepatic hilum hepatocellular (D >/= 3 cm): preliminary results. *Oncotarget* (2017) 8(45):79742–9. doi: 10.18632/oncotarget.19275
12. Imai Y, Hirooka M, Ochi H, Koizumi Y, Ohno Y, Watanabe T, et al. A case of hepatocellular carcinoma treated by radiofrequency ablation confirming the adjacent major bile duct under hybrid contrast mode through a biliary drainage catheter. *Clin J Gastroenterol* (2015) 8(5):318–22. doi: 10.1007/s12328-015-0599-2
13. Dominique E, El OA, Goharin A, Attalah D, de Baere T. Intraductal cooling of the main bile ducts during intraoperative radiofrequency ablation. *J Surg Oncol* (2001) 76(4):297–300. doi: 10.1002/jso.1049
14. Elias D, Sideris L, Pocard M, Dromain C, De Baere T. Intraductal cooling of the main bile ducts during radiofrequency ablation prevents biliary stenosis. *J Am Coll Surg* (2004) 198(5):717–21. doi: 10.1016/j.jamcollsurg.2003.12.026
15. Ogawa T, Kawamoto H, Kobayashi Y, Nakamura S, Miyatake H, Harada R, et al. Prevention of biliary complication in radiofrequency ablation for hepatocellular carcinoma-Cooling effect by endoscopic nasobiliary drainage tube. *Eur J Radiol* (2010) 73(2):385–90. doi: 10.1016/j.ejrad.2008.10.021
16. Minami Y, Kudo M. Ultrasound fusion imaging of hepatocellular carcinoma: a review of current evidence. *Dig Dis* (2014) 32(6):690–5. doi: 10.1159/000368001
17. Makino Y, Imai Y, Igura T, Kogita S, Sawai Y, Fukuda K, et al. Feasibility of Extracted-Overlay Fusion Imaging for Intraoperative Treatment Evaluation of Radiofrequency Ablation for Hepatocellular Carcinoma. *Liver Cancer* (2016) 5(4):269–79. doi: 10.1159/000449338
18. Xu EJ, Lv SM, Li K, Long YL, Zeng QJ, Su ZZ, et al. Immediate evaluation and guidance of liver cancer thermal ablation by three-dimensional ultrasound/contrast-enhanced ultrasound fusion imaging. *Int J Hyperthermia* (2018) 34 (6):870–6. doi: 10.1080/02656736.2017.1373306
19. Xu E, Li K, Long Y, Luo L, Zeng Q, Tan L, et al. Intra-Procedural CT/MR-Ultrasound Fusion Imaging Helps to Improve Outcomes of Thermal Ablation for Hepatocellular Carcinoma: Results in 502 Nodules. *Ultraschall Med* (2019). doi: 10.1055/a-1021-1616
20. Song KD, Lee MW, Rhim H, Kang TW, Cha DI, Sinn DH, et al. Percutaneous US/MRI Fusion-guided Radiofrequency Ablation for Recurrent Subcentimeter Hepatocellular Carcinoma: Technical Feasibility and Therapeutic Outcomes. *Radiology* (2018) 288(3):878–86. doi: 10.1148/radiol.2018172743
21. Ahn SJ, Lee JM, Lee DH, Lee SM, Yoon JH, Kim YJ, et al. Real-time US-CT/MR fusion imaging for percutaneous radiofrequency ablation of hepatocellular carcinoma. *J Hepatol* (2017) 66(2):347–54. doi: 10.1016/j.jhep.2016.09.003
22. European Society of Radiology (ESR). Abdominal applications of ultrasound fusion imaging technique: liver, kidney, and pancreas. *Insights Imaging* (2019) 10(1):6. doi: 10.1186/s13244-019-0692-z
23. Hakime A, Yevich S, Tselikas L, Deschamps F, Petrover D, De Baere T. Percutaneous Thermal Ablation with Ultrasound Guidance. Fusion Imaging Guidance to Improve Conspicuity of Liver Metastasis. *Cardiovasc Intervent Radiol* (2017) 40(5):721–7. doi: 10.1007/s00270-016-1561-5
24. Mauri G, Cova L, De Beni S, Ierace T, Tondolo T, Cerri A, et al. Real-time US-CT/MRI image fusion for guidance of thermal ablation of liver tumors undetectable with US: results in 295 cases. *Cardiovasc Intervent Radiol* (2015) 38(1):143–51. doi: 10.1007/s00270-014-0897-y
25. Li K, Su Z, Xu E, Guan P, Li LJ, Zheng R. Computer-Assisted Hepatocellular Carcinoma Ablation Planning Based on 3-D Ultrasound Imaging. *Ultrasound Med Biol* (2016) 42(8):1951–7. doi: 10.1016/j.ultrasmedbio.2016.03.013
26. Liu F, Liang P, Yu X, Lu T, Cheng Z, Lei C, et al. A three-dimensional visualisation preoperative treatment planning system in microwave ablation for liver cancer: a preliminary clinical application. *Int J Hyperthermia* (2013) 29(7):671–7. doi: 10.3109/02656736.2013.834383
27. Ren H, An C, Liang P, Yu J, Cheng Z, Han Z, et al. Ultrasound-guided percutaneous microwave ablation assisted by athree-dimensional visualization treatment platform combined with transcatheter arterial chemoembolization for a single large hepatocellular carcinoma 5 cm or larger: a preliminary clinical application. *Int J Hyperthermia* (2019) 36(1):44–54. doi: 10.1080/02656736.2018.1530459
28. Costello JR, Kalb B, Chundru S, Arif H, Petkovska I, Martin DR. MR imaging of benign and malignant biliary conditions. *Magn Reson Imaging Clin N Am* (2014) 22(3):467–88. doi: 10.1016/j.mric.2014.05.002
29. Zhou J, Sun HC, Wang Z, Cong WM, Wang JH, Zeng MS, et al. Guidelines for Diagnosis and Treatment of Primary Liver Cancer in China (2017 Edition). *Liver Cancer* (2018) 7(3):235–60. doi: 10.1159/000488035
30. Lin MX, Ye JY, Tian WS, Xu M, Zhuang BW, Lu MD, et al. Risk Factors for Bile Duct Injury After Percutaneous Thermal Ablation of Malignant Liver Tumors: A Retrospective Case-Control Study. *Dig Dis Sci* (2017) 62(4):1086–94. doi: 10.1007/s10620-016-4312-1
31. Kunishi Y, Numata K, Morimoto M, Okada M, Kaneko T, Maeda S, et al. Efficacy of fusion imaging combining sonography and hepatobiliary phase MRI with Gd-EOB-DTPA to detect small hepatocellular carcinoma. *AJR Am J Roentgenol* (2012) 198(1):106–14. doi: 10.2214/ajr.10.6039
32. Facciorusso A, Serviddio G, Muscatiello N. Local ablative treatments for hepatocellular carcinoma: An updated review. *World J Gastrointest Pharmacol Ther* (2016) 7(4):477–89. doi: 10.4292/wjgpt.v7.i4.477
33. Chu KF, Dupuy DE. Thermal ablation of tumours: biological mechanisms and advances in therapy. *Nat Rev Cancer* (2014) 14(3):199–208. doi: 10.1038/nrc3672

34. Zhong-Zhen S, Kai L, Rong-Qin Z, Er-Jiao X, Ting Z, Ao-Hua Z, et al. A feasibility study for determining ablative margin with 3D-CEUS-CT/MR image fusion after radiofrequency ablation of hepatocellular carcinoma. *Ultraschall Med* (2012) 33(7):E250–e5. doi: 10.1055/s-0032-1325466
35. Calandri M, Mauri G, Yevich S, Gazzera C, Basile D, Gatti M, et al. Fusion Imaging and Virtual Navigation to Guide Percutaneous Thermal Ablation of Hepatocellular Carcinoma: A Review of the Literature. *Cardiovasc Intervent Radiol* (2019) 42(5):639–47. doi: 10.1007/s00270-019-02167-z

Conflict of Interest: The authors declare that the research was conducted in the absence of any commercial or financial relationships that could be construed as a potential conflict of interest.

frontiers in Oncology

REVIEW
published: 05 March 2021
doi: 10.3389/fonc.2021.593636

Image Guidance in Ablation for Hepatocellular Carcinoma: Contrast-Enhanced Ultrasound and Fusion Imaging

Yasunori Minami and Masatoshi Kudo*

Department of Gastroenterology and Hepatology, Faculty of Medicine, Kindai University, Osaka, Japan

The ultrasound (US) imaging technology, including contrast-enhanced US (CEUS) and fusion imaging, has experienced radical improvement, and advancement in technology thus overcoming the problem of poor conspicuous hepatocellular carcinoma (HCC). On CEUS, the presence or absence of enhancement distinguishes the viable portion from the ablative necrotic portion. Using volume data of computed tomography (CT) or magnetic resonance imaging (MRI), fusion imaging enhances the three-dimensional relationship between the liver vasculature and HCC. Therefore, CT/MR-US fusion imaging provides synchronous images of CT/MRI with real-time US, and US-US fusion imaging provides synchronous US images before and after ablation. Moreover, US-US overlay fusion can visualize the ablative margin because it focuses the tumor image onto the ablation zone. Consequently, CEUS and fusion imaging are helpful to identify HCC with little conspicuity, and with more confidence, we can perform ablation therapy. CEUS/fusion imaging guidance has improved the clinical effectiveness of ablation therapy in patients with poor conspicuous HCCs. Therefore; this manuscript reviews the status of CEUS/fusion imaging guidance in ablation therapy of poor conspicuous HCC.

Keywords: ablation therapy, contrast-enhanced ultrasound, fusion imaging, hepatocellular carcinoma, poor conspicuity, precise ablation

OPEN ACCESS

Edited by:
Wei Yang,
Peking University Cancer Hospital, China

Reviewed by:
Hong Wang,
Peking University Cancer Hospital, China
Jie Wu,
Guizhou Provincial People's Hospital, China

****Correspondence:***
Yasunori Minami
minkun@med.kindai.ac.jp

Specialty section:
This article was submitted to Cancer Imaging and Image-directed Interventions, a section of the journal Frontiers in Oncology

Received: *11 August 2020*
Accepted: *19 January 2021*
Published: *05 March 2021*

Citation:
Minami Y and Kudo M (2021) Image Guidance in Ablation for Hepatocellular Carcinoma: Contrast-Enhanced Ultrasound and Fusion Imaging. Front. Oncol. 11:593636. doi: 10.3389/fonc.2021.593636

INTRODUCTION

Ablation therapy is a minimally invasive treatment option, and percutaneous ultrasound (US)-guided ablative treatments, including radiofrequency ablation (RFA), and microwave ablation (MWA), have successfully managed hepatocellular carcinoma (HCC) (1–6). However, patients with difficult conditions for ablation therapy require multiple treatment sessions due to the limitation of US guidance. Poorly conspicuous HCC is not easily targeted on B-mode US guidance and accounts for 5.2–38.8% of planning US for ablation therapy (7–10). The success of

Abbreviations: CEUS, contrast-enhanced ultrasound; CT, computed tomography; HCC, hepatocellular carcinoma; MPR, multiplanar reconstruction; MRI, magnetic resonance imaging; MWA, microwave ablation; RFA, radiofrequency ablation; US, ultrasound; 2D, two-dimensional; 3D, three-dimensional.

percutaneous ablation therapies primarily depends on correct targeting through an imaging technique and the suitable placement of the needle electrode into the target tumor thereby optimizing local tumor control.

The US imaging technology has experienced radical improvement, and advances in hardware and software have helped to overcome the problem of poor conspicuity on US. Presently, contrast-enhanced ultrasound (CEUS) is widely used in clinical practice and it provides significant contribution to the diagnosis of HCC (11, 12). On CEUS, we can distinguish the viable portion of HCC from the ablative necrotic one by the presence or absence of enhancement, and we can perform an image-guided ablation of this viable HCC. In addition, other technological advancements allow two-dimensional (2D) multiplanar reconstruction (MPR) images of CT or MRI to display in the same plane as US images. Consequently, fusion imaging becomes a powerful technique to detect poor conspicuous HCC on US. Moreover, image fusion technology contributes to the progress of ablation therapy as well as other fields.

This article reviews the principles, clinical applications, and techniques of US image-guidance in ablation therapy including CEUS and fusion imaging.

CEUS-GUIDED ABLATION

Contrast Agents and Pharmacokinetics

Contrast agents, such as SonoVue/Lumason (Bracco, Milan, Italy) and Sonazoid (GE Healthcare, Waukesha, WI, USA), are microbubbles containing a low-solubility gas enveloped by a phospholipid shell. These microbubbles provide stable non-linear oscillation in a low-power acoustic field because of their hard shells, thereby displaying vascular pattern in real-time. However, Kupffer cells of the liver engulf the contrast agent (especially sonazoid). Therefore, sonazoid microbubbles can accumulate in the liver parenchyma, thereby displaying enhancement of the liver parenchyma for a considerable period (13).

Regarding CEUS, the standard protocol for the examination of the liver consists of two main phases: the vascular and Kupffer phases (14–17). The vascular phase can be divided into three phases. These include the arterial phase (15 s after injection and lasting for 25–30 s), portal phase (30 s after injection and lasting for 2–3 min), and late vascular phase (4–7 min). The Kupffer phase starts 10 min post-injection of Sonazoid. The key diagnostic feature of HCC with SonoVue/Lumason is the hyper-enhancement seen in the arterial phase followed by a clearance seen in the portal and/or late phase. Similarly, we observe a hyper-enhancement in the arterial phase followed by defect in the Kupffer phase with sonazoid. In addition, repeated contrast injections are also useful for diagnosis of HCC. This procedure termed "defect reperfusion imaging" or "the re-injection technique" can diagnose HCC in the presence of arterial enhancement(s) in a defective lesion/wash-out (18–20).

Technique of CEUS Guidance

Prior to ablation therapy, we can use CEUS to assess the HCC lesion size, number, margins, and relationship with the surrounding liver vasculature. The diagnostic accuracy of CEUS (using SonoVue or Sonazoid) for poorly conspicuous HCC is 93.8–100%, similar to contrast-enhanced CT or MRI (21–24). Thus, CEUS facilitates needle placement in HCC poorly conspicuous on B-mode US, such that the defect/wash-out lesion signifies the target insertion point. Moreover, we can administer US contrast agents repeatedly in order to guide percutaneous ablation of multiple lesions.

Sometimes, it is difficult to differentiate local HCC tumor progression from ablative necrotic areas because both similarly show hypoenhancement lesions in the late vascular/Kupffer phase. Consequently, the defect reperfusion imaging becomes very useful in the confirmation of viable HCCs that are otherwise undetectable on US (20). Nevertheless, it is sometimes difficult to depict HCC with low-contrast images in the late vascular/Kupffer phase in severe liver cirrhosis. In other words, we experience a weak contrast brightness intensity of liver parenchyma due to a decrease of portal blood flow and number of Kupffer cells in the liver. Therefore, in such situations, we must administer a higher dose of US contrast agent to patients in order to improve contrast brightness intensity.

Evidence of CEUS-Guided Ablation Therapy

CEUS guidance in ablation therapy has increased operators' confidence and improved the outcome. It was reported that the success rate at first session of CEUS was significantly higher than that in B-mode US guidance for poor conspicuous HCC (94.7 *versus* 65.0%, $p = 0.043$) (25). Some previous cohort studies found that the number of sessions was significantly smaller with CEUS guidance than with B-mode US guidance (26, 27). Another study demonstrated that the local control rate was higher with CEUS guidance than with B-mode US guidance (85.3 *versus* 66.4% at 2 years, $p = 0.044$) (28). Moreover, CEUS easily recognizes serious acute complications including active bleeding or hepatic infarction, which is not the case with B-mode US guidance (29). CEUS may show active hemorrhage as extravasation of microbubbles through the needle tract and hepatic infarction as a hypoenhancement lesion.

FUSION IMAGING-GUIDED ABLATION

Applications of Fusion Imaging

The commercial image fusion platforms include Real-Time Virtual Sonography (RVS) (Hitachi, Tokyo, Japan), volume navigation (v-nav) (GE Healthcare, Waukesha, WI, USA), SmartFusion (Canon Medical systems, Tokyo, Japan), eSie Fusion Imaging (Siemens Healthcare, Erlangen, Germany), and PercuNav (Philips, Andover, MA, USA).

Cross-sectional MPR images from 3D-volume data allow virtual sonographic images, and magnetic tracking based on mapping of a 3D magnetic field. When using fusion imaging,

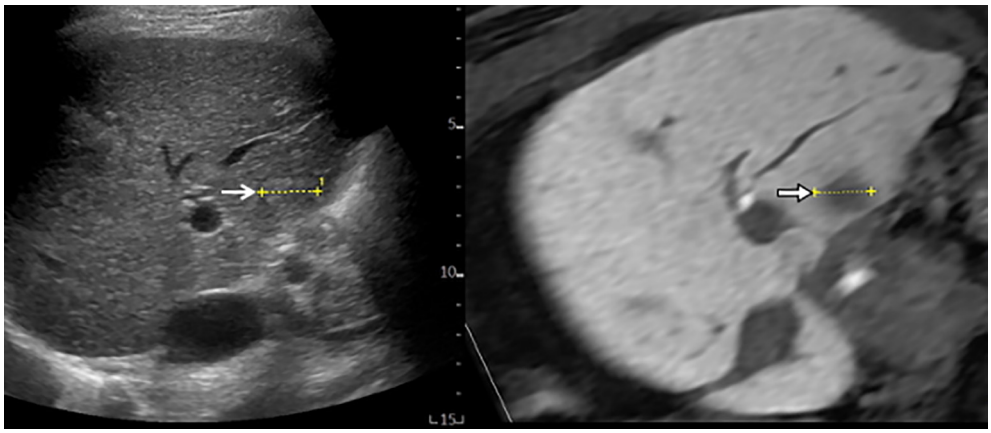

FIGURE 1 | MR-US fusion imaging. MRI and US images with HCC measuring 1.8 cm in diameter are well-matched. B-mode US (left) shows a slightly hyperechoic nodule with ill-defined HCC (open arrow) from intercostal view. Hepatobiliary phase image of gadoxetic acid-enhanced MRI (right) shows low signal intensity with ill-defined HCC (arrow).

we can obtain spatial information from the relationship between the magnetic field generator and the magnetic sensor attached to the US probe. By integrating the spatial information between the US probe and 3D volume data, a 2D-MPR image can show the same plane and move synchronously with real-time US images (30–32). CT/MR-US fusion imaging provides synchronous images of CT/MRI with real-time US (**Figure 1**). US-US fusion imaging provides synchronous US images before and after ablation (**Figure 2**). Moreover, it can visualize the ablative margins on US before ablation because it projects the tumor image onto the ablation zone.

Technique of Fusion Imaging Guidance

To operate effectively using fusion imaging technology, there is a need to match (co-register) the 3D image datasets with the real-time US; that is, we need to register the reference points near the tumor carefully. When the CT/MRI and US images are well-matched, inconspicuous HCC can be identified. Thus, CT/MR-US fusion imaging can increase the detectability of small HCCs compared to B-mode US. However, the gap in co-registration can persist in some situations. For example, imaging gap occurs because the depths of breath-holds in CT and sonographic examinations vary. Originally, CT/MR-US fusion imaging offer no support for synchronized action of breathing with any diagnostic US scanners at present. However, the priority is for the operator to catch the tumor location on US because the operator inserts the therapeutic needle watching on an US monitor under patients' breathing. Not so strictly image matching is necessary for inserting the therapeutic needle into the tumor in fact.

In contrast, succinct co-registration accuracy (in mm) can be required when assessing an ablative margin. For high quality images, a 3D-UD volume has to be obtained by a swing scanning with slow and steady speed. For high-quality image matching, we need to register the reference points near the tumor before and after the ablation more carefully.

Evidence of Fusion Imaging-Guided Ablation Therapy

CT/MR-US Fusion Imaging

According to some retrospective studies, the success and local tumor progression rates using RFA guided by CT/MR-US fusion imaging (for poorly conspicuous HCC on B-mode US) were 94.4–100% and 0–8.3%, respectively (33–37). According to a prospective study by Ahn et al. (38), CT/MR-US fusion imaging significantly improved the tumor visibility and operators' confidence compared to B-mode US alone ($p < 0.001$). Consequently, the recurrence-free survival rates were 86.0 and 75.8% at 12- and 24-months, respectively. The cumulative incidences of local tumor progression were 3.2 and 4.7% at 12- and 24-months, respectively.

US-US Fusion Imaging and US-US Overlay Fusion

Successful ablation therapy requires a wide ablation zone (including the tumor with ablative safety margin) in order to restrain local tumor progression. Although fusion imaging improves the visualization of HCC, some factors limit a 5-mm safety margin. These include large tumor size, tumor morphology, vasculature around the tumor, subcapsular tumor location, and gas bubbles in ablation zone (39, 40). Gas formation in particular, could envelope the tumor leading to a blind assessment of the ablative margin on US. Therefore, this ablative margin assessment technique was revised in order to overcome this challenging issue of a 5-mm safety margin.

US-US fusion imaging is used to compare images before and after ablation in a side-by-side manner, and US-US overlay fusion visualizes the ablative margin by focusing on the ablation zone of the projected tumor image (41–45). We achieved 5-mm safety margins in 89.3% (108/121) of HCC nodules using the US-US overlay fusion technique compared to 47.0% (213/453) in the conventional guidance group ($P < 0.01$). Two-year local tumor progression rates were 0.8% (1/121) with US-US overlay fusion and 6.0% (27/453) with conventional guidance ($P = 0.022$) (46).

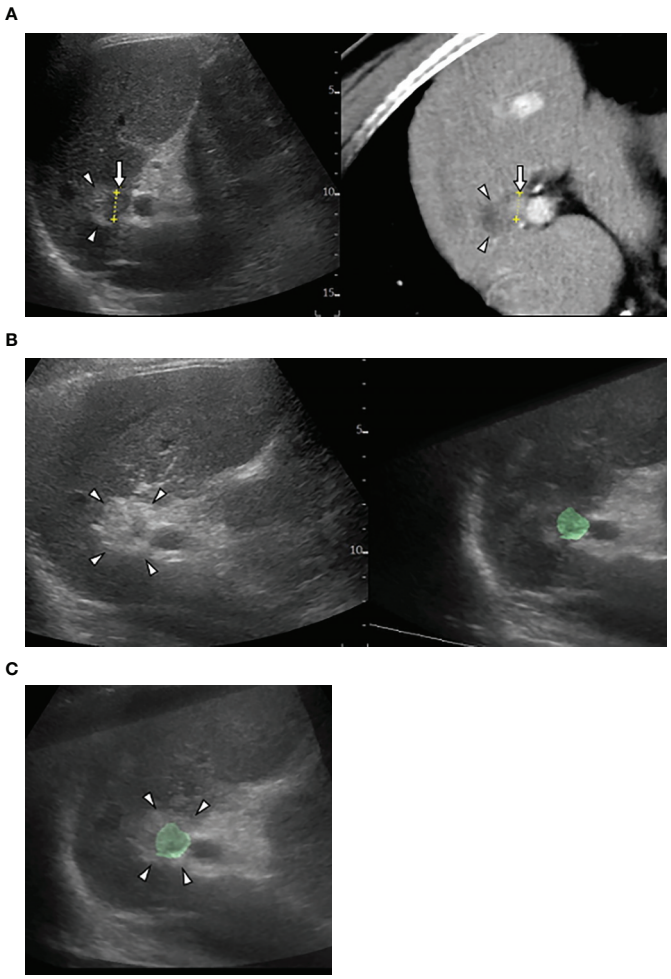

FIGURE 2 | US-US fusion imaging and US-US overlay fusion. **(A)** CT-US fused image shows locally progressed hepatocellular carcinoma (HCC) (arrows) touching ablative necrosis (arrow heads) due to previous ablation. **(B)** US-US fusion imaging displays HCC colorized as green before ablation (right) and ablative hyperechoic zone (arrowheads) due to the present ablaion (left). **(C)** US-US overlay fusion demonstrates the green colorized HCC inside the ablative hyperechoic zone concentrically.

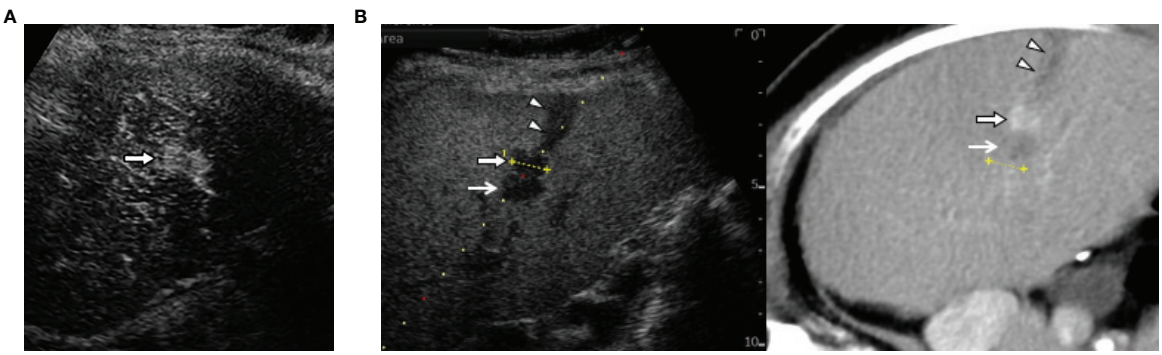

FIGURE 3 | The combination of contrast-enhanced US (CEUS) and fusion imaging. **(A)** CEUS with Sonazoid shows arterial enhancement of locally progressed hepatocellular carcinoma **(HCC)** (arrow). **(B)** The combination of Kupffer image on contrast-enhanced US (CEUS) and fused CT image demonstrates viable HCC (arrow) sandwiched between an ablated tract (arrow heads) and a necrotic tumor (open arrows).

THE COMBINATION GUIDANCE OF CEUS AND FUSION IMAGING

Operators may attempt CEUS fused with CT/MR image when CT/MR-US fusion imaging fails to identify HCCs. Either CEUS or fusion imaging provides an inadequately favorable condition for ablation therapy. Therefore, the combination of fusion imaging and CEUS is the last option (**Figure 3**). Even in difficult situations, we observed no significant differences in the number of treatment sessions required to obtain technical success of ablation between CEUS, fusion imaging, and the combination guidance (47). In addition, the combined guidance could be preferred for recurrent subcentimeter HCCs (48–50). This technique ablation may be expanded to intermediate stage HCC (51). However, CEUS has some detection limits for deep lesion, hypovascular HCC in a cirrhotic liver and lesions located in the subdiaphragrnatic regions. Therefore, we would like to recommend you choose fusion imaging guidance first.

CONCLUSION

CEUS and fusion imaging are relevant to identify HCC with poor conspicuity. Therefore, operators can perform ablation therapy with more confidence. CEUS/fusion imaging guidance has improved the clinical effectiveness of ablation therapy in poorly conspicuous HCC patients. However, CEUS or fusion imaging is limited in some situations. For example, HCC is unclear on CEUS either because the tumor location is deeper than 10 cm, the CT/MRI and US images could not be finally well-matched, or HCC is hidden behind bone or lung/bowl air. To overcome such situations, understanding the characteristics of each imaging guidance technique is key to identifying and managing poor conspicuous HCCs. No hostile relationship for ablation guidance between CEUS and fusion imaging. Occasionally, we can choose the combined guidance CEUS with fusion imaging in the most difficult situations. At least, we have to refrain from performing ablation therapy for poor conspicuous HCC with a simplistic strategy. CEUS/fusion imaging guided ablation therapy can provide longer recurrence-free survival rates and lower local tumor progression rates. Therefore, CEUS and fusion imaging can support the development of so-called "precise ablation."

AUTHOR CONTRIBUTIONS

All authors listed have made a substantial, direct, and intellectual contribution to the work and approved it for publication.

REFERENCES

1. Lin SM, Lin CJ, Lin CC, Hsu CW, Chen YC. Randomised controlled trial comparing percutaneous radiofrequency thermal ablation, percutaneous ethanol injection, and percutaneous acetic acid injection to treat hepatocellular carcinoma of 3 cm or less. *Gut* (2005) 54(8):1151–6. doi: 10.1136/gut.2004.045203
2. Chen MS, Li JQ, Zheng Y, Guo RP, Liang HH, Zhang YQ, et al. A prospective randomized trial comparing percutaneous local ablative therapy and partial hepatectomy for small hepatocellular carcinoma. *Ann Surg* (2006) 243:321–8. doi: 10.1097/01.sla.0000201480.65519.b8
3. Takayama T, Makuuchi M, Hasegawa K. Single HCC smaller than 2 cm: surgery or ablation?: surgeon's perspective. *J Hepatobiliary Pancreat Sci* (2010) 17(4):422–4. doi: 10.1007/s00534-009-0239-7
4. Peng ZW, Lin XJ, Zhang YJ, Liang HH, Guo RP, Shi M, et al. Radiofrequency ablation versus hepatic resection for the treatment of hepatocellular carcinomas 2 cm or smaller: a retrospective comparative study. *Radiology* (2012) 262(3):1022–33. doi: 10.1148/radiol.11110817
5. Feng K, Yan J, Li X, Xia F, Ma K, Wang S, et al. A randomized controlled trial of radiofrequency ablation and surgical resection in the treatment of small hepatocellular carcinoma. *J Hepatol* (2012) 57(4):794–802. doi: 10.1016/j.jhep.2012.05.007
6. Kudo M. Management of Hepatocellular Carcinoma in Japan: Current Trends. *Liver Cancer* (2020) 9:1–5. doi: 10.1159/000505370
7. Lee MW, Lim HK, Kim YJ, Choi D, Kim YS, Lee WJ, et al. Percutaneous sonographically guided radio frequency ablation of hepatocellular carcinoma: causes of mistargeting and factors affecting the feasibility of a second ablation session. *J Ultrasound Med* (2011) 30(5):607–15. doi: 10.7863/jum.2011.30.5.607
8. Minami Y, Kudo M, Kawasaki T, Chung H, Ogawa C, Shiozaki H. Treatment of hepatocellular carcinoma with percutaneous radiofrequency ablation: usefulness of contrast harmonic sonography for lesions poorly defined with B-mode sonography. *AJR Am J Roentgenol* (2004) 183:153–6. doi: 10.2214/ajr.183.1.1830153
9. Kim AY, Lee MW, Rhim H, Cha DI, Choi D, Kim YS, et al. Pretreatment evaluation with contrast-enhanced ultrasonography for percutaneous radiofrequency ablation of hepatocellular carcinomas with poor conspicuity on conventional ultrasonography. *Korean J Radiol* (2013) 14(5):754–63. doi: 10.3348/kjr.2013.14.5.754
10. Rajesh S, Mukund A, Arora A, Jain D, Sarin SK. Contrast-enhanced US-guided radiofrequency ablation of hepatocellular carcinoma. *J Vasc Interv Radiol* (2013) 24(8):1235–40. doi: 10.1016/j.jvir.2013.04.013
11. Kudo M, Ueshima K, Osaki Y, Hirooka M, Aso K, Numata K, et al. for the SELECTED Study Group Japan. B-Mode ultrasonography versus contrast-enhanced ultrasonography for surveillance of hepatocellular carcinoma: A prospective multicenter randomized controlled trial. *Liver Cancer* (2019) 8:271–80. doi: 10.1159/000501082
12. Liu F, Liu D, Wang K, Xie X, Su L, Kuang M, et al. Deep learning radiomics based on contrast-enhanced ultrasound might optimize curative treatments for very-early or early-stage hepatocellular carcinoma patients. *Liver Cancer* (2020) 9(4):397–413. doi: 10.1159/000505694
13. Shunichi S, Hiroko I, Fuminori M, Waki H. Definition of contrast enhancement phases of the liver using a perfluoro-based microbubble agent, perflubutane microbubbles. *Ultrasound Med Biol* (2009) 35:1819–27. doi: 10.1016/j.ultrasmedbio.2009.05.013
14. Dietrich CF, Nolsøe CP, Barr RG, Berzigotti A, Burns PN, Cantisani V, et al. Guidelines and Good Clinical Practice Recommendations for Contrast-Enhanced Ultrasound (CEUS) in the Liver-Update 2020 WFUMB in Cooperation with EFSUMB, AFSUMB, AIUM, and FLAUS. *Ultrasound Med Biol* (2020) 46(10):2579–604. doi: 10.1016/j.ultrasmedbio.2020.04.030
15. Terminology and Diagnostic Criteria Committee. Japan Society of Ultrasonics in Medicine. Ultrasound diagnostic criteria for hepatic tumors. *J Med Ultrason* (2001) 41(1):113–23. doi: 10.1007/s10396-013-0500-1
16. Lee JY, Minami Y, Choi BI, Lee WJ, Chou YH, Jeong WK, et al. The AFSUMB Consensus Statements and Recommendations for the Clinical Practice of Contrast-Enhanced Ultrasound Using Sonazoid. *Ultrasonography* (2020) 39 (3):191–220. doi: 10.14366/usg.20057

17. Kudo M. Breakthrough Imaging in Hepatocellular Carcinoma. *Liver Cancer* (2016) 5(1):47–54. doi: 10.1159/000367761
18. Minami Y, Kudo M. Contrast-enhanced ultrasonography with Sonazoid in hepatocellular carcinoma diagnosis. *Hepatoma Res* (2020) 6:46. doi: 10.20517/2394-5079.2020.32
19. Kudo M, Hatanaka K, Maekawa K. Newly developed novel ultrasound technique, defect reperfusion ultrasound imaging, using sonazoid in the management of hepatocellular carcinoma. *Oncology* (2010) 78:40–5. doi: 10.1159/000315229
20. Kudo M. Defect reperfusion imaging with Sonazoid®: a breakthrough in hepatocellular carcinoma. *Liver Cancer* (2016) 5:1–7. doi: 10.1159/000367760
21. Kang TW, Lee MW, Song KD, Kim M, Kim SS, Kim SH, et al. Added Value of contrast-enhanced ultrasound on biopsies of focal hepatic lesions invisible on fusion imaging guidance. *Korean J Radiol* (2017) 18(1):152–61. doi: 10.3348/kjr.2017.18.1.152
22. Korenaga K, Korenaga M, Furukawa M, Yamasaki T, Sakaida I. Usefulness of sonazoid contrast-enhanced ultrasonography for hepatocellular carcinoma: comparison with pathological diagnosis and superparamagnetic iron oxide magnetic resonance images. *J Gastroenterol* (2009) 44(7):733–41. doi: 10.1007/s00535-009-0053-7
23. Tanaka H. Current role of ultrasound in the diagnosis of hepatocellular carcinoma. *J Med Ultrason* (2001) 47(2):239–55. doi: 10.1007/s10396-020-01012-y
24. Wei Y, Ye Z, Yuan Y, Huang Z, Wei X, Zhang T, et al. A new diagnostic criterion with gadoxetic acid-enhanced MRI may improve the diagnostic performance for hepatocellular carcinoma. *Liver Cancer* (2020) 9(4):414–25. doi: 10.1159/000505696
25. Minami Y, Kudo M, Chung H, Kawasaki T, Yagyu Y, Shimono T, et al. Contrast harmonic sonography-guided radiofrequency ablation therapy versus B-mode sonography in hepatocellular carcinoma: prospective randomized controlled trial. *AJR Am J Roentgenol* (2007) 188:489–94. doi: 10.2214/AJR.05.1286
26. Minami Y, Kudo M, Hatanaka K, Kitai S, Inoue T, Hagiwara S, et al. Radiofrequency ablation guided by contrast harmonic sonography using perfluorocarbon microbubbles (Sonazoid) for hepatic malignancies: an initial experience. *Liver Int* (2010) 30:759–64. doi: 10.1111/j.1478-3231.2010.02226.x
27. Masuzaki R, Shiina S, Tateishi R, Yoshida H, Goto E, Sugioka Y, et al. Utility of contrast-enhanced ultrasonography with Sonazoid in radiofrequency ablation for hepatocellular carcinoma. *J Gastroenterol Hepatol* (2011) 26:759–64. doi: 10.1111/j.1440-1746.2010.06559.x
28. Dohmen T, Kataoka E, Yamada I, Miura K, Ohshima S, Shibuya T, et al. Efficacy of contrast-enhanced ultrasonography in radiofrequency ablation for hepatocellular carcinoma. *Intern Med* (2012) 51:1–7. doi: 10.2169/internalmedicine.51.6042
29. Huang DY, Yusuf GT, Daneshi M, Ramnarine R, Deganello A, Sellars ME, et al. Contrast-enhanced ultrasound (CEUS) in abdominal intervention. *Abdom Radiol (NY)* (2018) 43:960–76. doi: 10.1007/s00261-018-1473-8
30. Minami Y, Kudo M. Ultrasound fusion imaging technologies for guidance in ablation therapy for liver cancer. *J Med Ultrason* (2001) 47(2):257–63. doi: 10.1007/s10396-020-01006-w
31. Hirooka M, Iuchi H, Kurose K, Kumagi T, Horiike N, Onji M. Abdominal virtual ultrasonographic images reconstructed by multi-detector row helical computed tomography. *Eur J Radiol* (2005) 53:312–7. doi: 10.1016/j.ejrad.2004.03.026
32. Hirooka M, Iuchi H, Kumagi T, Shigematsu S, Hiraoka A, Uehara T, et al. Virtual sonographic radiofrequency ablation of hepatocellular carcinoma visualized on CT but not on conventional sonography. *AJR Am J Roentgenol* (2006) 186:S255–60. doi: 10.2214/AJR.04.1252
33. Minami Y, Kudo M, Chung H, Inoue T, Takahashi S, Hatanaka K, et al. Percutaneous radiofrequency ablation of sonographically unidentifiable liver tumors. Feasibility and usefulness of a novel guiding technique with an integrated system of computed tomography and sonographic images. *Oncology* (2007) 72 Suppl 1:111–6. doi: 10.1159/000111716
34. Kitada T, Murakami T, Kuzushita N, Minamitani K, Nakajo K, Osuga K, et al. Effectiveness of real-time virtual sonography-guided radiofrequency ablation treatment for patients with hepatocellular carcinomas. *Hepatol Res* (2008) 38(6):565–71. doi: 10.1111/j.1872-034X.2007.00308.x
35. Minami Y, Chung H, Kudo M, Kitai S, Takahashi S, Inoue T, et al. Radiofrequency ablation of hepatocellular carcinoma: value of virtual CT sonography with magnetic navigation. *AJR Am J Roentgenol* (2008) 190(6):W335–341. doi: 10.2214/AJR.07.3092
36. Nakai M, Sato M, Sahara S, Takasaka I, Kawai N, Minamiguchi H, et al. Radiofrequency ablation assisted by real-time virtual sonography and CT for hepatocellular carcinoma undetectable by conventional sonography. *Cardiovasc Intervent Radiol* (2009) 32(1):62–9. doi: 10.1007/s00270-008-9462-x
37. Song KD, Lee MW, Rhim H, Cha DI, Chong Y, Lim HK. Fusion imaging-guided radiofrequency ablation for hepatocellular carcinomas not visible on conventional ultrasound. *AJR Am J Roentgenol* (2013) 201(5):1141–7. doi: 10.2214/AJR.13.10532
38. Ahn SJ, Lee JM, Lee DH, Lee SM, Yoon JH, Kim YJ, et al. Real-time US-CT/MR fusion imaging for percutaneous radiofrequency ablation of hepatocellular carcinoma. *J Hepatol* (2017) 66(2):347–54. doi: 10.1016/j.jhep.2016.09.003
39. Nishikawa H, Osaki Y, Iguchi E, Takeda H, Matsuda F, Nakajima J, et al. Radiofrequency ablation for hepatocellular carcinoma: the relationship between a new grading system for the ablative margin and clinical outcomes. *J Gastroenterol* (2013) 48(8):951–65. doi: 10.1007/s00535-012-0690-0
40. Calandri M, Mauri G, Yevich S, Gazzera C, Basile D, Gatti M, et al. Fusion imaging and virtual navigation to guide percutaneous thermal ablation of hepatocellular carcinoma: a review of the literature. *Cardiovasc Intervent Radiol* (2019) 42(5):639–47. doi: 10.1007/s00270-019-02167-z
41. Toshikuni N, Tsutsumi M, Takuma Y, Arisawa T. Real-time image fusion for successful percutaneous radiofrequency ablation of hepatocellular carcinoma. *J Ultrasound Med* (2014) 33(11):2005–10. doi: 10.7863/ultra.33.11.2005
42. Minami Y, Minami T, Chishina H, Kono M, Arizumi T, Takita M, et al. US-US Fusion Imaging in Radiofrequency Ablation for Liver Metastases. *Dig Dis* (2016) 34(6):687–91. doi: 10.1159/000448857
43. Minami Y, Minami T, Hagiwara S, Ida H, Ueshima K, Nishida N, et al. Ultrasound-ultrasound image overlay fusion improves real-time control of radiofrequency ablation margin in the treatment of hepatocellular carcinoma. *Eur Radiol* (2018) 28(5):1986–93. doi: 10.1007/s00330-017-5162-8
44. Xu EJ, Lv SM, Li K, Long YL, Zeng QJ, Su ZZ, et al. Immediate evaluation and guidance of liver cancer thermal ablation by three-dimensional ultrasound/contrast-enhanced ultrasound fusion imaging. *Int J Hyperthermia* (2018) 34(6):870–6. doi: 10.1080/02656736.2017.1373306
45. Lv S, Long Y, Su Z, Zheng R, Li K, Zhou H, et al. Investigating the accuracy of ultrasound-ultrasound fusion imaging for evaluating the ablation effect via special phantom-simulated liver tumors. *Ultrasound Med Biol* (2019) 45(11):3067–74. doi: 10.1016/j.ultrasmedbio.2019.07.415
46. Minami Y, Minami T, Takita M, Hagiwara S, Ida H, Ueshima K, et al. Radiofrequency ablation for hepatocellular carcinoma: Clinical value of ultrasound-ultrasound overlay fusion for optimal ablation and local controllability. *Hepatol Res* (2020) 50(1):67–74. doi: 10.1111/hepr.13407
47. Minami T, Minami Y, Chishina H, Arizumi T, Takita M, Kitai S, et al. Combination guidance of contrast-enhanced US and fusion imaging in radiofrequency ablation for hepatocellular carcinoma with poor conspicuity on contrast-enhanced US/fusion imaging. *Oncology* (2014) 87 Suppl 1:55–62. doi: 10.1159/000368146
48. Song KD, Lee MW, Rhim H, Kang TW, Cha DI, Sinn DH, et al. Percutaneous US/MRI fusion-guided radiofrequency ablation for recurrent subcentimeter hepatocellular carcinoma: technical feasibility and therapeutic outcomes. *Radiology* (2018) 288:878–86. doi: 10.1148/radiol.2018172743
49. Lee MW, Lim HK. Management of sub-centimeter recurrent hepatocellular carcinoma after curative treatment: Current status and future. *World J Gastroenterol* (2018) 24:5215–22. doi: 10.3748/wjg.v24.i46.5215
50. Numata K, Fukuda H, Morimoto M, Kondo M, Nozaki A, Oshima T, et al. Use of fusion imaging combining contrast-enhanced ultrasonography with a perflubutane-based contrast agent and contrast-enhanced computed tomography for the evaluation of percutaneous radiofrequency ablation of hypervascular hepatocellular carcinoma. *Eur J Radiol* (2012) 81(10):2746–53. doi: 10.1016/j.ejrad.2011.11.052

51. Kariyama K, Nouso K, Wakuta A, Oonishi A, Toyoda H, Tada T, et al. Treatment of intermediate-stage hepatocellular carcinoma in Japan: Position of curative therapies. *Liver Cancer* (2020) 9:41–9. doi: 10.1159/000502479

Conflict of Interest: The authors declare that the research was conducted in the absence of any commercial or financial relationships that could be construed as a potential conflict of interest.

frontiers in Oncology

SYSTEMATIC REVIEW
published: 09 March 2021
doi: 10.3389/fonc.2021.600800

Comparative Effectiveness and Safety of High-Intensity Focused Ultrasound for Uterine Fibroids: A Systematic Review and Meta-Analysis

Yi Wang[1], Jinsong Geng[2], Haini Bao[2], Jiancheng Dong[2], Jianwei Shi[3] and Qinghua Xi[4]*

[1] Department of Radiology, Zhongshan Hospital, Fudan University, Shanghai, China, [2] Ministry of Education Virtual Research Center of Evidence-Based Medicine at Nantong University, Medical School of Nantong University, Nantong, China, [3] Shanghai Jiaotong University School of Medicine, Shanghai, China, [4] Affiliated Hospital of Nantong University, Nantong, China

OPEN ACCESS

Edited by:
Wei Yang,
Peking University Cancer Hospital, China

Reviewed by:
Song Wang,
Peking University Cancer Hospital, China
Hao Wu,
Peking University Cancer Hospital, China
Jinyun Chen,
Chongqing Medical University, China

***Correspondence:**
Jinsong Geng
gjs@ntu.edu.cn

Specialty section:
This article was submitted to Cancer Imaging and Image-directed Interventions, a section of the journal Frontiers in Oncology

Received: 31 August 2020
Accepted: 04 February 2021
Published: 09 March 2021

Citation:
Wang Y, Geng J, Bao H, Dong J, Shi J and Xi Q (2021) Comparative Effectiveness and Safety of High-Intensity Focused Ultrasound for Uterine Fibroids: A Systematic Review and Meta-Analysis. Front. Oncol. 11:600800. doi: 10.3389/fonc.2021.600800

Background: Uterine fibroids are common benign tumors among premenopausal women. High- intensity focused ultrasound (HIFU) is an emerging non-invasive intervention which uses the high-intensity ultrasound waves from ultrasound probes to focus on the targeted fibroids. However, the efficacy of HIFU in comparison with that of other common treatment types in clinical procedure remains unclear.

Objective: To investigate the comparative effectiveness and safety of HIFU with other techniques which have been widely used in clinical settings.

Methods: We searched the Cochrane Central Register of Controlled Trials, PubMed, EMBASE, Cumulative Index to Nursing & Allied Health Literature, Web of Science, ProQuest Nursing & Allied Health Database, and three Chinese academic databases, including randomized controlled trials (RCTs), non-RCTs, and cohort studies. The primary outcome was the rate of re-intervention, and the GRADE approach was used to interpret the findings.

Results: About 18 studies met the inclusion criteria. HIFU was associated with an increased risk of re-intervention rate in comparison with myomectomy (MYO) [pooled odds ratio (OR): 4.05, 95% confidence interval (CI): 1.82–8.9]. The results favored HIFU in comparison with hysterectomy (HYS) on the change of follicle-stimulating hormone [pooled mean difference (MD): −7.95, 95% CI: −8.92–6.98), luteinizing hormone (MD: −4.38, 95% CI: −5.17−3.59), and estradiol (pooled MD: 43.82, 95% CI: 36.92–50.72)]. HIFU had a shorter duration of hospital stay in comparison with MYO (pooled MD: −4.70, 95% CI: −7.46−1.94, $p < 0.01$). It had a lower incidence of fever (pooled OR: 0.15, 95% CI: 0.06–0.39, $p < 0.01$) and a lower incidence of major adverse events (pooled OR: 0.04, 95% CI: 0.00–0.30, $p < 0.01$) in comparison with HYS.

Conclusions: High-intensity focused ultrasound may help maintain feminity and shorten the duration of hospital stay. High-quality clinical studies with a large sample size, a long-term follow-up, and the newest HIFU treatment protocol for evaluating the re-intervention rate are suggested to be carried out. Clinical decision should be based on the specific situation of the patients and individual values.

Keywords: high intensity focused ultrasound (HIFU), uterine fibroids, meta-analysis, myomectomy, uterine arterial embolisation

INTRODUCTION

Uterine fibroids are common benign tumors which are rich in extracellular matrix among premenopausal women (1, 2). Fibroids can cause severe menstrual bleeding and menorrhagia, which may lead to iron deficiency anemia. Large fibroids can lead to pelvic pain and pressure on the rectum with painful or difficult defecation. Fibroids are the potential causes of recurrent miscarriages (3, 4). The conventional surgical approaches to fibroid treatment comprise hysterectomy (HYS) or abdominal myomectomy (MYO) for those desiring uterine preservation. Physicians are seeking new ways to treat uterine fibroids, which may allow patients to avoid invasive surgery. Minimally invasive techniques for the treatment of uterine fibroids have been developed in recent years, such as high-intensity focused ultrasound (HIFU), laparoscopic MYO, uterine artery embolization (UAE), and radiofrequency ablation (RFA) (5–7).

High-intensity focused ultrasound is an emerging intervention which uses the high-intensity ultrasound waves from ultrasound probes to focus on the targeted fibroids. It is a non-invasive technique that causes instant coagulated necrosis in a well-circumscribed area of a few millimeters in diameter and can be performed under the guidance of either MRI or ultrasound. HIFU has been increasingly performed in China and has now become a preferred therapy of uterine fibroids in some hospitals, especially for women with fibroid-associated bulk symptoms who desire for uterine-sparing and fertility-sparing surgeries.

Recent studies have compared the effectiveness of HIFU with that of some treatment techniques. Nevertheless, the results obtained from individual studies are sometimes contradictory. At present, the comparative benefits and risks of HIFU for the treatment of uterine fibroids remain unclear. The objective of the present systematic review and meta-analysis is to evaluate the comparative effectiveness and safety of HIFU in the treatment of uterine fibroids. We specifically aimed to compare HIFU with different techniques which have been widely used in clinical practice.

Abbreviations: HIFU, high-intensity focused ultrasound; UAE, uterine artery embolization; MYO, myomectomy; HYS, hysterectomy; RFA, radiofrequency ablation; FSH, follicle-stimulating hormone; LH, luteinizing hormone; E2, estradiol; MRIgHIFU, magnetic resonance image-guided HIFU; USgHIFU, ultrasound-guided HIFU.

MATERIALS AND METHODS

Search Strategy and Study Selection

Trials were identified by searching the Cochrane Central Register of Controlled Trials (CENTRAL), PubMed, EMBASE, Cumulative Index to Nursing & Allied Health Literature (CINAHL), Web of Science, and ProQuest Nursing & Allied Health Database. A search of Chinese academic databases, including Wanfang Data, VIP Chinese Science and Technique Journals Database (VIP-CSTJ), and China National Knowledge Infrastructure (CNKI), was also carried out. Among the studies published in Chinese journals, only the journals indexed by the ExLibris Chinese Core Journal Searching System were considered to reduce publication bias. The protocol of this systematic review has been registered at PROSPERO (No. CRD42018115773). Databases were searched on July 8, 2020. A detailed search strategy was given (**Appendix 1**). There were no limitations to languages of the included studies. Reference lists were examined for any additional relevant studies which were not identified through the search. Randomized controlled trials (RCTs), non-RCTs, and cohort studies were included in the review.

Two review authors (Wang Y and Geng JS) independently screened all titles and abstracts of publications identified by the search to assess their eligibility. We excluded at this stage the publications that did not meet the criteria. Following the screening, we assessed the full texts of eligible citations for inclusion. We reached a consensus on the selection of trials and the final list of studies. We consulted a third member of our review team (Dong JC) when a consensus could not be reached. The inclusion criteria for the full text were observational studies, RCTs, or non-RCTs published in English before July 8, 2020, which provide data on the clinical assessment of outcomes of patients with uterine fibroids after being treated with HIFU and the other clinically used techniques as comparison groups. In order to build a more comprehensive database concerning this subject, there is a need for the inclusion of publications in Chinese or other languages in our study. The following criteria were used for exclusion: (1) reviews, conference abstracts, case reports, opinions, and comments; (2) patients having undergone earlier treatment for uterine fibroids; (3) no outcome of interest was found; and (4) no suitable data (no standard deviation or interquartile range) can be used for statistical analysis.

Eligibility Criteria

(a) Types of participants: Women with a definite diagnosis of uterine fibroids, regardless of age, were included. Patients

who had previous intervention for fibroids were excluded; (b) Types of intervention and comparison: Both MRI-guided HIFU (MRIgHIFU) and ultrasound-guided HIFU (USgHIFU) were included. Comparison groups comprised of techniques other than HIFU, which were usually used in clinical practice, such as UAE, RFA, MYO (including laparoscopy MYO), and HYS.

Data Extraction

The following metrics were extracted from the eligible articles: (a) study characteristics: first author name, publication date, participant factors (patient's age, number, fibroid size), trial design, details of intervention and control, and follow-up information; (b) primary outcome: the rate of re-intervention after using HIFU or comparative techniques; and (c) secondary outcomes: defining the incidence of abnormal pregnancy in the abnormal pregnancy percentage for those patients with uterine fibroids who got pregnant after the treatment with HIFU or comparative techniques. The change of serum sex hormones, including follicle-stimulating hormone (FSH), luteinizing hormone (LH), and estradiol (E2), was assessed. The days of hospital stay for patients with uterine fibroids during the treatment period were calculated. The incidence of complications and adverse events were noted. Significant clinical complications were defined as fever within 2–3 days after the treatment, and the incidence of patients experiencing at least one major adverse event within 6 weeks after the treatment. Studies without having any of the abovementioned outcomes were excluded from the meta-analysis.

Assessment of Risk of Bias

The risk of bias of RCTs was assessed according to "The Cochrane Collaboration's tool" (8). The characteristics of RCTs were evaluated as follows: randomization, allocation concealment, blinding of outcome assessment, incomplete outcome data, and selective reporting. The risk of bias of non-RCTs was assessed according to "Methodological Index for Non-randomized Studies" (MINOS) (9). We deleted the item "'endpoints appropriate to the aim of the study" from MINOS since not every end point of the published papers was included in our systematic review. Therefore, the remaining 11 characteristics of non-RCTs were evaluated. Cohort studies were assessed in accordance with a "Newcastle-Ottawa Quality Assessment Scale" (NOS) (10). Characteristics of cohort studies including the selection of cohorts, comparability of cohorts, and the outcomes were evaluated.

The GRADE approach (11) was used to interpret findings for the primary outcomes, and the GRADE profile allowed us to import data from Review Manager 5.3 to create "Summary of findings" tables. We downgraded the evidence quality from "high quality" by one level for serious (or by two for very serious) study limitations (risk of bias), inconsistency, indirectness of evidence, imprecision of effect estimates, or potential publication bias.

Data Synthesis and Statistical Analysis

Data synthesis and statistical analysis were presented using Review Manager 5.3 (RevMan, Review Manager 5.3). We used odds ratio (OR) with 95% confidence interval (CI) for dichotomous data. We used mean difference (MD) with 95% CI for continuous data when data were provided as mean and SD. The heterogeneity of intervention has effects among the studies using the standard Chi-square test (p-value). We considered a value of $p < 0.10$ as evidence of heterogeneity (8). In case of no substantial or considerable heterogeneity, we utilized a fixed-effects model in the data synthesis. Otherwise, we used a random-effects model. Moreover, a subgroup analysis was designed for each outcome according to the different types of comparisons. In addition, a sensitivity analysis was performed to evaluate the stability of this meta-analysis, and an intention-to-treat analysis was conducted when available to test the robustness of the results. Finally, the Begg–Mazumdar's rank test and the Egger's regression test were used to assess publication bias, in which a value of $p < 0.05$ was considered statistically significant. We only evaluated the publication bias of fever rate, since the number of included studies of other outcomes was less than seven, which was considered not sufficient for an analysis.

RESULTS

Study Characteristics

About 18 studies were included in the review (12–27). About three were RCTs (16, 18, 21), seven were non-RCTs (12, 15, 17, 22–24, 26), and eight were cohort studies (13, 14, 19, 20, 25, 27–29). In Barnard et al. (19), only the cohort data were included in the meta-analysis. One study (17) was carried out in 14 medical centers in USA, Israel, UK, and Germany, and the other studies were conducted in China ($n = 13$), USA ($n = 1$), Germany ($n = 1$), The Netherlands ($n = 1$), and Israel ($n = 1$). The average age of women who participated in the included studies ranged from 33.60 to 46.54 years. PRISMA Flow diagram of study selection is listed in **Figure 1**. Characteristics of included studies are listed in **Table 1**.

About three RCTs with unclear risk of bias were included in the systematic review. For seven non-RCTs, the average score was 15.4 according to MINOS, indicating the moderate quality. Blinding was not used in the non-RCTs, and some objective outcomes, such as abnormal pregnancy and serum sex hormones, were unlikely to be influenced by the lack of blinding. However, according to MINOS, only the reported and adequate items could be given two scores. Seven of the eight included cohort studies were equal to or more than six stars according to NOS, which suggested a moderate quality. Detailed information on the summary of the risk of bias is presented in **Supplementary Tables 1–3**.

Meta-Analysis

Primary Outcomes

Rate of Re-intervention

High-intensity focused ultrasound was associated with an increased risk of re-intervention rate in comparison with UAE (pooled OR: 11.99, 95% CI: 5.17–27.83, $p < 0.01$) and MYO (pooled OR: 4.05, 95% CI: 1.82–8.99, $p < 0.01$) (**Figure 2**).

The results from the intention-to-treat analysis also found an increased risk of re-intervention for HIFU in comparison

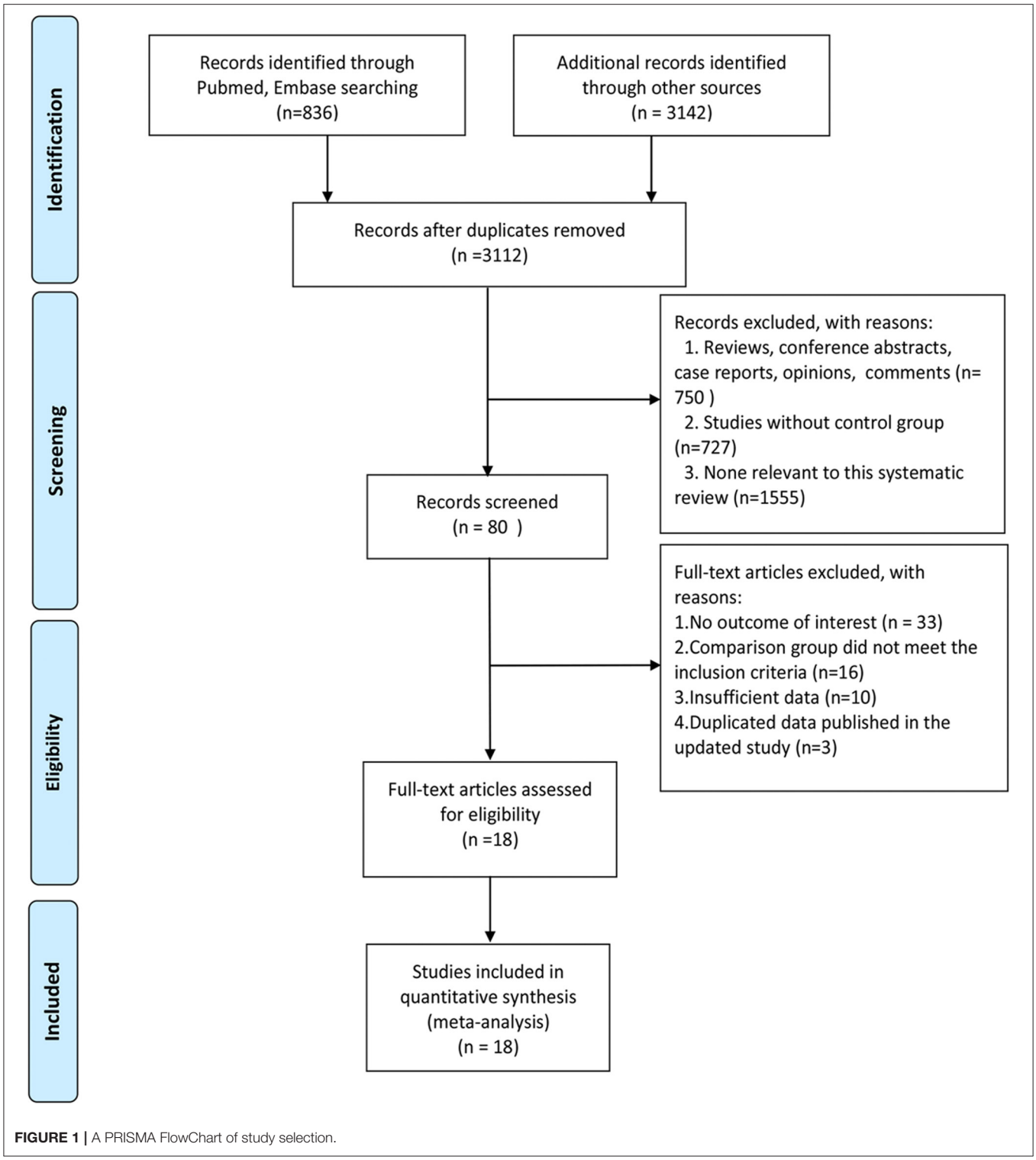

FIGURE 1 | A PRISMA FlowChart of study selection.

with UAE (pooled OR: 9.33, 95% CI: 4.26–20.47, $p < 0.01$) and MYO (pooled OR: 4.51, 95% CI: 2.02–10.07, $p < 0.01$) (**Supplementary Figure 1**). The sensitivity analysis did not change the increased re-intervention rate for HIFU in comparison with UAE and MYO (**Supplementary Figure 2**).

The GRADE evidence profile is given in **Supplementary Table 4**, which lists the results of relative effects and absolute effects. The overall quality of evidence regarding HIFU vs. UAE and HIFU vs. MYO was moderate and low, respectively.

TABLE 1 | Characteristics of included studies.

References	Study design	Setting	No. of patients	Age of participants (years)*	Manufactures of HIFU	Outcomes of interests (duration of follow-up after treatment)
Taran et al. (17)	Non-RCT	14 medical centers in USA, Israel, UK and Germany	HIFU:109 HYS: 83	HIFU:44.8 ± 4.9; HYS:44.4 ± 5.6	InSightec	Fever (2 days)
Meng et al. (16)	RCT	China	HIFU: 50 RFA: 50	HIFU:35.6 ± 6.0; RF:39.2 ± 5.7	Shanghai Aishen Technology	Fever (2 days)
Chen et al. (12)	Non-RCT	China	HIFU: 30 MYO(abdominal/laparoscopic MYO):30 HYS: 30	HIFU:38.8; MYO:38.4; HYS:39.1	Chongqing Haifu Technology	Change of serum sex hormones (6 months)
Froeling et al. (13)	Retrospectivecohort study	Germany	HIFU: 36 UAE: 41	HIFU:36.2(29.2–41.0); UAE:42.7(33.6–52.2)	InSightec	Rate of re-intervention (60.7–61.9 months)
Liu et al. (15)	Non-RCT	China	HIFU: 30 HYS: 30	HIFU:39.25 ± 3.08; HYS:41.13 ± 3.22	Chongqing Haifu Technology	Change of serum sex hormones (1 year)
Wang et al. (18)	RCT	China	HIFU: 60 MYO (abdominal MYO): 60	HIFU:39.92 ± 5.07; MYO:38.60 ± 4.36	Chongqing Haifu Technology	Fever (3 days)
Ikink et al. (14)	Retrospective cohort study	Netherlands	HIFU: 51 UAE: 68	HIFU:46(43–49); UAE:43(41–46)	Philips Healthcare	Rate of re-intervention (1 year)
Wang et al. (23)	Non-RCT	China	HIFU: 89 MYO (laparoscopic MYO): 41	HIFU:37.9 ± 5.5; MYO:38.4 ± 5.0	Chongqing Haifu Technology	Days of hospital stay; Fever (2 days); Major adverse events (42 days)
Wang et al. (24)	Non-RCT	China	HIFU: 86 HYS: 81	HIFU:33.6 ± 4.6; HYS:34.1 ± 4.7	Chongqing Haifu Technology	Fever (2 days); Major adverse events (42 days)
Xu et al. (26)	Non-RCT	China	HIFU: 30 MYO (laparoscopic MYO): 34	Both groups:37.7	Chongqing Haifu Technology	Change of serum sex hormones (6 months)
Barnard et al. (19) *	Prospective cohort study	USA	HIFU: 43 UAE: 40	HIFU:44.0 ± 4.3; UAE:44.3 ± 5.2	InSightec	Rate of re-intervention (42 days); Major adverse events (42 days)
Lin et al. (22)	Non-RCT	China	HIFU: 60 UAE: 54	HIFU:39.5 ± 7.4; UAE: 38.7 ± 6.2	Chongqing Haifu Technology	Incidence of abnormal pregnancy (2 years); Change of serum sex hormones (2 years); Fever (2 days)
Xiong et al. (25)	Retrospective cohort study	China	HIFU: 206 MYO (laparoscopic MYO): 317	HIFU:41.37 ± 5.68; MYO:40.48 ± 5.58	Chongqing Haifu Technology	Rate of re-intervention (1.5–4 years); Incidence of abnormal pregnancy (1.5–4 years); Days of hospital stay
Chen et al. (20)	Prospective cohort study	China	HIFU: 1,353 MYO (abdominal/laparoscopic MYO): 586 HYS: 472	HIFU:41.31 ± 5.08; MYO:40.93 ± 5.02; HYS:46.54 ± 3.48	Chongqing Haifu Technology	Rate of re-intervention (1 year); Days of hospital stay; Fever (2 days); Major adverse events (30 days)
Li et al. (21)	RCT	China	HIFU: 60 MYO (laparoscopic MYO): 60	HIFU:38.4 ± 5.4; MYO:39.3 ± 6.82	Chongqing Haifu Technology	Incidence of abnormal pregnancy (3 years); Days of hospital stay
Mohr-Sasson et al. (27)	Retrospective cohort study	Israel	HIFU: 68 MYO#(laparoscopic MYO): 64	HIFU:44(38–47); MYO:38(34–43)	InSightec	Rate of re-intervention (31–36 months)

(Continued)

TABLE 1 | Continued

References	Study design	Setting	No. of patients	Age of participants (years)*	Manufactures of HIFU	Outcomes of interests (duration of follow-up after treatment)
Wu et al. (28)	Retrospective cohort study	China	HIFU: 219 MYO (laparoscopic MYO): 224	HIFU:31.6 (22–42); MYO:32.4 (25–41)	Chongqing Haifu Technology	Incidence of abnormal pregnancy (1–8 years)
Hu et al. (29)	Prospective cohort study	China	HIFU: 39 MYO (hysteroscopic MYO): 42	HIFU:43.0 ± 5.6 MYO:41.3 ± 4.4	Chongqing Haifu Technology	Days of hospital stay

HIFU, high intensity focused ultrasound; UAE, uterine artery embolization; MYO, myomectomy; HYS, hysterectomy; RFA, radio frequency ablation.

**Mean ± SD or Median(range).*

#*In the myomectomy group, 29 women (45.3%) received robotically assisted laparoscopic myomectomy (Da Vinci Surgical system).*

Secondary Outcomes

Incidence of Abnormal Pregnancy

Lin et al. (22) analyzed the incidence of abnormal pregnancy between HIFU and UAE. The results obtained from this study did not find any statistical differences between these two techniques (OR: 1.20, 95% CI: 0.42–3.40, $p = 0.73$) (**Figure 3**).

Statistically significant differences were not found when comparing HIFU with MYO (pooled OR: 0.82, 95% CI: 0.46–1.46, $p = 0.50$). The results obtained from the intention-to-treat analysis did not present any change to the conclusion (**Supplementary Figure 3**).

Change of Serum Sex Hormones From Baseline

There were no statistically significant differences between HIFU and MYO on the FSH, LH, and E2 levels (**Table 2**, **Supplementary Figures 4–6**).

However, HIFU seemed to be better in terms of maintaining the serum FSH, LH, and E2 levels in comparison with HYS (**Table 3**, **Supplementary Figures 4–6**).

Furthermore, Lin et al. (22) compared the change of serum sex hormones between HIFU and UAE. Data from this study did not find any statistically significant differences between these two techniques for FSH (MD: −0.20, 95% CI: −0.91–0.51, $p = 0.58$), LH (MD: 0.10, 95% CI: −0.55–0.75, $p = 0.76$), and E2 (MD: −1.00, 95% CI: −7.42–5.42, $p = 0.76$) (**Supplementary Figures 4–6**).

Days of Hospital Stay

Although statistical heterogeneity was found for the included studies ($p < 0.01$, $I^2 = 93\%$) (**Figure 4**), the direction of the individual studies remains the same and the results of meta-analysis favored the shorter duration of hospital stay for HIFU in comparison with MYO (pooled MD: −4.70, 95% CI: −7.46−1.94, $p < 0.01$).

The results from the included study (20) also favored HIFU in comparison with HYS (MD: −6.90, 95% CI: −7.24−6.56, $p < 0.01$).

Incidence of Complications and Adverse Events

Incidence of Fever

Meta-analysis showed a lower incidence of fever in HIFU in comparison with MYO (pooled OR: 0.13, 95% CI: 0.04–0.50, $p < 0.01$); HIFU could also decrease the incidence of fever in comparison with HYS (pooled OR: 0.15, 95% CI: 0.06–0.39, $p < 0.01$) (**Figure 5**).

The sensitivity analysis showed the beneficial effects of HIFU in comparison with HYS (**Supplementary Figure 7**). However, only one study (23) was included in the sensitivity analysis to compare the incidence of fever between HIFU and MYO, and no significant statistical differences were identified.

Lin et al. (22) investigated the incidence of fever in HIFU in comparison with UAE, and the results favored HIFU (OR: 0.09, 90% CI: 0.04–0.21, $p < 0.01$). The results obtained from the study by Meng et al. (16) favored HIFU in comparison with RFA (OR: 0.19, 90% CI: 0.04–0.93, $p = 0.04$).

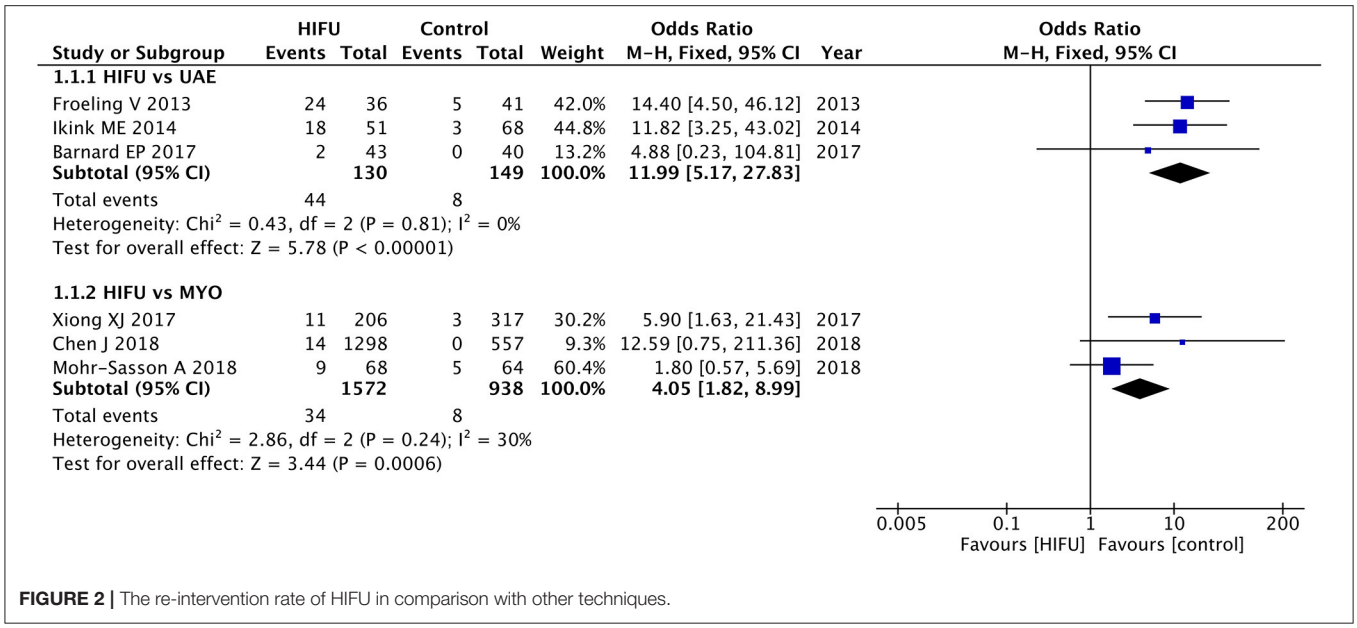

FIGURE 2 | The re-intervention rate of HIFU in comparison with other techniques.

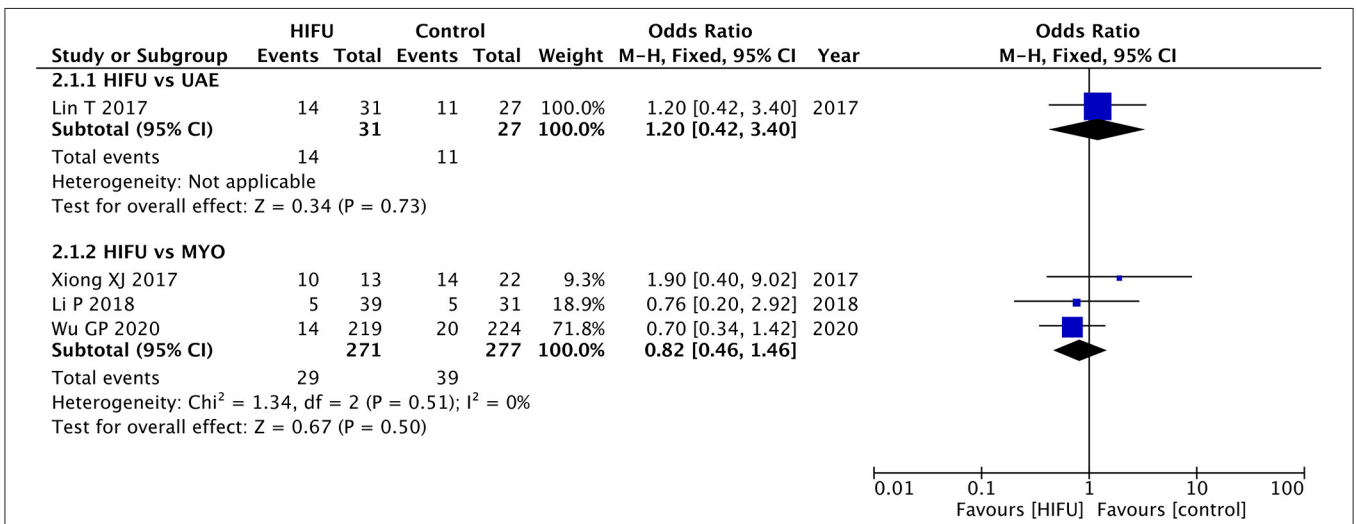

FIGURE 3 | Abnormal pregnancy incidence of HIFU in comparison with other techniques.

TABLE 2 | Meta-analysis of serum sex hormones change between HIFU and MYO.

Outcome measure	Number of studies	Test for heterogeneity (*P*-value)	Pooled MD (95% CI)	Test for overall effect (*P*-value)
FSH	2 (12, 26)	0.93	0.00 (−0.58 0.59)	0.99
LH	2 (12, 26)	0.65	−0.11 (−0.73 0.51)	0.73
E2	2 (12, 26)	0.61	1.14 (−3.29 5.57)	0.24

TABLE 3 | Meta-analysis of serum sex hormones change between HIFU and HYS.

Outcome measure	Number of studies	Test for heterogeneity (*P*-value)	Pooled MD (95% CI)	Test for overall effect (*P*-value)
FSH	2 (12, 26)	0.60	−7.95 (−8.92 −6.98)	<0.01
LH	2 (12, 26)	0.02	−4.38 (−5.17 −3.59)	<0.01
E2	2 (12, 26)	0.73	43.82 (36.92 50.72)	<0.01

Incidence of Major Adverse Events

The results of the meta-analysis did not found statistical significant differences between HIFU and MYO (pooled OR: 0.11, 95% CI: 0.00–4.41, $p < 0.01$) (**Figure 6**). However, significant heterogeneity among the included studies was identified ($p < 0.01$).

The meta-analysis favored the lower incidence of major adverse events in HIFU in comparison with HYS (pooled OR:

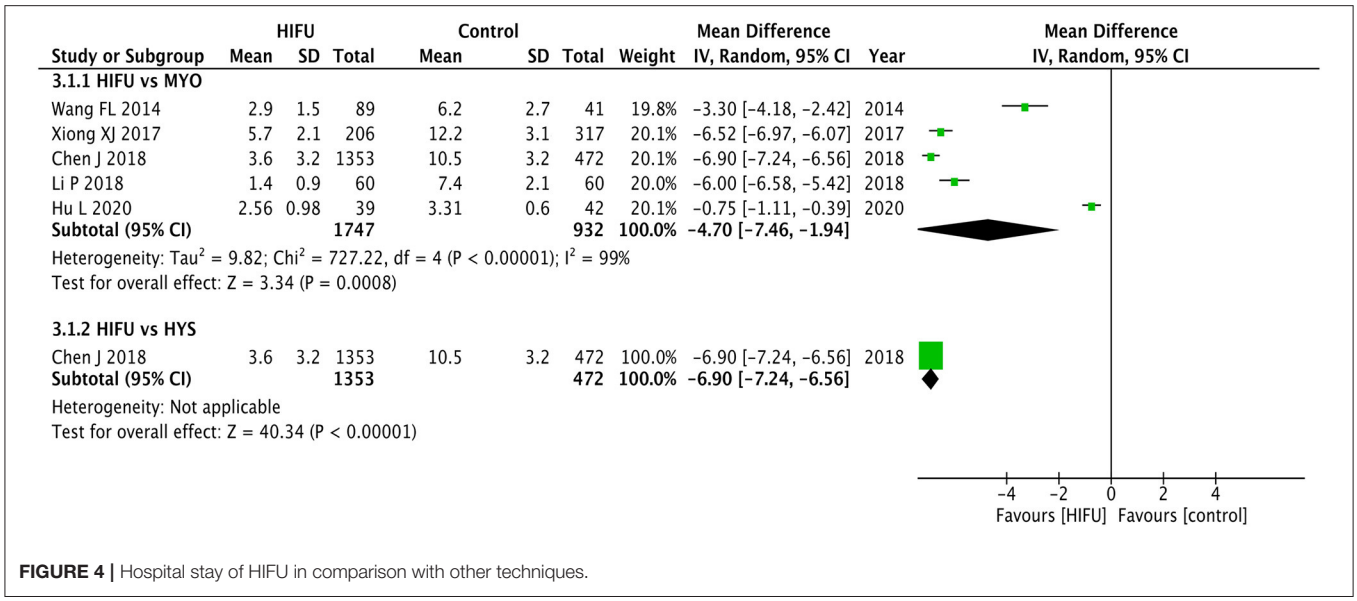

FIGURE 4 | Hospital stay of HIFU in comparison with other techniques.

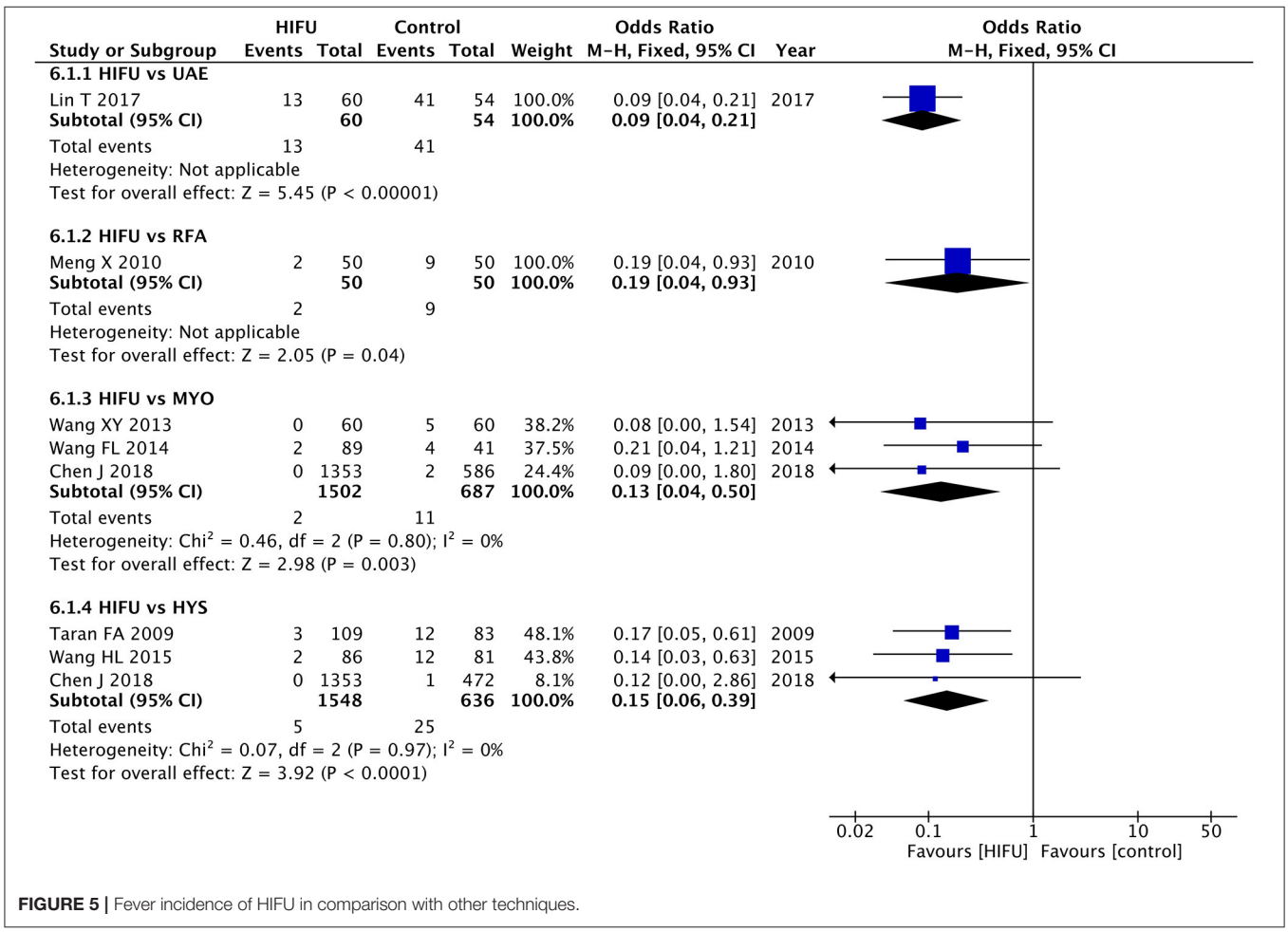

FIGURE 5 | Fever incidence of HIFU in comparison with other techniques.

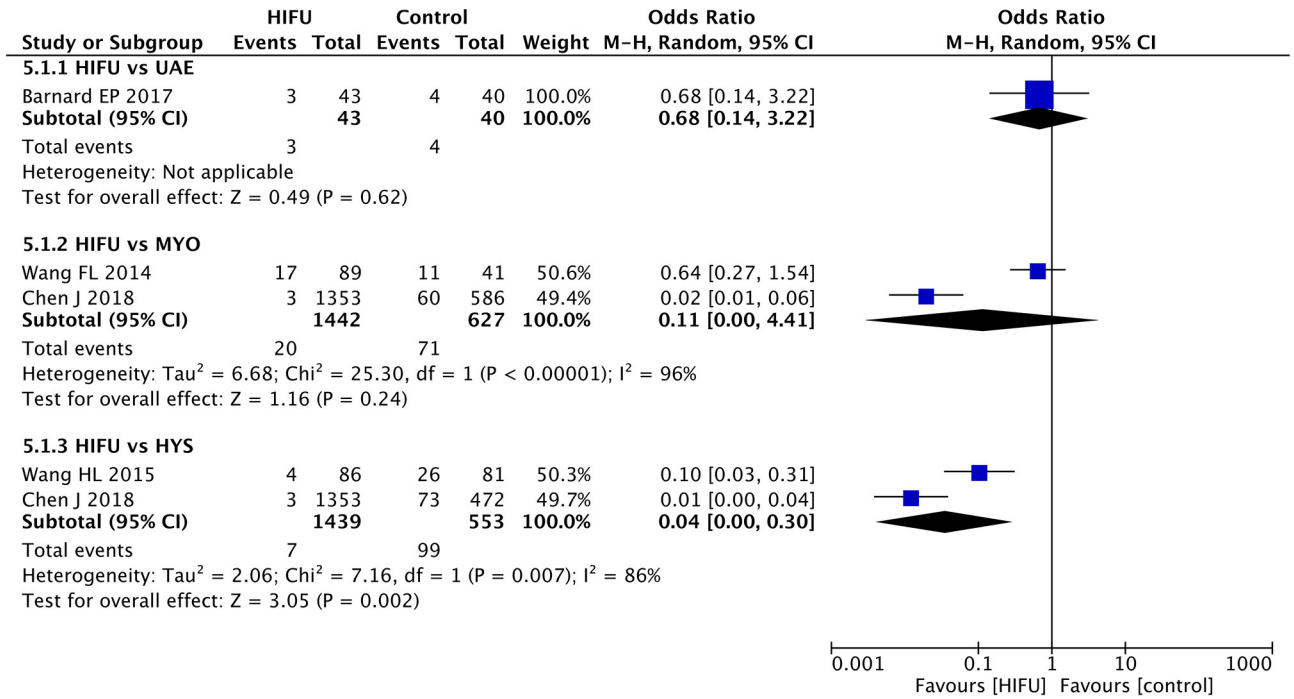

FIGURE 6 | Major adverse events of HIFU in comparison with other techniques.

0.04, 95% CI: 0.00–0.30, $p < 0.01$). Although heterogeneity of the included studies was identified ($p < 0.01$), the results of the individual studies were consistent with those of the meta-analysis.

No statistical significant difference was identified between HIFU and UAE from the included study (19) (OR: 0.68, 95% CI: 0.14–3.22, $p = 0.62$).

Assessment of Bias Across Included Studies

No significant publication bias was observed in the outcome of fever rate (Begg–Mazumdar's test: $p = 0.81$, Egger's test: $p = 0.58$).

DISCUSSION

Uterine fibroids are the most common tumors of the female reproductive tract. Due to lack of the latest published synthesized evidence on primary studies on the relative efficacy and safety of the different types of treatment techniques, choosing the best option for a patient might sometimes become difficult. When counseling a patient about the different treatment options, the re-intervention risk is a crucial aspect to consider. We demonstrated that HIFU had the least promising outcome regarding the re-intervention incidence in comparison with UAE and MYO. Our results are consistent with another meta-analysis (30), which showed that the cumulative risk of re-intervention for UAE is 14.4% and for HIFU is 54% at 60 months after initial therapy. Previous studies (31–33) have demonstrated that the non-perfused volume (NPV) ratio is an optimal predictor of re-intervention rates, and the fibroids with NPVs more than 50–60% were less likely to need additional treatments. Verpalen et al. (33) conducted subgroup analyses of HIFU stratified by treatment protocols and found that the re-intervention rates in an unrestrictive protocol of HIFU are significantly lower than those of a restrictive protocol after a 7-years follow-up. However, the studies included in the review did not classify patients from the HIFU group according to characteristics of fibroids and a specific HIFU treatment option. Hence, the outcomes of our study should be interpreted cautiously, which possibly cause an underlying confoundingresult. In the future, high-quality clinical studies should be implemented to achieve more specific results to guarantee further modification of treatment protocol after evaluating the individual condition. Wang et al. (34) compared the efficacy of HIFU and other uterine-sparing surgeries for the treatment of submucosal fibroids with an deep intramural extension, concluding that HIFU had lower re-intervention rates. Simon et al. (35) implemented a novel HIFU treatment using a modified energy transmission and oxytocin augmentation, which resulted in lower re-intervention rates in comparison with UAE. Moreover, a few studies (36, 37) pointed out that the ablation effect of HIFU could be enhanced by using a microbubble contrast agent, which could significantly increase the post-operative NPV ratio and reduce the incidence of recurrence of uterine fibroids.

Hysterectomy is the most common treatment for symptomatic fibroids and is considered to be the definitive therapy. HYS was recommended for premenopausal women who had no wish to preserve their fertility (38). However,

childbearing-age women with multiple submucosal and intramural fibroids presented with menorrhagia and pelvic pain also desire future pregnancies and was concerned about the loss of femininity. To date, MYO remains the gold standard for treating fibroid-related symptoms in women who desire fertility preservation. It was recommended by the guideline that MYO might be considered to optimize pregnancy outcomes in women with asymptomatic cavity-distorting myomas (39). In a systematic review (40), MYO has higher successful pregnancy rates (75.6%) in comparison with UAE (60.6%), which might be explained by a high risk of disruption of blood supply to the ovary and intima after the UAE treatment. Liu et al. (41) reported that a successful vaginal delivery rate after the HIFU ablation had reached 80.8%. Other studies (28, 42) reported that pregnancy outcomes of HIFU were not compromised, and in comparison with laparoscopic MYO, HIFU is conducive to decreasing cesarean delivery rate since HIFU focuses on the lesion without damaging the surrounding normal tissue of the uterine. On the contrary, conventional surgery would have a high risk of pelvic cavity adhesion. However, HIFU has a higher incidence of preterm birth, through fetal distress.

Lee et al. (43) and Cheung et al. (44) assessed the changes in anti-mullerian hormone levels after the ablation of uterine fibroids, which also showed that HIFU did not impair ovarian function. We found that HIFU presented an obviously advantage over HYS with significantly less fluctuations in hormonal mediators, and it is non-inferior to UAE and MYO. However, the results should be interpreted with caution, since two of the included studies (12, 26) analyzed the hormone levels only at 6 months after the treatment, and only one study (22) was included to compare the change of serum sex hormones between HIFU and UAE.

High-intensity focused ultrasound is associated with fewer adverse events; therefore, the duration of hospital stay is shorter. The reduction of the days of hospital stay has widely attracted attention from policymakers as an important way to improve efficiency and quality of medical care (45, 46). High cost effectiveness of the protocol can largely alleviate the economic and social burden. Nevertheless, there are no current studies reporting the days of hospital stay by comparing HIFU and other minimally invasive therapies like UAE or RFA.

Patients have different preferences in regard to surgical procedures and the potential risk of adverse outcomes. Therefore, we analyzed the incidence of serious adverse events. HIFU was also more favorable in comparison with MYO and HYS on the incidence of major adverse events after the treatment. In a multicenter large cohort study (47), a total of 0.408% major complications of HIFU have been observed, while in another study (48), laparoscopic MYO had an incidence of 3.5% significant complications. Meanwhile, it is worth noting that Verpalen et al. (49) demonstrated that there is a significant difference between Sonalleve (17.6%) and Exblate (5.7%) when evaluating the rate of adverse events.

Evidence for the use of HIFU in our systematic review was mainly Available online at non-randomized studies, and robust evidence of evaluating comparative efficacy and safety of HIFU for the treatment of uterine fibroids in these studies remains lacking. However, data from cohort studies and non-RCTs could not be underestimated, since these studies can better mimic the real clinical setting in comparison with RCTs (50–52). Furthermore, RCTs are not always feasible to be conducted in certain clinical circumstances. RCTs, non-RCTs, and cohort studies are valuable to determine more accurate outcomes in clinical practice.

CONCLUSION

This study provides clinicians with latest published comparative evidence between HIFU and other widely used clinical treatment methods. Currently, patients usually prefer less invasive options for the treatment regardless of pregnancy. Our results found that HIFU seemed to be safer and more effective than HYS. HIFU was non-inferior to MYO in maintaining the serum sex hormone levels, as well as the prevention of abnormal pregnancy, and was more effective than MYO in reducing the incidence of fever. HIFU could become a potential efficient technique to shorten the duration of hospital stay. The comparative efficacy and safety of HIFU with other types of minimally invasive techniques, such as UAE, still deserve to be further assessed. High-quality clinical studies with a large sample size and a long-term follow-up are suggested to be performed in future to further evaluate the re-intervention rate of HIFU, utilizing the advanced treatment protocol and equipment in comparison with the other treatment techniques.

It is crucial to realize the function of these treatment options in various clinical scenarios so that appropriate consultation could be performed. Patients should be informed of potential benefits and harms and should be actively involved in the choice of surgery. The treatment decision depends on the clinical symptoms the desire of patients for subsequent fertility and pregnancy, as well as efficacy and need for repeated interventions.

DATA AVAILABILITY STATEMENT

The original contributions presented in the study are included in the article/**Supplementary Material**, further inquiries can be directed to the corresponding author/s.

DISCLOSURE

National Natural Science Foundation of China (Grant No. 71603138) was used for this research project. The authors declare that the research was conducted in the absence of any commercial or financial relationships that could be construed as a potential conflict of interest.

AUTHOR CONTRIBUTIONS

YW, JG, and HB contributed to the conception and design of the study. HB and QX were responsible for data acquisition and interpretation. YW and QX performed the statistical analysis. YW and JG wrote sections of the manuscript. All authors contributed to manuscript revision, read, and approved the submitted version.

SUPPLEMENTARY MATERIAL

The Supplementary Material for this article can be found online at: https://www.frontiersin.org/articles/10.3389/fonc.2021.600800/full#supplementary-material

Supplementary Figure 1 | Re-intervention rate of high-intensity focused ultrasound (HIFU) in comparison with other techniques: intention to treat (ITT) analysis.

Supplementary Figure 2 | Re-intervention rate of HIFU in comparison with other techniques: sensitivity analysis.

Supplementary Figure 3 | Abnormal pregnancy incidence of HIFU in comparison with other techniques: ITT analysis.

Supplementary Figure 4 | Follicle-stimulating hormone (FSH) change of HIFU in comparison with other techniques.

Supplementary Figure 5 | Luteinizing hormone (LH) change of HIFU in comparison with other techniques.

Supplementary Figure 6 | Estradiol (E2) change of HIFU in comparison with other techniques.

Supplementary Figure 7 | Fever incidence of HIFU in comparison with other techniques: sensitivity analysis.

Supplementary Table 1 | Risk of bias of included randomized controlled trials.

Supplementary Table 2 | Risk of bias of included non-randomized controlled trials. *For outcomes which were included in the systematic review. The items were scored as 0 (not reported), 1 (reported but inadequate), or 2 (reported and adequate).

Supplementary Table 3 | Risk of bias of included cohort studies. *For outcomes which were included in the systematic review. # Study controlled for: number of fibroid tumors/volume of all fibroid tissues or the maximal fibroid diameter, and age of patients. A study could be awarded a maximum of one star for each numbered item within the "Selection" and "Outcome" categories, and a maximum of two stars could be given for "Comparability."

Supplementary Table 4 | GRADE evidence profile of the outcome of rate of re-intervention. 1. Cohort studies were assessed in accordance with the Newcastle-Ottawa Quality Assessment Scale (NOS), and the best quality of cohort studies should be those with nine stars. However, six stars were given to the three included studies. 2. The results from Barnard et al. (19), which only observed the short-term outcomes, did not find any statistical significant differences between HIFU and UAE. 3. Pooled odds ratio (OR) was 11.99 (95% confidence interval: 5.17–27.83, $p < 0.001$). 4. For Froeling et al. (13), volume of all fibroid tissues was significantly larger ($p = 0.005$) in the uterine artery embolization (UAE) group at baseline. However, in Ikink et al. (14), the maximum fibroid diameter and age at baseline were significantly higher ($p < 0.005$) in the MR-HIFU group. 5. Cohort studies were assessed in accordance with the NOS, and the best quality of cohort studies should be those with nine stars. Eight, seven, and five stars were given to the three included studies. 6. The results from Chen et al. (20) and Mohr-Sasson et al. (27) did not find any statistical significant differences between high-intensity focused ultrasound (HIFU) and myomectomy (MYO). 7. Pooled OR was 4.05 (95% CI 1.82–8.99, $p < 0.001$). 8. In Chen et al. (20), the mean age of the HIFU group was lower than that of the surgery group, and the uterine volume was smaller. In Mohr-Sasson et al. (27), women in the laparoscopic MYO group were younger ($p < 0.001$), and multiple uterine fibroid tumors were more common in the laparoscopic MYO group ($p < 0.001$).

REFERENCES

1. Donnez J, Dolmans MM. Uterine fibroid management: from the present to the future. *Hum Reprod Update.* (2016) 22:665–86. doi: 10.1093/humupd/dmw023
2. Stewart EA, Laughlin-Tommaso SK, Catherino WH, Lalitkumar S, Gupta D, Vollenhoven B. Uterine fibroids. *Nat Rev Dis Primers.* (2016) 2:16043. doi: 10.1038/nrdp.2016.43
3. Stewart EA. Clinical practice. Uterine fibroids. *N Engl J Med.* (2015) 372:1646–55. doi: 10.1056/NEJMcp1411029
4. Chen YH, Lin HC, Chen SF, Lin HC. Increased risk of preterm births among women with uterine leiomyoma: a nationwide population-based study. *Hum Reprod.* (2009) 24:3049–56. doi: 10.1093/humrep/dep320
5. Iversen H, Dueholm M. Radiofrequency thermal ablation for uterine myomas: long-term clinical outcomes and reinterventions. *J Minim Invas Gynecol.* (2017) 24:1020–8. doi: 10.1016/j.jmig.2017.05.021
6. Zhao WP, Han ZY, Zhang J, Liang P. A retrospective comparison of microwave ablation and high intensity focused ultrasound for treating symptomatic uterine fibroids. *Europ J Radiol.* (2015) 84:413–7. doi: 10.1016/j.ejrad.2014.11.041
7. Vilos GA, Allaire C, Laberge PY, Leyland N. The management of uterine leiomyomas. *J Obstetr Gynaecol Canada.* (2015) 37:157–78. doi: 10.1016/S1701-2163(15)30338-8
8. Cochrane Handbook for Systematic Reviews of Interventions Version 5.1.0 [updated March 2011]. *The Cochrane Collaboration.* (2011). Available online at: http://handbook-5-1.cochrane.org/
9. Slim K, Nini E, Forestier D, Kwiatkowski F, Panis Y, Chipponi J. Methodological index for non-randomized studies (minors): development and validation of a new instrument. *ANZ J Surg.* (2003) 73:712–6. doi: 10.1046/j.1445-2197.2003.02748.x
10. Wells GA, D O'Connell BS, Peterson J, Welch V, Losos M, Tugwell P. The Newcastle-Ottawa Scale (NOS) for assessing the quality of nonrandomised studies in meta-analyses (2013). Available online at: http://www.ohri.ca/programs/clinical_epidemiology/oxford.asp
11. Guyatt G, Oxman AD, Akl EA, Kunz R, Vist G, Brozek J, et al. GRADE guidelines: 1. Introduction-GRADE evidence profiles and summary of findings tables. *J Clin Epidemiol.* (2011) 64:383–94. doi: 10.1016/j.jclinepi.2010.04.026
12. Chen H, Huang Y, Zhang W, LI S, Chen X. Study of influence on ovarian function by HIFU and surgical treatment for uterine fibroids. *Chin J Obstet Gynecol Pediatr.* (2012) 8:392–4.
13. Froeling V, Meckelburg K, Schreiter NF, Scheurig-Muenkler C, Kamp J, Maurer MH, et al. Outcome of uterine artery embolization versus MR-guided high-intensity focused ultrasound treatment for uterine fibroids: long-term results. *Europ J Radiol.* (2013) 82:2265–9. doi: 10.1016/j.ejrad.2013.08.045
14. Ikink ME, Nijenhuis RJ, Verkooijen HM, Voogt MJ, Reuwer PJHM, Smeets AJ, et al. Volumetric MR-guided high-intensity focused ultrasound versus uterine artery embolisation for treatment of symptomatic uterine fibroids: comparison of symptom improvement and reintervention rates. *Europ Radiol.* (2014) 24:2649–57. doi: 10.1007/s00330-014-3295-6
15. Liu X, He J, He M, Zhang L. Comparison on ovarian functions of premenopausal women between HIFU and hysterectomy for treating uterine fibroids. *Chongq Med.* (2013) 42:3552–4.
16. Meng X, He G, Zhang J, Han Z, Yu M, Zhang M, et al. A comparative study of fibroid ablation rates using radio frequency or high-intensity focused ultrasound. *Cardiovasc Intervent Radiol.* (2010) 33:794–9. doi: 10.1007/s00270-010-9909-8
17. Taran FA, Tempany CM, Regan L, Inbar Y, Revel A, Stewart EA. Magnetic resonance-guided focused ultrasound (MRgFUS) compared with abdominal hysterectomy for treatment of uterine leiomyomas. *Ultrasound Obstetr Gynecol.* (2009) 34:572–8. doi: 10.1002/uog.7435

18. Wang X, Qin J, Chen J, Wang L, Chen W, Tang L. The effect of high-intensity focused ultrasound treatment on immune function in patients with uterine fibroids. *Int J Hyperther.* (2013) 29:225–33. doi: 10.3109/02656736.2013.775672
19. Barnard EP, AbdElmagied AM, Vaughan LE, Weaver AL, Laughlin-Tommaso SK, Hesley GK, et al. Periprocedural outcomes comparing fibroid embolization and focused ultrasound: a randomized controlled trial and comprehensive cohort analysis. *Am J Obstetr Gynecol.* (2017) 216:500.e1-.e11. doi: 10.1016/j.ajog.2016.12.177
20. Chen J, Li Y, Wang Z, McCulloch P, Hu L, Chen W, et al. Evaluation of high-intensity focused ultrasound ablation for uterine fibroids: an IDEAL prospective exploration study. *BJOG.* (2018) 125:354–64. doi: 10.1111/1471-0528.14689
21. Li P, Xiang L, Li L. Comparison on gravidity of post-operative patients between uterine fibroid ablation of high intensity focused ultrasound and laparoscopic myomectomy. *China Med Equip.* (2018) 15:59–62.
22. Lin T, Fu X, Chen M. Comparison of curative effects of UAE and HIFU in treatment of intramural hysteromyoma. *Med J Natl Def Forces Southwest China.* (2017) 27:57–9.
23. Wang F, Tang L, Wang L, Wang X, Chen J, Liu X, et al. Ultrasound-guided high-intensity focused ultrasound vs laparoscopic myomectomy for symptomatic uterine myomas. *J Minim Invas Gynecol.* (2014) 21:279–84. doi: 10.1016/j.jmig.2013.09.004
24. Wang H, Qin R, Wang S, Wang Y, Hua C, Yang Y. Comparison on effects of high intensity focused ultrasound and abdominal hysterectomy for treating uterine fibroids. *Chongq Med.* (2015) 44:2060–5.
25. Xiong X, Fu Y, Hu B, Wen R, Zhang Y. Comparison of high intensity focused ultrasound, laparoscopic and open abdomen in the treatment of long-term recurrence and pregnancy in uterine fibroids. *Chinese J Family Plann Gynecotok.* (2017) 9:40–3.
26. Xu L, Wang Y, Han X. Analysis of sex hormones changes after high intensity focused ultrasound treatment on patients who are less than 45 years old with uterine fibroids. *Med Pharm Yunnan.* (2016) 37:172–5.
27. Mohr-Sasson A, Machtinger R, Mashiach R, Nir O, Inbar Y, Maliyanker N, et al. Long-term outcome of MR-guided focused ultrasound treatment and laparoscopic myomectomy for symptomatic uterine fibroid tumors. *Am J Obstetr Gynecol.* (2018) 219:375.e1-.e7. doi: 10.1016/j.ajog.2018.09.002
28. Wu G, Li R, He M, Pu Y, Wang J, Chen J, et al. A comparison of the pregnancy outcomes between ultrasound-guided high-intensity focused ultrasound ablation and laparoscopic myomectomy for uterine fibroids: a comparative study. *Int J Hyperthermia.* (2020) 37:617–23. doi: 10.1080/02656736.2020.1774081
29. Hu L, Zhao JS, Xing C, Xue XL, Sun XL, Dang RF, et al. Comparison of focused ultrasound surgery and hysteroscopic resection for treatment of submucosal uterine fibroids (FIGO Type 2). *Ultrasound Med Biol.* (2020) 46:1677–85. doi: 10.1016/j.ultrasmedbio.2020.02.018
30. Sandberg EM, Tummers FHMP, Cohen SL, van den Haak L, Dekkers OM, Jansen FW. Reintervention risk and quality of life outcomes after uterine-sparing interventions for fibroids: a systematic review and meta-analysis. *Fertil Steril.* (2018) 109:698–707.e1. doi: 10.1016/j.fertnstert.2017.11.033
31. Suomi V, Komar G, Sainio T, Joronen K, Perheentupa A, Blanco Sequeiros R. Comprehensive feature selection for classifying the treatment outcome of high-intensity ultrasound therapy in uterine fibroids. *Sci Rep.* (2019) 9:10907. doi: 10.1038/s41598-019-47484-y
32. Keserci B, Duc NM. The role of T1 perfusion-based classification in magnetic resonance-guided high-intensity focused ultrasound ablation of uterine fibroids. *Eur Radiol.* (2017) 27:5299–308. doi: 10.1007/s00330-017-4885-x
33. Verpalen IM, de Boer JP, Linstra M, Pol RLI, Nijholt IM, Moonen CTW, et al. The Focused Ultrasound Myoma Outcome Study (FUMOS); a retrospective cohort study on long-term outcomes of MR-HIFU therapy. *Eur Radiol.* (2020) 30:2473–82. doi: 10.1007/s00330-019-06641-7
34. Wang Y, Liu X, Wang W, Tang J, Song L. Long-term clinical outcomes of us-guided high-intensity focused ultrasound ablation for symptomatic submucosal fibroids: a retrospective comparison with uterus-sparing surgery. *Acad Radiol.* (2020) doi: 10.1016/j.acra.2020.05.010
35. Yu SC, Cheung EC, Leung VY, Fung LW. Oxytocin-Augmented and non-sedating high-intensity-focused ultrasound (HIFU) for uterine fibroids showed promising outcome as compared to hifu alone or uterine artery embolization. *Ultrasound Med Biol.* (2019) 45:3207–13. doi: 10.1016/j.ultrasmedbio.2019.07.410
36. Chen Y, Jiang J, Zeng Y, Tian X, Zhang M, Wu H, et al. Effects of a microbubble ultrasound contrast agent on high-intensity focused ultrasound for uterine fibroids: a randomised controlled trial. *Int J Hyperthermia.* (2018) 34:1311–5. doi: 10.1080/02656736.2017.1411620
37. Jiang N, Xie B, Zhang X, He M, Li K, Bai J, et al. Enhancing ablation effects of a microbubble-enhancing contrast agent ("SonoVue") in the treatment of uterine fibroids with high-intensity focused ultrasound: a randomized controlled trial. *Cardiovasc Intervent Radiol.* (2014) 37:1321–8. doi: 10.1007/s00270-013-0803-z
38. Pérez-López FR, Ornat L, Ceausu I, Depypere H, Erel CT, Lambrinoudaki I, et al. EMAS position statement: management of uterine fibroids. *Maturitas.* (2014) 79:106–16. doi: 10.1016/j.maturitas.2014.06.002
39. Practice Committee of the American Society for Reproductive Medicine. Electronic address Aao, Practice Committee of the American Society for Reproductive M. Removal of myomas in asymptomatic patients to improve fertility and/or reduce miscarriage rate: a guideline. *Fertil Steril.* (2017) 108:416–25.
40. Khaw SC, Anderson RA, Lui MW. Systematic review of pregnancy outcomes after fertility-preserving treatment of uterine fibroids. *Reprod Biomed Online.* (2020) 40:429–44. doi: 10.1016/j.rbmo.2020.01.003
41. Liu X, Xue L, Wang Y, Wang W, Tang J. Vaginal delivery outcomes of pregnancies following ultrasound-guided high-intensity focused ultrasound ablation treatment for uterine fibroids. *Int J Hyperthermia.* (2018) 35:510–7. doi: 10.1080/02656736.2018.1510548
42. Zou M, Chen L, Wu C, Hu C, Xiong Y. Pregnancy outcomes in patients with uterine fibroids treated with ultrasound-guided high-intensity focused ultrasound. *Bjog.* (2017) 124 (Suppl. 3):30–5. doi: 10.1111/1471-0528.14742
43. Lee JS, Hong GY, Lee KH, Kim TE. Changes in anti-müllerian hormone levels as a biomarker for ovarian reserve after ultrasound-guided high-intensity focused ultrasound treatment of adenomyosis and uterine fibroid. *Bjog.* (2017) 124 S(uppl. 3):18–22. doi: 10.1111/1471-0528.14739
44. Cheung VY, Lam TP, Jenkins CR, Cheung GK, Chan SS, Choi WK. Ovarian reserve after ultrasound-guided high-intensity focused ultrasound for uterine fibroids: preliminary experience. *J Obstet Gynaecol Can.* (2016) 38:357–61. doi: 10.1016/j.jogc.2016.02.006
45. Suriyawongpaisal P, Kamlungkuea T, Chiawchantanakit N, Charoenpipatsin N, Sriturawanit P, Kreesang P, et al. Relevance of using length of stay as a key indicator to monitor emergency department performance: case study from a rural hospital in Thailand. *Emerg Med Australas.* (2019). doi: 10.1111/1742-6723.13254
46. Moore L, Stelfox HT, Turgeon AF, Nathens AB, Lavoie A, Emond M, et al. Derivation and validation of a quality indicator of acute care length of stay to evaluate trauma care. *Ann Surg.* (2014) 260:1121–7. doi: 10.1097/SLA.0000000000000648
47. Liu Y, Zhang WW, He M, Gong C, Xie B, Wen X, et al. Adverse effect analysis of high-intensity focused ultrasound in the treatment of benign uterine diseases. *Int J Hyperthermia.* (2018) 35:56–61. doi: 10.1080/02656736.2018.1473894
48. Bean EM, Cutner A, Holland T, Vashisht A, Jurkovic D, Saridogan E. Laparoscopic myomectomy: a single-center retrospective review of 514 patients. *J Minim Invasive Gynecol.* (2017) 24:485–93. doi: 10.1016/j.jmig.2017.01.008
49. Verpalen IM, Anneveldt KJ, Nijholt IM, Schutte JM, Dijkstra JR, Franx A, et al. Magnetic resonance-high intensity focused ultrasound (MR-HIFU) therapy of symptomatic uterine fibroids with unrestrictive treatment protocols: a systematic review and meta-analysis. *Eur J Radiol.* (2019) 120:108700. doi: 10.1016/j.ejrad.2019.108700
50. Vinogradova Y, Coupland C, Hill T, Hippisley-Cox J. Risks and benefits of direct oral anticoagulants versus warfarin in a real world setting: cohort study in primary care. *BMJ.* (2018) 362:k2505. doi: 10.1136/bmj.k2505
51. Ezzat VA, Lee V, Ahsan S, Chow AW, Segal O, Rowland E, et al. A systematic review of ICD complications in randomised controlled trials versus registries: is our 'real-world' data an underestimation? *Open Heart [Internet].* (2015) 2:e000198. doi: 10.1136/openhrt-2014-000198
52. Elliott L, Fidler C, Ditchfield A, Stissing T. Hypoglycemia event rates: a comparison between real-world data and

randomized controlled trial populations in insulin-treated diabetes. *Diabetes Ther.* (2016) 7:45–60. doi: 10.1007/s13300-016-0157-z

Conflict of Interest: The authors declare that the research was conducted in the absence of any commercial or financial relationships that could be construed as a potential conflict of interest.

frontiers in Oncology

ORIGINAL RESEARCH
published: 07 December 2021
doi: 10.3389/fonc.2021.584265

Long-Term Follow-Up of Single-Fiber Multiple Low-Intensity Energy Laser Ablation Technique of Benign Thyroid Nodules

*Mattia Squarcia[1,2], Mireia Mora[2,3,4], Gloria Aranda[2,3], Enrique Carrero[5], Daniel Martínez[6], Ramona Jerez[5], Ricard Valero[5], Joan Berenguer[1], Irene Halperin[2,3,4] and Felicia A. Hanzu[2,3,4]**

[1] Department of Neuroradiology, Hospital Clínic, Barcelona, Spain, [2] Group of Endocrine Disorders, Institut d'Investigacions Biomèdiques August Pi i Sunyer (IDIBAPS), Barcelona, Spain, [3] Endocrinology and Nutrition Department, Hospital Clinic, Barcelona, Spain, [4] Department of Medicine, Faculty of Medicine, University of Barcelona, Barcelona, Spain, [5] Department of Anesthesia and Critical Care Hospital Clinic, Barcelona, Spain, [6] Department of Pathology and Anatomy, Hospital Clinic, Barcelona, Spain

OPEN ACCESS

Edited by:
Hugo Alexandre Ferreira,
University of Lisbon, Portugal

Reviewed by:
Yue Zhang,
Xijing Hospital, China
Jason David Prescott,
New York University, United States

***Correspondence:**
Felicia A. Hanzu
fhanzu@clinic.cat

Specialty section:
This article was submitted to Cancer Imaging and Image-directed Interventions, a section of the journal Frontiers in Oncology

Received: 16 July 2020
Accepted: 08 November 2021
Published: 07 December 2021

Citation:
Squarcia M, Mora M, Aranda G, Carrero E, Martínez D, Jerez R, Valero R, Berenguer J, Halperin I and Hanzu FA (2021) Long-Term Follow-Up of Single-Fiber Multiple Low-Intensity Energy Laser Ablation Technique of Benign Thyroid Nodules. Front. Oncol. 11:584265. doi: 10.3389/fonc.2021.584265

Aim: The short-term and long-term efficacy of different thermal percutaneous ablation techniques remains a topical issue. Our group implemented percutaneous laser ablation (LA), a moving-shot technique to increase efficiency and reduce costs and variability of LA by applying multiple lower-intensity energy illuminations (MLIEI) covering the nodular volume (V) through changes in position of a single laser fiber within the thyroid nodule. The aim of the present study was to evaluate the efficacy of the single-fiber LA-MLIEI during a 5-year follow-up and to identify possible predictors of the final outcome.

Methods: *Prospective study*: Thirty outpatients (23 women and seven men) with benign symptomatic thyroid nodules were assigned to single-fiber LA-MLIEI, between 2012 and 2015. A single LA session was performed under real-time ultrasound (US) guidance using a 1,064-nm continuous-wave laser at 3 W. A 400-μm optical fiber was inserted through a 21-gauge needle, and 3–10 illuminations were performed per nodule, administering between 400 and 850 J/illumination. The total administered energy was calculated on the initial V of the nodule and the estimated ablation area. US evaluation was performed after LA-MLIEI at 1 week and 1, 3, 6, and 12 months and after that annually up to 5 years. Clinical symptoms, laboratory thyroid function during follow-up, and acute and chronic complications of treatment were registered.

Results: On follow-up, 67% (n: 20) were responders to single-fiber LA-MLIEI, while 33% (n: 10) were non-responders. The responder group initiated V reduction (ΔV) at 1 month, with remission of symptoms, and presented a 50% ΔV at 3 months of treatment; the maximum response was achieved at 24 months and remained stable until the end of the study. The non-responder group presented a ΔV of less than 50% at 12 months; though a tendency to >50% ΔV was observed at 24–36 months, there was subsequent regrowth, and 40% of this group required surgery. ΔV was positively correlated with the total

administered energy/V (J/V) and inversely with nodule V. No severe adverse effects were observed. Thyroid function remained normal in all patients. Remission of symptoms occurred rapidly after 1 month.

Conclusions: LA with multiple fractional discharges employing a single fiber in a unique session is a safe and inexpensive technique that allows rapid reduction of thyroid nodules, with a stable response up to 5 years, similarly to what has been reported with the conventional LA. Total nodule volume appears as a predictive factor of the reduction.

Keywords: single fiber, unique session, thyroid nodules, long-term response, short-term response

INTRODUCTION

Thermal ablation of thyroid nodules with laser ablation (LA), radiofrequency ablation (RFA), and very recently microwaves are nowadays increasing minimally invasive percutaneous non-surgical techniques employed in the treatment of symptomatic thyroid nodules that are benign at cytological assessment (1–5). Moreover, they are under evaluation in the local treatment of malignant nodules (6–11).

Initial results from heterogeneous studies comparing RFA and LA showed significantly better results in volume (V) reduction for RFA than LA, but LA included patients with larger nodules, and RFA included patients with a higher cyst component. In the last years, results from both prospective and retrospective multicentric studies showed that both techniques induced a clinically significant 1–5 years of long-lasting V reduction, as well as symptom improvement and preserved thyroid function in treated benign thyroid nodules (12–22). The probability of regrowth needing retreatment was lower after RFA and was associated with a younger age, larger baseline V, and treatment with lower energy delivery (18). Moreover, nodule decrease seemed to initiate earlier for RFA (12, 20).

Both LA and RFA thermal percutaneous techniques are well tolerated and demonstrated to be safe with an extremely low incidence of major local acute or chronic side effects, depending more on the operator experience and the intensity of the applied treatment than on the type of the technique (22–25).

RFA technique consists of moving-shot ablation using a sole probe (5, 12, 14, 16, 18, 20, 26). During LA, the number of fibers employed during each treatment session depends on the nodule V, with mostly one to two illuminations for each fiber (5, 13, 15, 17, 18, 20, 22, 25, 27). Although LA is considered a cost-effective technique in a sole treatment, the use of multiple fibers per session and the eventual need for retreatment increases the costs, generating significant limitations for its use by public healthcare systems.

The aim of the present study was to assess a modified LA technique that intends to improve treatment response, reduce costs, and, therefore, increase efficiency. We employed a single active LA fiber in a unique session treatment covering the nodular V through moving shots and repositioning the optic fiber with multiple lower-intensity energy illuminations (MLIEI). In this work, we report the clinical results, safety, and possible predictors of the outcome of LA-MLIEI during a 5-year follow-up.

MATERIAL AND METHODS

Study Design

A prospective one-center non-randomized pilot study was performed in patients with thyroid nodules with benign cytology (single thyroid nodule or a multinodular goiter with a dominant nodule) requiring permanent treatment due to the size and/or compressive symptoms and who either rejected surgery or could not be operated for medical reasons.

Patients

Patients with symptomatic benign thyroid nodules who rejected surgery or presented a contraindication for surgery due to their comorbidities were admitted between 2012 and 2015 at the hospital outdoor clinic of the Endocrinology Department of Hospital Clinic Barcelona. All nodules showed benign ultrasound (US) characteristics. Fine-needle aspiration (FNA) cytology was performed twice, and Bethesda 2 cytology was required in all LA-treated nodules. The study was approved by the Hospital's Ethics Committee, and written informed consent was obtained from all participants.

Inclusion criteria comprised patients with benign symptomatic solid nodules superior to 25 mm in at least one diameter with local compressive symptoms due to the anatomical position regarding esophagus or trachea or cosmetic symptoms; benign cytological findings (at least two, one in the last 12 months); normal free thyroxine (T4); and normal or low thyrotropin [thyroid-stimulating hormone (TSH)].

Exclusion criteria were a history of previous external radiotherapy or radioiodine exposure, multinodular goiter without a dominant nodule, overt hyperthyroidism, V, and diameter below inclusion criteria.

Initial and Follow-Up Evaluations

Clinical evaluation and US assessment of all patients were performed before LA at 1 week and 1, 3, 6, and 12 months after the procedure, and afterward annually. In addition, laboratory follow-up was performed at 1, 6, and 12 months and annually after that.

Local symptoms were evaluated through a questionnaire assessing the presence/absence of one or more of the following symptoms: neck constriction, cervical tenderness, dysphagia, dyspnea, and dysphonia. The clinical assessment of the signs of

the nodular goiter was performed by visual inspection (presence of a cervical lump visible at a distance of 1 m from the patient).

Thyroid US was performed using a commercially available US scanner (Siemens Acuson S2000) with a 7.5- to 13.0-MHz linear transducer. The nodule volumes were calculated by the ellipsoid formula by three experienced sonographers in the center at all examination time points.

Laboratory tests included the following: TSH, serum-free thyroxine (FT4), triiodothyronine (T3), and anti-thyroid peroxidase antibodies (anti-TPOAb). Coagulation was evaluated before the procedure. All laboratory tests were performed following standard assays in the central core laboratory of the center.

Treatment: Ablation Technique

A continuous-wave multidiode surgical laser (Intermedic, 30 W) operating at 1.064 mm at an output power of 3 W was used for the procedures.

According to the protocols and specific guidelines, anticoagulant therapy was switched to heparin, and antiplatelet therapy was discontinued before the procedure.

The procedure was performed under local anesthesia (2% lidocaine at the point of the puncture) and with conscious sedation with intravenous propofol, fentanyl bolus, and ketamine if required.

LA-MLIEI treatment was performed by one operator with the patient lying in a supine position with the neck in hyperextension by introducing one guiding 21-gauge needle from the isthmus to the targeted nodule (**Figure 1A1**). Under US guidance, the entire length of the needle was visualized in a transverse US view, and the tip of the needle was initially positioned in the most inferior part of the nodule. A 400-μm optic fiber was then inserted through the needle until the distal active 5 to 7 mm of the fiber was in direct contact with the thyroid tissue (**Figure 1A2**).

LA-MLIEI consists of multiple sequential overlapping low and intermediate energy laser illuminations (between 400 and 850 J/illumination) using a single active optic fiber in an RFA moving shot-like technique. At the end of each illumination, the active tip of the optic fiber was pulled back, and a new illumination was performed in the part of the nodule adjacent to the previously treated area, thus permitting the overlap of the

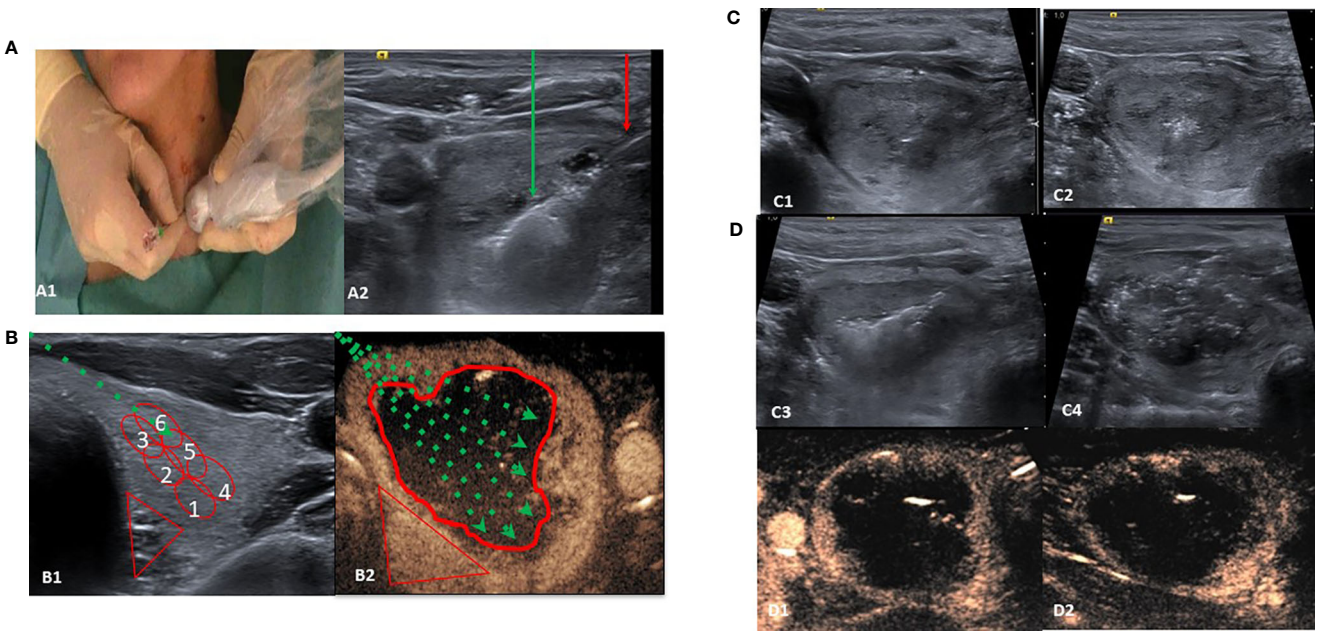

FIGURE 1 | Single-fiber laser ablation multiple lower-intensity energy illuminations (LA-MLIEI) technique. **(A, A1)** Positions of the operator and patient. The patient is placed in a supine position with mild neck extension, and the operator stands close to the patient's head. The operator's left hand holds the ultrasound (US) probe and the right hand the electrode. **(A2)** US image of the LA-MLIEI with trans-isthmic approach. This transverse US image shows the needle shaft (red arrow), in the thyroid nodule, and the hyperechoic area (green arrow) from tissue heating and vaporization during illuminations. **(B, B1)** B-mode and drawing of the LA-MLIEI technique. The optic fiber (dotted green arrow) is inserted through the isthmus to visualize the entire length. Illuminations are sequentially performed from the deepest portion of the nodule (red circles Nr. 1 and 4) to the superficial area (red circles Nr. 3 and 6) by pulling back the tip of the optic fiber. **(B2)** Contrast-enhanced US imaging and drawing of the LA-MLIEI technique. The procedure is repeated with different optic fiber angulations (dotted green arrows) to cover all the volume (V) of the target nodule. Illuminations are performed with lower energies in the proximities of the peripheral danger triangle (in red) and higher energies in the central area. **(C)** Sequential US images of the LA-MLIEI technique. **(C1)** Transverse US image showing the tip of the optic fiber. **(C2)** Hyperechoic area in the thyroid nodule appearing during optic fiber firing. **(C3)** Overlapping areas of gas formation during optic fiber moving shot. **(C4)** At the end of the procedure, the complete volume of the nodule appears diffusely hypoechogenic with multiple hyperechogenic gas bubbles dispersed in the treated area. **(D)** Postprocedural axial **(D1)** and sagital **(D2)** contrast-enhanced US images showing complete ablation of the target nodule with the presence of enhancing tissue in the location of the danger triangle, indicating preserved safety margins.

ablated regions. The total number of intranodular repositions of the fiber's active tip, subsequent illuminations, and administered energy were calculated according to the initial V and the estimated ablation area.

Usually, the procedure began with the trans-isthmic approach at the most inferior part of the nodule, and subsequently, the tip of the needle was withdrawn medially and superiorly for about 8–10 mm with the moving-shot technique. After the ablation of the inferior third of the nodule was completed, the tip of the needle was repositioned at the middle and the superior third of the nodule. Then multiple overlapping illuminations were performed with the moving-shot technique in these locations (**Figures 1B1, B2**).

The single-fiber LA-MLIEI technique allows spreading laser energy in the complete V of the nodule, thus permitting the use of reduced energy illuminations. The peripheral 10 mm of the nodule or the regions of the nodule close to the trachea and the danger triangle were treated by low energy illumination (up to 400 J) to ensure a safe procedure, while the central part of the nodule was treated with higher energy illuminations (between 600 and 850 J) (**Figures 1C1–C4**). To assess the ablated area, a B-mode US, color Doppler, and contrast-enhanced US evaluation (28) were performed immediately after the procedure (**Figures 1D1, D2**).

Methylprednisolone (0.5 mg/kg/*ev*) was administered together with 40 mg pantoprazole *ev* at the beginning of the procedure to prevent airway obstruction by edema. If requested, analgesia was complemented with 1 g of paracetamol. After the procedure, oral corticosteroids were given in a short downward schedule for 5 days (e.g., Urbason® 32 mg/day × 1 day; 16 mg/day × 1 day; and 8 mg/day × 2 days, 4 mg for 1 day) and optional analgesia (paracetamol 1 g/8 h and dexketoprofen 25 mg/8 h vo) if pain persisted.

Tolerability, major/minor complications, and acute/chronic side effects of the treatment were evaluated and registered following previously established criteria. Symptoms were evaluated using symptom questionnaires, and pain intensity was rated by a numeric scale (categorized as mild (<4 of 10), moderate (4–7 of 10), or severe (>7 of 10) (15). The need for subsequent home analgesic treatment or outpatient clinic checkup due to local pain was also registered.

Statistical Analysis

Continuous variables were expressed as mean ± SD, categorical variables were displayed as frequencies, and the appropriate parametric or non-parametric test was used to assess the significance of the differences between subgroups. All data are expressed as mean ± SD unless otherwise specified. Timing differences within subjects were analyzed through repeated-measures ANOVA or Kruskal–Wallis test for normally or not normally distributed variables, respectively. The correlation between percentage reduction of the nodular V and energy per volume supplies was assessed using Pearson's method. All the tests were two-sided, and statistical significance was set at $p < 0.05$. Statistical analysis was performed using the SPSS 20 software package (SPSS, Inc.).

RESULTS

Patients and Treatment Characteristics

Thirty patients, 23 women and seven men, fulfilling the inclusion criteria were included in the study. The patients' clinical, demographic, and laboratory findings are reported in **Table 1**; 36% presented nodular goiter with a single dominant nodule, while 72% presented a unique thyroid nodule. Ablated nodules were localized in the left thyroid lobe in 34% of the patients, in the right thyroid lobe in 25% of the cases, in the isthmus in 28% of the cases, and at the junction of the isthmus left thyroid lobe in 15%. In addition, 6.6% of the patients presented subclinical hyperthyroidism while the rest were euthyroid, and 43.3% presented low (<100 mUI/L) positive TPOAb levels. During follow-up, thyroid function remained normal in all patients. The three patients with subclinical hyperthyroidism normalized thyroid function 6 months after the LA session, without further changes during follow-up. No relationship between thyroid antibodies and treatment or treatment response was observed.

The nodules' largest diameter ranged from 26 to 92 mm (median 38.4 mm), and the median volume was 18.9 ± 21.2 ml. Minimal symptomatic diameters were registered for isthmic nodules.

The mean procedure time for LA-MLIEI was of 45 ± 6 min. Between one and five insertions of the unique fiber and between 3 and 10 illuminations were performed for each nodule, releasing between 400 and 850 J/illumination.

Tolerability and Side Effects

One patient (3.3%) presented stridor during the procedure that remitted with lidocaine administration. Intra- and periprocedural

TABLE 1 | Clinical, demographic, and laboratory features of all patients at baseline and overall treatment characteristics and side effects.

Variable	
Sex, male/female (n)	7/23
Age (years)	62.3 ± 15.6
BMI (kg/m^2)	28.2 ± 5.9
Uninodular/multinodular Goiter (%)	72/36
Nodule type (solid/microcystic)	21/7
Thyroid nodule volume (ml)	18.9 ± 21.2
TSH (mU/ml)[a]	2.8 ± 2.3
FT4 (ng/dl)[b]	1.1 ± 0.1
FT3 (ng/dl)[c]	1.1 ± 0.2
TPOAb (mUI/ml) (n/%)[d]	13/43.3
Treatment duration (min)	45 ± 6
Total administered energy (J)	2,954.7 ± 1,689.4
Energy/V (J/ml)	231.9 ± 179.0
Number of illuminations	5.1 ± 7.7
Intraprocedural events (n/%)	1/3.3
Side effects (n/%)	3/9.9

Values are expressed as mean ± SD unless otherwise specified.
BMI, body mass index; TSH, thyrotropin; FT4, free T4; FT3, free T3; TPOAb, anti-thyroid peroxidase antibodies; V, volume; n, number.
[a]*Normal range TSH 0.4–4.0 mUI/L.*
[b]*Normal range FT4: 0.8–2.0 ng/dl.*
[c]*Normal range FT3: 0.7–1.9 ng/ml.*
[d]*TPOAb < 60 mUI/ml.*

pain was low to moderate in 93% (<7), while in 7%, it was severe. Of the patients, 3% needed complementary analgesia in the first 3–7 days after the treatment.

Of the patients, 9.8% (n = 3) presented an anterior nodular rupture at 6–7 weeks after treatment that remitted with oral anti-inflammatory therapy and prophylactic antibiotic therapy. No other complications regarding treatment or medical examination were registered along with follow-up (**Table 1**).

Change of Thyroid Nodule Volume During Follow-Up

The overall mean V reduction for LA-MLIEI was 35% at 1 month after the procedure, increasing up to 63% at 12 months, and remained 60% at 60 months. Remission of compressive symptoms occurred rapidly after 1 month in 75% of the patients and esthetic symptoms after 3–6 months in 80% of the cases. Four patients (13.3%) were referred to surgery due to persistent symptoms or regrowth during follow-up. One patient was operated because his/her regrowth presented a malignant follicular neoplasia (**Figure 2**).

Two distinct groups of patients were observed according to ΔV reduction in the first 12 months after LA-MLIEI: responders 70% (n: 20) and non-responders 33% (n: 10).

Table 2 summarizes the clinical and demographic features of responders and non-responders. In the responder group, nodules tended to be more solid and smaller than for non-responders. Furthermore, an increased total energy delivery per nodular V (J/V) during the LA was also observed for the responder group.

Table 3 shows the nodular volume progression in responders and non-responders to LA during 5 years of follow-up. The difference between both groups was statistically significant at every point of evaluation.

The responder group initiated V decrease at 1 month, with remission of symptoms, and presented a 50% V reduction at 3 months of treatment, with a maximum response (74% of V reduction) at 24 months, which remained stable until the end of the follow-up period (**Figure 2**).

The non-responder group presented a V reduction of less than 50% at 12 months, with a later tendency to >50% V decrease at 24–36 months, and subsequent regrowth. Surgical treatment was required by four patients (40%) of this group (**Figure 2**).

Probable Predictors of Laser Ablation Treatment

Several parameters were analyzed to define probable predictors of nodule reduction: US features (type of nodule), nodular volume, the coexistence of thyroid autoimmunity, and the energy delivered per ml of nodule tissue. Higher energy supplied by thyroid nodule volume (J/V) was correlated with a lower thyroid nodule volume during follow-up (r: −0.477, p: 0.039). Higher total administered energy/V (J/V) and nodule V ≤ 20 ml (p: 0.034) were correlated with a greater ΔV. In other words, the greater the energy applied per thyroid volume, the greater the decrease in the nodule V.

DISCUSSION

In the present study, we report the short- and long-term results of the single-fiber LA-MLIEI approach to optimize efficiency and reduce conventional LA costs.

Overall, US-guided thermal ablation of thyroid nodules with LA is a safe minimally invasive percutaneous non-surgical technique employed in treating symptomatic benign thyroid nodules and for the local treatment of malignant ones. Various reports regarding the long-term efficacy have been recently published (1–22). What is more, very recently, long-term follow-up compared with RFA showed that both LA and RFA results are clinically similar in volume reduction and sparing thyroid function of benign thyroid nodules with minimal side effects (18, 20, 29).

Conventional LA technique has been implemented using either a variable number of fibers according to the V of the thyroid nodule in one unique treatment or just one in several sessions of LA. The LA technique was improved by the "pull-back technique", in which one or more laser fibers are subsequently retracted (29). However, generally more than one fiber is required for ablation of each nodule (5, 18, 20, 29–34). Very recently, there has been a report on an intent to standardize the LA technique with a single fiber in a few patients with a 12-month follow-up, with promising results (35).

In contrast, the development of unipolar RFA probes for thyroid nodule ablation and the trans-isthmic moving-shot approach have enabled an outstanding improvement concerning the fixed-electrode RFA technique so that just one probe is required for the ablation of larger nodules (12, 14, 26, 36). As thyroid nodules are often ellipsoidal or exophytic, they are difficult to ablate, and retreatments are sometimes needed to achieve volume reduction or symptomatic remission in LA and RFA (21, 26).

In this work, by applying a standardized approach, we observed a rapid and stable remission of symptoms and a long-term persistent volume reduction of benign thyroid nodules using the LA-MLIEI modified single active LA fiber technique in a single treatment session. The LA-MLIEI technique allows spreading laser energy in the complete V of the nodule, thus permitting reduced energy for each illumination as compared with other reported single- or double-fiber LA techniques (30, 35, 37). We used the LA fiber in a similar trans-isthmic approach, like an RFA probe covering the nodular V through multiple overlapping lower-intensity energy illuminations (MLIEI), repositioning the optic fiber inside the nodule by moving shot. The total number of intranodular moving shot and repositioning of the active tip of the fiber, subsequent illuminations, and administered energy were calculated according to the initial V and the estimated ablation area. At the end of each illumination, the active tip of the optic fiber was relocated, and a new illumination was performed in the part of the nodule adjacent to the previously treated area, thus permitting the overlap of the ablated regions.

During LA-MLIEI, we observed no increase in intraprocedural side effects regarding conventional LA and RFA (23–25, 30, 37).

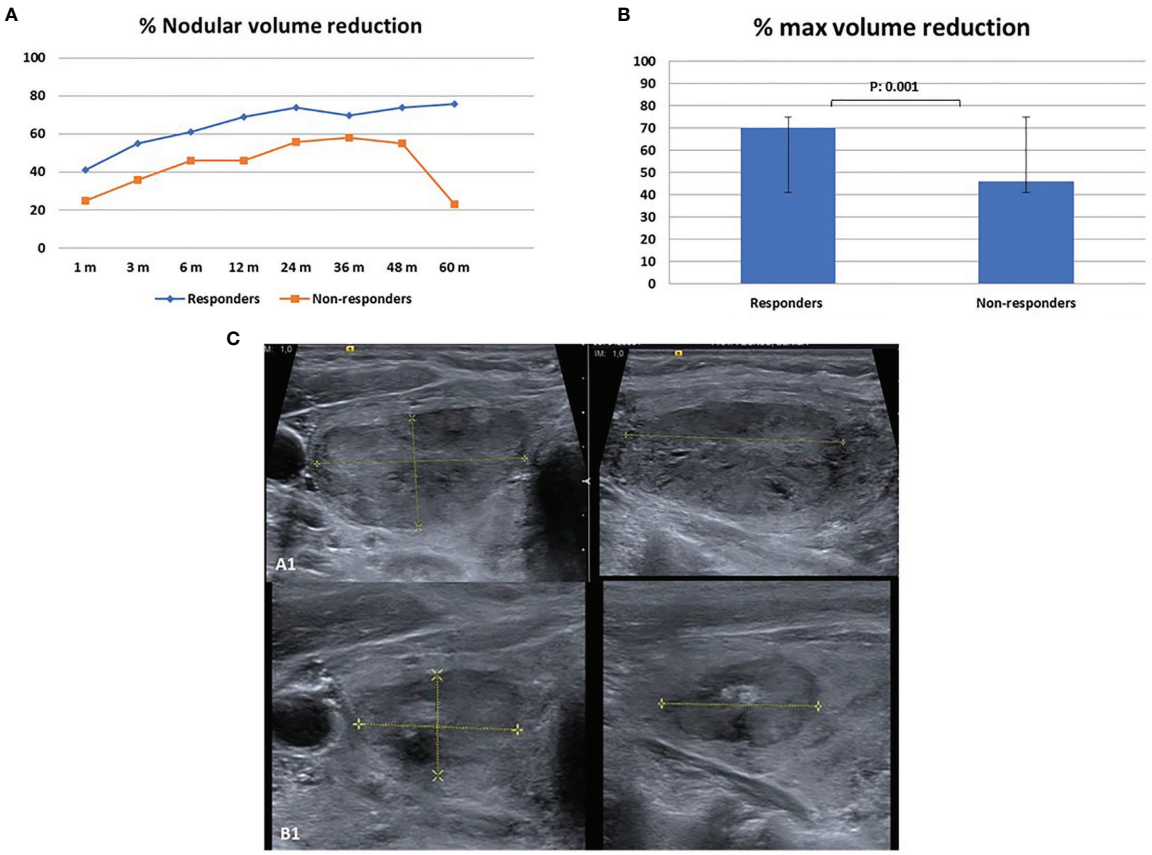

FIGURE 2 | Nodule reduction during follow-up after single-fiber laser ablation multiple lower-intensity energy illumination (LA-MLIEI) technique. **(A)** Percent (%) of nodule volume (V) reduction in the responder and non-responder groups during the 60 months' follow-up. Values are expressed as mean of % V reduction ± SD. **(B)** Maximum percent (%) of nodule V reduction in the responder and non-responder groups during the 60 months' follow-up. Values are expressed as mean of % V reduction ± SD. **(C)** Axial and sagittal US images of the target nodule obtained before the treatment and 12 months after the treatment showing a significant volume (V) decrease.

TABLE 2 | Clinical and treatment characteristics in responders and non-responders to the single-fiber laser ablation multiple lower-intensity energy illuminations (LA-MLIEI) treatment.

Clinical features	Responders	Non-responders	p-Value
Sex, female/male (n)	16/4 (20)	7/3 (10)	ns
Age (years)	60.5 ± 15.1	65.9 ± 16.8	ns
Nodule type (solid/microcystic)	16/4	5/5	0.05
Thyroid nodule volume (ml)	14.2 ± 8.6	30.4 ± 31.6	0.03
Total administered energy (J)	2,816.1 ± 1,840.9	3,232.0 ± 1,383.3	ns
Energy/V (J/ml)	268.3 ± 203.8	159.3 ± 82.3	ns
Number of illuminations	5.5 ± 2.6	6.2 ± 3.8	ns
Intraprocedural events (n/%)	1/3.3	–	ns
Side effects (n/%)	2/6.6	1/3.3	ns

Values are expressed as mean ± SD unless otherwise specified. Statistical significance was set at $p < 0.05$.
V, volume; n, number.

Interestingly, and probably due to the repeated movements with the fiber through the same initial insert point, the only subacute complication registered was an anterior nodule rupture, a complication that has been described for the RFA technique (25, 38).

Still, nodule rupture did not prevent V reduction, and surgery was not required. The use of conscious sedation can be considered biased for the intraprocedural perceived pain but has allowed us to apply the LA-MLIEI technique following our center's requirements for minimally invasive procedures. The laryngeal nerves were not affected or there was no dysphonia observed despite the trans-isthmic approach, as the danger triangle was avoided, and a safe distance was carefully kept.

Overall, the volume reduction observed through LA-MLIEI was approximately 50%, in line with the results generally reported for

TABLE 3 | Progression in volume (V) decrease after single-fiber laser ablation multiple lower-intensity energy illuminations (LA-MLIEI) treatment in responders and non-responders during follow-up.

	V 0m (ml)	V 1m (ml)	V 3m (ml)	V 6m (ml)	V 12m (ml)	V 24m (ml)	V 36m (ml)	V 48m (ml)	V 60m (ml)
LA Responder (n: 20)	14.2 ± 8.7	9.4 ± 7.5	7.7 ± 6.3	6.6 ± 5.0	5.0 ± 2.7	4.4 ± 2.6	3.7 ± 1.3	3.9 ± 2.0	4.1 ± 2.1
LA Non-responders (n: 10)	30.4 ± 31.6	22.3 ± 21.9	20.5 ± 20.3	21.2 ± 26.1	19.8 ± 21.0	18.8 ± 22.8	16.3 ± 4.6	16.7 ± 19.0	17.2 ± 13.6
p-Value	0.03	0.02	0.01	0.02	<0.01	0.04	0.03	<0.01	<0.01

Values are expressed as mean ± SD unless otherwise specified.
V, volume; m, months; LA, laser ablation.

long-time follow-up of LA ablated nodules (15, 18, 22, 29–31, 39). Similar to the RFA technique (12, 16, 20, 30, 36), clinical and US significant reduction started as early as 1 month after treatment. As a result, symptoms improved in more than 75% of the patients. Furthermore, stability of the V reduction was maintained between 6 and 48 months of follow-up, when late regrowth was observed. Treatment did not affect the baseline autoimmunity thyroid reactivity and did not significantly change thyroid function except for the increase of TSH level to the low normal range in the two patients with subclinical hyperthyroidism.

By analyzing the distribution of V decrease and searching for factors predicting V reduction, we observed, just like a recently reported long-term study from conventional LA technique did (39), a dual pattern among treated patients.

The responder group presented a decrease in V starting 1 month after treatment achieving up to 76% of V reduction, which was stable till the end of the follow-up period. The non-responder group showed a slower and inconstant reduction in volume with a significant difference at the 12 months' follow-up. Moreover, along with the follow-up, the non-responders group showed a tendency for regrowth starting at 36 months, so that more than one-third of this group was finally referred to surgery. One of the four patients who underwent surgery had a final diagnosis of follicular encapsulated thyroid cancer.

Unlike in some previous reports (40), a tendency to produce more solid nodules in the responder group was observed as compared with microcystic nodules in the non-responder group.

Non-responder nodules were larger and received lower energy applied per thyroid volume. These results strongly indicate that probably an increase of at least 30% of the total administered energy for large nodules could improve the LA-MLIEI technique results. This could be achieved either by increasing the level of energy/illuminations in some of the illuminations during the same treatment session or by increasing the number of illuminations by reducing the distance between applications to less than 10 mm.

The LA-MLIEI single-fiber technique permits a flexible nodule ablation, increasing the possibility of approaching the nodule by the operator. Furthermore, in comparison with the multifiber procedure, the time of ablation of the LA-MLIEI single-fiber procedure is longer (50 min in comparison with 30 min), something utterly compatible with ambulatory treatment, while the expenses due to the costs of the optical fiber are significantly lower (300 € in comparison with 600 € or 900 € for multiple fibers).

The relatively small number of patients and the absence of a comparative group are to be considered as the limitations of the present study. However, the strength of this study is its extensive follow-up. Multicenter studies employing the single-fiber LA-MLIEI technique are expected for large-scale use.

In conclusion, LA-MLIEI allows rapid reduction of thyroid nodules and is a safe, effective, and well-tolerated procedure in the treatment of benign thyroid nodules with similar results in V reduction and symptom remission to those reported with conventional LA at 1, 6, and 12 months and up to 5 years of follow-up. Moreover, LA-MLIEI is a cost-effective and easily reproducible procedure since only one active fiber is used in each treatment. Therefore, it should be considered for the treatment of large V nodule candidates who need retreatment.

DATA AVAILABILITY STATEMENT

The raw data supporting the conclusions of this article will be made available by the authors, without undue reservation.

ETHICS STATEMENT

The studies involving human participants were reviewed and approved by Comite Etico Hospital Clinic Barcelona. The patients/participants provided their written informed consent to participate in this study.

AUTHOR CONTRIBUTIONS

MS and FH: primary investigators, involved in study planning, data collection, data analysis and interpretation, and manuscript writing. MM, GA, EC, RJ, RV, and DM: involved in study planning, data collection, data analysis and interpretation, and proofreading of the manuscript. IH and JB: involved in study planning, data collection, data analysis and interpretation, manuscript writing, and proofreading of the manuscript. All authors contributed to the article and approved the submitted version.

FUNDING

The project was funded by the Institut d'Investigacions Biomèdiques August Pi i Sunyer (IDIBAPS) by the Instituto de Salud Carlos III (ISCIII) PROMIS II12/00003 grant and from own research funds of the group.

REFERENCES

1. Gharib H, Papini E, Garber JR, Duick DS, Harrell RM, Hegedüs L, et al. AACE/ACE/AME Task Force on Thyroid Nodules. AMERICAN ASSOCIATION OF CLINICAL ENDOCRINOLOGISTS, AMERICAN COLLEGE OF ENDOCRINOLOGY, AND ASSOCIAZIONE MEDICI ENDOCRINOLOGI MEDICAL GUIDELINES FOR CLINICAL PRACTICE FOR THE DIAGNOSIS AND MANAGEMENT OF THYROID NODULES–2016 UPDATE. *Endocr Pract* (2016) 22(5):622–39. doi: 10.4158/EP161208.GL
2. Kim JH, Baek JH, Lim HK, Ahn HS, Baek SM, Choi YJ, et al. Guideline Committee for the Korean Society of Thyroid Radiology (KSThR) and Korean Society of Radiology. 2017 Thyroid Radiofrequency Ablation Guideline: Korean Society of Thyroid Radiology. *Korean J Radiol* (2018) 19(4):632–55. doi: 10.3348/kjr.2018.19.4.632
3. Wang B, Han ZY, Yu J, Cheng Z, Liuu F, Yu XL, et al. Factors Related to Recurrence of the Benign Non-Functioning Thyroid Nodules After Percutaneous Microwave Ablation. *Int J Hyperthermia* (2017) 33(4):459–64. doi: 10.1080/02656736.2016.1274058
4. Papini E, Pacella CM, Solbiati LA, Achille G, Barbaro D, Bernardi S, et al. Minimally-Invasive Treatments for Benign Thyroid Nodules: A Delphi-Based Consensus Statement From the Italian Minimally-Invasive Treatments of the Thyroid (MITT) Group. *Int J Hyperthermia* (2019) 36(1):376–82. doi: 10.1080/02656736.2019.1575482
5. Valcavi R, Bertani A, Pesenti M, Al Jandali Rifa'Y, Frasoldati A, Formisano D, et al. Laser and Radiofrequency Ablation Procedures. In: Baskin HJ, Duick DS, Levine RA, editors. *Thyroid US and US Guided FNA Biopsy, 2nd ed.* New York: Springer (2008).
6. Haugen BR, Alexander EK, Bible KC, Doherty GM, Mandel SJ, Nikiforov YE, et al. American Thyroid Association Management Guidelines for Adult Patients With Thyroid Nodules and Differentiated Thyroid Cancer: The American Thyroid Association Guidelines Task Force on Thyroid Nodules and Differentiated Thyroid Cancer. *Thyroid* (2016) 26(1):1–133. doi: 10.1089/thy.2015.0020
7. Valcavi R, Barbieri V, Negro R. Ultrasound-Guided Percutaneous Laser Ablation of Papillary Thyroid Microcarcinoma: A Feasibility Study on Three Cases With Pathological and Immunohistochemical Evaluation. *Thyroid* (2013) 23(12):1578–82. doi: 10.1089/thy.2013.0279
8. Mauri G, Cova L, Ierace T, Baroli A, Di Mauro E, Pacella CM, et al. Treatment of Metastatic Lymph Nodes in the Neck From Papillary Thyroid Carcinoma With Percutaneous Laser Ablation. *Cardiovasc Intervent Radiol* (2016) 39 (7):1023–30. doi: 10.1007/s00270-016-1313-6
9. Zhou W, Jiang S, Zhan W, Zhou J, Xu S, Zhang L. Ultrasound-Guided Percutaneous Laser Ablation of Unifocal T1N0M0 Papillary Thyroid Microcarcinoma: Preliminary Results. *Eur Radiol* (2017) 27(7):2934–40. doi: 10.1007/s00330-016-4610-1
10. Persichetti A, Bizzarri G, Guglielmi R, Barnabei A, Bianchini A, Coccaro C, et al. Ultrasound- Guided Laser Ablation for Local Control of Neck Recurrences of Medullary Thyroid Cancer. Afeasibility Study. *Int J Hyperthermia* (2018) 35(1):480–92. doi: 10.1080/02656736.2018.1508759
11. Ji L, Wu Q, Gu J, Deng X, Zhou W, Fan X, et al. Ultrasound-Guided Percutaneous Laser Ablation for Papillary Thyroid Microcarcinoma: A Retrospective Analysis of 37 Patients. *Cancer Imaging* (2019) 19(1):16. doi: 10.1186/s40644-019-0204-x
12. Jeong WK, Baek JH, Rhim H, Kim YS, Kwak MS, Jeong HJ, et al. Radiofrequency Ablation of Benign Thyroid Nodules: Safety and Imaging Follow-Up in 236 Patients. *Eur Radiol* (2008) 18(6):1244–50. doi: 10.1007/s00330-008-0880-6
13. Cakir B, Ugras NS, Gul K, Ersoy R, Korukluoglu B. Initial Report of the Results of Percutaneous Laser Ablation of Benign Cold Thyroid Nodules: Evaluation of Histopathological Changes After 2 Years. *Endocr Pathol* (2009) 20(3):170–6. doi: 10.1007/s12022-009-9081-3
14. Spiezia S, Garberoglio R, Milone F, Ramundo V, Caiazzo C, Assanti AP, et al. Thyroid Nodules and Related Symptoms are Stably Controlled Two Years After Radiofrequency Thermal Ablation. *Thyroid* (2009) 19(3):219–25. doi: 10.1089/thy.2008.0202
15. Papini E, Rago T, Gambelunghe G, Valcavi R, Bizzarri G, Vitti P, et al. Long-Term Efficacy of Ultrasound-Guided Laser Ablation for Benign Solid Thyroid Nodules. Results of a Three-Year Multicenter Prospective Randomized Trial. *J Clin Endocrinol Metab* (2014) 99(10):3653–9. doi: 10.1210/jc.2014-1826
16. Cesareo R, Pasqualini V, Simeoni C, Sacchi M, Saralli E, Campagna G, et al. Prospective Study of Effectiveness of US-Guided Radiofrequency Ablation Versus Control Group in Patients Affected by Benign TN. *J Clin Endocrinol Metab* (2015) 100(2):460–6. doi: 10.1210/jc.2014-2186
17. Valcavi R, Riganti F, Bertani A, Formisano D, Pacella CM. Percutaneous Laser Ablation of Cold Benign Thyroid Nodules: A 3-Year Follow-Up Study in 122 Patients. *Thyroid* (2010) 20(11):1253–61. doi: 10.1089/thy.2010.0189
18. Bernardi S, Giudici F, Cesareo R, Antonelli G, Cavallaro M, Deandrea M, et al. Five-Year Results of Radiofrequency and Laser Ablation of Benign Thyroid Nodules: A Multicenter Study From the Italian Minimally-Invasive Treatments of the Thyroid Group. *Thyroid* (2020) 30(12):1759–70. doi: 10.1089/thy.2020.0202
19. Ha EJ, Baek JH, Kim KW, Pyo J, Lee JH, Baek SH, et al. Hegedüs L Comparative Efficacy of Radiofrequency and Laser Ablation for the Treatment of Benign Thyroid Nodules: Systematic Review Including Traditional Pooling and Bayesian Network Meta-Analysis. *J Clin Endocrinol Metab* (2015) 100(5):1903–11. doi: 10.1210/jc.2014-4077
20. Cesareo R, Pacella CM, Pasqualini V, Campagna G, Iozzino M, Gallo A, et al. Laser Ablation Versus Radiofrequency Ablation for Benign Non- Functioning Thyroid Nodules: Six-Month Results of a Randomized, Parallel, Open- Label, Trial (LARA Trial). *Thyroid* (2020) 30(6):847–56. doi: 10.1089/thy.2019.0660
21. Sui WF, Li JY, Fu JH. Percutaneous Laser Ablation for Benign Thyroid Nodules: A Meta- Analysis. *Oncotarget* (2017) 8(47):83225–36. doi: 10.18632/oncotarget.17928
22. Pacella CM, Mauri G, Cesareo R, Paqualini V, Cianni R, De Feo P, et al. A Comparison of Laser With Radiofrequency Ablation for the Treatment of Benign Thyroid Nodules: A Propensity Score Matching Analysis. *Int J Hyperthermia* (2017) 33(8):911–9. doi: 10.1080/02656736.2017.1332395
23. Valcavi R, Tsamatropoulos P. Health-Related Quality of Life After Percutaneous Radiofrequency Ablation of Cold, Sòlid, Bening Thyroid Nodules: A 2-Years Follow-Up Study in 40 Patients. *Endocr Pract* (2015) 21(8):887–96. doi: 10.4158/EP15676.OR
24. Pacella CM, Mauri G, Achille G, Barbaro D, Bizzarri G, De Feo P, et al. Outcomes and Risk Factors for Complications of Laser Ablation for Thyroid Nodules: A Multicenter Study on 1531 Patients. *J Clin Endocrinol Metab* (2015) 100(10):3903–10. doi: 10.1210/jc.2015-1964
25. Baek JH, Lee JH, Sung JY, Bae JI, Kim KT, Sim I, et al. Complications Encountered in the Treatment of Benign TN With US-Guided Radiofrequency Ablation: A Multicenter Study. *Radiology* (2012) 262 (1):335–42. doi: 10.1148/radiol.11110416
26. Huh JY, Baek JH, Choi H, Kim JK, Lee JH. Symptomatic Benign Thyroid Nodules: Efficacy of Additional Radiofrequency Ablation Treatment Session —Prospective Randomized Study. *Radiology* (2012) 263(3):909–16. doi: 10.1148/radiol.12111300
27. Amabile G, Rotondi M, Pirali B, Dionisio R, Agozzino L, Lanza M, et al. Interstitial Laser Photocoagulation for Benign TN: Time to Treat Large TN. *Lasers Surg Med* (2011) 43(8):797– 803. doi: 10.1002/lsm.21114
28. Ma S, Zhou P, Wu X, Tian S, Zhao Y. Detection of the Single-Session Complete Ablation Rate by Contrast-Enhanced Ultrasound During Ultrasound-Guided Laser Ablation for Benign Thyroid Nodules: A Prospective Study. *BioMed Res Int* (2016) 2016:9565364. doi: 10.1155/2016/9565364
29. Døssing H, Bennedbæk FN, Hegedüs L. Long-Term Outcome Following Interstitial Laser Photocoagulation of Benign Cold Thyroid Nodules. *Eur J Endocrinol* (2011) 165(1):123–8. doi: 10.1530/EJE-11-0220
30. Cesareo R, Manfrini S, Pasqualini V, Ambrogi C, Sanson G, Gallo A, et al. Laser Ablation Versus Radiofrequency Ablation for Thyroid Nodules: 12-Month Results of a Randomized Trial (LARA II Study). *J Clin Endocrinol Metab* (2021) 106(6):1692–701. doi: 10.1210/clinem/dgab102
31. Spiezia S, Vitale G, Di Somma C, Assanti AP, Ciccarelli A, Lombardi G. US-Guided Laser Thermal Ablation in the Treatment of Autonomous Hyperfunctioning TN and Compressive Nontoxic Nodular Goiter. *Thyroid* (2003) 13(10):941–7. doi: 10.1089/105072503322511346
32. Dössing H, Bennedbaek FN, Bonnema SJ, Grupe P, Hegedüs L. Randomized Prospective Study Comparing a Single Radioiodine Dose and a Single Laser Therapy Session in Autonomously Functioning Thyroid Nodules. *Eur J Endocrinol* (2007) 157(1):95–100. doi: 10.1530/EJE-07

33. Papini E, Guglielmi R, Bizzarri G, Pacella CM. Ultrasound-Guided Laser Thermal Ablation for Treatment of Benign Thyroid Nodules. *Endocr Pract* (2004) 10(3):276–83. doi: 10.4158/EP.10.3.276
34. Gambelunghe G, Fatone C, Ranchelli A, Fanelli C, Lucidi P, Fanelli C, et al. A Randomized Controlled Trial to Evaluate the Efficacy of Ultrasound-Guided Laser Photocoagulation for Treatment of Benign Thyroid Nodules. *J Endocrinol Invest* (2006) 29(9):RC23–6. doi: 10.1007/BF03347368
35. Guo Y, Li Z, Wang S, Liao X, Li C. Single-Fiber Laser Ablation in Treating Selected Metastatic Lymph Nodes of Papillary Thyroid Carcinoma and Benign Cold Thyroid Nodules-Preliminary Results. *Lasers Surg Med* (2020) 52(5):408–18. doi: 10.1002/lsm.23150
36. Kim YS, Rhim H, Tae K, Park DW, Kim ST. Radiofrequency Ablation of Benign Cold Thyroid Nodules: Initial Clinical Experience. *Thyroid* (2006) 16 (4):361–7. doi: 10.1089/thy.2006.16.361
37. de Freitas RMC, Miazaki AP, Tsunemi MH, de Araujo Filho VJF, Marui S, Danilovic DLS, et al. Laser Ablation of Benign Thyroid Nodules: A Prospective Pilot Study With a Preliminary Analysis of the Employed Energy. *Lasers Surg Med* (2020) 52(4):323–32. doi: 10.1002/lsm.23144
38. Chung SR, Baek JH, Sung JY, Ryu JH, Jung SL. Revisiting Rupture of Benign Thyroid Nodules After Radiofrequency Ablation: Various Types and Imaging Features. *Endocrinol Metab (Seoul)* (2019) 34(4):415–21. doi: 10.3803/EnM.2019.34.4.415
39. Magri F, Chytiris S, Molteni M, Croce L, Coperchini F, Rotondi M, et al. Laser Photocoagulation Therapy for Thyroid Nodules: Long-Term Outcome and Predictors of Efficacy. *J Endocrinol Invest* (2020) 43(1):95–100. doi: 10.1007/s40618-019-01085-8
40. Negro R, Salem TM, Greco G. Laser Ablation is More Effective for Spongiform Than Solid Thyroid Nodules. A 4-Year Retrospective Follow-Up Study. *Int J Hyperthermia* (2016) 32(7):822–8. doi: 10.1080/02656736.2016.1212279

Conflict of Interest: The authors declare that the research was conducted in the absence of any commercial or financial relationships that could be construed as a potential conflict of interest.

Publisher's Note: All claims expressed in this article are solely those of the authors and do not necessarily represent those of their affiliated organizations, or those of the publisher, the editors and the reviewers. Any product that may be evaluated in this article, or claim that may be made by its manufacturer, is not guaranteed or endorsed by the publisher.

Advantages of publishing in Frontiers

OPEN ACCESS
Articles are free to read for greatest visibility and readership

FAST PUBLICATION
Around 90 days from submission to decision

HIGH QUALITY PEER-REVIEW
Rigorous, collaborative, and constructive peer-review

TRANSPARENT PEER-REVIEW
Editors and reviewers acknowledged by name on published articles

Frontiers
Avenue du Tribunal-Fédéral 34
1005 Lausanne | Switzerland

Visit us: www.frontiersin.org
Contact us: frontiersin.org/about/contact

REPRODUCIBILITY OF RESEARCH
Support open data and methods to enhance research reproducibility

DIGITAL PUBLISHING
Articles designed for optimal readership across devices

FOLLOW US
@frontiersin

IMPACT METRICS
Advanced article metrics track visibility across digital media

EXTENSIVE PROMOTION
Marketing and promotion of impactful research

LOOP RESEARCH NETWORK
Our network increases your article's readership